Physics and Astronomy

Impact of biomass burning emissions and dust on soluble iron deposition to Australian waters, the Southern Ocean and Antarctica

Victoria Holly Liberty Winton

This thesis is presented for the Degree of
Doctor of Philosophy
of
Curtin University

February 2016

Declaration

To the best of my knowledge and belief this thesis contains no material previously published by any other person except where due acknowledgment has been made.

This thesis contains no material which has been accepted for the award of any other degree or diploma in any university.

Signature: 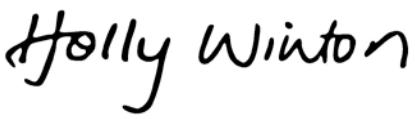

Date: 9 February 2016

Abstract

This research investigates sources of soluble atmospheric iron in the Australian sector of the Southern Hemisphere. The deposition and dissolution of aerosols containing iron into the ocean may alter macro-nutrient utilisation and thus phytoplankton, and nitrogen production by diazotrophs. In pelagic surface waters with abundant nitrate and phosphate, but low levels of iron and chlorophyll (i.e. high-nutrient, high-chlorophyll (HNLC) waters, such as the Southern Ocean), small additions of iron have been shown to result in substantial phytoplankton blooms and increased levels of marine productivity. In contrast, additions of iron to tropical waters with low levels of fixed nitrogen may result in higher rates of nitrogen fixation by diazotrophs, such as the cyanobacteria *Trichodesmium erythraeum*. Iron enhanced nitrogen fixation has been implicated in the initiation of toxic algae blooms impacting marine ecosystems and fisheries. Given the important interaction between iron and marine biogeochemistry it is not surprising that the addition of iron to HNLC waters has been proposed as a geoengineering solution to remove carbon dioxide from the atmosphere. However, very little is known with respect to natural atmospheric inputs of iron to the surface ocean. For example, the variability of fractional iron solubility in the literature (0.01 to 80 %) is larger than changes in the atmospheric iron deposition rate to the Southern Ocean on glacial-interglacial time scales. Iron bioavailability is likely a product of iron solubility, at least in the first order, and is a primary variable determining the impact of atmospheric iron deposition in marine ecosystems.

In this research, I have investigated differences in atmospheric iron solubility over tropical northern Australia, the Southern Ocean and in Antarctic snowfall. These locations were used to investigate iron in aerosols transported over continental and marine areas at different spatial scales relative to sources. The primary hypothesis tested by this research is that the variance in the observed fractional iron solubility is due to a combination of different soluble iron sources including mineral dust and biomass burning emissions. The results of the study suggest that aerosol iron derived from mineral dust is relatively insoluble regardless of atmospheric transport time. However, the interaction of mineral dust with biomass burning emission plumes may increase fractional iron solubility episodically. The results of this research do not suggest that fire emissions are a major source of soluble iron, but that they may indirectly enhance the solubility of iron derived from mineral dust. An inverse

hyperbolic relationship was observed between total iron concentration and fractional iron solubility at all the study areas, including tropical continental, marine and remote polar locations. Differences in this relationship were observed with respect to the constant fractional iron solubility at high total iron concentrations. Contrary to expectations, higher constant fractional iron solubility was found in northern tropical Australia and may be due to the presence of higher concentrations of organic acids emitted by biomass burning. The study has implications for future climate scenarios, which suggests increased biomass burning globally, for interpreting paleo records of iron deposition to the ocean and for predicating toxic algae blooms initiated by iron-fertilised nitrogen fixation.

Acknowledgments

First and most importantly, I'd like to thank my supervisors A/Prof. Ross Edwards and A/Prof. Andrew Bowie for your ongoing support, time, encouragement and open door policy for this project. Thank you, Ross, for your friendship, mentorship and taking me into your family home when I first moved to Perth. I am truly grateful for you continual input, passion and investment in this project, for teaching me publishing skills and "hyper-trace" analytical skills and for the HR-ICP-MS training you have given me. Thank you especially for teaching me to think out of the box and the importance of generating new ideas. I always looked forward to our discussions about big picture ice core and biogeochemical science and the never ending new project possibilities. These discussions kept up my enthusiasm in this project and desire to continue a career in environmental research. I am grateful that we have learnt to work effectively together, as a team, over the last three plus years, and that our professional relationship has grown. Thank you, Andy, for your dedication, continual input, and enthusiasm for this project. Your support during this time has been especially evident while you have been at sea and yet still managed to find time for this project in the extremely busy schedule and rough seas. I have thoroughly enjoyed all my research visits to UTAS. I have benefited from observing your proficient and professional project management skills over the past plus three years. Thank you for giving me the opportunity to coordinate and lead aerosol sampling projects at Cape Grim and on board the RV Investigator.

Thank you to my collaborators for your generous support. To Dr Barbara Delmonte for the open invitation to your lab, and hosting me at the University of Milano-Bicocca to carry out coulter-counter dust measurements on Roosevelt Island Climate Evolution (RICE) snow pit samples, and for your continued support regarding Antarctic dust provenance. To Dr Per Andersson for hosting me twice at the Department of Geosciences, Swedish Museum of Natural History (NRM) to carry out isotopic analyses on Antarctic dust and potential source area samples, for tutoring me in an isotope geochemistry short course, and for your continued guidance regarding Sr and Nd isotopic systems. To Dr Melita Keywood for opening up fieldwork opportunities in atmospheric campaigns for the collection of aerosols at Cape Grim, Gunn Point and on the RV Investigator. This project would not have been possible without the support of the CSIRO Ocean and Atmosphere Flagship in collecting these

samples. Thank you to Dr Akinori Ito for stimulating soluble iron concentrations at the Gunn Point using your global chemical transport model for comparison to my measurements.

This project was a contribution to a number of large international and national science projects, and I was fortunate to participate in ice core drilling and atmospheric campaigns throughout my candidature. Thank you to A/Prof Nancy Bertler and the 2012/2013 RICE ice core drilling team for allowing me to sample a snow pit at Roosevelt Island and for stable isotope measurements in the snow pit. Thank you to Dr Mark Curran and the Aurora Bain North (ABN) ice core drilling team for help digging and sampling a snow pit at ABN. In particular, to Dr Mana Inoue, Chris Plummer and Dr Olivia Maselli for your dedication to completing the snow pit in atrocious weather conditions and to Dr Andrew Moy for providing stable isotopes data from the snow pit. To the Savannah Fires in the Early Dry Season (SAFIRED) team who opened up opportunities to sample aerosols at Gunn Point. In particular, thanks to Jason Ward for technical support, to Rob Gillet and Maximilien Desservettaz for changing filters, to Dr Alastair Williams and Dr Scott Chambers for generating air mass back trajectories and sharing the radon data to help interpret aerosol sources, to Paul Selleck for providing the elemental carbon and oxalate data measured on Gunn Point filters and to Maximilien Desservettaz for providing the carbon monoxide time series data at Gunn Point.

Thank you to Karin Wallner and Hans Schöberg at NRM for technical support with Sr and Nd ion chromatography and TIMS analysis of tiny Antarctic dust samples; to Dr Pier van der Merwe and Dr Ashley Townsend at UTAS for technical support with iron solubility experiments, aerosol digestions and ICP-MS analysis; to Jason Ward at CSIRO, Nigel Somerville, Jeremy Ward and Sam Cleland at the Bureau of Meteorology (BOM) for your continued support with filter collection at Cape Grim and troubleshooting the high-volume sampler failures and advice with aerosol sampling; to Dr Sylvester Werczynski at ANSTO for generating air mass back trajectories at Cape Grim and Gunn Point, to the late Dr Kevin Rosman for the dedication and establishment of the TRACE lab and ultra-clean practices within; to Dr Phillip Boyd and Dr Edward Butler for use of the high-volume aerosol sampler that was installed at Cape Grim Baseline Air Pollution Station (CGBAPS); to Dr Alex Baker for helpful discussions on contamination issues with high-volume aerosol collection; to Dr David Carslaw for assistance with plotting back trajectories using the OpenAir package in R; to Prof. Robert Dunbar for providing Chinstrap sediment trap samples from the ROAVERRS

mooring program; to Jane Chewings, A/Prof. Brent Alloway and A/Prof. Ana Aguilar-Islas for the collection of McMurdo Sound and Granite Harbour samples; to Prof. Paul Augustinus at the University of Auckland, Prof. C. Baroni at the University of Pisa and Dr Luca Lanci and the University of Urbino for providing samples from Bunger Hills and Taylor Glacier Valley for Sr and Nd isotopic characterisation; to Ming Lim at Curtin for 3D printing; to Dr Kevin Jarrett, Gwyn Hughes, Emily Baker, Jarrad Raddon, and Dr Jing Ming for technical support in the TRACE lab; to Dr Brendan McGann for administration and project management advice; and to Melat Habtemariam and the Physics admin team for your willingness to help.

The completion of the PhD would not have been possible without the never ending encouragement and love of my family, my parents Jeannine and James, my Grandmother Grace and my brother Harry, even though you live are far away. Simon, thank you for your constant love, friendship and companionship. Words cannot express my gratitude for your moral support during the final push. A massive thank you to my officemate, colleague and dear friend Aja Ellis for your motivation, advice, daily company and laughter. Thank you to Diana Blackwood for your friendship and mentorship over the past three years. And to old and new friends I have made during my candidature for helping me achieve a work-life balance and putting perspective on things.

A final thank you to Curtin University and the University of Tasmania for making this project possible, and to the following organisations for scholarships: Curtin University and the Australia Government (Australian Postgraduate Award and Curtin Research Scholarship), Swedish Museum of Natural History (Friends of the Museum Grant), Antarctic Science Ltd (Antarctic Science Bursary), Curtin University Postgraduate Association (CUPSA) (CUPSA Data Collection Grant, and 2x CUPSA Conference Grants). Additional financial support was provided through Physics and Astronomy, Curtin University and the Association of Polar Early Career Researchers (APECS) for participation in the APECS World Summit: Shaping the Future of Polar Science in Sofia, Bulgaria, from Surface Ocean Lower Atmosphere Study (SOLAS) to attend the 2013 SOLAS summer school in Xiamen, China; from Goldschmidt for the 2015 Goldschmidt conference travel grant, and from the International Partnerships in Ice Core Science (IPICS) 2016 for travel support to attend the IPICS2016 conference in Hobart.

This project was funded through Curtin University (Curtin Research Fellowship RES-SE-DAP-AW-47679-1 to R.E.) the University of Tasmania (Rising Stars contract B0019024 to A.R.B.) the Australian Research Council (FT130100037 to A.R.B.), the Antarctic Climate and Ecosystems Cooperative Research Centre, and New Zealand Ministry of Science and Innovation through contracts to Victoria University of Wellington (Contracts: VUW0704; RDF-VUW1103) and GNS Science (Contracts: 540GCT32; C05X1001). Access to ICP-MS instrumentation at UTAS and Curtin University was facilitated through ARC LIEF funding (LE0989539 and LE130100029 respectively). CSIRO and the Australian Bureau of Meteorology in Australia are also thanked for their continuous support of the CGBAPS. Isotopic analyses for dust provenance characterisation were carried out at the Swedish Museum of Natural History and were supported by the Department of Geosciences, Swedish Museum of Natural History. Coulter counter dust measurements were carried out and supported by the University of Milano-Bicocca. The use of equipment, scientific and technical assistance of the Curtin University Electron Microscope Facility, which has been partially funded by the University, State and Commonwealth Governments is acknowledged. Wind speed data from Cape Grim was sourced from the Australian Bureau of Meteorology. Wind roses were created using OpenAir package in R and meteorological data from the Bureau of Meteorology. Acknowledgement to the NOAA Air Resources Laboratory (ARL) for the provision of the HYSPLIT transport and dispersion model and READY website (http://www.arl.noaa.gov/ready.html). Additional acknowledgements to the Norwegian Polar Institute for the use of the Qantarctica package. CSIRO Ocean and Atmosphere Flagship is acknowledged for the use of their high-volume aerosol sampler at Gunn Point. This work is a contribution to the Roosevelt Island Climate Evolution (RICE) Programme, funded by national contributions from New Zealand, Australia, Denmark, Germany, Italy, the People's Republic of China, Sweden, U.K., and the U.S.A. Logistic support was provided by Antarctica New Zealand (K049) and the US Antarctic Program. Thank you to Scott Base and Casey Station personnel, Antarctica New Zealand, the Australian Antarctic Division, CSIRO and the Marine National Facility for fieldwork and logistical support.

Table of Contents

List of publications included as part of this thesis

This thesis compiles a collection of research papers and data publications that were either published or in preparation at the time of submission. The objectives and relationship between the papers are described in the introduction. The final chapter summarises the papers as a whole and places them into a wider context of iron biogeochemistry in the Southern Hemisphere. A statement of co-authorship for each paper is located in Appendix A. Published paper 1 is reprinted in Appendix A1. As *Atmospheric Measurement Techniques Discussions* is an open access journal, no copy write license is required for paper 1. Published paper 3 is reprinted in Appendix A2 along with the copy write license. Published paper 4 is reprinted in Appendix A3 along with the copy write license. Published paper 5 is reprinted in Appendix A4. No copyright agreement is required for paper 4. The formatting of each chapter in this thesis may appear to vary, and may differ to the published form based on the requirements and formatting guidelines of each individual journal and the Curtin University PhD thesis guidelines. The list of journal and data publications included as part of this thesis is below:

Paper 1: **V.H.L. Winton**, A. Bowie, M. Keywood, P. van der Merwe, R. Edwards, 2016. Suitability of high-volume aerosol samplers for ultra-trace aerosol iron measurements in pristine air masses: blanks, recoveries and bugs. *Atmospheric Measurement Techniques Discussions*, doi:10.5194/amt-2016-12, in review.

Data publication 1: **V.H.L. Winton**, A. Bowie, M. Keywood, P. van der Merwe, R. Edwards, 2015. HR-ICP-MS soluble and total trace element data for blank Whatman 41 filters. *Curtin University Research Data*, http://doi.org/10.4225/06/564AB348340D5.

Paper 2: **V.H.L. Winton**, R. Edwards, A.R. Bowie, M. Keywood, A.G. Williams, S. Chambers, M. Desservettaz, P. Selleck, et al. Dry season aerosol iron solubility in tropical northern Australia. In prep. Plan to submit to *Atmospheric Chemistry and Physics.*

Data publication 2: **V.H.L. Winton**, R. Edwards, A.R. Bowie, M. Keywood, A.G. Williams, S. Chambers, M. Desservettaz, P. Selleck, 2015. HR-ICP-MS soluble and total trace element data for Gunn Point, Northern Territory filters, June 2014. *Curtin University Research Data*, http://doi.org/10.4225/06/5671012A48C2A.

Paper 3: **Winton, V.H.L**., A.R. Bowie, R. Edwards, M. Keywood, A.T. Townsend, P. van der Merwe, Bollhofer, A., 2015. Fractional iron solubility of atmospheric iron inputs to the Southern Ocean, *Mar. Chem*., 177, Part 1, 20-32, http://dx.doi.org/10.1016/j.marchem.2015.06.006.

Data publication 3: **Winton, V.H.L**., A.R. Bowie, R. Edwards, M. Keywood, A.T. Townsend, P. van der Merwe, Bollhofer, A., 2015. SF-ICP-MS soluble and total iron data for Cape Grim aerosols. *Curtin University Research Data*, http://doi.org/10.4225/06/565E7702F1E12.

Paper 4: **V.H.L. Winton**, R. Edwards, B. Delmonte, A. Ellis, P.S. Andersson, A. Bowie, N.A.N. Bertler, P. Neff, A. Tuohy., 2016. Multiple sources of soluble atmospheric iron to Antarctic waters. *Global Biogeochemical Cycles*, 29, doi:10.1002/2015GB005265.

Data publication 4: **V.H.L. Winton**, R. Edwards, B. Delmonte, A. Ellis, P.S. Andersson, A. Bowie, N.A.N. Bertler, P. Neff, A. Tuohy, 2015. Roosevelt Island 2012/2013 1.5 m snow pit data set. *Curtin University Research Data*, http://doi.org/10.4225/06/565BCE14467D0.

Paper 5: **V.H.L. Winton**, G.B. Dunbar, C.B. Atkins, N.A.N. Bertler, B. Delmonte, P. S. Andersson, A. Bowie, R. Edwards, 2016. The origin of lithogenic sediment in the south western Ross Sea and implications for iron fertilization. *Antarctic Science*, available on CJO2016. doi:10.1017/S095410201600002X.

Data publication 5: **V.H.L Winton**, G.B. Dunbar, C. Atkins, N.A.N. Bertler, B. Delmonte, P. Andersson, A. Bowie, and R. Edwards, 2015. McMurdo Sound dust Sr and Nd isotopic data, *Curtin University Research Data*, http://doi.org/10.4225/06/5643EBA1C8473.

List of additional publications relevant to this thesis

Additional papers and conference proceedings were published during the time of the doctoral thesis but were either not wholly researched during the thesis timeframe, or I was not the lead author. The publications are listed below, as well as the reason for their inclusion as part of the additional publications.

Papers

Paper 6: Marc Mallet, Maximilien Desservettaz, Branka Miljevic, Zoran Ristovski, Andelija Milic, Joel Alroe, Luke Cravigan, Rohan Jayaratne, Clare Paton-Walsh, David Griffith, Steve Wilson, Graham Kettlewell, Marcel Vanderschoot, Paul Selleck, Fabienne Reisen, Sarah Lawson, Jason Ward, James Harnwell, Min Cheng, Rob Gillett, Suzie Molloy, Dean Howard, Peter Nelson, Anthony Morrisson, Grant Edwards, Alastair Williams, Scott Chambers, Sylvester Werczynski, Leah Williams, Holly Winton, and Brad Atkinson, Xianyu Wang, Melita Keywood. Emissions from north Australian savannah fires in the early dry season: Project Overview. In prep. Plan to submit to *Atmospheric Chemistry and Physics.*

> This paper provides an overview to the multi-institutional Savannah Fires in the Early Dry Season campaign in which paper 2 was a contribution. I participated for two weeks in the field campaign.

Conference proceedings

Conference presentation 1: **Winton H**, Edwards R and Bowie A (2015). Latitudinal Gradients in Southern Hemispheric Soluble Iron Deposition. Goldschmidt Abstracts, 2015, 3431, *Goldschmidt*, Prague, Czech Republic, 16-21 August 2015.

> This oral presentation at an international conference is for the work in papers 2 to 4.

Conference presentation 2: Ellis. A, Edwards. R, Bertler. N, **Winton. H**, Goodwin. I, Neff. N, Tuohy. A, Proemse. B, Hogan. C, Feiteng. W. RICE ice core: Black Carbon reflects climate variability at Roosevelt Island, West Antarctica. Poster presented at *European Geophysical Union*, Vienna, Austria, 12-17 April 2014.

This poster presentation at an international conference contributed to the work in paper 4.

Conference presentation 3: **Winton H**, B. Delmonte, P. Andersson, C. Atkins, N. Bertler, A. Bowie, G. Dunbar, R. Edwards. Aeolian Dust in the Ross Sea: Local versus Distal Sources. SCAR Open Science Conference, Auckland, New Zealand, 25-28 August 2014.

This poster presentation at an international conference is for the work in papers 4 and 5.

Conference presentation 4: **Winton. H**, Edwards. R, Bowie. A, Chambers. S, Keywood. M, Wercynski. S, Williams. A.G., 2014. Aerosol iron solubility: comparison between the Australian subtropics and Southern Ocean. Oral presentation at *Atmospheric Composition & Chemistry Observations & Modelling Conference incorporating the Cape Grim Annual Science Meeting*, Melbourne, Australia, 12-14 November 2014.

This oral presentation at a national conference is for the work in paper 3.

Conference presentation 5: **Winton. H**, Edwards. R, Bowie. A, Townsend. A, van der Merwe. P, 2013. Aerosol iron over the Southern Ocean: Observations from the Cape Grim Baseline Air Pollution Station. Poster presented at *Strategic Science in Antarctica: A joint Australian & New Zealand Conference 2013*, Hobart, Australia, 24-26 June 2013.

This poster presentation at a national conference is for the work in paper 3.

Conference presentation 6: **Winton. H.**, Edwards. R, Bowie. A, Townsend. A, van der Merwe. P, Keywood. M, 2013. Seasonality of soluble aerosol iron in the Southern Ocean. Poster presented at *Atmospheric Composition & Chemistry Observations & Modelling Conference incorporating the Cape Grim Annual Science Meeting*, Melbourne, Australia, 27-29 November 2013.

This poster presentation at a national conference is for the work in paper 3.

List of fieldwork conducted as part of this thesis

Antarctic fieldwork

1. *Roosevelt Island Climate Evolution ice core drilling program*
   Ice core processing and snow pit sampling
   Roosevelt Island, Antarctica, October 2012 - January 2013
2. *Aurora Basin North ice core drilling program*
   Ice core processing, snow pit sampling and water isotope analysis
   Aurora Basin North, East Antarctic Plateau, Antarctica, December 2013 - January 2014

Ship time

1. *RV Investigator trial voyage (IN05)*
   Trace metal clean aerosol sampling
   Southern Ocean south of Tasmania, March 2015
2. *Surface Ocean Lower Atmosphere summer school cruise*
   Xiamen River, China, September 2013

Aerosol collection

1. *Savannah Fires in the Early Dry Season campaign*
   Trace metal aerosol sampling
   Gunn Point, Northern Territory, Australia, June 2014
2. *Cape Grim Baseline Air Pollution Station*
   Site survey, March 2013
   Installation and setup of long-term trace metal aerosol sampling program, May 2013
   Cape Grim, northwest Tasmania, Australia

List of abbreviations

ε	Epsilon
µm	micrometre
µg kg^{-1}	micrograms per kilo
µmol m^{-2} d^{-1}	micromolar per metre squared per day
$\delta^{18}O$	oxygen isotope ratio
δCO_2	carbon dioxide isotope ratio
$\varepsilon_{Nd}(0)$	Epsilon neodymium normalised to CHUR
$^{87}Sr/^{86}Sr$	strontium isotopic ratio
ABN	Aurora Basin North
ACE	Antarctic Climate and Ecosystems
A.D.	Anno Domino
AESOPS	Antarctic Environment and Southern Ocean Process Study
a.g.l.	above ground level
AIMS	Australian Institute of Marine Science
Al	aluminium
AR	analytical reagent
ARC	Australian Research Council
ARL	Air Resources Laboratory
ANSTO	Australian Nuclear Science and Technology Organisation
APECS	Association of Polar early Career Scientists
a.s.l.	above sea level
ATARS	Australian Tropical Atmospheric Research Station
AWS	Automatic Weather Station
AWST	Australian Western Standard Time
Ba	barium
BOM	Bureau of Meteorology
BC	black carbon

BCR	Basalt Columbia River
BSD	backscatter electron detector
Ca	calcium
$C_{aerosol}$	concentration of the aerosol
CEA	coastal East Antarctica
CGBAPS	Cape Grim Baseline Air Pollution Station
CHUR	chondritic uniform reservoir
Cl	chloride
CO	carbon monoxide
Co	cobalt
CO_2	carbon dioxide
cm s^{-1}	centimetre per second
CPP	coarse particle percentage
CR	Cape Roberts
CRC	Cooperative Research Centre
CRM	certified reference material
CSIRO	Commonwealth Scientific and Industrial Research Organisation
CT	Chinstrap sediment trap
CT1	Chinstrap sediment trap top 1
Cu	copper
CUPSA	Curtin University Postgraduate Association
DAl	dissolved aluminium
DFe	dissolved iron
DISAT	Department of Earth and Environmental Sciences
DL	detection limit
DMA	differential mobility analyser
DSI_3	Dust Strom Index
EAIS	East Antarctic Ice Shelf
EAP	East Antarctic Plateau

EAST	Australian Eastern Standard Time
EC	Elemental Carbon
EDML	EPICIA Dronning Maud Land
EDS	energy dispersive X-ray system
EPA	Environmental protection Agency
EF	enrichment factor
e.g.	for example
EPA	Environmental Protection Agency
EPICA	European Project for Ice Coring in Antarctica
ESI	Elemental Scientific Inc.
F_{dry}	dry deposition rate
Fe	iron
Fe_{BIO}	bioavailable iron
Fe_L	labile iron
FPP	fine particle percentage
Fe_R	refractory iron
Fe_S	soluble iron
Fig.	Figure
GDAS	global data assimilation system
GH	Granite Harbour
g m^{-2} yr^{-1}	grams per metre squared per year
g m^{-2} d^{-1}	grams per metre squared per day
GMT	Greenwich mean time
GNS	Geological and Nuclear Sciences
GP	Gunn Point
HAc	acetic acid
HCl	hydrochloric acid
$HClO_4$	perchloric acid
HEPA	high-efficiency particulate arrestance

HF	hydrofluoric acid
Hi-vol	high-volume
HNHC	high-nutrient, high-chlorophyll
HNLC	high-nitrate, low-chlorophyll
HNO_3	nitric acid
HR-ICP-MS	high-resolution inductively coupled plasma mass spectrometer
i.e.	that is
In	indium
IC	ion chromatography
IMAS	Institute for Marine and Antarctic Studies
IQ	Instrument Quality
ITCZ	intertropical convergence zone
K	potassium
km h^{-1}	kilometres per hour
kyr	thousand years
LIEF	Linkage Infrastructure, Equipment and Facilities
IPCC	Intergovernmental Panel on Climate Change
LGM	Last Glacial Maximum
LIL	large ion lithophile
LDPE	low density polyethylene
LNLC	low-nitrate, low-chlorophyll
LSA	Lear-Siegler
m^3	metres cubed
MP	Marble Point
m.a.s.l.	metres above sea level
mbsl	meters below sea level
MED	mobility equivalent diameters
MESS-3	Marine Sediment Reference Materials for Trace Metals and other Constituents
MDV	McMurdo Dry Valleys

MIS	McMurdo Sea Ice
Mg	magnesium
mg kg^{-1}	milligram per kilo
mg g^{-1}	milligram per gram
mg m^{-2} yr^{-1}	milligram per metre squared per year
mg m^{-2} d^{-1}	milligram per metre squared per day
mL	millilitre
Mn	manganese
MP	Marble Point
MQ	Milli-Q
MS3	Multisizer 3
MVG	McMurdo Volcanic Group
N/A	not applicable
n/d	no data
n	number
NaCl	sodium chloride
NBS	National Bureau of Standards
Nd	neodymium
NH2OH·HCl	hydroxylamine hydrochloride
Ni	nickel
NIST	National Institute of Standards and Technology
ng g^{-1}	nanogram per gram
ng m^{-3}	nanogram per cubic metre
nM	nanomolar
nmol g^{-1}	nanomole per gram
nmol L^{-1}	nanomole per litre
nmol m^{-2} d^{-1}	nanomole per meter squared per day
NOAA	National Oceanographic and Atmospheric Administration
NRM	Swedish Museum of Natural History

nss	non-sea salt sulfer
OC	organic carbon
PAH	polycyclic aromatic hydrocarbons
Pb	lead
PFA	fluorinated ethylene propylene
Pg	picograms
pg cm^{-2}	picograms per squared centimetre
pg m^{-3}	picograms per cubic metre
POM	particulate organic material
PM10	particulate matter less than ten micrometres
PP	polypropylene
ppb	parts per billion
ppm	parts per million
ppt	parts per trillion
PSA	potential source area
PTFE	polytetrafluoroethylene
PVDF	Polyvinylidene Fluoride
QC	quality control
R^2	coefficient of determination
Rb	rubidium
rBC	refractory black carbon
REE	Rare Earth Elements
RI	Roosevelt Island
RICE	Roosevelt Island Climate Evolution
Rn	radon
ROAVEERS	Research on Ocean - Atmosphere Variability and Ecosystem Response in the Ross Sea
RV	research vessel
S	Sulphur
SAFIRED	Savannah Fires in the Early Dry Season

Sd	standard deviation
SE	standard error
SE	secondary electron
SeaWiFS	Sea-Viewing Wide Field-of-View Sensor
SEM	scanning electron microscope
SF-ICP-MS	sector field inductively coupled plasma mass spectrometer
Si	silica
Sm	samarium
SOA	secondary organic aerosol
SOLAS	Surface Ocean Lower Atmosphere
SP2	single particle intracavity laser-induced incandescence photometer
SPM	suspended particulate matter
Sr	strontium
SRM	standard reference material
SW	south-western
TAM	Transantarctic Mountains
TDAl	total dissolvable aluminium
TDFe	total dissolvable iron
Tg	teragram
Tg a^{-1}	teragram per year
Th	thorium
Ti	titanium
TIMS	thermal ionisation mass spectrometer
TMF	trace metal on filter
TSP	Total suspended particulates
TSPM	total suspended particulate matter
UTAS	University of Tasmania
UTC	current local time
V^*_t	threshold velocity for particle diameter

v/v	percent by volume
V	vanadium
VFC	volume flow controlled
VSMOW	Vienna Mean Standard Ocean Water
VUW	Victoria University of Wellington
v_t	fluid threshold velocity
V_{dry}	dry deposition velocity
VFC	Volumetric Flow Controlled
VOCs	volatile organic compounds
W41	Whatman 41
WAIS	West Antarctic Ice Shelf
w.e.	water equivalent
Wt	weight
Zn	zinc

List of Figures

List of Tables

Chapter 1. Exegesis introduction

1.1 Aerosol iron and its biogeochemical importance in the Southern Hemisphere

The marine iron biogeochemical cycle and the distribution of bioavailable iron in surface waters plays a key role in marine primary productivity through iron-limitation and nitrogen fixation. Iron inputs to iron-limited surface waters of the Southern Ocean enhance macronutrient utilisation and primary productivity while inputs of iron to nitrogen poor tropical and sub-tropical waters may modulate nitrogen fixation. Globally, the atmospheric deposition of mineral dust is thought to be the primary source of new bioavailable iron to the pelagic ocean. The distribution of atmospheric iron deposition is well known, but its solubility and bioavailability is not. To date, most studies have assumed that mineral dust aerosols represent the primary source of soluble iron in the atmosphere. However, fire emissions and oil combustion are other potential sources.

1.2 Research aims and objectives of this thesis

1.2.1 Description of research aims

The over-arching aim of the project was to investigate sources of soluble atmospheric iron in the Australian tropics, the Southern Ocean and Antarctica. This project tested the hypothesis that a substantial fraction of soluble iron in the atmosphere originates from biomass burning rather than mineral dust, which is relatively insoluble. To achieve this, equipment, expertise and methodology were developed to sample and measure extremely low concentrations of soluble and total iron in aerosols and snow samples from the Australian section of the Southern Hemisphere. This study was based on; i) exposure blank aerosol filters from the Cape Grim Baseline Air Pollution Station (CGBAPS) (Chapter 3), ii) a time series of archived aerosol samples from CGBAPS from 1999-2000 [*Bollhöfer et al.*, 2005] (Chapter 5), iii) a time series of aerosol samples from Gunn Point, Northern Territory collected during the Savannah Fires in the Early Dry Season (SAFIRED) campaign in June 2014 (Chapter 4), iv) snow samples from a snow pit at Roosevelt Island, Ross Sea as part of the Roosevelt Island Climate Evolution Project (RICE) (Chapter 6), and v) a suite of surface snow samples collected from the McMurdo sea ice in November 2009 [*Winton et al.*, 2014] (Chapter 7).

The aerosol and snow pit samples contained a record of spatial variability in soluble iron deposition across a latitudinal gradient in the Southern Hemisphere. The snow pit contained a high-resolution record of variable dust fluxes, long-range transported refractory black carbon (rBC; fire tracer) concentrations, and dissolved and total dissolvable iron concentrations over the past few years, including an exceptionally large rBC event in 2012. These samples are important as Australia is a large potential source area (PSA) of both mineral dust and biomass burning emissions in the Southern Hemisphere, and there is a dearth of soluble iron measurements in this region.

1.2.2 Objectives of this thesis

Specific project objectives and the steps undertaken to achieve them were:

1. *Assess the suitability of high-volume aerosol samplers for ultra-trace aerosol iron measurements in low aerosol iron loading environments.*

    a) Establish a high-volume aerosol sampling program at the CGBAPS, northwest Tasmania using trace metal protocols to sample baseline marine air over the Southern Ocean. Determine exposure, procedural and instrumental blank exposure filters.

    b) Assess the cleanliness of the sampling system by carrying out microscope observations, iron solubility experiments and total aerosol iron digestions of the exposure blank filters. Determine a blank iron budget for the blank exposure filters.

2. *Investigate soluble aerosol iron in fresh smoke in the Australian tropics.*

    a) Collect a time series of aerosol samples during the dry season from the Australian Tropical Atmospheric Research Station (ATARS), Gunn Point, Northern Territory.

    b) Measure the soluble and total iron concentration in the samples.

    c) Determine potential sources of aerosol iron using a combination of air mass back trajectories, enrichment factor analysis, and radon222 concentrations.

    d) Compare the soluble iron data to elemental carbon (fire tracer) concentrations, and global chemical transport models [*Ito*, 2015] of soluble aerosol iron.

3. *Investigate soluble aerosol iron in Southern Ocean baseline air.*

    a) Measure the soluble, labile and total iron concentration in archived samples collected from a 70 m telecommunications tower at CGBAPS.

    b) Compare the soluble iron data to atmospheric organic acids to assess their influence on fractional iron solubility.

4. *Investigate soluble aerosol iron sources to the eastern Ross Sea.*

a) Sample a two year high-resolution record of soluble iron from a snow pit at Roosevelt Island.

b) Measure dissolved and total dissolvable iron concentrations, dust concentrations, stable water isotope ratios and refractory black carbon (rBC; fire tracer) concentrations in the samples.

c) Investigate the provenance of mineral dust to the site using particle counts, particle size distribution and Nd and Sr isotopic ratios of mineral dust.

5. *Investigate the provenance of lithogenic sediment in the southwestern Ross Sea and assess the implications for natural iron-fertilisation by local dust.*

a) Investigate the provenance of dust deposited on sea ice in McMurdo Sound, southwestern (SW) Ross Sea and the lithogenic fraction of sediment suspended in the water column from a sediment trap in the SW Ross Sea (collected by R. Dunbar, 1997) using Nd and Sr isotopic ratios and mixing models.

b) Assess the importance of local dust as a source of new dissolved iron to the SW Ross Sea.

1.2.3 Note on elemental/black carbon terminology

Within the literature, there is a difference in the terminology between refractory black carbon (rBC) and elemental carbon: rBC is often referred to as elemental or graphitic carbon, although the nomenclature is dependent on the analytical method [*Andreae and Gelencsér*, 2006]. *Andreae and Gelencsér* [2006] suggest that elemental carbon refers to the fraction of carbon that is oxidized in combustion analysis above a certain temperature threshold, and only in the presence of oxygen. Refractory black carbon is a carbonaceous material formed during combustion of carbon based fuels [*Bond et al.*, 2013]. Refractory black carbon can be determined by light absorbing carbon methods using the optical adoption technique as it's physical properties allows it to be distinguished from other forms of aerosol carbon. These physical properties include: strong visible light absorption, insolubility in water, refraction, and aggregation of small carbon spherules [*Bond et al.*, 2013]. The terminology used in this thesis reflects that of the original author, as it is difficult to convert between black and elemental carbon. These terms are used interchangeably in this thesis.

1.3 Layout of this thesis

This research has produced a number of manuscripts and peer-reviewed publications. One publication is published, two publications are in press, one manuscript is currently under review and another is in the process of submission. These manuscripts and publications make

up the body of this thesis. Copyright agreements to reproduce publications resulting from this thesis can be found in Appendices A. This thesis is organised into the following sections:

1. *Introduction*

Chapter 1 describes the context of this research, the research aims and objectives, the layout of this thesis and outlines the analyses conducted.

2. *Literature review*

Chapter 2 reviews the literature regarding the importance of iron for primary production in the Southern Ocean and tropical waters, the deposition of aeolian dust and black carbon, and the bioavailability of aerosol iron.

3. *Paper 1*

V.H.L. Winton, A. Bowie, M. Keywood, P. van der Merwe, R. Edwards, 2016. Suitability of high-volume aerosol samplers for ultra-trace aerosol iron measurements in pristine air masses: blanks, recoveries and bugs. *Atmospheric Measurement Techniques Discussions*, doi:10.5194/amt-2016-12, in review.

4. *Paper 2*

V.H.L. Winton, R. Edwards, A.R. Bowie, M. Keywood, A.G. Williams, S. Chambers, M. Desservettaz, C. Selleck, et al. Dry season aerosol iron solubility in tropical northern Australia. To be submitted to *Atmospheric Chemistry and Physics*.

5. *Paper 3*

Winton, V.H.L., A.R. Bowie, R. Edwards, M. Keywood, A.T. Townsend, P. van der Merwe, Bollhofer, A., 2015. Fractional iron solubility of atmospheric iron inputs to the Southern Ocean, *Mar. Chem.*, 177, Part 1, 20-32, http://dx.doi.org/10.1016/j.marchem.2015.06.006.

6. *Paper 4*

V.H.L. Winton, R. Edwards, B. Delmonte, A. Ellis, P.S. Andersson, A. Bowie, N.A.N. Bertler, P. Neff, A. Tuohy, 2016. Multiple sources of soluble atmospheric iron to Antarctic waters. *Global Biogeochemical Cycles,* 29, doi:10.1002/2015GB005265.

7. Paper 5

V.H.L. Winton, G.B. Dunbar, C.B. Atkins, N.A.N. Bertler, B. Delmonte, P. S. Andersson, A. Bowie, R. Edwards, 2016. The origin of lithogenic sediment in the south western Ross Sea and implications for iron fertilization. *Antarctic Science*, available on CJO2016. doi:10.1017/S095410201600002X.

8. Exegesis and future work and recommendations

The exegesis reviews and discusses the linkages between the manuscripts and publications. This chapter answers the objectives set above by; a) compiling and assessing latitudinal trends in soluble aerosol iron data from low latitude locations in the Northern Territory, Australia to high latitude locations on the East Antarctic Plateau, b) evaluating the impact of biomass burning to soluble iron deposition in the Australian sector of the Southern Hemisphere by comparing refractory black carbon (rBC), dust and soluble aerosol iron, and comparing the data to global chemical transport models, and c) applying a simple two component mixing model of data produced in this thesis to ice core dust records of the last 800,00 years to estimate how soluble iron concentrations and fractional iron solubility may have changed during glacial-interglacial periods.

References

Andreae, M., and A. Gelencsér (2006), Black carbon or brown carbon? The nature of light-absorbing carbonaceous aerosols, *Atmospheric Chemistry and Physics*, *6*(10), 3131-3148.

Bollhöfer, A., K. J. R. Rosman, A. L. Dick, W. Chisholm, G. R. Burton, R. D. Loss, and W. Zahorowski (2005), Concentration, isotopic composition, and sources of lead in Southern Ocean air during 1999/2000, measured at the Cape Grim Baseline Air Pollution Station, Tasmania, *Geochimica et Cosmochimica Acta*, *69*(20), 4747-4757.

Bond, T. C., et al. (2013), Bounding the role of black carbon in the climate system: A scientific assessment, *Journal of Geophysical Research: Atmospheres*, *118*(11), 5380-5552.

Winton, V. H. L., G. B. Dunbar, N. A. N. Bertler, M. A. Millet, B. Delmonte, C. B. Atkins, J. M. Chewings, and P. Andersson (2014), The contribution of aeolian sand and dust to iron fertilization of phytoplankton blooms in southwestern Ross Sea, Antarctica, *Global Biogeochemical Cycles*, *28*(4), 2013GB004574.

Chapter 2. Literature review

2.1 Introduction

Iron-fertilisation of the Southern Ocean has been proposed as one of the drivers initiating glacial cycles. *Martin* [1990] suggested that increased iron supply, by higher dust fluxes, during glacial maxima triggered higher rates of primary production and thus carbon sequestration to the ocean. Consequently, global climate was impacted by reducing the atmospheric carbon dioxide (CO_2) concentration. Subsequent analysis of Antarctic ice cores supported the "iron hypothesis" and showed that over glacial-interglacial cycles the rate of dust deposition is inversely correlated to atmospheric concentrations of CO_2, however there are some questions with respect to leads and lags [*Lambert et al.*, 2008; *Petit et al.*, 1999]. Co-variation of iron and mineral dust proxies in Antarctic ice cores display higher deposition rates during glacial stages [*Edwards et al.*, 2006; *Gaspari et al.*, 2006; *Vallelonga et al.*, 2013]. Southern Ocean marine sediments from several regions also link enhanced glacial atmosphere iron deposition to higher rates of primary productivity [*Anderson et al.*, 2014; *Martínez-Garcia et al.*, 2009; *Martínez-García et al.*, 2014; *Moore et al.*, 2000]. While other studies postulate that higher rates of iron input to the Southern Ocean during glacial periods were sourced from the upwelling of water enriched by sediments [*Latimer and Filippelli*, 2001; *Latimer et al.*, 2006]. Recently, *Conway et al.* [2015] suggest that soluble iron deposition to the Southern Ocean during the Last Glacial Maximum (LGM) would have been at least ten times greater than modern deposition, with similar rates to an upwelling supply of iron. Most recently, numerical modelling by *Lambert et al.* [2015] shows that higher LGM dust deposition may have only reduced atmospheric CO_2 by <10 ppm, however, greater carbon burial and carbonate compensation would have further decreased atmospheric CO_2 around 10 ppm over millennial timescales. It is now well established that primary productivity in the modern Southern Ocean is limited due to low iron availability [e.g. *Blain et al.*, 2007; *Boyd et al.*, 2007; *Boyd et al.*, 2000; *Martin et al.*, 1991]. *In situ* iron-fertilisation experiments have shown that carbon can be exported to deep sediments following phytoplankton blooms induced by iron relief to iron-limited waters [*Smetacek et al.*, 2012].

The current literature suggests that while at present mineral dust is an important source of new iron to remote ocean waters, it not the only one [e.g. *Boyd and Ellwood*, 2010]. Aerosol

iron deposition rates to the remote Southern Ocean surface waters are the lowest on earth ranging from 0.3-2.5 mg m^{-2} d^{-1} [*Winton et al*., 2015; and references within]. Iron deposition to the region has been investigated in relation to the distribution and transport of mineral dust [*Bowie et al.*, 2009; *Donaghay et al.*, 1991; *Gao et al.*, 2013; *Luo et al.*, 2005; *Mahowald et al.*, 2005; *Wagener et al.*, 2008]. Atmospheric iron deposition events associated with dust storms have been reported to relieve iron-limitation and trigger phytoplankton blooms in the Southern Ocean [*Boyd et al.*, 2004; *Gabric et al.*, 2010; *Johnson et al.*, 2010; *Mackie et al.*, 2008]. This is in contrast to dust deposition events in the Atlantic Ocean [e.g. *Banerjee and Prasanna Kumar*, 2014]. Nevertheless, aerosol iron is an important contributor to the supply of new iron in remote iron-depleted waters. Despite several decades of research, the atmospheric deposition of iron to the ocean is not well quantified, especially around water adjacent to Australia and in the Southern Ocean. The first section of this literature review assesses the importance of mineral dust as a source of new iron to the Australian sector of the Southern Ocean (area defined in Fig. 2.1), by examining i) the sources of iron and the delivery mechanisms to the ocean, and ii) the bioavailability of aerosol iron. The second and third sections review potential dust and biomass burning sources of iron to the Australian sector of the Southern Ocean.

2.1.1 Regional setting

2.1.1.1 Iron-limitation: Australian tropical waters

Waters surrounding Australia are not generally thought of as being directly iron-limited. However, nitrogen fixers, such as nonheterocystous cyanobacteria *Trichodesmium* [*Berman-Frank et al.*, 2001; *Paerl et al.*, 1994], reside in some oligotrophic, low nitrate, low chlorophyll (LNLC) tropical waters north of Australia (Fig. 2.1). In these waters, iron availability is a primary factor limiting nitrogen fixation by diazotrophic phytoplankton [*Falkowski*, 1997; *Mills et al.*, 2004; *Rueter*, 1988; *Rueter et al.*, 1992]. The addition of bioavailable iron can influence inputs of newly fixed nitrogen into surface waters [*Paerl et al.*, 1987; *Rueter*, 1988], and trigger toxic algal blooms [*Abram et al.*, 2003; *LaRoche and Breitbarth*, 2005]. The high iron requirement for nitrogen fixation is reflected in higher Fe:C quotas of *Trichodesmium*, compared with other marine phytoplankton such as diatoms [*Johnson et al.*, 1997; *Kustka et al.*, 2003; *Rueter et al.*, 1992]. High iron requirements were

observed during a phytoplankton bloom in coastal waters north of Australia [*Berman-Frank et al.*, 2001].

Little is known about how atmospheric inputs of iron impact biota and modify the carbon balance in oligotrophic waters. In the oligotrophic waters of the north Tasman Sea, a ten-fold increase in nitrogen fixation was observed in response to a cyclone. The cyclone stimulated diazotrophic phytoplankton by enhanced phosphate availability in the absence of nitrate, and increased the dissolved iron supply by wet deposition of Australian dust [*Law et al.*, 2011]. In other tropical regions, studies have shown that large toxic algal blooms, such as dinoflagellate Gymnodinium and cyanobacteria have been stimulated by atmospheric deposition of nutrients. For example, the deposition of volcanic ash and Saharan dust may have alleviated the iron-limitation of toxic diazotrophs, thus fuelling nitrogen fixation of red tides in the eastern Gulf of Mexico [*Lenes et al.*, 2008; *Walsh and Steidinger*, 2001]. *Guieu et al.* [2014] investigated episodic inputs of aerosol iron to LNLC waters and found that the overall impact was not a simple fertilisation effect of increasing phytoplankton biomass as observed in HNLC regions. The authors found that although phytoplankton growth could be enhanced by additions of aerosol iron, increased bacterial activity, and respiration resulted in a weakening of biological carbon sequestration.

2.1.1.1 Iron-limitation: waters south of Australia

The Southern Ocean is characterized by high nitrate, low chlorophyll (HNLC) waters, where diatoms typically reside. These waters are characteristically replete with nitrate and phosphate and depleted with iron (Fig. 2.1). However, nitrate and phosphate macro-nutrients are not fully utilised, resulting in usually low primary production [e.g. *Arrigo et al.*, 2008a]. In HNLC waters, mesoscale perturbation experiments have demonstrated that low iron availability limits primary production [*Boyd et al.*, 2007]. Dissolved iron (DFe) concentrations in the Southern Ocean are variable [*de Baar and de Jong*, 2001], with typical DFe concentrations in waters south of Australia around 0.1-0.7 nmol L^{-1} [*Bowie et al.*, 2009]. In contrast to the Southern Ocean, the Ross Sea is the most biologically productive continental shelf region in Antarctica and experiences intense seasonal phytoplankton blooms [e.g. *Arrigo and McClain*, 1994; *Smith and Gordon*, 1997]. The Ross Sea is seasonally iron-limited and has a high-nutrient high-chlorophyll (HNHC) regime compared to the chronically iron-limited HNLC regime of the Southern Ocean. The Ross Sea is dominated by *Phaeocystis antarctica* and diatoms [*Arrigo et al.*, 2000].

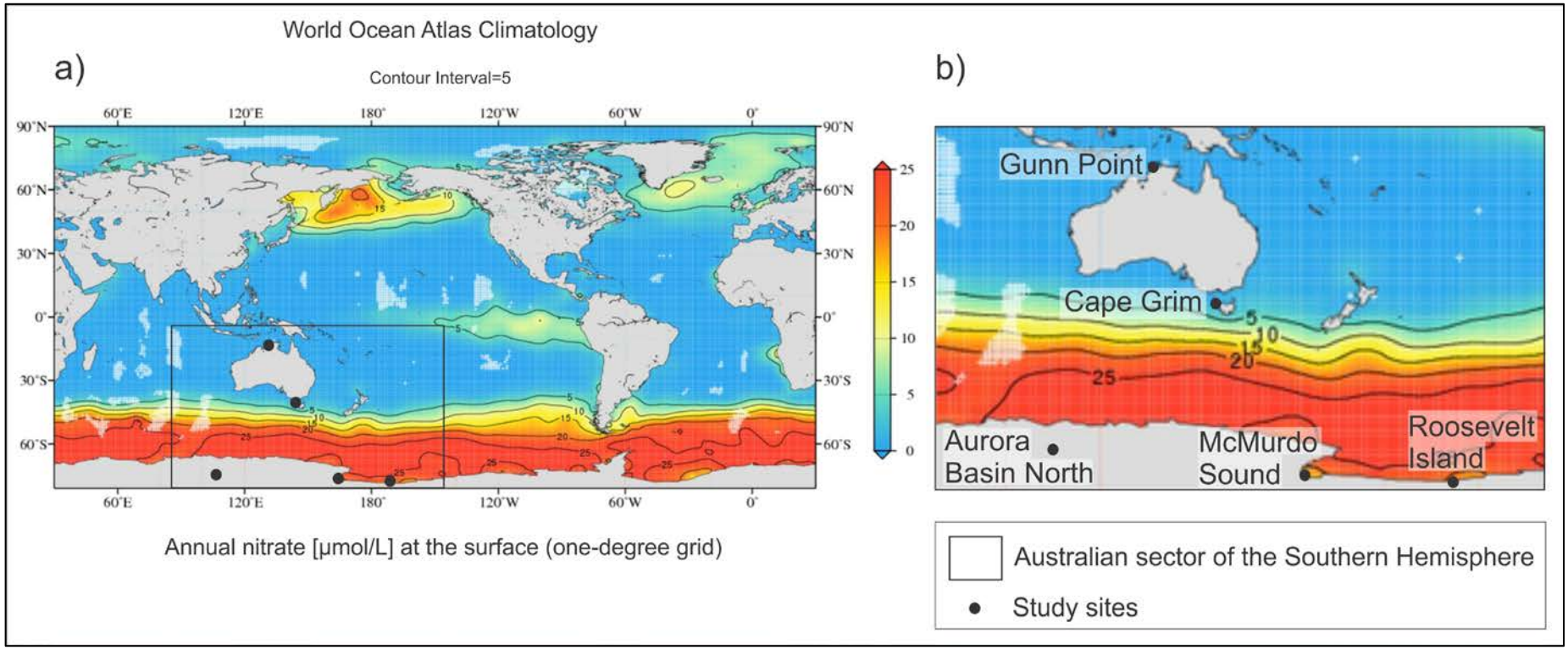

Fig. 2.1: a) Global ocean surface nitrate concentrations. b) Insert of the region defined as the "Australian sector of the Southern Hemisphere", and the study sites that cross a latitudinal gradient in ocean nitrate concentrations in this research. Source: World Ocean Atlas 2013 V2 (https://www.nodc.noaa.gov/OC5/woa13/).

2.2 Iron biogeochemistry

2.2.1 Modes of iron supply to the Southern Ocean, Antarctica and Australian waters

Mineral dust as a source of iron to the open ocean has been the focus of many studies on a global scale [*Sholkovitz et al.*, 2012]. Other potential iron sources include; upwelling of deep ocean waters [*de Baar et al.*, 1995; *Grand et al.*, 2015c; *Robinson et al.*, 2014], deep winter mixing and entrainment [*Bowie et al.*, 2014; *Tagliabue et al.*, 2014], transport from continental margins by ocean currents [*Elrod et al.*, 2004; *Johnson et al.*, 1999], from sea-ice, ice bergs and ice shelve melting [*Gerringa et al.*, 2012; *Lannuzel et al.*, 2010; *Raiswell et al.*, 2008a; *Raiswell et al.*, 2008b; *Sedwick and DiTullio*, 1997], and hydrothermal vents [*Frants et al.*, 2016; *Resing et al.*, 2015; *Tagliabue et al.*, 2010]. These sources are illustrated in Fig. 2.2a. The relative importance of each source varies spatially (shown in the global marine iron cycle from a simple inverse model in Fig. 2.3) and temporally.

Until a year ago, little was known about sources of iron to the Ross Sea. *Sedwick et al.* [2011] observed that the winter reserve of DFe in the Ross Sea is consumed by phytoplankton early in the season (Fig. 2.2b) and that the resulting iron limitation must be overcome by new sources to sustain the major biomass observed over summer. The authors identified possible sources of new DFe as episodic vertical exchange, lateral advection, aerosol input, and reductive dissolution of particulate iron. In the last year, a number of new studies have emerged and have confirmed that upwelling of iron-rich waters is the primary source of iron to surface waters in the Ross Sea [*Gerringa et al.*, 2015; *Kustka et al.*, 2015; *Marsay et al.*, 2014; *McGillicuddy et al.*, 2015; *Sedwick et al.*, 2011]. A few studies have quantified local dust [*Bhattachan et al.*, 2015; *de Jong et al.*, 2013; *Winton et al.*, 2014] and sea ice [*de Jong et al.*, 2013; *McGillicuddy et al.*, 2015] as additional sources that supply DFe to the Ross Sea in the austral summer.

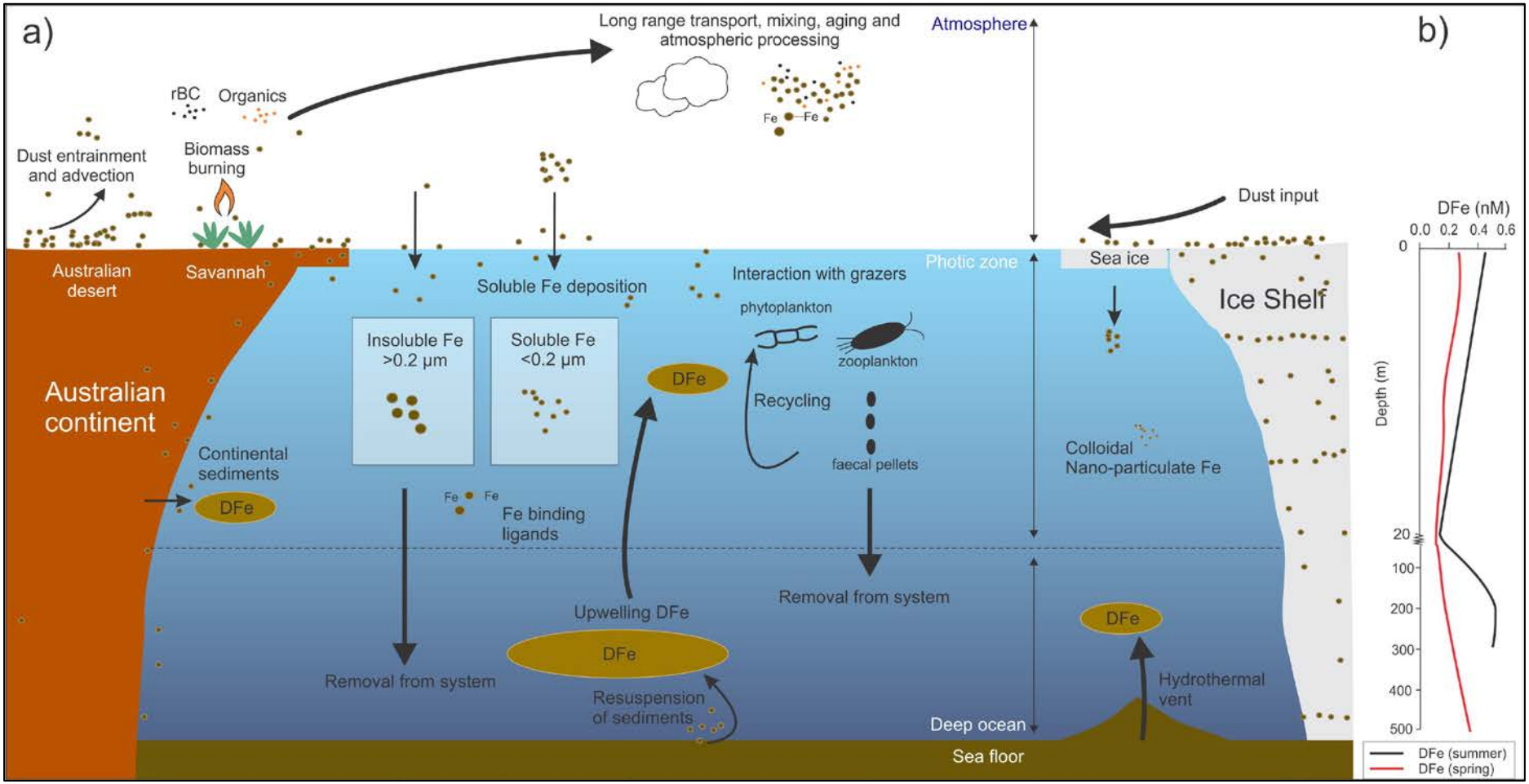

Fig. 2.2: Schematic illustrating sources of iron to the surface ocean. a) Sources of new iron and the processes that impact iron solubility in the atmosphere and ocean. b) Example of a dissolved iron (DFe) profile for the Ross Sea. The profile illustrates that surface ocean DFe is consumed early in the phytoplankton growing season [*Sedwick et al.*, 2011].

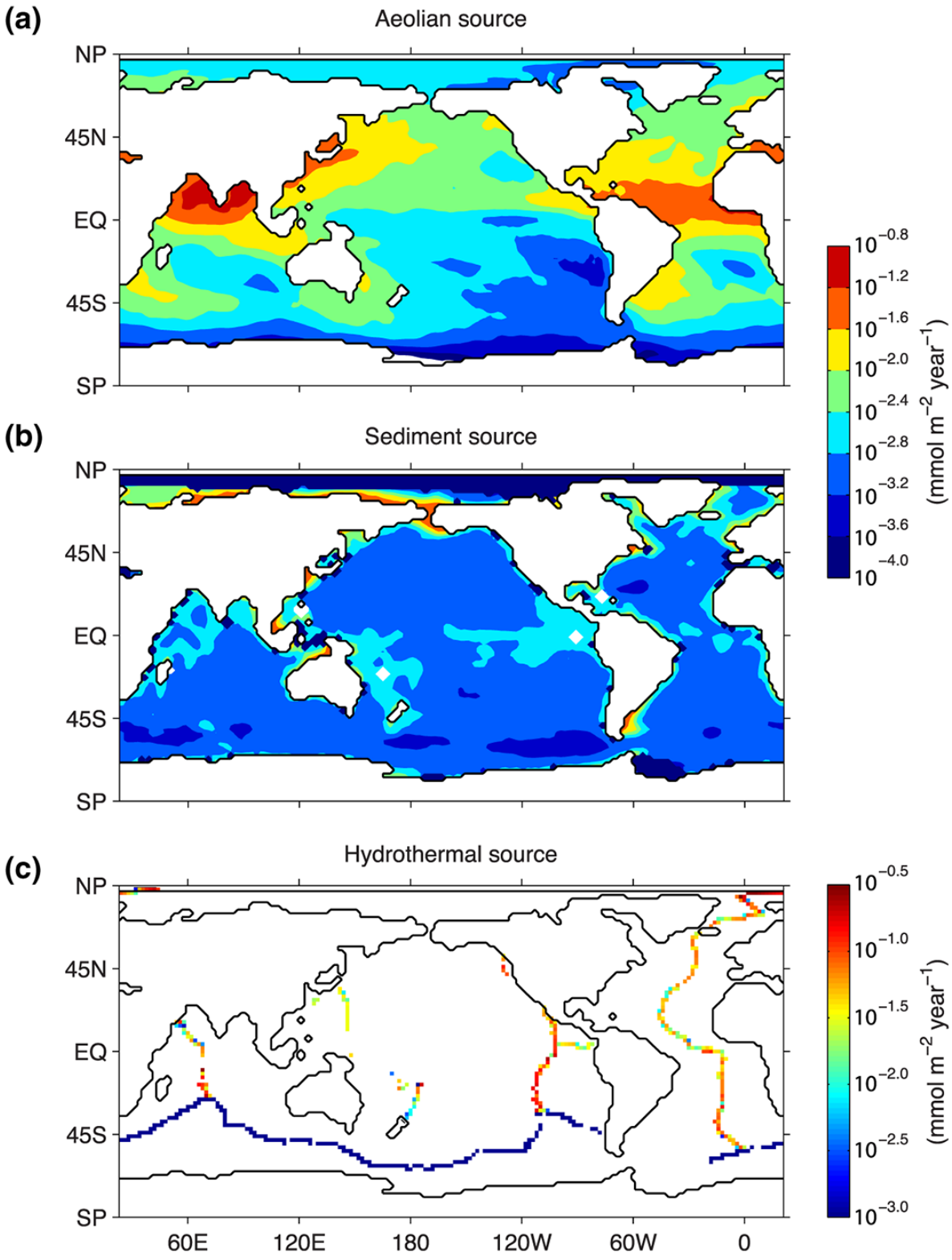

Fig. 2.3: The global modelled distribution of iron sources. a) Aeolian source from dust and combustion sources. b) Sediment source. c) Hydrothermal source. Note the logarithmic colour scales. Source: *Frants et al.* [2016].

2.2.2 Aerosol iron

The iron biogeochemistry section of this literature review focuses on aerosol iron as a source of new iron to oceanic waters. Firstly, the terminology of bioavailable versus soluble iron is clarified, secondly the variability in estimates of soluble iron and the factors influencing this variability are examined, and thirdly multiple sources of soluble iron are discussed as an explanation for the large variability of soluble iron observed on a global scale.

2.2.2.1 Note on bioavailability versus solubility and the measurement of soluble iron

From a biogeochemical perspective, it is not the total amount of aerosol iron supplied to the ocean that is important but the amount that is bioavailable, i.e., the amount available for uptake and utilisation by living cells. However, a major difficulty in assessing the bioavailability of aerosol iron in marine environments is the lack of consistency in the operational definition of soluble or bioavailable iron. The most common approach to understanding the delivery of iron-bearing aerosols to biota has been to quantify the solubility of iron from aerosols and assume that all iron that is soluble is bioavailable. There are limitations to this approach as not all soluble iron is necessarily bioavailable [*Boyd et al.*, 2010]. The operational definition of soluble iron is determined by the available methods. Such methods include iron leaching experiments and numerical models [e.g. *Baker et al.*, 2006; *Ito and Shi*, 2015]. In this thesis, soluble iron is operationally defined as iron that passes through a 0.2 or 0.45 μm filter.

Reported values of the percentage of iron in aerosols that are soluble (i.e., fractional iron solubility defined by equation (2.1)) range from 0.01 to 90 % [*Mahowald et al.*, 2005; *Sholkovitz et al.*, 2012; and references within].

$$Fractional\ Fe\ solubility = \frac{Soluble\ Fe}{Total\ Fe} x\ 100 \qquad \text{(Equation 2.1)}$$

This variation in fractional iron solubility reflects differences in the properties of aerosol (e.g. source and mineralogy, see section below), but also due to the inconsistency in aerosol iron leaching methods and the operational definitions of soluble iron. Leaching methods involve the extraction of soluble iron from aerosols, collected on a filter, via exposure to a leaching solution. There is a wide variation in the iron extraction method in the literature e.g. from leaching solution type and volume (ultra-pure water, seawater, weak acid) to leaching time

(instantaneous to 3 months [e.g. *Buck et al.*, 2006; *Edwards and Sedwick*, 2001]). *Aguilar-Islas et al.* [2010] showed that the variability of fractional iron solubility derived from leaching schemes was less than the variability derived from the chemical and physical proprieties of the aerosol. To mimic aerosol iron dissolution in nature, seawater is the preferred leaching solution. However, the heterogonous chemistry of seawater is likely to contribute to the large variation in reported fractional iron solubility. *Baker and Croot* [2010] highlight that as seawater is heterogonous in time and space; reproducibility of iron leaching results using seawater is difficult. The authors suggest the use of a standardised method with an artificial seawater standard. Recently, progress toward a standardised method has been made through the GEOTRACES aerosol intercalibration experiment [*Morton et al.*, 2013] however, the implementation of a standardised method is still ongoing. Previous studies have recommended using a simple ultra-pure water leach for easy comparison among different research groups and standardising of results from different aerosols source regions [e.g. *Desboeufs et al.*, 2005b; *Spokes et al.*, 1994]. Thus, I adopt the ultra-pure water leach method in this research. New aerosol iron leaching methods employ the use of ligands, reducing agents and photochemistry to mimic the dissolution of iron in seawater. For example, organic acids have been used to mimic mineral dust and organic aerosol interactions during atmospheric transport [*Ito and Shi*, 2015] and cloud processing [*Shi et al.*, 2015], and also variations temperature, pH and oxygen levels to mimic changing surface ocean conditions [*Fishwick et al.*, 2014].

2.2.2.2 Factors affecting the variability in fractional iron solubility

Aside from the complexities in measuring soluble iron, there are a number of environmental controls than have an impact on fractional iron solubility. Some of these processes, illustrated in Fig. 2.2a, occur in the atmosphere while other take place in the ocean [*Boyd et al.*, 2010].

Atmospheric controls on fractional iron solubility

Some studies have proposed a physical control on fractional iron solubility, i.e., the preferential removal via settling of large particles during long-range transport. Thus, at lower dust concentrations distal from the source, the modal particle size is smaller and has a correspondingly larger surface area to volume ratio. A greater proportion of the iron content at the surface led *Baker and Jickells* [2006] to propose that fine particles would have a higher fractional iron solubility. However, other field studies were not able to confirm this [*Buck et*

al., 2006; *Luo et al.*, 2005], and it appears fractional iron solubility is not a simple function of particle size. Some studies have observed fractional iron solubility as a function of aerosol particle concentration with higher iron solubility observed at lower suspended particle concentrations [*Baker and Jickells*, 2006; *Bonnet and Guieu*, 2004; *Chen and Siefert*, 2004; *Spokes and Jickells*, 1995; *Trapp et al.*, 2010].

Laboratory studies suggest dust and aerosols under atmospheric transport can undergo a number of atmospheric physio-chemical processes that can enhance the dissolution of iron, for example in clouds [e.g. *Desboeufs et al.*, 2005a], and over several cycles of evaporation and hydration with associated changes in pH [*Mackie et al.*, 2005; *Spokes and Jickells*, 1995]. Internal mixing of acidic and mineral dust components of an aerosol population enhances fractional iron solubility, and has been demonstrated in laboratory studies that simulate changes in aerosol pH [*Spokes et al.*, 1994; *Zhu et al.*, 1992]. Atmospheric processing under acidic conditions outside clouds can also increase soluble iron in mineral dust [*Shi et al.*, 2015; *Zhu et al.*, 1992; *Zhu et al.*, 1993].

Mineral dust can be mixed with organic acids and humic material in the atmosphere (Fig. 2.2a) [*Alexander et al.*, 2015; *Huang et al.*, 2014]. Sulfates, nitrates and carboxylic acids, e.g. oxalic acid, are common in aerosol populations derived from anthropogenic contamination or biomass burning emissions, and could enhance the solubility of mineral dust [*Huang et al.*, 2006; *Ito*, 2015; *Ito and Shi*, 2015; *Zuo and Zhan*, 2005]. However, in remote areas in the Southern Ocean, oxalic acid concentrations (measured as oxalate as the conjugate base throughout this research), are typically 20-100 times lower than urban air (10-50 ng m^{-3} compared to 900 ng m^{-3}; [*Warneck*, 2003]). Therefore, organic compounds, such as oxalate, may be less relevant in the less polluted air masses in the Australian southeast dust path compared to the northwest dust path where substantial biomass burning derived oxalate aerosols are produced (see section 2.3.3 for dust paths). Solubility enhancing pollutants, such as SO_x and NO_x, are low in the Southern Hemisphere [*Ayers et al.*, 1997]. In addition, studies in other regions found no correlation between the concentration of acidic species and fractional iron solubility [*Baker et al.*, 2006; *Spokes and Jickells*, 1995].

Perhaps the most important variable controlling fractional iron solubility is the aerosol source. Fractional iron solubility is dependent on the mineral composition of dust [*Baker et al.*, 2006; *Raiswell et al.*, 2008b], and on the type of aerosol e.g. mineral dust versus anthropogenic aerosol [*Aguilar-Islas et al.*, 2010; *Sedwick et al.*, 2007; *Sholkovitz et al.*,

2009; *Sholkovitz et al.*, 2012]. Iron speciation can vary considerably among sources and could be a driver of iron solubility [e.g. *Schroth et al.*, 2009]. Furthermore, glacial weathering of sediments can enhance iron solubility [*Raiswell et al.*, 2008a; *Schroth et al.*, 2009].

Oceanographic controls on fractional iron solubility

Post-depositional processes can also solubilise iron from aerosols in surface waters (Fig. 2.2a). *Boyd et al.* [2005] suggests two mechanisms by which dust dissolution occurs in the surface ocean: physio-chemically mediated dissolution on the order of hours (estimated using instantaneous leaching schemes) and microbial/photo-chemically mediated dissolution on the order of weeks (estimated using reducing agents in leaching schemes [e.g. *Berger et al.*, 2008]). *Wu et al.* [2001] and *Aguilar-Islas et al.* [2010] suggest that aerosol iron deposition was mainly released in the colloidal pool, and there is evidence that colloidal iron is bioavailable [*Barbeau and Moffett*, 1998; *Chen and Siefert*, 2003; *Rich and Morel*, 1990; *Wells et al.*, 1983]. Nano-particles are also potentially bioavailable [*Raiswell et al.*, 2008a; *Raiswell et al.*, 2008b]. Photochemical reactions in the surface ocean are also important for maintaining bioavailable iron in the mixed layer, and can influence iron solubility when the surface ocean is sunlit. Iron-fertilisation experiments in the Southern Ocean show that photo-reduction extends the lifetime of Fe(II) [*Croot et al.*, 2001; *Croot et al.*, 2005; *Johnson et al.*, 1994]. Grazing by zooplankton, bacteria and whales recycles iron in the water column [*Boyd and Ellwood*, 2010; *Nicol et al.*, 2010; *Smetacek et al.*, 2004]. Iron contained in colloids and particulates may be ingested by zooplankton. The action of digestive enzymes results in a fraction of the iron becoming soluble. Grazing of phytoplankton and zooplankton may release iron-binding ligands, further increasing the solubility of iron [*Sato et al.*, 2007]. Furthermore, excretion of iron as faeces from zooplankton may be consequently taken up by phytoplankton [*Barbeau et al.*, 1996; *Hutchins et al.*, 1993]. Organic complexation is another factor; the concentration of particulate iron in seawater is controlled by the presence of strong iron-binding ligands [*Kraemer*, 2004; *Kraemer et al.*, 2005]. Complexation of Fe(II) by organic ligands such as formate, acetate, and oxalate promotes the photo-reduction of more soluble Fe(II). When Fe(II) complexes form on the surface of particles, photo-reduction results in the release of Fe(II) into solution.

Furthermore, little is known about how a changing climate might affect these factors and inputs of soluble iron to oceanic waters [*Boyd*, 2015; *Boyd et al.*, 2015a]. *Fishwick et al.* [2014] investigated the impact of predicted changes in surface ocean conditions on the

dissolution of aerosol iron and found that temperature, pH and oxygen had little effect on iron solubility compared to the aerosol source. Episodic changes in mineral dust deposition to the Southern Ocean have been linked to 20th-century climate change and Australian land use modification [*Bhattachan and D'Odorico*, 2014]. *Boyd et al.* [2015b] investigated subantarctic phytoplankton response to changing oceanographic conditions predicted for future climate change and found that climate change could enhance diatom growth due to warming and iron enrichment. Concentrations of iron in the ocean in a warmer climate are predicted to be two-fold higher than the present day conditions [*Boyd et al.*, 2008; *Moore et al.*, 2013]. Modelling by *Mahowald et al.* [2010] show that dust deposition trends could increase ocean productivity by 6 % over the 20th century, drawing down an additional 4 ppm of CO_2 into the oceans.

2.2.2.3 Two component mixing of aerosol iron sources

To date, most studies have assumed that mineral dust represents the primary source of soluble iron in the atmosphere [e.g. *Jickells et al.*, 2005]. However, fire emissions, oil combustion and extra-terrestrial iron are other potential sources. *Sholkovitz et al.* [2012] complied a global set of fractional iron solubility data, and found that the large variability in fractional iron solubility is related to a mixing of aerosol sources, i.e. mineral dust with a low fractional iron solubility (0.5-2 %) and combustion aerosol with a high fractional iron solubility (up to 95 %; Fig. 7.2a). The inverse hyperbolic curve resulting from fractional iron solubility and total aerosol iron loading can best be explained by the conservative mixing of two end-members each characterised by distinct atmospheric concentrations of fractional iron solubility and total aerosol iron [*Sedwick et al.*, 2007; *Sholkovitz et al.*, 2012]. The first end member “mineral dust” is characterised by relatively high aerosol iron loading and relatively low fractional iron solubility. The second end member “combustion aerosol” is characterised by relatively low total aerosol iron loading and relatively high fractional iron solubility.

Combustion aerosol iron estimates

There is a large range in fractional iron solubility of combustion sources e.g. ship exhaust (>10 %; *Ito* [2013]; *Sholkovitz et al.* [2009]; *Siefert et al.* [1999]), oil fly ash (~36 %; *Desboeufs et al.* [2005b]), coal fly ash (~0.2 %; *Desboeufs et al.* [2005b]), coal burning [*Lin et al.*, 2015], and oil combustion (~77-81 %; *Schroth et al.* [2009]). Biomass burning sources of soluble iron have received relatively less attention and also have a large range in fractional

iron solubility e.g. 2-40 % [*Bowie et al.*, 2009; *Guieu et al.*, 2005; *Ito*, 2011; *Ito*, 2012; 2015; *Paris et al.*, 2010]. *Chang-Graham et al.* [2011] suggests that biomass may accumulate metal-containing species that are re-emitted during biomass burning. The authors report that 45–75 % of the organic matter in biomass burning aerosols are water soluble, and water soluble metal-organic compounds (e.g., $C_7H_6N_2O_4Fe$) were emitted during biomass burning [*Chang-Graham et al.*, 2011]. Biomass burning aerosols can undergo long-range atmospheric transport [*Bisiaux et al.*, 2012b; *McConnell et al.*, 2002] and deposition to the open ocean [*Ito*, 2011]. Fractional iron solubility also displays a large range (1–42 %) in Antarctica during the LGM [*Conway et al.*, 2015].

Australian mineral dust and Southern Ocean aerosol iron estimates

Mackie et al. [2008] syntheses the processes influencing the biogeochemistry of Australian dust and compares them to processes from other dust sources. The stand out concern arising from this review is that there are virtually no *in situ* measurements of soluble iron from Australian dust or aerosol sources, despite Australia being the largest dust source in the Southern Hemisphere for the current climate. One measurement of fractional iron solubility (0.9 %) and fractional acid leachable iron (15 %) from dust from Thargomindah, southwest Queensland [*Mackie et al.*, 2006], and a few measurements of soluble ferrous Fe(II) (0.5-0.24 mg g^{-1}) and total soluble Fe (0.14-1.9 mg g^{-1}) from Mallee, southeast Australia [*Bhattachan and D'Odorico*, 2014] exist. Iron oxides were investigated in mineral dust from the Red Dawn storm event in eastern Australia in September 2009 (total Fe content was 4.7 %) [*Reynolds et al.*, 2014]. The authors speculate that the mixing of Australian desert dust plumes (with iron in the form of Fe^{3+}) and iron-bearing industrial effluent (iron in the form of Fe^{2+}) could be a source of soluble iron to downwind oceans.

The few measurements of soluble iron from aerosol collected at sea over the Southern Ocean show that the soluble iron concentrations are extremely low. Soluble iron fluxes over the Southern Ocean range from 0.04-7.4 nmol m^{-2} d^{-1} [*Baker et al.*, 2013; *Bowie et al.*, 2009; *Wagener et al.*, 2008]. Recently, *Chance et al.* [2015] reported soluble and total iron fluxes for the southeast Atlantic ranging from 2-135 nmol m^{-2} d^{-1} and 22-2100 nmol m^{-2} d^{-1} respectively for remote South Atlantic air masses. The highest total iron concentrations were associated with air masses close to South Africa and the lowest concentrations from air masses originating from Antarctica. Iron solubility ranged from 1-22 %, with higher fractional iron solubility in samples collected south of 40° S [*Chance et al.*, 2015]. Using

dissolved Al (DAl) concentrations of surface seawater as a proxy for dust deposition, *Grand et al.* [2015b] estimate DFe fluxes for the southern Indian Ocean to be considerably higher (1.7-20 µmol m^{-2} d^{-1}), and suggest DFe and DAl concentrations in the subtropical Indian Gyre are primality influenced by dust deposition. The authors used a number of assumptions in their estimates for dust DFe fluxes, i.e., constant fractional iron solubility and total iron content, which actually vary depending on aerosol source. Thus, caution should be used when comparing these estimates to *in situ* aerosol iron measurements. Nevertheless, these are the only known estimates for the south Indian Ocean sector of the Southern Ocean. Estimates at Kerguelen Island are higher than the broader Southern Ocean due to the influence of local dust [*Heimburger et al.*, 2013b]. Soluble iron concentrations in coastal East Antarctica (0.13-1.3 ng m^{-3}) are also influenced by local dust sources but the concentrations are still low [*Gao et al.*, 2013]. While total aerosol iron concentrations south of Tasmania range between 5 and 17 ng m^{-3} [*Bowie et al.*, 2009]. Even less data exits for wet deposition iron fluxes over the Southern Ocean [*Chance et al.*, 2015; *Heimburger et al.*, 2013a]. Estimates of 1000 ± 1200 nmol m^{-2} d^{-1} for the southeast Atlantic have been reported by *Chance et al.* [2015], and are greater than dry deposition fluxes. However, due to the large uncertainty, the authors were not able to conclude which form of deposition is dominant. There is a need for more information on the solubility of aerosol iron, in order to better parameterise models [*Baker et al.*, 2013; *Mahowald et al.*, 2009; *Schulz et al.*, 2012].

2.3 Aerosol iron end member one: Atmospheric dust

Originally, aeolian dust was thought to be the main source of aerosol iron to the open ocean [*Jickells et al.*, 2005; *Martin*, 1990]. The dust section of this literature review, reviews the physical processes of atmospheric dust transport, dust deposition rates in the Australian sector of the Southern Hemisphere, potential sources areas (PSA) of dust to Antarctica and the Southern Ocean, and the geochemical methods for characterising the provenance of dust.

2.3.1 Physical transport of dust by wind

Wind is critical for the dispersal of dust. Particle entrainment, dispersion and deposition processes are influenced by the properties of low-level airflow and the surface over which air moves.

2.3.1.1 Particle entrainment

Particles begin to move under the influence of a moving fluid (this review focusses on air). The friction velocity above which particles move is defined as the threshold velocity and is a function of surface roughness, particle size and density, and whether the airflow is laminar or turbulent. The entrainment of particles by air can be described by Shield's criterion, which is equivalent to *Bagnold's* [1941] "fluid threshold" and is given by equation (2.2):

$$V_{*t} = A\frac{\sqrt{\sigma-\rho}}{\rho}gd \qquad \text{(Equation 2.2)}$$

where V_{*t} is the threshold wind velocity for movement of particles of diameter *d*; σ: density of the particle, typically assumed to be 2.65 g cm^{-3}; *p*: density of air; *g*: acceleration due to gravity; *d*: particle diameter; *A*: empirical coefficient equal to 0.1 for particle friction Reynolds number which describes whether air flow is laminar or turbulent. Turbulent conditions (Re_p >3.5) generally prevail when the transporting fluid is wind.

As wind velocity increases logarithmically with height above the bed (as friction between the air column and the surface diminishes with height) equation (2.2) can be modified to calculate the fluid threshold velocity for a given particle size for wind measured at any height above the surface (*z*) as long as the surface roughness (*k*) and relative particle density as known. Equation (2.3) is a practical extension of equation (2.2) [*Bagnold*, 1941]:

$$V_t = 5.75A\sqrt{\frac{\sigma-\rho}{\rho}gd}\ \log\frac{z}{k} \qquad \text{(Equation 2.3)}$$

where v_t is the fluid threshold velocity; *z*: height above the surface; *k*: surface roughness.

The threshold velocity as described by equations (2.2) and (2.3) indicates that larger particles require higher wind velocity to initiate movement. Particles >50 µm are infrequently suspended into the vertical flux and typically remain in the horizontal saltation flux [*Greeley and Iversen*, 1985]. For small particles, <50 µm, equations (2.2) and (2.3) may not adequately describe the threshold velocity due to strong particle cohesion forces [*Bagnold*, 1941]. Instead, where inter-particle cohesive forces are important, the threshold velocity for entrainment increases with decreasing particle size. These two effects lead to an optimum particle size of around 80 µm for which the threshold velocity is a minimum [*Bagnold*, 1941; *Pye*, 1989].

After particle size, surface roughness is an important factor for particle entrainment. Surface roughness (*k*) is defined as the height below which there is zero fluid velocity. Surface roughness depends on the properties of the surface above which the flow occurs and is approximately equal to 1/30 of the diameter of the roughness elements on the surface [*Bagnold*, 1941]. High surface roughness causes turbulence and exerts friction on the overflowing air mass [*Pye*, 1989].

2.3.1.2 Particle dispersion

The dispersion of aeolian dust describes how particles move. The mechanism by which a particle is transported depends on the particle shape and size, or more specifically the relationship between the particle settling velocity and fluid turbulence [*Bagnold*, 1941; *Pye*, 1989]. The settling velocity of a particle depends on its size and shape. Wind transports dust by three mechanisms: i) surface creep (sliding and rolling), ii) saltation and iii) suspension [*Pye*, 1989]. These dispersion processes are illustrated in Fig. 2.4. Particles with a diameter >500 µm are transported mainly along the surface by surface creep. They remain on the surface because the settling velocity is much greater than the upward motion of turbulence unless saltating particles eject them to greater heights in the airflow (Fig. 2.4). Saltation transports particles between 70-500 µm in diameter. Particles enter the air stream, are transported on the order of meters to tens of meters, and then impact the bed leading to other particles being ejected from the surface. A particle will remain in suspension if the vertical velocity is greater than the settling velocity (Fig. 2.4) [*Pye*, 1989]. Suspension of particles for up to several weeks occurs at a particle size of <20 µm [*Pye*, 1989], where the low settling velocity can be overcome by air turbulence for long periods of time [*Kalinske*, 1943]. Dust records from polar ice cores show that dust originating from remote regions, such as South America and Australia, travelled thousands of kilometres from the source [*Delmonte et al.*, 2002; *Delmonte et al.*, 2004a; *Delmonte et al.*, 2008]. Estimates of tropospheric transport age to Antarctica vary, for example over 5.5 days from Patagonia, 6.5 days from Australia and 8.5 days from Southern Africa [*Krinner and Genthon*, 2003]. During transport, dust is exposed to a number of environmental conditions that can enhance the solubility of iron contained in the particle (see section 2.2.2).

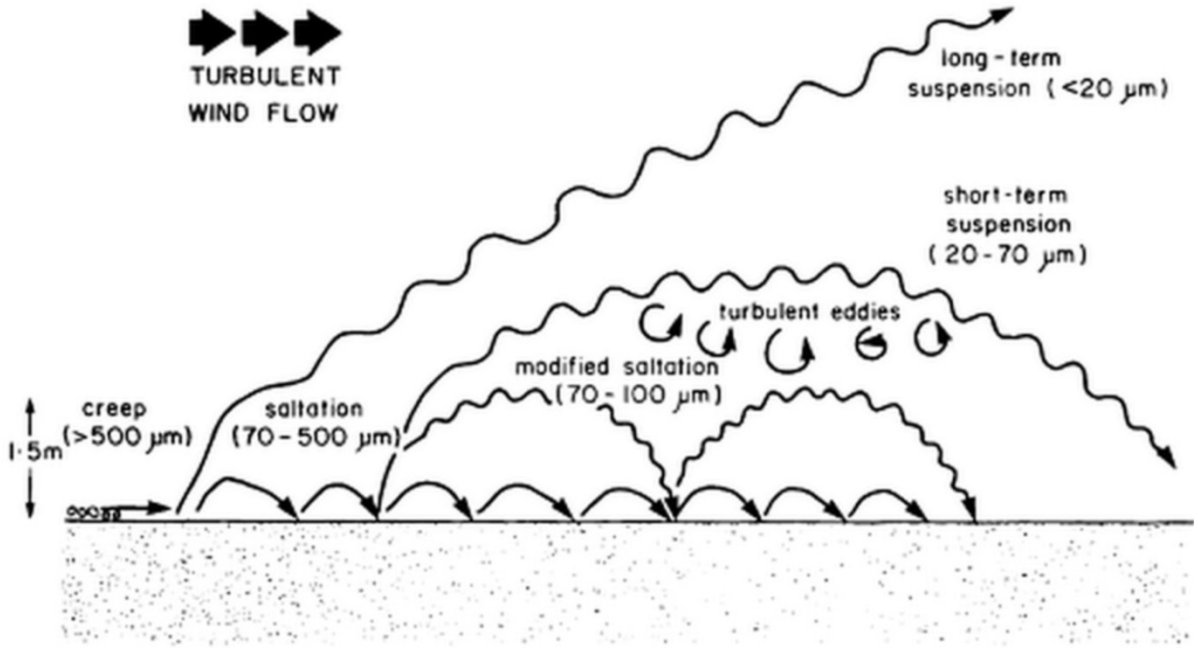

Fig. 2.4: Modes of particle transport by wind. The indicated particle size range in different transport modes are typically found during moderate windstorms ($\varepsilon=10^4 - 10^5$ cm^2 s^{-1}). Source: *Pye* [1989].

2.3.1.3 Particle deposition

Dust deposition can either be by dry or wet deposition. However, few data on the proportion of wet versus dry deposition exist for the Southern Hemisphere [e.g. *Chance et al.*, 2015; *Heimburger et al.*, 2013a; *Wagener et al.*, 2008]. Furthermore, there are large uncertainties in deposition velocities [*Arimoto and Duce*, 1986; *Slinn and Slinn*, 1980] for the Southern Hemisphere and a wide range of deposition velocities, ranging from 0.2-1.3 cm s^{-1}, have been applied to soluble iron fluxes [*Baker et al.*, 2003; *Chance et al.*, 2015; *Duce et al.*, 1991; *Heimburger et al.*, 2012; *Schulz et al.*, 2012].

2.3.2 The emission of dust in Australia and deposition of dust in the Southern Ocean and Antarctica

Modelled and observed global dust deposition patterns for the current climate are illustrated in Fig. 2.5. Estimates suggest that there is an order of magnitude uncertainty in deposition from models and observations [*Albani et al.*, 2012a; *Jickells et al.*, 2005; *Luo et al.*, 2005]. Studies of dust transport and deposition are dominated by observations from the Northern Hemisphere as this is where the largest dust emissions (Sahara and China) are sourced (Fig. 2.5). Dust transport in the Southern Hemisphere is different to that in the Northern

Hemisphere, whereby Southern Hemispheric dust transport is constrained by circumpolar westerlies. In contrast, Saharan dust in the Northern Hemisphere is transported by the northeast trade winds and deposited in the equatorial North Atlantic. Global dust models predict that <20 % of global oceanic dust deposition occurs in Southern Hemispheric waters [*Mahowald et al.*, 2009], due to its remoteness from continents. In the Southern Hemisphere, dust deposition is highest in waters adjacent to Australia, southern South America and southern Africa (Fig. 2.5).

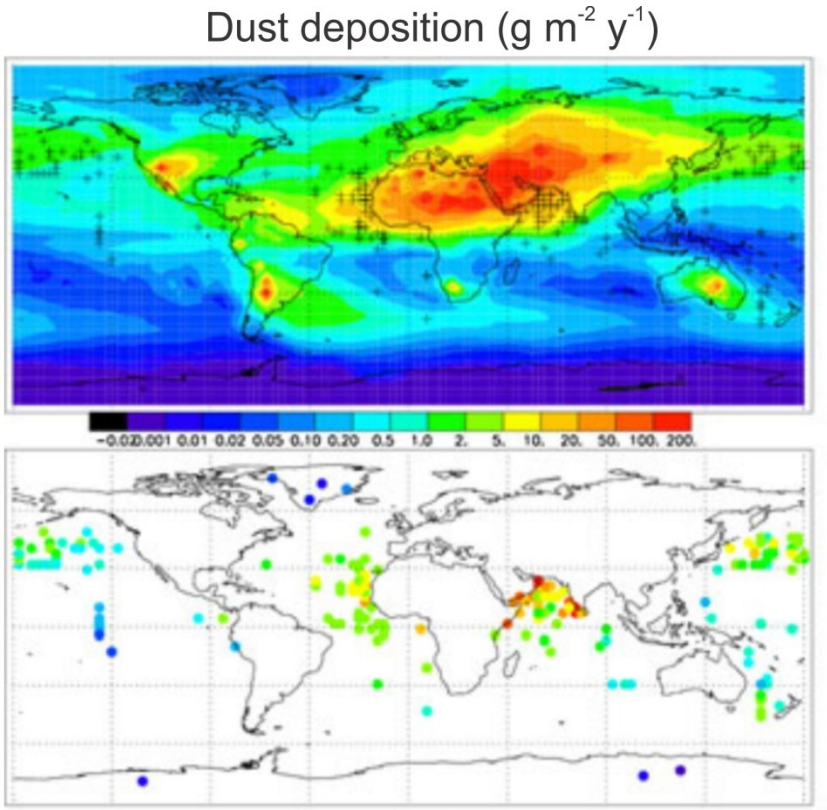

Fig. 2.5: Comparisons between global dust deposition models (upper panel) and observations from DIRTMAP [*Kohfeld and Harrison,* 2001] (central panel) for the current climate. Source: *Albani et al.* [2012a].

2.3.2.1 Dust emission in Australia

Mackie et al. [2008] provide a thorough synthesis of Australian dust biogeochemistry and the processes from dust emission to deposition in the ocean. The *Mackie et al.* [2008] synthesis highlights that there are very few actual Australian dust deposition data, and remote sensing studies can underestimate Australian dust emissions [*McGowan et al.*, 2005]. Global models also have difficulty in accurate predictions of Australian dust emissions due to the complex

spatial variability of Australian potential source areas (PSA) and the episodic nature of Australian dust processes (see below). Australian dust plumes can carry large loads of sediment, for example in the October 2002 storm, around 4.9 Tg of soil was transported off the east coast of Australia [*Knight et al.*, 1995].

2.3.2.2 Dust deposition in the Southern Ocean

Data on Southern Ocean dust fluxes come from aerosol capture [e.g. *Bowie et al.*, 2009; *Gao et al.*, 2013; *Wagener et al.*, 2008], modelling studies [e.g. *Arimoto and Duce*, 1986], surface dissolved aluminium (Al) concentrations [*Grand et al.*, 2015a; *Grand et al.*, 2015b], long-lived thorium isotopes (^{232}Th and ^{230}Th) in seawater [*Hayes et al.*, 2015], and derived atmospheric fluxes from ^{7}Be [*Kadko et al.*, 2015]. Modern dust fluxes range between 0.001-0.2 g m^{-2} y^{-1} [e.g. *Duce et al.*, 1991; *Mahowald et al.*, 2005; *Wagener et al.*, 2008]. Dust fluxes in the Southern Ocean vary with latitude (Fig. 2.5), for example, high dust fluxes of 66 ± 60 mg $m^{-2}yr^{-1}$ by *Grand et al.* [2015a] were estimated for Antarctic regions of the eastern Indian Ocean using surface dissolved DAl concentrations. Surface dissolved DAl concentrations were also used to estimate the high dust fluxes for the eastern and western South Indian Subtropical Gyre Ocean which range between 60 - 685 mg $m^{-2}yr^{-1}$ and are influenced by Australian and South African dust respectively [*Grand et al.*, 2015b]. Caution should be applied when interpreting DAl in surface waters as a proxy for dust deposition, especially as the fractional aluminium solubility can vary as much as fractional iron solubility in the Southern Ocean [*Chance et al.*, 2015].

2.3.2.3 Dust deposition rates in Antarctica

Until recently, the main focus of research on dust in Antarctic ice has been on investigations of ice cores from the Antarctic interior, such as European Project for Ice Coring in Antarctica (EPICA) Dome C and Vostok. These deep ice cores cover geological time spans of several hundreds of thousands of years, and dust extracted from them represents Southern Hemispheric derived material that has travelled long distances [*Basile et al.*, 1997; *Delmonte et al.*, 2002; *Delmonte et al.*, 2008; *Delmonte et al.*, 2004b; *Grousset and Biscaye*, 2005; *Grousset et al.*, 1992a]. Due to the remoteness of continental sources, the concentration of dust on the East Antarctica Plateau is extremely low. Dust concentrations at EPICA Dome C and Vostok during the Holocene and earlier interglacials are around 15 mg kg^{-1}. Whereas, concentrations were 50 times higher (800 mg kg^{-1}) during full glacial conditions [*Lambert et*

al., 2008]. Glacial concentrations of dust can exceed interglacial concentrations by a factor of 25-50 [*Petit et al.*, 1981; *Petit et al.*, 1999; *Wegner et al.*, 2015]. Changes in dust concentrations in the EPICA Dronning Maud Land (EDML) ice core, in the Atlantic sector of the East Antarctic Ice Sheet (EAIS), have recently been attributed to changes in source conditions [*Wegner et al.*, 2015]. The effect of the change in the seasonality of the source emission strength and the transport intensity on the dust, decrease over the transition and significantly contribute to the large decrease of dust concentration from the glacial to the Holocene. Dust fluxes for the East Antarctic Plateau during the Holocene are 0.0002-0.0006 g m^{-2} yr^{-1} [*Albani et al.*, 2012b; *Delmonte et al.*, 2005]. However, small pockets of exposed rock and sediment exist, of which the McMurdo Dry Valleys (MDV) are the largest in aerial extent and the dustiness known area in Antarctica [*Chewings et al.*, 2014]. These isolated ice-free areas on the margin of Antarctica can represent a non-negligible dust (and iron) source to the local atmosphere [*Bory et al.*, 2010; *Delmonte et al.*, 2010a; *Delmonte et al.*, 2013; *Delmonte et al.*, 2010b; *Gao et al.*, 2013; *Winton et al.*, 2014].

Data on dust provenance and fluxes to Antarctica come from surface snow and ice cores [*Bory et al.*, 2010; *Delmonte et al.*, 2002; *Delmonte et al.*, 2005; *Delmonte et al.*, 2008; *Delmonte et al.*, 2004b; *Delmonte et al.*, 2010a; *Delmonte et al.*, 2013; *Delmonte et al.*, 2010b; *Koffman et al.*, 2014b; *Lambert et al.*, 2008; *Revel-Rolland et al.*, 2006], sediment traps, marine sediment cores [e.g. *Barrett et al.*, 1983; *Collier et al.*, 2000], and modelling studies [e.g. *Albani et al.*, 2012b; *Albani et al.*, 2015; *Krinner et al.*, 2010; *Wegner et al.*, 2015]. These studies show that dust can be divided into two end member categories (Fig. 2.6, Table 2.1):

1. Remote "Southern Hemispheric" dust, characterised by modern dust fluxes ranging between 0.001-0.2 g m^{-2} y^{-1} [e.g. *Duce et al.*, 1991; *Mahowald et al.*, 2005; *Wagener et al.*, 2008] and 0.0002-0.0006 g m^{-2} yr^{-1} during the Holocene (Fig. 2.6) [*Albani et al.*, 2012b; *Delmonte et al.*, 2005], a long atmospheric residence time [e.g. *Albani et al.*, 2012a; *Krinner et al.*, 2010], a modal particle size <5 µm [*Wegner et al.*, 2015] and a geochemical fingerprint showing it is derived from arid regions of Patagonia and/or Australia [*De Deckker et al.*, 2010; *Delmonte et al.*, 2008; *Delmonte et al.*, 2004b; *Vallelonga et al.*, 2010].

2. "Local" dust characterised by dust fluxes 3 to 4 orders of magnitude higher than the East Antarctic Plateau (1 g m^{-2} y^{-1}; *Chewings et al.* [2014]; *Winton et al.*

[2014]), a modal particle size in the fine sand range, and a geochemical affinity with local rocks [*Winton et al.*, 2014].

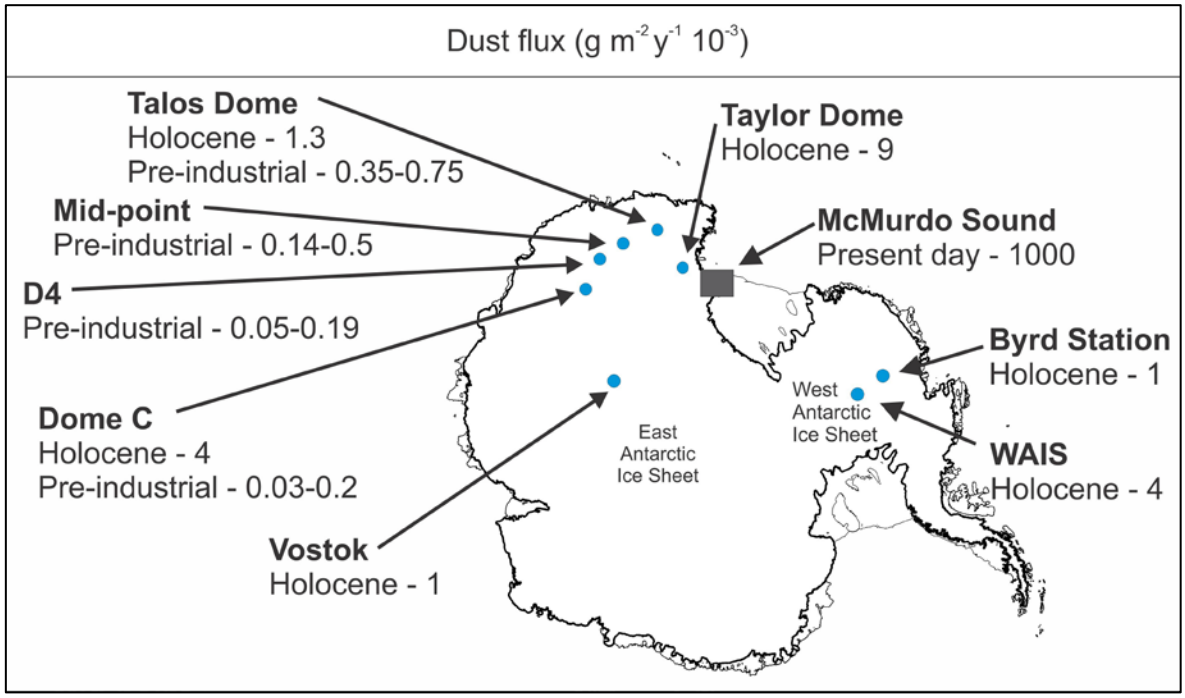

Fig. 2.6: Holocene, pre-industrial and present day dust fluxes (g m^{-2} yr^{-1} 10^{-3}) at ice core sites in Antarctica. Particle size distribution and references for each site can be found in Table 2.1.

Table 2.1: Dust fluxes at various Antarctic ice core sites. The location of ice core sites is illustrated in Fig. 2.6. EAIS: East Antarctic Ice Sheet, WAIS: West Antarctic Ice Sheet.

Site	Dust flux ($g\ m^{-2}\ yr^{-1}$)	Primary modal size (µm)	Reference
Range "Southern Hemispheric" dust	**$3\ 10^{-5}$ to 0.2**	**<5**	[*Delmonte et al.*, 2004a; *Delmonte et al.*, 2013; *Duce et al.*, 1991; *Gao et al.*, 2001; *Mahowald et al.*, 2005; *Marticorena and Bergametti*, 1995; *Wagener et al.*, 2008]
Taylor Dome, EAIS	Holocene - $9\ 10^{-3}$		[*Hinkley and Matsumoto*, 2001]
Vostok, EAIS	Holocene – $4\ 10^{-3}$	1	[*Delmonte et al.*, 2004b; *Kohfeld and Harrison*, 2001]
Talos Dome, EAIS	Holocene – $1.3\ 10^{-3}$ Pre-industrial – 0.35 to $0.75\ 10^{-3}$		[*Delmonte et al.*, 2013]
Dome C, EAIS	Pre-industrial – 0.03 to $0.20\ 10^{-3}$ Holocene – $4\ 10^{-3}$	1	[*Delmonte et al.*, 2004b; *Delmonte et al.*, 2013]
Berkner Island	Present day – not reported	1-9	[*Bory et al.*, 2010]
Mid-point, EAIS	Pre-industrial – 0.14 to $0.5\ 10^{-3}$		[*Delmonte et al.*, 2013]
D4, EAIS	Pre-industrial – 0.05 to $0.19\ 10^{-3}$		[*Delmonte et al.*, 2013]
Dronning Maud Land, EAIS	-	2-3	[*Wegner et al.*, 2015]
Byrd Station, WAIS	Holocene - $1\ 10^{-3}$		[*Windom*, 1969]
West Antarctic Divide, WAIS	Holocene - $4\ 10^{-3}$	5-8	[*Koffman et al.*, 2014b]
Southern Ocean: - Dust distribution models - Aerosol sampling	 Present day - $1\ 10^{-3}$ to 0.2 Present day - 0.2 to $4\ 10^{-3}$	 <5 <5	[*Gao et al.*, 2013; *Mahowald et al.*, 2005; *Wagener et al.*, 2008]
Range "Local" dust	**<25**	**20-250**	[*Atkins and Dunbar*, 2009; *Dunbar et al.*, 2009]
Windless Bight, McMurdo Ice Shelf	Present day - 0.8	40-100	[*Dunbar et al.*, 2009]
Southern McMurdo Sound	Present day - 8 to 24	76-130	[*Atkins and Dunbar*, 2009]
Granite Harbour, McMurdo Sound	Present day - 2		[*Macpherson*, 1987]
Victoria Lower Glacier, Southern Victoria Land	Present day - 25	63-200	[*Alying*, 2001; *Schuck*, 2009]
Sea ice, southern McMurdo Sound	Present day – 1	20-250	[*Chewings et al.*, 2014; *Winton et al.*, 2014]

2.3.3 Potential source areas

2.3.3.1 Methods for determination of dust provenance

The connection between dust source and sink can be made by several techniques, for example numerical model simulations of dust erosion, deposition and air circulation [e.g. *Mahowald et al.*, 1999], remote sensing, archived meteorological data to estimate air mass back trajectories from appoint of dust deposition upwind to PSA [e.g. *Neff and Bertler*, 2015a], and geochemical fingerprints such as trace element concentrations, rare earth elements (REE) [e.g. *Gabrielli et al.*, 2010a], and/or ratios and mineralogy [*Grousset and Biscaye*, 2005]. In some cases, particle size frequency distributions might reflect a given origin [*Barrett et al.*, 1983; *le Roux*, 1994; *McLaren*, 1981; *Wegner et al.*, 2015]. Other traces can be used in combination with geochemistry, such as pollen, diatoms, and other biomarkers to indicate relative marine or terrestrial origin. Trace element concentrations are often not unique to a single area; hence their ability to discriminate PSA is limited.

The isotopic composition of dust has been used to discriminate variability between geographic provinces [e.g. *Bollhöfer and Rosman*, 2000; *Grousset and Biscaye*, 2005]. Common radiogenic isotopes that are used to fingerprint the provenance of dust are $^{87}Sr/^{86}Sr$, $\varepsilon_{Nd}(0)$[1], [e.g. *Bory et al.*, 2010; *Delmonte et al.*, 2010b; *Grousset et al.*, 1988] and $^{206}Pb/^{204}Pb$ [e.g. *Bollhöfer and Rosman*, 2000; *Vallelonga et al.*, 2010]. The combination of multiple isotopic systems are useful in tracing PSA because different geographic provinces can be discriminated by variations in radiogenic isotopes of mantle-derived (basaltic rocks, tephra and soils derived from them, weathered and eroded mafic rocks) or crustal (soils, sediments) derived dust [*Grousset and Biscaye*, 2005]. For example, Antarctica is one of the four

[1] Rocks in the Earth are extremely variable in their isotopic composition and a comparison can be made only if samples are of the same age. In order to make the samples comparable, the $^{143}Nd/^{144}Nd$ ratios are normalized to the chondritic model of Earth composition (CHUR), which evolves over time. For this reason, DePaolo, D. J., and G. J. Wasserburg (1976), Inferences about magma sources and mantle structure from variations of 143Nd/144Nd, *Geophys. Res. Lett.*, *3*(12), 743-746. introduced the Epsilon (ε) parameter, normalizing the isotopic ratio of $^{143}Nd/^{144}Nd$ measured in the rocks at present time $(^{143}Nd/^{144}Nd)_{measured}$ to the value of CHUR at the same time:
$\varepsilon_{Nd}(0) = ((^{143}Nd/^{144}Nd)_{measured}/(^{143}Nd/^{144}Nd)_{CHUR}^{-1}) \times 10^4$
with present time $(^{143}Nd/^{144}Nd)_{CHUR} = 0.512638$ Jacobsen, S. B., and G. J. Wasserburg (1980), Sm-Nd isotopic evolution of chondrites, *Earth and Planetary Science Letters*, *50*(1), 139-155. A positive εNd value indicates that rocks were derived from sources that were depleted in large ion lithophile (LIL) elements, while negative ε_{Nd} values indicate that the rocks were derived from sources enriched in LIL elements, i.e. that the rocks derived or assimilated old crustal rocks whose Sm/Nd ratio had been originally lowered when they separated from the uniform reservoir. The Sm and Nd isotopic system is not altered by geological processes in the crust such as metamorphism, sedimentation, erosion.

principle domains on a global scale and is represented by particles derived from old, crustal Antarctic rocks and exposed sand dunes. These are characterised by a wide range of $^{87}Sr/^{86}Sr$ isotopic signatures (0.713-0.770) and non-radiogenic $\varepsilon_{Nd}(0)$ values (-25 $\varepsilon_{Nd}(0)$>-47) [*Grousset and Biscaye*, 2005]. In this thesis, $^{87}Sr/^{86}Sr$ and $\varepsilon_{Nd}(0)$ isotopic ratios are used to identify the PSA of dust deposited in Antarctic snow. The rational is that dust keeps the Sr and Nd isotopic imprint of rocks from which they derive, which depends on lithology and geologic history [*Biscaye et al.*, 1997].

2.3.3.2 Australian dust

There are two major Australian PSA of active wind erosion: the Lake Eyre Basin and the western sector of the Murray-Darling Basin [*Prospero et al.*, 2002]. These two basins can supply large volumes of fine particles to central Australia as the internal drainage systems continuously renew the supply of fine particles [*McTainsh*, 1989]. Sand dunes in Alice Springs and the Simpson Desert in the Northern Territory and in the north of South Australia are additional PSA. Western Australian deserts, consisting mainly of sand dunes, are not considered to be a major atmospheric source for long-range transportable dust [*Prospero et al.*, 2002]. Sand dunes are not good sources for long-range transport of dust as they are devoid of the fine fraction and contain larger particles with high settling velocities [*Hesse and McTainsh*, 2003; *Prospero et al.*, 2002]. However, little attention has been given to this region in terms of a PSA. Therefore, it appears that dominant source of dust in Australia, for the current climate, corresponds to the two major drainage systems, Lake Eyre and Murray-Darling [*Hesse and McTainsh*, 2003]. In contrast to South America, Australia is characterised by an extremely variable Sr and Nd isotopic composition [*Delmonte et al.*, 2004b; *Gingele and De Deckker*, 2005; *Grousset et al.*, 1992c; *Martin and McCulloch*, 1999; *Revel-Rolland et al.*, 2006]. The contribution of each PSA to a long-range transportable "Australian" aeolian dust composition is still unresolved. The smaller PSA within Australia become active at different times [*Butler et al.*, 2001]. This intermittency has large implications for the interpretation of dust provenance in Antarctic ice core records.

There are two general dust pathways in Australia [*Bowler*, 1976; *Lu and Shao*, 2001; *Magee et al.*, 1995; *Prospero et al.*, 2002; *Shao and Leslie*, 1997] (Fig. 2.7):

1. Southeast dust path

The southeast dust path moves across the southeast landmass and passes over the Coral Sea, the Tasman Sea and the Southern Ocean (Fig. 2.7). Within this pathway, there are three dust trajectories with distinct source regions and seasonality (Fig. 2.7) [*McTainsh and Leys*, 1993]: i) northeast over Coral Sea, most active between September and December, with a source region in the northern Lake Eyre Basin, ii) southeast over Tasman Sea, most active between December and March, with a source region in the southeastern sector of the Lake Eyre Basin and the southern Murray-Darling Basin, iii) and south over the Southern Ocean, most active between December and March, with a source region in the southern section of the Lake Eyre and Murry-Darling Basins [*Li et al.*, 2008; *McTainsh*, 1989; *McTainsh and Lynch*, 1996; *Prospero et al.*, 2002]. Other PSA of the southeastern dust path are the Simpson Desert-Channel Country regions of southwest Queensland, the Strzelecki Desert in South Australia and in western NSW extending south to the Mallee region in northwest Victoria. The southeast dust path has been observed at several locations along its trajectory; in soil [*Hesse and McTainsh*, 2003] and on snow in southeastern Australia [*Johnston*, 2001], in sediment in the southwest Pacific region [*Hesse*, 1994], and in glaciers in New Zealand [*Marx et al.*, 2005]. Few studies have attempted to document the geochemical composition of the aeolian dust and to identify its sources on a continental scale [*Gatehouse et al.*, 2001; *Hesse*, 1997; *McGowan et al.*, 2005; *Walker and Costin*, 1971], and even fewer studies have investigated the composition of Australian dust in terms of iron biogeochemistry [*Bhattachan and D'Odorico*, 2014; *Mackie et al.*, 2006; *Mackie et al.*, 2005; *Mackie et al.*, 2008].

ii) Northwest dust path

Easterly trade winds supply the northwest dust path, and this dust path is even less documented [*Hesse and McTainsh*, 2003]. This path crosses the northwest landmass and then over the Indian Ocean (Fig. 2.7).

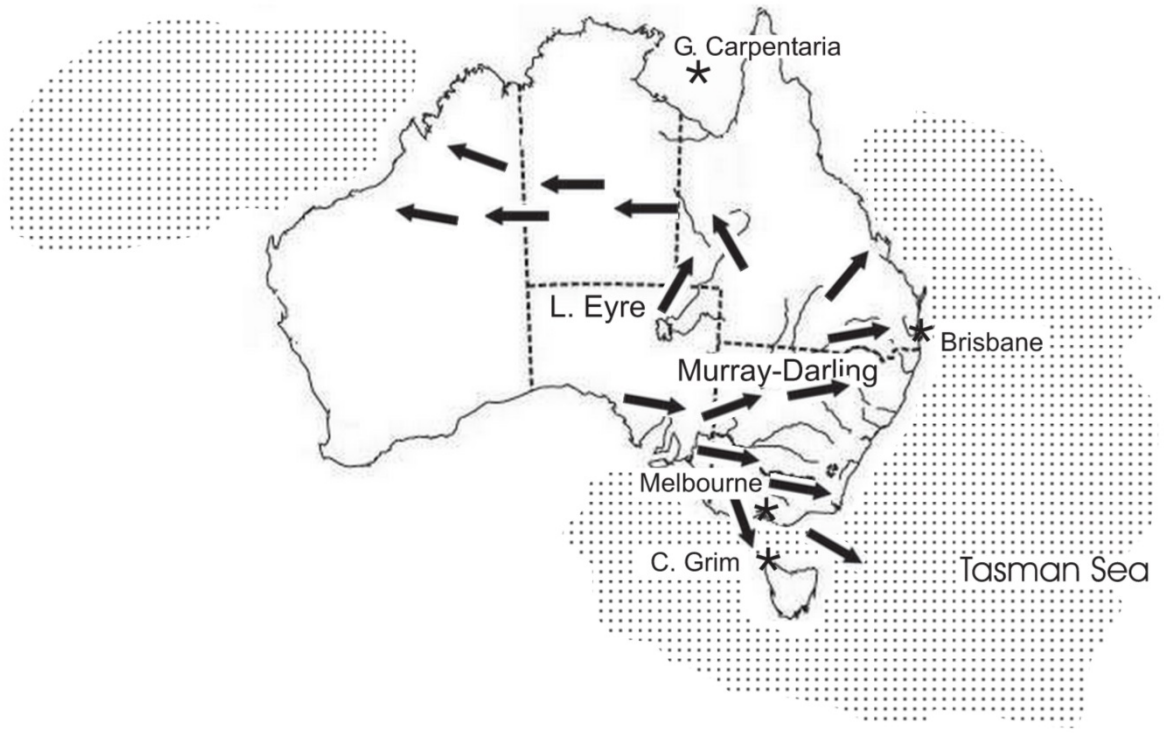

Fig. 2.7: Australian dust transport pathways. Source: *Mackie et al.* [2008].

It is interesting to note that these two dust paths, with different dust sources, are transported to the two contrasting oceanographic environments (as discussed in section 2.1.1), i.e. the northwest dust path is transported to low-iron LNLC waters north of Australia, where the southwest dust path is transported to the low-iron HNLC waters south of Australia.

Australian dust storm activity is highly episodic, and large dust storms occur during periods of drought. For example, suspended dust was collected during the 2002 Canberra dust storm and showed that, during a dust storm, several potential sources can contribute to a dust plume (as wind direction can change from northerly pre-frontal to westerly winds within minutes during the same storm) [*Revel-Rolland et al.*, 2006]. Spatial and temporal patterns of dust activity have been measured in various ways. The Dust Strom Index (DSI_3), which measures the frequency and intensity of dust entrainment using records of dust events weighed according to the extent to which they reduce visibility. *McTainsh et al.* [2006] shows that most dust activity occurs in the centre of the Australian continent which reflects rainfall and dust entrainment (Fig. 2.8).

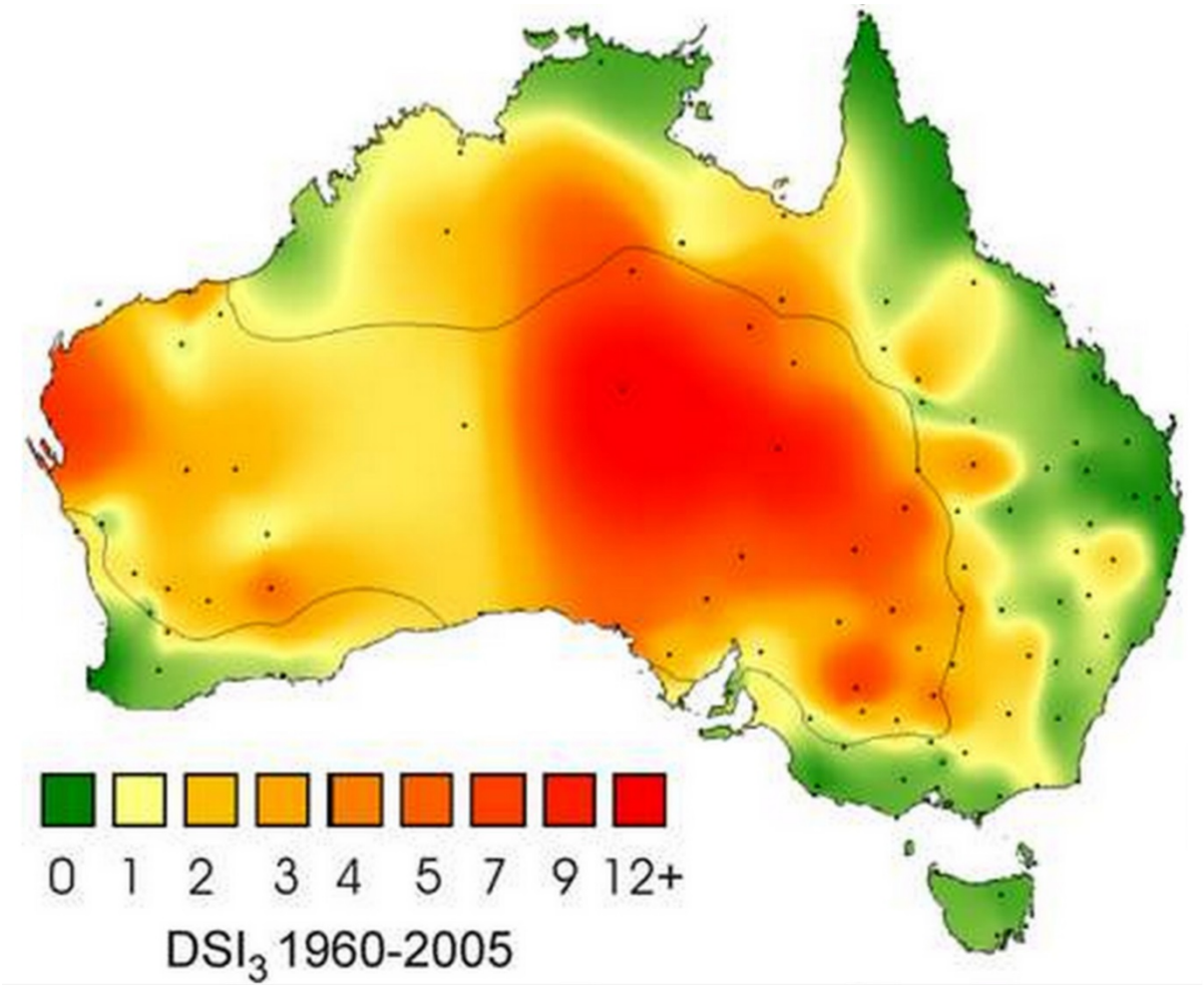

Fig. 2.8: Annual mean DSI_3 for Australia, 1960-2005. The 400 mm isohyet indicated by solid black line. Black dots present observing stations. Note that this is a smoothed temporal record because of intersectoral differences in rainfall and resultant dust activity between the west and eastern sectors of the continent which tend to cancel each other out. Generally speaking, when the east is in drought, the west is experiencing higher than average rainfall and vice versa. Source: *Mackie et al.* [2008].

2.3.3.3 Remote dust sources to Antarctica

Changes in dust deposition to the East Antarctic Plateau can be related to changes in source intensity and seasonality, atmospheric aerosol lifetime, atmospheric pathway and deposition processes, or a combination of these factors [*Krinner et al.*, 2010; *Petit et al.*, 1981; *Petit and Delmonte*, 2011; *Wegner et al.*, 2015]. Radiogenic isotope studies using combinations of Sr and Nd isotopes of dust extracted from ice cores (Dome C, old Dome C, Dome B, Vostok, Talos Dome, Komsomolskaia), have shown that the bulk of the dust deposited on the East Antarctic Plateau during glacial periods originated from mixed dust sources in Patagonia and the Puna-Altiplano plateau in southern South America [*Basile et al.*, 1997; *Delmonte et al.*,

2008; *Delmonte et al.*, 2004b; *Delmonte et al.*, 2010a; *Grousset et al.*, 1992b]. However, the dataset for interglacials, i.e. when dust input to Antarctica is low, is less certain [*Delmonte et al.*, 2007]. Measurements of Holocene dust suggest that Australia is an additional source [*De Deckker et al.*, 2010; *Delmonte et al.*, 2007; *Delmonte et al.*, 2008; *Gaiero*, 2008; *Gingele and De Deckker*, 2005; *Revel-Rolland et al.*, 2006; *Vallelonga et al.*, 2010], as also supported by changes in mineralogical [*Gaudichel et al.*, 1992] and elemental [*Gabrielli et al.*, 2010a; *Gaudichel et al.*, 1992; *Marino et al.*, 2008] compositions, as well as in magnetic properties [*Lanci et al.*, 2008]. Seasonal timing of dust transport to Antarctica is poorly documented [e.g. *Weller et al.*, 2008], but could vary depending on the location in Antarctica. For example, at EDML the modern dust concentration maxima is thought to occur during winter [*Sommer et al.*, 2000] while at Berkner Island concentrations are higher in spring-summer [*Bory et al.*, 2010].

Revel-Rolland et al. [2006] suggested that the Lake Eyre region in central Australia was a PSA of Antarctic dust based on Sr and Nd isotopic ratios of lacustrine and 'loessic' deposits from central Australia. *De Deckker et al.* [2010] argue that some parts of the Murray-Darling Basin are also a PSA for dust in the EPICA Dome C ice core during interglacial periods which is based primarily on Pb isotopic compositions and meteorological observations of atmospheric dust transport trajectories from Australia. Lead isotopic values for pre-industrial ice core samples from EPICA Dome C and several regolith samples from south-central Australia showed that Antarctic dust represents mixtures of locally-derived and remote sources [*Vallelonga et al.*, 2005; *Vallelonga et al.*, 2010]. The authors concluded that southern South America was the dominant source of remote dust despite the relative similarity of Australian and southern South American signatures.

Little is known about the vertical and lateral dispersion of Australian dust plumes following uplift. However, modelling of transport, distribution and deposition of Southern Hemisphere dust to Antarctica can shed light on these processes [*Krinner et al.*, 2010; *Li et al.*, 2008]. Modelling by *Li et al.* [2008] indicated the importance of Australia as a source of dust to Antarctica as well as the Pacific and Southern Oceans for the present climate. The authors show that dust in the Southern Hemisphere originates primarily from Australia (120 Tg a^{-1}), Patagonia (38 Tg a^{-1}) and a small fraction from inter-hemispheric transport from the Northern Hemisphere (31 Tg a^{-1}). A small fraction (7 Tg a^{-1}) is transported and deposited in the Southern Ocean and Antarctica, whereas dust from South America, Australia, and Northern

Hemisphere is essentially located in the boundary layer, mid-troposphere, and upper-troposphere, respectively. Australia contributes to most of the dust deposited in the South Pacific Ocean (86 %) and pacific sector of the Antarctic continent (Fig. 2.9) [*Li et al.*, 2008]. In the current climatic, dust transport from Australia to Antarctica preferentially occurs at high altitude (above 5000 m), while transport of South American dust occurs at lower levels [*Krinner et al.*, 2010; *Li et al.*, 2008]. A modelling study of dust sources and deposition during the LGM by *Mahowald et al.* [1999] attributes half of dust deposited at Vostok from Patagonia, but with a noteworthy contribution from Australia. *Luo et al.* [2003] showed that, for the present climate, the contribution from Australian sources is even higher (70–100 % of the dust loading). However, modelling by *Albani et al.* [2012a] suggests that South America is the most important source of dust transported to Antarctica in the current climate, with Australia also an important contributor. Both *Albani et al.* [2012a]; *Li et al.* [2008] and *Krinner et al.* [2010] show spatial variability in the relative importance of these major dust sources (Fig. 2.9).

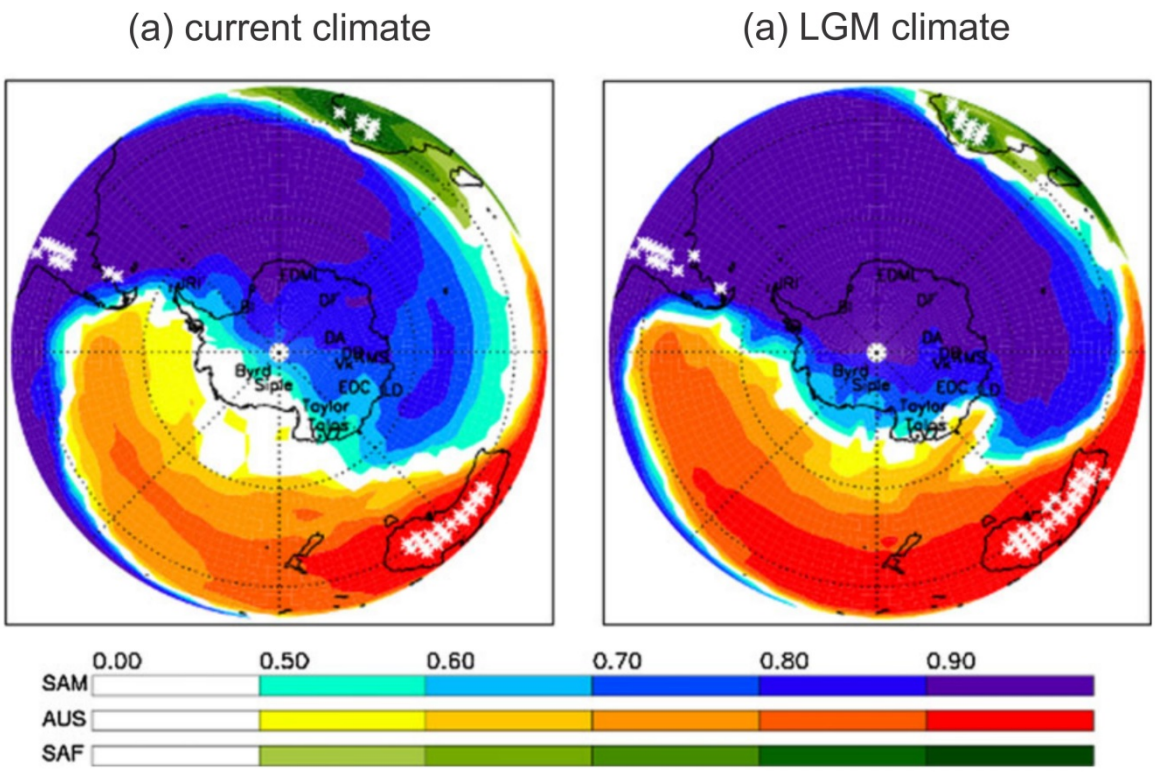

Fig. 2.9: Source apportionment in dust deposition, represented by the relative fractions to the total deposition flux, of dust originated from South America (blue colour scale), Australia (red colour scale) and South Africa (green colour scale). Coloured areas indicate that at least half of the deposited dust was originated from the corresponding macro-area. White stars represent active sources for dust mobilization. a) Current climate. b) LGM climate. Source: *Albani et al.* [2012a].

2.3.3.4 Local Antarctic dust sources

In addition, local dust sources occur around ice-free areas of Antarctica. The upper bound being the debris bands in McMurdo Sound, SW Ross Sea where the dust flux is around 1 g m^{-2} yr^{-1} [*Chewings et al.*, 2014; *Winton et al.*, 2014].

2.3.3.5 Mixed dust sources

Mixtures of these two end members exits, where Antarctic sourced dust is an important contributor of the total dust flux although the concentrations remain low [*Bory et al.*, 2002; *Delmonte et al.*, 2010b]. For example, dust concentration and origin was investigated in a two-year high-resolution snow pit from Berkner Island, Weddell Sea with the highest dust concentrations occurring in summer with additional episodic inter-annual variability [*Bory et al.*, 2010]. The isotopic composition of dust displayed a distinct isotopic range and most

likely represents a mixture of Patagonian (summer), Australian (spring) and an unidentified East Antarctic source. Although the dust in the Talos Dome ice core (Pacific/western Ross Sea Sector) and other ice cores from the East Antarctic Plateau, originated from South America during the last two glacial periods, [*Delmonte et al.*, 2010a; *Delmonte et al.*, 2010b], Holocene and pre-industrial dust in the Talos Dome, Mid-Point and D4 ice cores originated mainly from proximal of northern Victoria Land (Fig. 2.6). These ice-free areas are located at a similar altitude to the Talos Dome drilling site and were transported to the site via advection of maritime air masses from the Pacific/Ross Sea region [*Albani et al.*, 2012b; *Delmonte et al.*, 2013; *Delmonte et al.*, 2010b]. Both of these studies highlight the spatial variability of dust provenance in Antarctica, and that local dust sources can play an important role on the periphery of the ice sheet.

The provenance of the dust deposited in other regions of the Antarctic and the Southern Ocean remains unquantified. Improving the understanding of the provenance of the dust deposited in Antarctica, both at present and throughout the last climatic cycles, is required. The Ross Sea region, where a new intermediate depth ice core, Roosevelt Island Climate Evolution (RICE), has recently been recovered in West Antarctica is among one of the most sensitive regions to climate change according to the 2013 Intergovernmental Panel on Climate Change (IPCC) report.

2.4 Aerosol iron end member two: combustion aerosol

Combustion, from biomass burning and fossil fuel (oil and coal) combustion, is the second end member source of soluble iron.

2.4.1 Introduction

Biomass burning is the burning of living and dead vegetation. It is estimated that around 8700 Tg yr^{-1} of dry matter is burnt annually [*Andreae*, 1991]. Emissions from biomass burning are a significant source of trace gases and aerosols emitted to the atmosphere, and large biomass burning events may have a major effect on atmospheric chemistry due to the presence of reactive species. Biomass smoke aerosols effectively scatter and absorb solar radiation [*Ramanathan and Carmichael*, 2008], and smoke aerosols are good cloud condensation nuclei [*Zuberi et al.*, 2005]. Smoke properties vary between fires depending on fuel type and

moisture, combustion phase and wind conditions. The physical, chemical, and optical properties of biomass-burning aerosols can change rapidly as the aerosols disperse in the atmosphere. The biomass burning section of the literature review will briefly discuss the sources and processes of biomass combustion, and then focus on the chemistry and aging of aerosols associated with biomass burning, focusing primarily on rBC aerosols.

2.4.2 Sources

The majority (~65 %) of global biomass is burnt in savannah and agricultural regions [*Koppmann et al.*, 2005]. Seasonality drives savannah burning; during the wet season, biomass is produced and during the dry season, the biomass is turned into a highly flammable material. Despite the high frequency of savannah fires, there are only a few studies that have investigated the emissions from savannah fires [*Andreae*, 1991; 1993; *Crutzen and Andreae*, 1990; *Hao and Liu*, 1994]. Previous studies have focused on biomass burning emissions from various sources mainly in tropical regions e.g. Southeast Asia, Africa, Brazil, Indonesia and Malaysia [*Andreae*, 1991; *Crutzen and Andreae*, 1990; *Hao and Liu*, 1994; *Seiler and Crutzen*, 1980]. An exceptionally large biomass burning during the 1997/1998 Indonesia fires were attributed to the combined strength of El Nino and the Indian Ocean Dipole [*Field et al.*, 2009], with potential iron-fertilisation effects [*Abram et al.*, 2003]. A dry season annual haze in Southeast Asia is an annual phenomenon, but was intense in October 2015 where Indonesia experienced severe forest fires as a result of slash and burn methods to clear land for plantations.

In the Southern Hemisphere, biomass burning generally occurs between August and October [*Duncan et al.*, 2003; *Hao and Liu*, 1994; *Hoelzemann et al.*, 2004; *Ito and Penner*, 2004; *van der Werf et al.*, 2006]. Australia experiences biomass burning events on an annual basis. In most years, fires are restricted to the tropical savannah forests of northern Australia, contributing about 8 % of global carbon emissions from biomass burning [*Kasischke and Penner*, 2004]. In addition, episodic austral summer wildfires occur in southern and eastern Australia [e.g. *Iinuma et al.*, 2015], including the Black Saturday fires of February 2009 that burned 450,000 hectares [*Cruz et al.*, 2012]. Aerosols from Australian forest fires are known to circle the Southern Hemisphere [*Dirksen et al.*, 2009].

Refractory black carbon (rBC; a proxy for biomass burning, see sections 2.4.4-2.4.5) displays large spatial and temporal gradients (Fig. 2.10). The highest atmospheric concentrations of

rBC are found in the tropics due to the combustion of biomass and biofuels. In the Southern Hemisphere, rBC emissions are primarily from dry seasonal biomass burning in Australia, southern Africa and South America [*Mouillot and Field*, 2005]. Refractory black carbon is transported long-range in the atmosphere from low to mid-latitudes to the poles and deposited on surface snow preserving a history of rBC emissions. Concentrations of rBC in Antarctic ice cores are low. For example, at West Antarctic Ice Sheet (WAIS) Divide rBC concentrations are 0.08 µg kg^{-1}, at Law Dome rBC concentrations are 0.09 µg kg^{-1} [*Bisiaux et al.*, 2012b], and at Dronning Maud Land rBC concentrations are 0.1-0.18 µg kg^{-1} [*Bisiaux et al.*, 2012a]. At WAIS Divide, concentrations displayed a seasonal cycle with higher concentrations during the austral winter-spring [*Bisiaux et al.*, 2012b].

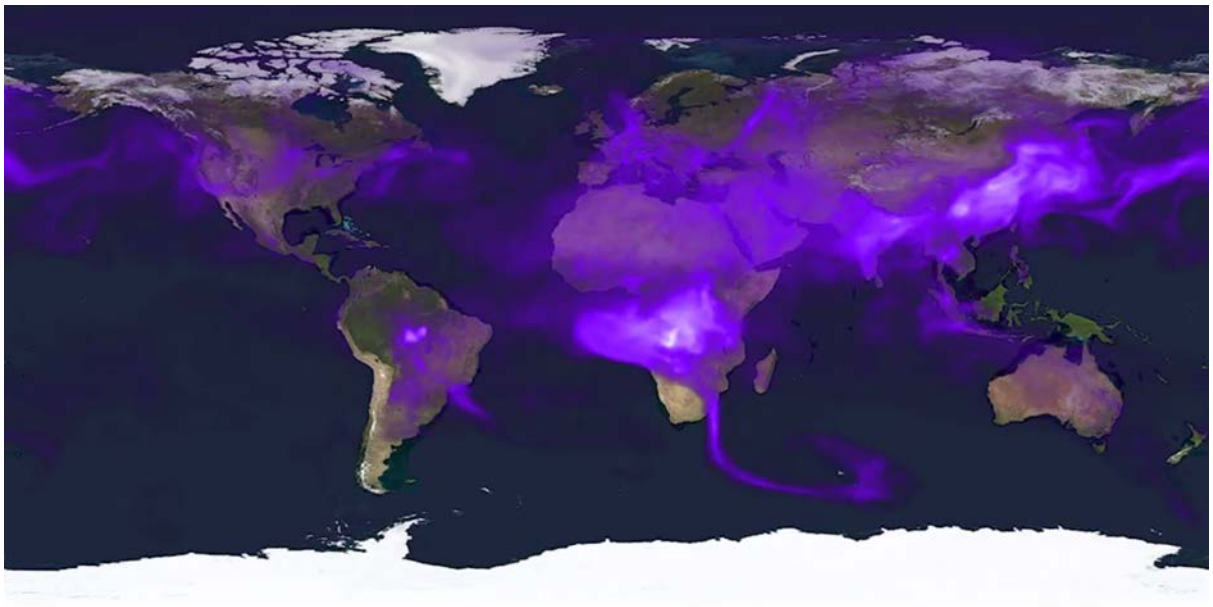

Fig. 2.10: Example of the global distribution of atmospheric black carbon density, around September 2009. Source: GOCART model (https://svs.gsfc.nasa.gov/cgi-bin/details.cgi?aid=3668).

2.4.3 Processes of combustion and emission

Physical and chemical processes occur during biomass burning, and these can be divided into three phases of combustion: ignition, flaming and smouldering. During the ignition phase, biomass is set alight and most of the water contained within the vegetation is out-gassed. During this phase, large quantities of highly volatile organics are released [*Reid et al.*, 2005]. Combustion proceeds from the ignition phase to the flaming phase when the fuel is dry. The fuel components in the flaming phase are cellulose, hemicellulose, lignin, organic species and trace minerals. Products of complete combustion are carbon dioxide and water. Incomplete

combustion leads to the emission of carbon monoxide and a number of organic compounds [*Nussbaumer*, 1989]. Plant matter contains a large abundance of volatile organic material that is released as volatile organic compounds (VOCs) [*Marutzky*, 1991. During the drying process, wood is cracked into hundreds of gaseous and solid products consisting mainly of charcoal. Gaseous compounds can be separated into primary and secondary emission products. The organic composition of the emissions is determined by temperature [*Struschka*, 1993; *Nussbaumer*, 1989]. Smouldering combustion begins when most of the volatiles have been expelled from the cellulose fuel [*Chandler et al.*, 1983]. The smouldering phase is characterised by flameless combustion of charcoal. Carbon monoxide is the predominate organic compound emitted in this phase.

The rest of this biomass burning review will focus on aerosols. Fires produce both solid and liquid aerosol particles. Particle formation during biomass burning is a condensation process. Particle formation in flames begins with the creation of condensation nuclei, such as polycyclic aromatic hydrocarbons (PAH) [*Frenklach*, 2002; *Glassman*, 1989] and a variety of soot-like species [*Turns*, 1996]. As the PAH molecules grow, they become condensation nuclei for other pyrolized species. If there is insufficient oxygen to the flame or if the temperature is too low to complete oxidation, many of these particles may undergo a secondary condensation growth phase and be emitted in the form of smoke. Particle formation can also occur in the smouldering phase. However, the mass fraction of soot in smoke particles is extremely low during this phase. These particles form by the condensation of volatilized organics around other nuclei [*Ward*, 1990].

2.4.4 Biomass burning aerosol chemistry

Aerosols generated by biomass burning have three principal components:

1. Particulate organic material (POM; carbon with associated organic matter such as H, N, and O)

2. Black or elemental carbon

3. Trace inorganic species

Reported data indicates that POM accounts for around 80 % of the mass of fresh dry smoke aerosol, followed by 5-9 % for rBC, and 12-15 % for other trace inorganic species. In

addition, a small non-combustible matter around vegetation is often entrained into fire plumes by pyro-convection. Pyro-convection occurs when heat and water vapour emissions from strong fires support the development of extremely deep convection. The entrainment of dust by pyro-convection has been attributed to the high surface winds associated with the convective updraft [*Maenhaut et al.*, 1996; *Palmer*, 1981]. This mobilises large amounts of soil particles into suspension [*Radke et al.*, 1991]. The convective transport into troposphere allows aerosols to be dispersed over long distances [*Cammas et al.*, 2009].

Organic carbon (OC) is the carbon in molecules of chained carbon atoms with hydrogen and other elements and functional groups. Whereas, rBC/elemental carbon is highly light absorbing carbon, such as soot, that has a graphitic-like structure [*Novakov*, 1982]. The IPCC AR5 estimates the total rBC inventory to be 7.7 Tg yr^{-1} [*Lamarque et al.*, 2010]. Refractory black carbon particles range from 10 to 1000 nm in particle diameter and are ubiquitous in the troposphere. Refractory black carbon aerosols are highly absorbing compared to other aerosol species, and thus rBC is thought to absorb all the wavelengths of short-wave radiation in polluted air [*Chakrabarty et al.*, 2007]. Often this material is referred to as elemental carbon, although the nomenclature is dependent on the analytical method employed (see section 1.2.3).

Refractory black carbon measurements are based upon two indirect techniques; i) thermal combustion, and ii) light absorption properties. Thermal combustion techniques involve the collection of smoke on a quartz filter, which is then heated in steps to temperatures <800°C where the carbon in the sample is oxidized to measurable CO_2 [e.g. *Chow et al.*, 2007]. The result is a thermogram of evolved carbon as a function of temperature. The second technique to measure rBC concentrations in aerosol samples is optical absorption. Refractory black carbon concentrations are based on the transmission or reflection of light off a sample, and a specific absorption factor is applied to convert absorption into a rBC concentration. Laser-induced incandescence instruments, such as the single particle intracavity laser-induced incandescence photometer (SP2), also exist. The SP2 works by simultaneous laser-induced incandescence and measurement of elastically scattered light to determine the size and the boiling point of single particles [*Stephens et al.*, 2003]. The SP2 is well suited to applications involving low concentrations of particles such as Antarctic snow and ice, and real-time measurements of ambient air or continuous flow analysis of ice cores [e.g. *Bisiaux et al.*, 2012b]. Both black and elemental carbon are used in this research; black carbon is

determined by the SP2 method and is referred to refractory black carbon (rBC), while elemental carbon is determined by the thermal combustion technique. Refectory black carbon is the principal tracer for smoke in Antarctic snow samples, while elemental carbon is the principle tracer for smoke in aerosol filters.

Trace inorganic species include potassium, chlorine, and calcium. Potassium and chloride each account for ~2-5 % of the fine particle mass [e.g. *Pósfai et al.*, 2003]. Trace inorganic species are useful for apportionment studies of ambient pollution, for example, potassium and chloride have been used as smoke tracers [*Artaxo et al.*, 1994; *Calloway et al.*, 1989; *Reid and Hobbs*, 1998], although in regions with more complicated aerosol chemistry such as Asia, co-linearity issues can prevent its use [*Gao et al.*, 2003]. Sulfur, in the form of sulfate, is also present at around 1 % of the fine particle mass. Trace metals make up a small fraction of the trace inorganic species. For example, between 0.02-1.9 % of iron has been measured in fresh smoke from biomass burning (Table 2.2) [*Turn et al.*, 1997; *Ward et al.*, 1992; *Ward et al.*, 1991; *Yamasoe et al.*, 2000]. Smoke particles are usually internally mixed, typically with a core of rBC and alkali earth compounds (such as potassium chloride) coated with organic compounds.

Table 2.2: Mass percentage of iron in aerosols associated with biomass burning. Modified from: [*Reid et al.*, 2005]

Location	Biomass type	Fe mass (%)	Reference
African Savanna	Fresh smoke, flaming	0.02	[*Maenhaut et al.*, 1996]
African Savanna	Fresh smoke, smouldering	0.03	[*Maenhaut et al.*, 1996]
Cerrado	Fresh smoke, flaming	1.2	[*Ward et al.*, 1992]
Cerrado	Fresh smoke, flaming	0.9	[*Ward et al.*, 1991]
Cerrado	Fresh smoke, flaming	0.08	[*Yamasoe et al.*, 2000]
Cerrado	Fresh smoke, smouldering	0.05	[*Yamasoe et al.*, 2000]
NA Temperate	Fresh smoke, mixed	0.1	[*Ward et al.*, 1991]
Trop. Broadleaf	Fresh smoke, flaming	0.1	[*Ward et al.*, 1992]
Trop. Broadleaf	Fresh smoke, flaming	0.9	[*Ward et al.*, 1991]
Trop. Broadleaf	Fresh smoke, flaming	0.03	[*Yamasoe et al.*, 2000]
Trop. Broadleaf	Fresh smoke, smouldering	0.05	[*Yamasoe et al.*, 2000]
Trop. Broadleaf	Fresh smoke, smouldering	0.1	[*Ward et al.*, 1992]
Agricultural	Fresh smoke, flaming	0.017	[*Turn et al.*, 1997]
South America-Rhondonia	Regions heavily impacted by smoke	0.3	[*Artaxo et al.*, 1998]
South America-Rhondonia	Regions heavily impacted by smoke	0.2	[*Artaxo et al.*, 1994]
South America-Rhondonia	Regions heavily impacted by smoke	0.42	[*Echalar et al.*, 1998]
South America-Rhondonia	Regions heavily impacted by smoke	0.4	[*Pereira et al.*, 1996]
South America-Rhondonia	Regions heavily impacted by smoke	0.5	[*Reid and Hobbs*, 1998]
South America: Mato Grosso	Regions heavily impacted by smoke	0.9	[*Artaxo et al.*, 1994]
South America: Mato Grosso	Regions heavily impacted by smoke	0.5	[*Reid and Hobbs*, 1998]
South Africa	Regions heavily impacted by smoke	0.5	[*Maenhaut et al.*, 1996]

2.4.5 Aging of biomass burning aerosols

Smoke particles undergo physical and chemical processes during transport, which have been observed on timescales ranging from minutes to days. These processes can alter the properties of smoke. Biomass burning plumes can mix with materials from other sources, for example, downwind of Africa aged biomass burning aerosol plumes are often mixed with desert dust [*Johnson et al.*, 2008]. The presence of reactive species within biomass burning emissions can have a substantial effect on atmospheric chemistry. Freshly emitted rBC aerosols are usually hydrophobic [*Shiraiwa et al.*, 2007; *Zuberi et al.*, 2005], and therefore, less likely to be removed from the atmosphere by wet deposition. Refractory black carbon can become hydrophilic when coated with soluble material [*Petters et al.*, 2006]. Both modelling studies and observations suggest that most rBC transported from its source region is internally mixed with soluble materials [*Riemer et al.*, 2004; *Shiraiwa et al.*, 2007]. Global rBC models suggest the aging process of converting hydrophobic rBC to hydrophilic rBC takes 1-2 days [e.g. *Cooke et al.*, 2002; *Liu et al.*, 2009]. Observations have shown that rBC

aerosols are typically coated with soluble materials, such as sulfate and organic matter [*Friedman et al.*, 2009; *Hasegawa and Ohta*, 2002; *Khalizov et al.*, 2009; *Moteki and Kondo*, 2007; *Zhang et al.*, 2008]. Aerosol microphysics models have attempted to understand the rBC coating mechanism by simulating the processes associated with rBC ageing e.g. nucleation, condensation, coagulation, evaporation, chemistry [*Jacobson*, 2003; *Oshima et al.*, 2009; *Riemer et al.*, 2004; *Riemer et al.*, 2010]. Modelling of long-range transportable rBC showed that aging of rBC, by the coating of soluble materials, can vary the residence time of rBC in the atmosphere on diurnal and seasonal scales, i.e., slow aging can allow rBC to remain largely hydrophobic during long range transport [*Liu et al.*, 2011].

The size distribution of smoke aerosols are modified during wet and dry removal processes and smoke aerosols increase in size with age [*Reid et al.*, 1999]. Dry deposition accounts for 15-40 % of total removal of rBC [*Textor et al.*, 2006]. Aged aerosols are also more spherical than fresh particles [*Ruellan et al.*, 1999]. Aged smoke is often mixed with other anthropogenic emissions. Several studies have shown significant enrichment of secondary inorganic species in aged smoke, such as ammonium, nitrate, sulfate, and other "semi-volatile" organic species [*Formenti et al.*, 2003; *Reid and Hobbs*, 1998]. In a study of biomass burning aerosol plumes at Aspendale, Victoria, Australia, *Keywood et al.* [2015] found that older smoke plumes (age 30 hours) displayed higher concentrations of a number of gaseous and aerosol species relative to the younger smoke plumes (age 3 hours). The authors found that secondary organic aerosol (SOA) compounds made up a greater fraction of speciated organic mass in the older plume than in the younger plume where speciated biomass burning compounds dominated.

2.4.6 Future predictions of biomass burning

Keywood et al. [2013] reviewed the impacts of biomass burning in a changing climate and discussed the uncertainties and limitations of the current state of knowledge. Under a warming climate, it is likely that fire frequency and severity will increase. The type and quantity of fuel, required for fire, is influenced by climate. Periods of high precipitation can result in increased biomass growth and greater fuel loads are available for future biomass burning seasons. Conversely, drought may result in drier biomass that is more easily burned. Higher temperatures may increase the likelihood of fire ignition [*Running*, 2006]. Furthermore, the atmospheric transport of biomass burning emissions can be influenced by changes in climatic phenomena, for example El Nino Southern Oscillation (ENSO). In

Australia, a 55 % increase in the probability of extreme fire risk by 2100 has been projected under an emission scenario of 621 ppm CO_2 [*Pitman et al.*, 2007].

References

Abram, N. J., M. K. Gagan, M. T. McCulloch, J. Chappell, and W. S. Hantoro (2003), Coral reef death during the 1997 Indian Ocean dipole linked to Indonesian wildfires, *Science*, *301*(5635), 952-955.

Aguilar-Islas, A. M., J. Wu, R. Rember, A. M. Johansen, and L. M. Shank (2010), Dissolution of aerosol-derived iron in seawater: Leach solution chemistry, aerosol type, and colloidal iron fraction, *Marine Chemistry*, *120*(1-4), 25-33.

Albani, S., N. Mahowald, B. Delmonte, V. Maggi, and G. Winckler (2012), Comparing modeled and observed changes in mineral dust transport and deposition to Antarctica between the Last Glacial Maximum and current climates, *Climate Dynamics*, *38*(9-10), 1731-1755.

Albani, S., B. Delmonte, V. Maggi, C. Baroni, J. R. Petit, B. Stenni, C. Mazzola, and M. Frezzotti (2012), Interpreting last glacial to Holocene dust changes at Talos Dome (East Antarctica): implications for atmospheric variations from regional to hemispheric scales, *Clim. Past Discuss.*, *8*(1), 145-168.

Albani, S., et al. (2015), Twelve thousand years of dust: the Holocene global dust cycle constrained by natural archives, *Clim. Past*, *11*(6), 869-903.

Alexander, J. M., V. H. Grassian, M. A. Young, and P. D. Kleiber (2015), Optical properties of selected components of mineral dust aerosol processed with organic acids and humic material, *Journal of Geophysical Research: Atmospheres*, *120*(6), 2437-2452.

Alying, B. (2001), Dust accumulation on the Victoria Lower Glacier and Wilson Piedmont, coastal South Victoria Land, Antarctica, and its potential as a paleowind indicator, Victoria University of Wellington, Wellington.

Anderson, R. F., S. Barker, M. Fleisher, R. Gersonde, S. L. Goldstein, G. Kuhn, P. G. Mortyn, K. Pahnke, and J. P. Sachs (2014), Biological response to millennial variability of dust and nutrient supply in the Subantarctic South Atlantic Ocean, *Philosophical Transactions of the Royal Society of London A: Mathematical, Physical and Engineering Sciences*, *372*(2019).

Andreae, M., and A. Gelencsér (2006), Black carbon or brown carbon? The nature of light-absorbing carbonaceous aerosols, *Atmospheric Chemistry and Physics*, *6*(10), 3131-3148.

Andreae, M. O. (1991), Biomass burning: Its history, use and distribution and its impact on environmental quality and global climate, *Global Biomass Burning: Atmospheric, Climatic, and Biospheric Implications, edited by J. S. Levine, pp. 3-21, MIT Press, Cambridge, Mass.*

Andreae, M. O. (1993), The influence of tropical biomass burning on climate and the atmospheric environment, in *Biogeochemistry of Global Change*, edited, pp. 113-150, Springer.

Arimoto, R., and R. A. Duce (1986), DRY DEPOSITION MODELS AND THE AIR/SEA EXCHANGE OF TRACE ELEMENTS, *J. Geophys. Res.*, *91*(D2), 2787-2792.

Arrigo, K. R., and C. R. McClain (1994), Spring Phytoplankton Production in the Western Ross Sea, *Science*, *266*(5183), 261-263.

Arrigo, K. R., G. L. van Dijken, and S. Bushinsky (2008), Primary production in the Southern Ocean, 1997-2006, *J. Geophys. Res.*, *113*(C8), C08004.

Arrigo, K. R., G. R. DiTullio, R. B. Dunbar, D. H. Robinson, M. VanWoert, D. L. Worthen, and M. P. Lizotte (2000), Phytoplankton taxonomic variability in nutrient utilization and primary production in the Ross Sea, *J. Geophys. Res.*, *105*(C4), 8827-8846.

Artaxo, P., F. Gerab, M. A. Yamasoe, and J. V. Martins (1994), Fine mode aerosol composition at three long-term atmospheric monitoring sites in the Amazon Basin, *Journal of Geophysical Research: Atmospheres (1984–2012)*, *99*(D11), 22857-22868.

Artaxo, P., E. T. Fernandas, J. V. Martins, M. A. Yamasoe, P. V. Hobbs, W. Maenhaut, K. M. Longo, and A. Castanho (1998), Large-scale aerosol source apportionment in Amazonia, *Journal of Geophysical Research: Atmospheres (1984–2012)*, *103*(D24), 31837-31847.

Atkins, C. B., and G. B. Dunbar (2009), Aeolian sediment flux from sea ice into Southern McMurdo Sound, Antarctica, *Global and Planetary Change*, *69*(3), 133-141.

Ayers, G., J. Cainey, R. Gillett, and J. Ivey (1997), Atmospheric sulphur and cloud condensation nuclei in marine air in the Southern Hemisphere, *Philosophical Transactions of the Royal Society of London B: Biological Sciences*, *352*(1350), 203-211.

Bagnold, R. (1941), *The physics of blown sand and desert dunes*, Methuen, London.

Baker, A., S. Kelly, K. Biswas, M. Witt, and T. Jickells (2003), Atmospheric deposition of nutrients to the Atlantic Ocean, *Geophysical Research Letters*, *30*(24).

Baker, A., C. Adams, T. Bell, T. Jickells, and L. Ganzeveld (2013), Estimation of atmospheric nutrient inputs to the Atlantic Ocean from 50° N to 50° S based on large-scale field sampling: Iron and other dust-associated elements, *Global Biogeochemical Cycles*, *27*(3), 755-767.

Baker, A. R., and T. D. Jickells (2006), Mineral particle size as a control on aerosol iron solubility, *Geophys. Res. Lett.*, *33*(17), L17608.

Baker, A. R., and P. L. Croot (2010), Atmospheric and marine controls on aerosol iron solubility in seawater, *Marine Chemistry*, *120*(1-4), 4-13.

Baker, A. R., T. D. Jickells, M. Witt, and K. L. Linge (2006), Trends in the solubility of iron, aluminium, manganese and phosphorus in aerosol collected over the Atlantic Ocean, *Marine Chemistry*, *98*(1), 43-58.

Banerjee, P., and S. Prasanna Kumar (2014), Dust-induced episodic phytoplankton blooms in the Arabian Sea during winter monsoon, *Journal of Geophysical Research: Oceans*, *119*(10), 7123-7138.

Barbeau, K., J. W. Moffett, D. A. Caron, P. L. Croot, and D. L. Erdner (1996), Role of protozoan grazing in relieving iron limitation of phytoplankton, *Nature*, *380*(6569), 61-64.

Barbeau, K. A., and J. W. Moffett (1998), Dissolution of Iron Oxides by Phagotrophic Protists: Using a Novel Method To Quantify Reaction Rates, *Environmental Science & Technology*, *32*(19), 2969-2975.

Barrett, P., A. Pyne, and B. Ward (1983), Modern sedimentation in McMurdo Sound, Antarctica In: Oliver, R.L., James, P.R., Jago, J.B. (Eds.), *Antarctic Earth Science*, 550-554.

Basile, I., F. E. Grousset, M. Revel, J. R. Petit, P. E. Biscaye, and N. I. Barkov (1997), Patagonian origin of glacial dust deposited in East Antarctica (Vostok and Dome C) during glacial stages 2, 4 and 6, *Earth and Planetary Science Letters*, *146*(3-4), 573-589.

Berger, C. J., S. M. Lippiatt, M. G. Lawrence, and K. W. Bruland (2008), Application of a chemical leach technique for estimating labile particulate aluminum, iron, and manganese in the Columbia River plume and coastal waters off Oregon and Washington, *Journal of Geophysical Research: Oceans (1978–2012)*, *113*(C2).

Berman-Frank, I., J. T. Cullen, Y. Shaked, R. M. Sherrell, and P. G. Falkowski (2001), Iron availability, cellular iron quotas, and nitrogen fixation in Trichodesmium, *Limnology and Oceanography*, *46*(6), 1249-1260.

Bhattachan, A., and P. D'Odorico (2014), Can land use intensification in the Mallee, Australia increase the supply of soluble iron to the Southern Ocean?, *Scientific reports*, *4*.

Bhattachan, A., L. Wang, M. F. Miller, K. J. Licht, and P. D'Odorico (2015), Antarctica's Dry Valleys: A potential source of soluble iron to the Southern Ocean?, *Geophysical Research Letters*, *42*(6), 1912-1918.

Biscaye, P. E., F. E. Grousset, M. Revel, S. Van der Gaast, G. A. Zielinski, A. Vaars, and G. Kukla (1997), Asian provenance of glacial dust (stage 2) in the Greenland Ice Sheet Project 2 Ice Core, Summit, Greenland, *J. Geophys. Res.*, *102*(C12), 26765-26781.

Bisiaux, M., R. Edwards, J. McConnell, M. Albert, H. Anschütz, T. Neumann, E. Isaksson, and J. Penner (2012a), Variability of black carbon deposition to the East Antarctic Plateau, 1800–2000 AD, *Atmospheric Chemistry and Physics*, *12*(8), 3799-3808.

Bisiaux, M., R. Edwards, J. McConnell, M. Curran, T. Van Ommen, A. Smith, T. Neumann, D. Pasteris, J. Penner, and K. Taylor (2012b), Changes in black carbon deposition to Antarctica from two high-resolution ice core records, 1850–2000 AD, *Atmospheric Chemistry and Physics*, *12*(9), 4107-4115.

Blain, S., et al. (2007), Effect of natural iron fertilization on carbon sequestration in the Southern Ocean, *Nature*, *446*(7139), 1070-1074.

Bollhöfer, A., and K. Rosman (2000), Isotopic source signatures for atmospheric lead: the Southern Hemisphere, *Geochimica et Cosmochimica Acta*, *64*(19), 3251-3262.

Bonnet, S., and C. Guieu (2004), Dissolution of atmospheric iron in seawater, *Geophys. Res. Lett.*, *31*(3), L03303.

Bory, A., E. Wolff, R. Mulvaney, E. Jagoutz, A. Wegner, U. Ruth, and H. Elderfield (2010), Multiple sources supply eolian mineral dust to the Atlantic sector of coastal Antarctica: Evidence from recent snow layers at the top of Berkner Island ice sheet, *Earth and Planetary Science Letters, 291*(1-4), 138-148.

Bory, A. J. M., P. E. Biscaye, A. Svensson, and F. E. Grousset (2002), Seasonal variability in the origin of recent atmospheric mineral dust at NorthGRIP, Greenland, *Earth and Planetary Science Letters, 196*(3-4), 123-134.

Bowie, A., P. van der Merwe, F. Quéroué, T. Trull, M. Fourquez, F. Planchon, G. Sarthou, F. Chever, A. Townsend, and I. Obernosterer (2014), Iron budgets for three distinct biogeochemical sites around the Kerguelen archipelago (Southern Ocean) during the natural fertilisation experiment KEOPS-2, *Biogeosciences Discussions, 11*(12), 17861-17923.

Bowie, A. R., D. Lannuzel, T. A. Remenyi, T. Wagener, P. J. Lam, P. W. Boyd, C. Guieu, A. T. Townsend, and T. W. Trull (2009), Biogeochemical iron budgets of the Southern Ocean south of Australia: Decoupling of iron and nutrient cycles in the subantarctic zone by the summertime supply, *Global Biogeochem. Cycles, 23*(4), GB4034.

Bowler, J. (1976), Aridity in Australia: age, origins and expression in aeolian landforms and sediments, *Earth-Science Reviews, 12*(2), 279-310.

Boyd, P., P. Dillingham, C. McGraw, E. Armstrong, C. Cornwall, Y.-y. Feng, C. Hurd, M. Gault-Ringold, M. Roleda, and E. Timmins-Schiffman (2015), Physiological responses of a Southern Ocean diatom to complex future ocean conditions, *Nature Climate Change*.

Boyd, P. W., and M. J. Ellwood (2010), The biogeochemical cycle of iron in the ocean, *Nature Geosci, 3*(10), 675-682.

Boyd, P. W., D. S. Mackie, and K. A. Hunter (2010), Aerosol iron deposition to the surface ocean - Modes of iron supply and biological responses, *Marine Chemistry, 120*(1-4), 128-143.

Boyd, P. W., S. C. Doney, R. Strzepek, J. Dusenberry, K. Lindsay, and I. Fung (2008), Climate-mediated changes to mixed-layer properties in the Southern Ocean: assessing the phytoplankton response, *Biogeosciences, 5*(3), 847-864.

Boyd, P. W., G. McTainsh, V. Sherlock, K. Richardson, S. Nichol, M. Ellwood, and R. Frew (2004), Episodic enhancement of phytoplankton stocks in New Zealand subantarctic waters: Contribution of atmospheric and oceanic iron supply, *Global Biogeochem. Cycles, 18*(1), GB1029.

Boyd, P. W., et al. (2007), Mesoscale Iron Enrichment Experiments 1993-2005: Synthesis and Future Directions, *Science, 315*(5812), 612-617.

Boyd, P. W., et al. (2005), FeCycle: Attempting an iron biogeochemical budget from a mesoscale SF6 tracer experiment in unperturbed low iron waters, *Global Biogeochem. Cycles, 19*(4), GB4S20.

Boyd, P. W., et al. (2000), A mesoscale phytoplankton bloom in the polar Southern Ocean stimulated by iron fertilization, *Nature, 407*(6805), 695-702.

Buck, C. S., W. M. Landing, J. A. Resing, and G. T. Lebon (2006), Aerosol iron and aluminum solubility in the northwest Pacific Ocean: Results from the 2002 IOC cruise, *Geochem. Geophys. Geosyst.*, *7*(4), Q04M07.

Butler, H., W. L. Hogarth, and G. H. McTainsh (2001), Effects of spatial variations in source areas upon dust concentration profiles during three wind erosion events in Australia, *Earth Surface Processes and Landforms*, *26*(10), 1039-1048.

Calloway, C., S. Li, J. Buchanan, and R. Stevens (1989), A refinement of the potassium tracer method for residential wood smoke, *Atmospheric Environment (1967)*, *23*(1), 67-69.

Cammas, J.-P., J. Brioude, J.-P. Chaboureau, J. Duron, C. Mari, P. Mascart, P. Nédélec, H. Smit, H.-W. Pätz, and A. Volz-Thomas (2009), Injection in the lower stratosphere of biomass fire emissions followed by long-range transport: a MOZAIC case study, *Atmospheric Chemistry and Physics*, *9*(15), 5829-5846.

Chakrabarty, R. K., H. Moosmüller, W. P. Arnott, M. A. Garro, J. G. Slowik, E. S. Cross, J.-H. Han, P. Davidovits, T. B. Onasch, and D. R. Worsnop (2007), Light scattering and absorption by fractal-like carbonaceous chain aggregates: Comparison of theories and experiment, *Applied optics*, *46*(28), 6990-7006.

Chance, R., T. D. Jickells, and A. R. Baker (2015), Atmospheric trace metal concentrations, solubility and deposition fluxes in remote marine air over the south-east Atlantic, *Marine Chemistry*.

Chandler, C., P. Cheney, P. Thomas, L. Trabaud, and D. Williams (1983), Fire in forestry. Forest fire behaviour and effects, *Ed. John Wiley & Sons*, *1*.

Chang-Graham, A. L., L. T. Profeta, T. J. Johnson, R. J. Yokelson, A. Laskin, and J. Laskin (2011), Case study of water-soluble metal containing organic constituents of biomass burning aerosol, *Environmental science & technology*, *45*(4), 1257-1263.

Chen, Y., and R. L. Siefert (2003), Determination of various types of labile atmospheric iron over remote oceans, *J. Geophys. Res.*, *108*(D24), 4774.

Chen, Y., and R. L. Siefert (2004), Seasonal and spatial distributions and dry deposition fluxes of atmospheric total and labile iron over the tropical and subtropical North Atlantic Ocean, *J. Geophys. Res.*, *109*(D9), D09305.

Chewings, J. M., C. B. Atkins, G. B. Dunbar, and N. R. Golledge (2014), Aeolian sediment transport and deposition in a modern high latitude glacial marine environment, *Sedimentology*.

Collier, R., J. Dymond, S. Honjo, S. Manganini, R. Francois, and R. Dunbar (2000), The vertical flux of biogenic and lithogenic material in the Ross Sea: moored sediment trap observations 1996-1998, *Deep Sea Research Part II: Topical Studies in Oceanography*, *47*(15-16), 3491-3520.

Conway, T., E. Wolff, R. Röthlisberger, R. Mulvaney, and H. Elderfield (2015), Constraints on soluble aerosol iron flux to the Southern Ocean at the Last Glacial Maximum, *Nature Communications*, *6*.

Cooke, W., V. Ramaswamy, and P. Kasibhatla (2002), A general circulation model study of the global carbonaceous aerosol distribution, *Journal of Geophysical Research: Atmospheres (1984–2012)*, *107*(D16), ACH 2-1-ACH 2-32.

Croot, P. L., A. R. Bowie, R. D. Frew, M. T. Maldonado, J. A. Hall, K. A. Safi, J. La Roche, P. W. Boyd, and C. S. Law (2001), Retention of dissolved iron and Fe II in an iron induced Southern Ocean phytoplankton bloom, *Geophys. Res. Lett.*, *28*(18), 3425-3428.

Croot, P. L., et al. (2005), Spatial and temporal distribution of Fe(II) and H2O2 during EisenEx, an open ocean mescoscale iron enrichment, *Marine Chemistry*, *95*(1-2), 65-88.

Crutzen, P. J., and M. O. Andreae (1990), Biomass burning in the tropics: Impact on atmospheric chemistry and biogeochemical cycles, *Science*, *250*(4988), 1669-1678.

Cruz, M., A. Sullivan, J. Gould, N. Sims, A. Bannister, J. Hollis, and R. Hurley (2012), Anatomy of a catastrophic wildfire: the Black Saturday Kilmore East fire in Victoria, Australia, *Forest Ecology and Management*, *284*, 269-285.

de Baar, H. J. W., and J. T. M. de Jong (2001), Distribution, sources and sinks of iron in seawater, *The Biogeochemistry of Iron in Seawater*, 123 - 253.

de Baar, H. J. W., J. T. M. de Jong, D. C. E. Bakker, B. M. Loscher, C. Veth, U. Bathmann, and V. Smetacek (1995), Importance of iron for plankton blooms and carbon dioxide drawdown in the Southern Ocean, *Nature*, *373*(6513), 412-415.

De Deckker, P., M. Norman, I. D. Goodwin, A. Wain, and F. X. Gingele (2010), Lead isotopic evidence for an Australian source of aeolian dust to Antarctica at times over the last 170,000 years, *Palaeogeography, Palaeoclimatology, Palaeoecology*, *285*(3-4), 205-223.

de Jong, J., V. Schoemann, N. Maricq, N. Mattielli, P. Langhorne, T. Haskell, and J.-L. Tison (2013), Iron in land-fast sea ice of McMurdo Sound derived from sediment resuspension and wind-blown dust attributes to primary productivity in the Ross Sea, Antarctica, *Marine Chemistry*, *157*(0), 24-40.

Delmonte, B., J. R. Petit, and V. Maggi (2002), Glacial to Holocene implications of the new 27000-year dust record from the EPICA Dome C (East Antarctica) ice core, *Climate Dynamics*, *18*(8), 647-660.

Delmonte, B., J. Robert Petit, I. Basile-Doelsch, E. Jagoutz, and V. Maggi (2007), 6. Late quaternary interglacials in East Antarctica from ice-core dust records, in *Developments in Quaternary Sciences*, edited by M. C. M. F. S. G. Frank Sirocko and L. Thomas, pp. 53-73, Elsevier.

Delmonte, B., J. R. Petit, K. K. Andersen, I. Basile-Doelsch, V. Maggi, and V. Ya Lipenkov (2004a), Dust size evidence for opposite regional atmospheric circulation changes over east Antarctica during the last climatic transition, *Climate Dynamics*, *23*(3), 427-438.

Delmonte, B., J. R. Petit, G. Krinner, V. Maggi, J. Jouzel, and R. Udisti (2005), Ice core evidence for secular variability and 200-year dipolar oscillations in atmospheric circulation over East Antarctica during the Holocene, *Climate Dynamics*, *24*(6), 641-654.

Delmonte, B., P. S. Andersson, M. Hansson, H. Schöberg, J. R. Petit, I. Basile-Doelsch, and V. Maggi (2008), Aeolian dust in East Antarctica (EPICA-Dome C and Vostok): Provenance during glacial ages over the last 800 kyr, *Geophys. Res. Lett.*, *35*(7), L07703.

Delmonte, B., I. Basile-Doelsch, J. R. Petit, V. Maggi, M. Revel-Rolland, A. Michard, E. Jagoutz, and F. Grousset (2004b), Comparing the Epica and Vostok dust records during the last 220,000 years: stratigraphical correlation and provenance in glacial periods, *Earth-Science Reviews*, *66*(1-2), 63-87.

Delmonte, B., P. S. Andersson, H. Schöberg, M. Hansson, J. R. Petit, R. Delmas, D. M. Gaiero, V. Maggi, and M. Frezzotti (2010a), Geographic provenance of aeolian dust in East Antarctica during Pleistocene glaciations: preliminary results from Talos Dome and comparison with East Antarctic and new Andean ice core data, *Quaternary Science Reviews*, *29*(1-2), 256-264.

Delmonte, B., C. Baroni, P. Andersson, B. Narcisi, M. Salvatore, J. Petit, C. Scarchilli, M. Frezzotti, S. Albani, and V. Maggi (2013), Modern and Holocene aeolian dust variability from Talos Dome (Northern Victoria Land) to the interior of the Antarctic ice sheet, *Quaternary Science Reviews*, *64*, 76-89.

Delmonte, B., et al. (2010b), Aeolian dust in the Talos Dome ice core (East Antarctica, Pacific/Ross Sea sector): Victoria Land versus remote sources over the last two climate cycles, *Journal of Quaternary Science*, *25*(8), 1327-1337.

DePaolo, D. J., and G. J. Wasserburg (1976), Inferences about magma sources and mantle structure from variations of 143Nd/144Nd, *Geophys. Res. Lett.*, *3*(12), 743-746.

Desboeufs, K., A. Sofikitis, R. Losno, J. Colin, and P. Ausset (2005), Dissolution and solubility of trace metals from natural and anthropogenic aerosol particulate matter, *Chemosphere*, *58*(2), 195-203.

Desboeufs, K. V., A. Sofikitis, R. Losno, J. L. Colin, and P. Ausset (2005), Dissolution and solubility of trace metals from natural and anthropogenic aerosol particulate matter, *Chemosphere*, *58*(2), 195-203.

Dirksen, R. J., K. Folkert Boersma, J. De Laat, P. Stammes, G. R. Van Der Werf, M. Val Martin, and H. M. Kelder (2009), An aerosol boomerang: Rapid around-the-world transport of smoke from the December 2006 Australian forest fires observed from space, *Journal of Geophysical Research: Atmospheres (1984–2012)*, *114*(D21).

Donaghay, P., P. Liss, R. A. Duce, D. Kester, A. Hanson, T. Villareal, N. W. Tindale, and D. Gifford (1991), The role of episodic atmospheric nutrient input in the chemical and biological dynamics of ocean ice ecosystems, *Oceanography*, *4*, 62-70.

Duce, R. A., et al. (1991), The atmospheric input of trace species to the world ocean, *Global Biogeochem. Cycles*, *5*(3), 193-259.

Dunbar, G. B., N. A. N. Bertler, and R. M. McKay (2009), Sediment flux through the McMurdo Ice Shelf in Windless Bight, Antarctica, *Global and Planetary Change*, *69*(3), 87-93.

Duncan, B. N., R. V. Martin, A. C. Staudt, R. Yevich, and J. A. Logan (2003), Interannual and seasonal variability of biomass burning emissions constrained by satellite observations, *Journal of Geophysical Research: Atmospheres (1984–2012)*, *108*(D2), ACH 1-1-ACH 1-22.

Echalar, F., P. Artaxo, J. V. Martins, M. Yamasoe, F. Gerab, W. Maenhaut, and B. Holben (1998), Long-term monitoring of atmospheric aerosols in the Amazon Basin: Source identification and apportionment, *Journal of Geophysical Research: Atmospheres (1984–2012)*, *103*(D24), 31849-31864.

Edwards, R., and P. Sedwick (2001), Iron in East Antarctic snow: Implications for atmospheric iron deposition and algal production in Antarctic waters, *Geophys. Res. Lett.*, *28*(20), 3907-3910.

Edwards, R., P. Sedwick, V. Morgan, and C. Boutron (2006), Iron in ice cores from Law Dome: A record of atmospheric iron deposition for maritime East Antarctica during the Holocene and Last Glacial Maximum, *Geochemistry, Geophysics, Geosystems*, *7*(12), Q12Q01.

Elrod, V., W. Berelson, K. Coale, and K. Johnson (2004), The flux of iron from continental shelf sediments: a missing source for global budgets, *Geophys Res Lett*, *31*, L12307.

Falkowski, P. G. (1997), Evolution of the nitrogen cycle and its influence on the biological sequestration of CO 2 in the ocean, *Nature*, *387*(6630), 272-275.

Field, R. D., G. R. van der Werf, and S. S. Shen (2009), Human amplification of drought-induced biomass burning in Indonesia since 1960, *Nature Geoscience*, *2*(3), 185-188.

Fishwick, M. P., P. N. Sedwick, M. C. Lohan, P. J. Worsfold, K. N. Buck, T. M. Church, and S. J. Ussher (2014), The impact of changing surface ocean conditions on the dissolution of aerosol iron, *Global Biogeochemical Cycles*, 2014GB004921.

Formenti, P., W. Elbert, W. Maenhaut, J. Haywood, S. Osborne, and M. Andreae (2003), Inorganic and carbonaceous aerosols during the Southern African Regional Science Initiative (SAFARI 2000) experiment: Chemical characteristics, physical properties, and emission data for smoke from African biomass burning, *Journal of Geophysical Research: Atmospheres (1984–2012)*, *108*(D13).

Frenklach, M. (2002), Reaction mechanism of soot formation in flames, *Physical Chemistry Chemical Physics*, *4*(11), 2028-2037.

Friedman, B., H. Herich, L. Kammermann, D. S. Gross, A. Arneth, T. Holst, and D. J. Cziczo (2009), Subarctic atmospheric aerosol composition: 1. Ambient aerosol characterization, *Journal of Geophysical Research: Atmospheres (1984–2012)*, *114*(D13).

Gabric, A. J., R. A. Cropp, G. H. McTainsh, B. M. Johnston, H. Butler, B. Tilbrook, and M. Keywood (2010), Australian dust storms in 2002–2003 and their impact on Southern Ocean biogeochemistry, *Global Biogeochemical Cycles*, *24*(2).

Gabrielli, P., A. Wegner, J. R. Petit, B. Delmonte, P. De Deckker, V. Gaspari, H. Fischer, U. Ruth, M. Kriews, and C. Boutron (2010), A major glacial-interglacial change in aeolian dust composition inferred from Rare Earth Elements in Antarctic ice, *Quaternary Science Reviews*, *29*(1), 265-273.

Gaiero, D. M. (2008), Reply to comment by B. Delmonte et al. on "Dust provenance in Antarctic ice during glacial periods: From where in southern South America?", *Geophysical Research Letters*, *35*(8).

Gao, S., D. A. Hegg, and H. Jonsson (2003), Aerosol chemistry, and light-scattering and hygroscopicity budgets during outflow from East Asia, *Journal of Atmospheric Chemistry*, *46*(1), 55-88.

Gao, Y., Y. J. Kaufman, D. Tanré, D. Kolber, and P. G. Falkowski (2001), Seasonal distributions of aeolian iron fluxes to the global ocean, *Geophys. Res. Lett.*, *28*(1), 29-32.

Gao, Y., G. Xu, J. Zhan, J. Zhang, W. Li, Q. Lin, L. Chen, and H. Lin (2013), Spatial and particle size distributions of atmospheric dissolvable iron in aerosols and its input to the Southern Ocean and coastal East Antarctica, *Journal of Geophysical Research: Atmospheres*, *118*(22), 12,634-612,648.

Gaspari, V., C. Barbante, G. Cozzi, P. Cescon, C. F. Boutron, P. Gabrielli, G. Capodaglio, C. Ferrari, J. R. Petit, and B. Delmonte (2006), Atmospheric iron fluxes over the last deglaciation: Climatic implications, *Geophys. Res. Lett.*, *33*(3), L03704.

Gatehouse, R. D., I. Williams, and B. Pillans (2001), Fingerprinting windblown dust in south-eastern Australian soils by uranium-lead dating of detrital zircon, *Soil Research*, *39*(1), 7-12.

Gaudichel, A., M. De Angelis, S. Joussaume, J. Petit, Y. Korotkevitch, and V. Petrov (1992), Comments on the origin of dust in East Antarctica for present and ice age conditions, *Journal of atmospheric chemistry*, *14*(1-4), 129-142.

Gerringa, L. J. A., P. Laan, G. L. van Dijken, H. van Haren, H. J. W. De Baar, K. R. Arrigo, and A. C. Alderkamp (in press), Sources of iron in the Ross Sea polynya in early summer, *Marine Chemistry*, http://dx.doi.org/10.1016/j.marchem.2015.06.002.

Gerringa, L. J. A., A.-C. Alderkamp, P. Laan, C.-E. Thuróczy, H. J. W. De Baar, M. M. Mills, G. L. van Dijken, H. v. Haren, and K. R. Arrigo (2012), Iron from melting glaciers fuels the phytoplankton blooms in Amundsen Sea (Southern Ocean): Iron biogeochemistry, *Deep Sea Research Part II: Topical Studies in Oceanography*, *71–76*(0), 16-31.

Gingele, F., and P. De Deckker (2005), Clay mineral, geochemical and Sr–Nd isotopic fingerprinting of sediments in the Murray–Darling fluvial system, southeast Australia, *Australian Journal of Earth Sciences*, *52*(6), 965-974.

Glassman, I. (1989), Soot formation in combustion processes, paper presented at Symposium (international) on combustion, Elsevier.

Grand, M. M., C. I. Measures, M. Hatta, W. T. Hiscock, C. S. Buck, and W. M. Landing (2015a), Dust deposition in the eastern Indian Ocean: The ocean perspective from Antarctica to the Bay of Bengal, *Global Biogeochemical Cycles*.

Grand, M. M., C. I. Measures, M. Hatta, P. L. Morton, P. Barrett, A. Milne, J. A. Resing, and W. M. Landing (2015b), The impact of circulation and dust deposition in controlling the distributions of dissolved Fe and Al in the south Indian subtropical gyre, *Marine Chemistry*, *176*, 110-125.

Grand, M. M., C. I. Measures, M. Hatta, W. T. Hiscock, W. M. Landing, P. L. Morton, C. S. Buck, P. M. Barrett, and J. A. Resing (2015), Dissolved Fe and Al in the upper 1000 m of the eastern Indian Ocean: A high-resolution transect along 95°E from the Antarctic margin to the Bay of Bengal, *Global Biogeochemical Cycles*, *29*(3), 375-396.

Greeley, R., and J. Iversen (1985), Wind as a geological process, no. 4 in Cambridge Planetary Science Series, *Cambridge Univ. Press, New York, NY*, *3*(3), 3.2.

Grousset, F., P. Rognon, G. Coudé-Gaussen, and P. Pédemay (1992), Origins of peri-Saharan dust deposits traced by their Nd and Sr isotopic composition, *Palaeogeography, Palaeoclimatology, Palaeoecology*, *93*(3), 203-212.

Grousset, F. E., and P. E. Biscaye (2005), Tracing dust sources and transport patterns using Sr, Nd and Pb isotopes, *Chemical Geology*, *222*(3-4), 149-167.

Grousset, F. E., P. E. Biscaye, A. Zindler, J. Prospero, and R. Chester (1988), Neodymium isotopes as tracers in marine sediments and aerosols: North Atlantic, *Earth and Planetary Science Letters*, *87*(4), 367-378.

Grousset, F. E., P. E. Biscaye, M. Revel, J.-R. Petit, K. Pye, S. Joussaume, and J. Jouzel (1992), Antarctic (Dome C) ice-core dust at 18 ky BP: Isotopic constraints on origins, *Earth and Planetary Science Letters*, *111*(1), 175-182.

Grousset, F. E., P. E. Biscaye, M. Revel, J.-R. Petit, K. Pye, S. Joussaume, and J. Jouzel (1992), Antarctic (Dome C) ice-core dust at 18 k.y. B.P.: Isotopic constraints on origins, *Earth and Planetary Science Letters*, *111*(1), 175-182.

Guieu, C., S. Bonnet, T. Wagener, and M. D. Loÿe-Pilot (2005), Biomass burning as a source of dissolved iron to the open ocean?, *Geophysical Research Letters*, *32*(19).

Guieu, C., et al. (2014), The significance of the episodic nature of atmospheric deposition to Low Nutrient Low Chlorophyll regions, *Global Biogeochemical Cycles*, 2014GB004852.

Hao, W. M., and M. H. Liu (1994), Spatial and temporal distribution of tropical biomass burning, *Global biogeochemical cycles*, *8*(4), 495-503.

Hasegawa, S., and S. Ohta (2002), Some measurements of the mixing state of soot-containing particles at urban and non-urban sites, *Atmospheric Environment*, *36*(24), 3899-3908.

Heimburger, A., R. Losno, and S. Triquet (2013), Solubility of iron and other trace elements in rainwater collected on the Kerguelen Islands (South Indian Ocean), *Biogeosciences*, *10*(10).

Heimburger, A., R. Losno, S. Triquet, and E. B. Nguyen (2013), Atmospheric deposition fluxes of 26 elements over the Southern Indian Ocean: Time series on Kerguelen and Crozet Islands, *Global Biogeochemical Cycles*, *27*(2), 440-449.

Heimburger, A., R. Losno, S. Triquet, F. Dulac, and N. Mahowald (2012), Direct measurements of atmospheric iron, cobalt, and aluminum-derived dust deposition at Kerguelen Islands, *Global Biogeochemical Cycles*, *26*(4).

Hesse, P. P. (1994), The record of continental dust from Australia in Tasman Sea sediments, *Quaternary Science Reviews*, *13*(3), 257-272.

Hesse, P. P. (1997), Mineral magnetic 'tracing'of aeolian dust in southwest Pacific sediments, *Palaeogeography, Palaeoclimatology, Palaeoecology*, *131*(3), 327-353.

Hesse, P. P., and G. H. McTainsh (2003), Australian dust deposits: modern processes and the Quaternary record, *Quaternary Science Reviews*, *22*(18), 2007-2035.

Hinkley, T. K., and A. Matsumoto (2001), Atmospheric regime of dust and salt through 75,000 years of Taylor Dome ice core: Refinement by measurement of major, minor, and trace metal suites, *J. Geophys. Res.*, *106*(D16), 18487-18493.

Hoelzemann, J. J., M. G. Schultz, G. P. Brasseur, C. Granier, and M. Simon (2004), Global Wildland Fire Emission Model (GWEM): Evaluating the use of global area burnt satellite data, *Journal of Geophysical Research: Atmospheres (1984–2012)*, *109*(D14).

Huang, X., T. Gordon, W. N. Rom, and R. B. Finkelman (2006), Interaction of iron and calcium minerals in coals and their roles in coal dust-induced health and environmental problems, *Reviews in mineralogy and geochemistry*, *64*(1), 153-178.

Huang, X., Y. Song, C. Zhao, M. Li, T. Zhu, Q. Zhang, and X. Zhang (2014), Pathways of sulfate enhancement by natural and anthropogenic mineral aerosols in China, *Journal of Geophysical Research: Atmospheres*.

Hutchins, D. A., G. R. DiTullio, and K. W. Bruland (1993), Iron and Regenerated Production: Evidence for Biological Iron Recycling in Two Marine Environments, *Limnology and Oceanography*, *38*(6), 1242-1255.

Ito, A. (2011), Mega fire emissions in Siberia: potential supply of bioavailable iron from forests to the ocean, *Biogeosciences*, *8*(6).

Ito, A. (2012), Contrasting the effect of iron mobilization on soluble iron deposition to the ocean in the Northern and Southern Hemispheres, *Meteorol. Soc. Japan*, *90*(0), 167-188.

Ito, A. (2013), Global modeling study of potentially bioavailable iron input from shipboard aerosol sources to the ocean, *Global Biogeochemical Cycles*, *27*(1), 1-10.

Ito, A. (2015), Atmospheric Processing of Combustion Aerosols as a Source of Bioavailable Iron, *Environmental Science & Technology Letters*, *2*(3), 70-75.

Ito, A., and J. E. Penner (2004), Global estimates of biomass burning emissions based on satellite imagery for the year 2000, *Journal of Geophysical Research: Atmospheres (1984–2012)*, *109*(D14).

Ito, A., and Z. Shi (2015), Delivery of anthropogenic bioavailable iron from mineral dust and combustion aerosols to the ocean, *Atmospheric Chemistry and Physics Discussions*, *15*(16), 23051-23088.

Jacobsen, S. B., and G. J. Wasserburg (1980), Sm-Nd isotopic evolution of chondrites, *Earth and Planetary Science Letters*, *50*(1), 139-155.

Jacobson, M. Z. (2003), Development of mixed-phase clouds from multiple aerosol size distributions and the effect of the clouds on aerosol removal, *Journal of Geophysical Research: Atmospheres (1984–2012)*, *108*(D8).

Jickells, T., et al. (2005), Global iron connections between desert dust, ocean biogeochemistry, and climate, *Science*, *308*, 67 - 73.

Johnson, B., B. Heese, S. McFarlane, P. Chazette, A. Jones, and N. Bellouin (2008), Vertical distribution and radiative effects of mineral dust and biomass burning aerosol over West Africa during DABEX, *Journal of Geophysical Research: Atmospheres (1984–2012)*, *113*(D23).

Johnson, K., F. Chavez, and G. Friederich (1999), Continental-shelf sediment as a primary source of iron for coastal phytoplankton, *Nature*, *398*, 697 - 700.

Johnson, K., K. Coale, V. Elrod, and W. Tindale (1994), Iron photochemistry in seawater from the equatorial Pacific, *Mar Chem*, *46*, 319 - 334.

Johnson, K. S., R. M. Gordon, and K. H. Coale (1997), What controls dissolved iron concentrations in the world ocean?, *Marine Chemistry*, *57*(3), 137-161.

Johnson, M. S., N. Meskhidze, V. P. Kiliyanpilakkil, and S. Gassó (2010), Understanding the transport of Patagonian dust and its influence on marine biological activity in the South Atlantic Ocean, *Atmos. Chem. Phys. Discuss.*, *10*(11), 27283-27320.

Johnston, S. W. (2001), The influence of aeolian dust deposits on alpine soils in south-eastern Australia, *Soil Research*, *39*(1), 81-88.

Kadko, D., W. M. Landing, and R. U. Shelley (2015), A novel tracer technique to quantify the atmospheric flux of trace elements to remote ocean regions, *Journal of Geophysical Research: Oceans*.

Kalinske, A. A. (1943), Turbulence and the transport of sand and silt by wind, *Annals of the New York Academy of Sciences*, *44*(1), 41-54.

Kasischke, E. S., and J. E. Penner (2004), Improving global estimates of atmospheric emissions from biomass burning, *Journal of Geophysical Research: Atmospheres (1984–2012)*, *109*(D14).

Keywood, M., M. Cope, C. M. Meyer, Y. Iinuma, and K. Emmerson (2015), When smoke comes to town: The impact of biomass burning smoke on air quality, *Atmospheric Environment*.

Keywood, M., M. Kanakidou, A. Stohl, F. Dentener, G. Grassi, C. Meyer, K. Torseth, D. Edwards, A. M. Thompson, and U. Lohmann (2013), Fire in the air: biomass burning impacts in a changing climate, *Critical Reviews in Environmental Science and Technology*, *43*(1), 40-83.

Khalizov, A. F., H. Xue, L. Wang, J. Zheng, and R. Zhang (2009), Enhanced light absorption and scattering by carbon soot aerosol internally mixed with sulfuric acid, *The Journal of Physical Chemistry A*, *113*(6), 1066-1074.

Knight, A. W., G. McTainsh, and R. Simpson (1995), Sediment loads in an Australian dust storm: implications for present and past dust processes, *Catena*, *24*(3), 195-213.

Koffman, B., K. Kreutz, D. Breton, E. Kane, D. Winski, S. Birkel, A. Kurbatov, and M. Handley (2014), Centennial-scale variability of the Southern Hemisphere westerly wind belt in the eastern Pacific over the past two millennia, *Climate of the Past*, *10*(3), 1125-1144.

Kohfeld, K. E., and S. P. Harrison (2001), DIRTMAP: the geological record of dust, *Earth-Science Reviews*, *54*(1-3), 81-114.

Koppmann, R., K. v. Czapiewski, and J. Reid (2005), A review of biomass burning emissions, part I: gaseous emissions of carbon monoxide, methane, volatile organic compounds, and nitrogen containing compounds, *Atmospheric Chemistry and Physics Discussions*, *5*(5), 10455-10516.

Kraemer, S. (2004), Iron oxide dissolution and solubility in the presence of siderophores, *Aquatic Sciences - Research Across Boundaries*, *66*(1), 3-18.

Kraemer, S. M., A. Butler, P. Borer, and J. Cervini-Silva (2005), Siderophores and the Dissolution of Iron-Bearing Minerals in Marine Systems, *Reviews in Mineralogy and Geochemistry*, *59*(1), 53-84.

Krinner, G., and C. Genthon (2003), Tropospheric transport of continental tracers towards Antarctica under varying climatic conditions, *Tellus B*, *55*(1), 54-70.

Krinner, G., J.-R. Petit, and B. Delmonte (2010), Altitude of atmospheric tracer transport towards Antarctica inpresent and glacial climate, *Quaternary science reviews*, *29*(1), 274-284.

Kustka, A. B., S. A. Sañudo-Wilhelmy, E. J. Carpenter, D. Capone, J. Burns, and W. G. Sunda (2003), Iron requirements for dinitrogen-and ammonium-supported growth in cultures of Trichodesmium (IMS 101): Comparison with nitrogen fixation rates and iron: Carbon ratios of field populations, *Limnology and Oceanography*, *48*(5), 1869-1884.

Kustka, A. B., et al. (2015), The roles of MCDW and deep water iron supply in sustaining a recurrent phytoplankton bloom on central Pennell Bank (Ross Sea), *Deep Sea Research Part I: Oceanographic Research Papers*, *105*, 171-185.

Lamarque, J.-F., T. C. Bond, V. Eyring, C. Granier, A. Heil, Z. Klimont, D. Lee, C. Liousse, A. Mieville, and B. Owen (2010), Historical (1850–2000) gridded anthropogenic and biomass burning emissions of reactive gases and aerosols: methodology and application, *Atmospheric Chemistry and Physics*, *10*(15), 7017-7039.

Lambert, F., A. Tagliabue, G. Shaffer, F. Lamy, G. Winckler, L. Farias, L. Gallardo, and R. De Pol-Holz (2015), Dust fluxes and iron fertilization in Holocene and Last Glacial Maximum climates, *Geophysical Research Letters*, n/a-n/a.

Lambert, F., B. Delmonte, J. R. Petit, M. Bigler, P. R. Kaufmann, M. A. Hutterli, T. F. Stocker, U. Ruth, J. P. Steffensen, and V. Maggi (2008), Dust-climate couplings over the past 800,000[thinsp]years from the EPICA Dome C ice core, *Nature*, *452*(7187), 616-619.

Lanci, L., B. Delmonte, V. Maggi, J. R. Petit, and D. V. Kent (2008), Ice magnetization in the EPICA-Dome C ice core: Implication for dust sources during glacial and interglacial periods, *J. Geophys. Res.*, *113*(D14), D14207.

Lannuzel, D., V. Schoemann, J. de Jong, B. Pasquer, P. van der Merwe, F. Masson, J.-L. Tison, and A. Bowie (2010), Distribution of dissolved iron in Antarctic sea ice: Spatial, seasonal, and inter-annual variability, *J. Geophys. Res.*, *115*(G3), G03022.

LaRoche, J., and E. Breitbarth (2005), Importance of the diazotrophs as a source of new nitrogen in the ocean, *Journal of Sea Research*, *53*(1), 67-91.

Latimer, J. C., and G. M. Filippelli (2001), Terrigenous input and paleoproductivity in the Southern Ocean, *Paleoceanography*, *16*(6), 627-643.

Latimer, J. C., G. M. Filippelli, I. L. Hendy, J. D. Gleason, and J. D. Blum (2006), Glacial-interglacial terrigenous provenance in the southeastern Atlantic Ocean: The importance of deep-water sources and surface currents, *Geology*, *34*(7), 545-548.

Law, C., E. Woodward, M. Ellwood, A. Marriner, S. Bury, and K. Safi (2011), Response of surface nutrient inventories and nitrogen fixation to a tropical cyclone in the southwest Pacific, *Limnology and Oceanography*, *56*(4), 1372-1385.

le Roux, J. P. (1994), An alternative approach to the identification of net sediment transport paths based on grain-size trends, *Sedimentary Geology*, *94*(1-2), 97-107.

Lenes, J., B. Darrow, J. Walsh, J. Prospero, R. He, R. Weisberg, G. Vargo, and C. Heil (2008), Saharan dust and phosphatic fidelity: A three-dimensional biogeochemical model of Trichodesmium as a nutrient source for red tides on the West Florida Shelf, *Continental Shelf Research*, *28*(9), 1091-1115.

Li, F., P. Ginoux, and V. Ramaswamy (2008), Distribution, transport, and deposition of mineral dust in the Southern Ocean and Antarctica: Contribution of major sources, *J. Geophys. Res.*, *113*(D10), D10207.

Lin, Y. C., J. P. Chen, T. Y. Ho, and I. Tsai (2015), Atmospheric iron deposition in the northwestern Pacific Ocean and its adjacent marginal seas: The importance of coal burning, *Global Biogeochemical Cycles*, *29*(2), 138-159.

Liu, J., S. Fan, L. W. Horowitz, and H. Levy (2011), Evaluation of factors controlling long-range transport of black carbon to the Arctic, *Journal of Geophysical Research: Atmospheres (1984–2012)*, *116*(D4).

Liu, J., D. L. Mauzerall, L. W. Horowitz, P. Ginoux, and A. M. Fiore (2009), Evaluating inter-continental transport of fine aerosols:(1) Methodology, global aerosol distribution and optical depth, *Atmospheric Environment*, *43*(28), 4327-4338.

Lu, H., and Y. Shao (2001), Toward quantitative prediction of dust storms: an integrated wind erosion modelling system and its applications, *Environmental Modelling & Software*, *16*(3), 233-249.

Luo, C., N. M. Mahowald, and J. del Corral (2003), Sensitivity study of meteorological parameters on mineral aerosol mobilization, transport, and distribution, *J. Geophys. Res.*, *108*(D15), 4447.

Luo, C., N. M. Mahowald, N. Meskhidze, Y. Chen, R. L. Siefert, A. R. Baker, and A. M. Johansen (2005), Estimation of iron solubility from observations and a global aerosol model, *J. Geophys. Res.*, *110*(D23), D23307.

Mackie, D., J. Peat, G. H. McTainsh, P. Boyd, and K. Hunter (2006), Soil abrasion and eolian dust production: Implications for iron partitioning and solubility, *Geochemistry, Geophysics, Geosystems*, *7*(12).

Mackie, D. S., P. W. Boyd, K. A. Hunter, and G. H. McTainsh (2005), Simulating the cloud processing of iron in Australian dust: pH and dust concentration, *Geophys. Res. Lett.*, *32*(6), L06809.

Mackie, D. S., P. W. Boyd, G. H. McTainsh, N. W. Tindale, T. K. Westberry, and K. A. Hunter (2008), Biogeochemistry of iron in Australian dust: From eolian uplift to marine uptake, *Geochem. Geophys. Geosyst.*, *9*(3), Q03Q08.

Macpherson, A. (1987), The MacKay Glacier/Granite Harbour system (Ross Dependency, Antarctica). A study in nearshore glacial marine sedimentation, 85 pp, Victoria University of Wellington, Wellington.

Maenhaut, W., I. Salma, J. Cafmeyer, H. J. Annegarn, and M. O. Andreae (1996), Regional atmospheric aerosol composition and sources in the eastern Transvaal, South Africa, and impact of biomass burning, *JOURNAL OF GEOPHYSICAL RESEARCH-ALL SERIES-*, *101*, 23,631-623,650.

Magee, J., J. Bowler, G. Miller, and D. Williams (1995), Stratigraphy, sedimentology, chronology and palaeohydrology of Quaternary lacustrine deposits at Madigan Gulf, Lake Eyre, South Australia, *Palaeogeography, Palaeoclimatology, Palaeoecology*, *113*(1), 3-42.

Mahowald, N., K. Kohfeld, M. Hansson, Y. Balkanski, S. P. Harrison, I. C. Prentice, M. Schulz, and H. Rodhe (1999), Dust sources and deposition during the last glacial maximum and current climate: A comparison of model results with paleodata from ice cores and marine sediments, *J. Geophys. Res.*, *104*(D13), 15895-15916.

Mahowald, N. M., A. R. Baker, G. Bergametti, N. Brooks, R. A. Duce, T. D. Jickells, N. Kubilay, J. M. Prospero, and I. Tegen (2005), Atmospheric global dust cycle and iron inputs to the ocean, *Global Biogeochem. Cycles*, *19*(4), GB4025.

Mahowald, N. M., S. Engelstaedter, C. Luo, A. Sealy, P. Artaxo, C. Benitez-Nelson, S. Bonnet, Y. Chen, P. Y. Chuang, and D. D. Cohen (2009), Atmospheric iron deposition: Global distribution, variability, and human perturbations*, *Marine Science*, *1*.

Mahowald, N. M., et al. (2010), Observed 20th century desert dust variability: impact on climate and biogeochemistry, *Atmos. Chem. Phys.*, *10*(22), 10875-10893.

Marino, F., E. Castellano, D. Ceccato, P. De Deckker, B. Delmonte, G. Ghermandi, V. Maggi, J. R. Petit, M. Revel-Rolland, and R. Udisti (2008), Defining the geochemical

composition of the EPICA Dome C ice core dust during the last glacial-interglacial cycle, *Geochem. Geophys. Geosyst., 9*(10), Q10018.

Marsay, C., P. N. Sedwick, M. Dinniman, P. Barrett, S. Mack, and D. J. McGillicuddy (2014), Estimating the benthic efflux of dissolved iron on the Ross Sea continental shelf, *Geophysical Research Letters, 41*(21), 7576-7583.

Marticorena, B., and G. Bergametti (1995), Modeling the atmospheric dust cycle: 1. Design of a soil-derived dust emission scheme, *J. Geophys. Res., 100*(D8), 16415-16430.

Martin, C. E., and M. T. McCulloch (1999), Nd-Sr isotopic and trace element geochemistry of river sediments and soils in a fertilized catchment, New South Wales, Australia, *Geochimica et cosmochimica acta, 63*(2), 287-305.

Martin, J. H. (1990), Glacial-interglacial CO2 change: the iron hypothesis, *Paleoceanography, 5*, 1-11.

Martin, J. H., R. M. Gordon, and S. E. Fitzwater (1991), The Case for Iron, *Limnology and Oceanography, 36*(8), 1793-1802.

Martínez-Garcia, A., A. Rosell-Melé, W. Geibert, R. Gersonde, P. Masqué, V. Gaspari, and C. Barbante (2009), Links between iron supply, marine productivity, sea surface temperature, and CO2 over the last 1.1 Ma, *Paleoceanography, 24*(1), PA1207.

Martínez-García, A., D. M. Sigman, H. Ren, R. F. Anderson, M. Straub, D. A. Hodell, S. L. Jaccard, T. I. Eglinton, and G. H. Haug (2014), Iron Fertilization of the Subantarctic Ocean During the Last Ice Age, *Science*, *343*(6177), 1347-1350.

Marx, S. K., B. S. Kamber, and H. A. McGowan (2005), Estimates of Australian dust flux into New Zealand: Quantifying the eastern Australian dust plume pathway using trace element calibrated< sup> 210</sup> Pb as a monitor, *Earth and Planetary Science Letters, 239*(3), 336-351.

McConnell, J. R., G. W. Lamorey, and M. A. Hutterli (2002), A 250-year high-resolution record of Pb flux and crustal enrichment in central Greenland, *Geophysical Research Letters, 29*(23), 45-41-45-44.

McGillicuddy, D., P. Sedwick, M. Dinniman, K. Arrigo, T. Bibby, B. Greenan, E. Hofmann, J. Klinck, W. Smith, and S. Mack (2015), Iron supply and demand in an Antarctic shelf ecosystem, *Geophysical Research Letters*.

McGowan, H. A., B. Kamber, G. H. McTainsh, and S. K. Marx (2005), High resolution provenancing of long travelled dust deposited on the Southern Alps, New Zealand, *Geomorphology, 69*(1), 208-221.

McLaren, P. (1981), An interpretation of trends in grain size measures, *JOURNAL OF SEDIMENTARY RESEARCH, 51*(2), 611-624.

McTainsh, G. (1989), Quaternary aeolian dust processes and sediments in the Australian region, *Quaternary Science Reviews, 8*(3), 235-253.

McTainsh, G., and J. Leys (1993), Soil erosion by wind, *Land Degradation Processes in Australia*, 188-233.

McTainsh, G., and A. Lynch (1996), Quantitative estimates of the effect of climate change on dust storm activity in Australia during the Last Glacial Maximum, *Geomorphology*, *17*(1), 263-271.

McTainsh, G., J. Leys, and E. Tews (2006), Wind erosion trends for the National State of the Environment Report: Data and Methods, *Australia State of the Environment 2006*.

Mills, M. M., C. Ridame, M. Davey, J. La Roche, and R. J. Geider (2004), Iron and phosphorus co-limit nitrogen fixation in the eastern tropical North Atlantic, *Nature*, *429*(6989), 292-294.

Moore, J. K., M. R. Abbott, J. G. Richman, and D. M. Nelson (2000), The southern ocean at the Last Glacial Maximum: A strong sink for atmospheric carbon dioxide, *Global Biogeochem. Cycles*, *14*(1), 455-475.

Moore, J. K., K. Lindsay, S. C. Doney, M. C. Long, and K. Misumi (2013), Marine ecosystem dynamics and biogeochemical cycling in the Community Earth System Model [CESM1 (BGC)]: Comparison of the 1990s with the 2090s under the RCP4. 5 and RCP8. 5 scenarios, *Journal of Climate*, *26*(23), 9291-9312.

Morton, P. L., W. M. Landing, S.-C. Hsu, A. Milne, A. M. Aguilar-Islas, A. R. Baker, A. R. Bowie, C. S. Buck, Y. Gao, and S. Gichuki (2013), Methods for the sampling and analysis of marine aerosols: results from the 2008 GEOTRACES aerosol intercalibration experiment, *Limnology and Oceanography: Methods*, *11*(FEB), 62-78.

Moteki, N., and Y. Kondo (2007), Effects of mixing state on black carbon measurements by laser-induced incandescence, *Aerosol Science and Technology*, *41*(4), 398-417.

Mouillot, F., and C. B. Field (2005), Fire history and the global carbon budget: a 1× 1 fire history reconstruction for the 20th century, *Global Change Biology*, *11*(3), 398-420.

Neff, P. D., and N. A. Bertler (2015), Trajectory modeling of modern dust transport to the Southern Ocean and Antarctica, *Journal of Geophysical Research: Atmospheres*.

Nicol, S., A. Bowie, S. Jarman, D. Lannuzel, K. M. Meiners, and P. Van Der Merwe (2010), Southern Ocean iron fertilization by baleen whales and Antarctic krill, *Fish and Fisheries*, *11*(2), 203-209.

Novakov, T. (1982), Soot in the atmosphere, in *Particulate Carbon*, edited, pp. 19-41, Springer.

Oshima, N., M. Koike, Y. Zhang, and Y. Kondo (2009), Aging of black carbon in outflow from anthropogenic sources using a mixing state resolved model: 2. Aerosol optical properties and cloud condensation nuclei activities, *Journal of Geophysical Research: Atmospheres (1984–2012)*, *114*(D18).

Paerl, H. W., K. M. Crocker, and L. E. Prufert (1987), Limitation of N2 fixation in coastal marine waters: Relative importance of molybdenum, iron, phosphorus, and organic matter availability1, *Limnology and Oceanography*, *32*(3), 525-536.

Paerl, H. W., L. E. Prufert-Bebout, and C. Guo (1994), Iron-stimulated N2 fixation and growth in natural and cultured populations of the planktonic marine cyanobacteria Trichodesmium spp, *Applied and Environmental Microbiology*, *60*(3), 1044-1047.

Palmer, T. Y. (1981), Large fire winds, gases and smoke, *Atmospheric Environment (1967)*, *15*(10), 2079-2090.

Paris, R., K. Desboeufs, P. Formenti, S. Nava, and C. Chou (2010), Chemical characterisation of iron in dust and biomass burning aerosols during AMMA-SOP0/DABEX: implication for iron solubility, *Atmospheric Chemistry and Physics*, *10*(9), 4273-4282.

Pereira, E., A. Setzer, F. Gerab, P. Artaxo, M. Pereira, and G. Monroe (1996), Airborne measurements of aerosols from burning biomass in Brazil related to the TRACE A experiment, *Journal of Geophysical Research: Atmospheres (1984–2012)*, *101*(D19), 23983-23992.

Petit, J.-R., M. Briat, and A. Royer (1981), Ice age aerosol content from East Antarctic ice core samples and past wind strength, *Nature*, *293*(5831), 391-394.

Petit, J. R., et al. (1999), Climate and atmospheric history of the past 420,000 years from the Vostok ice core, Antarctica, *Nature*, *399*(6735), 429-436.

Petters, M. D., A. J. Prenni, S. M. Kreidenweis, P. J. DeMott, A. Matsunaga, Y. B. Lim, and P. J. Ziemann (2006), Chemical aging and the hydrophobic-to-hydrophilic conversion of carbonaceous aerosol, *Geophysical research letters*, *33*(24).

Pitman, A., G. Narisma, and J. McAneney (2007), The impact of climate change on the risk of forest and grassland fires in Australia, *Climatic Change*, *84*(3-4), 383-401.

Pósfai, M., R. Simonics, J. Li, P. V. Hobbs, and P. R. Buseck (2003), Individual aerosol particles from biomass burning in southern Africa: 1. Compositions and size distributions of carbonaceous particles, *Journal of Geophysical Research: Atmospheres (1984–2012)*, *108*(D13).

Prospero, J. M., P. Ginoux, O. Torres, S. E. Nicholson, and T. E. Gill (2002), Environmental characterization of global sources of atmospheric soil dust identified with the Nimbus 7 Total Ozone Mapping Spectrometer (TOMS) absorbing aerosol product, *Reviews of geophysics*, *40*(1), 2-1-2-31.

Pye, K. (1989), *Aeolian dust and dust deposits*, Academic Press, Harcourt Brace Jovanovich, Publishers.

Radke, L. F., D. A. Hegg, P. V. Hobbs, J. D. Nance, J. H. Lyons, K. K. Laursen, R. E. Weiss, P. J. Riggan, and D. E. Ward (1991), Particulate and trace gas emissions from large biomass fires in North America, *Global biomass burning: Atmospheric, climatic, and biospheric implications*, 209-224.

Raiswell, R., L. G. Benning, L. Davidson, and M. Tranter (2008a), Nanoparticulate bioavailable iron minerals in icebergs and glaciers, *Mineral Mag*, *72*(1), 345-348.

Raiswell, R., L. G. Benning, M. Tranter, and S. Tulaczyk (2008b), Bioavailable iron in the Southern Ocean: the significance of the iceberg conveyor belt, *Geochemical Transactions*, *9*(1), 7.

Ramanathan, V., and G. Carmichael (2008), Global and regional climate changes due to black carbon, *Nature geoscience*, *1*(4), 221-227.

Reid, J., R. Koppmann, T. Eck, and D. Eleuterio (2005), A review of biomass burning emissions part II: intensive physical properties of biomass burning particles, *Atmospheric Chemistry and Physics*, *5*(3), 799-825.

Reid, J. S., and P. V. Hobbs (1998), Physical and optical properties of young smoke from individual biomass fires in Brazil, *Journal of Geophysical Research: Atmospheres (1984–2012)*, *103*(D24), 32013-32030.

Reid, J. S., T. F. Eck, S. A. Christopher, P. V. Hobbs, and B. Holben (1999), Use of the Angstrom exponent to estimate the variability of optical and physical properties of aging smoke particles in Brazil, *Journal of Geophysical Research*, *104*(D22), 27,473-427,489.

Resing, J. A., P. N. Sedwick, C. R. German, W. J. Jenkins, J. W. Moffett, B. M. Sohst, and A. Tagliabue (2015), Basin-scale transport of hydrothermal dissolved metals across the South Pacific Ocean, *Nature*, *523*(7559), 200-203.

Revel-Rolland, M., P. De Deckker, B. Delmonte, P. P. Hesse, J. W. Magee, I. Basile-Doelsch, F. Grousset, and D. Bosch (2006), Eastern Australia: A possible source of dust in East Antarctica interglacial ice, *Earth and Planetary Science Letters*, *249*(1-2), 1-13.

Reynolds, R. L., S. R. Cattle, B. M. Moskowitz, H. L. Goldstein, K. Yauk, C. B. Flagg, T. S. Berquó, R. F. Kokaly, S. Morman, and G. N. Breit (2014), Iron oxide minerals in dust of the Red Dawn event in eastern Australia, September 2009, *Aeolian Research*.

Rich, H. W., and F. M. M. Morel (1990), Availability of Well-Defined Iron Colloids to the Marine Diatom Thalassiosira weissflogii, *Limnology and Oceanography*, *35*(3), 652-662.

Riemer, N., H. Vogel, and B. Vogel (2004), Soot aging time scales in polluted regions during day and night, *Atmospheric Chemistry and Physics*, *4*(7), 1885-1893.

Riemer, N., M. West, R. Zaveri, and R. Easter (2010), Estimating black carbon aging time-scales with a particle-resolved aerosol model, *Journal of Aerosol Science*, *41*(1), 143-158.

Robinson, R. S., M. A. Brzezinski, C. P. Beucher, M. G. Horn, and P. Bedsole (2014), The changing roles of iron and vertical mixing in regulating nitrogen and silicon cycling in the Southern Ocean over the last glacial cycle, *Paleoceanography*.

Ruellan, S., H. Cachier, A. Gaudichet, P. Masclet, and J. P. Lacaux (1999), Airborne aerosols over central Africa during the Experiment for Regional Sources and Sinks of Oxidants (EXPRESSO), *Journal of Geophysical Research: Atmospheres (1984–2012)*, *104*(D23), 30673-30690.

Rueter, J. G. (1988), IRON STIMULATION OF PHOTOSYNTHESIS AND NITROGEN FIXATION IN ANABAENA 7120 AND TRICHODESMIUM (CYANOPHYCEAE) 1, *Journal of Phycology*, *24*(2), 249-254.

Rueter, J. G., D. A. Hutchins, R. W. Smith, and N. L. Unsworth (1992), Iron nutrition of Trichodesmium, in *Marine pelagic cyanobacteria: Trichodesmium and other Diazotrophs*, edited, pp. 289-306, Springer.

Running, S. W. (2006), Is global warming causing more, larger wildfires?, *SCIENCE-NEW YORK THEN WASHINGTON-*, *313*(5789), 927.

Sato, M., S. Takeda, and K. Furuya (2007), Iron regeneration and organic iron(III)-binding ligand production during in situ zooplankton grazing experiment, *Marine Chemistry*, *106*(3-4), 471-488.

Schroth, A. W., J. Crusius, E. R. Sholkovitz, and B. C. Bostick (2009), Iron solubility driven by speciation in dust sources to the ocean, *Nature Geosci*, *2*(5), 337-340.

Schuck, I. (2009), Mineralogical characterisation and geographic provenance of atmospheric particles in coastal Antarctic ice cores – indicators of past climatic variability, *Diploma thesis, Universitat Karlsruhe, Karlsruhe, Germany*.

Schulz, M., J. M. Prospero, A. R. Baker, F. Dentener, L. Ickes, P. S. Liss, N. M. Mahowald, S. Nickovic, C. P. r. García-Pando, and S. Rodríguez (2012), Atmospheric transport and deposition of mineral dust to the ocean: implications for research needs, *Environmental science & technology*, *46*(19), 10390-10404.

Sedwick, P. N., and G. R. DiTullio (1997), Regulation of algal blooms in Antarctic Shelf Waters by the release of iron from melting sea ice, *Geophys. Res. Lett.*, *24*(20), 2515-2518.

Sedwick, P. N., E. R. Sholkovitz, and T. M. Church (2007), Impact of anthropogenic combustion emissions on the fractional solubility of aerosol iron: Evidence from the Sargasso Sea, *Geochem. Geophys. Geosyst.*, *8*(10), Q10Q06.

Sedwick, P. N., et al. (2011), Early season depletion of dissolved iron in the Ross Sea polynya: Implications for iron dynamics on the Antarctic continental shelf, *J. Geophys. Res.*, *116*(C12), C12019.

Seiler, W., and P. J. Crutzen (1980), Estimates of gross and net fluxes of carbon between the biosphere and the atmosphere from biomass burning, *Climatic change*, *2*(3), 207-247.

Shao, Y., and L. M. Leslie (1997), Wind erosion prediction over the Australian continent, *JOURNAL OF GEOPHYSICAL RESEARCH-ALL SERIES-*, *102*, 30,091-030,105.

Shi, Z., M. D. Krom, S. Bonneville, and L. G. Benning (2015), Atmospheric Processing Outside Clouds Increases Soluble Iron in Mineral Dust, *Environmental Science & Technology*, *49*(3), 1472-1477.

Shiraiwa, M., Y. Kondo, N. Moteki, N. Takegawa, Y. Miyazaki, and D. Blake (2007), Evolution of mixing state of black carbon in polluted air from Tokyo, *Geophysical Research Letters*, *34*(16).

Sholkovitz, E. R., P. N. Sedwick, and T. M. Church (2009), Influence of anthropogenic combustion emissions on the deposition of soluble aerosol iron to the ocean: Empirical estimates for island sites in the North Atlantic, *Geochimica et Cosmochimica Acta*, *73*(14), 3981-4003.

Sholkovitz, E. R., P. N. Sedwick, T. M. Church, A. R. Baker, and C. F. Powell (2012), Fractional solubility of aerosol iron: Synthesis of a global-scale data set, *Geochimica et cosmochimica acta, 89*, 173-189.

Siefert, R. L., A. M. Johansen, and M. R. Hoffmann (1999), Chemical characterization of ambient aerosol collected during the southwest monsoon and intermonsoon seasons over the Arabian Sea: Labile-Fe(II) and other trace metals, *J. Geophys. Res.*, *104*(D3), 3511-3526.

Slinn, S., and W. Slinn (1980), Predictions for particle deposition on natural waters, *Atmospheric Environment (1967)*, *14*(9), 1013-1016.

Smetacek, V., P. Assmy, and J. Henjes (2004), The role of grazing in structuring Southern Ocean pelagic ecosystems and biogeochemical cycles, *Antarctic Science*, *16*(04), 541-558.

Smetacek, V., et al. (2012), Deep carbon export from a Southern Ocean iron-fertilized diatom bloom, *Nature*, *487*(7407), 313-319.

Smith, W. O., and L. I. Gordon (1997), Hyperproductivity of the Ross Sea (Antarctica) polynya during austral spring, *Geophys. Res. Lett.*, *24*(3), 233-236.

Spokes, L. J., and T. D. Jickells (1995), Factors controlling the solubility of aerosol trace metals in the atmosphere and on mixing into seawater, *Aquatic Geochemistry*, *1*(4), 355-374.

Spokes, L. J., T. D. Jickells, and B. Lim (1994), Solubilisation of aerosol trace metals by cloud processing: A laboratory study, *Geochimica et Cosmochimica Acta*, *58*(15), 3281-3287.

Stephens, M., N. Turner, and J. Sandberg (2003), Particle identification by laser-induced incandescence in a solid-state laser cavity, *Applied optics*, *42*(19), 3726-3736.

Tagliabue, A., J.-B. Sallee, A. R. Bowie, M. Levy, S. Swart, and P. W. Boyd (2014), Surface-water iron supplies in the Southern Ocean sustained by deep winter mixing, *Nature Geosci*, *7*(4), 314-320.

Tagliabue, A., et al. (2010), Hydrothermal contribution to the oceanic dissolved iron inventory, *Nature Geosci*, *3*(4), 252-256.

Textor, C., M. Schulz, S. Guibert, S. Kinne, Y. Balkanski, S. Bauer, T. Berntsen, T. Berglen, O. Boucher, and M. Chin (2006), Analysis and quantification of the diversities of aerosol life cycles within AeroCom, *Atmospheric Chemistry and Physics*, *6*(7), 1777-1813.

Trapp, J. M., F. J. Millero, and J. M. Prospero (2010), Trends in the solubility of iron in dust-dominated aerosols in the equatorial Atlantic trade winds: Importance of iron speciation and sources, *Geochem. Geophys. Geosyst.*, *11*(3), Q03014.

Turn, S., B. Jenkins, J. Chow, L. Pritchett, D. Campbell, T. Cahill, and S. Whalen (1997), Elemental characterization of particulate matter emitted from biomass burning: Wind tunnel derived source profiles for herbaceous and wood fuels, *Journal of Geophysical Research: Atmospheres (1984–2012)*, *102*(D3), 3683-3699.

Turns, S. R. (1996), *An introduction to combustion*, McGraw-hill New York.

Vallelonga, P., P. Gabrielli, K. J. R. Rosman, C. Barbante, and C. F. Boutron (2005), A 220 kyr record of Pb isotopes at Dome C Antarctica from analyses of the EPICA ice core, *Geophys. Res. Lett.*, *32*(1), L01706.

Vallelonga, P., C. Barbante, G. Cozzi, J. Gabrieli, S. Schüpbach, A. Spolaor, and C. Turetta (2013), Iron fluxes to Talos Dome, Antarctica, over the past 200 kyr, *Climate of the Past*, *9*(2), 597-604.

Vallelonga, P., et al. (2010), Lead isotopic compositions in the EPICA Dome C ice core and Southern Hemisphere Potential Source Areas, *Quaternary Science Reviews*, *29*(1-2), 247-255.

van der Werf, G. R., J. T. Randerson, L. Giglio, G. J. Collatz, P. S. Kasibhatla, and A. F. Arellano Jr (2006), Interannual variability in global biomass burning emissions from 1997 to 2004, *Atmospheric Chemistry and Physics*, *6*(11), 3423-3441.

Wagener, T., C. Guieu, R. Losno, S. Bonnet, and N. Mahowald (2008), Revisiting atmospheric dust export to the Southern Hemisphere ocean: Biogeochemical implications, *Global Biogeochem. Cycles*, *22*(2), GB2006.

Walker, P., and A. Costin (1971), Atmospheric dust accession in South-Eastern Australia, *Soil Research*, *9*(1), 1-5.

Walsh, J. J., and K. A. Steidinger (2001), Saharan dust and Florida red tides: the cyanophyte connection, *Journal of Geophysical Research: Oceans (1978–2012)*, *106*(C6), 11597-11612.

Ward, D. (1990), Factors influencing the emissions of gases and particulate matter from biomass burning, in *Fire in the Tropical Biota*, edited, pp. 418-436, Springer.

Ward, D., R. Susott, J. Kauffman, R. Babbitt, D. Cummings, B. Dias, B. Holben, Y. Kaufman, R. Rasmussen, and A. Setzer (1992), Smoke and fire characteristics for cerrado and deforestation burns in Brazil: BASE-B experiment, *Journal of Geophysical Research: Atmospheres (1984–2012)*, *97*(D13), 14601-14619.

Ward, D. E., A. W. Setzer, Y. J. Kaufman, and R. A. Rasmussen (1991), Characteristics of smoke emissions from biomass fires of the Amazon region-BASE-A experiment, *Global Biomass Burning: Atmospheric, Climatic, and Biospheric Implications*, 394-402.

Warneck, P. (2003), In-cloud chemistry opens pathway to the formation of oxalic acid in the marine atmosphere, *Atmospheric Environment*, *37*(17), 2423-2427.

Weller, R., J. Wöltjen, C. Piel, R. Resenberg, D. Wagenbach, G. KÖNIG-LANGLO, and M. Kriews (2008), Seasonal variability of crustal and marine trace elements in the aerosol at Neumayer station, Antarctica, *Tellus B*, *60*(5), 742-752.

Wells, M., N. Zorkin, and A. Lewis (1983), The role of colloidal chemistry in providing a source of iron to phytoplankton, *J Mar Res*, *41*, 731 - 746.

Wegner, A., H. Fischer, B. Delmonte, J.-R. Petit, T. Erhardt, U. Ruth, A. Svensson, B. Vinther, and H. Miller (2015), The role of seasonality of mineral dust concentration and size on glacial/interglacial dust changes in the EPICA Dronning Maud Land ice core, *Journal of Geophysical Research: Atmospheres*, *120*(19), 9916-9931.

Windom, H. L. (1969), Atmospheric Dust Records in Permanent Snowfields: Implications to Marine Sedimentation, *Geological Society of America Bulletin*, *80*(5), 761-782.

Winton, V. H. L., G. B. Dunbar, N. A. N. Bertler, M. A. Millet, B. Delmonte, C. B. Atkins, J. M. Chewings, and P. Andersson (2014), The contribution of aeolian sand and dust to iron fertilization of phytoplankton blooms in southwestern Ross Sea, Antarctica, *Global Biogeochemical Cycles*, *28*(4), 2013GB004574.

Wu, J., E. Boyle, W. Sunda, and L.-S. Wen (2001), Soluble and Colloidal Iron in the Oligotrophic North Atlantic and North Pacific, *Science*, *293*(5531), 847-849.

Yamasoe, M. A., P. Artaxo, A. H. Miguel, and A. G. Allen (2000), Chemical composition of aerosol particles from direct emissions of vegetation fires in the Amazon Basin: water-soluble species and trace elements, *Atmospheric Environment*, *34*(10), 1641-1653.

Zhang, R., A. F. Khalizov, J. Pagels, D. Zhang, H. Xue, and P. H. McMurry (2008), Variability in morphology, hygroscopicity, and optical properties of soot aerosols during atmospheric processing, *Proceedings of the National Academy of Sciences*, *105*(30), 10291-10296.

Zhu, X., J. M. Prospero, F. J. Millero, D. L. Savoie, and G. W. Brass (1992), The solubility of ferric ion in marine mineral aerosol solutions at ambient relative humidities, *Marine Chemistry*, *38*(1-2), 91-107.

Zhu, X., J. M. Prospero, D. L. Savoie, F. J. Millero, R. G. Zika, and E. S. Saltzman (1993), Photoreduction of Iron(III) in Marine Mineral Aerosol Solutions, *J. Geophys. Res.*, *98*(D5), 9039-9046.

Zuberi, B., K. S. Johnson, G. K. Aleks, L. T. Molina, M. J. Molina, and A. Laskin (2005), Hydrophilic properties of aged soot, *Geophysical research letters*, *32*(1).

Zuo, Y., and J. Zhan (2005), Effects of oxalate on Fe-catalyzed photooxidation of dissolved sulfur dioxide in atmospheric water, *Atmospheric Environment*, *39*(1), 27-37.

Chapter 3. Suitability of high-volume aerosol samplers for ultra-trace aerosol iron measurements in pristine air masses: blanks, recoveries and bugs

This chapter been published in *Atmospheric Measurement Techniques Discussions*. Co-author contributions can be found in Appendix A1. The data has been published in the *Curtin University Research Data Repository*.

V.H.L. Winton, A. Bowie, M. Keywood, P. van der Merwe, R. Edwards, 2016. Suitability of high-volume aerosol samplers for ultra-trace aerosol iron measurements in pristine air masses: blanks, recoveries and bugs. *Atmospheric Measurement Techniques Discussions*, doi:10.5194/amt-2016-12, in review.

V.H.L. Winton, A. Bowie, M. Keywood, P. van der Merwe, R. Edwards, 2015. HR-ICP-MS soluble and total trace element data for blank Whatman 41 filters. *Curtin University Research Data*, http://doi.org/10.4225/06/564AB348340D5.

Abstract

Atmospheric inputs of soluble iron (Fe) to the global ocean are an important factor determining marine primary productivity and nitrogen fixation. To investigate soluble aerosol Fe and fractional Fe solubility, marine aerosol sampling has been conducted from a number of platforms including aerosol towers, ship and buoy platforms. A number of these studies have used commercially available high-volume aerosol samplers to collect aerosols from large volumes of air. These samplers are attractive for sampling air from low Fe air masses since they can rapidly concentrate large volumes improving detection limits. Here we investigate the use of a high-volume sampler from the Cape Grim Baseline Air Pollution Station (CGBAPS), Tasmania, Australia to sample aerosol Fe from baseline Southern Ocean air-masses. The study followed the United States Environmental Protection Agency (EPA) standard for the sampling of ambient air using high-volume sampler, and the recommendations and protocols from GEOTRACES community for the sampling, sample preparation and digestion of trace element aerosols. Analysis and inspection of exposure blank (one month exposure) filters for Fe, and other metals, revealed major contamination

resulting from passive deposition of local soil, plants and insects. The results of the study suggest that high-volume aerosol samplers may not be suitable for low concentration air masses over the Southern Ocean aerosol without some mechanism to hermetically seal the sampler when the baseline sampling criteria are not met.

3.1 Introduction

Aerosols containing iron (Fe) have been investigated over the remote ocean to constrain Fe budgets in surface waters and related biological production. Aerosol sampling for metals such Fe is challenging in these regions where atmospheric concentrations are exceptionally low. Over the Southern Ocean, atmospheric Fe concentrations are extremely low with reported concentrations less than 60 ng m^{-2} of Fe [*Bowie et al.*, 2009; *Duce et al.*, 1991; *Gao et al.*, 2013; *Heimburger et al.*, 2013a; *Heimburger et al.*, 2013b; *Heimburger et al.*, 2012; *Prospero*, 1996]. The low atmospheric concentrations result in low atmospheric fluxes to surface waters. Fertilisation experiments in the Southern Ocean have shown that Fe is required for phytoplankton to efficiently undergo photosynthesis and respiration [e.g. *Boyd et al.*, 2007]. The Fe-hypothesis [*Martin*, 1990] has received a lot of interest in the past two decades, whereby the increases in Fe-laden dust, productivity and the degree of nitrate consumption are linked with lowering of atmospheric CO_2 during glacial periods [e.g. *Lambert et al.*, 2015; *Martínez-García et al.*, 2014]. Primary production may also be co-limited by other transition metals such as manganese (Mn) [*Middag et al.*, 2011], copper (Cu) [*Annett et al.*, 2008], cobalt (Cu) [*Saito et al.*, 2002], zinc (Zn) [*Morel et al.*, 1991] and nickel (Ni) [*Price and Morel*, 1991].

From a biogeochemical perspective, it is not the total amount of Fe supplied to the ocean that is important, but the amount that is bio-available, i.e., the amount available for uptake and utilisation by living cells. The most common approach to understanding the delivery of Fe-laden aerosols to phytoplankton has been to quantify the solubility of Fe from aerosols, using Fe leaching experiments. Extremely low soluble aerosol Fe concentrations have been observed in the Southern Ocean, for example 0.07-1.3 ng m^{-3} [*Gao et al.*, 2013; *Winton et al.*, 2015]. Fractional Fe solubility of mineral dust is typically only 1-2 % of the total Fe content [*Baker and Croot*, 2010]. Ultra-trace metal clean practices and methodologies to limit contamination are required for making reliable measurements of both soluble and total Fe in aerosols from the region. Low blank concentrations from sampling material and during analysis are crucial for reliable measurements [*Bollhöfer et al.*, 1999; *Vallelonga et al.*, 2002].

Very few estimates exist over the Southern Ocean, partly due to the difficulty of sampling clean baseline air. In remote areas, fixed sampling stations rarely exist due to access

difficulties or lack of suitable land masses; this covers the majority of the Southern Ocean. Southern Ocean aerosol Fe solubility estimates have resulted from a combination of ship-based and Subantarctic Island land-based aerosol sampling campaigns [e.g. *Bowie et al.*, 2009; *Chance et al.*, 2015; *Gao et al.*, 2013; *Wagener et al.*, 2008]. These studies have used wet and dry aerosol deposition samplers "open collector" [*Heimburger et al.*, 2012] and Volumetric Flow Controlled (VFC) high-volume aerosol samplers (e.g. Falkland Islands, *A Baker Pers. Comm.* [2013]). The recent GEOTRACES 2008 intercalibration experiment [*Morton et al.*, 2013] recommends the use of VFC high-volume aerosol samplers for ship-based marine aerosol sampling. In air masses with low particle loading, high volumes of filtered air are required to collect enough material for analysis. To ensure the required mass of sample is collected for analysis, filter substrates are often exposed for long periods of time requiring extra precautions to minimise contamination. Following an international intercalibration experiment between seven laboratories, *Morton et al.* [2013] recommended Whatman 41 (W41) cellulose fibre filters for low trace element background level applications. This filter substrate can be acid-cleaned to achieve low trace metal blank concentrations [*Baker et al.*, 2006; *Morton et al.*, 2013]. Furthermore, W41 filters have a high aerosol particle collection efficiency (e.g. 95 % efficiency for 0.2 µm diameter particles [*Stafford and Ettinger*, 1972], and 99 % for mineral dust [*Li-Jones and Prospero*, 1998]). Previous aerosol Fe solubility studies that have adopted these protocols and deployed high-volume aerosol samplers both on ships during marine cruises [e.g. *Baker et al.*, 2006; *Chance et al.*, 2015], and on land either at the top of a tower (for example, the clean air site at the Bermuda atmospheric observatory located 50 m a.s.l. [e.g. *Fishwick et al.*, 2014; *Kadko et al.*, 2015]) or deployed on the rooftop of a building [e.g. *Morton et al.*, 2013].

Most recently, Fe solubility in baseline air over the Southern Ocean has been estimated, using a short time series of archived aerosol filters from Cape Grim Baseline Air Pollution Station (CGBAPS) [*Winton et al.*, 2015]. CGBAPS has long been recognised for long-term monitoring of atmospheric species [e.g. *Keeling et al.*, 1996] that are representative of air masses over the remote Southern Ocean. Archived filters from CGBAPS were collected using ultra-trace sampling and methodology previously reported in [*Bollhöfer et al.*, 2005]. Samplers were deployed at a height of 70 m at the top of a communications tower at CGBAPS, above the turbulent layer. The *Bollhöfer et al.* [2005] sampler design prevented local soil contamination as filters were mounted inside a weather shelter i.e., cylindrical filter housing that was sealed pneumatically during non-baseline conditions. In order to extend the

short aerosol Fe solubility time series of *Winton et al.* [2015], we have established an Fe aerosol monitoring program at CGBAPS following GEOTRACES sampling and handling protocols for trace metal analysis [*Cutter et al.*, 2010; *Morton et al.*, 2013] and the United States Environmental Protection Agency (EPA) standard, described by [*Chow*, 1995], for the sampling of ambient air for total suspended particulates (TSP; all particle sizes) and PM10 (particulate matter diameter <10 µm) using high volume sampler for the instrument instalment, calibration and operating procedure. The sampling conditions in *Winton et al.* [2015] cannot be replicated due to new health and safety requirements at the station that prohibit sampling and personal climbing the tower. Therefore, a new method of sample collection was trialled during this study to assess the suitability of VFC high-volume aerosol samplers within the new framework of health and safety regulations. In the present study, a VFC high-volume aerosol sampler was located on the roof deck (90 m above sea level and 6 m above the ground) at CGBAPS where other VFC high-volume aerosol collectors are located, which collect samples for PM2.5 and PM10 (particulate matter diameter <2.5 µm and <10 µm respectively) aerosol composition using ion chromatography [*Selleck et al.*, 2014], multi-elemental analysis using accelerator based ion beam analysis [e.g. *Cohen et al.*, 2000] and black carbon using light-absorbing techniques [*Cohen and Stelcer*, 2014].

As the first step in developing a reliable multi-year Fe time series at the site we investigated a series of filter blanks and baseline aerosol samples. The samples were collected using the EPA standard and GEOTRACES recommended procedures and a VFC high-volume sampler. A combination of Fe leaching experiments, total aerosol digestions, optical light microscopy, scanning electron microscopy (SEM) and enrichment factor analysis were used to assess the reliability of the aerosol samples for Fe solubility studies in baseline Southern Ocean air.

3.2 Methods

3.2.1 Study site and aerosol collection

3.2.1.1 Site details

Cape Grim Baseline Air Pollution Station (40.68 S, 144.69 E) monitors long-term changes in a range of atmospheric species, including greenhouse gases, aerosols, and meteorological parameters. Monitoring occurs during baseline conditions i.e., when the wind direction is

between 190º and 280º (Fig. 3.1a) and the total aerosol particle counts are below a threshold concentration based on the 90th percentile of hourly medians for the previous five years. These conditions occur ~30 % of the time [*Keywood*, 2007] and are representative of air masses over the remote Southern Ocean.

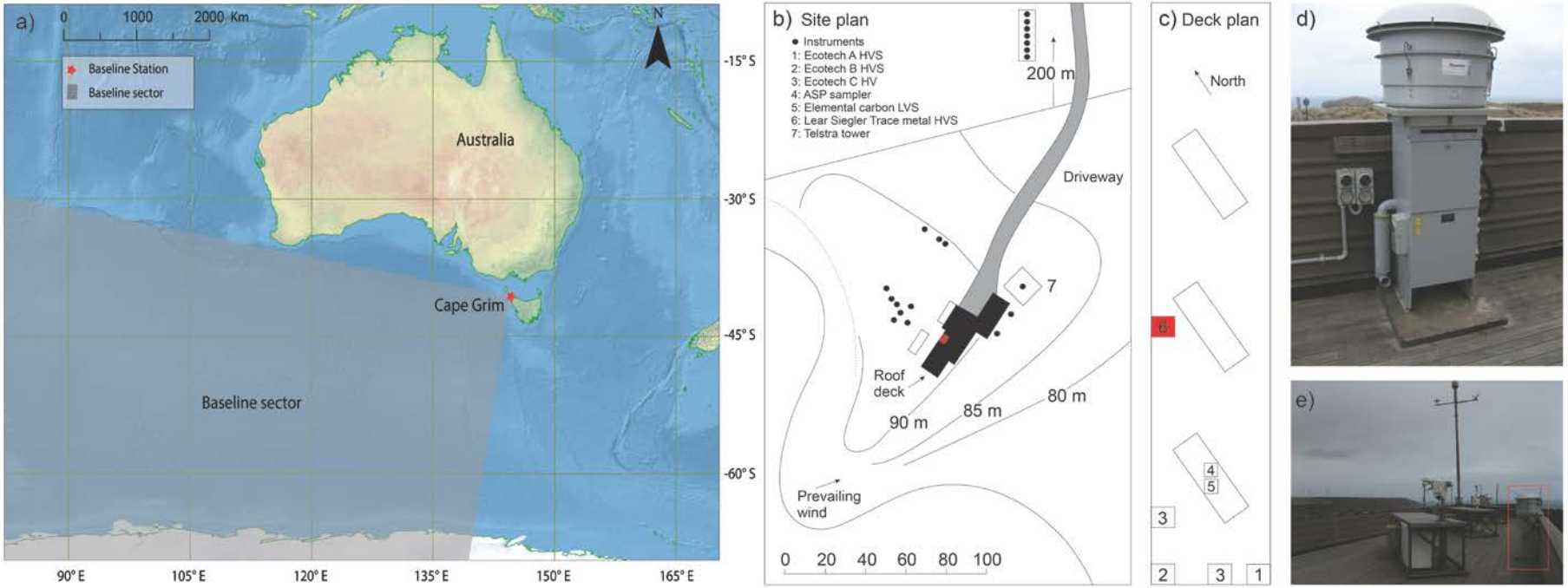

Fig. 3.1: a) Location of the CGBAPS and the high-volume aerosol sampler installed on the roof deck. Baseline conditions occur when the wind direction is between 190° and 280° and the total aerosol particle counts are below a threshold concentration based on the 90th percentile of hourly medians for the previous five years. b) CGBAPS site plan, b) roof deck plan, d-e) LSA high-volume aerosol sample attached with PM10 size selective inlet (photo credit: Jeremy Ward). Panels b) and c) modified from Baseline Report 2009-2010 [*Baseline,* 2014].

3.2.1.2 Aerosol sampler setup

Aerosols were sampled using a VFC high-volume aerosol collector (Lear-Siegler) located on the roof deck at CGBAPS (Fig. 3.1). We followed the United States EPA standard, described by [*Chow,* 1995], for the sampling of ambient air for TSP and PM10 using high volume sampler for the instrument instalment, calibration and operating procedure. The sampler was mounted against the northwest side of the roof deck wall. Prevailing winds at the site are from the southwest. Sampling airflow through the collector was automatically triggered during baseline conditions. At the onset of the project the collector was setup to collect TSP. However, optical light microscope inspection of the filters revealed large particles, up to 100 µm in diameter, (see Section 3.3.1.). Microscope images of the particles suggested that they were derived from local soil. Similar soil contamination of CGBAPS filters has been previously reported (Ayers, 2001). To minimise soil contamination a size-selective inlet was installed (PM10) on the sampler partway through the project (Fig. 3.1).

3.2.2 Laboratory environment, labware and reagents

3.2.2.1 Laboratory environment

All cleaning of labware, filters and sample preparation and analysis was conducted in the Curtin University TRACE facility. The TRACE facility is a large multi-stage clean room designed for ultra-trace metal measurements.

3.2.2.2 Reagents

All the apparatus that came in contact with the aerosol filters was acid cleaned following GEOTRACES protocols [*Cutter et al.*, 2010]. Nitric acid (HNO_3) and hydrochloric acid (HCl) used throughout the study was high purity (<10 ppt or 0.2 nmol L^{-1} Fe). Both acids were double distilled in-house from Seastar® Instrument Quality (IQ) grade acids (Choice Analytical Pty Ltd, Australia) using an all perfluoroalkoxy (PFA) acid purification system (DST-1000, Savillex®). Hereafter referred to as ultra-pure acid. This acid was used for both cleaning of labware and filters and for sample and standard preparation. Seastar Baseline® grade hydrofluoric acid (HF) and HNO_3 (Choice Analytical Pty Ltd, Australia) was used in the digestion of aerosol filters. Ultra-pure water (resistivity of 18.2 MΩ-cm, Purelab Classic, ELGA, Germany) was used throughout.

3.2.2.3 Labware preparation

Low-density polyethylene bottles (LDPE; Nalgene) and polypropylene (PP; Elemental Scientific Inc.) vials were rigorously acid-washed using the following procedure:

1. One week immersion in 3.2 mol L^{-1} IQ grade HNO_3. All labware was rinsed with copious quantities of ultra-pure water between acid baths;
2. One week in 1.2 mol L^{-1} ultra-pure HCl;
3. One week in 0.12 mol L^{-1} ultra-pure HCl;
4. One week in 0.16 mol L^{-1} ultra-pure HNO_3; and
5. One week in ultra-pure water.

Teflon filtration parts used in leaching experiments were cleaned in a series of acid baths on a hotplate at 80 °C for three days. The first bath consisted of 7.9 mol L^{-1} ultra-pure HNO_3, followed by 5.8 mol L^{-1} ultra-pure HCl, then 0.12 mol L^{-1} ultra-pure HCl and 0.16 mol L^{-1} ultra-pure HNO_3, and finally ultra-pure water. Filtration parts were rinsed with copious quantities of ultra-pure water between baths

3.2.2.4 Filter preparation

Aerosol collection substrates were all W41 paper sheets (20 x 25 cm; Whatman) acid-washed before use following the method of *Baker et al.* [2006] and GEOTRACES recommendations [*Morton et al.*, 2013]. Briefly, W41 filter sheets were arranged in layers, one at a time, between polypropylene (PP) mesh, in a series of three 0.5 mol L^{-1} ultra-pure HCl baths for 24 hours. Filters were then rinsed three times with ultra-pure water between baths and then placed in a fresh acid bath. Plastic ziplock bags and plastic tweezers were acid-washed using 3 % (0.5 mol L^{-1}) ultra-pure HNO_3 for 2 weeks. Acid-washed filters were stored in individual acid-washed ziplock bags until use.

3.2.3 Sampling procedures and quality control

3.2.3.1 Filter changing procedure

Loading and changing of aerosol collection substrates was carried out under a laminar flow clean bench at CGBAPS, and aerosol-laden filters were transferred into individual pre-acid-washed ziplock plastic bags immediately after collection and stored frozen until analysis.

3.2.3.2 Filter blanks and aerosol samples

Four types of filter blanks were analysed during the study: (i) untreated filter laboratory blanks, (ii) acid-washed filter laboratory blank, (iii) procedural filter blanks, and (iv) one-month exposure filter blanks. Procedural blanks consisted of acid-washed filters mounted in the aerosol collector for five minutes, with the air pump off. The one-month exposure blank, was collected by the same method as the procedural blank, but for one month duration. The exposure blank was carried out after the PM10 inlet was installed on the collector. Monthly aerosol sampling (TSP) began in June 2013 and the PM10 size selective inlet was installed in November 2013. Actual samples used for optical and Scanning Electron Microscopy (SEM) observations were CG13TM01 (TSP; sampled between 13 June 2013 and 16 July 2013) and CG13TM08 (PM10; sampled between 28 January 2014 and 25 February 2014). Sampling dates and volumes for blank filters and aerosol samples used in this study are reported in Table 3.1.

Table 3.1: Filter blank and aerosol sampling duration and volume.

	Inlet	Start	Finish	Total sampling time	Total sampling volume (m^3)
Procedural blank	TSP	8/08/2013	8/08/2013	5 minutes	0
Exposure blank	PM10	8/11/2013	10/12/2013	1 month	0
CG13TM01	TSP	12/06/2013	16/07/2013	814.7 hours	59473
CG13TM08	PM10	28/01/2014	25/02/2014	143.3 hours	10461

3.2.3.3 Certified Reference Materials and quality control filters

A certified reference material and a commercial quality control spiked filter were used to validate sample digestion procedures. These included the MESS-3 marine sediment (National Research Council, Canada) and a trace metal spiked quality control nitrocellulose filter (QC-TMFM-A, High Purity Standards).

3.2.3.4 Sample preparation

Soluble metals were extracted from each type of blank filter. Circular portions (47 mm diameter) were cut out of the blank filter sheets using a punch cutter (designed at Curtin University), which consisted of a sharpened titanium (Ti) circular blade and a PFA backing mount (both acid-washed). Soluble metals including aluminium (Al), Ti, Manganese (Mn), Fe, and lead (Pb) were extracted from the filter using an instantaneous flow-through water leach [e.g. *Aguilar-Islas et al.*, 2010] consisting of three separate passes of 10 mL of ultra-pure water. Three aliquots of each filter blank were leached with three repeated passes of ultra-pure water.

Total trace metal concentrations were determined following recommendations from the 2008 GEOTRACES intercalibration experiment for the analysis of marine aerosols [*Morton et al.*, 2013]. All digestions were carried out under high-efficiency particulate arresting (HEPA) filtered air, in a total-exhausting clean-air (ISO Class 5), hot block unit (SCP Science, Canada) fitted with an acid scrubber unit at the University of Tasmania. Circle portions (47 mm) of the filters were digested at 95 ºC for 12 hours with concentrated ultra-pure HNO_3 (1 mL, Seastar Baseline®) and ultra-pure HF (0.25 mL, Seastar Baseline®) in capped PFA vials (15 mL, acid cleaned Savillex®) following Bowie et al. (2010). At the end of the digestion, the samples were evaporated to dryness, reconstituted in 10 % (1.60 mol L^{-1}) ultra-pure HNO_3 (10 mL final volume, Seastar® IQ grade double distilled in-house) and stored at 40 ºC for ~48 hours before analysis. Two certified reference materials (MESS-3 marine sediment, National Research Council, Canada, and QC-TMFM-A spiked trace metals on nitrocellulose filter (TMF), High Purity Standards) were digested alongside the samples to test the digestion recovery procedure. Total digestion recovery for Fe from the MESS-3 CRM was 108 ± 8 % (n=3) and TFM was 99 ± 7 % (n=3). Recovery rates for other trace metals are reported in Table S3.1. Blank concentrations for Savillex® beakers, i.e. the digestion blank, are reported in Table 3.2.

Table 3.2: Average total trace metal concentration in filtrates. Data for blank filters are corrected for the digestion blank (Savillex® beaker blank). Errors are the standard deviation of the three sub-samples. DL: Detection limit, *: <0.001.

	Al				Ti				V				Mn				Fe				Pb			
	(ng cm^{-2})	±	(ng m^{-3})	±	(ng cm^{-2})	±	(ng m^{-3})	±	(ng cm^{-2})	±	(pg m^{-3})	±	(ng cm^{-2})	±	(ng m^{-3})	±	(ng cm^{-2})	±	(ng m^{-3})	±	(ng cm^{-2})	±	(pg m^{-3})	±
Instrumental blank (n=10)	0.01	0.004	*	*	*	*	*	*	*	*	0.002	0.002	*	*	*	*	*	*	*	*	*	*	0.005	0.0043
Digestion blank (n=3)	0.67	0.1	0.03	0.01	0.04	0.01	0.002	*	0.01	0.002	0.2	0.1	0.28	0.4	0.01	0.02	0.23	0.2	0.01	0.01	0.02	0.01	1	0.4
Unwashed filter (n=3)	5.6	0.3	0.2	0.01	23	10	0.9	0.4	0.01	0.003	0.52	0.1	<DL		<DL		15	2	0.6	0.1	0.08	0.05	3	2
Acid-washed filter (n=6)	4.1	1	0.2	0.05	3.6	1	0.1	0.01	0.01	0.01	0.56	0.3	<DL		<DL		8.0	5	0.3	0.2	0.004	0.01	0.2	0.2
Procedural blank (n=3) Exposed for 5 min: 8/8/2013 15:15 to 15:20	6.3	2	0.3	0.1	7.7	2	0.3	0.1	0.02	0.01	0.76	0.2	<DL		<DL		7.4	2	0.3	0.1	0.01	0.01	0.5	0.3
Exposure blank (n=3) Exposed for 1 month: 8/11/13 to 10/12/13	250	20	9.8	0.9	48	5	1.9	0.2	0.61	0.05	24	2	3.3	0.8	0.1	0.03	260	30	10	1	0.08	0.03	3	1

Filter blanks in units of "ng cm^{-2}" were calculated assuming the 47 mm aliquot is representative of the whole filter sheet sample.
Filter blanks in units of "ng m^{-3}" were calculated assuming a typical monthly filtered baseline air volume of 12600 m^3 assuming baseline conditions occur 30 % of the time [*Keywood*, 2007].

Table 3.3: Average trace metal soluble concentration in filtrates. Data for blank filters are corrected for the instrumental blank. Errors are the standard deviation of the three sub-samples.

		Al				Ti				V				Mn				Fe				Pb			
		(pg cm^{-2})	±	(pg m^{-3})	±	(pg cm^{-2})	±	(pg m^{-3})	±	(pg cm^{-2})	±	(pg m^{-3})	±	(pg cm^{-2})	±	(pg m^{-3})	±	(pg cm^{-2})	±	(pg m^{-3})	±	(pg cm^{-2})	±	(pg m^{-3})	±
Instrumental blank (n=9)		4.9	3	0.2	0.1	1.9	5	0.08	0.2	0.01	0.02	0.0004	0.0008	0.04	0.07	0.002	0.003	0.46	0.3	0.02	0.01	0.14	0.1	0.01	0.01
Unwashed filter	Leach 1	12	10	0.49	0.4	6.2	8	0.25	0.3	0.97	1	0.04	0.04	60	56	2.4	2	200	180	8.0	7	18	25	0.71	1
(n=3)	Leach 2	11	7	0.45	0.3	4.7	<DL	0.19	<DL	0.75	1	0.03	0.04	14	7	0.56	0.3	46	24	1.8	0.9	4.3	3	0.17	0.1
	Leach 3	0	0.02	<DL	<DL	1.1	<DL	0.04	<DL	0.14	0.2	0.01	0.01	3.6	2	0.14	0.06	9.4	7	0.37	0.3	0.74	0.6	0.03	0.02
Acid-washed	Leach 1	2600	180	100	7	1.1	2	0.05	0.07	0.94	0.9	0.04	0.03	7.5	3	0.30	0.1	30	16	1.2	0.6	1.3	1	0.05	0.04
filter (n=3)	Leach 2	930	650	37	26	<DL	<DL	<DL	<DL	0.54	0.7	0.02	0.03	4.0	3	0.16	0.1	17	14	0.68	0.6	4.6	7	0.18	0.3
	Leach 3	1700	2800	67	110	<DL	<DL	<DL	<DL	0.12	0.1	<DL	<DL	2.7	1	0.11	0.05	21	29	0.85	1	0.35	0.3	0.01	0.01
Procedural	Leach 1	620	330	25	13	12	8	0.46	0.3	3.3	2	0.13	0.07	9.7	4	0.38	0.2	16	9	0.63	0.3	2.4	0.4	0.10	0.02
blank (n=3)	Leach 2	420	120	17	5	1.9	1	0.07	0.04	0.62	0.2	0.02	0.01	2.0	0.5	0.08	0.02	6.2	3	0.25	0.1	0.92	0.4	0.04	0.02
	Leach 3	540	430	21	17	8.3	<DL	0.33	<DL	0.24	0.1	0.01	<DL	0.82	0.5	0.03	0.02	5.3	2	0.21	0.06	1.1	1	0.05	0.04
Exposure blank	Leach 1	54000	21000	2200	850	280	300	11	12	44	10	1.7	0.4	1800	300	70	12	870	490	35	20	26	10	1.0	0.5
(n=3)	Leach 2	14000	5600	580	220	50	16	2.0	0.6	8.6	4	0.34	0.2	110	100	4.2	4	290	110	12	5	1.6	0.6	0.06	0.03
	Leach 3	8400	3200	330	130	25	10	0.98	0.4	5.9	1	0.23	0.04	22	7	0.88	0.3	170	35	6.7	1	1.1	0.6	0.04	0.03

Filter blanks in units of "pg cm^{-2}" were calculated assuming the 47 mm aliquot is representative of the whole filter sheet sample.
Filter blanks in units of "pg m^{-3}" were calculated assuming a typical monthly filtered baseline air volume of 12600 m^3 assuming baseline conditions occur 30 % of the time [*Keywood*, 2007].

3.2.4 High-resolution inductively coupled plasma mass spectrometry analysis

Leachates and resuspended total digests were analysed using high-resolution inductively coupled plasma mass spectrometry (HR-ICP-MS, Element XR ThermoFisher). An auto sampler fitted with an acrylic sample enclosure was used to introduce the sample to the HR-ICP-MS. Measured isotopes and spectral resolutions, along with typical operating conditions, are reported in Table S3.2. The HR-ICP-MS was operated using Ni JET interface sampler and X-skimmer cones and an Apex desolvation unit (Elemental Scientific Inc, ESI) pumped with a Seafast II system syringe pumps (ESI). Samples were analysed in groups of ten bracketed by instrumental blanks (3% or 0.4 mol L^{-1} ultra-pure HCl (soluble) or HNO_3 (total)), and a quality control standard (QC). The QC standard was prepared from a commercial mixed elemental standard (Cat. #ICP-200.7-6 Solution A, High Purity Standards) by serial dilution. Partial procedural blanks were also determined. These included blanks for the leaching and total digestion procedures. Leaching and total digestion blanks consisted of ultra-pure water processed identically to filter leachates and total digestion samples. All samples and standards were prepared on a similar matrix basis. Leachates were acidified to 1 % (0.12 mol L^{-1}) HCl, and total digests were diluted and presented to the instrument as 3 % (0.5 mol L^{-1}) HNO_3. The sample introduction line was rinsed with 3 % (0.4 mol L^{-1}) ultra-pure HCl (3 % or 0.5 mol L^{-1} ultra-pure HNO_3) between leachate (digest) samples for 1.5 minutes. Standard solutions were prepared by serial dilution from 100 µg mL^{-1} stock solutions using ultra-pure water, with a final HCl (HNO_3) concentration of 1 % or 0.12 mol L^{-1} (3 % or 0.5 mol L^{-1}). Preparation of standards in 1 % 0.12 mol L^{-1} ultra-pure HCl (3 % or 0.5 mol L^{-1}ultra-pure HNO_3) matrix matched the leachates (digests). Ten-point calibration solutions were measured. Indium (In), at a concentration of 1.5 ppb, was used as an internal standard.

3.2.5 Optical and Scanning Electron Microscopy

Blank filters (acid-washed laboratory, procedural, and exposure) were examined using optical microscopy to investigate particulate contamination (morphology and particle size). Actual aerosol samples with visible contamination under the optical microscope were further investigated using a SEM (Zeiss Evo 40XVP and Zeiss Neon 40EsB FIBSEM). The SEM was fitted with secondary (SE) and backscatter (BSD) electron detectors and a SiLi energy dispersive X-ray system (EDS) to provide qualitative geochemistry of the particles. The

conditions used (kV, spot size, WD and detector) are shown on the SEM images. Filter blanks were carbon-coated prior to SEM examination.

3.2.6 Air mass back trajectory analysis

Air mass back trajectories were simulated using ANSTO's air mass back trajectory database, based on the NOAA's HYSPLIT v4.0 model [*Draxler and Rolph*, 2003] for the duration of the one-month exposure blank. Five-day air mass back trajectories were generated for the CGBAPS, based on a starting elevation of 200 m a.g.l., for every hour of every day between 8 November and 10 December 2013. Hindcasts were based on meteorological data of 0.5° x 0.5° resolution generated by the global data assimilation system (GDAS) model downloaded from the NOAA ARL website (ftp://arlftp.arlhq.noaa.gov/archives/gdas0p5).

3.3 Results

3.3.1 Optical and Scanning Electron microscopy

Filter blanks and baseline sample filters were inspected by a combination of optical microscopy and SEM. Inspection of acid-washed laboratory and procedural blank filters with an optical microscope showed no obvious sign of particulate contamination (Fig. 3.2). In contrast, the one-month exposure blank and aerosol samples from the aerosol collector (using both the TSP and PM10 inlets) were contaminated with particles up to 100 µm in diameter (Fig. 3.3-5). Visibly discoloured (orange) patches were also observed on a number of baseline TSP and PM10 filter samples (Fig. 3.4b). No discoloured patches were found on the blank filters. Baseline sample filters (both TSP and PM10 inlets) were inspected using a SEM. Particles were comprised of salt (NaCl, cubical crystals), gypsum, calcium carbonate, mineral dust (identified by the silicon (Si), Fe, Al, Ti EDS signals), and silica was identified on the PM10 filters (illustrated in Fig. 3.6). The TSP filters, were coated with a broader variety of material compared to the PM10 filters. Particles on the TSP filter were identified as carbonaceous particles, NaCl, mineral dust, silica sand, spores, and marine aerosol (particles containing magnesium (Mg), strontium (Sr) and barium (Ba); Fig. 3.7).

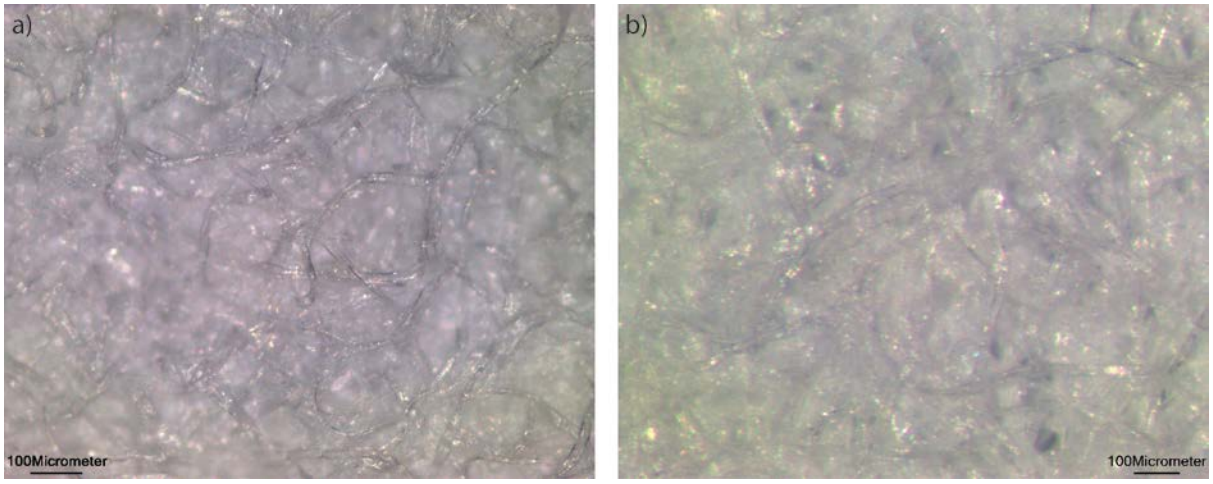

Fig. 3.2: Optical microscopy images of blank filters a) acid-washed blanks b), procedural banks.

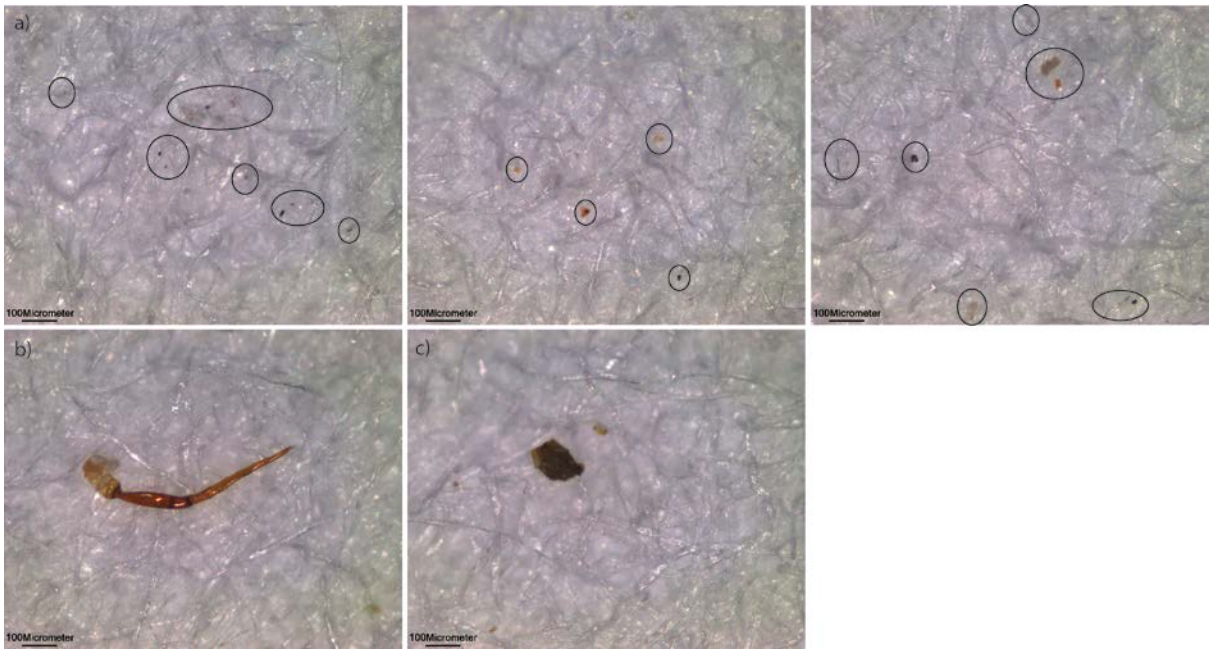

Fig. 3.3: Optical microscopy images of contaminated exposure blanks showing examples of particle son the filter, a) three examples of windblown particles, b) insect leg, c) large soil particle. Areas of interest are circled.

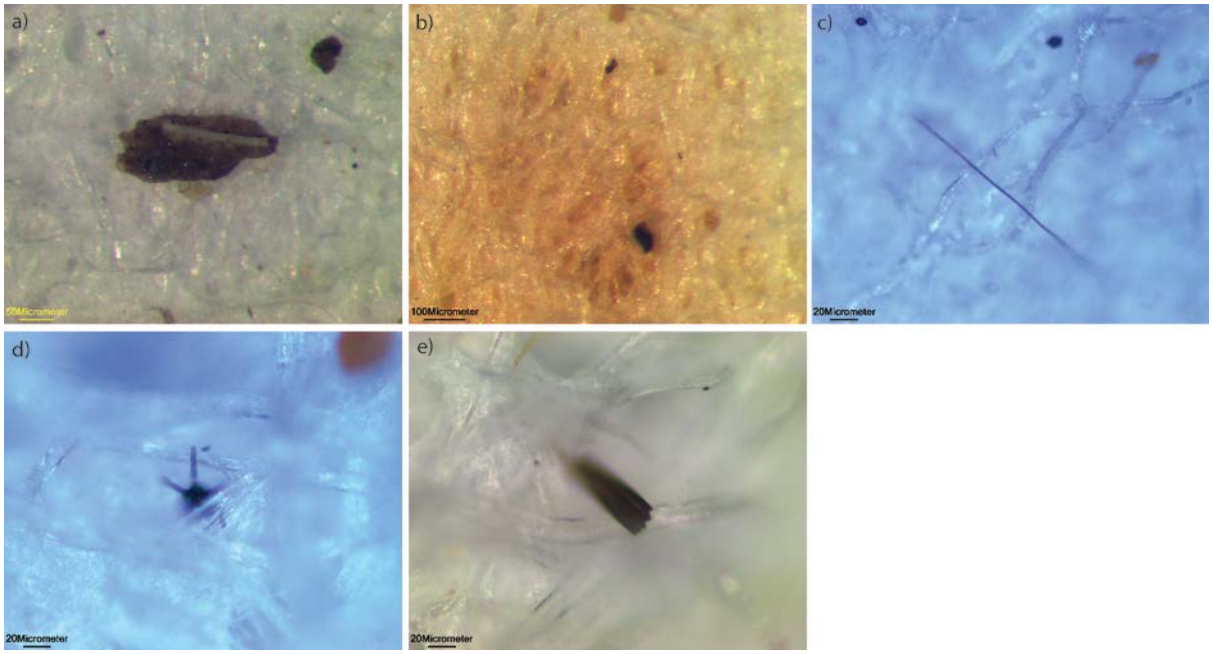

Fig. 3.4: Optical microscopy images of examples of particles collected on TSP filter (CG13TM01) a) large soil particle, b) orange spot common to many TSP filters, c) hair, d) spore, e) moth spare.

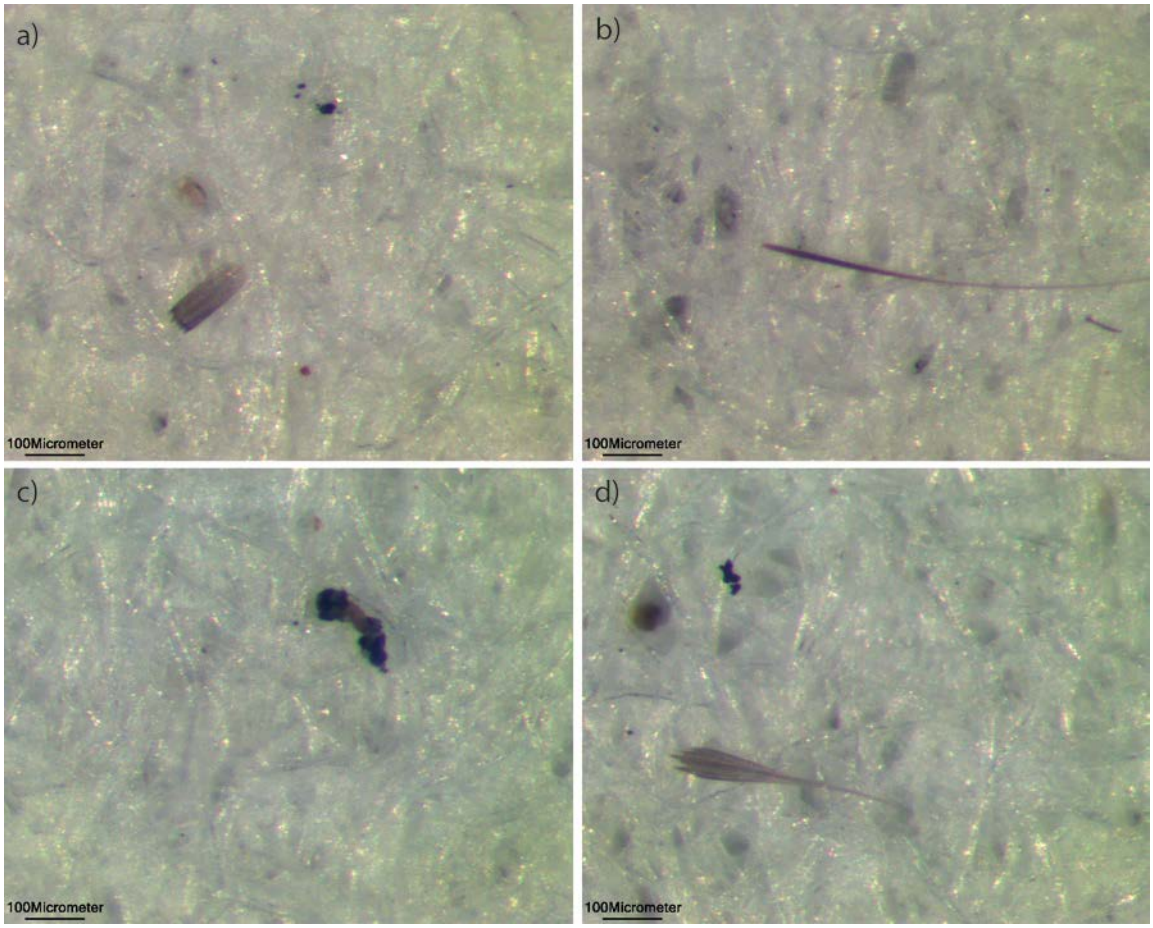

Fig. 3.5: Optical microscopy images of examples of particles collected on PM10 filter (CG13TM08) a) moth spare, b) grass, c-d) large windblown particles.

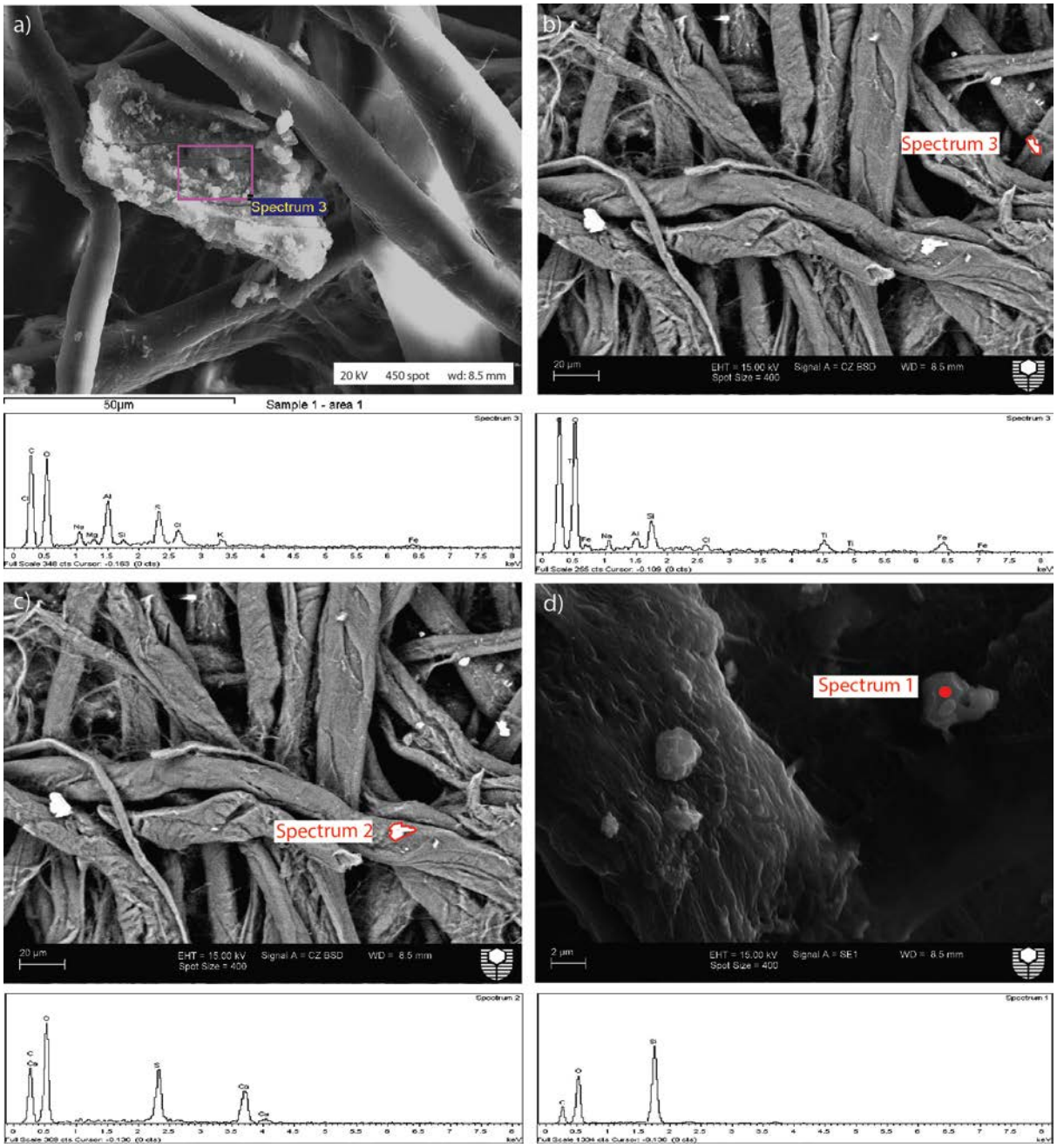

Fig. 3.6: Scanning Electron Microscope images and spectra of particles on a PM10 filter (CG13TM08) a) salt particle (sodium chloride) (detector: SE, instrument: EVO), b) soil (detector: BSD, instrument: EVO), c) calcium carbonate (detector: BSD, instrument: EVO), d) marine silica (detector: SE, instrument: EVO).

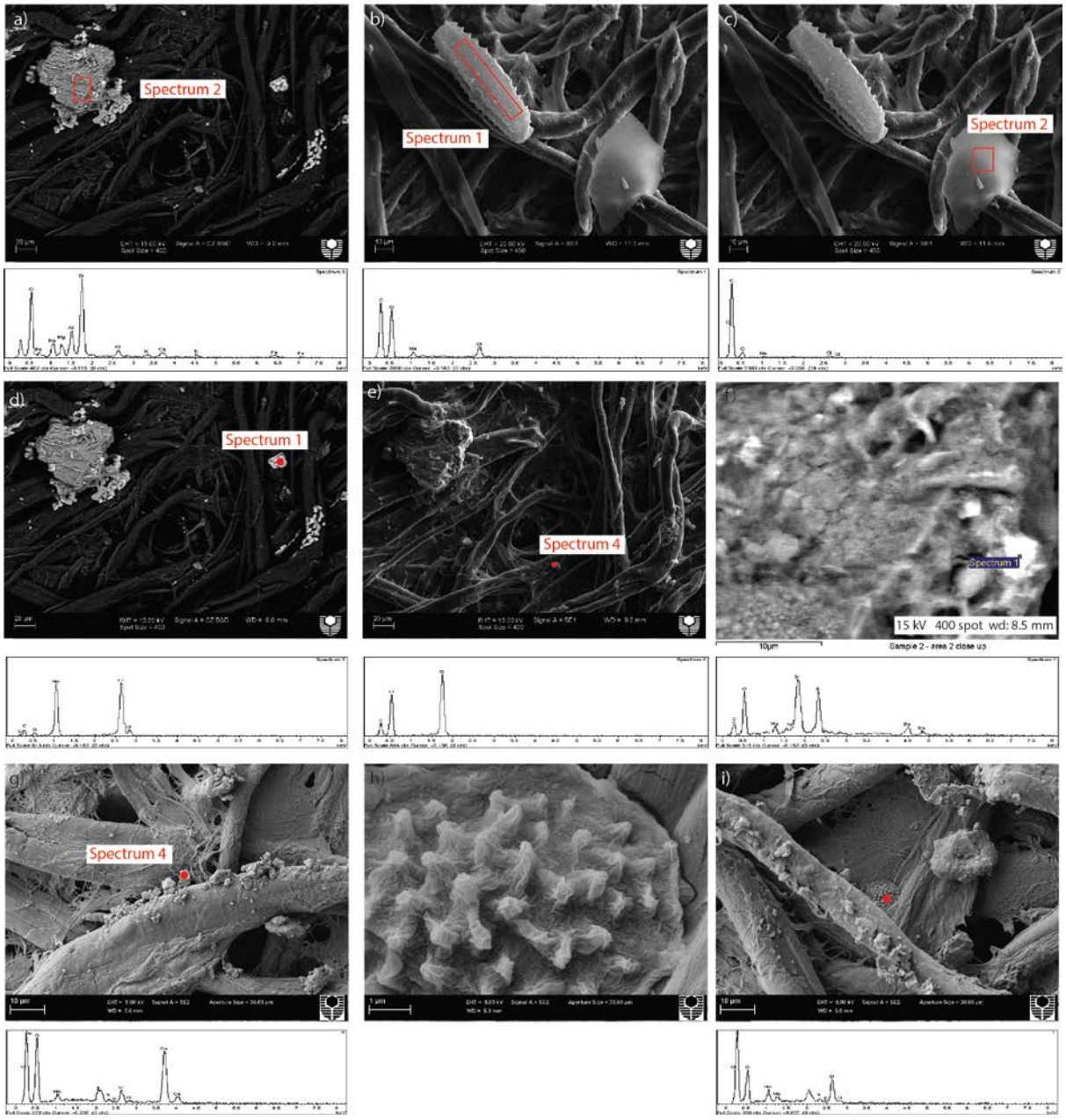

Fig. 3.7: Scanning Electron Microscope images and spectra of particles on a TSP filter (CG13TM01) a) mineral dust (Fe, Mg, Al, Si, Ti, K) (detector: BSD, instrument: EVO), b) organic material (detector: BC, instrument: NEO), c) organic carbonaceous particle (detector: BC, instrument: NEO), d) cubical salt (sodium chloride) (detector: BSD, instrument: EVO), e) silica sand (detector: BC, instrument: EVO), f) marine aerosol (detector: BSD, instrument: EVO), g) marine aerosol (Mg, Sr, Ba, Cl, Ca, Na) (detector: BC, instrument: EVO), h-i) spore (detector: BC, instrument: EVO).

3.3.2 Solubility of contamination-borne particles on blank filters

A typical volume of baseline air collected during a month deployment (ca. 12600 m^3, assuming baseline conditions occur for 30 % of the time [*Keywood*, 2007]) is used to

calculate filter blank concentrations for aerosol samples, and compare them to the aerosol concentrations on a "per cubic meter of air" basis [*Morton et al.*, 2013]. Leaching Fe from the blank filters with the use of ultra-pure water gave soluble Fe concentrations for the four types of blank filters, which can be used as a basis for comparison to other studies. The average soluble trace metal concentrations for the three subsamples of each type of filter are reported in Table 3.3 and Fig. 3.8. Soluble trace metal concentrations in all blank filters decreased with each additional sequential leach of ultra-pure water (Fig. 3.8). At least 50 % of soluble trace metals were leached within the first leach i.e., 65 % of soluble Fe, 53 % of soluble Al, 71 % of soluble Ti, 66 % of soluble V, 75% of soluble Mn, and 61% of soluble Pb for the exposure blank filter.

After acid-cleaning the filters, there was a substantial decrease in the concentration of soluble Fe, from 200 to 30 pg cm^{-2}. Acid-cleaning the filters also decreased the concentrations of soluble Mn, Pb, and Ti in the leachates, but there was no difference in the soluble V concentrations between acid-washed and untreated filters (Fig. 3.8). Soluble Al was the only element to increase (12 to 2600 pg cm^{-2}) after acid-washing the filter; perhaps, due to Al contained within the cellulose filter and further broken down by HCl.

For the procedural blank filters, i.e., those taken to the field and mounted in the VFC high-volume aerosol sampler for five minutes (Table 3.3), the soluble Fe concentrations (16 pg cm^{-2} of soluble Fe) were similar to the blank acid-washed filters (30 pg cm^{-2} of soluble Fe). This validates the cleanliness of our sample handling procedures. Soluble Ti, V, Mn, and Pb concentrations between acid-washed filter blanks and procedural blanks were also similar. Soluble Al was lower in the procedural blank.

In the month-long exposure blank, a considerable increase in the trace metal concentration was observed; for example, up to 870 pg cm^{-2} of soluble Fe. The concentration of all soluble trace metals was at least an order of magnitude greater in the exposure blank than in the procedural and acid-washed filter blank. Soluble Al displayed the highest concentrations in laboratory, procedure, and exposure blank filters.

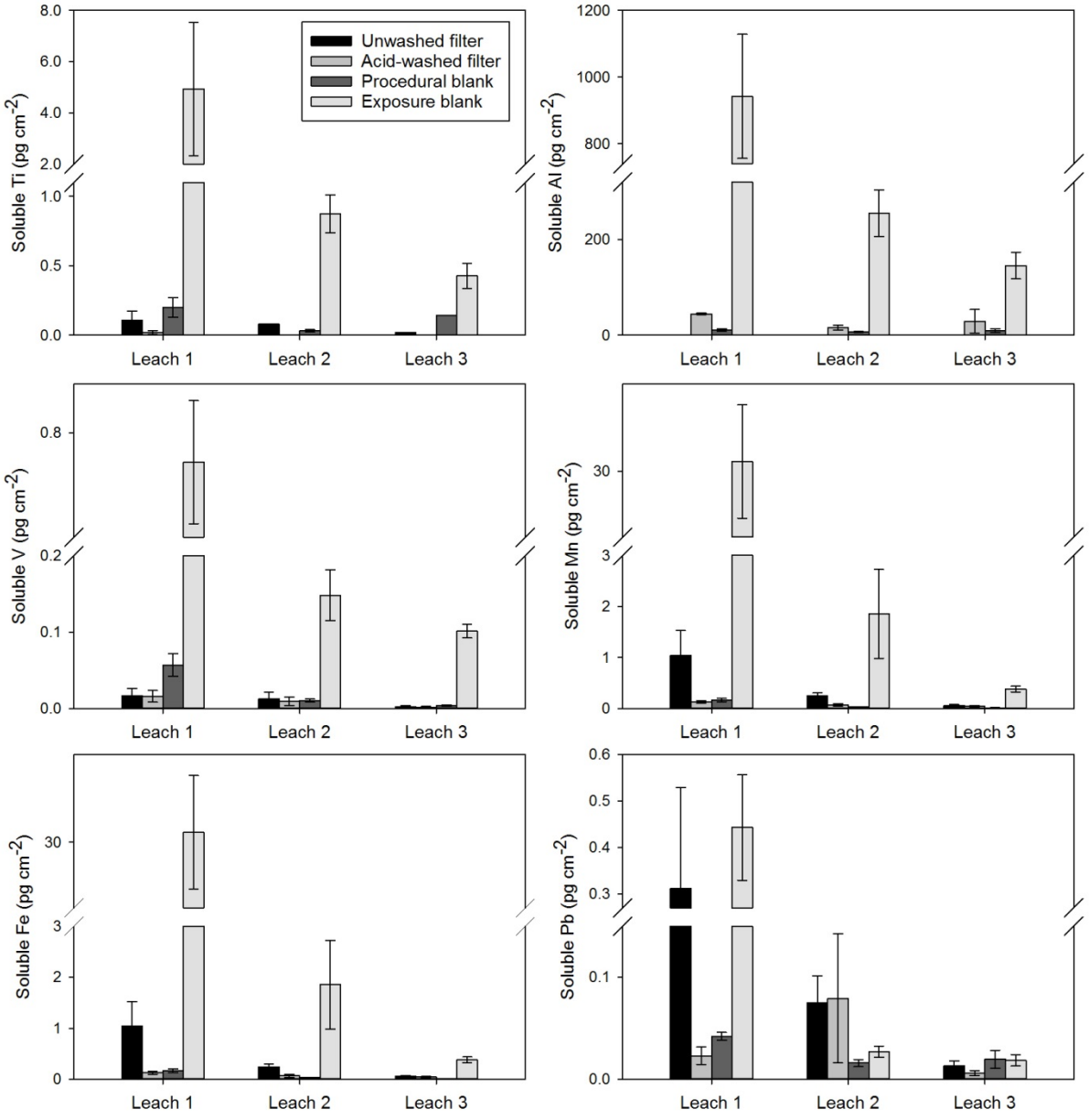

Fig. 3.8: Sequential leaching of soluble trace metals a) Al, b) Ti, c) V, d) Mn, e) Fe, f) Pb from blank filters.

3.3.3 Total trace metal concentrations of contamination-borne particles on blank filters

Similar to the soluble trace metal concentrations, acid-cleaning the filters substantially decreased in the total concentration of all trace metals, except for V where the concentration remained the same (Table 3.2). Procedural blank concentrations were slightly higher than the acid-washed filters for total Al, total Ti, total V, and total Pb concentrations. The procedural

blank total Fe concentration was ~7 pg cm^{-2} lower than the acid-washed filter. Exposure blank total trace metal concentrations were an order of magnitude higher than procedural blank concentrations for all trace metals.

3.4 Discussion

3.4.1 Contamination from laboratory procedures, filter handling and site exposure

We used a series of blank filter types to determine the source and quantity of soluble and total Fe contamination. The blank Fe budget consists of Fe introduced to the sample from reagents, ultra-pure water, leaching from plastic bottles and filter substrate, sample collection and handling, and the instrument (Table 3.4). The instrumental water blank gives an indication of contamination arising from the HR-ICP-MS vial, ultra-pure acids and the instrument. This contribution is ~0.4 pg cm^{-2}. Contamination from the W41 filter substrate is assessed by the difference in Fe between acid-washed and untreated filters. The W41 filters contributes 0.2 ng cm^{-2} (9 pg m^{-3}) of soluble Fe and 7 ng cm^{-2} (0.3 ng m^{-3}) of total Fe to the Fe budget. Thus, acid-washing the filters is crucial for baseline aerosol sampling. Acid-washing of the W41 filters is also necessary when analysing the trace solubility of Mn, Pb, and Ti as acid-washing substantially decreased the contamination arising from the filter substrate alone.

The Fe in the procedural blanks indicates the contamination acquired throughout the sampling process and handling of filters in the field. The sampling procedure contributes negligible total and soluble Fe to the budget (Table 3.4). By following ultra-trace protocols (GEOTRACES recommendations), contamination by personal or handling of filters was minimised; blank concentrations in acid-washed laboratory blank filters are similar to or less than procedural blank filters. Furthermore, no evidence of particulate contamination was observed in the acid-washed or procedural blank filters under an optical microscope.

There is considerable contamination derived from filter exposure at the sampling site. The largest source of soluble Fe contamination was evident in the month-long exposure blank. Contamination arising from one-month of site exposure is around 0.03 ng m^{-3} of soluble Fe and 10 ng m^{-3} of total Fe. This is considerable given water soluble Fe concentrations in contamination-free archived filters ranged from 0.01-0.3 ng m^{-3} of soluble Fe and 0.04-5.8 ng m^{-3} of total Fe [*Winton et al.*, 2015]. The contamination-free archived filters were sampled

using the *Bollhöfer et al*. [2005] aerosol sampler design (Fig. S3.1) and a similar Fe water solubility leaching scheme employed here. Thus, in the low concentration aerosol samples, contamination from site exposure (Tables 3.2 and 3.3) limits our ability to differentiate between the blank and 'real' signal. We suggest two processes by which contamination occurs during the month-long exposure. Firstly, by a passive deposition on the filters during a month-long sampling period at Cape Grim. Passive deposition contributes the majority (94 %) of Fe to the Fe budget (Table 3.4). Secondly, as there is no evidence of human-, sampler-, or building-derived (e.g., wood, paint) particles on the filters, the insect, soil, and marine particle contamination is likely a consequence of airborne particles hitting the sampler at high wind speeds. Additionally, insects could fly or crawl into to sampler, as the air inlet is not sealed during non-baseline conditions (Fig. 3.1). Insect contamination is likely at other sampling sites as indicated by the sampling procedure in the US EPA high-volume sampling standard for the determination of inorganic compounds in ambient air, which recommends that insects be removed with a pair of tweezers.

The total trace metal blank concentrations in acid-washed and untreated W41 filters are similar to those reported by *Morton et al.* [2013], who uses the same acid-washing procedure for cleaning the filters. It is interesting to note that *Morton et al.* [2013] reports a greater Al concentration on the acid-washed filter than the untreated filter. Our soluble Al blank concentrations were also greater for the acid-washed filter highlighting the need for a systematic study of blank aerosol filters in baseline air. The Whatman 41 filters are only suitable for trace metal aerosol studies when the sample concentration is above the detection limit. Aerosol Al concentrations have been reliably reported in regions where the aerosol loading is considerably greater than the Southern Ocean. However, if the sample concentration is too low in baseline air then we recommend that the sampling time is increased to collect a higher concentration of trace metal aerosols on the filter.

Table 3.4: Blank iron contamination budget.

	Total Fe (ng cm^{-2})	Soluble Fe (ng cm^{-2})	Fe blank contribution (ng cm^{-2})	Fe blank contribution (%)
Digestion	[1]0.2		0.2	0.1
Acid	[2]0.0006	[3]0.00004	0.0007	<0.001
Instrument	[4]0.0004	[5]0.0005	0.0009	<0.001
W41 filter	[6]6.6	[7]0.2	6.8	3
Sampling procedure	[8]negligible	[9]negligible	0	<0.001
Month exposure at field site	[10]254	[11]1	255	98
Total	261	1	262	

Method of determination: [1]Digested Savillex ® blank beaker with 0.5 mL of HNO_3 (Baseline Seastar®) and 0.25 of mL HF (Baseline Seastar®) (acid and instrument blank subtracted); [2]Assuming certified maximum specification of Seastar Baseline® of HNO_3 and HF is <10 ppt or 0.2 nmol L^{-1} of Fe; [3]Assuming concentration of double distilled in-house HCl from Seastar® IQ grade quality (Choice Analytical Pty Ltd, Australia) is <10 ppt or 0.2 nmol L^{-1} of Fe; [4]Vials filled with ultra-pure water acidified to 3 % or 0.5 mol L^{-1} HNO_3; [5]Vials filled with ultra-pure water acidified to 1 % or 0.12 mol L^{-1}HCl; [6]Total digestion of untreated filter (digestion, instrument and acid-washed filter blank subtracted); [7]Water soluble leach of untreated filter (instrument acid-washed filter blank subtracted); [8]Total digestion of procedural blank filter (digestion, instrument and acid-washed filter blank subtracted); [9]Water soluble leach of procedural blank filter (instrument and acid-washed filter blank subtracted); [10]Total digestion of exposure blank filter (digestion, instrument and procedural blank filter subtracted); [11]Water soluble leach of exposure blank filter (instrument and procedural blank filter subtracted).Negligible defined as <0.01 pg cm^3 of Fe.

3.4.2 Passive deposition and back trajectory analysis

The exposure blank, which was left in the aerosol collector with the motor switched off for a one-month collection period, reflects contamination derived from the atmospheric fallout or passive deposition. This type of blank gives an indication of the relative magnitudes of the in-sector active sampling (i.e., pump turned on and controlled by the baseline switch for a month) versus passive deposition. The deposition of particles, is thus, partly dependent on the mixture of in- and out-sector winds during the exposure blank period. The cluster means of five-day air mass back trajectories, for the duration of the month-long exposure blank, show that around half of the trajectories were transported from the non-baseline sector (i.e., over Tasmania) while the other half were baseline marine air (Fig. 3.9b). The frequency plot in Fig. 3.9c shows the fetch area of trajectories, which included Tasmania >10 % of the time, and occasionally, the Australian continent (>0.1 %). Furthermore, the high wind speeds at Cape Grim, up 80 km h^{-1} during the exposure blank period (Fig. 3.9a), potentially transport local dust and vegetation to the sampling site. The wind speed is most important when the sampler is turned off (i.e., non-baseline conditions) as it can transport and deposit local dust and insects through the unsealed air intake section of the sampler (visible in Fig. 3.1d).

Extreme weather conditions at this site are a concern for aerosol samplers that are not sealed during non-baseline conditions; contamination occurs regardless of whether the sampler is turned on or off. The *Bollhöfer et al.* [2005] sampler design minimised this source of contamination by pneumatically sealing the sampling when it was turned off.

We use optical microscopy to further assess the impact of passive deposition. Large particles up to 100 µm are observed in the exposure blank (Fig. 3.3). A mixture of mineral dust, vegetation, and even insects were observed on the exposure blank (Fig. 3.3). Large particles were still observed on filters after the installation of the PM10 size selective inlet (Fig. 3.5). An evaluation of PM10 size selective inlet performance in Australia found that PM10 inlets have a d_{50} of 10 µm, i.e., 50 % of particles greater than 10 µm are collected on the inlet [*Keywood*, 1999]. The calibration of the PM10 inlet collection efficiencies is done under certain wind speed conditions and it is likely that the extreme wind speeds at Cape Grim (80 km h^{-1}; Fig 3.9c) are higher than what the inlet was calibrated in. This may explain why some particles larger than 10 µm are observed on the PM10 sample filter (Fig. 3.5). These particles could have been deposited on the filter by a combination of high wind speeds when the sampler was running, which lowered the efficiency of PM10 inlet to separate particles <10 µm, and/or passive deposition when the sampler was turned off. Given the large particle size and the wind strength of non-baseline air (Fig. 3.9), the source of passive deposition is likely local.

Local contamination from the cliff face at Cape Grim has been known to occur for some time [*Ayers*, 2001], and elemental ratios are used to correct for this local cliff contamination for major ion measurements [*Ayers and Ivey*, 1988]. Due to the very weak signal at Cape Grim, fingerprinting (e.g. using elemental ratios or radiogenic isotope ratios) the cliff signal and separating it from the marine particles is challenging. As there is a clear indication of material from the cliff face being blown onto the roof deck during extreme wind events, the soil signal is likely to dominate the marine signal for trace metals. The high concentration of soluble Fe in the exposure blank, sampled at the roof deck height, is as high or higher than soluble trace metal sample (uncontaminated) collected up the 70 m communications tower [*Winton et al.*, 2015]. This local contamination will likely mask or dominate the true Fe solubility of baseline aerosols. At Cape Grim, there is no option to install the sampler elsewhere, e.g. higher up on a tower as has been done in the past [*Bollhöfer et al.*, 2005]. Using an impactor - for example, with a maximum of six upper stages and a backup filter - may aid in the

identification of contamination if the size distribution of the marine aerosol and the cliff debris were known and if those size distributions were significantly different. However, this is likely to result in detection problems of soluble trace metals since the aerosol would be deposited and spread across seven filters instead of one. To overcome this, a PM10 size selective head was installed at Cape Grim to remove the coarse particle size distribution that is not long-range or baseline transport. *Cohen and Stelcer* [2014] suggested that for non-baseline PM 2.5 samples, windblown soil (estimated from the oxides of Al, Si, Ti, Ca, and Fe) represents about 2 % of the total fine mass at Cape Grim. The remaining fine particle mass comprises sea salt (38 %), black carbon (4 %), and organic matter (5 %). Even if windblown soil only contributes 2 % of the total fine aerosol mass in samples, this could be a large fraction of the trace metal component due to their abundance in the soil particles [*Taylor and McLennan*, 1985] and considerably affect solubility. The passive deposition of locally-derived particles during out-sector winds will thus have a major influence on the overall aerosol Fe solubility in baseline samples.

The issue of local contamination has also been identified on Kerguelen Island, located in the Indian sector of the Southern Ocean during an aerosol sampling campaign. Using Al/Ti ratios as a tracer of local soil erosion, *Heimburger et al.* [2013a] found that out of 14 rain samples, only five were free of local contamination and representative of long-range transport particles deposited by rain events. The sampling location has been shown to be a major factor when designing trace metal studies in the Southern Ocean. Other Sub-Antarctic Island sites will likely face similar issues of local contamination such as at Cape Grim and Kerguelen Island. Thus, there is a need for future aerosol campaigns of baseline trace metal solubility to sample aerosols high above the turbulent layer, for example, Cape Verde (30 m) [e.g. *Fomba et al.*, 2012] and Tudor Hill, Bermuda (23 m) [e.g. *Fishwick et al.*, 2014; *Kadko et al.*, 2015].

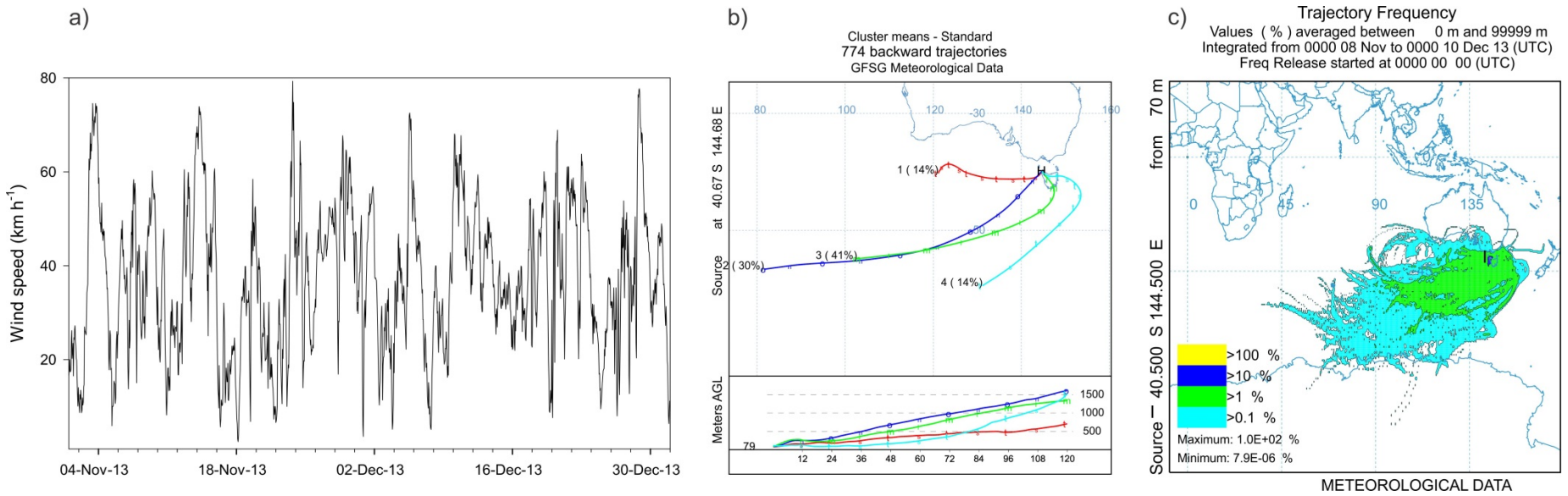

Fig. 3.9: Wind speed and fetch area of air masses associated with the whole duration of one month long exposure blank from 8 November to 10 December 2013. a) Time series of hourly wind speed (times are in the GMT+10 time zone; data sourced from the Australian Bureau of Meteorology), b) Cluster means of 5 day hourly air mass back trajectories.

3.4.3 Enrichment factor analysis

The *Wedepohl* [1995] compilation of continental crust composition was used to calculate crustal enrichment factors (EF) to determine the contribution of mineral dust to the observed total elemental concentrations in the blank filters. Total Al was used as a marker for mineral dust. For an element (Z) in a sample, the EF relative to Al is calculated using equation (3.1).

$$EF = \frac{(Z/Al)_{sample}}{(Z/Al)_{crust}} \quad \text{(Equation 3.1)}$$

The enrichment factors of exposure blank filters are used to gauge the level of mineral dust contamination from a month of exposure at the field site. For example, an EF between 0.7 and 2 is considered to be similar to the upper continental crust, implying that these trace metals might have originated from that source. From the EF in Table 3.5, trace metals had EF between 1.5 – 4.8 (Table 3.5); this is considered as a similar composition or moderate enrichment, in comparison to the upper continental crust (i.e. EF >0.7). Total Fe does not show Fe enrichment, suggesting that anthropogenic Fe was not a source of contamination to the exposure blank, although it is known to be a source of atmospheric soluble Fe [e.g. *Sholkovitz et al.,* 2012]. The low EF values of all trace metals suggest that the trace metals on the exposure blank could have originated from mineral dust sources. The low EFs of all trace metals in the month-long exposure blank that was subject to passive deposition and air masses crossing Tasmania (Fig. 3.9) are likely to reflect local contamination from crustal sources e.g. mineral dust from the cliff face.

Table 3.5: Enrichment factors of trace metals relative to Al measured in exposure and procedural blank filters. The composition of the upper continent crust is based from Wedepohl (1995).

	Ti	Fe	Mn	V	Pb
Exposure blank	4.8	2.7	2.0	3.6	1.5

3.4.4 Recommendations and future work

3.4.4.1 Importance of microscope observations in trace metal aerosol collection

The main concern when collecting marine-derived trace metal aerosol particles at CGBAPS is that the filters also collect dust from the local cliff-face directly below the sampler at the station, especially during stormy conditions. The filters are also subject to passive deposition

while the wind is out of baseline sector, which is noteworthy because of the already weak signal at CGBAPS. Therefore, microscope observations are a key tool in the identification of local contamination. We recommend that microscope observation becomes a routine practice when measuring the Fe content and solubility in aerosols from the Southern Ocean. For example, insect and vegetation contamination was found in our blank filters only through the use of microscope observations, and this source of contamination would not have been detected by the soluble geochemistry alone.

3.4.4.2 Bioactivity inside filters

Sporadic discolourations (orange spots) were identified on the PM10, TSP, and month-long exposure blanks. Microscope observations showed that these spots were located inside the 'depth' of the filter (Fig. 3.4b). A possible source for these spots is microbial growth inside the filters. Algae could be living off nutrients e.g. aerosol nitrate in the aerosol-laden filter. Microbes will also accumulate trace metals [*Morel and Price*, 2003] and affect the solubility. Further work is required to assess these orange spots and determine whether they are an additional source of trace metal contamination.

3.4.4.3 Aerosol sampler siting and closure requirements for low iron air sampling

Much of the passive deposition contamination found by this study was invisible to the naked eye. However, it was still a substantial source of the Fe blank budget compared to the expected Fe aerosol loading. In the case of this study, the sampler was on a platform ~6 m above the ground and exposed to extreme wind conditions. The contamination was primarily due to the lack of an air-tight closure at the sampler intake. As a result strong winds were able to force particles into the sampler and onto the filter. This form of contamination may be decreased by installing the sampler above the surface boundary layer (~50 m); however a hermetic closure is still desirable to keep out air that is out of sector [e.g. *Bollhöfer et al.*, 2005; *Winton et al.*, 2015] (Fig. S3.1). Due to new work health and safety requirements imposed on the field station, it is not possible to carry out a comparison of sampling on the 70 m tower and roof deck to determine if sampling above the turbulent layer decreases contamination. Ship based high-volume samplers are exposed to particulates from ship exhaust [*Edwards*, 1999]. For similar reasons they should be fitted with a hermetic closure to completely seal off the sampler when the winds are out of sector or the wind speed is too low. For example, *Edwards* [1999] investigated ship-derived contamination along an

upwind/downwind transect of snow on Antarctic sea ice. In contrast to the low upwind iron concentrations, downwind concentrations were up to two orders of magnitude higher than the upwind samples, suggesting that snow is substantially contaminated by material carried in the air from the ship.

3.5 Conclusions

A VFC high-volume aerosol sampler was installed at CGBAPS under new health and safety regulations, and following ultra-trace protocols and recommendations of the US EAP standard and GEOTRACES community for aerosol sampling. Using a series of blank filter types, we assessed the contribution of Fe contamination during different stages in the sampling, leaching and analysis of baseline Fe solubility at CGBAPS. To do this we used a combination of solubility experiments, microscope observations, and enrichment factor analysis of one-month exposure blank filters. Contamination arising from HR-ICP-MS, lab wear and handling of filters was negligible. Acid-washing the filters substantially decreased the Fe concentration leached from the W41 filter substrate. The greatest source of contamination was the passive deposition during aerosol sampling while the wind was out of the baseline sector. This source of contamination cannot be seen with the naked eye, but occurs regardless of whether the sampler is turned on or off. Exposure filters collect insects and dust from the local cliff-face directly below the sampler at the station, particularly during stormy conditions. This is a major concern for collecting marine-derived aerosol Fe particles in baseline air due to the very clean air (weak trace metal signal). As local aerosol debris may be found on filters deployed in high-volume aerosol samplers this type of sampler, in its current configuration, may not be appropriate for sampling marine aerosols representative of a broader region. For Southern Ocean studies, we recommend that (i) the use of microscope observations are a key tool for aiding in the identification of local contamination, (ii) land-based aerosol samplers are sealed during non-collection periods to prevent passive deposition, and (ii) ship based aerosol samplers are also sealed when the sector of interest is not being sampled to prevent ship exhaust contamination. Whilst this study shows substantial exposure blanks in clean air conditions, this may not be a problem at sites influenced by air-masses containing higher aerosol Fe loadings.

Acknowledgments

This project was funded through Curtin University (Curtin Research Fellowship to R.E.), the University of Tasmania (B0019024 to A.R.B.), the Australian Research Council (FT130100037 to A.R.B.) and the Antarctic Climate and Ecosystems CRC. Access to HR-ICP-MS instrumentation at Curtin University was facilitated through ARC LIEF funding (LE130100029). V.H.L.W. would like to acknowledge the following scholarship support: Australian Postgraduate Award and Curtin Research Scholarship. CSIRO and the Australian Bureau of Meteorology in Australia are also thanked for their continuous support of CGBAPS, and we also thank Sam Clelend, Nigel Somerville and Jeremy Ward who made the collection of aerosol samples possible. Wind speed data for Cape Grim was sourced from the Australian Bureau of Meteorology. The authors acknowledge the use of equipment, scientific and technical assistance of the Curtin University Electron Microscope Facility, which has been partially funded by the University, State and Commonwealth Governments. We thank Phillip Boyd and Edward Butler for use of the high-volume aerosol sampler that was installed at CGBAPS. We appreciate helpful discussion with Alex Baker on contamination issues with high-volume aerosol collection. We thank Alistair Williams, Scott Chambers and Sylvester Werczynski at ANSTO for their contribution to producing air mass back trajectories and plots. The dataset for blank filters is available through the Curtin University Research Data repository http://doi.org/10.4225/06/564AB348340D5. We thank and two anonymous reviewers who improved the paper.

References

Aguilar-Islas, A. M., Wu, J., Rember, R., Johansen, A. M., and Shank, L. M.: Dissolution of aerosol-derived iron in seawater: Leach solution chemistry, aerosol type, and colloidal iron fraction, Marine Chemistry, 120, 25-33, 2010.

Annett, A. L., Lapi, S., Ruth, T. J., and Maldonado, M. T.: The Effects of Cu and Fe Availability on the Growth and Cu:C Ratios of Marine Diatoms, Limnology and Oceanography, 53, 2451-2461, 2008.

Ayers, G. P.: Influence of local soil dust on composition of aerosol samples at Cape Grim Baseline Atmospheric Program (Australia) 1997-98, 2001. 50-56, 2001.

Ayers, G. P. and Ivey, J. P.: Precipitation composition at Cape Grim, 1977–1985, Tellus B, 40B, 297-307, 1988.

Baker, A. R. and Croot, P. L.: Atmospheric and marine controls on aerosol iron solubility in seawater, Marine Chemistry, 120, 4-13, 2010.

Baker, A. R., Jickells, T. D., Witt, M., and Linge, K. L.: Trends in the solubility of iron, aluminium, manganese and phosphorus in aerosol collected over the Atlantic Ocean, Marine Chemistry, 98, 43-58, 2006.

Baseline: Baseline Atmospheric Program Australia 2009-2010. Edited by Derek. N, Krummel. P. B, Cleland. S. J. Australian Bureau of Meteorology and CSIRO Marine and Atmospheric Research, 2014.

Bollhöfer, A., Chisholm, W., and Rosman, K. J. R.: Sampling aerosols for lead isotopes on a global scale, Analytica Chimica Acta, 390, 227-235, 1999.

Bollhöfer, A., Rosman, K., Dick, A., Chisholm, W., Burton, G., Loss, R., and Zahorowski, W.: Concentration, isotopic composition, and sources of lead in Southern Ocean air during 1999/2000, measured at the Cape Grim Baseline Air Pollution Station, Tasmania, Geochimica et cosmochimica acta, 69, 4747-4757, 2005a.

Bollhöfer, A. F., Rosman, K. J. R., Dick, A. L., Chisholm, W., Burton, G. R., Loss, R. D., and Zahorowski, W.: Concentration, isotopic composition, and sources of lead in Southern Ocean air during 1999/2000, measured at the Cape Grim Baseline Air Pollution Station, Tasmania, Geochimica et Cosmochimica Acta, 69, 4747-4757, 2005b.

Bowie, A. R., Lannuzel, D., Remenyi, T. A., Wagener, T., Lam, P. J., Boyd, P. W., Guieu, C., Townsend, A. T., and Trull, T. W.: Biogeochemical iron budgets of the Southern Ocean south of Australia: Decoupling of iron and nutrient cycles in the subantarctic zone by the summertime supply, Global Biogeochem. Cycles, 23, GB4034, 2009.

Boyd, P. W., Jickells, T., Law, C. S., Blain, S., Boyle, E. A., Buesseler, K. O., Coale, K. H., Cullen, J. J., de Baar, H. J. W., Follows, M., Harvey, M., Lancelot, C., Levasseur, M., Owens, N. P. J., Pollard, R., Rivkin, R. B., Sarmiento, J., Schoemann, V., Smetacek, V.,

Takeda, S., Tsuda, A., Turner, S., and Watson, A. J.: Mesoscale Iron Enrichment Experiments 1993-2005: Synthesis and Future Directions, Science, 315, 612-617, 2007.

Chance, R., Jickells, T. D., and Baker, A. R.: Atmospheric trace metal concentrations, solubility and deposition fluxes in remote marine air over the south-east Atlantic, Marine Chemistry, 2015. 2015.

Chow, J. C.: Measurement methods to determine compliance with ambient air quality standards for suspended particles, Journal of the Air & Waste Management Association, 45, 320-382, 1995.

Cohen, D. D., Garton, D., and Stelcer, E.: Multi-elemental methods for fine particle source apportionment at the global baseline station at Cape Grim, Tasmania, Nuclear Instruments and Methods in Physics Research Section B: Beam Interactions with Materials and Atoms, 161, 775-779, 2000.

Cohen, D. D. and Stelcer, E.: Fine particle sampling at Cape Grim, 2009-2010 Baseline report, 2014. 75, 2014.

Cutter, G., Andersson, P., Codispoti, L., Croot, P., Francois, R., Lohan, M., Obata, H., and Rutgers vd Loeff, M.: Sampling and sample-handling protocols for GEOTRACES Cruises, 2010. 2010.

Draxler, R. R. and Rolph, G. D.: Hybrid Single-Particle Lagrangian Integrated Trajectory (HYSPLIT), model, http://www.arl.noaa.gov/ready/hysplit4.html, 2003. 2003.

Duce, R. A., Liss, P. S., Merrill, J. T., Atlas, E. L., Buat-Menard, P., Hicks, B. B., Miller, J. M., Prospero, J. M., Arimoto, R., Church, T. M., Ellis, W., Galloway, J. N., Hansen, L., Jickells, T. D., Knap, A. H., Reinhardt, K. H., Schneider, B., Soudine, A., Tokos, J. J., Tsunogai, S., Wollast, R., and Zhou, M.: The atmospheric input of trace species to the world ocean, Global Biogeochem. Cycles, 5, 193-259, 1991.

Edwards, R.: Iron in modern and ancient East Antarctic snow: implications for phytoplankton production in the Southern Ocean, PhD thesis, University of Tasmania, Hobart, 1999. 1999.

Fishwick, M. P., Sedwick, P. N., Lohan, M. C., Worsfold, P. J., Buck, K. N., Church, T. M., and Ussher, S. J.: The impact of changing surface ocean conditions on the dissolution of aerosol iron, Global Biogeochemical Cycles, doi: 10.1002/2014GB004921, 2014. 2014GB004921, 2014.

Fomba, K., Müller, K., Pinxteren, D. v., and Herrmann, H.: Aerosol size-resolved trace metal composition in remote northern tropical Atlantic marine environment: case study Cape Verde Islands, Atmospheric Chemistry and Physics Discussions, 12, 29535-29569, 2012.

Gao, Y., Xu, G., Zhan, J., Zhang, J., Li, W., Lin, Q., Chen, L., and Lin, H.: Spatial and particle size distributions of atmospheric dissolvable iron in aerosols and its input to the Southern Ocean and coastal East Antarctica, Journal of Geophysical Research: Atmospheres, 118, 12,634-612,648, 2013.

Heimburger, A., Losno, R., and Triquet, S.: Solubility of iron and other trace elements in rainwater collected on the Kerguelen Islands (South Indian Ocean), Biogeosciences, 10, 2013a.

Heimburger, A., Losno, R., Triquet, S., Dulac, F., and Mahowald, N.: Direct measurements of atmospheric iron, cobalt, and aluminum-derived dust deposition at Kerguelen Islands, Global Biogeochemical Cycles, 26, 2012.

Heimburger, A., Losno, R., Triquet, S., and Nguyen, E. B.: Atmospheric deposition fluxes of 26 elements over the Southern Indian Ocean: Time series on Kerguelen and Crozet Islands, Global Biogeochemical Cycles, 27, 440-449, 2013b.

Kadko, D., Landing, W. M., and Shelley, R. U.: A novel tracer technique to quantify the atmospheric flux of trace elements to remote ocean regions, Journal of Geophysical Research: Oceans, 2015. 2015.

Keeling, R. F., Piper, S. C., and Heimann, M.: Global and hemispheric CO2 sinks deduced from changes in atmospheric O2 concentration, Nature, 381, 218-221, 1996.

Keywood, M.: An evaluation of PM10 and PM2. 5 size selective inlet performance using ambient aerosol, Aerosol Science & Technology, 30, 401-407, 1999.

Keywood, M. D.: Aerosol composition at Cape Grim : an evaluation of PM10 sampling program and baseline event switches., Baseline Atmospheric Program Australia 2005-2006. 2005-2006 ed. J. M. Cainey, N. Derek, and P. B. Krummel (editors). Melbourne: Australian Bureau of Meteorology and CSIRO Marine and Atmospheric Research, 2007. 31-36, 2007.

Lambert, F., Tagliabue, A., Shaffer, G., Lamy, F., Winckler, G., Farias, L., Gallardo, L., and De Pol-Holz, R.: Dust fluxes and iron fertilization in Holocene and Last Glacial Maximum climates, Geophysical Research Letters, doi: 10.1002/2015GL064250, 2015. n/a-n/a, 2015.

Li-Jones, X. and Prospero, J.: Variations in the size distribution of non-sea-salt sulfate aerosol in the marine boundary layer at Barbados: Impact of African dust, Journal of Geophysical Research: Atmospheres (1984–2012), 103, 16073-16084, 1998.

Martin, J. H.: Glacial-interglacial CO2 change: the iron hypothesis, Paleoceanography, 5, 1-11, 1990.

Martínez-García, A., Sigman, D. M., Ren, H., Anderson, R. F., Straub, M., Hodell, D. A., Jaccard, S. L., Eglinton, T. I., and Haug, G. H.: Iron Fertilization of the Subantarctic Ocean During the Last Ice Age, Science, 343, 1347-1350, 2014.

Middag, R., De Baar, H., Laan, P., Cai, P., and Van Ooijen, J.: Dissolved manganese in the Atlantic sector of the Southern Ocean, Deep Sea Research Part II: Topical Studies in Oceanography, 58, 2661-2677, 2011.

Morel, F. and Price, N.: The biogeochemical cycles of trace metals in the oceans, Science, 300, 944-947, 2003.

Morel, F. M., Hudson, R. J., and Price, N. M.: Limitation of productivity by trace metals in the sea, Limnology and Oceanography, 36, 1742-1755, 1991.

Morton, P. L., Landing, W. M., Hsu, S.-C., Milne, A., Aguilar-Islas, A. M., Baker, A. R., Bowie, A. R., Buck, C. S., Gao, Y., and Gichuki, S.: Methods for the sampling and analysis of marine aerosols: results from the 2008 GEOTRACES aerosol intercalibration experiment, Limnology and Oceanography: Methods, 11, 62-78, 2013.

Price, N. and Morel, F.: Colimitation of phytoplankton growth by nickel and nitrogen, LIMNOLOGY, 1991. 1991.

Prospero, J. M.: The atmospheric transport of particles to the ocean, in Particle Flux in the Ocean, John Wiley, Hoboken, N. J, 1996.

Saito, M. A., Moppett, J., Chisholm, S. W., and Waterbury, J. B.: Cobalt limitation and uptake in Prochlorococcus, Limnology and Oceanography, 47, 1629-1636, 2002.

Selleck, P. W., Keywood, M. D., Ward, J. P., Gillett, R. W., and Boast, K.: Aerosol samplers and chemical composition, 2009-2010 Baseline report, 76-79., 2014. 2014.

Sholkovitz, E. R., Sedwick, P. N., Church, T. M., Baker, A. R., and Powell, C. F.: Fractional solubility of aerosol iron: Synthesis of a global-scale data set, Geochimica et cosmochimica acta, 89, 173-189, 2012.

Stafford, R. G. and Ettinger, H. J.: Filter efficiency as a function of particle size and velocity, Atmospheric Environment (1967), 6, 353-362, 1972.

Taylor, S. R. and McLennan, S. M.: The continental crust: Its composition and evolution, 1985.

Vallelonga, P., Van de Velde, K., Candelone, J. P., Ly, C., Rosman, K. J. R., Boutron, C. F., Morgan, V. I., and Mackey, D. J.: Recent advances in measurement of Pb isotopes in polar ice and snow at sub-picogram per gram concentrations using thermal ionisation mass spectrometry, Analytica Chimica Acta, 453, 1-12, 2002.

Wagener, T., Guieu, C., Losno, R., Bonnet, S., and Mahowald, N.: Revisiting atmospheric dust export to the Southern Hemisphere ocean: Biogeochemical implications, Global Biogeochem. Cycles, 22, GB2006, 2008.

Wedepohl, K. H.: The composition of the continental crust, Geochimica et Cosmochimica Acta, 59, 1217-1232, 1995.

Winton, V. H. L., Bowie, A. R., Edwards, R., Keywood, M., Townsend, A. T., van der Merwe, P., and Bollhöfer, A.: Fractional iron solubility of atmospheric iron inputs to the Southern Ocean, Marine Chemistry, 177, Part 1, 20-32, http://dx.doi.org/10.1016/j.marchem.2015.06.006, 2015.

Supplementary information

Table S3.1: Recovery rates of total trace metals in certified reference materials (CRM).

CRM recovery %	Al	±	Ti	±	V	±	Mn	±	Fe	±	Pb	±
Marine sediment (MESS-3)	112	8	92	9	100	9	97	11	108	8	103	11
Trace metal on filter (TMF)	n/d		n/d		101	8	100	9	99	7	107	8

Table S3.2: Instrument conditions and measurement parameters.

Instrument	HR-ICPMS, Element XR (Thermo Fisher, Germany)
Torch	Precision type, quartz o-ring free, PFA injector (Element Scientific Inc.)
Spray chamber	Leachates: APEX with quartz spray chamber (ESI) Digests: PC^3 chilled cyclonic spray chamber (ESI)
Nebuliser	ST micro centric PFA (ESI)
RF power (W)	~1350
Cool gas flow (L min-1)	~16
Auxiliary gas flow (L min-1)	~0.7
Sample gas flow (L min-1)	~0.7
Additional gas (L min-1)	Leachates: ~0.2 N2 Digests: N/A
Additional gas (L min-1)	~~0.4 Ar
Guard electrode	Activated
Sample uptake	90 s (Seafast II pump auto-sampler with fast 3 sample injection valve)
Sample rinse	Leachates: 30 s, 3 % or 0.4 mol L^{-1}HCl Digests: 50 s, 3 % or 0.5 mol L^{-1} HNO3
Scan type	E-scan
Isotopes monitored in low resolution (m/Δm ~400)	^{208}Pb
Isotopes monitored in medium resolution (m/Δm ~4000)	^{27}Al, ^{47}Ti, ^{51}V , ^{55}Mn, ^{56}Fe

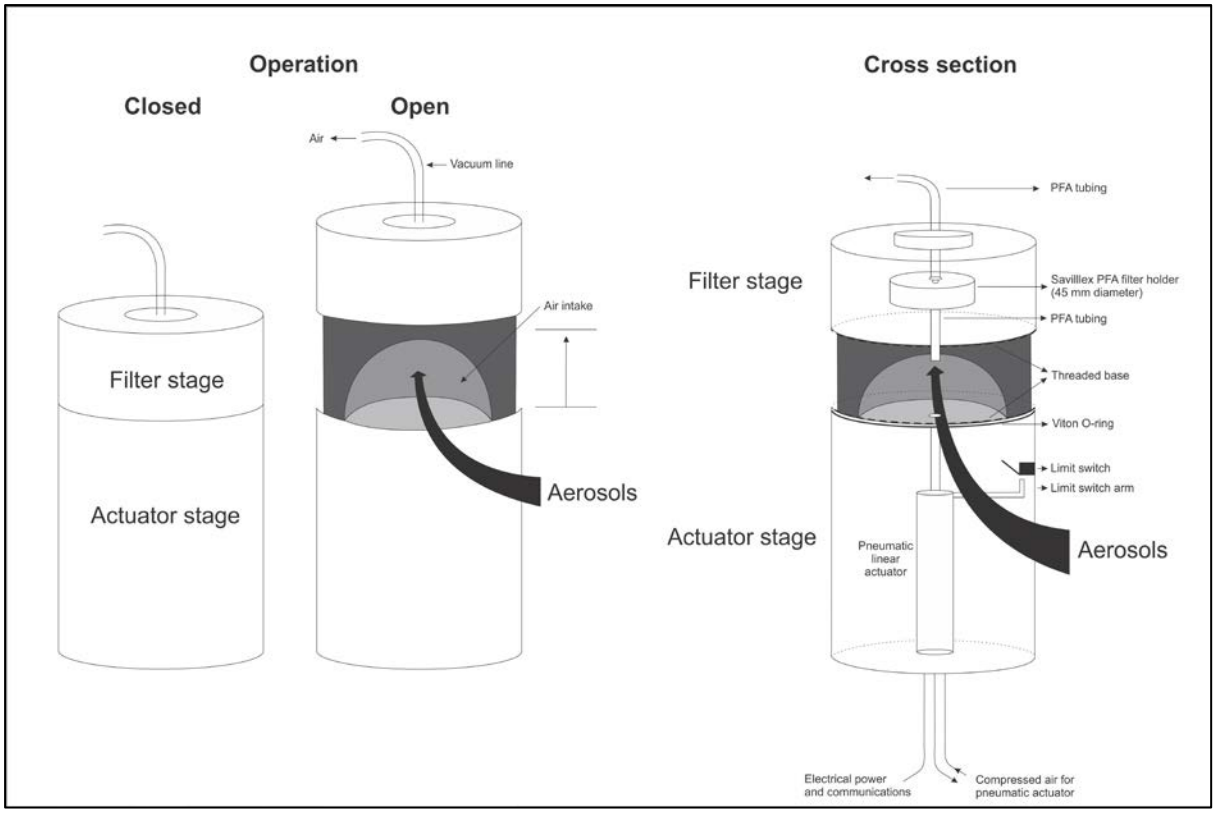

Fig. S3.1:Diagram to illustrate the hermetic seal of the *Bollhöfer et al.* [2005] aerosol sampler. Baseline conditions trigger the actuator to open the air intake. When the winds go out of the baseline sector, the air intake closes to minimise passive deposition of particles onto the filter during non-baseline conditions.

Chapter 4. Dry season aerosol iron solubility in tropical northern Australia

This chapter is in preparation for submission to *Atmospheric Chemistry and Physics*. The data has been published in the *Curtin University Research Data Repository*.

V.H.L. Winton, R. Edwards, A.R. Bowie, M. Keywood, A.G. Williams, S. Chambers, M. Desservettaz, P. Selleck, 2015. HR-ICP-MS soluble and total trace element data for Gunn Point, Northern Territory filters, June 2014. *Curtin University Research Data*, http://doi.org/10.4225/06/5671012A48C2A.

Abstract

Marine nitrogen fixation is co-limited by the supply of iron and phosphorus in large areas of the global ocean. Up to 75 % of marine nitrogen fixation may be limited by iron supply due to the relatively high iron requirements of planktonic diazotrophs. The deposition of soluble aerosol iron can initiate nitrogen fixation and trigger toxic algal blooms in nitrate-poor tropical waters. There is a large variability in estimates of soluble iron, related to the mixing of aerosol iron sources. Most studies assume that mineral dust represents the primary source of soluble iron in the atmosphere. However, seasonal biomass burning in tropical regions is a potential source of aerosol iron that could explain the large variability in soluble iron. To investigate aerosol iron sources to the adjacent tropical waters of Australia, the fractional solubility of aerosol iron was determined during the Savannah Fires in the Early Dry Season (SAFIRED) campaign at Gunn Point, Northern Territory, Australia during the dry season in 2014. The source of PM10 aerosol iron was a mixture of mineral dust, fresh biomass burning aerosol, sea spray and anthropogenic pollution. The mean soluble and total aerosol iron concentrations were 30 and 500 ng m^{-3} respectively. Fractional Fe solubility was relativity high for the majority of the campaign and averaged 8 % but dropped to 3 % during the largest and most proximal fire event. Fractional Fe solubility and proxies for biomass burning (elemental carbon, levoglucosan, oxalate and carbon monoxide) were unrelated throughout the campaign. An explanation to explain the lack of correlation between fractional Fe solubility and elemental carbon at the biomass burring source is due to the physical properties of elemental carbon, i.e., fresh elemental carbon aerosols are initially hydrophobic, however

they can disperse in water after aging in the atmosphere. Combustion aerosols are thought to have a high factional Fe solubility, which can increase during atmospheric transport from the source. Although, elemental carbon may not be a direct source of soluble iron, it can act indirectly as a surface for aerosols iron to bind during atmospheric transport and subsequently be released to the ocean upon deposition. In addition, biomass burning derived aerosols can indirectly impact the fractional solubility of mineral dust. Fractional Fe solubility was highest during dust events at Gunn Point, and could have been enhanced by the mixing of biomass burning derived species. Iron in dust may be more soluble in the tropics compared to higher latitudes due to the presence higher concentrations of biomass burring derived reactive organic species in the atmosphere, such as oxalate, and their potential to enhance the fractional Fe solubility of mineral dust. As the aerosol loading is dominated by biomass burning emissions over the tropical waters in the dry season, additions of biomass burning derived soluble iron could have harmful consequences for initiating nitrogen fixing toxic algal blooms. Future research is required to quantify elemental carbon sources of soluble iron over tropical waters.

4.1 Introduction

The deposition and dissolution of aerosols containing trace metals, such as iron (Fe), into the ocean may provide important micronutrients required for marine primary production in waters where they are depleted, such as the Southern Ocean [e.g. *Boyd et al.*, 2000]. Conversely, the deposition of soluble iron can trigger toxic algal blooms in nutrient-poor tropical waters [*LaRoche and Breitbarth*, 2005]. In these waters, iron availability is a primary factor limiting nitrogen fixation [*Falkowski*, 1997; *Rueter*, 1988; *Rueter et al.*, 1992], and the addition of bioavailable iron can influence inputs of newly fixed nitrogen into surface waters [*Paerl et al.*, 1987; *Rueter*, 1988]. A large fraction of nitrogen fixation is attributed to the filamentous, nonheterocystous cyanobacteria *Trichodesmium* [*Berman-Frank et al.*, 2001; *Paerl et al.*, 1994]. The high iron requirement for nitrogen fixation is reflected in higher Fe:C quotas of *Trichodesmium* (Fe:C quotas range between 180–214 µmol Fe mol^{-1} C) [*Berman-Frank et al.*, 2001], compared with other marine phytoplankton such as diatoms (Fe:C quotas range from 1 to 7 µmol mol^{-1}) [*Johnson et al.*, 1997; *Kustka et al.*, 2003; *Rueter et al.*, 1992]. Previous studies have investigated iron availability as a limiting factor to the oceans surrounding Australia. High iron quotas of *Trichodesmium*, consistent with high nitrogen fixation rates, have also been observed during bloom conditions from coastal waters north of Australia [*Berman-Frank et al.*, 2001]. *Berman-Frank et al.* [2001] calculated the potential of nitrogen fixation by *Trichodesmium* in the global ocean, and suggest that nitrogen fixation is essentially iron-limited in 75 % of the world oceans, given present aerosol iron fluxes and sea surface temperatures. In the oligotrophic waters of the north Tasman Sea, southwest Pacific, a 10-fold increase in nitrogen fixation was observed in response to a cyclone which stimulated diazotrophy by enhanced phosphate availability in the absence of nitrate, and increased dissolved iron supply by wet deposition of Australian dust [*Law et al.*, 2011].

Aerosols are an important source of new iron to the global ocean [*Boyd and Ellwood*, 2010; *Rubin et al.*, 2011]. In tropical waters, several studies have shown that large toxic algal blooms such as dinoflagellate Gymnodinium and cyanobacteria have been stimulated by an atmospheric deposition of nutrients. For example, the deposition of volcanic ash and Saharan dust may have alleviated the iron limitation of toxic diazotrophic cyanophytes, thus fuelling nitrogen fixation of red tides in the eastern Gulf of Mexico [*Lenes et al.*, 2008; *Walsh and Steidinger*, 2001]. In addition to mineral dust, biomass burning could be a source of

bioavailable iron supply fuelling toxic algal blooms in tropical waters. The mortality of a coral reef in 1997 in western Sumatra, Indonesia was linked to iron-fertilisation by Indonesian wildfires causing a giant red tide of *Trichodesmium* [*Abram et al.*, 2003].

Australia is the primary source of atmospheric dust in the Southern Hemisphere, supplying episodic dust deposition to the Tasman Sea [*McTainsh et al.*, 2005] and Southern Ocean. There are two general dust pathways from the Australian continent to the ocean [*Bowler*, 1976]. First, the transport of dust from the southeast aeolian dust path is associated with easterly-moving frontal systems within the zonal westerly winds, and its deposition has been observed in sediment in the southwest Pacific Ocean and glaciers in New Zealand [*Hesse*, 1994; *Hesse and McTainsh*, 2003; *Johnston*, 2001; *Marx et al.*, 2005]. Second, the transport of dust from the northwest aeolian dust path is associated with the easterly trade winds. In spite of the ubiquity of aeolian dust in Australia and surrounding oceans, there are few studies investigating the composition of the dust on a continental scale. Some, but not all, Australian dust storms are thought to stimulate phytoplankton blooms [*Cropp et al.*, 2013; *Gabric et al.*, 2010; *Mackie et al.*, 2008; *Shaw et al.*, 2008]. Soluble iron deposition models indicate that dust and combustion aerosols from the Australian continent can be deposited in other coastal regions of Australia, such as the Indian Ocean and waters north of Australia [*Ito*, 2015; *Mahowald et al.*, 2005]. Dust provenance and black carbon, a proxy for biomass burning, studies from ice cores show that Australian dust and black carbon can be transported long-range to Antarctica [*Bisiaux et al.*, 2012b; *De Deckker et al.*, 2010; *Revel-Rolland et al.*, 2006]. We note the difference in the terminology of black carbon versus elemental carbon in the literature: black carbon is often referred to as elemental or graphitic carbon, although the nomenclature is dependent on the analytical method [*Andreae and Gelencsér*, 2006]. *Andreae and Gelencsér* [2006] suggest that elemental carbon refers to the fraction of carbon that is oxidized in combustion analysis above a certain temperature threshold, and only in the presence of oxygen. Black carbon has optical properties and composition similar to soot and determined by light absorbing carbon measurements by the optical adoption technique. The terminology used here reflects that of the original author, as it is difficult to convert between black and elemental carbon as it is based on the analytical method [*Bond et al.*, 2013].

The fractional solubility of aerosol iron is an important variable determining iron availability for biological uptake. On a global scale, the large variability in the observed fractional iron solubility results, in part, from a mixture of different aerosol sources. To date most studies

have assumed that mineral dust aerosols represent the primary source of soluble iron in the atmosphere [e.g. *Baker and Croot*, 2010]. Mineral dust has a low fractional iron solubility (~0.5-2 %), whereas the presence of other soluble iron sources, such as those originating from biomass burning and oil combustion have higher fractional iron solubilities [*Chuang et al.*, 2005; *Guieu et al.*, 2005; *Ito*, 2011; *Schroth et al.*, 2009; *Sedwick et al.*, 2007]. Although, the total iron content of fresh smoke is small 0.01-1.2 % [*Maenhaut et al.*, 2002; *Reid et al.*, 2005; *Yamasoe et al.*, 2000], estimates of fractional iron solubility from fire combustion are large (1 to 60 %) and may vary in relationship to biomass and fire characteristics as well as that of the underlying terrain [*Ito*, 2011; *Paris et al.*, 2010].

Winton et al. [2016] investigated refractory black carbon deposition (fire tracer) to the Ross Sea, Antarctica and found that variability in annual deposition parallels austral dry season black carbon emissions, dust and soluble iron deposition. Thus, iron associated with biomass burning may be an important source of iron to the Southern Ocean. Over the time period investigated in the study, Southern Hemisphere biomass burning emissions primarily occurred in the intertropical convergence zone (ITCZ) of Africa, Australia and South America [*Giglio et al.*, 2013]. Of these regions, Australia is the closest to the Ross Sea. Biomass burning constitutes a large source of annual dry season aerosol emissions over northern and central Australia, and episodic austral summer wild fire in southern and eastern Australia [e.g. *Meyer et al.*, 2008]. To date, data for Australian aerosol soluble iron sources is sparse [e.g. *Mackie et al.*, 2005; *Mackie et al.*, 2008], and no soluble aerosol iron data exists for Australian fire sources. The dry seasonal tropical savannah burning region in northern Australian provides an ideal location to further investigate biomass burning derived fractional iron solubility at the source. This study reports fractional iron solubility as estimates of mixed dust and fresh biomass burning (elemental carbon) derived iron input to north Australian waters, as part of the Savannah Fires in the Early Dry Season (SAFIRED) campaign from the Australian Tropical Atmospheric Research Station (ATARS), Gunn Point, Northern Territory, Australia.

4.2 Methods

4.2.1 Study site

The Australian Bureau of Meteorology has established a station at the ATARS, Gunn Point, Northern Territory, Australia (12°14'56.6"S, 131°02'40.8"E) (Fig. 4.1) monitoring meteorological parameters since 2010. The SAFIRED campaign occurred at the ATARS throughout June 2014 to investigate the chemical and physical properties of aerosols and gases associated in fresh and aged smoke plumes from biomass burning. A range of atmospheric species including greenhouse gases, aerosols, and meteorological parameters were monitored during the campaign. An overview of the campaign and description of the Gunn Point study site can be found in *Mallet et al.* [in prep]. The Northern Territory of Australia experiences hot, humid and wet conditions during the summer months of December through to March, and dry conditions for the rest of the year. The savannah region gives rise to frequent fires between June and November. Indonesia and the tropical Timor Sea lie to the north of Gunn Point. The large desert regions of central Australia lie to the south. During the sampling campaign, strong winds from the southeast brought continental atmospheric conditions to the site (Fig. 4.1).

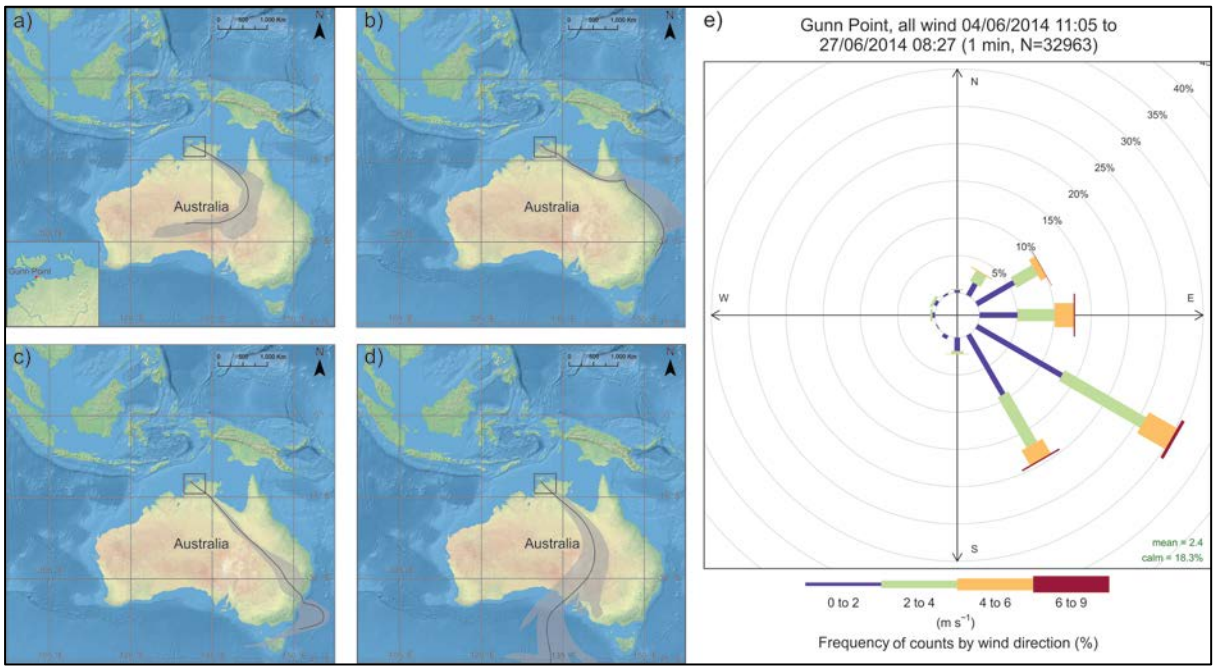

Fig. 4.1: Location of Gunn Point study site. Insert of the Northern Territory showing the Gunn Point site and the predominate fetch regions for the June 2014 Gunn Point campaign. a) Inland, low population density. b) Coastal, moderate urban/industrial activity. c) Major urban/industrial activity. d) Southerly. d) Wind rose corresponding to the aerosol sampling duration. Wind rose created using the OpenAir package in R [*Carslaw*, 2014; *Carslaw and Ropkins*, 2012].

4.2.2 Sampling and blanks

Daily aerosol filters were collected using two Volumetric Flow Controlled (VFC) high-volume aerosol samplers (Ecotech) attached with PM10 size selective inlets (Ecotech). The samplers were operated simultaneously. The first high-volume sampler was used to collect aerosols on acid cleaned cellulose Whatman 41 filters to determine the soluble and total fraction of aerosol iron and other trace elements. The second sampler was used to collect aerosol samples on quartz filters for elemental carbon and major cations and anions measurements. The aerosol samplers were located on the roof of a shipping container (at a height of 5 m above ground level (agl)) at the ATARS. A total of 23 aerosol filters were sampled daily for iron analysis between the 4 and 27 June 2014 and are described in Table 4.1.

All sample preparation and analysis was conducted in a trace metal clean laboratory (class 100 metal-free environment with high-efficiency particulate arrestance (HEPA) filtered air) at Curtin University following ultra-clean methodology. Nitric and hydrochloric acid used

throughout the study was high purity (<10 ppt Fe), double distilled in-house from Seastar® Instrument Quality (IQ) grade acids (Choice Analytical Pty Ltd, Australia) using an all perfluoroalkoxy (PFA) acid purification system (DST-1000, Savillex®), hereon referred to as "ultra-pure" acid. Ultra-pure water (resistivity of 18.2 MΩ-cm, Purelab Classic, ELGA, Germany) was used throughout. All apparatus coming in contact with the aerosol filters were pre-acid-washed. Teflon leaching apparatus parts and Savillex® digestion beakers were cleaned in a series of acid baths on a hotplate at 80 °C for three days. The first bath consisted of 50 % ultra-pure HNO_3, followed by 50 % ultra-pure HCl and then 1 % ultra-pure HCl and 1 % ultra-pure HNO_3 and finally ultra-pure water. Parts were rinsed with copious quantities of ultra-pure water between baths. Aerosol collection substrates were all Whatman 41 paper sheets (20 x 25 cm) acid-washed before use following the method of *Baker et al.* [2006]. Briefly, Whatman 41 filter sheets were arranged in layers, one at a time, between polypropylene (PP) mesh, in a series of three 0.5 M ultra-pure HCl baths for 24 hours. Filters were then rinsed three times with ultra-pure water between baths and then placed in a fresh acid bath. Plastic zip-lock bags and plastic tweezers were acid-washed using 3 % ultra-pure HNO_3 for 2 weeks. Acid-washed filters were stored in individual acid-washed zip-lock bags until use.

Loading and changing of aerosol collection substrates was carried out in a designated clean area at ATARS. Aerosol laden filters were transferred into the individual pre-acid-washed zip-lock plastic bags immediately after collection and stored frozen until analysis at Curtin University.

Three types of filter blanks were carried out; i) laboratory filter blanks (n=6) (acid-washed Whatman 41 filter papers that underwent the laboratory procedures without going into the field), ii) procedural filter blanks (n=4) (filters that had been treated as for normal samples i.e. acid-washed, but which were not otherwise used. Once a week, during daily filter change over, a procedural blank filter was mounted in the aerosol collector for 10 minutes without the collector pump in operation to give an indication of the operational blank associated with the sampling procedure), and iii) 24 hour exposure filter blanks sampled at the beginning and end of the field campaign (n=2) (filters treated like a procedural blank, but left it in the collector for 24 hours without switching the collector on).

Table 4.1:Trace metal aerosol samples (PM10) collected at Gunn Point, dry season 2014.

Sample time	[a]Start date/ time	[a]Finish date/ time	Total sampling duration (min)	[b]Total air volume (m3)	[c]Total air volume (m^3)
GP1	4/06/2014 11:05	5/06/2014 10:45	1117	1102	1122
GP2	5/06/2014 11:10	6/06/2014 12:30	1498	1458	1490
GP3	6/06/2014 12:55	7/06/2014 11:30	1355	1531	1572
GP4	7/06/2014 11:54	8/06/2014 8:47	1253	1416	1445
GP5	8/06/2014 9:08	9/06/2014 10:21	1512	1708	1715
GP6	9/06/2014 10:42	[d]10/06/2014	711	802	806
GP7	10/06/2014 2:41	11/06/2014 9:25	1112	1256	1278
GP8	11/06/2014 10:16	12/06/2014 10:43	1467	1658	1669
GP9	12/06/2014 11:03	13/06/2014 9:04	1322	1494	1518
GP10	13/06/2014 10:02	14/06/2014 10:56	1494	1688	1729
GP11	14/06/2014 11:31	15/06/2014 10:29	1378	1556	1584
GP12	15/06/2014 11:11	16/06/2014 10:16	1385	1565	1572
GP13	16/05/2014 10:45	17/06/2014 9:39	1374	1552	1550
GP14	17/06/2014 10:04	18/06/2014 10:18	1454	1643	1635
GP14	17/06/2014 10:04	18/06/2014 10:18	1454	1643	1635
GP15	18/06/2014 11:16	19/06/2014 10:15	1379	1559	1577
GP16	19/06/2014 10:41	20/06/2014 9:36	1375	1554	1584
GP17	20/06/2014 9:59	21/06/2014 9:58	1439	1626	1647
GP18	21/06/2014 10:31	22/06/2014 8:31	1319	1490	1508
GP19	22/06/2014 8:55	23/06/2014 9:32	1476	1668	1669
GP20	23/06/2014 10:39	24/06/2014 9:37	[c]1269	1429	1441
GP21	24/06/2014 10:04	25/06/2014 9:11	1387	1567	1569
GP22	25/06/2014 9:42	26/06/2014 9:05	1403	1499	1497
GP23	26/06/2014 9:46	27/06/2014 8:27	1360	1537	1536

[a]Australian Central Standard Time
[b]Total air volume calculated using STP.
[c]Total air volume corrected to ambient temperature and pressure.
[d]Fuse blown.

4.2.3 Trace metal analysis

4.2.3.1 Water solubility of aerosol iron

Soluble metals were extracted from aerosol filters (GP1-23), exposure blanks (EB1-2), and procedural blanks (PB1-4). Circle portions (47 mm diameter) of the filter were cut out of the filter sheet using a punch cutter, which consisted of a sharpened titanium (Ti) circular blade and PFA backing mount (both acid-washed). Soluble elements (Al, Ti, V, Mn, Fe, Pb) were extracted from the filter using an instantaneous flow-through water leach [e.g. *Aguilar-Islas et al.*, 2010] consisting of 20 separate passes of 50 mL of ultra-pure water. A total volume of

1000 mL was filtered through each aerosol filter. Only leaches 1-4, 6, 10 and 20 were collected and analysed, following a test where we determined the maximum number of leaches required to leach the majority of soluble iron from the aerosols. Here, we leached sample GP5 with 10 passes of 50 mL ultra-pure water. The experiment was repeated three times using three separate punches from the same sample. Leachates were collected in 50 mL acid-washed polypropylene (PP) Corning® tubes and acidified to 1 % ultra-pure HCl. The leachates from GP22 were filtered through 0.2 µm acid-cleaned Polyvinylidene Fluoride (PVDF) syringe filters. Blank concentrations for exposure blank and procedural blank filters averaged ~0.4 ng g^{-1} and 0.5 ng g^{-1} of soluble Fe respectively. Total water soluble trace elements were calculated by summing the soluble iron extracted from 20 leaches.

4.2.3.2 Total iron concentrations

Total PM10 trace element (Na, Al, K, Ti, V, Cr, Mn, Fe, Mo, Pb, As) concentrations were determined following recommendations from the 2008 GEOTRACES intercalibration experiment for the analysis of marine aerosols [*Morton et al.*, 2013]. All digestions were carried out under HEPA filtered air, in a total-exhausting clean-air (ISO Class 5), hot block unit (SCP Science, Canada) fitted with an acid scrubber unit at the University of Tasmania. Circle portions (47 mm diameter) of the filters were digested at 95 ºC for 12 hours with concentrated ultra-pure HNO_3 (1 mL, Seastar Baseline®) and ultra-pure HF (0.25 mL, Seastar Baseline®) in capped PFA vials (15 mL, acid cleaned Savillex®) following Bowie et al. (2010). At the end of the digestion, the samples were evaporated to dryness, reconstituted in 10 % ultra-pure HNO_3 (10 mL final volume, Seastar® IQ grade double distilled in-house) and stored at 40 ºC for ~48 hours before analysis. Two certified reference materials (MESS-3 marine sediment, National Research Council, Canada, and QC-TMFM-A spiked trace metals (1-10 µg of trace metal per filter) on nitrocellulose filter (TMF), High Purity Standards) were digested alongside the samples to test the digestion recovery procedure. Total digestion recovery for iron from the MESS-3 CRM was 108 ± 8 % (n=3) and TFM was 99 ± 7 % (n=3). Recovery rates for other trace metals are reported in Table S4.1. Blank concentrations for Savillex® digestion beakers, exposure blank, procedural blank and laboratory blank filters averaged ~4 ng g^{-1} (n=3), ~150 ng g^{-1} (n=2), ~140 ng g^{-1} (n=4), and ~140 ng g^{-1} (n=6) of total iron respectively.

4.2.3.3 High-resolution inductively coupled plasma mass spectrometry analysis

Leachates and resuspended total digests were analysed by high-resolution inductively coupled plasma mass spectrometry (HR-ICP-MS, Element XR ThermoFisher). An auto sampler housed in a laminar flow hood was used to introduce the sample to the HR-ICP-MS. Measured elements and the spectral resolutions, along with typical operating conditions, are reported in Table S4.2. The HR-ICP-MS was operated using Ni sample cones and pumped with a Seafast II system syringe pumps (ESI). During the course of the sample sequence an EPA standard (Cat. #ICP-200.7-6 Solution A, High Purity Standards) was measured regularly for quality control (QC). Laboratory vial blanks were also measured regularly during the course of the sample sequence determined by carrying out identical analytical procedures as the leachates but vials were filled with ultra-pure water rather than the leachate. Leachate concentrations were corrected for laboratory blanks, and the total digest concentrations corrected for the Savillex® digestion beaker blanks. All samples and standards were prepared on a similar matrix basis. Leachates were acidified to 1 % ultra-pure HCl, and total digests were diluted and presented to the instrument as 3 % ultra-pure HNO_3. The sample introduction line was rinsed with 3 % ultra-pure HCl (3 % ultra-pure HNO_3) between leachate (digest) samples for 1.5 minutes. Standard solutions were prepared by serial dilution from 100 µg mL^{-1} stock solutions using ultra-pure water, with a final ultra-pure HCl concentration of 1 %. Preparation of standards in 1 % ultra-pure HCl (HNO_3) matrix matched the leachates. Ten-point multiple calibration solutions were measured. Indium, at a concentration of 1.5 ppb, was used as an internal standard.

4.2.4 Air mass back trajectories

To identify the source region of air masses arriving at Gunn Point, we use hourly 5-day (120-hr) back trajectories (ending at 12 m agl) to reconstruct atmospheric circulation leading up to, and during, individual events. Air mass back trajectories were produced using the 'Trajectory program' based the NOAA ARL HYbrid Single-Particle Lagrangian Integrated Trajectory (HYsplit) model [*Draxler and Rolph*, 2003] (http://ready.arl.noaa.gov/HYSPLIT.php). Global Data Assimilation System model files (GDAS) obtained from NOAA ARL FTP (http://ready.arl.noaa.gov/gdas1.php) were used to drive the model. The resolution used was 0.5 degrees.

4.2.5 Radon concentrations

Natural radioactive noble gas radon-222 (radon) is a useful quantitative indicator of diurnal to synoptic scale mixing processes within the continental lower troposphere [*Chambers et al.*, 2014a], and a suitable tracer for continental air [e.g. *Dörr et al.*, 1983]. This is because radon has a half-life of 3.8 days and only one source and sink i.e. radon is solely produced from terrestrial surfaces and is lost from the atmosphere by radioactive decay. The ANSTO-built 700 L dual-flow-loop two-filter radon detector [e.g. *Chambers et al.*, 2014b; *Whittlestone and Zahorowski*, 1998] samples air from 12 m above ground level (a.g.l.). A coarse aerosol filter and dehumidifier are installed "upstream" of the detector, as well as a 400 L delay volume to ensure that thoron (^{220}Rn, half-life 55s) concentrations in the inlet air stream are reduced to less than 0.5 % of their ambient values. The detector's response time is around 45 minutes, and its lower limit of determination is 40 - 50 mBq m^{-3}. Calibrations are performed on a monthly basis by injecting radon from a PYLON 101.15±4% kBq Ra-226 source (12.745 Bq min^{-1} ^{222}Rn), traceable to NIST standards, and instrumental background is checked every 3 months. The time series for the Gunn Point campaign duration has been separated into contributions from a) advective (reflects the air mass fetch history over the last two weeks), and b) diurnal variability (indication of the change in mixing depth) following *Chambers et al.* [2014a]. The advective and diurnal components of the radon time series were integrated to daily values based on a noon-to-noon integration window.

4.2.7 Elemental carbon

Elemental carbon (EC) and organic carbon (OC) analysis was performed on the PM10 quartz filters at CSIRO Ocean and Atmosphere using a DRI Model 2001A Thermal-Optical Carbon Analyser following the IMPROVE-A temperature protocol [*Chow et al.*, 2007]. Laser reflectance is used to correct for charring, since reflectance has been shown to be less sensitive to the composition and extent of primary organic carbon. Prior to analysis of filter samples, the sample is baked in an oven to 910°C for 10 minutes to remove residual carbon. System blank levels are then tested until <0.20 µg C cm^{-2} is reported (with repeat oven baking if necessary). Twice daily calibration checks are performed to monitor possible catalyst degeneration. The analyser is reported to effectively measure carbon concentrations between 0.05 - 750 µg C cm^{-2}, with uncertainties in organic and elemental carbon of ± 10 %. The IMPROVE-A carbon method measures four OC fractions at four non-oxidizing heat ramps (OC1 at 140°C, OC2 at 280°C, OC3 at 480°C, OC4 at 580°C) and three elemental

carbon fractions at three oxidizing heat ramps (EC1 at 580°C, EC2 at 740°C, EC3 at 840°C). The quartz filter sample is held at the target temperature until all carbon is desorbed at that fraction. During the non-oxidizing heat ramps some of the organic carbon can be pyrolyzed and will not desorb until the oxidized stages. The quantity of organic carbon that was pyrolyzed (OC_{pyro}) during the non-oxidizing heat ramps is determined based on the time the reflectance of the filter rises back up to its initial value. Total organic carbon is then calculated from the addition of all the organic carbon fractions plus OC_{pyro}. Total elemental carbon is calculated from the addition of all the elemental carbon fractions minus OC_{pyro}.

4.2.7 Major cation and anion

Major cation and anion measurements, including oxalate and levoglucosan, were performed on the PM10 quartz filters at CSIRO Ocean and Atmosphere. The filter was wetted with methanol before being extracted in 5 ml of ultra-pure water. The sample was then preserved using 1 % chloroform. Anion and cation concentrations were determined by suppressed ion chromatography (IC) using a Dionex DX500 gradient ion chromatograph. Anions were determined using an AS11 column and an ASRS ultra-suppressor. Cations were determined using a CS12 column and a CSRS ultra-suppressor.

4.3 Results

4.3.1 Air mass back trajectories

We identified predominate fetch regions that gave rise to particular events; a) ‘inland, low population density,’ b) ‘coastal, moderate urban/industrial activity,’ c) ‘major urban/industrial activity,’ and d) ‘southerly.’ No trajectories fell in the ‘mainly oceanic’ category. The mean trajectory for each group was calculated and these representative trajectories are indicated in Fig. 4.1.

4.3.2 Biomass burning events during the campaign

A number of biomass burning markers were used to identify burn events during the campaign, including carbon monoxide (CO) [*M. Desservettaz, Pers. Comm.*, 2014], levoglucosan [*P. Selleck Pers. Comm.*, 2015], oxalate [*P. Selleck Pers. Comm.*, 2015] and elemental carbon [*P. Selleck Pers. Comm.*, 2015]. Six burn events were identified, with the

two major events occurring on the 9 June (fire event "G") and 25 June (fire event "FJAB") 2014 [*Mallet et al.*, in prep]. Smoke transported to the Gunn Point in fire event "G" was distally sourced i.e. >400 km, while smoke from the largest fire event "FJAB" was proximal i.e. within 15 km of the ATARS (fire locations from Sentinel Hotspot (MODIS and VIIRS satellites); *Mallet et al*. [in prep]). Due to the different time periods the CO data (minute) and aerosol samples (daily) integrate, we have grouped fire events "F", "J", "A" and "B" into one event (fire event "FJAB") for this study. C3 tree burning was identified from δCO_2 during the 25 June burn event [*C. Paton-Walsh Pers. Comm.*, 2014]. In addition, non-sea salt-potassium (nss-K) is a good indicator of biomass burning in terms of its elemental concentration, and also by normalising it relative to other elemental concentrations [*Maenhaut et al.*, 2002; *Yamasoe et al.*, 2000]. There is good agreement between nss-K concentrations and carbon monoxide (CO) (r^2=0.55) (Fig. S4.1). There is also a good correlation between nss-K and elemental carbon concentrations (r^2=0.74) (Fig. S4.1). Following *Guieu et al.* [2005] we normalise nss-K to Fe and compare the ratio to crustal aerosols (nss-K/Fe=0.49; *Wedepohl* [1995]) and polluted aerosols (nss-K/Fe=0.27; urban particulate patter – standard reference #1648, NIST). During the campaign the nss-K/Fe ratio ranged between 0.2-4.9. This relativity large range was similar to nss-K/Fe of 0.63-1.8 reported by *Guieu et al.* [2005] for Mediterranean summer fires in 2003. They suggested the higher ratio reflected a primarily fire origin for nss-K. The nss-K/Fe ratio was especially high during the two fire events in this study (nss-K/Fe ~4) and during the high elemental carbon concentrations between 21-27 June (nss-K/Fe~2.2), compared to non-fire events (nss-K/Fe ~1.3).

4.3.3 Sequential iron leaching

To determine the number of ultra-pure water leaches required to leach the majority of water soluble Fe from the Gunn Point aerosol filters, we conducted a test on the GP5 sample where three filter aliquots were leached with 10 sequential passes of 50 mL of water. The results in Fig. S4.2 shows that there is an exponential decrease in soluble Fe extracted with successive leaches. Even after 1 L of ultra-pure water was passed through the aerosol filter, soluble Fe was still being extracted. We therefore leached each sample with 20 passes of ultra-pure water totalling 1 L. We acknowledge that beyond 20 leaches, soluble Fe could continue to be leached out of the aerosol filter and thus the data reported here reflect "instantaneous" soluble Fe and may underestimate the total concentration of soluble Fe over greater leach volumes. Figure 4.2 highlights the percentage of soluble Fe in each leach. Around half of the soluble

Fe is extracted in the first leach. The leachates from GP22 were re-filtered through 0.2 µm membranes to calculate the <0.2 µm soluble Fe fraction of the total soluble Fe. The concentration of soluble Fe in the <0.2 µm fraction of the leachate contained 70 % of the total soluble Fe in GP22 and follows the same exponential decreases with successive leaches. Leachates showed a large variability in their colour, and visual observation after particle settling showed that they contained a large number of very fine particles even in the <0.2 µm fraction.

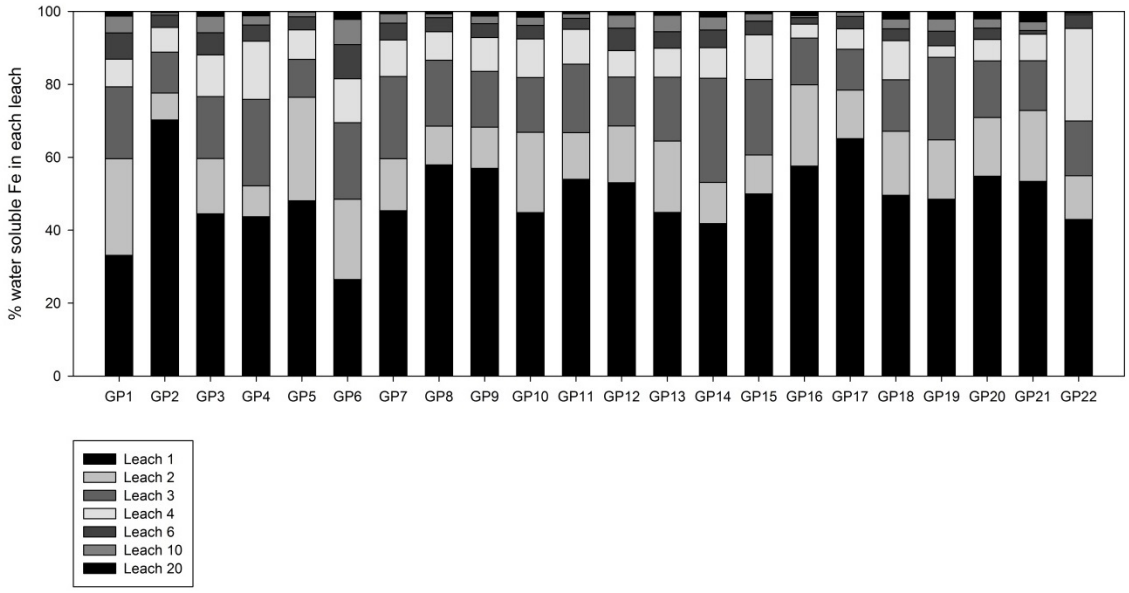

Fig. 4.2: Fraction of water soluble iron in sequential leaches of all PM10 samples.

4.3.4 Aerosol iron mass concentrations

Total and soluble PM10 trace element concentrations are illustrated in Figs. 4.3-4.5. Total PM10 aerosol Fe ranges from 60 - 1164 ng m^{-3}, while soluble aerosol Fe ranges from 4 - 123 ng m^{-3}. A strong linear correlation between in the soluble trace elements of Fe, Al, and Ti was found during the campaign (Fig. 4.5) i.e. soluble Fe and soluble Al (r^2=0.95), and soluble Fe and soluble Ti (r^2=0.81). Likewise, a strong linear correlation was found between the total PM10 trace elements of Fe, Al, V and Ti, i.e., total Fe and total Al (r^2=0.96), total Fe and total Ti (r^2=0.98), and total Fe and total V (r^2=0.99) (Fig. 4.3). There is considerable temporal variability in water soluble and total trace elements throughout the campaign. Two distinct events in soluble Al, Ti, and Fe and total Al, Ti, V, and Fe are observed on the 7-8 June 2014 (e.g. GP4-5; 52-124 ng m^{-3} of soluble Fe and 1158-1164 ng m^{-3} of total Fe), and 14-15 June

2014 (e.g. GP11-12; 39-76 ng m^{-3} of Fe and 677-928 ng m^{-3} of total Fe) (Figs. 4.4 and 4.6). On the 21 June 2014 high concentrations of these crustal like elements (total and soluble Al, Ti, V, Fe) were also observed (e.g. GP17; 64 ng m^{-3} of Fe and 1129 ng m^{-3} of total Fe) and are associated with marine air mass conditions. In addition, total Cr, As, Mo, V, and Na also peaked during the marine conditions on the 21 June (Fig. 4.5). This same set of total trace elements (Cr, As, Mo, V, and Na) also peaked on the 9 June during fire event "G" (Fig. 4.5). During the two fire events "G" and "FJAB" on the 9 and 25 June, daily integrated CO and nss-K are high at the same time as total As, Mn, Pb, and soluble V, Mn, Pb (Fig. 4.4).

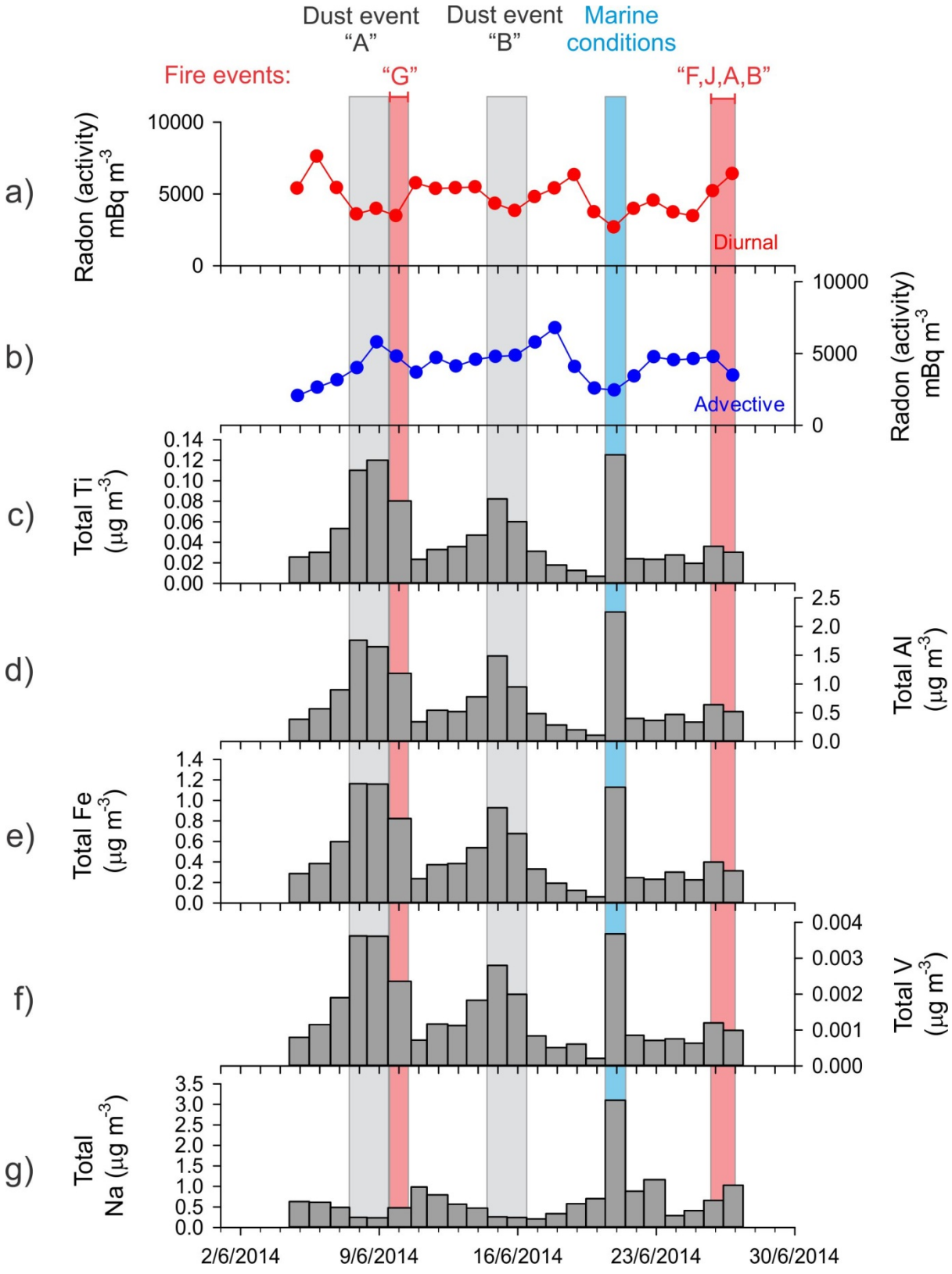

Fig. 4.3: Time series of a) diurnal radon, b) advective radon, and total PM10 trace element concentrations c) Ti, d) Al, e) Fe, f) V, and g) Na.

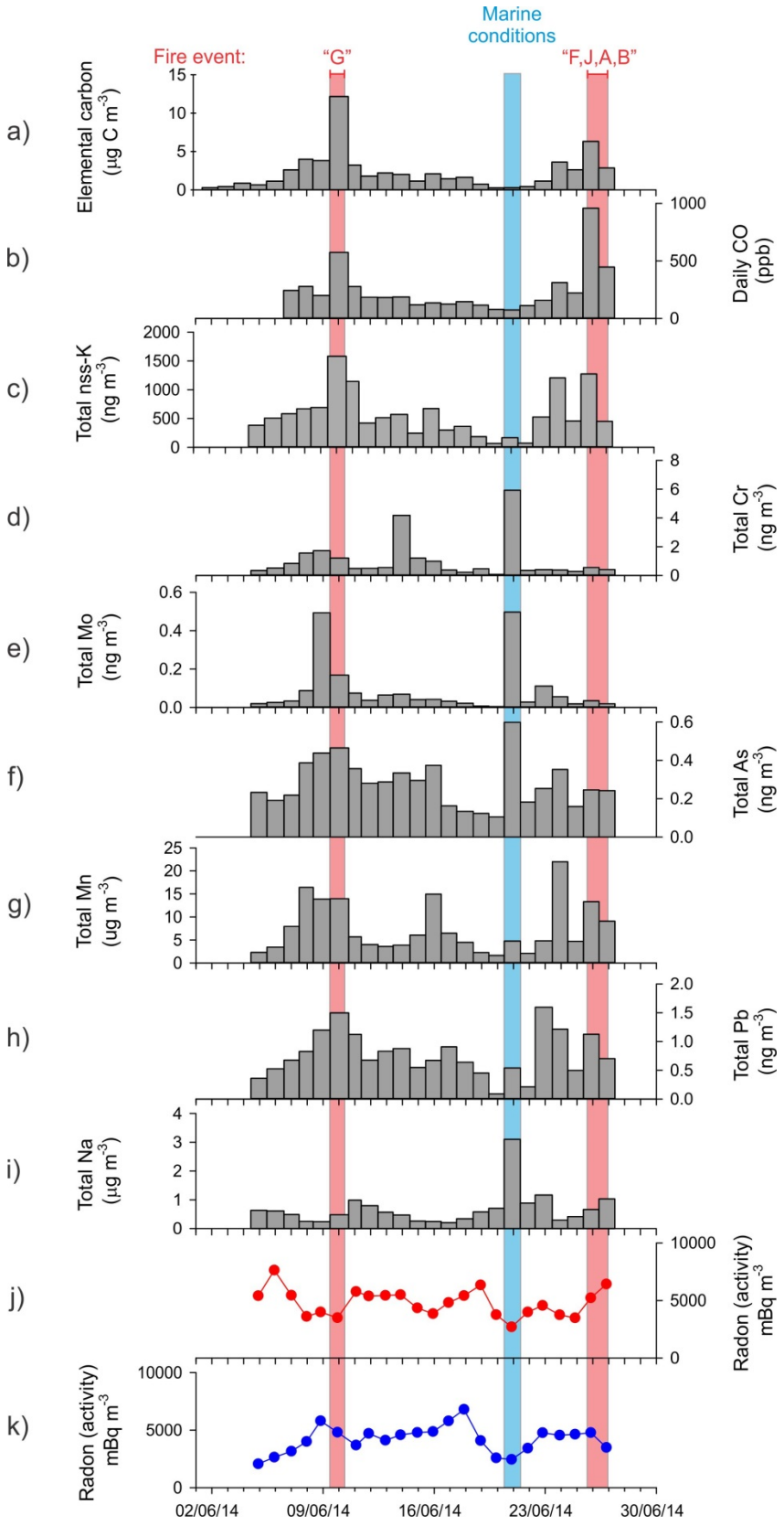

Fig. 4.4: Time series of a) elemental carbon, b) carbon monoxide, and total PM10 trace element concentrations c) nss-K, d) Cr, e) Mo, f), As, g) Mn, h) Pb, i) Na, j) diurnal radon, and k) advective radon.

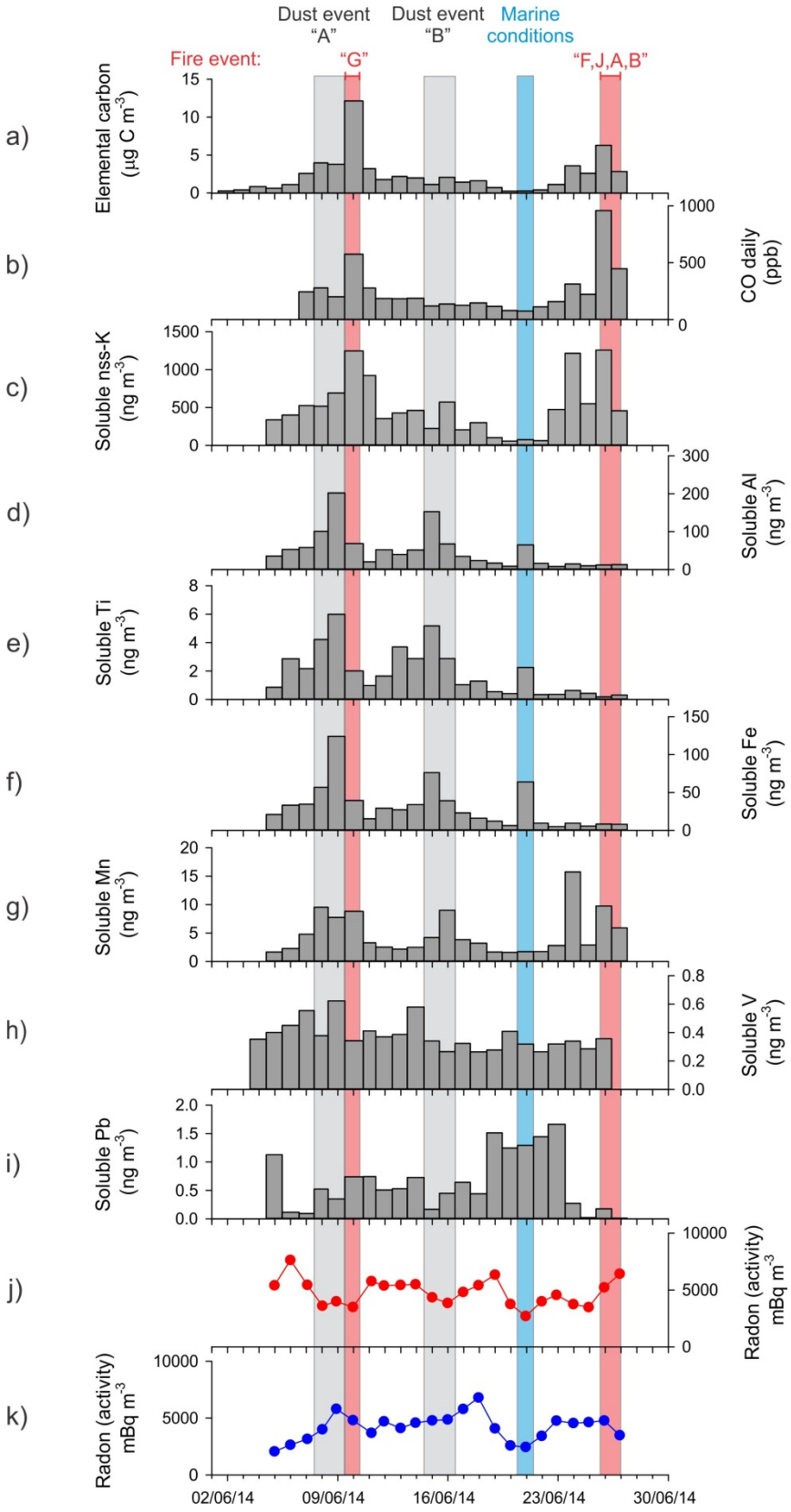

Fig. 4.5: Time series of a) elemental carbon, b) carbon monoxide, and soluble trace element concretions c) nss-K, d) Al, e) Ti, f), Fe, g) Mn, h) V, i) Pb and j) diurnal radon, k) advective radon.

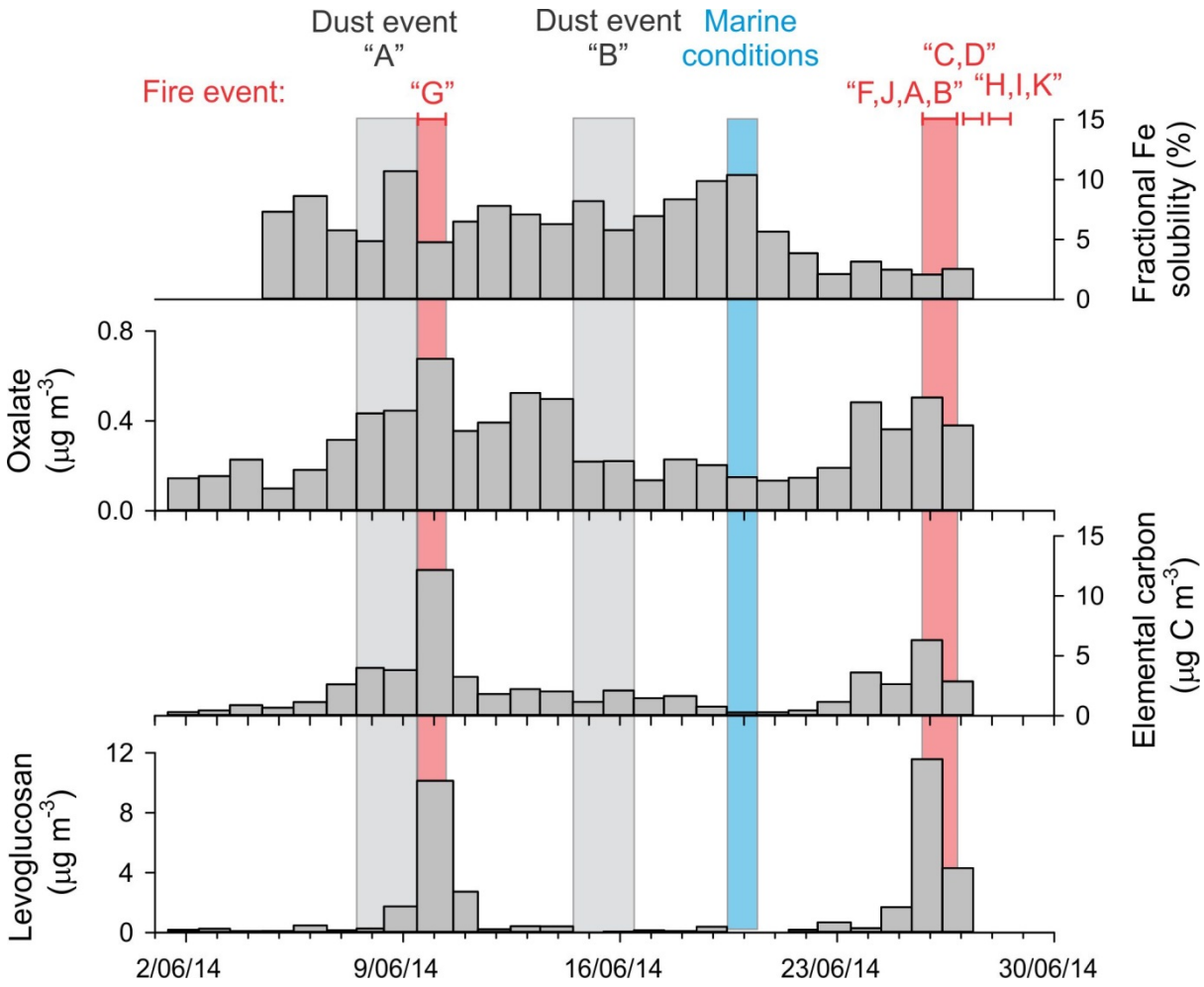

Fig. 4.6: Time series of fractional Fe solubility, oxalate, elemental carbon and levoglucosan concentrations.

4.3.5 Dry deposition iron flux

Estimates of the Fe dry deposition rate (F_{dry}) to adjacent north Australian surface waters were calculated using equation (4.1) from the total and soluble Fe concentrations ($C_{aerosol}$) using a dry deposition velocity (V_{dry}) of 2 cm s^{-1} for coastal areas [*Duce et al.*, 1991], following *Baker et al.* [2003] for aerosols collected along a transect in the Atlantic Ocean and *Baker et al.* [2007] for the tropical Atlantic atmosphere. Estimates of Fe dry deposition rates for Gunn Point aerosols are reported in Table 4.2.

$$F_{dry} = C_{aerosol} \, x \, V_{dry\ deposition} \qquad \text{(Equation 4.1)}$$

Table 4.2: Aerosol iron concentrations and dry deposition fluxes for Gunn Point PM10 aerosols.

Sample	Soluble Fe concentration (ng m^{-3})	±	*Soluble Fe flux (µmol m^{-2} d^{-1})	±	Total Fe concentration (ng m^{-3})	±	*Total Fe flux (µmol m^{-2} d^{-1})	±
GP1	21	2	0.6	0.3	286	9	9	4
GP2	33	1	1.0	0.5	384	12	12	6
GP3	34	1	1.1	0.5	598	19	18	9
GP4	57	2	1.8	0.9	1164	37	36	18
GP5	124	5	3.8	1.9	1158	37	36	18
GP6	39	2	1.2	0.6	823	26	25	13
GP7	15	0.6	0.5	0.2	236	7	7	4
GP8	29	1	0.9	0.5	374	12	12	6
GP9	27	1	0.8	0.4	385	12	12	6
GP10	34	1	1.0	0.5	539	17	17	8
GP11	76	3	2.4	1.2	928	29	29	14
GP12	39	2	1.2	0.6	677	21	21	10
GP13	23	1	0.7	0.4	331	10	10	5
GP14	16	0.6	0.5	0.2	192	6	6	3
GP15	12	0.5	0.4	0.2	123	4	4	2
GP16	6	0.2	0.2	0.1	60	2	2	1
GP17	64	3	2.0	1.0	1129	36	35	17
GP18	10	0.3	0.3	0.1	247	8	8	4
GP19	5	0.2	0.2	0.1	231	7	7	4
GP20	10	0.4	0.3	0.1	301	10	9	5
GP21	6	0.2	0.2	0.1	225	7	7	3
GP22	8	0.3	0.3	0.1	399	13	12	6
GP23	8	0.3	0.2	0.1	314	10	10	5

*The uncertainty in dry deposition fluxes was calculation by propagation of error of the analytical uncertainty and uncertainty in the deposition velocity assumed to be 50 %

4.4 Discussion

4.4.1 Iron mass concentrations

Total PM10 Fe concentrations during the fire events (Fig. 4.3) are in good agreement with fire aerosol studies reported from the Alta Floresta, Amazon forest, Brazil range between 1996-1998 which range from 270 to 1220 ng m^{-3} of total Fe [*Maenhaut et al.*, 2002]. The soluble Fe concentrations at Gunn Point (4 to 123 ng m^{3}) are less than soluble Fe concentrations reported in smoke from the Mediterranean and West African Sahel (350 ng

m^3; *Guieu et al.* [2005]) and (130 ng m^3; *Paris et al.* [2010]) respectively. There is sparse total and soluble aerosol Fe concentration data from Australian aerosols, however our estimates agree with reported total Fe concentrations at Jabiru, northern Australia (148 ng m^{-3}), at Sydney, New South Wales (150 ng m^{-3}) and modelled values for the north Australia coastal area (200-1000 ng m^{-3}) [*Mahowald et al.*, 2009; and references within]. Compared to aerosol Fe from other tropical regions, our estimates at the Australian source are greater than aerosol Fe concentrations reported for the tropical Atlantic open ocean (total Fe 0.1-1 nmol m^{-3} and soluble Fe 0.05-0.1 nmol m^{-3}) [*Baker et al.*, 2006].

4.4.2 Dry deposition estimates of soluble and total iron

Crude estimates of soluble and total PM10 Fe dry deposition fluxes associated with the aerosol samples are reported in Table 4.2 and range from 0.2 ± 0.1 to 4 ± 2 µmol m^{-2} d^{-1} for soluble Fe and 2 ± 1 to 36 ± 18 µmol m^{-2} d^{-1} for total PM10 Fe. The dry deposition Fe estimates for air over Gunn Point in this study are compared to other aerosol studies from the Southern Hemisphere and topical regions. The mean soluble Fe dry deposition flux (~1 µmol m^{-2} d^{-1}) is greater than soluble Fe dry deposition fluxes over open ocean tropical Atlantic waters (0.01-0.1 µmol m^{-2} d^{-1}) [*Baker et al.*, 2003]. The estimates at Gunn Point are also higher than those reported for the Southern Ocean, for example, 2 - 7 nmol m^{-2} d^{-1} reported by *Bowie et al.* [2009], 0.04 - 3 nmol m^{-2} d^{-1} reported by *Wagener et al.* [2008], 2 - 7 nmol m^{-2} d^{-1} reported by *Baker et al.* [2013] for the South Atlantic, and 0.1 - 7 nmol m^{-2} d^{-1} for baseline air over the Southern Ocean reported by *Winton et al.* [2015]. Estimates of total PM10 Fe dry deposition fluxes at Gunn Point are higher than those for the Southern Ocean (0.8 - 120 nmol m^{-2} d^{-1}) [*Winton et al.*, 2015] and the South Atlantic (100 – 300 nmol m^{-2} d^{-1}) [*Baker et al.*, 2013]. The Gunn Point data are in good agreement with estimates from global models for the north Australia coastal region. *Mahowald et al.* [2009] estimates total Fe deposition in the north Australia to be 0.04-1 g m^{-2} y^{-1}, and our mean total PM10 Fe flux of 0.3 g m^{-2} y^{-1} falls within this range.

4.4.3 Fractional iron solubility

The fractional Fe solubility ranged from 2 % to 11 % during the study (Figs. 4.6 and 4.7). These estimates are within the 0.6 to 40 % range of fractional Fe solubility reported for biomass burning [*Bowie et al.*, 2009; *Guieu et al.*, 2005; *Ito*, 2011; *Ito*, 2015; *Paris et al.*, 2010]. Fractional Fe solubility was highest between 4 and 20 June with a mean fractional Fe

solubility of 8 ± 2 %. After 20 June, the fractional Fe solubility dropped to 3 % between the 21 and 27 June when fires were proximal to the ATARS. These estimates are similar to dust estimates around 0.5-2 % at relatively high mass concentrations. During dust event "A" fractional Fe solubility peaked at ~11 %, fractional Al solubility at ~12 %, and fractional Ti solubility at ~5 %. Fractional Al and Ti solubility also decreased on 24 June from 8 ± 2 % to 3 ± 0.8 % for Al and from 5 ± 2 % to 1 ± 0.7 % for Ti. Fractional Mn solubility was relatively constant throughout the campaign and averaged ~65 % ± 10 %. Fractional Mn solubility was highest during fire event "F,J,A,B" when the fractional solubility of Al, Ti and Al was low. Fractional Pb solubility peaked during marine conditions.

Sholkovitz et al. [2012] reported a synthesis of global aerosol Fe solubility data sets and this compilation displayed an inverse hyperbolic relationship between the total Fe concentration and fractional Fe solubility (Fig. 4.7). The authors concluded that the characteristic inverse hyperbolic relationship is common over large regions of the global ocean. This relationship has been attributed to the mixing of low Fe solubility mineral dust and other soluble Fe aerosols from sources such as biomass burning and oil combustion [e.g. *Sedwick et al.*, 2007]. We have plotted the Gunn Point aerosol Fe data with the Southern Hemisphere compilation in Fig. 4.7. Our data sits within two narrow clusters i) moderate fractional Fe solubility and moderate total PM10 aerosol Fe loading between the 4 and 19 June and ii) low fractional Fe solubility and low total PM10 aerosol Fe loading between the 24 and 26 June (highlighted in Fig. 4.7).

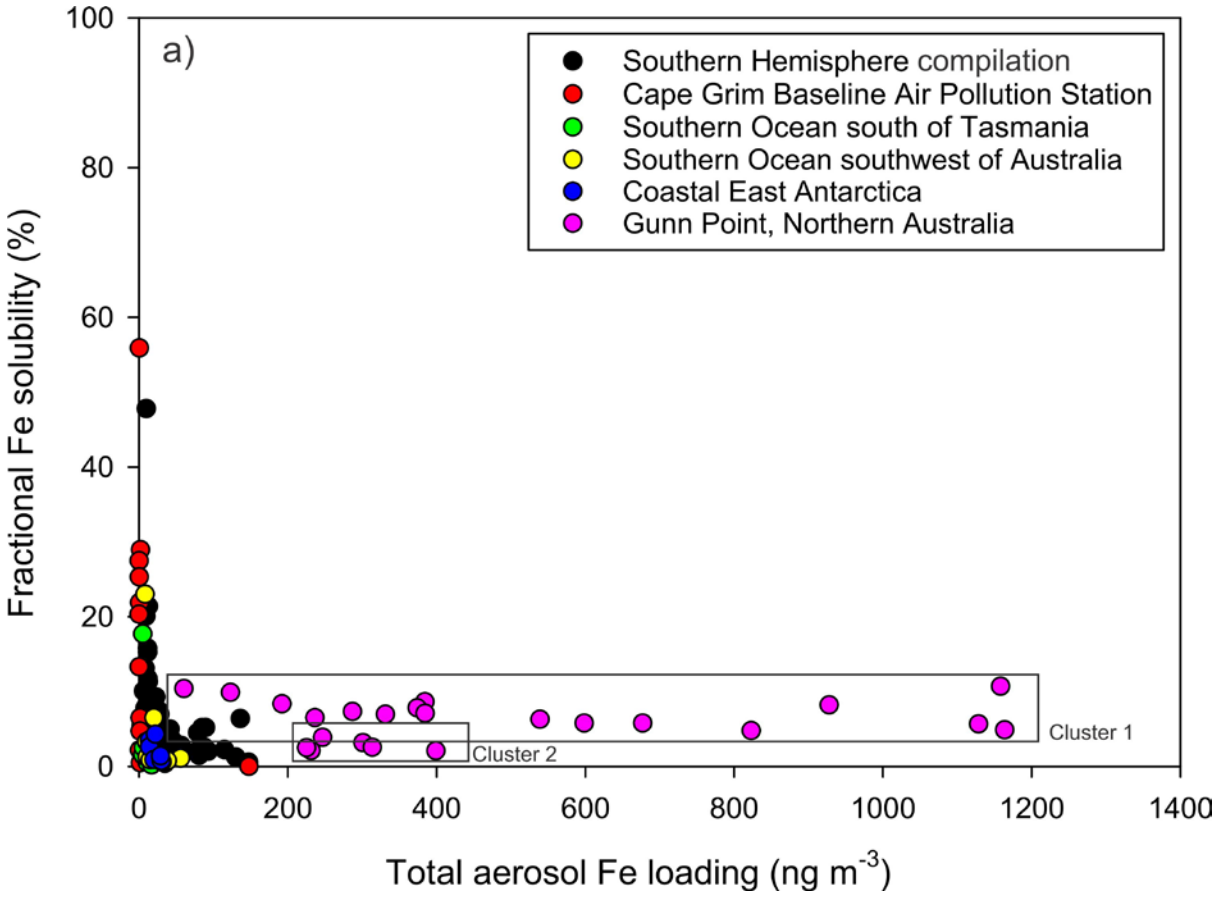

Fig. 4.7: Gunn Point total PM10 aerosol Fe mass concentration versus fractional Fe solubility superimposed upon the Southern Hemispheric data set [*Bowie et al.*, 2009; *Gao et al.*, 2013; *Sholkovitz et al.*, 2012; and references within; *Winton et al.*, 2015]. Boxes highlight the two clusters. Cluster 1: moderate fractional Fe solubility and moderate total aerosol Fe loading between the 4 and 19 June, and represents the upper bound of dust fractional Fe solubility for the topical dry season. Cluster 2: low fractional Fe solubility and low total aerosol Fe loading between the 24 and 26 June.

4.4.4 Enrichment factor analysis

The *Wedepohl* [1995] compilation of the continent crust composition was used to calculate crustal enrichment factors (EF) to determine the contribution of mineral dust to the observed total elemental concentrations. Total Ti was used as a marker for mineral dust. For an element (Z) in a sample, the EF relative to Ti is calculated using equation (4.2).

$$EF = \frac{(Z/Ti)_{sample}}{(Z/Ti)_{crust}} \qquad \text{Equation (4.2)}$$

The enrichment factors of Gunn Point filters are used to gauge the level of mineral dust contribution versus other sources. From the EF in Table 4.3, two groups of trace elements

were identified. The first was Al and Fe which have low EFs between 0.6 – 1.3 throughout the campaign; this is considered to be similar to the upper continental crust (i.e., EF between 0.7 and 2), implying that these trace metals might have originated from that source. Aerosol Fe has an EF between 0.9 and 1.3 and does not show Fe enrichment, suggesting that anthropogenic pollution was not a dominant source of Fe to Gunn Point.

The second group of trace elements consists of Cr, Mn, and Pb, and nss-K which had maximum EFs between 5 and 12 (i.e., moderate enrichment >2 EF <10 to enriched EF >10), indicating mixed sources. Cr showed moderate enrichment (EF of ~4) during the marine event, and also on the 13 June (EF of 8) when back trajectories crossed coastal Queensland (i.e., trajectory type "B"). Anthropogenic Cr could be sourced from industry and combustion [*Pacyna and Nriagu*, 1988].

Manganese, Pb and nss-K were enriched at three times throughout the campaign. Mn enrichment could be associated with particles that became airborne by soil dispersion or anthropogenic emissions (e.g., smelting and unleaded car fuel) [e.g. *Parekh*, 1990]. Atmospheric Pb originates from the geological weathering, smelting, burning of unleaded fuel, and coal combustion [e.g. *Bollhöfer and Rosman*, 2000; *Bollhöfer and Rosman*, 2001; *Bollhöfer et al.*, 1999]. The air mass back trajectories showed that during the elevated EF of Mn, Pb and nss-K, the wind direction was from the southeast and fetch area which included major cities and industrial areas in Brisbane (i.e. trajectory types "A" and C" (Fig. 4.1). Manganese (EF up to 5), Pb (EF between 5 and 12) and nss-K (EF between 3 and 6) showed moderate enrichment during fire events "G", and "F,J,A,B." Enrichment of these elements also occurred during the 16-18 June when trajectories came from the south and passed over major smelting sites i.e. Port Pire and Olympic Dam in South Australia and Mt Isa, Queensland (i.e., trajectory type "D"). The enrichment factors and air mass back trajectories suggest that both smelting and fire are sources of Mn, Pb and nss-K aerosols at these three times.

Lead can also originate from a resuspension of a contaminated material. Enrichment factors for Pb during dust events "A" and "B" were similar to the upper crust suggesting a dust source for aerosol Pb at this time. Enrichments factors of V were constant throughout the campaign, and ranged from 1.6 to 3 indicating the moderate EF for V could be related to contamination from both atmospheric mineral dust and fuel oil burning e.g. from ship exhaust [*Desboeufs et al.*, 2005b; *Hope*, 2008; *Jang et al.*, 2007].

Lower enrichment factors have been observed in marine air masses at Cape Verde (collected on a 30 m tower), indicating that the elements were likely of crustal origin. On the other hand, higher EFs have been reported in marine air masses that crossed Europe and North America, indicating that the elements were of anthropogenic origin [*Fomba et al.*, 2012]. The low EF in Al and Fe and higher EF in Mn, Cr, nss-K and Pb during fire events and air masses that passed over major smelting sites are likely to also reflect a combination of crustal, marine and anthropogenic aerosols.

Table 4.3: Enrichment factor analysis of Gunn Point aerosol samples.

	Sr	Pb	Al	V	Cr	Mn	Fe	K
GP1	0.37	2.57	0.60	1.81	1.22	0.53	1.12	1.72
GP2	0.37	3.18	0.76	2.24	1.54	0.67	1.28	1.91
GP3	0.40	2.32	0.68	2.09	1.41	0.88	1.13	1.23
GP4	0.34	1.38	0.64	1.93	1.26	0.88	1.07	0.67
GP5	0.24	1.83	0.55	1.77	1.28	0.68	0.97	0.64
GP6	0.31	3.42	0.59	1.72	1.34	1.03	1.03	2.17
GP7	0.71	8.81	0.59	1.81	1.88	1.44	1.02	5.50
GP8	0.42	3.77	0.66	2.08	1.34	0.72	1.15	1.49
GP9	0.29	4.25	0.58	1.85	1.38	0.60	1.08	1.63
GP10	0.23	3.42	0.67	2.29	7.93	0.49	1.16	1.37
GP11	0.17	1.22	0.73	2.00	1.32	0.44	1.14	0.34
GP12	0.43	2.05	0.64	1.95	1.48	1.47	1.14	1.23
GP13	0.39	5.32	0.62	1.57	1.09	1.22	1.07	1.07
GP14	0.68	6.55	0.64	1.67	1.16	1.48	1.08	2.30
GP15	0.76	6.60	0.65	2.84	3.37	1.07	0.99	1.79
GP16	1.43	2.39	0.62	1.77	0.99	1.40	0.88	1.49
GP17	0.33	0.79	0.72	1.73	4.22	0.23	0.91	0.25
GP18	0.52	1.63	0.67	2.09	1.34	0.52	1.04	0.48
GP19	0.66	12.46	0.63	1.78	1.55	1.22	1.00	2.65
GP20	1.38	8.05	0.68	1.60	1.25	4.70	1.10	4.79
GP21	0.50	4.65	0.69	1.90	1.32	1.43	1.16	2.63
GP22	1.16	5.72	0.71	1.96	1.37	2.18	1.12	3.92
GP23	1.04	4.25	0.69	1.92	1.22	1.77	1.04	1.76

4.4.5 Aerosol sources

Based on a combination of radon, air mass trajectories, enrichment factor analysis and biomass burning markers, trace elements have been grouped into three sources: dust, biomass burning and marine sources.

4.4.5.1 Dust events

Dust events “A” and “B” are characterised by peaks in total PM10 Al, Ti, Fe and V, and correspond to low diurnal radon i.e. when conditions are well mixed (Fig. 4.3). During these two dust events, back trajectories corresponded to times when the air mass passed over central Australian desert and low population areas of inland Australia, i.e., dust event “A”: trajectory type “c,” and dust event “ B”: trajectory type “d,” (Fig. 4.1). Enrichment factors for Al (EF of 0.6-0.7), V (EF of 1.8-2.0) and Fe (EF of 1.0-1.1) during these two dust events show that these trace metals have a similar composition to the upper crust (i.e. EF 0.7-2) and thus most likely originate from crustal material. Soluble concentrations of Fe, Al, Ti, Mn and V were high during dust events “A” and “B”. Fractional Fe solubility was highest in dust event “A” (11 %).

4.4.5.2 Anthropogenic and sea spray sources in marine conditions

On the 21 June 2014 marine conditions were identified by a decrease in aerosol particle counts and a change in the particle size distribution from unimodal to bimodal with modes at 20 nm and 70 nm [*Mallet et al*., in prep]. During these conditions, Na peaked to 107 ng m^{-3} indicative of sea spray (Figs. 4.4-4.6). The Na signal was greater during times of low advective radon i.e. when air masses were predominantly spending less time over land and more time over ocean regions. Total PM10 Al, Ti, Fe, V, as well as total PM10 Cr, Mo and As peaked during these conditions. There was a moderate rise in soluble Al, Ti and Fe. Enrichment factors for Al, V and Fe during marine conditions show that these trace metals have a similar composition to the upper crust (i.e. EF 0.7-2) and might originate from crustal material. Fractional Fe solubility was ~6 % in the marine air mass. During these conditions there were high concentrations of total PM10 Mo, Cr and As (Fig. 4.4), and the enrichment factor of Cr was moderately enriched (EF of 4.2). Small emissions of these three trace elements come from natural sources such as mineral dust, or volcanic emissions in the case of As. The greatest anthropogenic As emissions come from pyrometallurgical operations in the production of nonferrous metals, combustion of fossil fuels and the use of pesticides. Anthropogenic sources of aerosol Mo include the erosion of vehicle parts [*Lane et al.*, 2013], while anthropogenic Cr in the atmosphere is sourced from metallurgical and alloy steel, chemical, and refractory industry, coal and oil combustion, cement manufacturing, and refuse incineration [*Pacyna and Nriagu*, 1988]. Back trajectories passed over coastal regions of

Queensland i.e. type "b" (Fig. 4.1), suggesting that air masses could have been a mixture of dust and anthropogenic derived aerosols.

4.4.5.3 Fire events

The discussion of aerosol Fe during fire events focusses on the two major events occurring on the 9 June (fire event "G") and 25 June (fire event "FJAB") 2014 [*Mallet et al.*, in prep]. Both these events were comprised of C3 burning [*C. Paton-Walsh Pers. Comm.* [2014], and aerosol mass concentrations were higher than usual for the campaign. Concentrations of particulate matter less than 1 µm (PM1) increased up to 500 µg m^{-3} [*Mallet et al.*, in prep]. During these fire events, total PM10 Fe (400-800 ng m^{-3}) and soluble Fe (0.3-1.3 ng m^{-3}) concentrations and fractional Fe solubility (~3 %) were considerably less than the average concentration and fractional solubility throughout the campaign. For the first half of the campaign, from the 4-20 June, fractional Fe solubility averaged 8 % and then dropped to ~3 % between 21-27 June. During the drop in fractional Fe solubility, soluble and total PM10 Fe concentrations were the lowest found throughout the campaign.

We compare the fractional Fe solubility to biomass burring proxies during the campaign. There is no relationship between fractional Fe solubility and the biomass burning tracers (nss-K, elemental carbon, oxalate or levoglucosan; Fig. S4.2). However, fractional Fe solubility is typically higher when elemental carbon concentrations are low and vice versa, excluding dust event "A" (r^2=0.33). During the exceptionally large fire event "FJAB", fractional Fe solubility was the lowest (~3 %). In agreement with high concentrations of elemental carbon, oxalate and levoglucosan at this time, visual examination the aerosol filters showed that between the 21-27 June, filters were exceptionally caked with soot. The lowest fractional Fe solubility during fire event "FJAB" is related to proximal fires, where the fractional Fe solubility was relatively high during fire event "G" when fires were distantly sourced.

4.4.6 Biomass burning derived soluble iron – combustion and transport

Biomass burning is a potentially large source of soluble Fe to the open ocean [*Guieu et al.*, 2005; *Ito*, 2013; 2015]. *Ito* [2015] estimate that in the north Australian coastal region, biomass burning contributes around 60-70 % of the total soluble Fe deposition, where the dust contribution is less (40-50 %). Southern Hemisphere biomass burning emissions primarily occur in the intertropical convergence zone (ITCZ) of Africa, Australia and South

America [*Giglio et al.*, 2013]. Biomass burning constitutes a large source of annual dry season aerosol emissions over northern Australia, and episodic austral summer wildfire in southern and eastern Australia [e.g. *Meyer et al.*, 2008]. Modelling by *Ito* [2015] suggests biomass burning derived soluble Fe contributes substantial inputs of soluble Fe to tropical and Southern Ocean waters downwind of Australia. In the Southern Ocean, there is a larger contribution of biomass burning aerosol Fe than mineral dust and fossil fuel combustion derived aerosol Fe. Therefore biomass burning could be an important source of soluble Fe to both tropical and Southern Ocean waters surrounding Australia.

The particle size distribution of biomass burning aerosols was typically around 95 nm (with 95 % of all particles between 30-280 nm) for nearby fresh smoke at Gunn Point and around 120 nm (95 % of all particles were between 40-390 nm) for distant aged smoke at Gunn Point [*Mallet et al.*, in prep]. While the literature shows that for aged/long-range transported smoke, the particle sized distribution ranges between 75-540 nm [*Kipling et al.*, 2013]. As the particle size distribution for elemental/black carbon is in the nanometre range, any Fe associated with elemental/black carbon particles is operationally defined as soluble (i.e. <0.2 µm). The majority of soluble Fe in Gunn Point aerosols was within the <0.2 µm pool (i.e., the concentration of soluble Fe <0.2 µm was 6 ng m^{-3} compared to the bulk soluble Fe concentration of 8 ng m^{-3} in GP22). Leachates showed large variability in their colour, and visual observation after particle settling showed that they contained a large number of very fine particles in the <0.2 µm filtered fraction. Recent studies show that nanometre-sized Fe particles are potentially bioavailable [e.g. *Raiswell et al.*, 2008b], and thus future work should be directed to quantifying biomass burning sources of bioavailable Fe in tropical and remote oceanic regions.

Iron can be bound to long-range transportable black carbon aggregates deposited in Antarctic snow and ice [*Ellis et al.*, 2015]. Little is known about the process in which Fe is bound to black carbon aggregates, but Fe could originate from Fe contained within the biomass [*Maenhaut et al.*, 2002; *Reid et al.*, 2005; *Yamasoe et al.*, 2000], soil Fe incorporated into the aerosol mixture during combustion, or the binding of aerosol Fe to black carbon in the atmosphere during transport. Our samples comprised a mixture of elemental carbon and mineral dust. Using single particle analysis, mixed sources (e.g. black carbon and aluminosilicates) were detected in long-range transported aerosols to the Southern Ocean [*Ellis et al.*, 2015]. It is not surprising that the fractional Fe solubility data (2-11 %) plots

mid-range for aerosol Fe sources characteristic of dust and combustion in the Southern Hemisphere (Fig. 4.7).

Generally, the fractional Fe solubility was lower when fresh elemental carbon concentrations were high and sourced from proximal fires at Gunn Point (Fig. 4.6). This relationship could be related to the hydrophobic, i.e. water insoluble, nature of black carbon in water [e.g. *Chughtai et al.*, 1996]. The low soluble Fe concentrations, and hence low fractional Fe solubility, derived from the heavily caked soot filters between the 21 and 27 June could reflect the physical properties of fresh elemental carbon, i.e., fresh elemental carbon does not disperse in water thus any soluble Fe associated with fresh elemental carbon is not dispersed in the water leach. However, combustion aerosols are known to have a high factional Fe solubility [*Sholkovitz et al.*, 2012] and often these studies are based on aerosols collected shipboard in the remote open ocean where aerosol Fe has undergone transport and aging. Therefore, the fractional Fe solubility in these studies is not directly comparable to fresh combustion Fe reported in this study. Combustion aerosols can become more soluble with transport [*Ito*, 2015]. There is a growing body of work that suggests aerosol Fe solubility can be enhanced by cloud chemistry and acid processing [*Desboeufs et al.*, 1999; *Hoffer et al.*, 2005; *Kumar et al.*, 2010; *Meskhidze et al.*, 2003; *Spokes et al.*, 1994]. *Ito and Shi* [2015] show that enhanced Fe solubility of dust could be related to reactive organic species such as oxalate, in cloud water, which contains Fe-binding functionalities such as humic-like substances from biomass burning. Black/elemental carbon is initially insoluble, but can be aged into a soluble form following uptake of sulphuric acid and secondary organic material via condensation and coagulation in the atmosphere. Aged black/elemental carbon can also become hydrophilic and disperse in water when coated with acidic species or through the oxidation with functional groups during atmospheric transport over the remote ocean [*Chughtai et al.*, 1996; *Chughtai et al.*, 1991; *Decesari et al.*, 2002; *Lohmann et al.*, 2000]. If elemental/black carbon becomes hydrophilic in the atmosphere, soluble Fe bound to the black/elemental carbon particles would disperse in water and be captured in the water soluble Fe leach. This could explain why, i) the fractional Fe solubility was higher is distally sourced fire event “G” compared to the proximal fire event “FJAB”, and ii) the relatively high fractional Fe solubility observed in long-range transported aerosol to the remote Southern Ocean and Antarctica [*Conway et al.*, 2015; *Gaspari et al.*, 2006; *Winton et al.*, 2015]. The impact of transport time and distance on fractional Fe solubility should be further investigated.

Oxalate modification of mineral dust could be a leading factor enhancing the fractional Fe solubility of mineral dust [*Ito and Shi*, 2015] in regions where there are high oxalate concentrations in the atmosphere, such as the tropics. The higher fractional Fe solubility during dust events compared to fire events at Gunn Point could be related to biomass burning derived-oxalate enhancing the solubility of Australian mineral dust that has been transported to the Northern Territory and mixed with biomass burning plumes (Fig. 4.6). The fractional Fe solubility of mineral dust in the Southern Hemisphere is around 0.5-2 % [*Sholkovitz et al.*, 2012], which is relatively lower than our estimates of fractional Fe solubility during dust events in northern Australia. The air masses in lower latitudes over Antarctica and the Southern Ocean contain trace concentrations of oxalate [*Keywood*, 2007]. Although, little is known about the enhancement of fractional Fe solubility in these pristine air masses [*Chance et al.*, 2015], the concentrations of oxalate may be too low to enhance the fractional iron solubility of mineral dust. Therefore, biomass burning enhanced mineral dust fractional Fe solubility of ~8 % represents an upper bound of mineral dust fractional Fe solubility in the Australian tropics during the dry season as illustrated in Fig. 4.7.

The relatively low fractional Fe solubility in mixed dust and fresh biomass burning aerosols at Gunn Point, compared to other estimates of combustion aerosols (up to 60 %), could be related to the short aging time of fresh biomass in our samples. *Ito* [2015] model the transport of soluble Fe derived from combustion sources. The model indicates relatively low fractional Fe solubility near the sources of biomass burning and coal combustion. The fractional Fe solubility becomes higher as aerosols are transported to the open ocean. Therefore, transport time and distance could be an import factor in fractional Fe solubility. Alternatively, the relatively low fractional Fe solubility could be related to the type of biomass in northern Australia (i.e. savannah that is comprised of eucalypt dominated woodlands (10-30% foliage cover) and open-forests (30-70% foliage cover), with a diverse woody sub-canopy and grassy ground cover [*Edwards et al.*, 2015]). There is a wide range of fractional Fe solubility estimates for combustion aerosol in the literature and more studies are required to understand the chemical forms of Fe in different biomass types. On the other hand, low fractional Fe solubility during fire events and the inverse relationship between elemental carbon and soluble Fe questions whether biomass burning could be a bioavailable source of Fe. Clearly future work should be directed towards the solubility of Fe in fresh and aged smoke plumes.

4.5 Conclusions

Emissions of mineral dust and aged biomass burning from Australia are potential sources of soluble Fe to the Southern Ocean and Australian tropical waters. During the SAFIRED campaign, northern Australia in the dry season 2014, there was considerable temporal variability in soluble and total PM10 aerosol Fe concentrations that reflect mixed dust, fresh smoke and anthropogenic sources. Fractional Fe solubility was relatively high (2-12 %). Fractional Fe solubility was greatest during dust events, and was not correlated to biomass burning proxies. Iron in dust may be more soluble in the tropics, compared to higher latitudes, due to the higher concentrations of biomass burning derived reactive organic species in the atmosphere, such as oxalate, and their potential to enhance the fractional Fe solubility of mineral dust. Soluble Fe could be further enhanced during atmospheric transport and aging of black/elemental carbon that could explain the relatively high episodic fractional Fe solubility observed in long-range transportable aerosol Fe to the Southern Ocean and Antarctica. In addition, elemental carbon can act as a surface for aerosol iron to bind to during transport. Alternatively, due to the hydrophobic nature of fresh elemental carbon, biomass burning derived soluble Fe could be a negligible or non-bioavailable source of Fe to the ocean. Biomass burning constitutes a large fraction of the aerosol loading over the tropics which are a potential source of bioavailable Fe triggering nitrogen fixing toxic algal blooms. Such, toxic algal blooms have harmful consequences for humans and other vertebrates. The understanding of the factors that initiate algal blooms needs to be improved [*Abram et al.*, 2003; *Law et al.*, 2011], especially over tropical regions where inputs of biomass burning to the ocean are predicted to increase over the next century [*Keywood et al.*, 2013].

Acknowledgments

This project was funded through Curtin University (RES-SE-DAP-AW-47679-1 to R.E), the University of Tasmania (B0019024 to A.R.B.), the Australian Research Council (FT130100037 to A.R.B.), the Antarctic Climate and Ecosystems (ARC CRC) and the CSIRO. Access to HR-ICP-MS instrumentation at Curtin University was facilitated through ARC LIEF funding (LE130100029). V.H.L.W. would like to acknowledge the following scholarship support: Australian Postgraduate Award, Curtin Research Scholarship and CUPSA data collection grant. Thank you to CSIRO Ocean and Atmosphere for the use of their high-volume aerosol sampler and to the Bureau of Meteorology for the use of their site throughout the campaign. Thank you to the SAFIRED team, in particular to Rob Gillet and Jason Ward for assisting with the changeover of daily aerosol filters and to Brad Atkinson from BoM for assistance at Gunn Point. Thank you to Sylvester Werczynski from ANSTO for obtaining the back trajectories from HYSPLIT and cataloguing them in a data base for use with the Gunn Point data. Thank you to Pier van der Merwe for technical support with aerosol digestions. Wind roses were created using OpenAir package in R and meteorological data from the Bureau of Meteorology. The dataset for the trace metal filters is available through the Curtin University Research Data repository http://doi.org/10.4225/06/5671012A48C2A. We thank two anonymous reviewers who improved the paper.

References

Abram, N. J., Gagan, M. K., McCulloch, M. T., Chappell, J., and Hantoro, W. S.: Coral reef death during the 1997 Indian Ocean dipole linked to Indonesian wildfires, Science, 301, 952-955, 2003.

Aguilar-Islas, A. M., Wu, J., Rember, R., Johansen, A. M., and Shank, L. M.: Dissolution of aerosol-derived iron in seawater: Leach solution chemistry, aerosol type, and colloidal iron fraction, Marine Chemistry, 120, 25-33, 2010.

Andreae, M., and Gelencsér, A.: Black carbon or brown carbon? The nature of light-absorbing carbonaceous aerosols, Atmospheric Chemistry and Physics, 6, 3131-3148, 2006.

Baker, A., Kelly, S., Biswas, K., Witt, M., and Jickells, T.: Atmospheric deposition of nutrients to the Atlantic Ocean, Geophysical Research Letters, 30, 2003.

Baker, A., Weston, K., Kelly, S., Voss, M., Streu, P., and Cape, J.: Dry and wet deposition of nutrients from the tropical Atlantic atmosphere: Links to primary productivity and nitrogen fixation, Deep Sea Research Part I: Oceanographic Research Papers, 54, 1704-1720, 2007.

Baker, A., Adams, C., Bell, T., Jickells, T., and Ganzeveld, L.: Estimation of atmospheric nutrient inputs to the Atlantic Ocean from 50° N to 50° S based on large-scale field sampling: Iron and other dust-associated elements, Global Biogeochemical Cycles, 27, 755-767, 2013.

Baker, A. R., Jickells, T. D., Witt, M., and Linge, K. L.: Trends in the solubility of iron, aluminium, manganese and phosphorus in aerosol collected over the Atlantic Ocean, Marine Chemistry, 98, 43-58, 2006.

Baker, A. R., and Croot, P. L.: Atmospheric and marine controls on aerosol iron solubility in seawater, Marine Chemistry, 120, 4-13, 2010.

Berman-Frank, I., Cullen, J. T., Shaked, Y., Sherrell, R. M., and Falkowski, P. G.: Iron availability, cellular iron quotas, and nitrogen fixation in Trichodesmium, Limnology and Oceanography, 46, 1249-1260, 2001.

Bisiaux, M., Edwards, R., McConnell, J., Curran, M., Van Ommen, T., Smith, A., Neumann, T., Pasteris, D., Penner, J., and Taylor, K.: Changes in black carbon deposition to Antarctica from two high-resolution ice core records, 1850–2000 AD, Atmospheric Chemistry and Physics, 12, 4107-4115, 2012.

Bollhöfer, A., Chisholm, W., and Rosman, K. J. R.: Sampling aerosols for lead isotopes on a global scale, Analytica Chimica Acta, 390, 227-235, http://dx.doi.org/10.1016/S0003-2670(99)00182-8, 1999.

Bollhöfer, A., and Rosman, K.: Isotopic source signatures for atmospheric lead: the Southern Hemisphere, Geochimica et Cosmochimica Acta, 64, 3251-3262, 2000.

Bollhöfer, A., and Rosman, K.: Isotopic source signatures for atmospheric lead: the Northern Hemisphere, Geochimica et Cosmochimica Acta, 65, 1727-1740, 2001.

Bowie, A. R., Lannuzel, D., Remenyi, T. A., Wagener, T., Lam, P. J., Boyd, P. W., Guieu, C., Townsend, A. T., and Trull, T. W.: Biogeochemical iron budgets of the Southern Ocean south of Australia: Decoupling of iron and nutrient cycles in the subantarctic zone by the summertime supply, Global Biogeochem. Cycles, 23, GB4034, 10.1029/2009gb003500, 2009.

Bowler, J.: Aridity in Australia: age, origins and expression in aeolian landforms and sediments, Earth-Science Reviews, 12, 279-310, 1976.

Boyd, P. W., Watson, A. J., Law, C. S., Abraham, E. R., Trull, T., Murdoch, R., Bakker, D. C. E., Bowie, A. R., Buesseler, K. O., Chang, H., Charette, M., Croot, P. L., Downing, K., Frew, R., Gall, M., Hadfield, M., Hall, J., Harvey, M., Jameson, G., LaRoche, J., Liddicoat, M. I., Ling, R., Maldonado, M. T., McKay, R. M., Nodder, S., Pickmere, S., Pridmore, R., Rintoul, S., Safi, K., Sutton, P., Strzepek, R., Tanneberger, K., Turner, S., Waite, A., and Zeldis, J.: A mesoscale phytoplankton bloom in the polar Southern Ocean stimulated by iron fertilization, Nature, 407, 695-702, 2000.

Boyd, P. W., and Ellwood, M. J.: The biogeochemical cycle of iron in the ocean, Nature Geosci, 3, 675-682, http://www.nature.com/ngeo/journal/v3/n10/abs/ngeo964.html#supplementary-information, 2010.

Carslaw, D. C., and Ropkins, K.: Openair - An R package for air quality data analysis, Environmental Modelling & Software, 27, 52-61, 2012.

Carslaw, D. C.: The openair manual - open-source tools for analysing air pollution data., Manual for version 1.0, King's College London., 2014.

Chambers, S., Williams, A., Crawford, J., and Griffiths, A.: On the use of radon for quantifying the effects of atmospheric stability on urban emissions, Atmos. Chem. Phys. Discuss, 14, 25,411-425,452, 2014.

Chow, J. C., Watson, J. G., Chen, L.-W. A., Chang, M. O., Robinson, N. F., Trimble, D., and Kohl, S.: The IMPROVE_A temperature protocol for thermal/optical carbon analysis: maintaining consistency with a long-term database, Journal of the Air & Waste Management Association, 57, 1014-1023, 2007.

Chuang, P. Y., Duvall, R. M., Shafer, M. M., and Schauer, J. J.: The origin of water soluble particulate iron in the Asian atmospheric outflow, Geophys. Res. Lett., 32, L07813, 10.1029/2004gl021946, 2005.

Chughtai, A., Jassim, J., Peterson, J., Stedman, D., and Smith, D.: Spectroscopic and solubility characteristics of oxidized soots, Aerosol Science and Technology, 15, 112-126, 1991.

Chughtai, A., Brooks, M., and Smith, D.: Hydration of black carbon, Journal of Geophysical Research: Atmospheres (1984–2012), 101, 19505-19514, 1996.

Conway, T., Wolff, E., Röthlisberger, R., Mulvaney, R., and Elderfield, H.: Constraints on soluble aerosol iron flux to the Southern Ocean at the Last Glacial Maximum, Nature Communications, 6, 2015.

Cropp, R. A., Gabric, A. J., Levasseur, M., McTainsh, G. H., Bowie, A., Hassler, C. S., Law, C. S., McGowan, H., Tindale, N., and Viscarra Rossel, R.: The likelihood of observing dust-stimulated phytoplankton growth in waters proximal to the Australian continent, Journal of Marine Systems, 117–118, 43-52, http://dx.doi.org/10.1016/j.jmarsys.2013.02.013, 2013.

De Deckker, P., Norman, M., Goodwin, I. D., Wain, A., and Gingele, F. X.: Lead isotopic evidence for an Australian source of aeolian dust to Antarctica at times over the last 170,000 years, Palaeogeography, Palaeoclimatology, Palaeoecology, 285, 205-223, 2010.

Decesari, S., Facchini, M., Matta, E., Mircea, M., Fuzzi, S., Chughtai, A., and Smith, D.: Water soluble organic compounds formed by oxidation of soot, Atmospheric Environment, 36, 1827-1832, 2002.

Desboeufs, K. V., Losno, R., Vimeux, F., and Cholbi, S.: The pH-dependent dissolution of wind-transported Saharan dust, Journal of Geophysical Research: Atmospheres (1984–2012), 104, 21287-21299, 1999.

Desboeufs, K. V., Sofikitis, A., Losno, R., Colin, J. L., and Ausset, P.: Dissolution and solubility of trace metals from natural and anthropogenic aerosol particulate matter, Chemosphere, 58, 195-203, 2005.

Dörr, H., Kromer, B., Levin, I., Münnich, K., and Volpp, H. J.: CO2 and Radon 222 as tracers for atmospheric transport, Journal of Geophysical Research: Oceans (1978–2012), 88, 1309-1313, 1983.

Draxler, R. R., and Rolph, G. D.: Hybrid Single-Particle Lagrangian Integrated Trajectory (HYSPLIT), model, http://www.arl.noaa.gov/ready/hysplit4.html, 2003.

Duce, R. A., Liss, P. S., Merrill, J. T., Atlas, E. L., Buat-Menard, P., Hicks, B. B., Miller, J. M., Prospero, J. M., Arimoto, R., Church, T. M., Ellis, W., Galloway, J. N., Hansen, L., Jickells, T. D., Knap, A. H., Reinhardt, K. H., Schneider, B., Soudine, A., Tokos, J. J., Tsunogai, S., Wollast, R., and Zhou, M.: The atmospheric input of trace species to the world ocean, Global Biogeochem. Cycles, 5, 193-259, 10.1029/91gb01778, 1991.

Ellis, A., Edwards, R., Saunders, M., Chakrabarty, R. K., Subramanian, R., van Riessen, A., Smith, A. M., Lambrinidis, D., Nunes, L. J., Vallelonga, P., Goodwin, I. D., Moy, A. D., Curran, M. A. J., and van Ommen, T. D.: Characterizing black carbon in rain and ice cores using coupled tangential flow filtration and transmission electron microscopy, Atmos. Meas. Tech., 8, 3959-3969, 10.5194/amt-8-3959-2015, 2015.

Falkowski, P. G.: Evolution of the nitrogen cycle and its influence on the biological sequestration of CO 2 in the ocean, Nature, 387, 272-275, 1997.

Fomba, K., Müller, K., Pinxteren, D. v., and Herrmann, H.: Aerosol size-resolved trace metal composition in remote northern tropical Atlantic marine environment: case study Cape Verde Islands, Atmospheric Chemistry and Physics Discussions, 12, 29535-29569, 2012.

Gabric, A. J., Cropp, R. A., McTainsh, G. H., Johnston, B. M., Butler, H., Tilbrook, B., and Keywood, M.: Australian dust storms in 2002–2003 and their impact on Southern Ocean biogeochemistry, Global Biogeochemical Cycles, 24, 2010.

Gao, Y., Kaufman, Y. J., Tanré, D., Kolber, D., and Falkowski, P. G.: Seasonal distributions of aeolian iron fluxes to the global ocean, Geophys. Res. Lett., 28, 29-32, 10.1029/2000gl011926, 2001.

Gao, Y., Xu, G., Zhan, J., Zhang, J., Li, W., Lin, Q., Chen, L., and Lin, H.: Spatial and particle size distributions of atmospheric dissolvable iron in aerosols and its input to the Southern Ocean and coastal East Antarctica, Journal of Geophysical Research: Atmospheres, 118, 12,634-612,648, 2013.

Gaspari, V., Barbante, C., Cozzi, G., Cescon, P., Boutron, C. F., Gabrielli, P., Capodaglio, G., Ferrari, C., Petit, J. R., and Delmonte, B.: Atmospheric iron fluxes over the last deglaciation: Climatic implications, Geophys. Res. Lett., 33, L03704, 10.1029/2005gl024352, 2006.

Giglio, L., Randerson, J. T., and Werf, G. R.: Analysis of daily, monthly, and annual burned area using the fourth-generation global fire emissions database (GFED4), Journal of Geophysical Research: Biogeosciences, 118, 317-328, 2013.

Guieu, C., Bonnet, S., Wagener, T., and Loÿe-Pilot, M. D.: Biomass burning as a source of dissolved iron to the open ocean?, Geophysical Research Letters, 32, 2005.

Hesse, P. P.: The record of continental dust from Australia in Tasman Sea sediments, Quaternary Science Reviews, 13, 257-272, 1994.

Hesse, P. P., and McTainsh, G. H.: Australian dust deposits: modern processes and the Quaternary record, Quaternary Science Reviews, 22, 2007-2035, 2003.

Hoffer, A., Gelencsér, A., Guyon, P., Kiss, G., Schmid, O., Frank, G., Artaxo, P., and Andreae, M.: Optical properties of humiclike substances (HULIS) in biomass-burning aerosols, Atmos. Chem. Phys. Discuss, 5, 7341-7360, 2005.

Hope, B. K.: A dynamic model for the global cycling of anthropogenic vanadium, Global Biogeochemical Cycles, 22, 2008.

Ito, A.: Mega fire emissions in Siberia: potential supply of bioavailable iron from forests to the ocean, Biogeosciences, 8, 2011.

Ito, A.: Global modeling study of potentially bioavailable iron input from shipboard aerosol sources to the ocean, Global Biogeochemical Cycles, 27, 1-10, 2013.

Ito, A.: Atmospheric Processing of Combustion Aerosols as a Source of Bioavailable Iron, Environmental Science & Technology Letters, 2, 70-75, 10.1021/acs.estlett.5b00007, 2015.

Ito, A., and Shi, Z.: Delivery of anthropogenic bioavailable iron from mineral dust and combustion aerosols to the ocean, Atmospheric Chemistry and Physics Discussions, 15, 23051-23088, 2015.

Jang, H.-N., Seo, Y.-C., Lee, J.-H., Hwang, K.-W., Yoo, J.-I., Sok, C.-H., and Kim, S.-H.: Formation of fine particles enriched by V and Ni from heavy oil combustion: Anthropogenic sources and drop-tube furnace experiments, Atmospheric Environment, 41, 1053-1063, 2007.

Johnson, K. S., Gordon, R. M., and Coale, K. H.: What controls dissolved iron concentrations in the world ocean?, Marine Chemistry, 57, 137-161, 1997.

Johnston, S. W.: The influence of aeolian dust deposits on alpine soils in south-eastern Australia, Soil Research, 39, 81-88, 2001.

Kipling, Z., Stier, P., Schwarz, J., Perring, A., Spackman, J., Mann, G., Johnson, C., and Telford, P.: Constraints on aerosol processes in climate models from vertically-resolved aircraft observations of black carbon, Atmospheric Chemistry and Physics, 13, 5969, 2013.

Kumar, A., Sarin, M., and Srinivas, B.: Aerosol iron solubility over Bay of Bengal: Role of anthropogenic sources and chemical processing, Marine Chemistry, 121, 167-175, 2010.

Kustka, A. B., Sañudo-Wilhelmy, S. A., Carpenter, E. J., Capone, D., Burns, J., and Sunda, W. G.: Iron requirements for dinitrogen-and ammonium-supported growth in cultures of Trichodesmium (IMS 101): Comparison with nitrogen fixation rates and iron: Carbon ratios of field populations, Limnology and Oceanography, 48, 1869-1884, 2003.

Lane, S., Proemse, B. C., Tennant, A., and Wieser, M. E.: Concentration measurements and isotopic composition of airborne molybdenum collected in an urban environment, Analytical and bioanalytical chemistry, 405, 2957-2963, 2013.

LaRoche, J., and Breitbarth, E.: Importance of the diazotrophs as a source of new nitrogen in the ocean, Journal of Sea Research, 53, 67-91, 2005.

Law, C., Woodward, E., Ellwood, M., Marriner, A., Bury, S., and Safi, K.: Response of surface nutrient inventories and nitrogen fixation to a tropical cyclone in the southwest Pacific, Limnology and Oceanography, 56, 1372-1385, 2011.

Lenes, J., Darrow, B., Walsh, J., Prospero, J., He, R., Weisberg, R., Vargo, G., and Heil, C.: Saharan dust and phosphatic fidelity: A three-dimensional biogeochemical model of Trichodesmium as a nutrient source for red tides on the West Florida Shelf, Continental Shelf Research, 28, 1091-1115, 2008.

Lohmann, U., Feichter, J., Penner, J., and Leaitch, R.: Indirect effect of sulfate and carbonaceous aerosols- A mechanistic treatment, Journal of Geophysical Research, 105, 12193-12206, 2000.

Mackie, D. S., Boyd, P. W., Hunter, K. A., and McTainsh, G. H.: Simulating the cloud processing of iron in Australian dust: pH and dust concentration, Geophys. Res. Lett., 32, L06809, 10.1029/2004gl022122, 2005.

Mackie, D. S., Boyd, P. W., McTainsh, G. H., Tindale, N. W., Westberry, T. K., and Hunter, K. A.: Biogeochemistry of iron in Australian dust: From eolian uplift to marine uptake, Geochem. Geophys. Geosyst., 9, Q03Q08, 10.1029/2007gc001813, 2008.

Maenhaut, W., Fernández-Jiménez, M.-T., Rajta, I., and Artaxo, P.: Two-year study of atmospheric aerosols in Alta Floresta, Brazil: Multielemental composition and source apportionment, Nuclear Instruments and Methods in Physics Research Section B: Beam Interactions with Materials and Atoms, 189, 243-248, 2002.

Mahowald, N. M., Baker, A. R., Bergametti, G., Brooks, N., Duce, R. A., Jickells, T. D., Kubilay, N., Prospero, J. M., and Tegen, I.: Atmospheric global dust cycle and iron inputs to the ocean, Global Biogeochem. Cycles, 19, GB4025, 10.1029/2004gb002402, 2005.

Mahowald, N. M., Engelstaedter, S., Luo, C., Sealy, A., Artaxo, P., Benitez-Nelson, C., Bonnet, S., Chen, Y., Chuang, P. Y., and Cohen, D. D.: Atmospheric iron deposition: Global distribution, variability, and human perturbations*, Marine Science, 1, 2009.

Marx, S. K., Kamber, B. S., and McGowan, H. A.: Estimates of Australian dust flux into New Zealand: Quantifying the eastern Australian dust plume pathway using trace element calibrated< sup> 210</sup> Pb as a monitor, Earth and Planetary Science Letters, 239, 336-351, 2005.

McTainsh, G., Chan, Y.-c., McGowan, H., Leys, J., and Tews, K.: The 23rd October 2002 dust storm in eastern Australia: characteristics and meteorological conditions, Atmospheric Environment, 39, 1227-1236, 2005.

Meskhidze, N., Chameides, W., Nenes, A., and Chen, G.: Iron mobilization in mineral dust: Can anthropogenic SO2 emissions affect ocean productivity?, Geophysical Research Letters, 30, 2003.

Meyer, C. P., Luhar, A. K., and Mitchell, R. M.: Biomass burning emissions over northern Australia constrained by aerosol measurements: I—Modelling the distribution of hourly emissions, Atmospheric Environment, 42, 1629-1646, http://dx.doi.org/10.1016/j.atmosenv.2007.10.089, 2008.

Morton, P. L., Landing, W. M., Hsu, S.-C., Milne, A., Aguilar-Islas, A. M., Baker, A. R., Bowie, A. R., Buck, C. S., Gao, Y., and Gichuki, S.: Methods for the sampling and analysis of marine aerosols: results from the 2008 GEOTRACES aerosol intercalibration experiment, Limnology and Oceanography: Methods, 11, 62-78, 2013.

Pacyna, J., and Nriagu, J.: Atmospheric emissions of chromium from natural and anthropogenic sources, Chromium in the Natural and Human Environments, 105-123, 1988.

Paerl, H. W., Crocker, K. M., and Prufert, L. E.: Limitation of N2 fixation in coastal marine waters: Relative importance of molybdenum, iron, phosphorus, and organic matter availability1, Limnology and Oceanography, 32, 525-536, 1987.

Paerl, H. W., Prufert-Bebout, L. E., and Guo, C.: Iron-stimulated N2 fixation and growth in natural and cultured populations of the planktonic marine cyanobacteria Trichodesmium spp, Applied and Environmental Microbiology, 60, 1044-1047, 1994.

Parekh, P.: A study of manganese from anthropogenic emissions at a rural site in the eastern United States, Atmospheric Environment. Part A. General Topics, 24, 415-421, 1990.

Paris, R., Desboeufs, K., Formenti, P., Nava, S., and Chou, C.: Chemical characterisation of iron in dust and biomass burning aerosols during AMMA-SOP0/DABEX: implication for iron solubility, Atmospheric Chemistry and Physics, 10, 4273-4282, 2010.

Raiswell, R., Benning, L. G., Davidson, L., and Tranter, M.: Nanoparticulate bioavailable iron minerals in icebergs and glaciers, Mineral Mag, 72, 345-348, 10.1180/minmag.2008.072.1.345, 2008.

Reid, J., Koppmann, R., Eck, T., and Eleuterio, D.: A review of biomass burning emissions part II: intensive physical properties of biomass burning particles, Atmospheric Chemistry and Physics, 5, 799-825, 2005.

Revel-Rolland, M., De Deckker, P., Delmonte, B., Hesse, P. P., Magee, J. W., Basile-Doelsch, I., Grousset, F., and Bosch, D.: Eastern Australia: A possible source of dust in East Antarctica interglacial ice, Earth and Planetary Science Letters, 249, 1-13, 2006.

Rubin, M., Berman-Frank, I., and Shaked, Y.: Dust-and mineral-iron utilization by the marine dinitrogen-fixer Trichodesmium, Nature Geoscience, 4, 529-534, 2011.

Rueter, J. G.: IRON STIMULATION OF PHOTOSYNTHESIS AND NITROGEN FIXATION IN ANABAENA 7120 AND TRICHODESMIUM (CYANOPHYCEAE) 1, Journal of Phycology, 24, 249-254, 1988.

Rueter, J. G., Hutchins, D. A., Smith, R. W., and Unsworth, N. L.: Iron nutrition of Trichodesmium, in: Marine pelagic cyanobacteria: Trichodesmium and other Diazotrophs, Springer, 289-306, 1992.

Schroth, A. W., Crusius, J., Sholkovitz, E. R., and Bostick, B. C.: Iron solubility driven by speciation in dust sources to the ocean, Nature Geosci, 2, 337-340, http://www.nature.com/ngeo/journal/v2/n5/suppinfo/ngeo501_S1.html, 2009.

Sedwick, P. N., Sholkovitz, E. R., and Church, T. M.: Impact of anthropogenic combustion emissions on the fractional solubility of aerosol iron: Evidence from the Sargasso Sea, Geochem. Geophys. Geosyst., 8, Q10Q06, 10.1029/2007gc001586, 2007.

Shaw, E. C., Gabric, A. J., and McTainsh, G. H.: Impacts of aeolian dust deposition on phytoplankton dynamics in Queensland coastal waters, Marine and Freshwater Research, 59, 951-962, 2008.

Sholkovitz, E. R., Sedwick, P. N., Church, T. M., Baker, A. R., and Powell, C. F.: Fractional solubility of aerosol iron: Synthesis of a global-scale data set, Geochimica et cosmochimica acta, 89, 173-189, 2012.

Spokes, L. J., Jickells, T. D., and Lim, B.: Solubilisation of aerosol trace metals by cloud processing: A laboratory study, Geochimica et Cosmochimica Acta, 58, 3281-3287, 1994.

Stohl, A.: Computation, accuracy and applications of trajectories—a review and bibliography, Atmospheric Environment, 32, 947-966, 1998.

Wagener, T., Guieu, C., Losno, R., Bonnet, S., and Mahowald, N.: Revisiting atmospheric dust export to the Southern Hemisphere ocean: Biogeochemical implications, Global Biogeochem. Cycles, 22, GB2006, 10.1029/2007gb002984, 2008.

Walsh, J. J., and Steidinger, K. A.: Saharan dust and Florida red tides: the cyanophyte connection, Journal of Geophysical Research: Oceans (1978–2012), 106, 11597-11612, 2001.

Wedepohl, K. H.: The composition of the continental crust, Geochimica et Cosmochimica Acta, 59, 1217-1232, 1995.

Winton, V. H. L., Bowie, A. R., Edwards, R., Keywood, M., Townsend, A. T., van der Merwe, P., and Bollhöfer, A.: Fractional iron solubility of atmospheric iron inputs to the Southern Ocean, Marine Chemistry, 177, Part 1, 20-32, http://dx.doi.org/10.1016/j.marchem.2015.06.006, 2015.

Yamasoe, M. A., Artaxo, P., Miguel, A. H., and Allen, A. G.: Chemical composition of aerosol particles from direct emissions of vegetation fires in the Amazon Basin: water-soluble species and trace elements, Atmospheric Environment, 34, 1641-1653, 2000.

Supplementary information

Table S4.1: Recovery rates of total trace metals in certified reference materials (CRM).

CRM recovery %	Al	±	Ti	±	V	±	Mn	±	Fe	±	Pb	±
MESS-3	112	8	92	9	100	9	97	11	108	8	103	11
TMF	n/d		n/d		101	8	100	9	99	7	107	8

Table S4.2: Instrument conditions and measurement parameters.

Instrument	HR-ICP-MS, Element XR (Thermo Fisher, Germany)
Torch	Precision type, quartz o-ring free, PFA injector (Element Scientific Inc.)
Spray chamber	PC^3 chilled cyclonic spray chamber (ESI)
Nebuliser	ST micro centric PFA (ESI)
RF power (W)	~1350
Cool gas flow (L min^{-1})	~16
Auxiliary gas flow (L min^{-1})	~0.9
Sample gas flow (L min^{-1})	~0.9
Additional gas (L min^{-1})	~0.4 Ar
Guard electrode	Activated
Sample uptake	96 s (Seafast II pump auto-sampler with fast 3 sample injection valve)
Sample rinse	50 s, 3 % HCl (ultra-pure)
Pump speed during wash	10 rpm
Internal standard	1.5 ppb In, 5 % HCl (ultra-pure)
Scan type	E-scan
Elements monitored in low resolution ($m/\Delta m$ ~400)	Pb, Cd
Elements monitored in medium resolution ($m/\Delta m$ ~4000)	Na, Mg, Al, Ti, V ,Cr, Mn, Fe
Elements monitored in high resolution ($m/\Delta m$ ~4000)	K, As

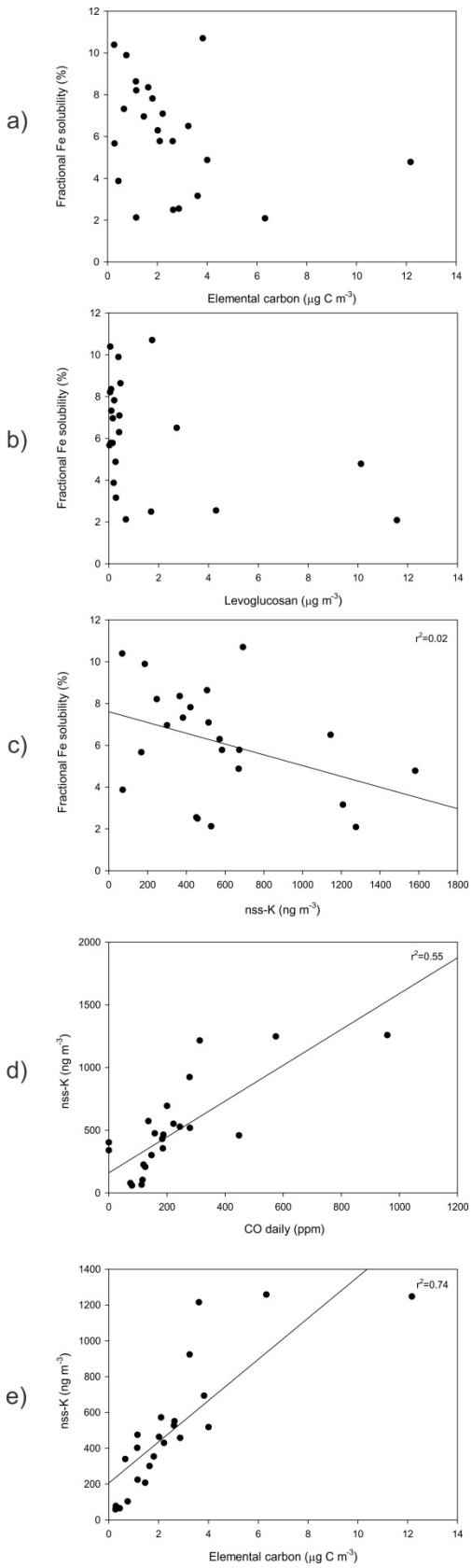

Fig. S4.1: Scatterplots of a) fractional Fe solubility versus elemental carbon concentrations, b) fractional Fe solubility versus nss-K concentrations, c) nss-K concentrations versus CO concentrations, d) nss-K concentrations versus elemental carbon concentrations.

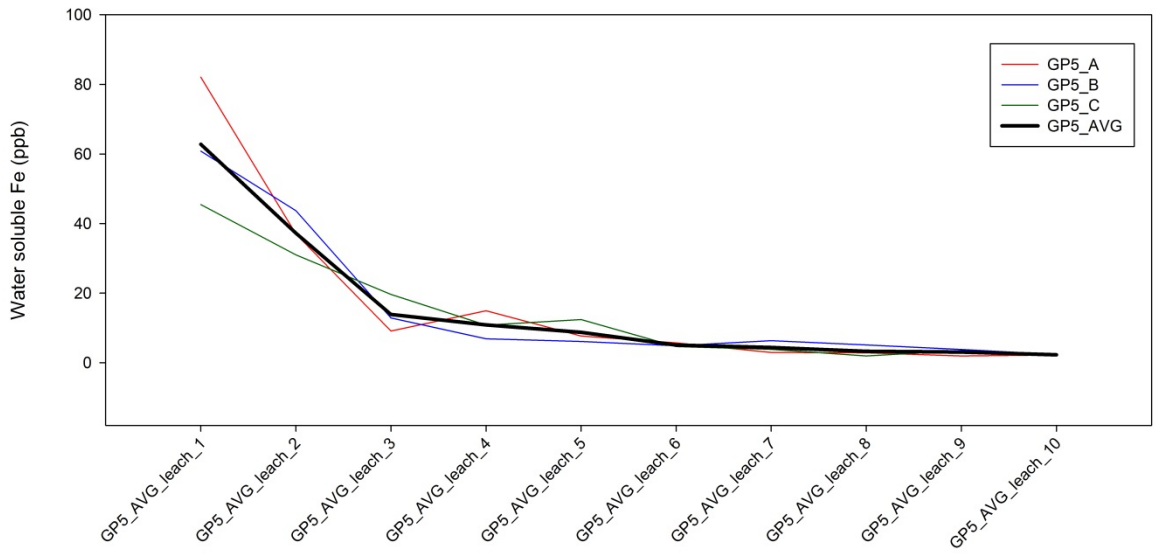

Fig. S4.2: Sequential ultra-pure water leaches of three aliquots of GP5.

Chapter 5. Fractional iron solubility of atmospheric iron inputs to the Southern Ocean

This chapter has been published in *Marine Chemistry*. Co-author contributions can be found in Appendix A2. The data has been published in the *Curtin University Research Data Repository*.

Winton, V.H.L., A.R. Bowie, R. Edwards, M. Keywood, A.T. Townsend, P. van der Merwe, Bollhofer, A., 2015. Fractional iron solubility of atmospheric iron inputs to the Southern Ocean, *Mar. Chem*., 177, Part 1, 20-32, http://dx.doi.org/10.1016/j.marchem.2015.06.006.

Winton, V.H.L., A.R. Bowie, R. Edwards, M. Keywood, A.T. Townsend, P. van der Merwe, Bollhofer, A., 2015. SF-ICP-MS soluble and total iron data for Cape Grim aerosols. *Curtin University Research Data*, http://doi.org/10.4225/06/565E7702F1E12.

Abstract

Deposition of iron (Fe) bearing aerosols to Fe deficient waters of the Southern Ocean may drive rapid changes in primary productivity, trophic structure and the biological uptake of carbon dioxide. The fractional solubility (i.e., the ratio of water leachable Fe to total Fe) of aerosol Fe is an important variable determining its availability for biological uptake, and is a function of both particle type and the experimental conditions used to leach the particles. There have been few studies of fractional Fe solubility over the Southern Ocean where the aerosol loading is the lowest in the world. To investigate Southern Ocean aerosol Fe solubility, the fractional solubility of Fe was determined in cryogenically archived Southern Ocean aerosols. Samples were collected at the Cape Grim Baseline Air Pollution Station (CGBAPS), Tasmania, Australia from February 1999 to April 2000. Fractions determined included water soluble Fe (<0.45 µm), labile Fe (>0.45 µm; acetic acid and hydroxylamine hydrochloride leachable Fe) and refractory Fe (>0.45 µm; total digestion using nitric and hydrofluoric acids). Extremely low Fe mass concentrations were observed for baseline Southern Ocean air during the study period. An inverse hyperbolic relationship was observed between fractional Fe solubility (0.5 to 56 %) and total Fe mass concentration (0.04 to 5.8 ng m^3; excluding an anomalously high sample). A peak of 4.6 ng m^3 of labile Fe occurred during

May/June 1999 and was linked to atmospheric transport from South Western Australia over the Southern Ocean. Bioavailable Fe was estimated by summing the water soluble and labile Fe fractions, and this likely represents the upper bound of long range transport aerosol over the Southern Ocean. The results confirm previous reports of a range of fractional Fe solubility within all atmospheric particles measured and also suggest that a large fraction of the Fe from Australian mineral aerosols is labile and potentially bioavailable.

5.1 Introduction

Limitation of Southern Ocean primary productivity due to low iron (Fe) availability is well established and has been the focus of a large body of research [e.g. *Blain et al.*, 2007; *Martin et al.*, 1990; 1991]. These waters are characteristically replete with nitrate and phosphate and depleted with respect to Fe. In-situ oceanic Fe-fertilisation experiments have demonstrated an almost explosive response of the ecosystem to relatively small additions of dissolved Fe [e.g. *Boyd et al.*, 2007; *Coale et al.*, 2004; *de Baar et al.*, 2005]. Inputs of new Fe to pelagic surface waters can occur through upwelling of deep waters [*de Baar et al.*, 1995], deep winter mixing and entrainment [*Bowie et al.*, 2014; *Tagliabue et al.*, 2014], transport from continental margins by ocean currents [*Elrod et al.*, 2004; *Johnson et al.*, 1999], from sea-ice and ice bergs [*Lannuzel et al.*, 2007; *Lannuzel et al.*, 2008; *Raiswell et al.*, 2008a; *Sedwick and DiTullio*, 1997], hydrothermal vents [*Frants et al.*, 2016; *Tagliabue et al.*, 2010], deep winter mixing [*Tagliabue et al.*, 2014], and atmospheric aerosol deposition [e.g. *Jickells et al.*, 2005]. Aerosol deposition to remote Southern Ocean surface waters is extremely low ranging from 0.3 to 2.5 mg m^{-2} d^{-1}, and has been investigated in relation to the distribution and transport of mineral dust [*Bowie et al.*, 2009; *Duce et al.*, 1991; *Luo et al.*, 2005; *Mahowald et al.*, 2005] and the episodic input of volcanic ash [*Narcisi et al.*, 2005]. Episodic changes in mineral dust deposition to the Southern Ocean have been linked to 20th-century climate change and land use modification [*Bhattachan and D'Odorico*, 2014]. Mineral dust proxy records from Antarctic ice cores [*Edwards et al.*, 2006; *Gaspari et al.*, 2006; *Spolaor et al.*, 2012; *Vallelonga et al.*, 2013] and Southern Ocean marine sediments from several regions [e.g. *Martínez-Garcia et al.*, 2009; *Moore et al.*, 2000; *Smetacek et al.*, 2012] display higher deposition rates during glacial stages. Recent Southern Ocean marine sediment studies link enhanced glacial atmospheric Fe deposition to higher rates of Southern Ocean primary productivity [*Martínez-García et al.*, 2014]. While other studies postulate that higher rates of Fe inputs to the Southern Ocean during glacial periods were sourced from the upwelling of water enriched by sediments [*Latimer and Filippelli*, 2001; *Latimer et al.*, 2006].

Aerosol Fe bioavailability data is required to constrain the biogeochemical impact of present and past atmospheric Fe variability. Aerosol Fe bioavailability will depend on the residence time of the Fe aerosol in the euphotic zone, and thus it is a function of its chemical composition and physical characteristics (e.g. particle size, surface area). Therefore, an upper

limit of aerosol Fe bioavailability can be estimated by measuring the instantaneous water solubility (i.e., the concentration of Fe that passes through a 0.2 or 0.45 μm aerosol-laden filter when leached with ultra-pure water) and the labile Fe fraction (i.e., a chemically defined measure using weak acid to estimate the portion of the particulate trace metal pool that is potentially bio-available on the time frame of phytoplankton generation (days) [*Berger et al.*, 2008]) from aerosol particles over longer time scales [*Berger et al.*, 2008; *Boyd et al.*, 2010]. Reported values of the Southern Ocean fractional Fe solubility (i.e., the ratio of water leachable Fe to total Fe) range from 0.01 to 90 % [*Baker and Croot*, 2010; *Bowie et al.*, 2009; *Edwards and Sedwick*, 2001; *Heimburger et al.*, 2013a; *Mahowald et al.*, 2005]. This large range may reflect differences in mineral dust concentrations, particle size, atmospheric weathering, cloud chemistry and aerosol leaching methods [*Aguilar-Islas et al.*, 2010; *Baker and Jickells*, 2006; *Bonnet and Guieu*, 2004; *Buck et al.*, 2006; *Chen and Siefert*, 2003; *Mackie et al.*, 2005; *Meskhidze and Nenes*, 2006; *Meskhidze et al.*, 2003; *Spokes and Jickells*, 1995; *Trapp et al.*, 2010; *Zhuang et al.*, 1990; *Zhuang et al.*, 1992]. Laboratory studies have indicated that aerosol Fe solubility is enhanced by acid processing [*Desboeufs et al.*, 1999; *Spokes et al.*, 1994], although this relationship was not observed in the remote Atlantic and Pacific ocean [*Baker et al.*, 2006; *Hand et al.*, 2004]. An alternative hypothesis for the observed solubility range is that it results from a mixture of aerosol Fe source types with different mineralogy and Fe solubilities [*Sholkovitz et al.*, 2012]. *Sholkovitz et al.* [2012] show that global scale fractional aerosol Fe solubility displays an inverse hyperbolic relationship with the total Fe mass concentration. This relationship is consistent with a low Fe solubility for mineral dust (~1-2 %) and the presence of other soluble Fe sources such as those originating from fire and oil combustion with higher Fe solubilities [*Chuang et al.*, 2005; *Gao et al.*, 2013; *Guieu et al.*, 2005; *Ito*, 2011; *Kumar et al.*, 2010; *Luo et al.*, 2008; *Paris et al.*, 2010; *Sedwick et al.*, 2007; *Sholkovitz et al.*, 2009]. *Gao et al.* [2013] recently measured soluble Fe as Fe(II) in the Southern Ocean southwest of Australia and this species of Fe has been operationally defined as labile [e.g. *Chen and Siefert*, 2004]. Studies of labile Fe species (Fe(II)) over the Atlantic Ocean show that the highest percentage of labile Fe (mean value of 32 %) was observed in winter corresponding to low mass concentrations of total Fe and air mass trajectories influenced by anthropogenic activities over North America [*Chen and Siefert*, 2004]. Conversely, the lowest concentrations of labile Fe (mean value 5 %) were observed in summer with higher mineral aerosol concentrations associated with African dust.

This study reports fractional Fe solubility and estimates of the upper bound of Fe bioavailability for Southern Ocean aerosols sampled from the Cape Grim Baseline Air Pollution Station (CGBAPS) in Tasmania, Australia. Data from the aerosol samples have previously been reported with respect to lead (Pb) pollution and its source apportionment [*Bollhöfer et al.*, 2005].

5.2 Methods

5.2.1 Sampling site

This study used archived aerosol filter samples collected from February 1999 to April 2000 at CGBAPS (40.68° S, 144.69° E), located at the northwest tip of Tasmania, Australia (Fig. 5.1). Fractions of filters were previously studied for Pb isotopic composition and are described in detail by *Bollhöfer et al.* [2005]. Samples were collected during baseline conditions using a sector-controlled ultra-trace clean aerosol filter system suspended 70 m above the ground (164 m a.s.l.) on a communication tower (~100 m from the ocean, adjacent to 94 m high coastal cliffs). Meteorological baseline air conditions for CGBAPS are described by *Ayers et al.* [1987] and occur when the winds are from the west to southwest (wind direction from 190 to 280º (Fig. 5.1) and total aerosol particle counts are <600 cm3. These conditions occur ~30 % of the time [*Keywood*, 2007] and are representative of air masses over the remote Southern Ocean.

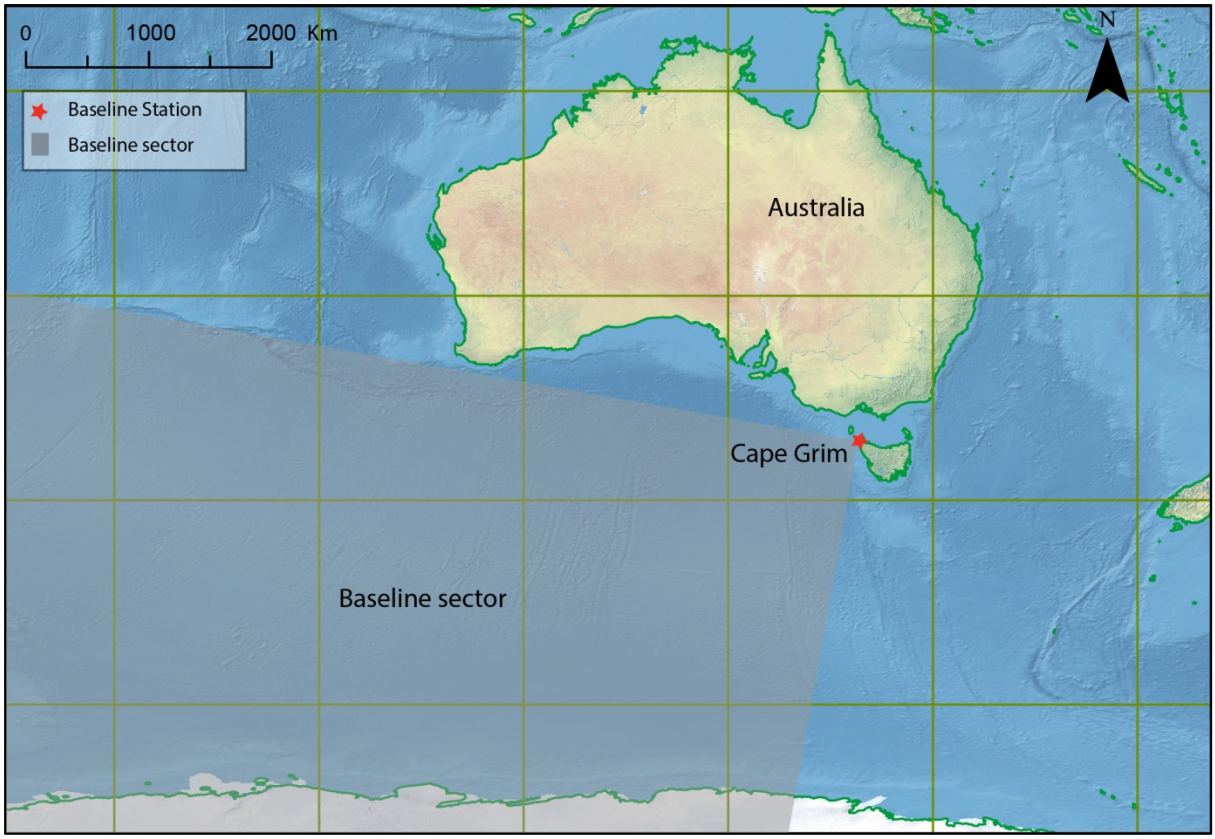

Fig. 5.1: Map of Australia and the Southern Ocean highlighting the baseline sector associated with CGBAPS. http://www.sciencedirect.com/science/article/pii/S0304420315001218

5.2.2 Sample collection

Stringent trace-metal clean techniques were used throughout the sampling campaign [*Bollhöfer et al.*, 2005]. Briefly, aerosols were collected on 47 mm acid-cleaned polytetrafluoroethylene (PTFE) filters (0.45 µm front, 60 µm back) in single-stage perfluroalkoxy alkane (PFA) filter assemblies (acid-cleaned). The filter assembly housing consisted of trace-metal clean cylindrical inlet units, with a baseline sector controlled pump at the tower base and a pneumatically actuated seal on the top of the inlet unit. The samples were collected over time periods varying from one to seven weeks. Exposure blanks (n = 5), collected with every 3rd to 4th sample, were run as for normal samples but the pump switched off [*Bollhöfer et al.*, 2005]. These exposure blanks were used to determine the Fe contribution from sampling, laboratory procedures and analysis. Air volumes were measured using a calibrated gas flow meter. Thirteen cryogenically archived (-18 ºC) filter sub-samples (Table S5.1) from the *Bollhöfer et al.* [2005] study were used in this work to investigate the aerosol Fe mass concentration and fractional Fe solubility.

5.2.3 Partial filter sizing

During the original study, the filters were cut into halves or quarters with an acid cleaned stainless steel scalpel blade [*Bollhöfer et al.*, 1999; *Bollhöfer et al.*, 2005]. These filter sub-samples were the focus of this aerosol Fe study. Filter samples were visually inspected in a laminar flow hood under clean-room conditions with minimal handling.

5.2.4 Aerosol iron leaching experiments

All bottles and filtration parts used in the Fe leaching experiments were acid-cleaned following GEOTRACES protocols [*Cutter et al.*, 2010]. Leaching experiments were conducted sequentially using a trace metal clean flow-through reactor (Fig. 5.2) [e.g. *Aguilar-Islas et al.*, 2010; *Wu et al.*, 2007]. This reactor consisted of the sub-sampled filter supported on acid-cleaned 0.45 µm backing filter that was mounted in a single-stage PFA filter assembly with a PFA funnel front face. Leaching solutions were pulled through the reactor under vacuum, into 250 ml low-density polyethylene bottles (LDPE). The PTFE filters were hydrophobic and required exposure to high-purity methanol to initiate water flow. Prior to the leaching experiments, the system was rinsed with several litres of ultra-pure water (>18 Mohm-cm) and ultra-pure 1 % HCl (baseline Seastar), followed by another ultra-pure water rinse.

5.2.4.1 Soluble iron

The instantaneous water soluble Fe fraction (Fig. 5.2) was investigated using two successive 50 ml aliquots ("a" and "b") of ultra-pure water. The mean procedural blank (n=10) for this Fe fraction was 0.07 ± 0.005 nmol g^{-1} of soluble Fe. The mean exposure blank (n=5) was 0.1 ± 0.003 nmol g^{-1} of soluble Fe. The mean ultra-pure water blank (n=5) was 0.001 ± 0.002 nmol g^{-1}. On average 90 % of the water soluble Fe was leached in the first leach. Other ultra-pure water leaching schemes using multiple leaches have shown that the concentration of soluble Fe exponentially decreases with each successive water leach [e.g. *Buck et al.*, 2006]. Thus, even the small volume of leaching solution in the first leach will have captured the majority of instantaneous water soluble Fe.

5.2.4.2 Labile iron

The method of *Berger et al.* [2008] was used to determine the labile Fe fraction (Fig. 5.2) of the aerosol samples. A similar weak acid leaching method to determine labile Fe in aerosols was carried out by *Chen and Siefert* [2003]. The *Berger et al.* [2008] method uses an acetic acid (HAc) and hydroxylamine hydrochloride ($NH_2OH \cdot HCl$) leach to determine the reactive Fe fraction. A similar method was used in this study with the exception that the filters were water leached prior to exposure to HAc and $NH_2OH \cdot HCl$. In this study, the water leached filters were placed in acid-washed vials, dried under a laminar flow hood and leached with 25 % ultra-high purity HAc (Seastar Baseline® 99.9%, <20 ppt Fe) and 0.02 M $NH_2OH \cdot HCl$ (Acros Organics, Belgium, 99 %) at 90 °C for 10 minutes. The short heating step of 90 - 95 °C is used to access metals found in intracellular proteins that are associated with phytoplankton [*Berger et al.*, 2008; *Hurst and Bruland*, 2007]. This leaching method liberates trace metals associated with biogenic material, Fe and manganese oxyhydroxides and metals that may be adsorbed onto the surface of aluminosilicate clay minerals. Windblown diatoms have been observed in high elevation ice cores significantly inland from the ocean (Burckle et al., 1988). Thus, the possibility that phytoplankton cells are transported in baseline marine air masses cannot be ruled out, although we acknowledge that they most likely constitute a relatively minor mass of the total aerosol loading. The mean labile procedural blank (n=5) and exposure blank (n=5) concentrations were 0.03 ± 0.003 and 0.8 ± 0.07 nmol g^{-1} of Fe, respectively. Two exposure blanks were found to have exceptionally high labile Fe concentrations possibly from random contamination (water solubility associated with those exposure blanks did not have high values). Excluding these two high values, exposure blanks averaged 0.2 ± 0.001 nmol g^{-1} of Fe, comparable to the labile procedural blank and water soluble exposure blank concentrations. This blank value was used in labile Fe calculations.

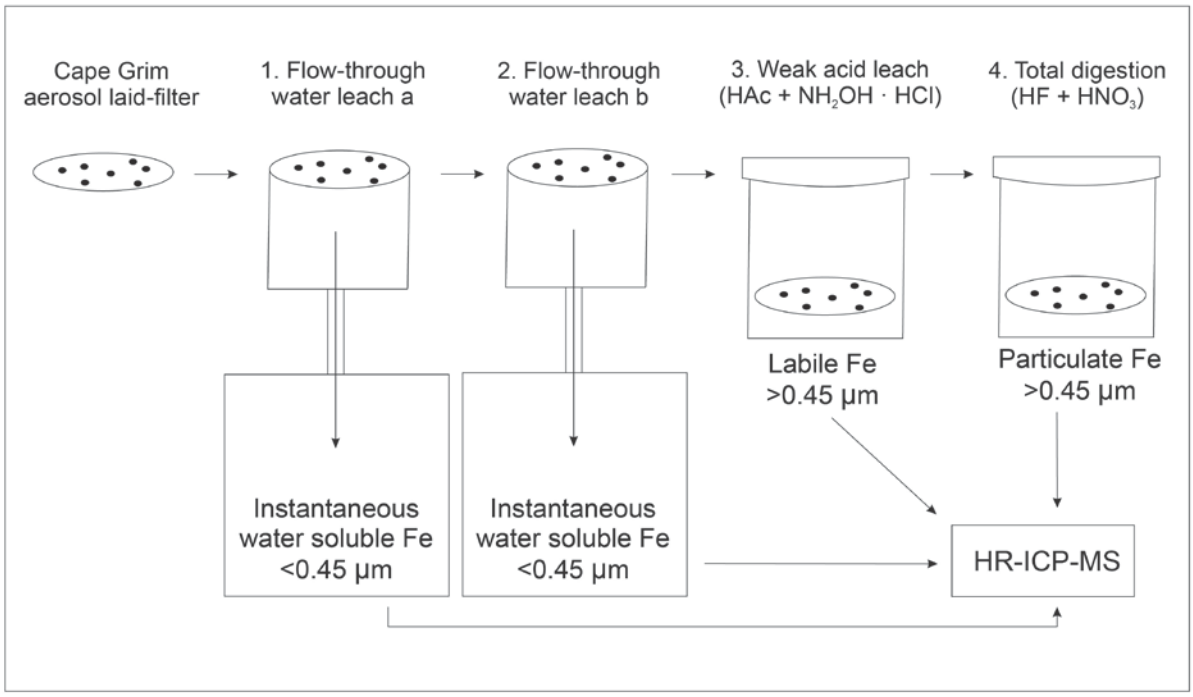

Fig. 5.2: Schematic showing the different extraction stages to leach soluble, labile and refractory iron from Cape Grim marine aerosols. **http://www.sciencedirect.com/science/article/pii/S0304420315001218**

5.2.4.3 Refractory iron

The refractory Fe fraction (>0.45 µm) was determined following recommendations from the 2008 GEOTRACES intercalibration experiment for the analysis of marine aerosols [*Morton et al.*, 2013]. All digestions were carried out under high-efficiency particulate arrestance (HEPA) filtered air, in a total-exhausting clean-air (ISO Class 5), hot block unit (SCP Science, Canada) fitted with an acid scrubber unit. The leached sample filters and filter blanks were digested at 95 ºC for 12 hours with concentrated ultra-pure nitric acid (HNO_3, 0.5 ml, Seastar Baseline®) and ultra-pure hydrofluoric acid (HF, 0.5 ml, Seastar Baseline®) in capped PFA vials (15 ml, Savillex) following *Bowie et al.* [2010]. At the end of the digestion, the samples were evaporated to dryness, reconstituted in 1 % ultra-pure HNO_3 (10 ml final volume, Seastar Baseline®) and stored at 25 ºC for ~12 hours before analysis. A certified reference material (MESS-3, National Research Council, Canada) of marine sediment was digested alongside the samples to test the digestion recovery procedure. Total digestion recovery for Fe from the CRM was ~90 ± 1.2 % (n=3). Mean refractory procedural blank (n=3) and exposure blank (n=5) concentrations were 0.2 ± 0.01 nmol g^{-1} of Fe and 1.0 ± 3.7 nmol g^{-1} of Fe respectively. Two filter blanks were found to have high Fe levels (8.0 nmol g^{-1}

and 1.7 nmol g^{-1} of Fe). The digestion of aerosol filters using concentrated HNO_3 and HF at 95 °C could have leached out additional impurities in the PTFE filter than the *Bollhöfer et al.* [1999] acid cleaning step employed specifically for Pb analysis. Therefore, the high blank levels possibly resulted from a lack of exposure of HF to the PTFE filter substrate prior to sampling [*Bollhöfer et al.*, 1999].

5.2.4.4 Total iron

The total Fe loading of the filters was estimated as the sum of the individual Fe fractional masses from each step and is given in equations (5.1) to (5.3).

$$Water\ soluble\ Fe = water\ soluble\ Fe\ leach\ \text{a} + water\ soluble\ Fe\ leach\ \text{b}$$

Equation (5.1)

$$Bioavailable\ Fe = water\ soluble\ Fe + labile\ Fe$$

Equation (5.2)

$$Fe\ total = bioavailable\ Fe + refractory\ Fe$$

Equation (5.3)

5.2.5 Iron determination by Sector-Field Inductively Coupled Plasma Mass Spectrometry

All samples and standards were prepared on a similar matrix basis. Water soluble Fe leachates and total digestion solutions were acidified to 1 % (v/v) with ultra-pure HNO_3 (Seastar Baseline®) and spiked with an Indium (In) internal standard. Labile leachates were diluted, and spiked with In and presented to the instrument as a 2.5 % (v/v) HAc and 0.02 M NH_2OH HCl solution and 1 % (v/v) ultra-pure HNO_3 (Seastar Baseline®). The analysis of the water soluble and labile Fe leachate fractions occurred within 24 hours of leaching. All samples were analysed by sector-field inductively coupled plasma mass spectrometry (SF-ICP-MS, Thermo Fisher Scientific ELEMENT 2) at the University of Tasmania. Samples were introduced using an auto-sampler housed in a laminar flow clean-air hood. Typical operating conditions are reported in Table S5.2. Isobaric ^{56}Fe interferences (e.g. $^{40}Ar^{16}O$ and $^{40}Ca^{16}O$) were resolved using a mass resolution of >4000 amu (10 % valley definition, medium resolution). Instrumental blanks (1 % HNO_3 and 2.5 % (v/v) HAc and 0.02 M $NH_2OH \cdot HCl$) and a QC standard were measured throughout the analysis sequence at regular intervals. Internal standard normalised ^{56}Fe intensities were quantified using "matrix

matched" external standards prepared by serial dilution from traceable commercial primary standards. The results were blank subtracted and corrected for dilution.

5.2.6 Major cation and anion

Major cation and anion measurements for the period between January 1999 and August 2000 have previously been reported in *Keywood et al.* [2004], and we use the sodium, sulfate and nitrate data here. Oxalate, not previously reported, was also measured in these samples following the same procedure. The major ion data were obtained using a "Goldtop sampler" installed with a PM10 (particle diameter <10 µm) inlet at CGBAPS [*Ayers et al.*, 1990]. Particles were collected on Pallflex filters (EMSB TX 4OH, 120-WW) on a weekly basis. The filter was wetted with methanol before being extracted in 5 ml of ultra-pure water. The sample was then preserved using 1 % chloroform. Anion and cation concentrations were determined by suppressed ion chromatography (IC) using a Dionex DX500 gradient ion chromatograph. Anions were determined using an AS11 column and an ASRS ultra-suppressor. Cations were determined using a CS12 column and a CSRS ultra-suppressor.

5.3 Results

5.3.1 Aerosol iron mass concentrations

Baseline aerosol concentrations for the different Fe fractions were estimated from the filters by equation 5.4 (assuming a uniform aerosol loading of the filters) and are summarised in Table 5.1.

$$Aerosol\ concentration = \frac{Fe\ fraction\ mass * filter\ sub\ sample\ fraction}{air\ volume\ (m^3,\ \ standard\ temperature\ and\ pressure\ )}$$

Equation (5.4)

With the exception of sample CG5 (4-16 March 1999), extremely low total Fe aerosol mass concentrations, compared to other aerosol Fe studies on a global scale [*Sholkovitz et al.*, 2012], were found and ranged from 0.034 to 5.86 ng m^{-3}. Sample CG5 sampled only 5 m^3 of air but displayed total Fe aerosol concentrations 25 times greater (147.81 ng m^{-3}) than the next largest aerosol sample. This sample was almost entirely comprised of refractory Fe and

may have been exposed to local (non-baseline) air. The sample was subsequently excluded from the estimates and further discussion.

Table 5.1: Fractional aerosol iron concentrations in Southern Ocean baseline air.

Fe Fraction	Range ($ng\ m^{-3}$)	*Geometric mean ($ng\ m^{-3}$)
Total Fe	0.04 to 5.8	0.8
Refractory Fe	<0.02 to 5.7	0.2
Labile Fe	0.01 to 4.6	0.1
Soluble Fe	0.01 to 0.3	0.07

*n=13

5.4.2 Aerosol iron fractions

The range and geometric mean for the different fractions are shown in Table 5.1. The total Fe geometric mean mass concentration of 0.77 ng m^{-3} was ~11 times that of soluble Fe (0.07 ng m^{-3}), ~4.8 times the labile Fe (0.16 ng m^{-3}) and ~3.1 times the refractory Fe (0.24 ng m^{-3}) mass concentrations. Fractional estimates relative to total Fe ranged from 0.5 % to 56 % for soluble Fe, 1.5 % to 94.0 % for labile Fe, and 4.6 % to 97.0 % for refractory Fe. The order of the geometric mean fractional estimates was soluble Fe (15 %) < labile Fe (32 %) < refractory Fe (48 %).

5.3.3 Atmospheric iron dry deposition flux estimates

Estimates of the Fe dry deposition rate (F_{dry}) to adjacent Southern Ocean surface waters were calculated using equation 5.5 from the total and soluble aerosol Fe concentrations ($C_{aerosol}$) using a dry deposition velocity (V_{dry}) of 1.3 cm s^{-1} [*Ezat and Dulac*, 1995] following *Heimburger et al.* [2012], and are reported in Table 5.2. This deposition velocity is based on the dry deposition model of *Slinn and Slinn* [1980] following the "100-step method" [*Dulac et al.*, 1989] which takes into consideration the size dispersion of particles. We assume a constant deposition velocity is appropriate for the Southern Ocean, as i) the particle size has a narrow size distribution and thus the dry deposition fluxes will exhibit little variability compared to a wide particle size distribution [*Arimoto et al.*, 1985], and ii) the mean wind speeds at Cape Grim have little temporal variability. Furthermore, *Duce et al.* [1991] report deposition velocities of 0.4 cm s^{-1} for the open ocean and 2 cm s^{-1} for coastal regions and the value of 1.3 cm s^{-1} is within this range.

$$F_{dry} = C_{aerosol} * V_{dry\ deposition}$$ Equation (5.5)

Table 5.2: Dry deposition iron fluxes of Southern Ocean baseline air.

Sample	Soluble Fe concentration (ng m^{-3})	*Soluble Fe flux (nmol m^{-2} d^{-1})	Total Fe concentration (ng m^{-3})	*Total Fe flux (nmol m^{-2} d^{-1})
CG4	0.55 ± 0.04	11 ± 6	1.9 ± 0.1	38 ± 20
CG9	0.17 ± 0.01	3.3 ± 2	0.76 ± 0.02	15 ± 8
CG10	0.34 ± 0.03	6.8 ± 3	5.1 ± 0.2	100 ± 50
CG14	0.01 ± 0.01	0.17 ± 0.1	1.8 ± 0.06	36 ± 20
CG15	0.07 ± 0.01	1.4 ± 0.7	0.26 ± 0.01	5.2 ± 3
CG17	0.04 ± 0.01	0.76 ± 0.4	0.28 ± 0.01	5.7 ± 3
CG18	0.08 ± 0.01	1.7 ± 0.9	0.33 ± 0.01	6.7 ± 3
CG26	0.01 ± 0.01	0.3 ± 0.2	0.68 ± 0.02	14 ± 7
CG28	0.01 ± 0.01	0.14 ± 0.1	0.04 ± 0.00	0.75 ± 0.4
CG23	0.08 ± 0.01	1.7 ± 0.8	5.8 ± 0.2	120 ± 60
CG35	0.25 ± 0.01	5.1 ± 3	0.45 ± 0.01	9.0 ± 5
CG37	0.09 ± 0.01	1.7 ± 0.9	1.4 ± 0.04	27 ± 10
CG40	0.06 ± 0.01	1.3 ± 0.6	1.3 ± 0.04	27 ± 10

*The uncertainty in dry deposition fluxes was calculation by propagation of error of the analytical uncertainty and uncertainty in the deposition velocity assumed to be 50 %.

5.4 Discussion

5.4.1 Baseline iron mass concentrations

Atmospheric Fe mass loadings from 1999 to 2000 are shown in Fig. 5.3a-3d. Total Fe displayed maximum concentrations during May/June 1999 and November 1999 with peak Fe mass concentrations of 5.15 ng m^{-3} and 5.86 ng m^{-3}, respectively. The lowest concentrations occurred from August to November 1999 (austral winter/spring), with a minimum mass concentration of 0.034 ng m^{-3}. The total Fe mass concentrations are amongst the lowest Fe mass concentrations reported in the literature. For example, *Bowie et al.* [2009] reported total Fe mass concentrations between 5 and 17 ng m^{-3} for marine aerosols collected in a similar region south of Tasmania but sampling all wind sectors. A global compilation of the total aerosol Fe mass data suggests concentrations can reach up to 147 ng m^{-3} for the Southern Hemisphere (Fig. 5.4) [*Sholkovitz et al.*, 2012]. Baseline total aerosol Fe mass loadings are similar to those reported for Syowa Station, coastal East Antarctica [*Kobayashi et al.*, 2010]. However, they are lower than estimates over the southwest Australian sector of the Southern

Ocean and coastal East Antarctica which average 19 ng m^{-3} and 26 ng m^{-3} respectively [*Gao et al.*, 2013]. The authors suggest that the air masses over coastal East Antarctica are influenced by local Antarctic dust, as the total aerosol Fe concentrations were higher than the Southern Ocean, and the aerosols have a coarse particle size distribution.

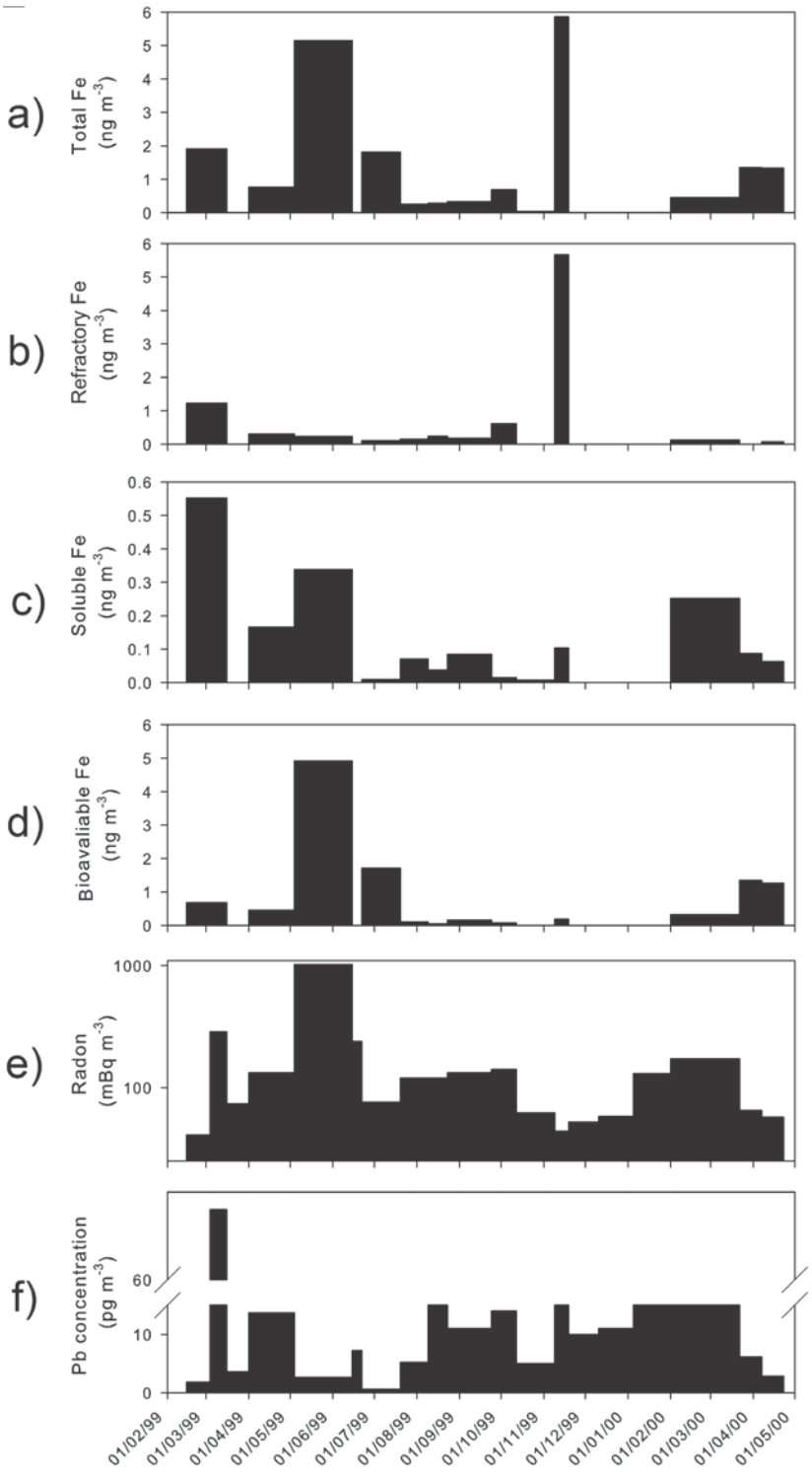

Fig. 5.3: Time series of aerosol Fe mass concentrations excluding CG5. a) Total Fe concentration, b) refractory Fe concentration, c) soluble Fe concentration, d) bioavailable Fe concentration (i.e., the sum of soluble and labile Fe fractions), e) radon concentration [data source: *Bollhöfer et al.*, 2005], and f) Pb concentration [data source: *Bollhöfer et al.*, 2005].
http://www.sciencedirect.com/science/article/pii/S0304420315001218

While the two total Fe peaks were similar with respect to mass concentration, they displayed different characteristics with respect to the leached Fe fractions suggesting different sources and bioavailability. For example, the May/June 1999 Fe peak was primarily composed of labile Fe (~90 %) with little refractory Fe (Fig. 5.3). Conversely, the November 1999 total Fe peak was comprised primarily of refractory Fe, however the contribution of labile Fe to the bioavailable Fe fraction was relatively minor compared to the water soluble contribution. Thus, while the total Fe mass concentrations were similar, the potential bioavailability of the Fe represented by the two peaks was not. The May/June peak was associated with a peak in radon (Fig. 5.3e) reported by *Bollhöfer et al.* [2005]. Radon is emitted from crustal materials and has a relatively short half-life (3.8 days) making it useful as a tracer of continental air masses [*Porstendorfer et al.*, 1994; *Zahorowski et al.*, 2004]. Air mass back trajectories reported by *Bollhöfer et al.* [2005] combined with the radon data suggest that the labile Fe peak is related to atmospheric transport over South Western Australia.

The highest soluble Fe mass concentrations occurred in February-March 1999 (0.55 ng m^{-3}) and February-March 2000 (0.25 ng m^{-3}; Fig. 5.3a). However, the soluble Fe concentrations exhibited an extremely low geometric mean soluble Fe concentration of 0.07 ng m^{-3} for the entire data set. These soluble Fe concentrations in baseline air are lower than those reported as Fe(II) for the southwest Australian sector of the Southern Ocean and coastal East Antarctica that range from 0.13 - 1.3 ng m^{-3} [*Gao et al.*, 2013]. Variability in soluble Fe, in this study, essentially tracked the radon concentrations demonstrating a link with continental air masses (Fig. S5.1a). These radon episodes (Fig. 5.3e) occurred during baseline intervals in May/June 1999, August/October 1999 and January/April 2000 [*Bollhöfer et al.*, 2005]. Not surprisingly these time periods encompass the highest Pb concentrations (Fig. 5.3f) reported by *Bollhöfer et al.* [2005] which further highlights the link between soluble Fe and continental air masses and potentially anthropogenic emissions.

While, the variability between the labile and soluble Fe with the *Bollhöfer et al.* [2005] radon and Pb data seemed consistent, the refractory Fe variability bore little resemblance to these time series. The independence of the refractory Fe from the other Fe fractions and radon data was unexpected and difficult to rationalise. For example, the highest refractory Fe concentration occurred during November 1999, coincident with low radon concentrations. A plausible explanation is that this peak was due to local material blown up to the tower from the cliff face rather than long range transport aerosol. A single mineral grain could

contaminate these low concentration samples. However, based on the sample's aerosol Fe mass concentration the data appears uncontaminated by sampling and handling procedures. *Bollhöfer et al.* [2005] ruled out local soil dust contamination in these aerosol samples by comparing the Pb isotopic composition of the aerosols with that of local soil. Nevertheless, as discussed in the results section, a filter sample from March 1999 was excluded from further assessment due to suspected contamination from local mineral dust sources. If the November 1999 data point is similarly excluded from the interpretation, the refractory Fe variability becomes similar to the soluble Fe and consistent with the radon data (Fig. S5.1b).

5.4.2 Dry deposition estimates of soluble and total iron

Crude estimates of soluble and total Fe dry deposition fluxes associated with the aerosol samples are reported in Table 5.2 and range from 0.1 ± 0.07 to 7 ± 3 nmol m^{-2} d^{-1} for soluble Fe and 0.8 ± 0.4 to 116 ± 60 nmol m^{-2} d^{-1} for total Fe over the period April 1999 to March 2000. This period was considered to include samples collected with the largest volumes of air over an entire 12 month period, and also closely aligns with the work of *Bollhöfer et al.* [2005] allowing comparison with their Pb data. The Fe flux estimates for baseline air over Southern Ocean in this study are compared to other aerosol studies from the Southern Ocean. The mean soluble Fe flux (~2 ± 1 nmol m^{-2} d^{-1}) is in good agreement with fluxes of 2.4 - 7.4 nmol m^{-2} d^{-1} reported by *Bowie et al.* [2009], 0.04 - 3.2 nmol m^{-2} d^{-1} reported by *Wagener et al.* [2008], and 1.8 - 7.3 nmol m^{-2} d^{-1} reported by *Baker et al.* [2013] for the South Atlantic. The estimates in this study are lower than those reported at Kerguelen Island, Southern Ocean (400 nmol m^{-2} d^{-1}) where local dust influences the aerosol sample [*Heimburger et al.*, 2013b]. Estimates in baseline air may be more representative of the broader Southern Ocean region south of Australia, as the marine air was collected at a higher elevation above the boundary layer and at a site free from local pollution. Estimates of total Fe dry deposition at CGBAPS are significantly lower than those estimated at Kerguelen Island (500 - 700 nmol m^{-2} d^{-1}) [*Heimburger et al.*, 2013b], at Crozet Island (900 nmol m^{-2} d^{-1}) [*Planquette et al.*, 2007], and in the South Atlantic (100 – 300 nmol m^{-2} d^{-1}) [*Baker et al.*, 2013]. *Heimburger et al.* [2012] suggest dust fluxes during 2009-2010 were higher during winter and spring, and that the aerosols were crustal in origin. Whereas *Heimburger et al.* [2013b] showed no seasonal variability in aerosol Fe, they did find an anthropogenic contribution to the Southern Ocean during winter as shown by elevated elemental concentrations of Pb, As, Cr, Cu, and V.

5.4.3 Fractional iron solubility

The baseline fractional Fe solubility ranged from 0.5 % to 56 % during the study. Estimates of fractional Fe solubility in the South Atlantic are within this range (2.4 % to 20 %) [*Baker et al.*, 2013]. The lowest values (0.5 % to ~3 %) at CGBAPS were comparable to the low Fe solubility (1 to 2 %) reported for mineral dust [e.g. *Baker and Croot*, 2010] at relatively high mass concentrations. Furthermore, the low fractional Fe solubility (0.58 % to 6.5 %) measured as Fe(II) over the southwest Australian sector of the Southern Ocean is thought to be influenced by local Antarctic dust sources [*Gao et al.*, 2013]. Mineral dust from Patagonia is also known to be transported into the southern South Atlantic Ocean and on the Antarctic Plateau [*Delmonte et al.*, 2008; *Gaiero et al.*, 2007; *Gaiero et al.*, 2003]. Similar to *Sholkovitz et al.* [2012], the data in this study displayed an inverse hyperbolic relationship (Fig. 5.4a) between the total Fe mass concentration and fractional Fe solubility. This relationship has been attributed to the mixing of low Fe solubility mineral dust and other soluble Fe aerosols from sources such as biomass burning and oil combustion [*Sedwick et al.*, 2007]. *Sholkovitz et al.* [2012] reported a synthesis of global aerosol Fe solubility data sets and concluded that the characteristic inverse hyperbolic relationship is common over large regions of the global ocean. Results here are different to other Southern Ocean data, i.e., at the 1 - 2 % fractional Fe solubility limit of mineral dust, the total Fe mass concentrations are very low (<6 ng m^{-3}) compared to the rest of the Southern Ocean where they have been observed up to 140 ng m^{-3}. This aspect of the data may be explained by a lack of both mineral dust and other soluble Fe sources, such as biomass burning, in the exceptionally clean baseline air. Alternatively it is possible that the long cryogenic storage of the aerosol filters resulted in lower concentrations of instantaneously soluble Fe. *Jeong et al.* [2012] found that the dissolution of iron oxides was enhanced during freezing of aqueous dispersions of Fe oxides. However, the aerosol filters used in this study were stored frozen in a dark and dry environment and are not directly comparable. However, aerosols are archived in ice cores for comparatively longer time periods (e.g. 1 to 1000 years), and Fe solubility studies of ice cores have been used to estimate Fe fluxes and bioavailability. With regards to the instantaneous solubility, Antarctic ice core leaching studies in dilute hydrochloric acid and nitric acid [*Edwards and Sedwick*, 2001; *Edwards et al.*, 2006; *Gaspari et al.*, 2006; *Koffman et al.*, 2014a] show that a large portion of the Fe bound in frozen mineral particles are not soluble and require up to three months to leach into solution. Furthermore, fractional Fe solubility estimates reported here are within the range of those reported for other studies [e.g. *Baker and Croot*, 2010] and in

particular for aerosols sampled in the Southern Ocean south of Tasmania (Fig. 5.4a) [*Bowie et al.*, 2009].

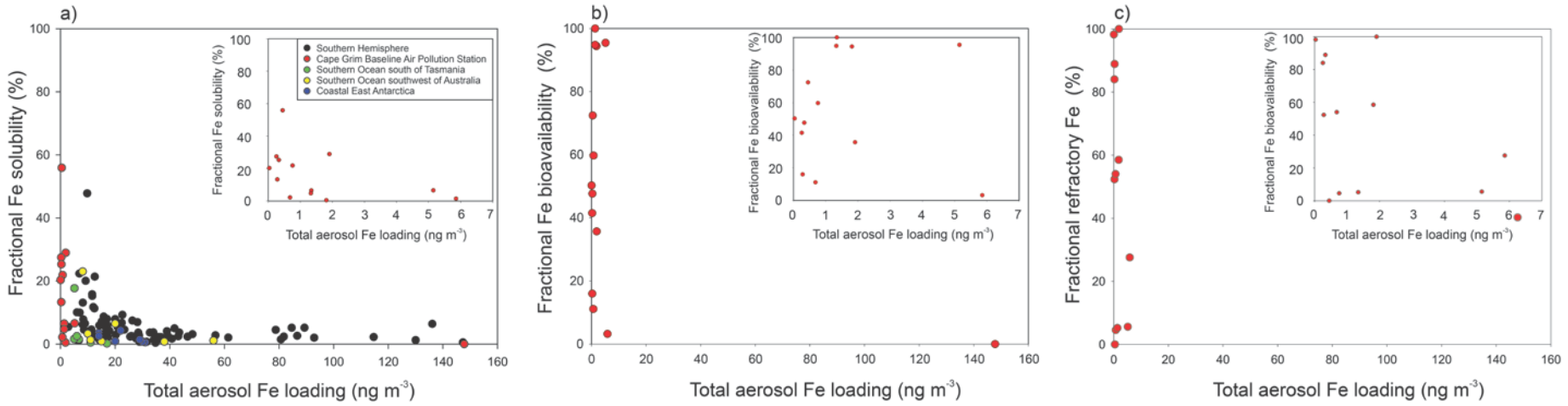

Fig. 5.4: a) Cape Grim total aerosol Fe mass concentration versus fractional Fe solubility superimposed upon Southern Hemispheric data set (data source: Bowie et al., 2009; Sholkovitz et al., 2012; Gao et al., 2013). Top right insert: Cape Grim data expanded excluding CG5 that sampled a low volume of air. b) Cape Grim total aerosol Fe mass concentration versus fractional Fe bioavailability. c) Cape Grim total aerosol Fe mass concentration versus fractional refractory Fe. http://www.sciencedirect.com/science/article/pii/S0304420315001218

5.4.4 Estimates of iron bioavailability

In order to determine the upper bound of bioavailable trace metals in seawater sourced from atmospheric particles, measurement of both the soluble and labile fractions are necessary [*Berger et al.*, 2008]. Commonly used instantaneous water leaching schemes have been suggested to underestimate the fraction of Fe that dissolves in the oceanic mixed layer, as they do not take into account the longer residence time of aerosols in the euphotic zone. Thus, an additional leach is needed to estimate the longer-term release of Fe from atmospheric particles during their residence time in the surface ocean mixed layer [*Boyd et al.*, 2010]. This study followed the *Berger et al.* [2008] rationale to estimate the fraction of labile Fe in aerosols. The heating step in this method may overestimate the labile fraction of Fe in aerosols, causing dissolution of Fe that would normally have low bioavailability. Iron solubility increases with temperature [*Schwertmann*, 1991], and thus the heating step may recover more Fe than the intracellular fraction alone. Despite this, leaching schemes employed to access the labile Fe pool are operationally defined. They are designed to mimic biological processes that take time, but do so in a much shorter and practical timescale in the laboratory. Currently, no leaching scheme takes into account all processes affecting the bioavailability of Fe upon its deposition in the upper water column. For example, grazing is known to impact the bioavailability of Fe contained in particles [*Barbeau et al.*, 1996]. Other studies have indicated that the conversion of Fe from particle to dissolved phase in seawater can take place due to photochemistry [*Croot et al.*, 2008; *Ellwood et al.*, 2015]. Recently, *Lis et al.* [2015] observed a relationship between the uptake rate constant of Fe and the surface area of several phytoplankton species. An upper limit to the rate at which Fe-limited phytoplankton can uptake Fe suggests that alternative uptake mechanisms are an advantage in Fe-limited waters, such as a reduction in cell size, or the utilization of Fe from the colloidal or particulate fraction [*Nodwell and Price*, 2001; *Rubin et al.*, 2011]. Colloidal Fe has been found to be an important fraction of the bioavailable Fe pool [*Aguilar-Islas et al.*, 2010; *Kuma and Matsunaga*, 1995], and further research is required to estimate this fraction over the Southern Ocean.

The leaching scheme used in this study mimics the bi-modal release of Fe, i.e., i) instantaneous soluble Fe and ii) longer term dissolution that is mediated by microbes and/or ligands and photochemistry in the surface mixed layer [*Wagener et al.*, 2008; *Wuttig et al.*, 2013], thereby allowing an estimate of the upper limit of Fe bioavailability over the Southern

Ocean. Fractional bioavailable Fe was calculated by summing the fractional Fe solubility and fractional Fe lability (equation 5.3). Fractional Fe bioavailability ranged from 3 to 100 % of the total Fe (Fig. 5.4b). More bioavailable Fe data is required to investigate the relationship between the total Fe mass concentration and fractional Fe bioavailability and mixing of mineral dust versus combustion aerosol sources (Fig. 5.4b).

New aerosol Fe supply by dry deposition to the Southern Ocean and the fractions of Fe (soluble, labile, bioavailable and refractory) that are leached from the aerosols upon deposition into surface waters is illustrated in Fig. 5.5. No wet deposition data is available at the CGBAPS, however estimates of Fe concentrations in rain at Kerguelen Island suggest a concentration of 17 to 32 µg m^{-2} with a fractional Fe solubility of ~70 % in rain water [*Heimburger et al.*, 2013a]. Wet deposition fluxes of 5.4 to 231 nmol m^{-2} d^{-1} of soluble Fe and 41-1100 nmol m^{-2} d^{-1} of total Fe for the South Atlantic have been estimated by *Baker et al.* [2013], and significantly higher wet deposition fluxes of 3700 µmol m^{-2} d^{-1} for the New Zealand region of the South Pacific westerlies have been estimated by *Halstead et al.* [2000]. Half of the upper bound of mean fractional Fe bioavailability (50 %) from dry deposition at CGBAPS could potentially be bio-available, while the other half is refractory or insoluble and is presumably lost from the surface ocean via settling (Figs. 4c and 5). Aerosol particles associated with instantaneous soluble Fe (i.e., <0.4 µm) will reside in the mixed layer for a time period on the order of years, assuming the mixed layer is between 50 and 200 m [*Bowie et al.*, 2011] and particles with a diameter of 0.4 µm have a settling velocity of 9.5 x 10^{-6} cm s^{-1} [*Gibbs et al.*, 1971]. The residence time of aerosol particles associated with labile Fe is orders of magnitude shorter, and may range between days and weeks (assuming labile Fe over the Southern Ocean range between 0.4 and 5 µm [*Delmonte et al.*, 2002; *Delmonte et al.*, 2013; *Koffman et al.*, 2014b], and this particle size range has a settling velocity between 9.5 x 10^{-6} cm s^{-1} and 1.5 x 10^{-3} cm s^{-1} [*Gibbs et al.*, 1971]). We acknowledge that processes in the ocean can alter sinking rates, such as aggregation of colloids. Moreover, particle dimensions can change, for example with bacterial attachment [*Yamada et al.*, 2013]. Labile Fe comprises a large component of total Fe, and this fraction may be slowly released from aerosol particles into the surface mixed layer. Estimates of labile Fe and water soluble Fe, in this study, represent an upper bound of the potential bioavailability of Fe deposited to Southern Ocean. The majority of estimates over the Southern Ocean are based on soluble Fe fractions alone and do not take into consideration labile Fe.

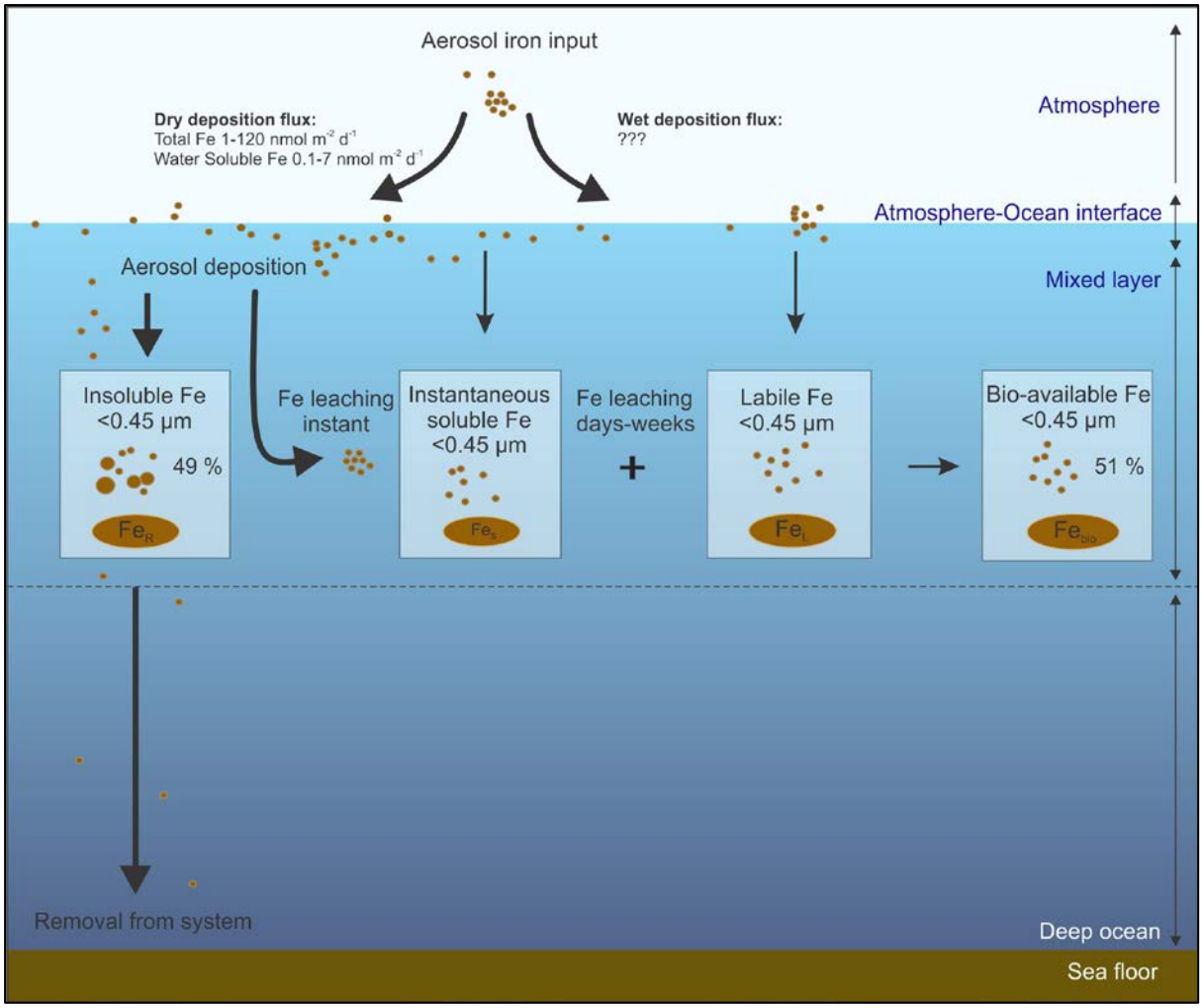

Fig. 5.5: Schematic of aerosol iron fractions that are potentially bioavailable for uptake by plankton in the Southern Ocean. Fe_R: refractory Fe, Fe_S: soluble Fe, Fe_L: labile Fe, Fe_{BIO}: bioavailable Fe. **http://www.sciencedirect.com/science/article/pii/S0304420315001218**

The estimates of bioavailable Fe reported here are relatively high and represent an upper bound of Fe bioavailability over the Southern Ocean. Several factors could account for the high Fe bioavailability found at CGBAPS. Aerosol Fe solubility could be enhanced by cloud chemistry and acid processing [*Desboeufs et al.*, 1999; *Kumar et al.*, 2010; *Meskhidze et al.*, 2003; *Spokes et al.*, 1994], and these processes may play a role in the lability of long range transport aerosol Fe over the Southern Ocean. We compare our fractional Fe bioavailability data to non-sea salt (nss)-sulfate and nitrate aerosol measurements made at CGBAPS [*Keywood et al.*, 2004] (Fig. 5.6a-d). No significant relationship was found between the acid species and fractional Fe bioavailability during the short time series at CGBAPS. However, in February-March 2000 water soluble Fe made a large contribution to the bioavailable Fe pool (Fig. 5.6a-b), at a time of high nitrate and nss-sulfate concentrations. During this period,

sodium was exceptionally high (Fig. 5.6g), suggesting the marine aerosol was comprised primarily of sea salt (Mg, K, Cl, and Ca concentrations were also high [*Keywood et al.*, 2004]. During this sampling period the average baseline wind speed measured at 10 m of 13. 8 m s^{-1} was in the 89^{th} percentile of wind speeds recorded for the period 1998-2005). No relationship between these acid species and fractional Fe solubility was found in other field studies in the remote Atlantic and Pacific Ocean [*Baker et al.*, 2006; *Hand et al.*, 2004]. *Baker et al.* [2013] suggest that the lack of correlation in real samples could be due to a low degree of internal mixing in the aerosol samples rather than due to the lack of acid influence on Fe solubility. Either, the enhancement of Fe bioavailability by acid processing on the surface of the aerosol is not a significant process in the atmosphere over the Southern Ocean, or that it has not occurred in the samples collected in this study because the acidic and Fe-laden aerosol fraction are not in contact with each other, or that our time series is too short to see any relationship, or that the high fractional Fe solubility observed in one sample is related to a large volume of sea salt derived air masses during a particularly strong storm event.

Recently, Fe solubility has been investigated in relation to carboxylic acids, whereby oxalate was most effective at enhancing the fractional Fe solubility in mineral dust [*Paris and Desboeufs*, 2013; *Paris et al.*, 2011]. *Paris et al.* [2011] show that oxalate complexation increases fractional Fe solubility of hematite, goethite and illite minerals in African dust from 0.0025 to 0.26 %. Furthermore, biomass burning is a major source of carboxylic acid and is known to enhance fractional Fe solubility [*Fu et al.*, 2014]. A biomass burning source was suggested by *Bowie et al.* [2009] to account for the high fractional Fe solubility of 17 % in an aerosol sample collected over the Southern Ocean south of Tasmania (Fig. 5.4). We compare the fractional Fe bioavailability data in this study to oxalate measurements made at Cape Grim using methods described in [*Keywood et al.*, 2004] in Fig. 5.6a-e. The highest concentration of oxalate occurred in March 1999. However, the corresponding sample archive was missing. The May/June peak in fractional Fe bioavailability (where labile Fe contributed a large fraction of the total Fe) corresponds to low oxalate and low nss-potassium (Figs. 6b and 6e-f). Non sea salt-potassium has been widely used as a biomass burning tracer [e.g. *Duan et al.*, 2004; *Echalar et al.*, 1995; *Paris et al.*, 2010], and the lack of correlation here suggests that biomass burring is not a large contributor to bioavailable Fe at CGBAPS during this study.

The lack of correlation with oxalate at CGBAPS may be related to the type of Fe-bearing minerals in the baseline aerosols. We are unable to determine the atmospheric processes that enhance the fractional Fe bioavailability of marine aerosols during long range transport over the Southern Ocean. This may be related to the extremely clean air masses at CGBAPS. Thus, a longer time series is needed to confirm whether organic complexation or acid processing affects the solubility and bioavailability of aerosol Fe in the Southern Ocean. The temporal variability in aerosol Fe at CGBAPS is most likely related to a mixture of aerosol sources from continental air masses, as discussed above.

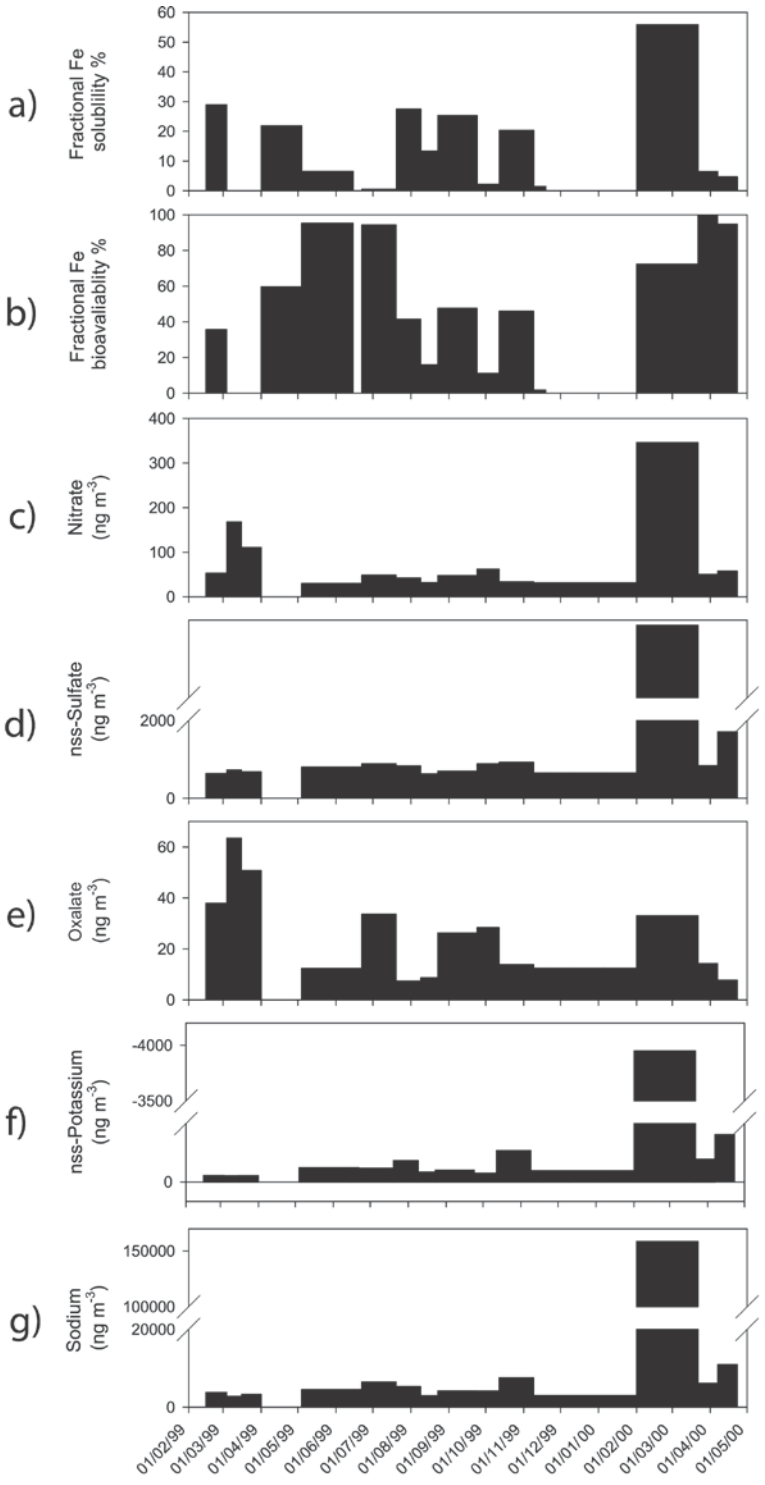

Fig. 5.6: Time series of major ions measured at CGBAPS. a) bioavailable Fe concentration (i.e., the sum of soluble and labile Fe fractions), b) nitrate, c) sulfate, d) oxalate, e) sodium (data source for nitrate, sulfate and sodium: Keywood et al. (2004). http://www.sciencedirect.com/science/article/pii/S0304420315001218

5.5 Conclusions

This paper shows extremely low aerosol Fe concentrations over the Southern Ocean during 1999 to early 2000 and provides estimates for the soluble and total atmospheric Fe flux by dry deposition. The temporal variability of soluble Fe was consistent with the intrusion of continental air masses over the Southern Ocean. The relationship between the fractional Fe solubility and total Fe mass concentration was comparable to other studies that postulated mixed soluble Fe aerosol sources and low mineral dust Fe solubility. Labile Fe comprised a large component of the total Fe and suggested that the soluble Fe may significantly underestimate the potential bioavailability of Fe deposited to Southern Ocean surface waters. However, further studies of labile of Fe are required to understand the significance of labile Fe as determined by the operational method here used here. Longer-term studies of Southern Ocean aerosol Fe bioavailability are also required to understand aerosol Fe variability and to characterise sources. Wet deposition Fe estimates remain relatively unknown over the Southern Ocean. Overall the data shows that the Fe bioavailability of present day aerosols is complex and not simply scaled to atmospheric concentrations of mineral dust. It is likely that past variability in the atmospheric deposition of bioavailable Fe to the Southern Ocean is just as complex and that our current understanding of its Quaternary variability may be in need of revision.

Acknowledgements

This project was funded through Curtin University (Curtin Research Fellowship to R.E.), the University of Tasmania (Rising Stars contract B0019024 to A.R.B.), the Australian Research Council (FT130100037) and the Antarctic Climate and Ecosystems Cooperative Research Centre. Access to SF-ICP-MS instrumentation at UTAS was facilitated through ARC LIEF funding (LE0989539). V.H.L.W. would like to acknowledge the following scholarship support: Australian Postgraduate Award and Curtin University Postgraduate Scholarship. This research would have been impossible without the support and dedication of the late Kevin Rosman. Useful discussions with Rachel Shelley over labile iron leaching methods are appreciated. CSIRO and the Australian Bureau of Meteorology in Australia are also thanked for their continuous support of CGBAPS, and we also thank the staff at CGBAPS who made the collection of monthly aerosol samples possible. The dataset for the filters is available through the Curtin University Research Data repository http://doi.org/10.4225/06/565E7702F1E12. We thank three anonymous reviewers for their constructive comments which improved this manuscript.

References

Aguilar-Islas, A.M., Wu, J., Rember, R., Johansen, A.M. and Shank, L.M., 2010. Dissolution of aerosol-derived iron in seawater: Leach solution chemistry, aerosol type, and colloidal iron fraction. Marine Chemistry, 120(1-4): 25-33.

Arimoto, R., Duce, R., Ray, B. and Unni, C., 1985. Atmospheric trace elements at Enewetak Atoll: 2. Transport to the ocean by wet and dry deposition. Journal of Geophysical Research: Atmospheres (1984–2012), 90(D1): 2391-2408.

Ayers, G., Ivey, J. and Goodman, H., 1987. Sulfate and Methanesulfonnate in the Maritime Aerosol at Cape Grim, Tasmania, Scientific Application of Baseline Observations of Atmospheric Composition (SABOAC). Springer, pp. 371-383.

Ayers, G.P., Ivey, J. and Gillett, R., 1990. High Volume Samplers in Baseline Atmospheric Program (Australia) 1988, edited by S.R. Wilson and G.P. Ayers, CSIRO Atmospheric Research, Melbourne, Australia, 45.

Baker, A., Adams, C., Bell, T., Jickells, T. and Ganzeveld, L., 2013. Estimation of atmospheric nutrient inputs to the Atlantic Ocean from 50° N to 50° S based on large-scale field sampling: Iron and other dust-associated elements. Global Biogeochemical Cycles, 27(3): 755-767.

Baker, A.R. and Croot, P.L., 2010. Atmospheric and marine controls on aerosol iron solubility in seawater. Marine Chemistry, 120(1-4): 4-13.

Baker, A.R. and Jickells, T.D., 2006. Mineral particle size as a control on aerosol iron solubility. Geophys. Res. Lett., 33(17): L17608.

Baker, A.R., Jickells, T.D., Witt, M. and Linge, K.L., 2006. Trends in the solubility of iron, aluminium, manganese and phosphorus in aerosol collected over the Atlantic Ocean. Marine Chemistry, 98(1): 43-58.

Barbeau, K., Moffett, J.W., Caron, D.A., Croot, P.L. and Erdner, D.L., 1996. Role of protozoan grazing in relieving iron limitation of phytoplankton. Nature, 380(6569): 61-64.

Berger, C.J., Lippiatt, S.M., Lawrence, M.G. and Bruland, K.W., 2008. Application of a chemical leach technique for estimating labile particulate aluminum, iron, and manganese in the Columbia River plume and coastal waters off Oregon and Washington. Journal of Geophysical Research: Oceans (1978–2012), 113(C2).

Bhattachan, A. and D'Odorico, P., 2014. Can land use intensification in the Mallee, Australia increase the supply of soluble iron to the Southern Ocean? Scientific reports, 4.

Blain, S., Queguiner, B., Armand, L., Belviso, S., Bombled, B., Bopp, L., Bowie, A., Brunet, C., Brussaard, C., Carlotti, F., Christaki, U., Corbiere, A., Durand, I., Ebersbach, F., Fuda, J.-L., Garcia, N., Gerringa, L., Griffiths, B., Guigue, C., Guillerm, C., Jacquet, S., Jeandel, C., Laan, P., Lefevre, D., Lo Monaco, C., Malits, A., Mosseri, J., Obernosterer, I., Park, Y.-H., Picheral, M., Pondaven, P., Remenyi, T., Sandroni, V., Sarthou, G., Savoye, N., Scouarnec,

L., Souhaut, M., Thuiller, D., Timmermans, K., Trull, T., Uitz, J., van Beek, P., Veldhuis, M., Vincent, D., Viollier, E., Vong, L. and Wagener, T., 2007. Effect of natural iron fertilization on carbon sequestration in the Southern Ocean. Nature, 446(7139): 1070-1074.

Bollhöfer, A., Chisholm, W. and Rosman, K., 1999. Sampling aerosols for lead isotopes on a global scale. Analytica chimica acta, 390(1): 227-235.

Bollhöfer, A.F., Rosman, K.J.R., Dick, A.L., Chisholm, W., Burton, G.R., Loss, R.D. and Zahorowski, W., 2005. Concentration, isotopic composition, and sources of lead in Southern Ocean air during 1999/2000, measured at the Cape Grim Baseline Air Pollution Station, Tasmania. Geochimica et Cosmochimica Acta, 69(20): 4747-4757.

Bonnet, S. and Guieu, C., 2004. Dissolution of atmospheric iron in seawater. Geophys. Res. Lett., 31(3): L03303.

Bowie, A., van der Merwe, P., Quéroué, F., Trull, T., Fourquez, M., Planchon, F., Sarthou, G., Chever, F., Townsend, A. and Obernosterer, I., 2014. Iron budgets for three distinct biogeochemical sites around the Kerguelen archipelago (Southern Ocean) during the natural fertilisation experiment KEOPS-2. Biogeosciences Discussions, 11(12): 17861-17923.

Bowie, A.R., Griffiths, F.B., Dehairs, F. and Trull, T.W., 2011. Oceanography of the subantarctic and polar frontal zones south of Australia during summer: setting for the SAZ-Sense study. Deep Sea Research Part II: Topical Studies in Oceanography, 58(21): 2059-2070.

Bowie, A.R., Lannuzel, D., Remenyi, T.A., Wagener, T., Lam, P.J., Boyd, P.W., Guieu, C., Townsend, A.T. and Trull, T.W., 2009. Biogeochemical iron budgets of the Southern Ocean south of Australia: Decoupling of iron and nutrient cycles in the subantarctic zone by the summertime supply. Global Biogeochem. Cycles, 23(4): GB4034.

Bowie, A.R., Townsend, A.T., Lannuzel, D., Remenyi, T.A. and Van der Merwe, P., 2010. Modern sampling and analytical methods for the determination of trace elements in marine particulate material using magnetic sector inductively coupled plasma–mass spectrometry. Analytica chimica acta, 676(1): 15-27.

Boyd, P.W., Jickells, T., Law, C.S., Blain, S., Boyle, E.A., Buesseler, K.O., Coale, K.H., Cullen, J.J., de Baar, H.J.W., Follows, M., Harvey, M., Lancelot, C., Levasseur, M., Owens, N.P.J., Pollard, R., Rivkin, R.B., Sarmiento, J., Schoemann, V., Smetacek, V., Takeda, S., Tsuda, A., Turner, S. and Watson, A.J., 2007. Mesoscale Iron Enrichment Experiments 1993-2005: Synthesis and Future Directions. Science, 315(5812): 612-617.

Boyd, P.W., Mackie, D.S. and Hunter, K.A., 2010. Aerosol iron deposition to the surface ocean - Modes of iron supply and biological responses. Marine Chemistry, 120(1-4): 128-143.

Buck, C.S., Landing, W.M., Resing, J.A. and Lebon, G.T., 2006. Aerosol iron and aluminum solubility in the northwest Pacific Ocean: Results from the 2002 IOC cruise. Geochem. Geophys. Geosyst., 7(4): Q04M07.

Chen, Y. and Siefert, R.L., 2003. Determination of various types of labile atmospheric iron over remote oceans. J. Geophys. Res., 108(D24): 4774.

Chen, Y. and Siefert, R.L., 2004. Seasonal and spatial distributions and dry deposition fluxes of atmospheric total and labile iron over the tropical and subtropical North Atlantic Ocean. J. Geophys. Res., 109(D9): D09305.

Chuang, P.Y., Duvall, R.M., Shafer, M.M. and Schauer, J.J., 2005. The origin of water soluble particulate iron in the Asian atmospheric outflow. Geophys. Res. Lett., 32(7): L07813.

Coale, K.H., Johnson, K.S., Chavez, F.P., Buesseler, K.O., Barber, R.T., Brzezinski, M.A., Cochlan, W.P., Millero, F.J., Falkowski, P.G., Bauer, J.E., Wanninkhof, R.H., Kudela, R.M., Altabet, M.A., Hales, B.E., Takahashi, T., Landry, M.R., Bidigare, R.R., Wang, X., Chase, Z., Strutton, P.G., Friederich, G.E., Gorbunov, M.Y., Lance, V.P., Hilting, A.K., Hiscock, M.R., Demarest, M., Hiscock, W.T., Sullivan, K.F., Tanner, S.J., Gordon, R.M., Hunter, C.N., Elrod, V.A., Fitzwater, S.E., Jones, J.L., Tozzi, S., Koblizek, M., Roberts, A.E., Herndon, J., Brewster, J., Ladizinsky, N., Smith, G., Cooper, D., Timothy, D., Brown, S.L., Selph, K.E., Sheridan, C.C., Twining, B.S. and Johnson, Z.I., 2004. Southern Ocean Iron Enrichment Experiment: Carbon Cycling in High- and Low-Si Waters. Science, 304(5669): 408-414.

Croot, P., Bluhm, K., Schlosser, C., Streu, P., Breitbarth, E., Frew, R. and Van Ardelan, M., 2008. Regeneration of Fe (II) during EIFeX and SOFeX. Geophysical Research Letters, 35(19).

Cutter, G., Andersson, P., Codispoti, L., Croot, P., Francois, R., Lohan, M., Obata, H. and Rutgers vd Loeff, M., 2010. Sampling and sample-handling protocols for GEOTRACES Cruises.

de Baar, H.J.W., Boyd, P.W., Coale, K.H., Landry, M.R., Tsuda, A., Assmy, P., Bakker, D.C.E., Bozec, Y., Barber, R.T., Brzezinski, M.A., Buesseler, K.O., Boyé, M., Croot, P.L., Gervais, F., Gorbunov, M.Y., Harrison, P.J., Hiscock, W.T., Laan, P., Lancelot, C., Law, C.S., Levasseur, M., Marchetti, A., Millero, F.J., Nishioka, J., Nojiri, Y., van Oijen, T., Riebesell, U., Rijkenberg, M.J.A., Saito, H., Takeda, S., Timmermans, K.R., Veldhuis, M.J.W., Waite, A.M. and Wong, C.S., 2005. Synthesis of iron fertilization experiments: From the Iron Age in the Age of Enlightenment. J. Geophys. Res., 110(C9): C09S16.

de Baar, H.J.W., de Jong, J.T.M., Bakker, D.C.E., Loscher, B.M., Veth, C., Bathmann, U. and Smetacek, V., 1995. Importance of iron for plankton blooms and carbon dioxide drawdown in the Southern Ocean. Nature, 373(6513): 412-415.

Delmonte, B., Andersson, P.S., Hansson, M., Schöberg, H., Petit, J.R., Basile-Doelsch, I. and Maggi, V., 2008. Aeolian dust in East Antarctica (EPICA-Dome C and Vostok): Provenance during glacial ages over the last 800 kyr. Geophys. Res. Lett., 35(7): L07703.

Delmonte, B., Baroni, C., Andersson, P., Narcisi, B., Salvatore, M., Petit, J., Scarchilli, C., Frezzotti, M., Albani, S. and Maggi, V., 2013. Modern and Holocene aeolian dust variability from Talos Dome (Northern Victoria Land) to the interior of the Antarctic ice sheet. Quaternary Science Reviews, 64: 76-89.

Delmonte, B., Petit, J.R. and Maggi, V., 2002. Glacial to Holocene implications of the new 27000-year dust record from the EPICA Dome C (East Antarctica) ice core. Climate Dynamics, 18(8): 647-660.

Desboeufs, K.V., Losno, R., Vimeux, F. and Cholbi, S., 1999. The pH-dependent dissolution of wind-transported Saharan dust. Journal of Geophysical Research: Atmospheres (1984–2012), 104(D17): 21287-21299.

Duan, F., Liu, X., Yu, T. and Cachier, H., 2004. Identification and estimate of biomass burning contribution to the urban aerosol organic carbon concentrations in Beijing. Atmospheric Environment, 38(9): 1275-1282.

Duce, R.A., Liss, P.S., Merrill, J.T., Atlas, E.L., Buat-Menard, P., Hicks, B.B., Miller, J.M., Prospero, J.M., Arimoto, R., Church, T.M., Ellis, W., Galloway, J.N., Hansen, L., Jickells, T.D., Knap, A.H., Reinhardt, K.H., Schneider, B., Soudine, A., Tokos, J.J., Tsunogai, S., Wollast, R. and Zhou, M., 1991. The atmospheric input of trace species to the world ocean. Global Biogeochem. Cycles, 5(3): 193-259.

Dulac, F., BUAT-MÉNARD, P., Ezat, U., Melki, S. and Bergametti, G., 1989. Atmospheric input of trace metals to the western Mediterranean: uncertainties in modelling dry deposition from cascade impactor data. Tellus B, 41(3): 362-378.

Echalar, F., Gaudichet, A., Cachier, H. and Artaxo, P., 1995. Aerosol emissions by tropical forest and savanna biomass burning: characteristic trace elements and fluxes. Geophysical research letters, 22(22): 3039-3042.

Edwards, R. and Sedwick, P., 2001. Iron in East Antarctic snow: Implications for atmospheric iron deposition and algal production in Antarctic waters. Geophys. Res. Lett., 28(20): 3907-3910.

Edwards, R., Sedwick, P., Morgan, V. and Boutron, C., 2006. Iron in ice cores from Law Dome: A record of atmospheric iron deposition for maritime East Antarctica during the Holocene and Last Glacial Maximum. Geochemistry, Geophysics, Geosystems, 7(12): Q12Q01.

Ellwood, M.J., Hutchins, D.A., Lohan, M.C., Milne, A., Nasemann, P., Nodder, S.D., Sander, S.G., Strzepek, R., Wilhelm, S.W. and Boyd, P.W., 2015. Iron stable isotopes track pelagic iron cycling during a subtropical phytoplankton bloom. Proceedings of the National Academy of Sciences, 112(1): E15-E20.

Elrod, V., Berelson, W., Coale, K. and Johnson, K., 2004. The flux of iron from continental shelf sediments: a missing source for global budgets. Geophys Res Lett, 31: L12307.

Ezat, U. and Dulac, F., 1995. Size distribution of mineral aerosols at Amsterdam-island and dry deposition rates in the Southern Indian Ocean. Comptes Rendus De L Acadmie Des Sciences Serie II, 320(1): 9-14.

Fu, H., Shang, G., Lin, J., Hu, Y., Hu, Q., Guo, L., Zhang, Y. and Chen, J., 2014. Fractional iron solubility of aerosol particles enhanced by biomass burning and ship emission in Shanghai, East China. Science of The Total Environment, 481: 377-391.

Gaiero, D.M., Brunet, F., Probst, J.-L. and Depetris, P.J., 2007. A uniform isotopic and chemical signature of dust exported from Patagonia: Rock sources and occurrence in southern environments. Chemical Geology, 238(1): 107-120.

Gaiero, D.M., Probst, J.-L., Depetris, P.J., Bidart, S.M. and Leleyter, L., 2003. Iron and other transition metals in Patagonian riverborne and windborne materials: geochemical control and transport to the southern South Atlantic Ocean. Geochimica et Cosmochimica Acta, 67(19): 3603-3623.

Gao, Y., Xu, G., Zhan, J., Zhang, J., Li, W., Lin, Q., Chen, L. and Lin, H., 2013. Spatial and particle size distributions of atmospheric dissolvable iron in aerosols and its input to the Southern Ocean and coastal East Antarctica. Journal of Geophysical Research: Atmospheres, 118(22): 12,634-12,648.

Gaspari, V., Barbante, C., Cozzi, G., Cescon, P., Boutron, C.F., Gabrielli, P., Capodaglio, G., Ferrari, C., Petit, J.R. and Delmonte, B., 2006. Atmospheric iron fluxes over the last deglaciation: Climatic implications. Geophys. Res. Lett., 33(3): L03704.

Gibbs, R., Mathews, M. and Unk, D., 1971. The relationship between sphere size and settling velocity. Journal of Sedimentary Petrology, 41(1): 7-18.

Guieu, C., Bonnet, S., Wagener, T. and Loÿe-Pilot, M.D., 2005. Biomass burning as a source of dissolved iron to the open ocean? Geophysical Research Letters, 32(19).

Halstead, M.J., Cunninghame, R.G. and Hunter, K.A., 2000. Wet deposition of trace metals to a remote site in Fiordland, New Zealand. Atmospheric Environment, 34(4): 665-676.

Hand, J.L., Mahowald, N.M., Chen, Y., Siefert, R.L., Luo, C., Subramaniam, A. and Fung, I., 2004. Estimates of atmospheric-processed soluble iron from observations and a global mineral aerosol model: Biogeochemical implications. J. Geophys. Res., 109(D17): D17205.

Heimburger, A., Losno, R. and Triquet, S., 2013a. Solubility of iron and other trace elements in rainwater collected on the Kerguelen Islands (South Indian Ocean). Biogeosciences, 10(10).

Heimburger, A., Losno, R., Triquet, S., Dulac, F. and Mahowald, N., 2012. Direct measurements of atmospheric iron, cobalt, and aluminum-derived dust deposition at Kerguelen Islands. Global Biogeochemical Cycles, 26(4).

Heimburger, A., Losno, R., Triquet, S. and Nguyen, E.B., 2013b. Atmospheric deposition fluxes of 26 elements over the Southern Indian Ocean: Time series on Kerguelen and Crozet Islands. Global Biogeochemical Cycles, 27(2): 440-449.

Hurst, M.P. and Bruland, K.W., 2007. An investigation into the exchange of iron and zinc between soluble, colloidal, and particulate size-fractions in shelf waters using low-abundance isotopes as tracers in shipboard incubation experiments. Marine chemistry, 103(3): 211-226.

Ito, A., 2011. Mega fire emissions in Siberia: potential supply of bioavailable iron from forests to the ocean. Biogeosciences, 8(6).

Jeong, D., Kim, K. and Choi, W., 2012. Accelerated dissolution of iron oxides in ice. Atmospheric Chemistry and Physics, 12(22): 11125-11133.

Jickells, T., An, Z., Anderson, K., Baker, A., Bergametti, G., Brooks, N., Cao, J., Boyd, P., Duce, R., Hunter, K., Kawaahata, H., Kubilay, N., LaRoche, J., Liss, P., Mahowald, N.,

Prospero, J., Ridgewell, A., Tegen, I. and Torres, R., 2005. Global iron connections between desert dust, ocean biogeochemistry, and climate. Science, 308: 67 - 73.

Johnson, K., Chavez, F. and Friederich, G., 1999. Continental-shelf sediment as a primary source of iron for coastal phytoplankton. Nature, 398: 697 - 700.

Keywood, M.D., 2007. Aerosol composition at Cape Grim : an evaluation of PM10 sampling program and baseline event switches. Baseline Atmospheric Program Australia 2005-2006. 2005-2006 ed. J. M. Cainey, N. Derek, and P. B. Krummel (editors). Melbourne: Australian Bureau of Meteorology and CSIRO Marine and Atmospheric Research: 31-36.

Keywood, M.D., Graham, B., Gillett, R.W., Gras, J.G. and Selleck, P.W., 2004. High volume aerosol sampler. Baseline Atmospheric Program (Australia) 2001-200 edited by J. Cainey, N.Derek and P.Krummel. .Bureau of Meteorology CSIRO Atmospheric Research and, Melbourne, Australia: 74-77.

Kobayashi, H., Hara, K., Shiobara, M., Yamanouchi, T., Osada, K. and Ohta, S., 2010. Seasonal variation of carbonaceous and metal compositions of atmospheric aerosols at Syowa Station, Antarctica in 2001. Antarctic Record(Tokyo), 54: 554-561.

Koffman, B., Kreutz, K., Breton, D., Kane, E., Winski, D., Birkel, S., Kurbatov, A. and Handley, M., 2014a. Centennial-scale variability of the Southern Hemisphere westerly wind belt in the eastern Pacific over the past two millennia. Climate of the Past, 10(3): 1125-1144.

Koffman, B.G., Handley, M.J., Osterberg, E.C., Wells, M.L. and Kreutz, K.J., 2014b. Dependence of ice-core relative trace-element concentration on acidification. Journal of Glaciology, 60(219): 103-112.

Kuma, K. and Matsunaga, K., 1995. Availability of colloidal ferric oxides to coastal marine phytoplankton. Marine Biology, 122(1): 1-11.

Kumar, A., Sarin, M. and Srinivas, B., 2010. Aerosol iron solubility over Bay of Bengal: Role of anthropogenic sources and chemical processing. Marine Chemistry, 121(1): 167-175.

Lannuzel, D., Schoemann, V., de Jong, J., Chou, L., Delille, B., Becquevort, S. and Tison, J., 2008. Iron study during a time series in the western Weddell pack ice. Marine Chemistry, 108(1-2): 85-95.

Lannuzel, D., Schoemann, V., de Jong, J., Tison, J. and Chou, L., 2007. Distribution and biogeochemical behaviour of iron in the East Antarctic sea ice. Marine Chemistry, 106(1-2): 18-32.

Latimer, J.C. and Filippelli, G.M., 2001. Terrigenous input and paleoproductivity in the Southern Ocean. Paleoceanography, 16(6): 627-643.

Latimer, J.C., Filippelli, G.M., Hendy, I.L., Gleason, J.D. and Blum, J.D., 2006. Glacial-interglacial terrigenous provenance in the southeastern Atlantic Ocean: The importance of deep-water sources and surface currents. Geology, 34(7): 545-548.

Lis, H., Shaked, Y., Kranzler, C., Keren, N. and Morel, F.M.M., 2015. Iron bioavailability to phytoplankton: an empirical approach. ISME J, 9(4): 1003-1013.

Luo, C., Mahowald, N., Bond, T., Chuang, P.Y., Artaxo, P., Siefert, R., Chen, Y. and Schauer, J., 2008. Combustion iron distribution and deposition. Global Biogeochem. Cycles, 22(1): GB1012.

Luo, C., Mahowald, N.M., Meskhidze, N., Chen, Y., Siefert, R.L., Baker, A.R. and Johansen, A.M., 2005. Estimation of iron solubility from observations and a global aerosol model. J. Geophys. Res., 110(D23): D23307.

Mackie, D.S., Boyd, P.W., Hunter, K.A. and McTainsh, G.H., 2005. Simulating the cloud processing of iron in Australian dust: pH and dust concentration. Geophys. Res. Lett., 32(6): L06809.

Mahowald, N.M., Baker, A.R., Bergametti, G., Brooks, N., Duce, R.A., Jickells, T.D., Kubilay, N., Prospero, J.M. and Tegen, I., 2005. Atmospheric global dust cycle and iron inputs to the ocean. Global Biogeochem. Cycles, 19(4): GB4025.

Martin, J.H., Gordon, R.M. and Fitzwater, S.E., 1990. Iron in Antarctic waters. Nature, 345(6271): 156-158.

Martin, J.H., Gordon, R.M. and Fitzwater, S.E., 1991. The Case for Iron. Limnology and Oceanography, 36(8): 1793-1802.

Martínez-Garcia, A., Rosell-Melé, A., Geibert, W., Gersonde, R., Masqué, P., Gaspari, V. and Barbante, C., 2009. Links between iron supply, marine productivity, sea surface temperature, and CO2 over the last 1.1 Ma. Paleoceanography, 24(1): PA1207.

Martínez-García, A., Sigman, D.M., Ren, H., Anderson, R.F., Straub, M., Hodell, D.A., Jaccard, S.L., Eglinton, T.I. and Haug, G.H., 2014. Iron Fertilization of the Subantarctic Ocean During the Last Ice Age. Science, 343(6177): 1347-1350.

Meskhidze, N., Chameides, W., Nenes, A. and Chen, G., 2003. Iron mobilization in mineral dust: Can anthropogenic SO2 emissions affect ocean productivity? Geophysical Research Letters, 30(21).

Meskhidze, N. and Nenes, A., 2006. Phytoplankton and cloudiness in the Southern Ocean. Science, 314(5804): 1419-1423.

Moore, J.K., Abbott, M.R., Richman, J.G. and Nelson, D.M., 2000. The southern ocean at the Last Glacial Maximum: A strong sink for atmospheric carbon dioxide. Global Biogeochem. Cycles, 14(1): 455-475.

Morton, P.L., Landing, W.M., Hsu, S.-C., Milne, A., Aguilar-Islas, A.M., Baker, A.R., Bowie, A.R., Buck, C.S., Gao, Y. and Gichuki, S., 2013. Methods for the sampling and analysis of marine aerosols: results from the 2008 GEOTRACES aerosol intercalibration experiment. Limnology and Oceanography: Methods, 11(FEB): 62-78.

Narcisi, B., Petit, J.-R., Delmonte, B., Basile-Doelsch, I. and Maggi, V., 2005. Characteristics and sources of tephra layers in the EPICA-Dome C ice record (East Antarctica): implications for past atmospheric circulation and ice core stratigraphic correlations. Earth and Planetary Science Letters, 239(3): 253-265.

Nodwell, L.M. and Price, N.M., 2001. Direct Use of Inorganic Colloidal Iron by Marine Mixotrophic Phytoplankton. Limnology and Oceanography, 46(4): 765-777.

Paris, R. and Desboeufs, K., 2013. Effect of atmospheric organic complexation on iron-bearing dust solubility. Atmospheric Chemistry and Physics, 13(9): 4895-4905.

Paris, R., Desboeufs, K., Formenti, P., Nava, S. and Chou, C., 2010. Chemical characterisation of iron in dust and biomass burning aerosols during AMMA-SOP0/DABEX: implication for iron solubility. Atmospheric Chemistry and Physics, 10(9): 4273-4282.

Paris, R., Desboeufs, K. and Journet, E., 2011. Variability of dust iron solubility in atmospheric waters: Investigation of the role of oxalate organic complexation. Atmospheric Environment, 45(36): 6510-6517.

Planquette, H., Statham, P.J., Fones, G.R., Charette, M.A., Moore, C.M., Salter, I., Nedelec, F.H., Taylor, S.L., French, M. and Baker, A.R., 2007. Dissolved iron in the vicinity of the Crozet Islands, Southern Ocean. Deep Sea Research Part II: Topical Studies in Oceanography, 54(18): 1999-2019.

Porstendorfer, J., Butterweck, G. and Reineking, A., 1994. Daily variation of the radon concentration indoors and outdoors and the influence of meteorological parameters. Health physics, 67(3): 283-287.

Raiswell, R., Benning, L.G., Tranter, M. and Tulaczyk, S., 2008. Bioavailable iron in the Southern Ocean: the significance of the iceberg conveyor belt. Geochemical Transactions, 9(1): 7.

Rubin, M., Berman-Frank, I. and Shaked, Y., 2011. Dust-and mineral-iron utilization by the marine dinitrogen-fixer Trichodesmium. Nature Geoscience, 4(8): 529-534.

Schwertmann, U., 1991. Solubility and dissolution of iron oxides, Iron nutrition and interactions in plants. Springer, pp. 3-27.

Sedwick, P.N. and DiTullio, G.R., 1997. Regulation of algal blooms in Antarctic Shelf Waters by the release of iron from melting sea ice. Geophys. Res. Lett., 24(20): 2515-2518.

Sedwick, P.N., Sholkovitz, E.R. and Church, T.M., 2007. Impact of anthropogenic combustion emissions on the fractional solubility of aerosol iron: Evidence from the Sargasso Sea. Geochem. Geophys. Geosyst., 8(10): Q10Q06.

Sholkovitz, E.R., Sedwick, P.N. and Church, T.M., 2009. Influence of anthropogenic combustion emissions on the deposition of soluble aerosol iron to the ocean: Empirical estimates for island sites in the North Atlantic. Geochimica et Cosmochimica Acta, 73(14): 3981-4003.

Sholkovitz, E.R., Sedwick, P.N., Church, T.M., Baker, A.R. and Powell, C.F., 2012. Fractional solubility of aerosol iron: Synthesis of a global-scale data set. Geochimica et cosmochimica acta, 89: 173-189.

Slinn, S. and Slinn, W., 1980. Predictions for particle deposition on natural waters. Atmospheric Environment (1967), 14(9): 1013-1016.

Smetacek, V., Klaas, C., Strass, V.H., Assmy, P., Montresor, M., Cisewski, B., Savoye, N., Webb, A., d'Ovidio, F., Arrieta, J.M., Bathmann, U., Bellerby, R., Berg, G.M., Croot, P., Gonzalez, S., Henjes, J., Herndl, G.J., Hoffmann, L.J., Leach, H., Losch, M., Mills, M.M., Neill, C., Peeken, I., Rottgers, R., Sachs, O., Sauter, E., Schmidt, M.M., Schwarz, J., Terbruggen, A. and Wolf-Gladrow, D., 2012. Deep carbon export from a Southern Ocean iron-fertilized diatom bloom. Nature, 487(7407): 313-319.

Spokes, L.J. and Jickells, T.D., 1995. Factors controlling the solubility of aerosol trace metals in the atmosphere and on mixing into seawater. Aquatic Geochemistry, 1(4): 355-374.

Spokes, L.J., Jickells, T.D. and Lim, B., 1994. Solubilisation of aerosol trace metals by cloud processing: A laboratory study. Geochimica et Cosmochimica Acta, 58(15): 3281-3287.

Spolaor, A., Vallelonga, P., Gabrieli, J., Cozzi, G., Boutron, C. and Barbante, C., 2012. Determination of Fe2+ and Fe3+ species by FIA-CRC-ICP-MS in Antarctic ice samples. Journal of Analytical Atomic Spectrometry, 27(2): 310-317.

Tagliabue, A., Bopp, L., Dutay, J.-C., Bowie, A.R., Chever, F., Jean-Baptiste, P., Bucciarelli, E., Lannuzel, D., Remenyi, T., Sarthou, G., Aumont, O., Gehlen, M. and Jeandel, C., 2010. Hydrothermal contribution to the oceanic dissolved iron inventory. Nature Geosci, 3(4): 252-256.

Tagliabue, A., Sallee, J.-B., Bowie, A.R., Levy, M., Swart, S. and Boyd, P.W., 2014. Surface-water iron supplies in the Southern Ocean sustained by deep winter mixing. Nature Geosci, 7(4): 314-320.

Trapp, J.M., Millero, F.J. and Prospero, J.M., 2010. Trends in the solubility of iron in dust-dominated aerosols in the equatorial Atlantic trade winds: Importance of iron speciation and sources. Geochem. Geophys. Geosyst., 11(3): Q03014.

Vallelonga, P., Barbante, C., Cozzi, G., Gabrieli, J., Schüpbach, S., Spolaor, A. and Turetta, C., 2013. Iron fluxes to Talos Dome, Antarctica, over the past 200 kyr. Climate of the Past, 9(2): 597-604.

Wagener, T., Guieu, C., Losno, R., Bonnet, S. and Mahowald, N., 2008. Revisiting atmospheric dust export to the Southern Hemisphere ocean: Biogeochemical implications. Global Biogeochem. Cycles, 22(2): GB2006.

Wu, J., Rember, R. and Cahill, C., 2007. Dissolution of aerosol iron in the surface waters of the North Pacific and North Atlantic oceans as determined by a semicontinuous flow-through reactor method. Global Biogeochem. Cycles, 21(4): GB4010.

Wuttig, K., Wagener, T., Bressac, M., Dammshäuser, A., Streu, P., Guieu, C. and Croot, P., 2013. Impacts of dust deposition on dissolved trace metal concentrations (Mn, Al and Fe) during a mesocosm experiment. Biogeosciences (BG), 10(4): 2583-2600.

Yamada, Y., Fukuda, H., Inoue, K., Kogure, K. and Nagata, T., 2013. Effects of attached bacteria on organic aggregate settling velocity in seawater. Aquatic microbial ecology, 70(3): 261-272.

Zahorowski, W., Chambers, S. and Henderson-Sellers, A., 2004. Ground based radon-222 observations and their application to atmospheric studies. Journal of environmental radioactivity, 76(1): 3-33.

Zhuang, G., Duce, R.A. and Kester, D.R., 1990. The Dissolution of Atmospheric Iron in Surface Seawater of the Open Ocean. J. Geophys. Res., 95(C9): 16207-16216.

Zhuang, G., Yi, Z., Duce, R.A. and Brown, P.R., 1992. Chemistry of iron in marine aerosols. Global Biogeochem. Cycles, 6(2): 161-17.

Supplementary information

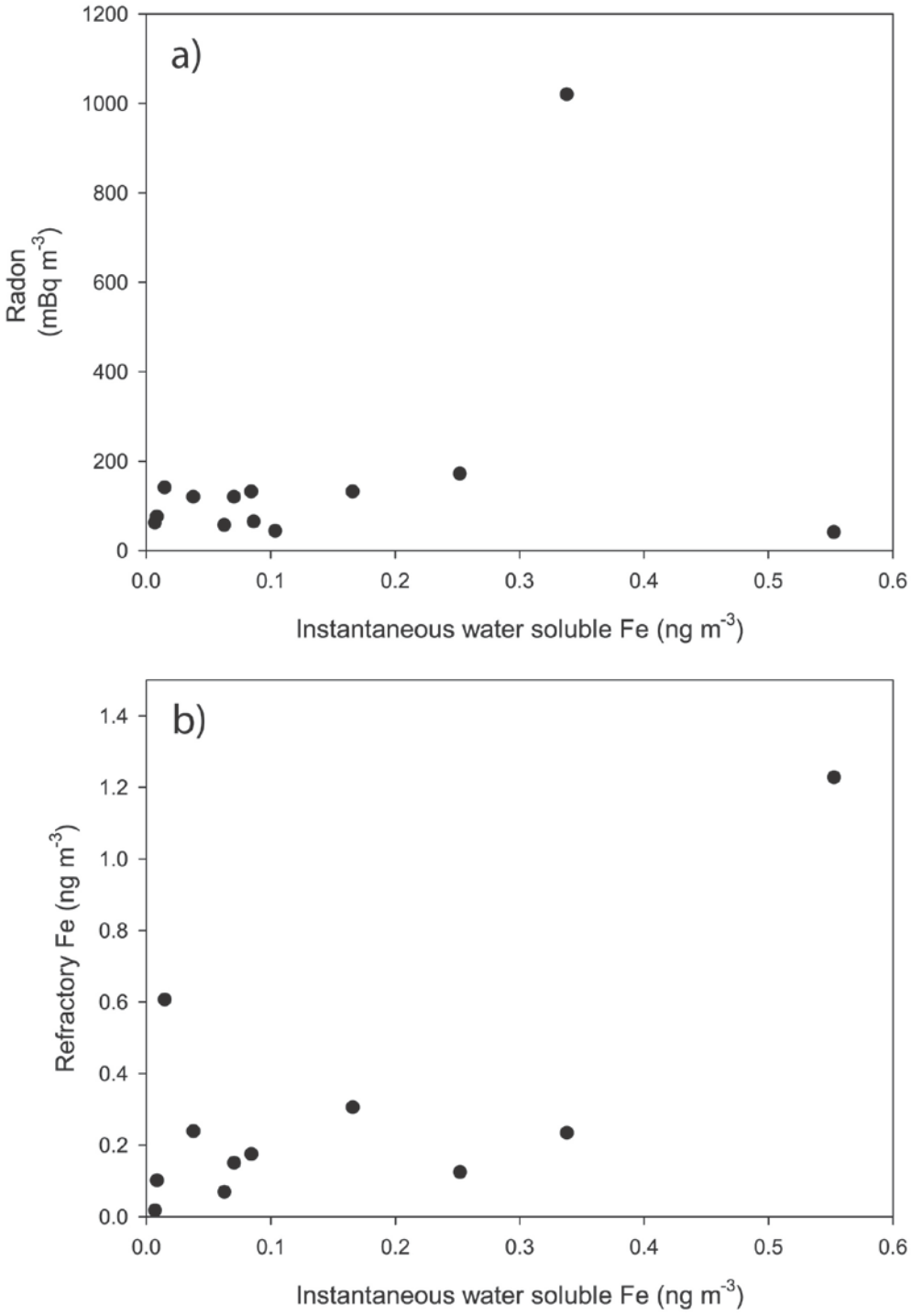

Fig. S5.1: Instantaneous water soluble iron mass concentration versus a) radon concentration, and b) refractory iron mass concentration. **http://www.sciencedirect.com/science/article/pii/S0304420315001218**

Table S5.1: Cape Grim archived aerosol samples used for iron analysis.

Sample	Fraction of filter	Date started sampling	Date finished sampling	Air volume (m^3)
CG4	0.25	15/02/1999	2/03/1999	28.9
G5	0.125	4/03/1999	16/03/1999	5.1
CG9	0.25	1/04/1999	4/05/1999	102
CG10	0.5	4/05/1999	15/06/1999	132
CG15	0.5	20/07/1999	2/08/1999	201
CG17	0.75	9/08/1999	23/08/1999	366
CG18	0.75	23/08/1999	24/09/1999	118
CG26	0.75	24/09/1999	12/10/1999	106
CG28	0.75	12/10/1999	9/11/1999	141
CG23	0.75	9/11/1999	16/11/1999	14
CG35	0.75	1/02/2000	21/03/2000	122
CG37	0.75	22/03/2000	7/04/2000	108
CG40	0.75	7/04/2000	26/04/2000	103

Table S5.2: SF-ICP-MS Instrument parameters.

Instrument	ELEMENT 2 sector field ICP-MS (Thermo Fisher, Germany)
Torch	Fassel type (Thermo Fisher, Germany)
Spray chamber	20 mL Quartz cyclonic (Glass Expansion, Australia)
Nebuliser	0.2 mL min-1 Micromist (Glass Expansion, Australia)
RF power (W)	1350
Cool gas flow (L min^{-1})	~15
Auxiliary gas flow (L min^{-1})	~0.7
Sample gas flow (L min^{-1})	~0.95
Guard electrode	Activated
Sample uptake	100 s, with pumping
Sample rinse	150 s, 1 % HNO3
Scan type	E-scan

Chapter 6. Multiple sources of soluble atmospheric iron to Antarctic waters

This chapter has been published in *Global Biogeochemical Cycles*. The data has been published in the *Curtin University Research Data Repository*. Co-author contributions can be found in Appendix A3.

V.H.L. Winton, R. Edwards, B. Delmonte, A. Ellis, P.S. Andersson, A. Bowie, N.A.N. Bertler, P. Neff, A. Tuohy., 2016. Multiple sources of soluble atmospheric iron to Antarctic waters. *Global Biogeochemical Cycles*, 29, doi:10.1002/2015GB005265.

V.H.L. Winton, R. Edwards, B. Delmonte, A. Ellis, P.S. Andersson, A. Bowie, N.A.N. Bertler, P. Neff, A. Tuohy, 2015. Roosevelt Island 2012/2013 1.5 m snow pit data set. *Curtin University Research Data*, http://doi.org/10.4225/06/565BCE14467D0.

Abstract

The Ross Sea, Antarctica, is a highly productive region of the Southern Ocean. Significant new sources of iron (Fe) are required to sustain phytoplankton blooms in the austral summer. Atmospheric deposition is one potential source. The fractional solubility of Fe is an important variable determining Fe availability for biological uptake. To constrain aerosol Fe inputs to the Ross Sea region, fractional solubility of Fe was analysed in a snow pit from Roosevelt Island, eastern Ross Sea. In addition, aluminium, dust, and refractory black carbon (rBC) concentrations were analysed, to determine the contribution of mineral dust and combustion sources to the supply of aerosol Fe. We estimate exceptionally high dissolved Fe (dFe) flux of 1.2 x 10^{-6} g m^{-2} y^{-1} and total dissolvable Fe (TDFe) flux of 140 x 10^{-6} g m^{-2} y^{-1} for 2011/2012. Deposition of dust, Fe, Al, and rBC occurs primarily during spring-summer. The observed background fractional Fe solubility of ~0.7 % is consistent with a mineral dust source. Radiogenic isotopic ratios and particle size distribution of dust indicates that the site is influenced by local and remote sources. In 2011/2012 summer, relatively high dFe concentrations paralleled both mineral dust and rBC deposition. Around half of the annual aerosol Fe deposition occurred in the austral summer phytoplankton growth season; however

the fractional Fe solubility was low. Our results suggest that the seasonality of dFe deposition can vary, and should be considered on longer glacial-interglacial timescales.

6.1 Introduction

The Ross Sea is the most biologically productive continental shelf region around Antarctica and an important region for atmospheric CO_2 sequestration [*Arrigo and Van Dijken*, 2007; *Arrigo et al.*, 1998; *Arrigo et al.*, 2008b; *Smith and Gordon*, 1997]. Each summer the Ross Sea blooms with phytoplankton [e.g. *Smith and Gordon*, 1997]. Two distinct blooms occur, with each characterized by differences in location, timing, water stratification and species [*Arrigo and van Dijken*, 2004]. The first bloom occurs in the central Ross Sea polynya north of the Ross Ice Shelf and is dominated by *Phaeocystis Antarctica*. This bloom develops in late October-November when sea ice is still present and terminates as early as mid-December. The second bloom occurs in the southwestern (SW) Ross Sea, is dominated by diatoms, and is much smaller in areal extent. In the Southern Ocean, environmental factors responsible for controlling the rates of phytoplankton production include: grazing [e.g. *Banse*, 1991], temperature [e.g. *Bunt*, 1963], light availability [e.g. *Mitchell et al.*, 1991], water stratification [*Tagliabue and Arrigo*, 2006], sea ice extent [*Smith and Nelson*, 1986], trace metal availability [e.g. Fe; *Martin et al.*, 1990; *Sedwick and DiTullio*, 1997; *Sedwick et al.*, 2011], or a combination of these [e.g. *Arrigo et al.*, 2000]. Due to the Ross Sea's capacity to support intense early summer phytoplankton blooms, the seasonally Fe-limited high-nutrient high-chlorophyll (HNHC) regime of the Ross Sea in summer is distinct from the chronically Fe-limited high nutrient, low chlorophyll (HNLC) offshore waters of the Southern Ocean [*Tagliabue and Arrigo*, 2005].

In-situ oceanic iron (Fe)-fertilization experiments have demonstrated a response of the ecosystem to relatively small additions of dissolved Fe (dFe) in the Ross Sea and other sections of the Southern Ocean [*Coale et al.*, 2003; *Martin et al.*, 1990]. The seasonally Fe-limited HNHC regime in the Ross Sea requires continuous new inputs of dissolved Fe (dFe) to sustain these phytoplankton blooms [e.g. *Fitzwater et al.*, 2000; *Sedwick et al.*, 2011]. Inputs of new Fe to surface waters in the Ross Sea can occur through upwelling of deep waters, transport from continental margins by ocean currents, melt from sea-ice, icebergs and ice shelves, and atmospheric aerosol deposition [*Atkins and Dunbar*, 2009; *de Jong et al.*, 2013; *Gerringa et al.*, 2015; *Jacobs et al.*, 1970; *Marsay et al.*, 2014; *Sedwick and DiTullio*, 1997; *Sedwick et al.*, 2011; *Winton et al.*, 2014].

In terms of an atmospheric source, the deposition of aerosol Fe to remote Southern Ocean surface waters is extremely low [e.g. *Winton et al.*, 2015], and has been investigated in relation to the distribution and transport of mineral dust. Little aerosol Fe data exists for the Ross Sea region. Total dissolvable Fe (TDFe) aerosol fluxes to the Ross Sea from long-range transport dust have been estimated to range between 0.007 to 0.1 mg m^{-2} yr^{-1} [*Edwards and Sedwick*, 2001]. Measurements of local soluble Fe from local dust on sea ice in McMurdo Sound [*Winton et al.*, 2014] show that this local Fe source is much larger (2-7 mg m^{-2} yr^{-1}) than that supplied by long-range transport sources [e.g. *Wagener et al.*, 2008]. The supplied Fe, however, only contributes to phytoplankton blooms within the localized McMurdo Sound region. On longer timescales, enhanced glacial atmospheric Fe deposition has been linked to higher rates of Southern Ocean primary productivity as observed from recent Southern Ocean marine sediment studies [e.g. *Martínez-García et al.*, 2014]. Furthermore, Antarctic ice core records associate higher dust deposition rates with Fe supply during glacial stages [*Conway et al.*, 2015; *Edwards et al.*, 2006; *Gaspari et al.*, 2006; *Vallelonga et al.*, 2013]. Dust deposition to Antarctica can be sourced from both remote and local sources [e.g. *Bory et al.*, 2010; *Delmonte et al.*, 2013]. Dust provenance can be determined from the $^{87}Sr/^{86}Sr$ and $^{143}Nd/^{144}Nd$ radiogenic isotope composition of dust in snow and ice by comparison with potential source areas (PSAs) [*Grousset and Biscaye*, 2005]. This is because the Sr and Nd isotopic composition of dust are primarily related to lithology and the geologic history of parent materials [*Faure*, 1986].

Aerosol Fe bioavailability information is required to constrain the biogeochemical impact of present and past atmospheric Fe variability. Reported values of fractional aerosol Fe solubility range from 0.01 to 90 % [*Baker and Croot*, 2010; *Bowie et al.*, 2009; *Edwards and Sedwick*, 2001; *Heimburger et al.*, 2013a; *Mahowald et al.*, 2005]. This large range may reflect differences in mineral dust concentrations, particle size, atmospheric weathering and aerosol leaching methods [*Aguilar-Islas et al.*, 2010; *Baker and Jickells*, 2006; *Bonnet and Guieu*, 2004; *Buck et al.*, 2006; *Chen and Siefert*, 2003; *Spokes and Jickells*, 1995; *Trapp et al.*, 2010; *Zhuang et al.*, 1990; *Zhuang et al.*, 1992]. An alternative hypothesis for the observed solubility range is that it results from a mixture of aerosol Fe sources with different mineralogy and fractional Fe solubility [*Sholkovitz et al.*, 2012]. *Sholkovitz et al.* [2012] showed that global scale fractional aerosol Fe solubility displays an inverse hyperbolic relationship with the total Fe concentration. This relationship is consistent with a low fractional Fe solubility for mineral dust (~1-2 %) and the presence of other soluble Fe

sources, such as those originating from biomass burning and oil combustion with higher fractional Fe solubility [*Chuang et al.*, 2005; *Guieu et al.*, 2005; *Ito*, 2011; *Kumar et al.*, 2010; *Luo et al.*, 2008; *Paris et al.*, 2010; *Sedwick et al.*, 2007; *Sholkovitz et al.*, 2009]. Estimates of fractional Fe solubility from fire combustion range from 1 to 60 % and may vary in relationship to biomass and fire characteristics as well as that of the underlying terrain [*Guieu et al.*, 2005; *Ito*, 2011; *Kumar et al.*, 2010; *Luo et al.*, 2008; *Paris et al.*, 2010]. Over the time period investigated (2010-2012) in this study, Southern Hemisphere biomass burning emissions primarily occurred in the intertropical convergence zone (ITCZ) of Africa, Australia and South America [*Giglio et al.*, 2013]. Of these regions, Australia is the closest to the Ross Sea. Biomass burning constitutes a large source of austral dry-season aerosol emissions over northern Australia, and episodic austral summer wildfires in southern and eastern Australia [e.g. *Meyer et al.*, 2008]. Refractory black carbon aerosols (rBC) are emitted by biomass burning and fossil fuels [*Reid et al.*, 2005]. In the Southern Hemisphere, rBC emissions are primarily from biomass burning [*Giglio et al.*, 2013] and can be used as a proxy for the long-range transport of biomass burning aerosols to Antarctica. *Bisiaux et al.* [2012b] investigated ice core records of rBC deposition to West Antarctica and found annual deposition consistent with austral dry season biomass burning. Thus, Fe associated with rBC may provide information with respect to biomass burning inputs of Fe to the Southern Ocean in this study.

An intermediate depth ice core (764 m) was recently drilled in the framework of the Roosevelt Island Climate Evolution (RICE) project Roosevelt Island (79.36086 ºS, 161.64600 ºW; Fig. 6.1), located on the opposite side of the Ross Sea to McMurdo Sound. Many aspects of atmospheric Fe deposition in marginal areas of Antarctica remain poorly known. In this respect, Roosevelt Island represents an ideal location to investigate the timing and source(s) of soluble Fe deposition to the eastern Ross Sea region. This study investigated the present-day seasonality of fractional Fe solubility, and potential sources from mineral dust and refractory black carbon (rBC) at Roosevelt Island.

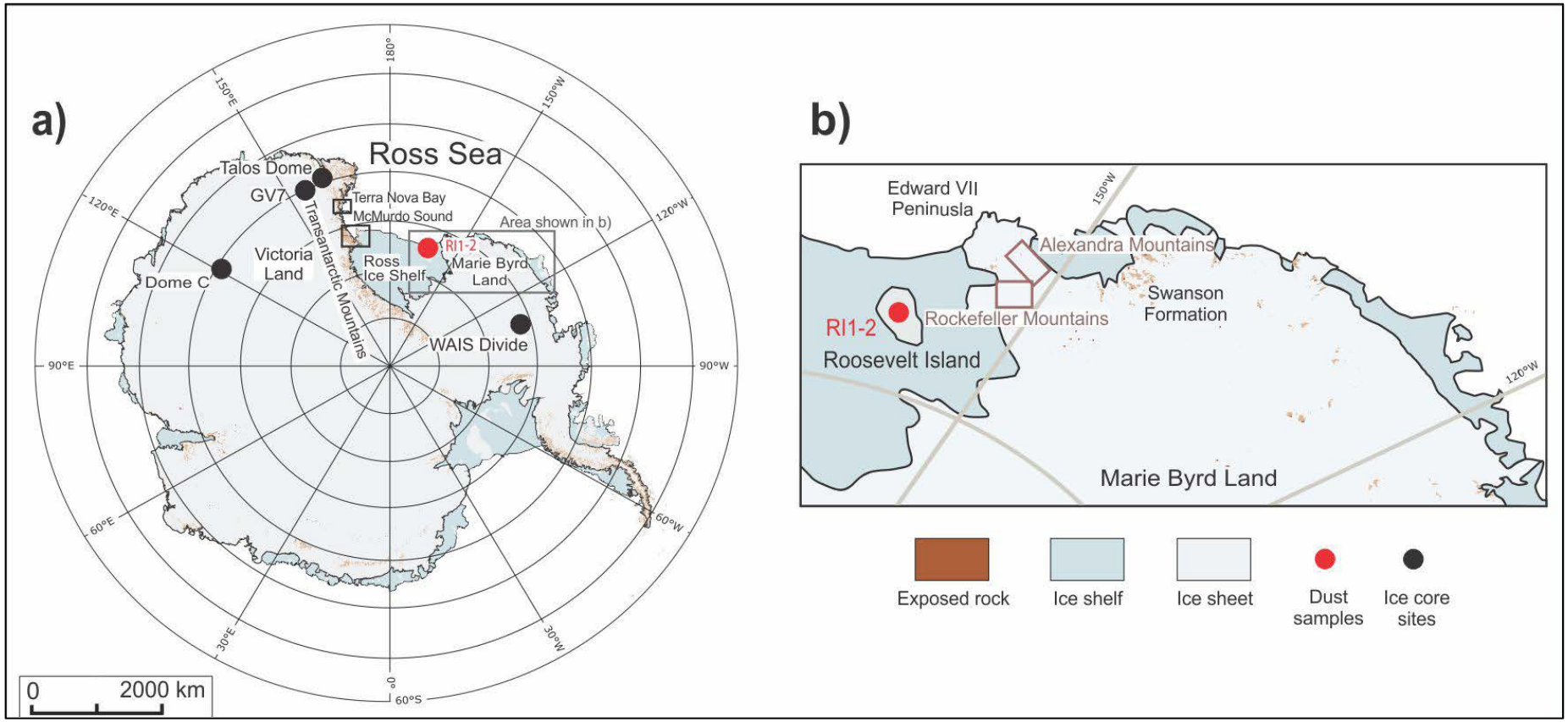

Fig. 6.1: a) Map of Antarctica showing the location of the Ross Sea. b) Insert of Marie Byrd Land showing West Antarctica potential source areas and Roosevelt Island dust sample locations (RI1-2). EAIS: East Antarctic Ice Sheet, MDV: McMurdo Dry Valleys, TAM: Transantarctic Mountains.

6.2 Methods

A detailed description of the snow sampling procedure, dust, rBC, trace metal solubility and Sr and Nd isotopic analysis can be found in Supplementary Information 1. Briefly, four parallel profiles of ultra-clean snow samples were collected at 3 cm resolution from a 1.5 m snow pit. The snow pit was located in a designated clean sector at Roosevelt Island during the 2012/13 RICE ice core drilling campaign. Parallel profile samples were measured for particle size and concentration (Coulter Counter [*Delmonte et al.*, 2002]), rBC concentration (single particle intracavity laser-induced incandescence photometer (SP2 [*Sterle et al.*, 2013]), $\delta^{18}O$ isotopes (high-resolution laser absorption spectroscopy; Los Gatos Research Liquid-Water Isotope Analyser), and dissolved and total dissolvable concentrations of sulfur (S), Fe and aluminium (Al). Dissolved Fe and Al fractions were determined by filtering a 10 mL aliquot of snow melt through a 0.2 µm filter [*Lannuzel et al.*, 2008]. The remaining (unfiltered) sample was leached with 1 % HCl (ultra-pure) for three months to determine the total dissolvable trace metal fraction following *Edwards et al.* [2006] who showed that a three-month leaching period was required for TDFe concentrations to plateau. Total dissolvable solutions and dissolved leachates were analysed by high resolution inductively coupled plasma mass spectrometry (HR-ICP-MS). HR-ICP-MS operating conditions and blank elemental levels are reported in Tables S6.1 and S6.2. Stringent trace metal practices were employed at all stages of sample processing and analysis. Sampling vials and filtration gear was rigorously acid cleaned prior to use following GEOTRACES protocols[2]. Fractional Fe solubility was calculated using equation 6.1:

$$Fractional\ Fe\ Solubility = \frac{dFe}{TDFe}\ x\ 100 \qquad \text{Equation (6.1)}$$

where dFe is the soluble or dissolved Fe fraction and TDFe is the total dissolvable fraction.

A reflected light optical microscope (BX51M) was used to confirm the presence of large particles (>10 µm) detected by Coulter Counter (Fig. S6.1). Adjacent to the snow pit, a large volume of surface snow was collected for Sr and Nd isotopic ratios and concentrations of dust for provenance attribution (Supplementary Information 1). Dust particles were separated from the snow, and two samples (RI1-2) were spiked, digested, separated from interfering

[2] http://www.geotraces.org/images/stories/documents/intercalibration/Cookbook.pdf

elements and analysed by TRITON Thermal Ionization Mass Spectrometer (TIMS) following *Delmonte et al.* [2008].

6.3 3. Results

6.3.1 Snow pit dating

The dating of the RICE snow pit was based on water stable isotope ratios $\delta^{18}O$ and on concentrations of total dissolved non-sea-salt sulfur (nss-S) (Fig. 6.2) following *Tuohy et al.* [2015]. Non-sea-salt sulfur shows sharp, well defined summer peaks. The $\delta^{18}O$ measurements in Antarctic snow and ice often reflect seasonal cycles in temperature [*Dansgaard*, 1954; *Johnsen et al.*, 1972]. However, the upper snow pack at Roosevelt Island contains $\delta^{18}O$ variability within seasons which reflects individual storm events [*Tuohy et al.*, 2015]. Summers were determined as 1 January and were positioned where nss-S peaks aligned with peaks or shoulders of peaks in the $\delta^{18}O$ record. Winters were determined as 1 July where a nss-S trough aligned with a $\delta^{18}O$ trough. Annual cycle counting of nss-S layers shows the snow pit spans a two year period from summer 2012/13 to summer 2010/11 (Fig. 6.2), with an age uncertainty of ±0.5 year at the base of the snow pit. The snow accumulation rate of the snow pit is estimated to be 0.33 m yr^{-1} water equivalent (w.e; estimated from nss-S concentration peaks between January 2011 and January 2012), assuming the average annual distribution of snowfall is uniform. These rates are consistent with an accumulation rate of ~0.27 m yr^{-1} ice equivalent from snow stake measurements ~700 m from the snow pit site at Roosevelt Island between 2010 and 2012 [*H. Conway*, unpublished data, 2015].

To constrain the seasonality of nss-S with known sulfate emissions from phytoplankton [e.g. *Rhodes et al.*, 2009], high-resolution chlorophyll-*a* satellite data were downloaded for the Ross Sea region (area defined by 161.175° to -151.125°, -70.078° to -80.0°) (Fig. 6.2k-l, SeaWiFS; http://disc.sci.gsfc.nasa.gov/giovanni). The temporal development of Ross Sea polynya phytoplankton bloom ("bloom 2," see Section 6.1) was used due to the dominant easterly transport within the Ross Sea [*Sinclair et al.*, 2010]. Comparison of chlorophyll-*a* concentration data over the Ross Sea region shows that the bloom develops in November and declines in December in both 2010 and 2011 (Fig. 6.2l). In addition, a hoar layer (with a low snow density of 0.20 g m^{-3}) at ~55 cm depth in the snow pit was compared to nss-S summer

maxima Fig. 6.2i-l). The age scale independently places this hoar layer in 2011 spring-summer, confirming the validity of the overall age model.

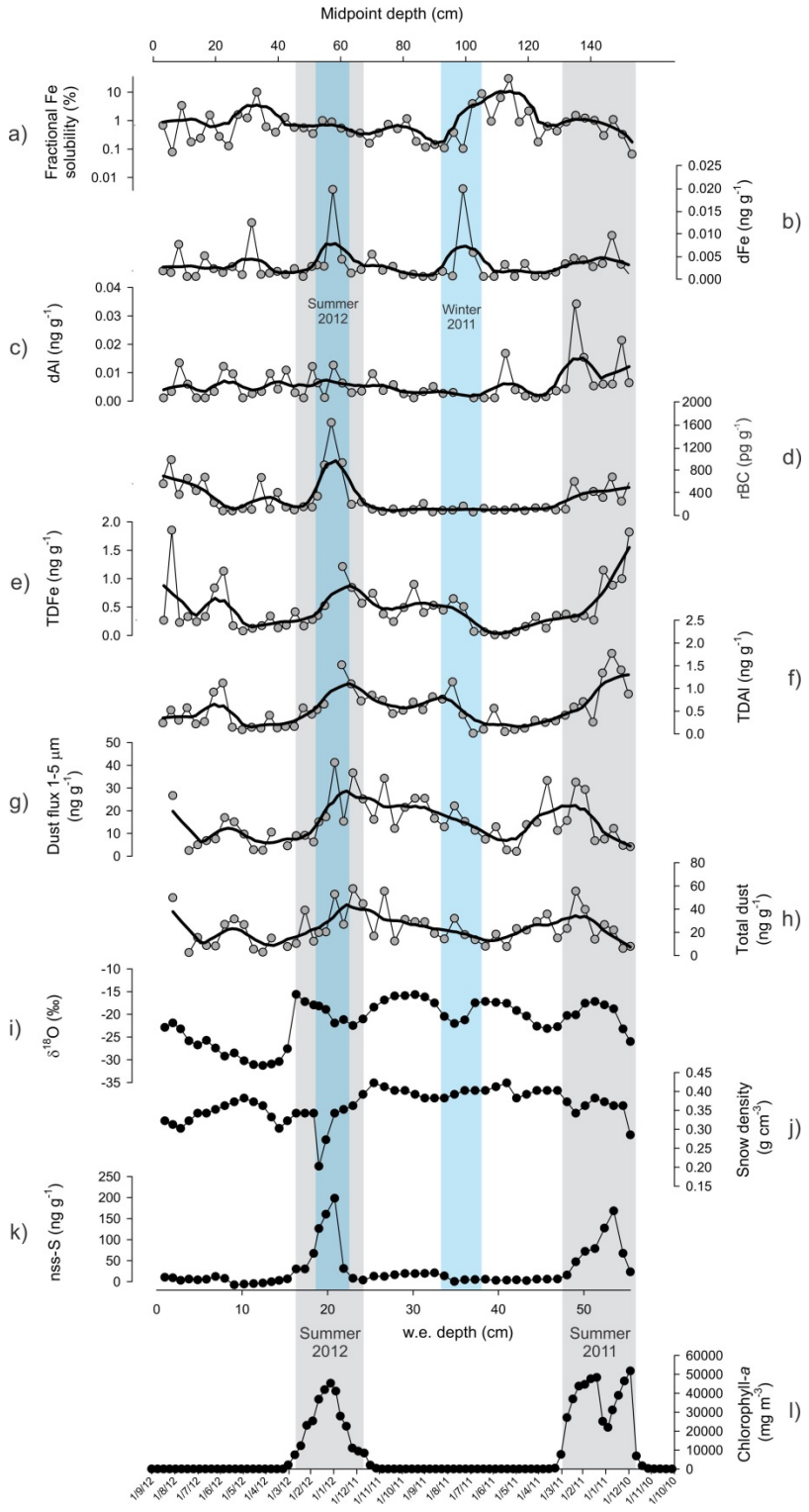

Fig. 6.2: Roosevelt Island snow pit profile showing a) fractional Fe solubility, b) dFe concentration, c) dAl concentration, d) rBC concentration, e) TDFe concentration, f) TDAl concentration, g) dust concentration for the 1-5 µm fraction, h) total dust concentration for the 1-30 µm fraction, i) $\delta^{18}O$, j) snow density, k) nss-S concentration, l) chlorophyll-*a* concentration. Grey bars indicate summer periods. Blue bars highlight the largest periods of dFe deposition. Black lines indicate smoothed data using a 0.15 loess model [*Cleveland and Devlin*, 1988].

6.3.2 Seasonal dust variability and particle size distribution

The Roosevelt Island snow pit records inter-annual variability in dust deposition over a two year period. The dust concentration in the snow pit ranges from 2 to 41 ng g^{-1} for the 1-5 µm fraction and 2 to 58 ng g^{-1} for the 1-30 µm particle size fraction. We note that two samples have low dust concentrations (<4 ng g^{-1}) close to exposure blank levels (~2 ng g^{-1}). Dust deposition in the snow pit is episodic. The dust record displays two maxima corresponding to summer-spring elevated levels of nss-S in January 2012 and January 2011 (Figs. 6.2g-h and 2k). Lower dust concentrations are observed in winter, however, an episodic dust event is captured during winter 2012. Seasonal dust deposition at Roosevelt Island, primarily during spring-summer, is coherent with an earlier snow pit study from the site that showed higher Al/Na ratios [*Cohen*, 2013] in correspondence with summer peaks of the $\delta^{18}O$ record. At GV7, a peripheral site located on the South Pacific margin of the East Antarctic ice sheet in Northern Victoria Land (Fig. 6.1), dust deposition from a snow pit clearly shows spring-summer maxima and winter minima *(B. Delmonte,* unpublished data, 2015). Dust deposition at other locations in Antarctica also exhibits seasonal variability with a maximum in summer (e.g. Berkner Island [*Bory et al.*, 2010], Windless Bight, McMurdo Sound [*Dunbar et al.*, 2009] and South Pole [*Legrand and Kirchner*, 1988]).

The particle size distribution of dust particles measured from 1 to 30 µm does not approximate a lognormal particle size distribution. Rather, the size distribution of dust particles approaches the theoretical dust emission particle size distribution, parameterized by [*Kok*, 2011a], for particles between 1 and 5 µm in diameter in samples with elevated dust concentrations in both spring-summer periods. The particle size can be seen in some of these highly concentrated spring-summer samples in Fig. 6.3 and compared to the lognormal particle size distribution of long-range transport dust to the East Antarctic Plateau. For very low concentration samples, the size distribution of microparticles typically does not show a clear mode. For this reason, other size indicators (fine particle percentage (FPP) and the coarse particle percentage (CPP) parameters) were introduced to study long-term dust size variations in central Antarctica [*Delmonte et al.*, 2002]. In this case, longer records of particle size distributions are required to investigate seasonality in particle size distribution at Roosevelt Island. Large particles with an equivalent spherical diameter between 5 and 10 µm were also observed (Fig. 6.3).

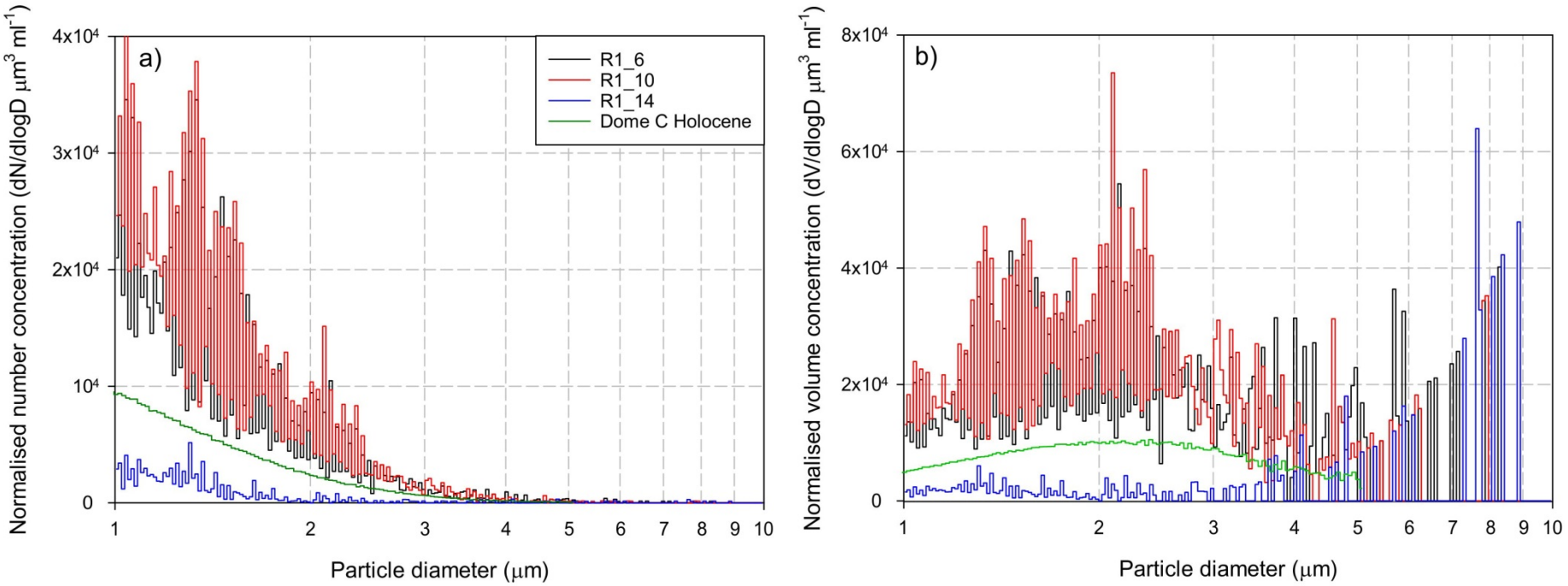

Fig. 6.3: Examples of particle size distributions in the snow pit from Roosevelt Island and comparison to the lognormal particles size distribution of Holocene dust from the Dome C ice core on the East Antarctic Plateau. Blue: a) Normalized size distribution of the number of particles (dN/dlogD), b) normalized volume size distribution (dV/dlogD). Samples shown are RI_14, Black: RI_6, Red: RI_10. Dome C Holocene particle size distribution from *Delmonte et al.* [2002].

6.3.3 Isotopic composition of dust

The Sr and Nd isotopic composition of the two Roosevelt Island dust samples (RI1-2) are $0.7122 < {}^{87}Sr/{}^{86}Sr < 0.7156$ and $\varepsilon_{Nd}(0) = -9.6$. These data are reported in Table 6.1 and Figs. 6.4-6.5 with additional isotopic data from Antarctic PSAs. PSAs in Fig. 6.4 are grouped by geographic location.

Table 6.1:Nd and Sr concentrations [in parentheses] and isotopic composition of Roosevelt Island surface snow samples analysed in this study. n.d.: no data.

Sample	Size (µm)	$^{143}Nd/^{144}Nd$	[a] $\pm 2\sigma_{mean} *10^6$	[b] $\varepsilon_{Nd}(0)$	[c] $\pm 2\sigma$	[Nd] (ppm)	[d] $\pm$ (ppm)	$^{87}Sr/^{86}Sr$	[e] $\pm 2\sigma_{mean} *10^6$	[f] $^{87}Sr/^{86}Sr$ corrected	[g] $\pm 2\sigma *10^6$	[Sr] (ppm)	[d] $\pm$ (ppm)
RI-1	Bulk	n.d.	n.d.	n.d.	n.d.	3	0.3	0.712173	17	0.712201	17	40	4
RI-2	Bulk	0.512146	50	-9.6	0.3	12	1.2	0.715560	48	0.715588	48	60	6

[a] Internal precision, 2 standard errors of the mean.
[b] Nd isotopic ratios expressed as epsilon units $\varepsilon_{Nd}(0) = [(^{143}Nd/^{144}Nd)_{sample}/(^{143}Nd/^{144}Nd)_{CHUR}-1]x10^4$; CHUR, chondritic uniform reservoir with $^{143}Nd/^{144}Nd=0.512638$.
[c] Uncertainty estimates based upon external precision for standard runs. Internal precision is used if it exceeds the external.
[d] Error due to difficulty of measuring small sample masses, estimated by repeat measuring of weighting BCR-2 standards (~0.3 mg).
[e] Internal precision, 2 standard errors of the mean.
[f] Corrected to a NBS 987 $^{87}Sr/^{86}Sr$ ratio of 0.710245.
[g] Uncertainty estimates based upon external precision for standard runs. Internal precision is used if it exceeds the external.

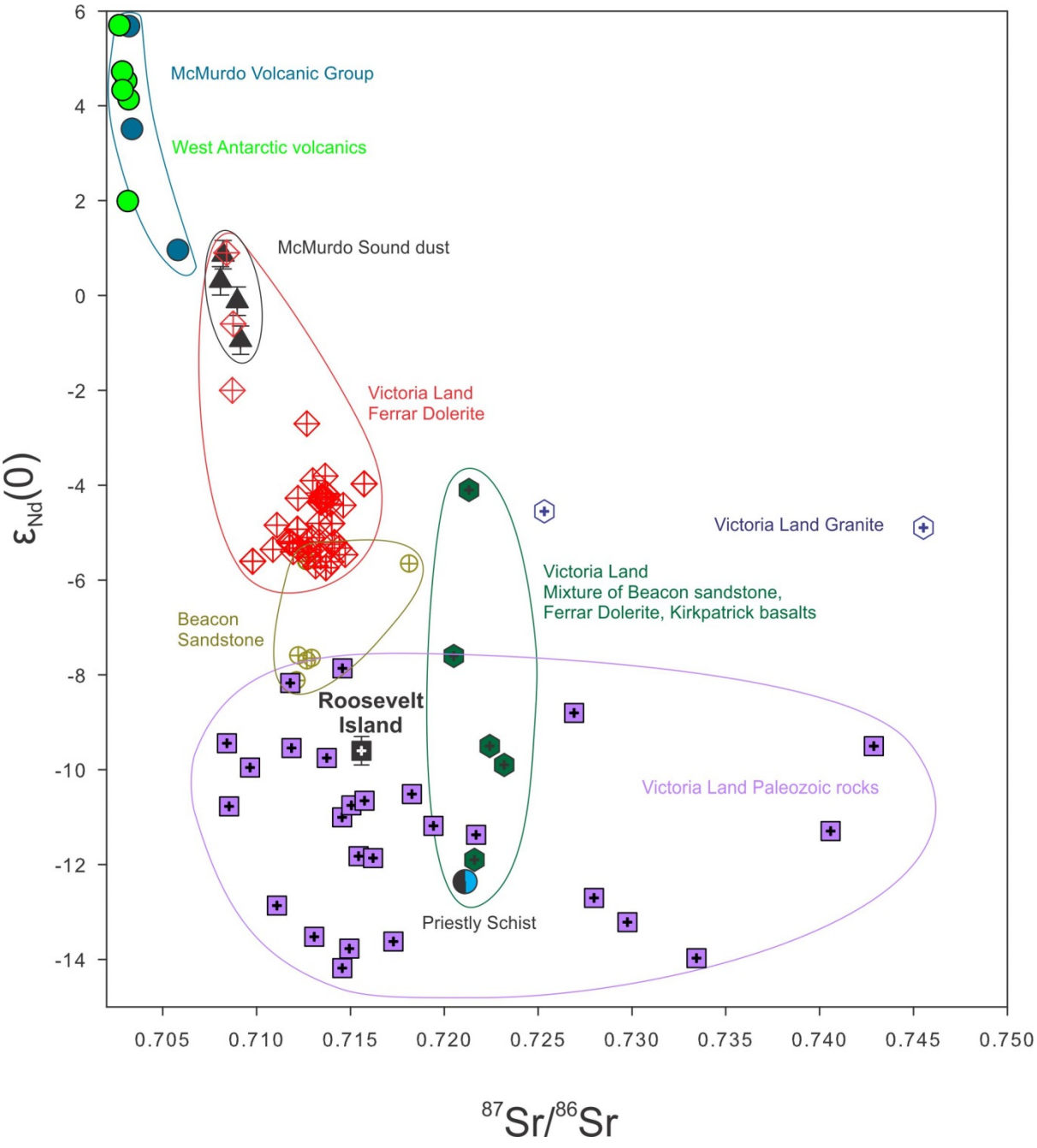

Fig. 6.4: Nd and Sr isotope signature of Roosevelt Island surface snow dust sample. Note only one sample is plotted as there is no Nd data for the second sample. Also plotted are data from Victoria Land sediments from potential dust sources (regolith, glacial deposits, aeolian sediments) [*Delmonte et al.*, 2004b; *Delmonte et al.*, 2013; *Delmonte et al.*, 2010b] that include different parent lithologies (Victoria Land Ferrar Igneous Provence [*Antonini et al.*, 1999; *Delmonte et al.*, 2004b; *Elliot et al.*, 1999; *Fleming et al.*, 1995] and Victoria Land Palaeozoic rocks [*Cox et al.*, 2000; *Schüssler et al.*, 1999; *Talarico et al.*, 1995]) and volcanic rocks from the McMurdo Volcanic Group and West Antarctica [*Delmonte et al.*, 2004b; *Futa and Le Masurier*, 1983; *Hole and LeMasurier*, 1994].

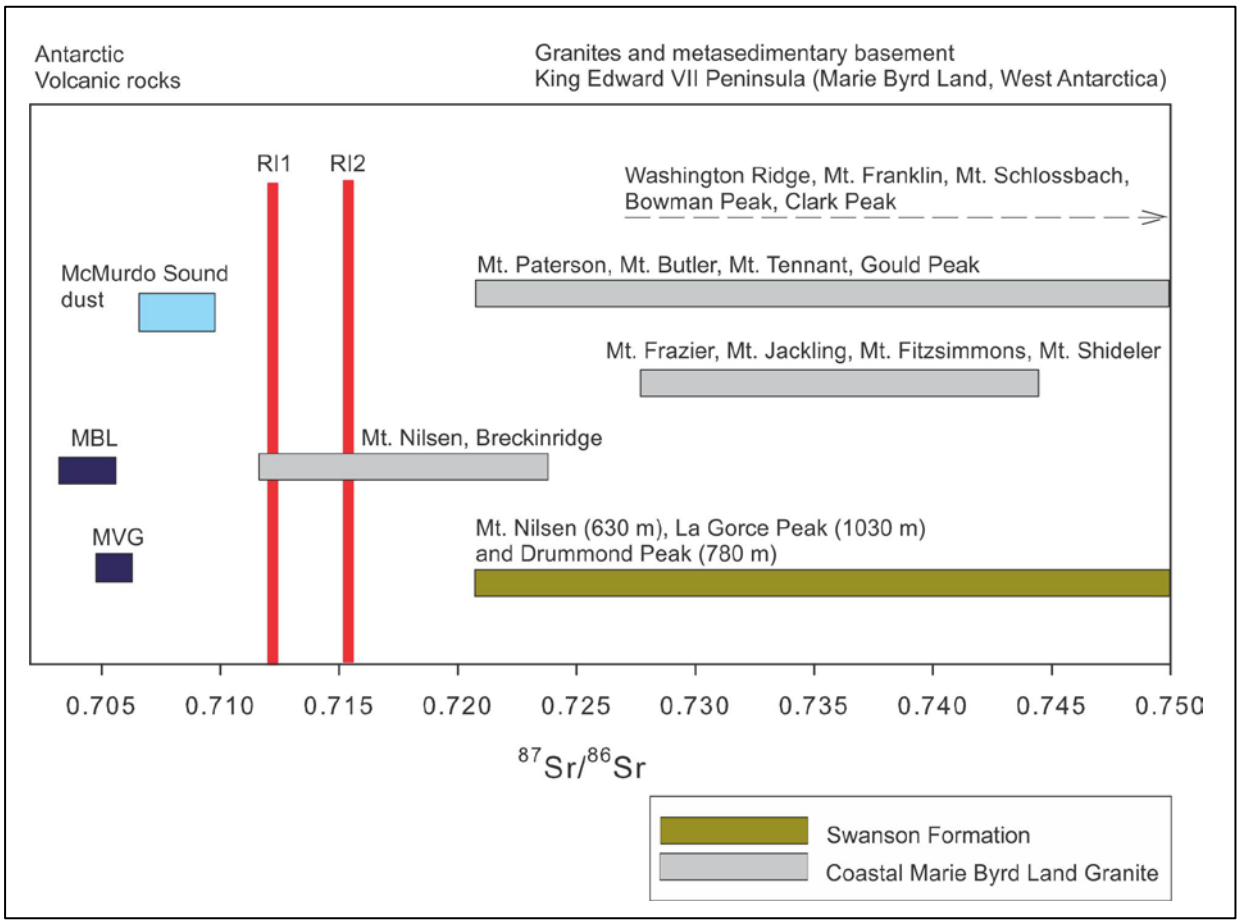

Fig. 6.5: $^{87}Sr/^{86}Sr$ isotopic composition of Roosevelt Island dust compared to McMurdo Sound dust [*Winton et al.*, 2014; Winton et al., in review], Antarctic volcanic rocks [*Delmonte et al.*, 2004b; *Futa and Le Masurier*, 1983; *Hole and LeMasurier*, 1994] and King Edward VII Peninsula, Marie Byrd Land, West Antarctic Granites and metasedimentary basement rocks [*Adams et al.*, 1995].

6.3.4 Microscope observations

Mineral dust and volcanic glass (~10 µm in diameter) was present in Roosevelt Island samples, but only a few qualitative optical observations were performed on selected samples from Roosevelt Island (Fig. S6.1). Volcanic glass is a common component of background dust in Antarctica [*Narcisi et al.*, 2005]. These microscopic observations were useful for confirming the presence of particles having a diameter between 5 and 10 µm, thus a) eliminating the possibility of particulate contamination of sampling equipment and laboratory procedures, and b) validating Coulter Counter observations of relatively coarse particles in the samples.

6.3.5 Refractory black carbon

Deposition of rBC in the Roosevelt Island snow pit is highest during the 2011/2012 summer (Fig. 6.2d). Austral winter background values in 2011 average ~100 pg g^{-1}, and the summer rBC concentrations reached four times above background levels in January 2011, and seven times the background levels in January 2012 (up to ~1.5 ng g^{-1}). The 2011/2012 summer peak in rBC was exceptionally high in comparison to rBC concentrations reported for the West Antarctic Ice Sheet (WAIS) Divide ice core (geometric mean ~80 pg g^{-1} [*Bisiaux et al.*, 2012b]). Additional smaller peaks of rBC concentrations were also found in late winter-spring in 2012 at Roosevelt Island, similar to the timing of rBC deposition at WAIS Divide.

6.3.6 Dissolved and total dissolvable iron and aluminium

With the exception of one layer (61.5 - 64.5 cm depth), TDFe and TDAl concentrations ranged from 0.01 ± 0.001 to 1.9 ± 0.1 ng g^{-1} and 0.01 ± 0.001 to 1.8 ± 0.1 ng g^{-1} respectively. The higher concentrations from the 61.5 - 64.5 cm layer were 5.4 ± 0.1 ng g^{-1} of TDFe and 6.7 ± 0.1 ng g^{-1} of TDAl. This depth also displayed high rBC concentrations of 1630 pg g^{-1}. TDFe and TDAl co-vary in the snow pit (Figs. 6.2e-f). A strong relationship was found between the two trace metals (r^2=0.86; Fig. 6.S3a), with maxima occurring in the summer at the same time as rBC and dust in 2011/2012 but not in 2010/2011.

Dissolved Fe concentrations were lower than TDFe, and ranged between 0.001 ± 0.0001 and 0.2 ± 0.001 ng g^{-1} (Fig. 6.2b). Although the exposure blank dFe and dAl concentrations are exceptionally low (Table S6.2), the dFe and dAl blank background is similar to some of the snow pit samples. Due to the extremely low dissolved concentration of the snow pit samples, it is possible that the uncertainty on the blank concentrations could be responsible for some of the temporal variation. Nevertheless, dFe peaked four times above the recorded dFe background of 0.02 ng g^{-1}. Two of these maxima occurred in summer 2011/2012 at the same time as peaks in TDFe, TDAl, dust and rBC concentrations at Roosevelt Island, while the other two peaks occur in the winter when dust rBC, TDFe and TDAl are low (Fig. 6.2).

6.4 Discussion

6.4.1 Atmospheric dust deposition and provenance

Ice cores from the high-elevation East Antarctic Plateau represent a unique archive to investigate long-range dust transport [e.g. *Delmonte et al.*, 2004b]. In contrast, around the margin of Antarctica, the occurrence of sparse ice-free areas can represent a non-negligible dust source to the local atmosphere [*Delmonte et al.*, 2013]. At these sites, the interpretation of ice core dust records is related to mesoscale dust entrainment, advection and deposition driven by regional circulation. Roosevelt Island is a low-altitude location (550 m.a.s.l.), well outside the high-elevation polar plateau. Large expanses of ice-free areas occur around the margins of the Ross Sea (Fig. 6.1), and thus the dust cycle there is widely different from the East Antarctic Plateau in terms of abundance and origin.

Known dust sources to the western Ross Sea include the Transantarctic Mountains, Terra Nova Bay and McMurdo Sound [*Atkins and Dunbar*, 2009; *Barrett et al.*, 1983; *Dunbar et al.*, 2009]. Of these, southern McMurdo Sound is known to be the dustiest location in Antarctica [*Chewings et al.*, 2014; *Winton et al.*, 2014]. In terms of the western Ross Sea, Sr and Nd isotopic data is only available for McMurdo Sound and some areas in the Transantarctic Mountains [*Cook et al.*, 2013; and refernces therein; *Delmonte et al.*, 2004b; *Delmonte et al.*, 2013; *Winton et al.*, 2014], although an expansion of the existing isotopic catalogue of Antarctic PSAs is in preparation [*Blakowski et al.*, submitted] in an effort to deepen the current understanding of Holocene dust input to the periphery of the EAIS. The isotopic signature of these PSAs in the western Ross Sea is plotted in Fig. 6.4 and compared to the signature of Roosevelt Island dust measured in this study. The isotopic composition of one sample representing modern summer snow at Roosevelt Island is markedly different from the fingerprint of McMurdo Sound (Table 6.1, Fig. 6.4), i.e., Roosevelt Island dust ($0.7122< {}^{87}Sr/{}^{86}Sr <0.7156$ and $\varepsilon_{Nd}(0)=-9.6$) has a more radiogenic ${}^{87}Sr/{}^{86}Sr$ signature and less radiogenic $\varepsilon_{Nd}(0)$ signature compared to the volcanic sediments from McMurdo Sound [*Winton et al.*, 2014]. Therefore, the isotopic data alone suggests that dust deposited on Roosevelt Island cannot be solely sourced from McMurdo Sound.

In addition, the dust concentrations at Roosevelt Island are lower and the particle size distribution is finer than the dusty McMurdo Sound [e.g. *Chewings et al.*, 2014]. An annual

dust flux at Roosevelt Island was estimated for the calendar year 2011 (the beginning of the calendar year was taken at each nss-S peak), and the water equivalent depth was calculated from the snow pit density measurements (Fig. 6.S2). The estimated dust flux of 6 mg m^{-2} yr^{-1} for the 1-5 µm particle fraction (8 mg m^{-2} yr^{-1} for the bulk 1-30 µm particle fraction) at Roosevelt Island in this study is seven times greater than the equivalent pre-industrial East Antarctic dust flux of 0.19-0.75 mg m^{-2} yr^{-1} [*Delmonte et al.*, 2013], and also greater than modern modelled and empirical fluxes of dust to the Southern Ocean (0.3 to 2.5 mg m^{-2} d^{-1}) [*Duce et al.*, 1991; *Mahowald et al.*, 2005; *Wagener et al.*, 2008]. The bulk 1-30 µm dust flux at Roosevelt Island is double that found in the WAIS Divide ice core: ~4 mg m^{-2} yr^{-1} over the past two millennia [*Koffman et al.*, 2014b]. By comparison, the dust fluxes for Roosevelt Island, East Antarctica and the Southern Ocean are orders of magnitude lower than the dust flux of the McMurdo Sound fine fraction reported by *Winton et al.* [2014], i.e. 460 mg m^{-2} yr^{-1} for the <10 µm fraction.

Larger dust particles (between 5-10 µm) represent a non-negligible contribution to the total dust input at Roosevelt Island. The particle size distribution of the dust at Roosevelt Island (Fig. 6.3) is coarser than the distally-sourced dust deposited on the East Antarctica Plateau. For example, at Dome C and other sites located in central Antarctica [*Delmonte et al.*, 2002], dust particles are mostly within the size interval 1-5 µm in diameter. The only large particles deposited on the central East Antarctic Plateau have been previously associated with tephra layers [*Basile et al.*, 2001; *Narcisi et al.*, 2005]. Furthermore, the particle size distribution curve can provide additional information about the proximity to the dust source [*Kok*, 2011a; b]. Dust follows a lognormal distribution in ice cores from regions that primarily receive long-range transport dust to the East Antarctic Plateau or central Greenland [*Delmonte et al.*, 2002; *Ruth*, 2002; *Steffensen*, 1997], for example, Dome C (Fig. 6.3). However, recent work by *Kok* [2011a; 2011b] has shown that dust near the emission source does not necessarily follow a lognormal distribution. The spring-summer snow pit samples that approach the theoretical dust emission particle size distribution, parameterized by [*Kok*, 2011a], at Roosevelt Island and other sites near the margin of the ice sheet (e.g. WAIS Divide [*Koffman et al.*, 2014b]), suggest that dust is not travelling as far as long-range transported dust reaching the East Antarctic Plateau which has a lognormal distribution [*Delmonte et al.*, 2002] (Fig. 6.3). These spring-summer samples that approach the theoretical dust emission distribution are indicative of local dust sources. Compared to the East Antarctic Plateau, the higher dust flux, particle size distribution approaching the theoretical dust emission

distribution and the presence of large particles (<10 μm) observed under the optical microscope and SEM suggests a local Antarctic dust input to Roosevelt Island. This local Antarctic dust input has a distinctly different isotopic fingerprint to modern McMurdo Sound dust emissions (Fig. 6.4).

The Sr and Nd isotopic signature of Roosevelt Island dust in Figs. 6.4 and 6.5 suggest that dust deposited at Roosevelt Island during summer 2012/2013 could be a mixture of at least two local sources. One end member is likely volcanic material with relatively high radiogenic Nd and less radiogenic Sr. The other end member is likely to be much older, with more radiogenic Sr and less radiogenic Nd. Given existing Sr and Nd isotopic data, the sources to Roosevelt Island include eastern Australia, parts of coastal Marie Byrd Land, and most of Victoria Land. Given the relatively high dust flux, the presence of large particles and particle size distribution approaching the theoretical dust emission distribution we first consider local dust sources upwind of Roosevelt Island. The fetch area of five-day air mass back trajectories for 2011 and 2012 arriving at Roosevelt Island are predominately from West Antarctica, the Pacific Ocean sector of Antarctica and Victoria Land [*Tuohy et al.*, 2015]. Air mass back trajectories and background climatological circulation shows prevailing winds cross exposed rock in Marie Byrd Land, West Antarctica before arriving at Roosevelt Island [*Koffman et al.*, 2014b; *Tuohy et al.*, 2015]. Air masses can also arrive at Roosevelt Island via synoptic cyclonic circulation in the Ross Sea [*Koffman et al.*, 2014b; *Neff and Bertler*, 2015b]. Therefore, two potential end member local dust sources for Roosevelt Island are West Antarctic volcanic material and Victoria Land Palaeozoic rocks (i.e., the bedrock that comprises most of northern Victoria Land, effectively upwind of Roosevelt). Figure 6.4 shows that the isotopic composition of Roosevelt Island dust falls between the isotopic fields of both these end members. Despite the isotopic similarity of Victoria Land Palaeozoic rocks and Roosevelt Island dust, we believe this West to East dust transport hypothesis very unlikely, because strong convective uplift would be necessary to uplift dust in the troposphere above the marine boundary layer, where dust is rapidly removed.

In terms of Victoria Land, previous studies have shown that although there is a high dust flux within the McMurdo Dry Valleys [*Ayling and McGowan*, 2006; *Gillies et al.*, 2013; *Lancaster et al.*, 2010; *Selby et al.*, 1974], little dust exits the valleys [*Winton et al.*, In Press]. The long exposure to katabatic winds has winnowed the surface sediment, resulting in a lack of dust and very fine sand-sized material over most of the valley floor [e.g. *Delmonte et al.*,

2010b; *Selby et al.*, 1974]. These air masses do not travel high in the troposphere and when they encounter humidity from the ocean, the dust is scavenged. Although *Bhattachan et al.* [2015] suggest that dust from Taylor Valley in the McMurdo Dry Valleys could supply soluble iron to the wider Southern Ocean, other studies have discounted the McMurdo Dry Valleys as a major dust (and dFe) source due to the limited transport in this region [*Barrett et al.*, 1983; *Bentley*, 1979; *Chewings et al.*, 2014; *Winton et al.*, 2014; *Winton et al.*, 2016]. Therefore, we suggest that dust sourced from Victoria Land is unlikely to be transported eastward to Roosevelt Island. While Victoria Land sources should not be completely discarded due to the large expanse of ice-free area and the isotopic signature Victoria Land Palaeozoic rocks potentially acting as an end member dust source, we also consider local sources from Marie Byrd Land that are immediately upwind of Roosevelt Island.

Although Roosevelt Island is completely ice-covered, there are patchy ice-free areas (Rockefeller Mountains and Alexandra Mountains, and extensive volcanics e.g. the Executive Committee Range) along the north-westernmost part of Marie Byrd Land, on the King Edward VII Peninsula (Fig. 6.1b), that is adjacent to the eastern Ross Sea. According to *Adams et al.* [1995], the King Edward VII Peninsula is characterized by presence of three main rock units: i) a low-grade metasedimentary suite of late Ordovician age, correlated with the Swanson Formation of the Ford Ranges; ii) a granitoid suite correlated to the Byrd Coast granite and particularly developed in the Rockefeller Mountains, which includes monzogranites and syenogranites, and iii) the Alexandra Metamorphic Complex formed by migmatitic paragneiss. The Sr isotopic signature of these ice-free areas on the eastern margin of the Ross Sea is compared to Roosevelt Island dust in Fig. 6.5. Whole-rock Rb-Sr geochemistry of the Rockefeller and Alexandra Mountains of Edward VII Peninsula show $^{87}Sr/^{86}Sr$ higher than about 0.721 (Swanson Formation) and higher than 0.712 (Byrd Coast Granite) (Fig. 6.5) while Nd isotopic data are not available [*Adams et al.*, 1995]. On the contrary, volcanic rocks from Marie Byrd Land and other volcanic provinces show very unradiogenic Sr (McMurdo Sound and Marie Byrd Land volcanic rocks ($0.7026< {}^{87}Sr/^{86}Sr <0.7032$ and $2.0< \varepsilon_{Nd}(0) <6.9$); Fig. 6.5) [*Futa and Le Masurier*, 1983; *Hole and LeMasurier*, 1994]. On the basis of Sr isotopic data and particle size distribution data indicating that dust at Roosevelt Island may be locally-sourced at present-day, we suggest that the summer 2012/2013 Roosevelt Island snow dust sample represents a mixture of local volcanic dust and crustal material likely deriving from the neighbouring granites and metasedimentary rocks of

western Marie Byrd Land and possibly Palaeozoic rocks from Victoria Land (Figs. 6.4 and 6.5).

We also consider a remote Southern Hemispheric contribution of long-range transported dust to Roosevelt Island. Distally-derived larger particles could reach Roosevelt Island but are not transported further inland to the high elevation Antarctic interior. The Roosevelt Island isotopic signature is distinctly different to dust deposited on East Antarctica during the pre-industrial (1400 A.D. - 1800 A.D.; $^{87}Sr/^{86}Sr$ ranging between 0.707468 - 0.708468) and Holocene periods ($^{87}Sr/^{86}Sr$ ranging between 0.707689 - 0.711200 [*Delmonte et al.*, 2013]), which suggests the eastern Ross Sea has a different dust source to the East Antarctica Plateau. Roosevelt Island falls within the Australian isotopic field, which is characterized by $^{87}Sr/^{86}Sr$ ratios ranging from 0.709 to 0.732 and $\varepsilon_{Nd}(0)$ between −3 and −15 [*Delmonte et al.*, 2004b; *Revel-Rolland et al.*, 2006]. *Revel-Rolland et al.* [2006] and *De Deckker et al.* [2010] suggested that Australia could contribute to the dust input in central East Antarctica. Modelling studies of dust transport to Antarctica from Southern Hemispheric continents [*Krinner et al.*, 2010] show that the annual mean concentration of dust in the eastern Ross Sea region of Antarctica is mostly represented by dust derived from Australia, in agreement with former modelling studies [*Albani et al.*, 2012b; *Li et al.*, 2008; *McGowan and Clark*, 2008]. We note, in addition, that the seasonality of Australian dust export to high southern latitudes occurs during spring and summer [*Boyd et al.*, 2004; *Mahowald et al.*, 2005], hence it is synchronous with the dust peaks we observed in the Roosevelt Island snow pit. *Krinner et al.* [2010] clearly showed that the concentration of Australian continental dust tracers is at a maximum at about 150 °W, close to Roosevelt Island. Although, dust appears to be mostly concentrated at higher tropospheric levels (about 6000 m) that are well above the altitude of the Roosevelt Island [*Krinner et al.*, 2010]. *Neff and Bertler* [2015b] and *Tuohy et al.* [2015] highlight the likelihood of air parcels transported to Roosevelt Island: both air mass back trajectories for the 2011/2012 summer season and the average seasonal air mass forward trajectories from Southern Hemisphere dust sources for the previous thirty-five six years indicate that air can be derived from the South Pacific which includes transport from Australia and New Zealand. Based on the Sr and Nd isotope data of Australian and New Zealand rocks [*Delmonte et al.*, 2004b; *Revel-Rolland et al.*, 2006], an Australian contribution is more likely.

In summary, geochemical evidence excludes McMurdo Sound dust inputs as the dominant dust source to Roosevelt Island at present. The isotopic data and the presence of coarse particles at Roosevelt Island, compared to East Antarctic Plateau dust, suggest a local contribution from coastal regions of Antarctica. Potential dust sources include Marie Byrd Land rock outcrops, West Antarctic outcrops which are currently not well characterized in terms of their Nd and Sr isotopic signature, or other ice-free areas that have an old crust-like signature. These ice-free areas could include Victoria Land, given that the synoptic cyclonic circulation pattern in the Ross Sea region could allow for dust transport from the western Ross Sea to the eastern Ross Sea. We cannot exclude the possibility of an Australian dust contribution, as the isotopic field overlaps with that of Marie Byrd Land and Victoria Land Palaeozoic rocks. Both *Bory et al.* [2010] and *Delmonte et al.* [2013] show that local dust sources on the periphery of the ice sheet can significantly influence the dust composition at coastal, low elevation Antarctic ice core sites. Thus, Roosevelt Island could similarly be sourced from a mixture of local and distal dust sources. Further geochemical measurements from the RICE ice core are required to better constrain the dust provenance in the Ross Sea.

6.4.2 Atmospheric iron in the Ross Sea region

6.4.2.1 Atmospheric iron fluxes

Annual dissolved and total dissolvable Fe and Al fluxes for 2011 were calculated using the same method for dust (see section 6.4.1). Summer and winter dissolved Fe and Al fluxes for the period 2011 to 2012 were also estimated and are reported in Table 6.2. We estimate an annual dFe flux of 1.2 x 10^{-6} g m^{-2} y^{-1} and annual TDFe flux of 140 x 10^{-6} g m^{-2} y^{-1}. The TDFe flux estimate for Roosevelt Island is higher than published Holocene values in Antarctic ice cores, for example, a TDFe flux of 45 x 10^{-6} g m^{-2} y^{-1} was reported for coastal Law Dome [*Edwards et al.*, 2006]. The TDFe flux at Roosevelt Island is also higher than acid leachable fluxes of 7 x 10^{-6} g m^{-2} y^{-1} at Dome C, East Antarctic Plateau [*Gaspari et al.*, 2006] and 90 x 10^{-6} g m^{-2} y^{-1} at Talos Dome [*Vallelonga et al.*, 2013]. Talos Dome is known to be influenced by local dust sources [*Delmonte et al.*, 2010b], and the higher TDFe flux at Roosevelt Island is likely due to the contribution of local dust sources from Marie Byrd Land and/or Victoria Land. Local dust sources located on the coast of East Antarctica are also known to influence the concentration of aerosol Fe samples collected over marginal waters [*Gao et al.*, 2013]. The TDFe flux at Roosevelt Island is orders of magnitude lower than locally derived aeolian

Fe from McMurdo Sound (HF and HNO_3 digestible total Fe: 37 - 121 mg m^{-2} yr^{-1}; water-soluble Fe: 2 - 7 mg m^{-2} yr^{-1} [*Winton et al.*, 2014]). We acknowledge that these studies are not directly comparable as different methods were employed to determine the total and soluble Fe fractions. It has been demonstrated that both the acid leachable Fe method [*Gaspari et al.*, 2006; *Vallelonga et al.*, 2013] and the TDFe method [*Edwards et al.*, 2006; this study] underestimate the total Fe fraction in snow and ice [*Conway et al.*, 2015].

Table 6.2: Summer and winter trace metal dissolved, total dissolvable and dust fluxes.

	dFe flux (10^{-6} g m^{-2} y^{-1})	TDFe flux (10^{-6} g m^{-2} y^{-1})	dAl flux (10^{-6} g m^{-2} y^{-1})	TDAl flux (10^{-6} g m^{-2} y^{-1})	Dust flux1-5 µm (mg m^{-2} y^{-1})	Dust flux1-30 µm (mg m^{-2} y^{-1})
Summer	0.4	39	0.5	50	2.7	4.1
Winter	0.2	50	0.4	63	2.4	3.2
Annual	1.2	140	2.9	195	5.9	8.8

6.4.2.2 Atmospheric fractional iron solubility

Fractional Fe solubility was calculated using equation (6.1). Fractional Fe solubility ranged from 0.1 - 30 %. Fractional Fe solubility was fairly constant at ~0.7 % throughout the record, however dramatically rose above this background to 10 and 30 % during winter in 2012 and 2011 respectively. The background fractional Fe solubility (Fig. 6.2a) parallels $\delta^{18}O$ (Fig. 6.2i) suggesting this variability in Fe deposition could be driven by synoptic weather conditions. We note that it is possible that the higher uncertainty associated with extremely low dFe and dAl concentrations in the snow pit could be responsible for some of the variability in the fractional Fe solubility. Additionally, precipitation of Fe(III) during sample melting or removal of oxyhydroxide complexes during filtration through a 0.2 µm filter could lead to under-estimation of dFe concentrations and fractional Fe solubility. However, these processes would have had to occur rapidly as snow melting took <2 hours and samples were filtered, acidified and analysed immediately after melting to minimise such processes.

The data in this study displayed an inverse hyperbolic relationship between the TDFe concentration in snow and fractional Fe solubility (Fig. 6.6). This relationship has been attributed to the mixing of low Fe solubility mineral dust and other soluble Fe aerosols from sources such as biomass burning and oil combustion [e.g. *Sedwick et al.*, 2007]. *Sholkovitz et al.* [2012] reported global fractional Fe solubility data sets and concluded that the characteristic inverse hyperbolic relationship is common over large regions of the global ocean. This relationship was also found for baseline air at the Cape Grim Baseline Air Pollution Station (CGBAPS), Tasmania, Australia representative of the Southern Ocean [*Winton et al.*, 2015]. Results here are similar to or greater than CGBAPS with respect to the extremely low TDFe in the exceptionally clean air. The inverse hyperbolic relationship at Roosevelt Island also suggests a mixture of mineral dust and combustion sources of Fe.

Reported values for global fractional Fe solubility of mineral dust are around 1 - 2 % [e.g. *Baker and Croot*, 2010]. Aerosol Fe deposition to remote Southern Ocean surface waters has previously been investigated in relation to the distribution and transport of mineral dust [e.g. *Edwards and Sedwick*, 2001; *Martínez-García et al.*, 2014; *Wagener et al.*, 2008; *Winton et al.*, 2014]. High-elevation East Antarctic ice core records also link higher rates of Fe and dust deposition during glacial periods [*Conway et al.*, 2015; *Vallelonga et al.*, 2013]. The background fractional Fe solubility of ~0.7 % at relatively high TDFe mass concentrations at Roosevelt Island is consistent with a mineral dust source.

Alternatively, the variability in fractional Fe solubility could be driven by changes in dust mineralogy and grain size without necessarily being related to biomass burning sources of soluble Fe. Changes in dust source could supply dust with a higher dFe fraction, or where the TDFe dissolves less easily in acid. Furthermore, TDFe can be a highly variable portion of total Fe [e.g. *Conway et al.*, 2015]. Seasonal changes in dust provenance at Roosevelt Island are an important topic that deserves further investigation. Some studies have shown that cloud chemistry and atmospheric processing by oxalate and sulfate can enhance the solubility of mineral dust [*Desboeufs et al.*, 1999; *Kumar et al.*, 2010; *Meskhidze et al.*, 2003; *Spokes et al.*, 1994]. However, in the remote Atlantic and Pacific Ocean and the Southern Ocean south of Australia, no relationship was observed between acid species and fractional Fe solubility [*Baker et al.*, 2006; *Hand et al.*, 2004; *Winton et al.*, 2015]. Even if the dust source to Roosevelt Island in 2012 was continental Antarctica, e.g. Marie Byrd Land, it is unlikely that atmospheric processing by combustion aerosols (observed in polluted air masses where concentrations of organic acids are high [*Chuang et al.*, 2005; *Ito*, 2015; *Ito and Shi*, 2015; *Kumar et al.*, 2010]) would enhance the solubility of the iron contained in the mineral dust. The air masses over Antarctica and the Southern Ocean contain trace concentrations of sulfate and oxalate [*Keywood*, 2007]. However, little is known about the enhancement of fractional Fe solubility in these pristine air masses [*Chance et al.*, 2015]. In addition, any enhancement of fractional iron solubility by oxalate may not be sufficient to account for the high fractional Fe solubility observed in the snow pit. For example, *Paris et al.* [2011] showed that although oxalate complexation increased fractional Fe solubility from 0.0025 to 0.26 % in African dust minerals, the fractional Fe solubility remained low. No relationship was found between the samples with a lognormal size distribution and high fractional Fe solubility. Longer records of particle size distribution and fractional Fe solubility at Roosevelt Island are required to investigate whether particle size can explain the variability in fractional Fe solubility.

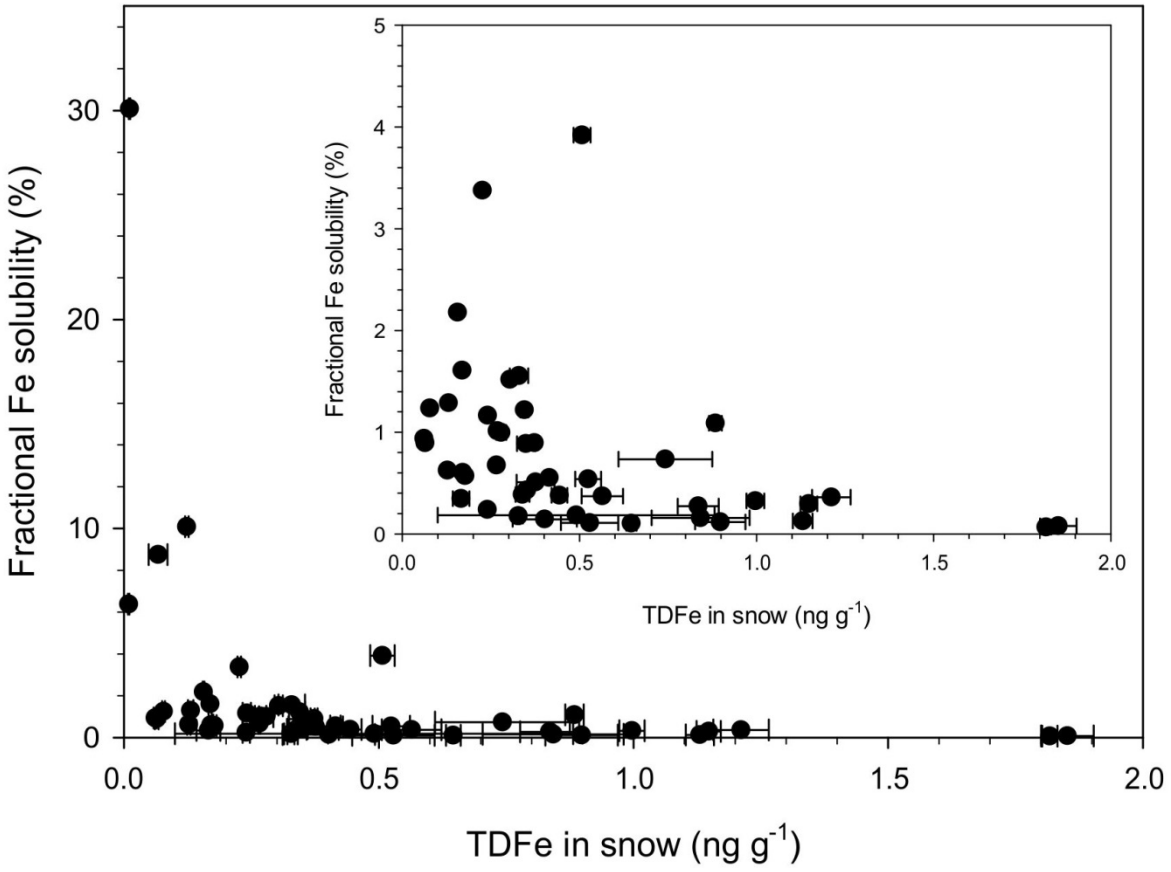

Fig. 6.6: Scatterplot of Roosevelt Island total dissolved Fe concentration versus fractional Fe solubility. Top right insert: low concentration data expanded.

6.4.3 Multiple sources of atmospheric dissolved iron to the Ross Sea

The temporal variability of mineral dust and the biomass burning tracer, rBC, parallels Roosevelt Island atmospheric dFe deposition (Fig. 6.2). Similar to TDFe concentrations, dust and rBC concentrations displayed an inverse hyperbolic relationship with fractional Fe solubility (Fig. 6.S3b-c). Dissolved Fe deposition to Roosevelt Island is semi-annual with elevated deposition in summer and winter during the study period (Fig. 6.2b). The rest of this discussion focusses on the two largest deposition events of dFe highlighted in blue in Fig. 6.2. There were two intervals with high dFe concentrations. There were exceptionally high rBC concentrations in the first interval in summer 2011/2012. While during the second interval in winter 2011, concentrations of rBC were near background levels. In both cases, dust deposition was high indicated by high concentrations of dust, TDFe and TDAl. During the study period, it appears that dust is the primary source of dFe with additional rBC

contributions. In both intervals, the excursion of $\delta^{18}O$ to more negative values suggests that the process by which dFe is deposited at the site is storm related [*Tuohy et al.*, 2015]. Multiple sources of dust and rBC may contribute to the atmospheric Fe supply to the Ross Sea, and the absence of an rBC source in winter highlights that the relative importance of the different sources varies seasonally.

6.4.3.1 Atmospheric iron sourced from mineral dust

A mineral dust source in summer is evident through i) co-variation of dFe maxima and high dust in 2011/2012 summer-spring (Figs. 6.2e and 6.2g), ii) strong correlation between the crustal elements TDFe and TDAl (r^2=0.86; Fig. 6.S3a), iii) co-variation of TDAl and dust in 2011 (Fig. 6.S3d-e), and iv) low fractional Fe solubility during summer (~0.7 %). For the majority of the record, TDFe and TDAl tracks dust concentration. However, not every dust deposition event leads to higher dFe, for example in spring 2011. This could be related to differences in the mineralogy of the dust, which varies depending on the dust provenance. Whether the dust provenance switches between seasons is unknown, but it is an important topic that deserves more attention in future. The coarser particle size distribution in summer-spring and Sr and Nd isotopic ratios matching that of nearby Marie Byrd Land, Victoria Land and Australia suggests that a mixture of different types of local and possibly remote dust sources influence dFe deposition at present.

6.4.3.2 Atmospheric iron sourced from biomass burning

Biomass burning may also contribute to the 2011/2012 summer deposition of dFe at Roosevelt Island. Refractory black carbon deposition to Antarctica is linked to Southern Hemispheric long-range transport of biomass burning [*Bisiaux et al.*, 2012b]. The high fractional Fe solubility during winter in 2011 and 2012 (up to 30 %; Figs. 6.2a and 6.6) indicates that additional atmospheric sources, other than mineral dust or biomass burning, are responsible for high fractional Fe solubility in the winter periods observed in this record. Thus, biomass burning can only account for the high fractional Fe solubility observed in background Southern Hemispheric air during the 2011/2012 summer period covered by the snow pit. Ice core records report rBC as a late winter-spring phenomena in West Antarctica [*Bisiaux et al.*, 2012b]. Consistent with WAIS Divide, a small late winter-spring-time rBC peak is observed in 2012 in this study. However, the exceptionally large 2011/2012 summer rBC peak does not overlap with the time period covered by WAIS Divide rBC record. Longer

records of rBC and fractional Fe solubility are needed to test the hypothesis that biomass burning sources of dFe can account for high fractional Fe solubility of aerosols over the Ross Sea.

6.4.3.3 Timing and supply of iron deposition

Sea ice is a source of dFe to the ocean in the SW Ross Sea, where high dFe concentrations have been observed in the surface waters after considerable sea ice melt [*de Jong et al.,* 2013; *McGillicuddy et al.,* 2015; *Sedwick and DiTullio,* 1997]. This snow pit record from Roosevelt Island demonstrates that spring-summer dFe deposition occurs during ice-free open water conditions in the Ross Sea, when phytoplankton is blooming (Fig. 6.2l). Around half of the annual TDFe and dFe for 2011 was deposited in the summer, and, therefore, the seasonality of dFe deposition needs to be considered on longer glacial-interglacial time scales. Despite high dFe and TDFe deposition in spring-summer, fractional Fe solubility was only ~0.7 % at this time. Higher fractional Fe solubility occurs in winter when TDFe is low, and the Ross Sea is seasonally ice covered. Snow on sea ice is a repository for aerosol Fe [*Lannuzel et al.*, 2010; *Winton et al.*, 2014]. Therefore, deposition of aerosol Fe, with relatively high dFe content, is stored in the surface snow of sea ice during winter. In spring-summer, aerosol Fe with a higher fractional Fe solubility is released and supplied to the ocean as sea ice melts. Regardless of the timing and mechanism in which aerosol dFe is supplied to the Ross Sea, i.e., deposition directly into open water in summer and deposition onto surface snow on sea ice in winter with subsequent release into the ocean during spring-summer sea ice melt, both mechanisms act as a new source of dFe to phytoplankton blooms in spring-summer.

6.5 Conclusions

A dust flux of 6 mg m^{-2} yr^{-1} for the 1-5 µm fraction and 8 mg m^{-2} yr^{-1} for the bulk 1-30 µm has been estimated for modern dust deposition at Roosevelt Island. Snow pit data from Roosevelt Island reveal dust deposition occurs primarily in the spring-summer season. The higher dust flux at Roosevelt Island compared to the East Antarctic Plateau, the presence of coarse dust particles (>10 µm), the particle size distribution that approaches the theoretical dust emission distribution and the Sr and Nd isotopic ratio of dust deposited on Roosevelt Island suggest a mixture of local and possibly remote dust sources for the present day. The Sr isotopic composition ($0.7122 < {}^{87}Sr/{}^{86}Sr < 0.7156$) of summer dust in the snow at Roosevelt

Island suggests a possible mixing of volcanic and crustal rocks of local origin (i.e., older material, e.g. Palaeozoic rock from Victoria Land and parts of Marie Byrd Land, and Mesozoic to Cenozoic volcanics). Additional input from remote dust sources cannot be discounted. In this respect, Australia best matches the Roosevelt Island isotopic composition of Sr and Nd. Advection of Australian dust is consistent with modelling studies of modern Australian aeolian transport for the present day. These dust data from Roosevelt Island provide useful context for the interpretation of the dust record in the 764 m long RICE ice core.

An annual dFe flux of 1.2 x 10^{-6} g m^{-2} y^{-1} and an annual TDFe flux of 140 x 10^{-6} g m^{-2} y^{-1} have been estimated for Roosevelt Island for 2011. Deposition of dFe is semi-annual occurring in the summer and winter, with half of dFe and TDFe deposition occurring in the summer. The inverse hyperbolic relationship between TDFe concentrations and fractional Fe solubility shows that additional atmospheric sources, other than mineral dust, are responsible for high Fe solubility at different times in the year. There were two intervals with high dFe concentrations in the snow pit: one with exceptionally high rBC concentrations in summer 2011/2012, and the other with rBC concentrations near background levels in winter 2011. In both cases, dust was high. Therefore, mineral dust, from both local and remote sources, is the primary source of dFe to Roosevelt Island with additional input from long-range transport of biomass burning aerosols. Biomass burning may account for the high fractional Fe solubility observed in background Southern Hemispheric air during the summer period. The semi-annual nature of Fe deposition to Antarctic waters should be considered when interpreting longer glacial-interglacial time scales of aerosol Fe deposition to the Southern Ocean.

Acknowledgements

This work is a contribution to the Roosevelt Island Climate Evolution (RICE) Programme, funded by national contributions from New Zealand, Australia, Denmark, Germany, Italy, the People's Republic of China, Sweden, U.K., and the U.S.A. Logistic support was provided by Antarctica New Zealand (K049) and the US Antarctic Program. We would like to thank Antarctica New Zealand and Scott Base personnel for logistics support. Thank you to the RICE 2012/2013 team for assisting in the collection of samples from Roosevelt Island. VHLW would like to thank Curtin University for scholarship support (Australian Postgraduate Award and Curtin Research Scholarship). This project was funded by Curtin University, Victoria University of Wellington (RDF-VUW1103), GNS Science (540GCT32), the University of Milano-Bicocca, and the Swedish Museum of Natural History. Access to HR-ICP-MS instrumentation at Curtin University was facilitated through ARC LIEF funding (LE130100029). Thank you to K. Jarrett for technical assistance. Isotopic analyses for dust provenance characterization were carried out at the Swedish Museum of Natural History and were supported by the Department of Geosciences, Swedish Museum of Natural History. The authors acknowledge the use of equipment, scientific and technical assistance of the Curtin University Electron Microscope Facility, which has been partially funded by the University, State and Commonwealth Governments. We would like to acknowledge the Norwegian Polar Institute for the use of the Qantarctica package. The snow pit dataset for the RICE 2012/2013 1.5 m snow pit is available through the Curtin University Research Data repository http://doi.org/10.4225/06/565BCE14467D0. Additional thanks for the helpful comments and suggestions of Bess Koffman and an anonymous reviewer that aided in revision of this manuscript.

References

Abram, N. J., Gagan, M. K., McCulloch, M. T., Chappell, J., and Hantoro, W. S.: Coral reef death during the 1997 Indian Ocean dipole linked to Indonesian wildfires, Science, 301, 952-955, 2003.

Adams, C., Seward, D., and Weaver, S.: Geochronology of Cretaceous granites and metasedimentary basement on Edward VII Peninsula, Marie Byrd Land, West Antarctica, Antarctic science, 7, 265-276, 1995.

Aguilar-Islas, A. M., Wu, J., Rember, R., Johansen, A. M., and Shank, L. M.: Dissolution of aerosol-derived iron in seawater: Leach solution chemistry, aerosol type, and colloidal iron fraction, Marine Chemistry, 120, 25-33, 2010.

Albani, S., Delmonte, B., Maggi, V., Baroni, C., Petit, J. R., Stenni, B., Mazzola, C., and Frezzotti, M.: Interpreting last glacial to Holocene dust changes at Talos Dome (East Antarctica): implications for atmospheric variations from regional to hemispheric scales, Clim. Past Discuss., 8, 145-168, 10.5194/cpd-8-145-2012, 2012a.

Albani, S., Mahowald, N., Delmonte, B., Maggi, V., and Winckler, G.: Comparing modeled and observed changes in mineral dust transport and deposition to Antarctica between the Last Glacial Maximum and current climates, Climate Dynamics, 38, 1731-1755, 10.1007/s00382-011-1139-5, 2012b.

Albani, S., Mahowald, N. M., Winckler, G., Anderson, R. F., Bradtmiller, L. I., Delmonte, B., François, R., Goman, M., Heavens, N. G., Hesse, P. P., Hovan, S. A., Kang, S. G., Kohfeld, K. E., Lu, H., Maggi, V., Mason, J. A., Mayewski, P. A., McGee, D., Miao, X., Otto-Bliesner, B. L., Perry, A. T., Pourmand, A., Roberts, H. M., Rosenbloom, N., Stevens, T., and Sun, J.: Twelve thousand years of dust: the Holocene global dust cycle constrained by natural archives, Clim. Past, 11, 869-903, 10.5194/cp-11-869-2015, 2015.

Alexander, J. M., Grassian, V. H., Young, M. A., and Kleiber, P. D.: Optical properties of selected components of mineral dust aerosol processed with organic acids and humic material, Journal of Geophysical Research: Atmospheres, 120, 2437-2452, 10.1002/2014JD022782, 2015.

Alying, B.: Dust accumulation on the Victoria Lower Glacier and Wilson Piedmont, coastal South Victoria Land, Antarctica, and its potential as a paleowind indicator, BSc Honours, School of Earth Sciences, Victoria University of Wellington, Wellington, 2001.

Anderson, R. F., Barker, S., Fleisher, M., Gersonde, R., Goldstein, S. L., Kuhn, G., Mortyn, P. G., Pahnke, K., and Sachs, J. P.: Biological response to millennial variability of dust and nutrient supply in the Subantarctic South Atlantic Ocean, Philosophical Transactions of the Royal Society of London A: Mathematical, Physical and Engineering Sciences, 372, 10.1098/rsta.2013.0054, 2014.

Andersson, P. S., Wasserburg, G., Ingri, J., and Stordal, M. C.: Strontium, dissolved and particulate loads in fresh and brackish waters: the Baltic Sea and Mississippi Delta, Earth and Planetary Science Letters, 124, 195-210, 1994.

Andreae, M., and Gelencsér, A.: Black carbon or brown carbon? The nature of light-absorbing carbonaceous aerosols, Atmospheric Chemistry and Physics, 6, 3131-3148, 2006.

Andreae, M. O.: Biomass burning: Its history, use and distribution and its impact on environmental quality and global climate, Global Biomass Burning: Atmospheric, Climatic, and Biospheric Implications, edited by J. S. Levine, pp. 3-21, MIT Press, Cambridge, Mass., 1991.

Andreae, M. O.: The influence of tropical biomass burning on climate and the atmospheric environment, in: Biogeochemistry of Global Change, Springer, 113-150, 1993.

Andreasen, R., and Sharma, M.: Solar nebula heterogeneity in p-process samarium and neodymium isotopes, Science, 314, 806-809, 2006.

Antonini, P., Piccirillo, E., Petrini, R., Civetta, L., D'Antonio, M., and Orsi, G.: Enriched mantle–Dupal signature in the genesis of the Jurassic Ferrar tholeiites from Prince Albert Mountains (Victoria Land, Antarctica), Contributions to Mineralogy and Petrology, 136, 1-19, 1999.

Arimoto, R., Duce, R., Ray, B., and Unni, C.: Atmospheric trace elements at Enewetak Atoll: 2. Transport to the ocean by wet and dry deposition, Journal of Geophysical Research: Atmospheres (1984–2012), 90, 2391-2408, 1985.

Arimoto, R., and Duce, R. A.: DRY DEPOSITION MODELS AND THE AIR/SEA EXCHANGE OF TRACE ELEMENTS, J. Geophys. Res., 91, 2787-2792, 10.1029/JD091iD02p02787, 1986.

Arrigo, K. R., and McClain, C. R.: Spring Phytoplankton Production in the Western Ross Sea, Science, 266, 261-263, 10.1126/science.266.5183.261, 1994.

Arrigo, K. R., Weiss, A. M., and Smith, W. O., Jr.: Physical forcing of phytoplankton dynamics in the southwestern Ross Sea, J. Geophys. Res., 103, 1007-1021, 10.1029/97jc02326, 1998.

Arrigo, K. R., DiTullio, G. R., Dunbar, R. B., Robinson, D. H., VanWoert, M., Worthen, D. L., and Lizotte, M. P.: Phytoplankton taxonomic variability in nutrient utilization and primary production in the Ross Sea, J. Geophys. Res., 105, 8827-8846, 10.1029/1998jc000289, 2000.

Arrigo, K. R., and van Dijken, G. L.: Annual changes in sea-ice, chlorophyll a, and primary production in the Ross Sea, Antarctica, Deep Sea Research Part II: Topical Studies in Oceanography, 51, 117-138, 2004.

Arrigo, K. R., and Van Dijken, G. L.: Interannual variation in air-sea CO2 flux in the Ross Sea, Antarctica: A model analysis, J. Geophys. Res., 112, C03020, 10.1029/2006jc003492, 2007.

Arrigo, K. R., van Dijken, G., and Long, M.: Coastal Southern Ocean: A strong anthropogenic CO2 sink, Geophys. Res. Lett., 35, L21602, 10.1029/2008gl035624, 2008a.

Arrigo, K. R., van Dijken, G. L., and Bushinsky, S.: Primary production in the Southern Ocean, 1997-2006, J. Geophys. Res., 113, C08004, 10.1029/2007jc004551, 2008b.

Artaxo, P., Gerab, F., Yamasoe, M. A., and Martins, J. V.: Fine mode aerosol composition at three long-term atmospheric monitoring sites in the Amazon Basin, Journal of Geophysical Research: Atmospheres (1984–2012), 99, 22857-22868, 1994.

Artaxo, P., Fernandas, E. T., Martins, J. V., Yamasoe, M. A., Hobbs, P. V., Maenhaut, W., Longo, K. M., and Castanho, A.: Large-scale aerosol source apportionment in Amazonia, Journal of Geophysical Research: Atmospheres (1984–2012), 103, 31837-31847, 1998.

Atkins, C. B., and Dunbar, G. B.: Aeolian sediment flux from sea ice into Southern McMurdo Sound, Antarctica, Global and Planetary Change, 69, 133-141, 2009.

Ayers, G., Ivey, J., and Goodman, H.: Sulfate and Methanesulfonnate in the Maritime Aerosol at Cape Grim, Tasmania, in: Scientific Application of Baseline Observations of Atmospheric Composition (SABOAC), Springer, 371-383, 1987.

Ayers, G., Cainey, J., Gillett, R., and Ivey, J.: Atmospheric sulphur and cloud condensation nuclei in marine air in the Southern Hemisphere, Philosophical Transactions of the Royal Society of London B: Biological Sciences, 352, 203-211, 1997.

Ayers, G. P., Ivey, J., and Gillett, R.: High Volume Samplers in Baseline Atmospheric Program (Australia) 1988, edited by S.R. Wilson and G.P. Ayers, CSIRO Atmospheric Research, Melbourne, Australia, 45., 1990.

Ayling, B., and McGowan, H.: Niveo-eolian Sediment Deposits in Coastal South Victoria Land, Antarctica: Indicators of Regional Variability in Weather and Climate, Arctic, Antarctic, and Alpine Research, 38, 313-324, 2006.

Bagnold, R.: The physics of blown sand and desert dunes, Methuen, London, 1941.

Baker, A., Kelly, S., Biswas, K., Witt, M., and Jickells, T.: Atmospheric deposition of nutrients to the Atlantic Ocean, Geophysical Research Letters, 30, 2003.

Baker, A., Adams, C., Bell, T., Jickells, T., and Ganzeveld, L.: Estimation of atmospheric nutrient inputs to the Atlantic Ocean from 50° N to 50° S based on large-scale field sampling: Iron and other dust-associated elements, Global Biogeochemical Cycles, 27, 755-767, 2013.

Baker, A. R., and Jickells, T. D.: Mineral particle size as a control on aerosol iron solubility, Geophys. Res. Lett., 33, L17608, 10.1029/2006gl026557, 2006.

Baker, A. R., Jickells, T. D., Witt, M., and Linge, K. L.: Trends in the solubility of iron, aluminium, manganese and phosphorus in aerosol collected over the Atlantic Ocean, Marine Chemistry, 98, 43-58, 2006.

Baker, A. R., and Croot, P. L.: Atmospheric and marine controls on aerosol iron solubility in seawater, Marine Chemistry, 120, 4-13, 2010.

Banerjee, P., and Prasanna Kumar, S.: Dust-induced episodic phytoplankton blooms in the Arabian Sea during winter monsoon, Journal of Geophysical Research: Oceans, 119, 7123-7138, 2014.

Banse, K.: Rates of Phytoplankton Cell Division in the Field and in Iron Enrichment Experiments, Limnology and Oceanography, 36, 1886-1898, 1991.

Barbeau, K., Moffett, J. W., Caron, D. A., Croot, P. L., and Erdner, D. L.: Role of protozoan grazing in relieving iron limitation of phytoplankton, Nature, 380, 61-64, 1996.

Barbeau, K. A., and Moffett, J. W.: Dissolution of Iron Oxides by Phagotrophic Protists: Using a Novel Method To Quantify Reaction Rates, Environmental Science & Technology, 32, 2969-2975, 10.1021/es9802549, 1998.

Barrett, P., Pyne, A., and Ward, B.: Modern sedimentation in McMurdo Sound, Antarctica In: Oliver, R.L., James, P.R., Jago, J.B. (Eds.), Antarctic Earth Science, 550-554, 1983.

Basak, C., Pahnke, K., Frank, M., Lamy, F., and Gersonde, R.: Neodymium isotopic characterization of Ross Sea Bottom Water and its advection through the southern South Pacific, Earth and Planetary Science Letters, 419, 211-221, 2015.

Basile, I., Grousset, F. E., Revel, M., Petit, J. R., Biscaye, P. E., and Barkov, N. I.: Patagonian origin of glacial dust deposited in East Antarctica (Vostok and Dome C) during glacial stages 2, 4 and 6, Earth and Planetary Science Letters, 146, 573-589, 1997.

Basile, I., Petit, J. R., Touron, S., Grousset, F. E., and Barkov, N.: Volcanic layers in Antarctic (Vostok) ice cores: Source identification and atmospheric implications, Journal of Geophysical Research: Atmospheres (1984–2012), 106, 31915-31931, 2001.

Berger, C. J., Lippiatt, S. M., Lawrence, M. G., and Bruland, K. W.: Application of a chemical leach technique for estimating labile particulate aluminum, iron, and manganese in the Columbia River plume and coastal waters off Oregon and Washington, Journal of Geophysical Research: Oceans (1978–2012), 113, 2008.

Berman-Frank, I., Cullen, J. T., Shaked, Y., Sherrell, R. M., and Falkowski, P. G.: Iron availability, cellular iron quotas, and nitrogen fixation in Trichodesmium, Limnology and Oceanography, 46, 1249-1260, 2001.

Bhattachan, A., and D'Odorico, P.: Can land use intensification in the Mallee, Australia increase the supply of soluble iron to the Southern Ocean?, Scientific reports, 4, 2014.

Bhattachan, A., Wang, L., Miller, M. F., Licht, K. J., and D'Odorico, P.: Antarctica's Dry Valleys: A potential source of soluble iron to the Southern Ocean?, Geophysical Research Letters, 42, 1912-1918, 2015.

Biscaye, P. E., Grousset, F. E., Revel, M., Van der Gaast, S., Zielinski, G. A., Vaars, A., and Kukla, G.: Asian provenance of glacial dust (stage 2) in the Greenland Ice Sheet Project 2 Ice Core, Summit, Greenland, J. Geophys. Res., 102, 26765-26781, 10.1029/97jc01249, 1997.

Bisiaux, M., Edwards, R., McConnell, J., Albert, M., Anschütz, H., Neumann, T., Isaksson, E., and Penner, J.: Variability of black carbon deposition to the East Antarctic Plateau, 1800–2000 AD, Atmospheric Chemistry and Physics, 12, 3799-3808, 2012a.

Bisiaux, M., Edwards, R., McConnell, J., Curran, M., Van Ommen, T., Smith, A., Neumann, T., Pasteris, D., Penner, J., and Taylor, K.: Changes in black carbon deposition to Antarctica from two high-resolution ice core records, 1850–2000 AD, Atmospheric Chemistry and Physics, 12, 4107-4115, 2012b.

Blain, S., Queguiner, B., Armand, L., Belviso, S., Bombled, B., Bopp, L., Bowie, A., Brunet, C., Brussaard, C., Carlotti, F., Christaki, U., Corbiere, A., Durand, I., Ebersbach, F., Fuda, J.-L., Garcia, N., Gerringa, L., Griffiths, B., Guigue, C., Guillerm, C., Jacquet, S., Jeandel, C., Laan, P., Lefevre, D., Lo Monaco, C., Malits, A., Mosseri, J., Obernosterer, I., Park, Y.-H., Picheral, M., Pondaven, P., Remenyi, T., Sandroni, V., Sarthou, G., Savoye, N., Scouarnec, L., Souhaut, M., Thuiller, D., Timmermans, K., Trull, T., Uitz, J., van Beek, P., Veldhuis, M., Vincent, D., Viollier, E., Vong, L., and Wagener, T.: Effect of natural iron fertilization on carbon sequestration in the Southern Ocean, Nature, 446, 1070-1074, http://www.nature.com/nature/journal/v446/n7139/suppinfo/nature05700_S1.html, 2007.

Bollhöfer, A., Chisholm, W., and Rosman, K.: Sampling aerosols for lead isotopes on a global scale, Analytica chimica acta, 390, 227-235, 1999.

Bollhöfer, A., and Rosman, K.: Isotopic source signatures for atmospheric lead: the Southern Hemisphere, Geochimica et Cosmochimica Acta, 64, 3251-3262, 2000.

Bollhöfer, A. F., Rosman, K. J. R., Dick, A. L., Chisholm, W., Burton, G. R., Loss, R. D., and Zahorowski, W.: Concentration, isotopic composition, and sources of lead in Southern Ocean air during 1999/2000, measured at the Cape Grim Baseline Air Pollution Station, Tasmania, Geochimica et Cosmochimica Acta, 69, 4747-4757, http://dx.doi.org/10.1016/j.gca.2005.06.024, 2005.

Bonnet, S., and Guieu, C.: Dissolution of atmospheric iron in seawater, Geophys. Res. Lett., 31, L03303, 10.1029/2003gl018423, 2004.

Bory, A., Wolff, E., Mulvaney, R., Jagoutz, E., Wegner, A., Ruth, U., and Elderfield, H.: Multiple sources supply eolian mineral dust to the Atlantic sector of coastal Antarctica: Evidence from recent snow layers at the top of Berkner Island ice sheet, Earth and Planetary Science Letters, 291, 138-148, 2010.

Bory, A. J. M., Biscaye, P. E., Svensson, A., and Grousset, F. E.: Seasonal variability in the origin of recent atmospheric mineral dust at NorthGRIP, Greenland, Earth and Planetary Science Letters, 196, 123-134, 2002.

Bowie, A., van der Merwe, P., Quéroué, F., Trull, T., Fourquez, M., Planchon, F., Sarthou, G., Chever, F., Townsend, A., and Obernosterer, I.: Iron budgets for three distinct biogeochemical sites around the Kerguelen archipelago (Southern Ocean) during the natural fertilisation experiment KEOPS-2, Biogeosciences Discussions, 11, 17861-17923, 2014.

Bowie, A. R., Lannuzel, D., Remenyi, T. A., Wagener, T., Lam, P. J., Boyd, P. W., Guieu, C., Townsend, A. T., and Trull, T. W.: Biogeochemical iron budgets of the Southern Ocean south of Australia: Decoupling of iron and nutrient cycles in the subantarctic zone by the summertime supply, Global Biogeochem. Cycles, 23, GB4034, 10.1029/2009gb003500, 2009.

Bowie, A. R., Townsend, A. T., Lannuzel, D., Remenyi, T. A., and Van der Merwe, P.: Modern sampling and analytical methods for the determination of trace elements in marine particulate material using magnetic sector inductively coupled plasma–mass spectrometry, Analytica chimica acta, 676, 15-27, 2010.

Bowie, A. R., Griffiths, F. B., Dehairs, F., and Trull, T. W.: Oceanography of the subantarctic and polar frontal zones south of Australia during summer: setting for the SAZ-Sense study, Deep Sea Research Part II: Topical Studies in Oceanography, 58, 2059-2070, 2011.

Bowler, J.: Aridity in Australia: age, origins and expression in aeolian landforms and sediments, Earth-Science Reviews, 12, 279-310, 1976.

Boyd, P., Dillingham, P., McGraw, C., Armstrong, E., Cornwall, C., Feng, Y.-y., Hurd, C., Gault-Ringold, M., Roleda, M., and Timmins-Schiffman, E.: Physiological responses of a Southern Ocean diatom to complex future ocean conditions, Nature Climate Change, 2015.

Boyd, P. W., Watson, A. J., Law, C. S., Abraham, E. R., Trull, T., Murdoch, R., Bakker, D. C. E., Bowie, A. R., Buesseler, K. O., Chang, H., Charette, M., Croot, P. L., Downing, K., Frew, R., Gall, M., Hadfield, M., Hall, J., Harvey, M., Jameson, G., LaRoche, J., Liddicoat, M. I., Ling, R., Maldonado, M. T., McKay, R. M., Nodder, S., Pickmere, S., Pridmore, R., Rintoul, S., Safi, K., Sutton, P., Strzepek, R., Tanneberger, K., Turner, S., Waite, A., and Zeldis, J.: A mesoscale phytoplankton bloom in the polar Southern Ocean stimulated by iron fertilization, Nature, 407, 695-702, 2000.

Boyd, P. W., McTainsh, G., Sherlock, V., Richardson, K., Nichol, S., Ellwood, M., and Frew, R.: Episodic enhancement of phytoplankton stocks in New Zealand subantarctic waters: Contribution of atmospheric and oceanic iron supply, Global Biogeochem. Cycles, 18, GB1029, 10.1029/2002gb002020, 2004.

Boyd, P. W., Law, C. S., Hutchins, D. A., Abraham, E. R., Croot, P. L., Ellwood, M., Frew, R. D., Hadfield, M., Hall, J., Handy, S., Hare, C., Higgins, J., Hill, P., Hunter, K. A., LeBlanc, K., Maldonado, M. T., McKay, R. M., Mioni, C., Oliver, M., Pickmere, S., Pinkerton, M., Safi, K., Sander, S., Sanudo-Wilhelmy, S. A., Smith, M., Strzepek, R., Tovar-Sanchez, A., and Wilhelm, S. W.: FeCycle: Attempting an iron biogeochemical budget from a mesoscale SF6 tracer experiment in unperturbed low iron waters, Global Biogeochem. Cycles, 19, GB4S20, 10.1029/2005gb002494, 2005.

Boyd, P. W., Jickells, T., Law, C. S., Blain, S., Boyle, E. A., Buesseler, K. O., Coale, K. H., Cullen, J. J., de Baar, H. J. W., Follows, M., Harvey, M., Lancelot, C., Levasseur, M., Owens, N. P. J., Pollard, R., Rivkin, R. B., Sarmiento, J., Schoemann, V., Smetacek, V., Takeda, S., Tsuda, A., Turner, S., and Watson, A. J.: Mesoscale Iron Enrichment Experiments 1993-2005: Synthesis and Future Directions, Science, 315, 612-617, 10.1126/science.1131669, 2007.

Boyd, P. W., Doney, S. C., Strzepek, R., Dusenberry, J., Lindsay, K., and Fung, I.: Climate-mediated changes to mixed-layer properties in the Southern Ocean: assessing the phytoplankton response, Biogeosciences, 5, 847-864, 2008.

Boyd, P. W., and Ellwood, M. J.: The biogeochemical cycle of iron in the ocean, Nature Geosci, 3, 675-682, http://www.nature.com/ngeo/journal/v3/n10/abs/ngeo964.html#supplementary-information, 2010.

Boyd, P. W., Mackie, D. S., and Hunter, K. A.: Aerosol iron deposition to the surface ocean - Modes of iron supply and biological responses, Marine Chemistry, 120, 128-143, 2010.

Buck, C. S., Landing, W. M., Resing, J. A., and Lebon, G. T.: Aerosol iron and aluminum solubility in the northwest Pacific Ocean: Results from the 2002 IOC cruise, Geochem. Geophys. Geosyst., 7, Q04M07, 10.1029/2005gc000977, 2006.

Bunt, J. S.: Microbiology of Antarctic Sea-ice: Diatoms of Antarctic Sea-ice as Agents of Primary Production, Nature, 199, 1255-1257, 1963.

Bunt, J. S., and Wood, E. J. F.: Microbiology of Antarctic Sea-ice: Microalgae and Antarctic Sea-ice, Nature, 199, 1254-1255, 1963.

Butler, H., Hogarth, W. L., and McTainsh, G. H.: Effects of spatial variations in source areas upon dust concentration profiles during three wind erosion events in Australia, Earth Surface Processes and Landforms, 26, 1039-1048, 2001.

Calloway, C., Li, S., Buchanan, J., and Stevens, R.: A refinement of the potassium tracer method for residential wood smoke, Atmospheric Environment (1967), 23, 67-69, 1989.

Cammas, J.-P., Brioude, J., Chaboureau, J.-P., Duron, J., Mari, C., Mascart, P., Nédélec, P., Smit, H., Pätz, H.-W., and Volz-Thomas, A.: Injection in the lower stratosphere of biomass fire emissions followed by long-range transport: a MOZAIC case study, Atmospheric Chemistry and Physics, 9, 5829-5846, 2009.

Chakrabarty, R. K., Moosmüller, H., Arnott, W. P., Garro, M. A., Slowik, J. G., Cross, E. S., Han, J.-H., Davidovits, P., Onasch, T. B., and Worsnop, D. R.: Light scattering and absorption by fractal-like carbonaceous chain aggregates: Comparison of theories and experiment, Applied optics, 46, 6990-7006, 2007.

Chance, R., Jickells, T. D., and Baker, A. R.: Atmospheric trace metal concentrations, solubility and deposition fluxes in remote marine air over the south-east Atlantic, Marine Chemistry, 2015.

Chandler, C., Cheney, P., Thomas, P., Trabaud, L., and Williams, D.: Fire in forestry. Forest fire behaviour and effects, Ed. John Wiley & Sons, 1, 1983.

Chang-Graham, A. L., Profeta, L. T., Johnson, T. J., Yokelson, R. J., Laskin, A., and Laskin, J.: Case study of water-soluble metal containing organic constituents of biomass burning aerosol, Environmental science & technology, 45, 1257-1263, 2011.

Chen, Y., and Siefert, R. L.: Determination of various types of labile atmospheric iron over remote oceans, J. Geophys. Res., 108, 4774, 10.1029/2003jd003515, 2003.

Chen, Y., and Siefert, R. L.: Seasonal and spatial distributions and dry deposition fluxes of atmospheric total and labile iron over the tropical and subtropical North Atlantic Ocean, J. Geophys. Res., 109, D09305, 10.1029/2003jd003958, 2004.

Chewings, J. M., Atkins, C. B., Dunbar, G. B., and Golledge, N. R.: Aeolian sediment transport and deposition in a modern high latitude glacial marine environment, Sedimentology, 2014a.

Chewings, J. M., Atkins, C. B., Dunbar, G. B., and Golledge, N. R.: Aeolian sediment transport and deposition in a modern high-latitude glacial marine environment, Sedimentology, n/a-n/a, 10.1111/sed.12108, 2014b.

Chuang, P. Y., Duvall, R. M., Shafer, M. M., and Schauer, J. J.: The origin of water soluble particulate iron in the Asian atmospheric outflow, Geophys. Res. Lett., 32, L07813, 10.1029/2004gl021946, 2005.

Cleveland, W. S., and Devlin, S. J.: Locally weighted regression: an approach to regression analysis by local fitting, Journal of the American Statistical Association, 83, 596-610, 1988.

Coale, K. H., Wang, X., Tanner, S. J., and Johnson, K. S.: Phytoplankton growth and biological response to iron and zinc addition in the Ross Sea and Antarctic Circumpolar Current along 170 W, Deep Sea Research Part II: Topical Studies in Oceanography, 50, 635-653, 2003.

Coale, K. H., Johnson, K. S., Chavez, F. P., Buesseler, K. O., Barber, R. T., Brzezinski, M. A., Cochlan, W. P., Millero, F. J., Falkowski, P. G., Bauer, J. E., Wanninkhof, R. H., Kudela, R. M., Altabet, M. A., Hales, B. E., Takahashi, T., Landry, M. R., Bidigare, R. R., Wang, X., Chase, Z., Strutton, P. G., Friederich, G. E., Gorbunov, M. Y., Lance, V. P., Hilting, A. K., Hiscock, M. R., Demarest, M., Hiscock, W. T., Sullivan, K. F., Tanner, S. J., Gordon, R. M., Hunter, C. N., Elrod, V. A., Fitzwater, S. E., Jones, J. L., Tozzi, S., Koblizek, M., Roberts, A. E., Herndon, J., Brewster, J., Ladizinsky, N., Smith, G., Cooper, D., Timothy, D., Brown, S. L., Selph, K. E., Sheridan, C. C., Twining, B. S., and Johnson, Z. I.: Southern Ocean Iron Enrichment Experiment: Carbon Cycling in High- and Low-Si Waters, Science, 304, 408-414, 10.1126/science.1089778, 2004.

Cohen, L.: Atmospheric Variability and Precipitation in the Ross Sea Region, Antarctica, PhD thesis, Victoria University of Wellington, Wellington, 2013.

Collier, R., Dymond, J., Honjo, S., Manganini, S., Francois, R., and Dunbar, R.: The vertical flux of biogenic and lithogenic material in the Ross Sea: moored sediment trap observations 1996-1998, Deep Sea Research Part II: Topical Studies in Oceanography, 47, 3491-3520, 2000.

Conway, H., Hall, B. L., Denton, G. H., Gades, A. M., and Waddington, E. D.: Past and Future Grounding-Line Retreat of the West Antarctic Ice Sheet, Science, 286, 280-283, 10.1126/science.286.5438.280, 1999.

Conway, T., Wolff, E., Röthlisberger, R., Mulvaney, R., and Elderfield, H.: Constraints on soluble aerosol iron flux to the Southern Ocean at the Last Glacial Maximum, Nature Communications, 6, 2015.

Cook, C. P., van de Flierdt, T., Williams, T., Hemming, S. R., Iwai, M., Kobayashi, M., Jimenez-Espejo, F. J., Escutia, C., Gonzalez, J. J., Khim, B.-K., McKay, R. M., Passchier, S., Bohaty, S. M., Riesselman, C. R., Tauxe, L., Sugisaki, S., Galindo, A. L., Patterson, M. O., Sangiorgi, F., Pierce, E. L., Brinkhuis, H., Klaus, A., Fehr, A., Bendle, J. A. P., Bijl, P. K., Carr, S. A., Dunbar, R. B., Flores, J. A., Hayden, T. G., Katsuki, K., Kong, G. S., Nakai, M., Olney, M. P., Pekar, S. F., Pross, J., Rohl, U., Sakai, T., Shrivastava, P. K., Stickley, C. E., Tuo, S., Welsh, K., and Yamane, M.: Dynamic behaviour of the East Antarctic ice sheet during Pliocene warmth, Nature Geosci, 6, 765-769, 10.1038/ngeo1889

http://www.nature.com/ngeo/journal/v6/n9/abs/ngeo1889.html#supplementary-information, 2013.

Cooke, W., Ramaswamy, V., and Kasibhatla, P.: A general circulation model study of the global carbonaceous aerosol distribution, Journal of Geophysical Research: Atmospheres (1984–2012), 107, ACH 2-1-ACH 2-32, 2002.

Cox, S. C., Parkinson, D. L., Allibone, A. H., and Cooper, A. F.: Isotopic character of Cambro-Ordovician plutonism, southern Victoria Land, Antarctica, New Zealand Journal of Geology and Geophysics, 43, 501-520, 2000.

Croot, P., Bluhm, K., Schlosser, C., Streu, P., Breitbarth, E., Frew, R., and Van Ardelan, M.: Regeneration of Fe (II) during EIFeX and SOFeX, Geophysical Research Letters, 35, 2008.

Croot, P. L., Bowie, A. R., Frew, R. D., Maldonado, M. T., Hall, J. A., Safi, K. A., La Roche, J., Boyd, P. W., and Law, C. S.: Retention of dissolved iron and Fe II in an iron induced Southern Ocean phytoplankton bloom, Geophys. Res. Lett., 28, 3425-3428, 10.1029/2001gl013023, 2001.

Croot, P. L., Laan, P., Nishioka, J., Strass, V., Cisewski, B., Boye, M., Timmermans, K. R., Bellerby, R. G., Goldson, L., Nightingale, P., and de Baar, H. J. W.: Spatial and temporal distribution of Fe(II) and H2O2 during EisenEx, an open ocean mescoscale iron enrichment, Marine Chemistry, 95, 65-88, 2005.

Crutzen, P. J., and Andreae, M. O.: Biomass burning in the tropics: Impact on atmospheric chemistry and biogeochemical cycles, Science, 250, 1669-1678, 1990.

Cruz, M., Sullivan, A., Gould, J., Sims, N., Bannister, A., Hollis, J., and Hurley, R.: Anatomy of a catastrophic wildfire: the Black Saturday Kilmore East fire in Victoria, Australia, Forest Ecology and Management, 284, 269-285, 2012.

Cutter, G., Andersson, P., Codispoti, L., Croot, P., Francois, R., Lohan, M., Obata, H., and Rutgers vd Loeff, M.: Sampling and sample-handling protocols for GEOTRACES Cruises, 2010.

Dansgaard, W.: The O18- abundance in fresh water, Geochimica et Cosmochimica Acta 6, 241-260, 1954.

de Baar, H. J. W., de Jong, J. T. M., Bakker, D. C. E., Loscher, B. M., Veth, C., Bathmann, U., and Smetacek, V.: Importance of iron for plankton blooms and carbon dioxide drawdown in the Southern Ocean, Nature, 373, 412-415, 1995.

de Baar, H. J. W., and de Jong, J. T. M.: Distribution, sources and sinks of iron in seawater, The Biogeochemistry of Iron in Seawater, 123 - 253, 2001.

de Baar, H. J. W., Boyd, P. W., Coale, K. H., Landry, M. R., Tsuda, A., Assmy, P., Bakker, D. C. E., Bozec, Y., Barber, R. T., Brzezinski, M. A., Buesseler, K. O., Boyé, M., Croot, P. L., Gervais, F., Gorbunov, M. Y., Harrison, P. J., Hiscock, W. T., Laan, P., Lancelot, C., Law, C. S., Levasseur, M., Marchetti, A., Millero, F. J., Nishioka, J., Nojiri, Y., van Oijen, T., Riebesell, U., Rijkenberg, M. J. A., Saito, H., Takeda, S., Timmermans, K. R., Veldhuis, M. J. W., Waite, A. M., and Wong, C. S.: Synthesis of iron fertilization experiments: From the Iron Age in the Age of Enlightenment, J. Geophys. Res., 110, C09S16, 10.1029/2004jc002601, 2005.

De Deckker, P., Norman, M., Goodwin, I. D., Wain, A., and Gingele, F. X.: Lead isotopic evidence for an Australian source of aeolian dust to Antarctica at times over the last 170,000 years, Palaeogeography, Palaeoclimatology, Palaeoecology, 285, 205-223, 2010.

de Jong, J., Schoemann, V., Maricq, N., Mattielli, N., Langhorne, P., Haskell, T., and Tison, J.-L.: Iron in land-fast sea ice of McMurdo Sound derived from sediment resuspension and wind-blown dust attributes to primary productivity in the Ross Sea, Antarctica, Marine Chemistry, 157, 24-40, http://dx.doi.org/10.1016/j.marchem.2013.07.001, 2013.

Delmonte, B., Petit, J. R., and Maggi, V.: Glacial to Holocene implications of the new 27000-year dust record from the EPICA Dome C (East Antarctica) ice core, Climate Dynamics, 18, 647-660, 10.1007/s00382-001-0193-9, 2002.

Delmonte, B., Basile-Doelsch, I., Petit, J. R., Maggi, V., Revel-Rolland, M., Michard, A., Jagoutz, E., and Grousset, F.: Comparing the Epica and Vostok dust records during the last 220,000 years: stratigraphical correlation and provenance in glacial periods, Earth-Science Reviews, 66, 63-87, 2004a.

Delmonte, B., Petit, J. R., Andersen, K. K., Basile-Doelsch, I., Maggi, V., and Ya Lipenkov, V.: Dust size evidence for opposite regional atmospheric circulation changes over east Antarctica during the last climatic transition, Climate Dynamics, 23, 427-438, 10.1007/s00382-004-0450-9, 2004b.

Delmonte, B., Petit, J. R., Krinner, G., Maggi, V., Jouzel, J., and Udisti, R.: Ice core evidence for secular variability and 200-year dipolar oscillations in atmospheric circulation over East Antarctica during the Holocene, Climate Dynamics, 24, 641-654, 10.1007/s00382-005-0012-9, 2005.

Delmonte, B., Robert Petit, J., Basile-Doelsch, I., Jagoutz, E., and Maggi, V.: 6. Late quaternary interglacials in East Antarctica from ice-core dust records, in: Developments in Quaternary Sciences, edited by: Frank Sirocko, M. C. M. F. S. G., and Thomas, L., Elsevier, 53-73, 2007.

Delmonte, B., Andersson, P. S., Hansson, M., Schöberg, H., Petit, J. R., Basile-Doelsch, I., and Maggi, V.: Aeolian dust in East Antarctica (EPICA-Dome C and Vostok): Provenance during glacial ages over the last 800 kyr, Geophys. Res. Lett., 35, L07703, 10.1029/2008gl033382, 2008.

Delmonte, B., Andersson, P. S., Schöberg, H., Hansson, M., Petit, J. R., Delmas, R., Gaiero, D. M., Maggi, V., and Frezzotti, M.: Geographic provenance of aeolian dust in East Antarctica during Pleistocene glaciations: preliminary results from Talos Dome and comparison with East Antarctic and new Andean ice core data, Quaternary Science Reviews, 29, 256-264, 2010a.

Delmonte, B., Baroni, C., Andersson, P. S., Schoberg, H., Hansson, M., Aciego, S., Petit, J. R., Albani, S., Mazzola, C., Maggi, V., and Frezzotti, M.: Aeolian dust in the Talos Dome ice core (East Antarctica, Pacific/Ross Sea sector): Victoria Land versus remote sources over the last two climate cycles, Journal of Quaternary Science, 25, 1327-1337, 10.1002/jqs.1418, 2010b.

Delmonte, B., Baroni, C., Andersson, P., Narcisi, B., Salvatore, M., Petit, J., Scarchilli, C., Frezzotti, M., Albani, S., and Maggi, V.: Modern and Holocene aeolian dust variability from Talos Dome (Northern Victoria Land) to the interior of the Antarctic ice sheet, Quaternary Science Reviews, 64, 76-89, 2013.

DePaolo, D. J., and Wasserburg, G. J.: Inferences about magma sources and mantle structure from variations of 143Nd/144Nd, Geophys. Res. Lett., 3, 743-746, 10.1029/GL003i012p00743, 1976.

Desboeufs, K., Sofikitis, A., Losno, R., Colin, J., and Ausset, P.: Dissolution and solubility of trace metals from natural and anthropogenic aerosol particulate matter, Chemosphere, 58, 195-203, 2005a.

Desboeufs, K. V., Losno, R., Vimeux, F., and Cholbi, S.: The pH-dependent dissolution of wind-transported Saharan dust, Journal of Geophysical Research: Atmospheres (1984–2012), 104, 21287-21299, 1999.

Desboeufs, K. V., Sofikitis, A., Losno, R., Colin, J. L., and Ausset, P.: Dissolution and solubility of trace metals from natural and anthropogenic aerosol particulate matter, Chemosphere, 58, 195-203, 2005b.

Dirksen, R. J., Folkert Boersma, K., De Laat, J., Stammes, P., Van Der Werf, G. R., Val Martin, M., and Kelder, H. M.: An aerosol boomerang: Rapid around-the-world transport of smoke from the December 2006 Australian forest fires observed from space, Journal of Geophysical Research: Atmospheres (1984–2012), 114, 2009.

Donaghay, P., Liss, P., Duce, R. A., Kester, D., Hanson, A., Villareal, T., Tindale, N. W., and Gifford, D.: The role of episodic atmospheric nutrient input in the chemical and biological dynamics of ocean ice ecosystems, Oceanography, 4, 62-70, 1991.

Duan, F., Liu, X., Yu, T., and Cachier, H.: Identification and estimate of biomass burning contribution to the urban aerosol organic carbon concentrations in Beijing, Atmospheric Environment, 38, 1275-1282, 2004.

Duce, R. A., Liss, P. S., Merrill, J. T., Atlas, E. L., Buat-Menard, P., Hicks, B. B., Miller, J. M., Prospero, J. M., Arimoto, R., Church, T. M., Ellis, W., Galloway, J. N., Hansen, L., Jickells, T. D., Knap, A. H., Reinhardt, K. H., Schneider, B., Soudine, A., Tokos, J. J., Tsunogai, S., Wollast, R., and Zhou, M.: The atmospheric input of trace species to the world ocean, Global Biogeochem. Cycles, 5, 193-259, 10.1029/91gb01778, 1991.

Dulac, F., BUAT-MÉNARD, P., Ezat, U., Melki, S., and Bergametti, G.: Atmospheric input of trace metals to the western Mediterranean: uncertainties in modelling dry deposition from cascade impactor data, Tellus B, 41, 362-378, 1989.

Dunbar, G. B., Bertler, N. A. N., and McKay, R. M.: Sediment flux through the McMurdo Ice Shelf in Windless Bight, Antarctica, Global and Planetary Change, 69, 87-93, 2009.

Duncan, B. N., Martin, R. V., Staudt, A. C., Yevich, R., and Logan, J. A.: Interannual and seasonal variability of biomass burning emissions constrained by satellite observations, Journal of Geophysical Research: Atmospheres (1984–2012), 108, ACH 1-1-ACH 1-22, 2003.

Echalar, F., Gaudichet, A., Cachier, H., and Artaxo, P.: Aerosol emissions by tropical forest and savanna biomass burning: characteristic trace elements and fluxes, Geophysical research letters, 22, 3039-3042, 1995.

Echalar, F., Artaxo, P., Martins, J. V., Yamasoe, M., Gerab, F., Maenhaut, W., and Holben, B.: Long-term monitoring of atmospheric aerosols in the Amazon Basin: Source identification and apportionment, Journal of Geophysical Research: Atmospheres (1984–2012), 103, 31849-31864, 1998.

Edwards, R., and Sedwick, P.: Iron in East Antarctic snow: Implications for atmospheric iron deposition and algal production in Antarctic waters, Geophys. Res. Lett., 28, 3907-3910, 10.1029/2001gl012867, 2001.

Edwards, R., Sedwick, P., Morgan, V., and Boutron, C.: Iron in ice cores from Law Dome: A record of atmospheric iron deposition for maritime East Antarctica during the Holocene and Last Glacial Maximum, Geochemistry, Geophysics, Geosystems, 7, Q12Q01, 10.1029/2006GC001307, 2006.

Elderfield, H.: Strontium isotope stratigraphy, Palaeogeography, Palaeoclimatology, Palaeoecology, 57, 71-90, 1986.

Elliot, D. H., Fleming, T. H., Kyle, P. R., and Foland, K. A.: Long-distance transport of magmas in the Jurassic Ferrar Large Igneous Province, Antarctica, Earth and Planetary Science Letters, 167, 89-104, http://dx.doi.org/10.1016/S0012-821X(99)00023-0, 1999.

Ellwood, M. J., Hutchins, D. A., Lohan, M. C., Milne, A., Nasemann, P., Nodder, S. D., Sander, S. G., Strzepek, R., Wilhelm, S. W., and Boyd, P. W.: Iron stable isotopes track pelagic iron cycling during a subtropical phytoplankton bloom, Proceedings of the National Academy of Sciences, 112, E15-E20, 2015.

Elrod, V., Berelson, W., Coale, K., and Johnson, K.: The flux of iron from continental shelf sediments: a missing source for global budgets, Geophys Res Lett, 31, L12307, 2004.

Ezat, U., and Dulac, F.: Size distribution of mineral aerosols at Amsterdam-island and dry deposition rates in the Southern Indian Ocean, Comptes Rendus De L Acadmie Des Sciences Serie II, 320, 9-14, 1995.

Falkowski, P. G.: Evolution of the nitrogen cycle and its influence on the biological sequestration of CO 2 in the ocean, Nature, 387, 272-275, 1997.

Faure, G.: Principles of Isotope Geology (2nd ed.)Wiley, New York (1986), p. 589, 1986.

Field, R. D., van der Werf, G. R., and Shen, S. S.: Human amplification of drought-induced biomass burning in Indonesia since 1960, Nature Geoscience, 2, 185-188, 2009.

Fishwick, M. P., Sedwick, P. N., Lohan, M. C., Worsfold, P. J., Buck, K. N., Church, T. M., and Ussher, S. J.: The impact of changing surface ocean conditions on the dissolution of aerosol iron, Global Biogeochemical Cycles, 2014GB004921, 10.1002/2014GB004921, 2014.

Fitzwater, S. E., Johnson, K. S., Gordon, R. M., Coale, K. H., and Smith, W. O.: Trace metal concentrations in the Ross Sea and their relationship with nutrients and phytoplankton growth, Deep Sea Research Part II: Topical Studies in Oceanography, 47, 3159-3179, 2000.

Fleming, T., Foland, K., and Elliot, D.: Isotopic and chemical constraints on the crustal evolution and source signature of Ferrar magmas, north Victoria Land, Antarctica, Contributions to Mineralogy and Petrology, 121, 217-236, 10.1007/BF02688238, 1995.

Formenti, P., Elbert, W., Maenhaut, W., Haywood, J., Osborne, S., and Andreae, M.: Inorganic and carbonaceous aerosols during the Southern African Regional Science Initiative (SAFARI 2000) experiment: Chemical characteristics, physical properties, and emission data for smoke from African biomass burning, Journal of Geophysical Research: Atmospheres (1984–2012), 108, 2003.

Frenklach, M.: Reaction mechanism of soot formation in flames, Physical Chemistry Chemical Physics, 4, 2028-2037, 2002.

Freydier, R., Michard, A., De Lange, G., and Thomson, J.: Nd isotopic compositions of Eastern Mediterranean sediments: tracers of the Nile influence during sapropel S1 formation?, Marine Geology, 177, 45-62, 2001.

Friedman, B., Herich, H., Kammermann, L., Gross, D. S., Arneth, A., Holst, T., and Cziczo, D. J.: Subarctic atmospheric aerosol composition: 1. Ambient aerosol characterization, Journal of Geophysical Research: Atmospheres (1984–2012), 114, 2009.

Fu, H., Shang, G., Lin, J., Hu, Y., Hu, Q., Guo, L., Zhang, Y., and Chen, J.: Fractional iron solubility of aerosol particles enhanced by biomass burning and ship emission in Shanghai, East China, Science of The Total Environment, 481, 377-391, 2014.

Futa, K., and Le Masurier, W.: Nd and Sr isotopic studies on Cenozoic mafic lavas from West Antarctica: Another source for continental alkali basalts, Contributions to Mineralogy and Petrology, 83, 38-44, 1983.

Gabric, A. J., Cropp, R. A., McTainsh, G. H., Johnston, B. M., Butler, H., Tilbrook, B., and Keywood, M.: Australian dust storms in 2002–2003 and their impact on Southern Ocean biogeochemistry, Global Biogeochemical Cycles, 24, 2010.

Gabrielli, P., Wegner, A., Petit, J. R., Delmonte, B., De Deckker, P., Gaspari, V., Fischer, H., Ruth, U., Kriews, M., and Boutron, C.: A major glacial-interglacial change in aeolian dust composition inferred from Rare Earth Elements in Antarctic ice, Quaternary Science Reviews, 29, 265-273, 2010.

Gaiero, D. M., Probst, J.-L., Depetris, P. J., Bidart, S. M., and Leleyter, L.: Iron and other transition metals in Patagonian riverborne and windborne materials: geochemical control and transport to the southern South Atlantic Ocean, Geochimica et Cosmochimica Acta, 67, 3603-3623, 2003.

Gaiero, D. M., Brunet, F., Probst, J.-L., and Depetris, P. J.: A uniform isotopic and chemical signature of dust exported from Patagonia: Rock sources and occurrence in southern environments, Chemical Geology, 238, 107-120, 2007.

Gaiero, D. M.: Reply to comment by B. Delmonte et al. on “Dust provenance in Antarctic ice during glacial periods: From where in southern South America?”, Geophysical Research Letters, 35, 2008.

Gao, S., Hegg, D. A., and Jonsson, H.: Aerosol chemistry, and light-scattering and hygroscopicity budgets during outflow from East Asia, Journal of Atmospheric Chemistry, 46, 55-88, 2003.

Gao, Y., Kaufman, Y. J., Tanré, D., Kolber, D., and Falkowski, P. G.: Seasonal distributions of aeolian iron fluxes to the global ocean, Geophys. Res. Lett., 28, 29-32, 10.1029/2000gl011926, 2001.

Gao, Y., Xu, G., Zhan, J., Zhang, J., Li, W., Lin, Q., Chen, L., and Lin, H.: Spatial and particle size distributions of atmospheric dissolvable iron in aerosols and its input to the Southern Ocean and coastal East Antarctica, Journal of Geophysical Research: Atmospheres, 118, 12,634-612,648, 2013.

Gaspari, V., Barbante, C., Cozzi, G., Cescon, P., Boutron, C. F., Gabrielli, P., Capodaglio, G., Ferrari, C., Petit, J. R., and Delmonte, B.: Atmospheric iron fluxes over the last deglaciation: Climatic implications, Geophys. Res. Lett., 33, L03704, 10.1029/2005gl024352, 2006.

Gatehouse, R. D., Williams, I., and Pillans, B.: Fingerprinting windblown dust in south-eastern Australian soils by uranium-lead dating of detrital zircon, Soil Research, 39, 7-12, 2001.

Gaudichel, A., De Angelis, M., Joussaume, S., Petit, J., Korotkevitch, Y., and Petrov, V.: Comments on the origin of dust in East Antarctica for present and ice age conditions, Journal of atmospheric chemistry, 14, 129-142, 1992.

Gerringa, L. J. A., Alderkamp, A.-C., Laan, P., Thuróczy, C.-E., De Baar, H. J. W., Mills, M. M., van Dijken, G. L., Haren, H. v., and Arrigo, K. R.: Iron from melting glaciers fuels the phytoplankton blooms in Amundsen Sea (Southern Ocean): Iron biogeochemistry, Deep Sea Research Part II: Topical Studies in Oceanography, 71–76, 16-31, 10.1016/j.dsr2.2012.03.007, 2012.

Gerringa, L. J. A., Laan, P., van Dijken, G. L., van Haren, H., De Baar, H. J. W., Arrigo, K. R., and Alderkamp, A. C.: Sources of iron in the Ross Sea Polynya in early summer, Marine Chemistry, 177, Part 3, 447-459, http://dx.doi.org/10.1016/j.marchem.2015.06.002, 2015.

Gerringa, L. J. A., Laan, P., van Dijken, G. L., van Haren, H., De Baar, H. J. W., Arrigo, K. R., and Alderkamp, A. C.: Sources of iron in the Ross Sea polynya in early summer, Marine Chemistry, http://dx.doi.org/10.1016/j.marchem.2015.06.002, http://dx.doi.org/10.1016/j.marchem.2015.06.002, in press.

Gibbs, R., Mathews, M., and Unk, D.: The relationship between sphere size and settling velocity, Journal of Sedimentary Petrology, 41, 7-18, 1971.

Giglio, L., Randerson, J. T., and Werf, G. R.: Analysis of daily, monthly, and annual burned area using the fourth-generation global fire emissions database (GFED4), Journal of Geophysical Research: Biogeosciences, 118, 317-328, 2013.

Gillies, J. A., Nickling, W. G., and Tilson, M.: Frequency, magnitude, and characteristics of aeolian sediment transport: McMurdo Dry Valleys, Antarctica, Journal of Geophysical Research: Earth Surface, 118, 461-479, 2013.

Gingele, F., and De Deckker, P.: Clay mineral, geochemical and Sr–Nd isotopic fingerprinting of sediments in the Murray–Darling fluvial system, southeast Australia, Australian Journal of Earth Sciences, 52, 965-974, 2005.

Glassman, I.: Soot formation in combustion processes, Symposium (international) on combustion, 1989, 295-311.

Grand, M. M., Measures, C. I., Hatta, M., Hiscock, W. T., Buck, C. S., and Landing, W. M.: Dust deposition in the eastern Indian Ocean: The ocean perspective from Antarctica to the Bay of Bengal, Global Biogeochemical Cycles, 2015a.

Grand, M. M., Measures, C. I., Hatta, M., Hiscock, W. T., Landing, W. M., Morton, P. L., Buck, C. S., Barrett, P. M., and Resing, J. A.: Dissolved Fe and Al in the upper 1000 m of the eastern Indian Ocean: A high-resolution transect along 95°E from the Antarctic margin to the Bay of Bengal, Global Biogeochemical Cycles, 29, 375-396, 10.1002/2014GB004920, 2015b.

Grand, M. M., Measures, C. I., Hatta, M., Morton, P. L., Barrett, P., Milne, A., Resing, J. A., and Landing, W. M.: The impact of circulation and dust deposition in controlling the distributions of dissolved Fe and Al in the south Indian subtropical gyre, Marine Chemistry, 176, 110-125, 2015c.

Greeley, R., and Iversen, J.: Wind as a geological process, no. 4 in Cambridge Planetary Science Series, Cambridge Univ. Press, New York, NY, 3, 3.2, 1985.

Grousset, F., Rognon, P., Coudé-Gaussen, G., and Pédemay, P.: Origins of peri-Saharan dust deposits traced by their Nd and Sr isotopic composition, Palaeogeography, Palaeoclimatology, Palaeoecology, 93, 203-212, 1992a.

Grousset, F. E., Biscaye, P. E., Zindler, A., Prospero, J., and Chester, R.: Neodymium isotopes as tracers in marine sediments and aerosols: North Atlantic, Earth and Planetary Science Letters, 87, 367-378, 1988.

Grousset, F. E., Biscaye, P. E., Revel, M., Petit, J.-R., Pye, K., Joussaume, S., and Jouzel, J.: Antarctic (Dome C) ice-core dust at 18 k.y. B.P.: Isotopic constraints on origins, Earth and Planetary Science Letters, 111, 175-182, 1992b.

Grousset, F. E., Biscaye, P. E., Revel, M., Petit, J.-R., Pye, K., Joussaume, S., and Jouzel, J.: Antarctic (Dome C) ice-core dust at 18 ky BP: Isotopic constraints on origins, Earth and Planetary Science Letters, 111, 175-182, 1992c.

Grousset, F. E., and Biscaye, P. E.: Tracing dust sources and transport patterns using Sr, Nd and Pb isotopes, Chemical Geology, 222, 149-167, 2005.

Guieu, C., Bonnet, S., Wagener, T., and Loÿe-Pilot, M. D.: Biomass burning as a source of dissolved iron to the open ocean?, Geophysical Research Letters, 32, 2005.

Guieu, C., Aumont, O., Paytan, A., Bopp, L., Law, C. S., Mahowald, N., Achterberg, E. P., Marañón, E., Salihoglu, B., Crise, A., Wagener, T., Herut, B., Desboeufs, K., Kanakidou, M., Olgun, N., Peters, F., Pulido-Villena, E., Tovar-Sanchez, A., and Völker, C.: The significance of the episodic nature of atmospheric deposition to Low Nutrient Low Chlorophyll regions, Global Biogeochemical Cycles, 2014GB004852, 10.1002/2014GB004852, 2014.

Gysel, M., Laborde, M., Olfert, J., Subramanian, R., and Gröhn, A.: Effective density of Aquadag and fullerene soot black carbon reference materials used for SP2 calibration, Atmospheric Measurement Techniques, 4, 2851-2858, 2011.

Halstead, M. J., Cunninghame, R. G., and Hunter, K. A.: Wet deposition of trace metals to a remote site in Fiordland, New Zealand, Atmospheric Environment, 34, 665-676, 2000.

Hand, J. L., Mahowald, N. M., Chen, Y., Siefert, R. L., Luo, C., Subramaniam, A., and Fung, I.: Estimates of atmospheric-processed soluble iron from observations and a global mineral aerosol model: Biogeochemical implications, J. Geophys. Res., 109, D17205, 10.1029/2004jd004574, 2004.

Hao, W. M., and Liu, M. H.: Spatial and temporal distribution of tropical biomass burning, Global biogeochemical cycles, 8, 495-503, 1994.

Hasegawa, S., and Ohta, S.: Some measurements of the mixing state of soot-containing particles at urban and non-urban sites, Atmospheric Environment, 36, 3899-3908, 2002.

Heimburger, A., Losno, R., Triquet, S., Dulac, F., and Mahowald, N.: Direct measurements of atmospheric iron, cobalt, and aluminum-derived dust deposition at Kerguelen Islands, Global Biogeochemical Cycles, 26, 2012.

Heimburger, A., Losno, R., and Triquet, S.: Solubility of iron and other trace elements in rainwater collected on the Kerguelen Islands (South Indian Ocean), Biogeosciences, 10, 2013a.

Heimburger, A., Losno, R., Triquet, S., and Nguyen, E. B.: Atmospheric deposition fluxes of 26 elements over the Southern Indian Ocean: Time series on Kerguelen and Crozet Islands, Global Biogeochemical Cycles, 27, 440-449, 2013b.

Hesse, P. P.: The record of continental dust from Australia in Tasman Sea sediments, Quaternary Science Reviews, 13, 257-272, 1994.

Hesse, P. P.: Mineral magnetic ‘tracing’of aeolian dust in southwest Pacific sediments, Palaeogeography, Palaeoclimatology, Palaeoecology, 131, 327-353, 1997.

Hesse, P. P., and McTainsh, G. H.: Australian dust deposits: modern processes and the Quaternary record, Quaternary Science Reviews, 22, 2007-2035, 2003.

Hinkley, T. K., and Matsumoto, A.: Atmospheric regime of dust and salt through 75,000 years of Taylor Dome ice core: Refinement by measurement of major, minor, and trace metal suites, J. Geophys. Res., 106, 18487-18493, 10.1029/2000jd900550, 2001.

Hoelzemann, J. J., Schultz, M. G., Brasseur, G. P., Granier, C., and Simon, M.: Global Wildland Fire Emission Model (GWEM): Evaluating the use of global area burnt satellite data, Journal of Geophysical Research: Atmospheres (1984–2012), 109, 2004.

Hole, M., and LeMasurier, W.: Tectonic controls on the geochemical composition of Cenozoic, mafic alkaline volcanic rocks from West Antarctica, Contributions to Mineralogy and Petrology, 117, 187-202, 1994.

Huang, X., Gordon, T., Rom, W. N., and Finkelman, R. B.: Interaction of iron and calcium minerals in coals and their roles in coal dust-induced health and environmental problems, Reviews in mineralogy and geochemistry, 64, 153-178, 2006.

Huang, X., Song, Y., Zhao, C., Li, M., Zhu, T., Zhang, Q., and Zhang, X.: Pathways of sulfate enhancement by natural and anthropogenic mineral aerosols in China, Journal of Geophysical Research: Atmospheres, 2014.

Hurst, M. P., and Bruland, K. W.: An investigation into the exchange of iron and zinc between soluble, colloidal, and particulate size-fractions in shelf waters using low-abundance isotopes as tracers in shipboard incubation experiments, Marine chemistry, 103, 211-226, 2007.

Hutchins, D. A., DiTullio, G. R., and Bruland, K. W.: Iron and Regenerated Production: Evidence for Biological Iron Recycling in Two Marine Environments, Limnology and Oceanography, 38, 1242-1255, 1993.

Ito, A., and Penner, J. E.: Global estimates of biomass burning emissions based on satellite imagery for the year 2000, Journal of Geophysical Research: Atmospheres (1984–2012), 109, 2004.

Ito, A.: Mega fire emissions in Siberia: potential supply of bioavailable iron from forests to the ocean, Biogeosciences, 8, 2011.

Ito, A.: Contrasting the effect of iron mobilization on soluble iron deposition to the ocean in the Northern and Southern Hemispheres, Meteorol. Soc. Japan, 90, 167-188, 2012.

Ito, A.: Global modeling study of potentially bioavailable iron input from shipboard aerosol sources to the ocean, Global Biogeochemical Cycles, 27, 1-10, 2013.

Ito, A.: Atmospheric Processing of Combustion Aerosols as a Source of Bioavailable Iron, Environmental Science & Technology Letters, 2, 70-75, 10.1021/acs.estlett.5b00007, 2015.

Ito, A., and Shi, Z.: Delivery of anthropogenic bioavailable iron from mineral dust and combustion aerosols to the ocean, Atmospheric Chemistry and Physics Discussions, 15, 23051-23088, 2015.

Jacobs, S. S., Amos, A. F., and Bruchhausen, P. M.: Ross sea oceanography and antarctic bottom water formation, Deep Sea Research and Oceanographic Abstracts, 17, 935-962, 1970.

Jacobsen, S. B., and Wasserburg, G. J.: Sm-Nd isotopic evolution of chondrites, Earth and Planetary Science Letters, 50, 139-155, 1980.

Jacobson, M. Z.: Development of mixed-phase clouds from multiple aerosol size distributions and the effect of the clouds on aerosol removal, Journal of Geophysical Research: Atmospheres (1984–2012), 108, 2003.

Jeong, D., Kim, K., and Choi, W.: Accelerated dissolution of iron oxides in ice, Atmospheric Chemistry and Physics, 12, 11125-11133, 2012.

Jickells, T., An, Z., Anderson, K., Baker, A., Bergametti, G., Brooks, N., Cao, J., Boyd, P., Duce, R., Hunter, K., Kawaahata, H., Kubilay, N., LaRoche, J., Liss, P., Mahowald, N., Prospero, J., Ridgewell, A., Tegen, I., and Torres, R.: Global iron connections between desert dust, ocean biogeochemistry, and climate, Science, 308, 67 - 73, 2005.

Jochum, K. P., Nohl, U., Herwig, K., Lammel, E., Stoll, B., and Hofmann, A. W.: GeoReM: A New Geochemical Database for Reference Materials and Isotopic Standards, Geostandards and Geoanalytical Research, 29, 333-338, 10.1111/j.1751-908X.2005.tb00904.x, 2005.

Johnsen, S. J., Dansgaard, W., Clausen, H. B., and Langway, C. C.: Oxygen Isotope Profiles through the Antarctic and Greenland Ice Sheets, Nature, 235, 429-434, 1972.

Johnson, B., Heese, B., McFarlane, S., Chazette, P., Jones, A., and Bellouin, N.: Vertical distribution and radiative effects of mineral dust and biomass burning aerosol over West Africa during DABEX, Journal of Geophysical Research: Atmospheres (1984–2012), 113, 2008.

Johnson, K., Coale, K., Elrod, V., and Tindale, W.: Iron photochemistry in seawater from the equatorial Pacific, Mar Chem, 46, 319 - 334, 1994.

Johnson, K., Chavez, F., and Friederich, G.: Continental-shelf sediment as a primary source of iron for coastal phytoplankton, Nature, 398, 697 - 700, 1999.

Johnson, K. S., Gordon, R. M., and Coale, K. H.: What controls dissolved iron concentrations in the world ocean?, Marine Chemistry, 57, 137-161, 1997.

Johnson, M. S., Meskhidze, N., Kiliyanpilakkil, V. P., and Gassó, S.: Understanding the transport of Patagonian dust and its influence on marine biological activity in the South Atlantic Ocean, Atmos. Chem. Phys. Discuss., 10, 27283-27320, 10.5194/acpd-10-27283-2010, 2010.

Johnston, S. W.: The influence of aeolian dust deposits on alpine soils in south-eastern Australia, Soil Research, 39, 81-88, 2001.

Kadko, D., Landing, W. M., and Shelley, R. U.: A novel tracer technique to quantify the atmospheric flux of trace elements to remote ocean regions, Journal of Geophysical Research: Oceans, 2015.

Kalinske, A. A.: Turbulence and the transport of sand and silt by wind, Annals of the New York Academy of Sciences, 44, 41-54, 1943.

Kasischke, E. S., and Penner, J. E.: Improving global estimates of atmospheric emissions from biomass burning, Journal of Geophysical Research: Atmospheres (1984–2012), 109, 2004.

Kellogg, T. B., Kellogg, D., and Stuiver, M.: Late Quaternary History of the Southwestern Ross Sea: Evidence from Debris Bands on the McMurdo Ice Shelf, Antarctica, Antarctic Res. Ser. (AGU), 50, 25-56, 1990.

Keywood, M., Kanakidou, M., Stohl, A., Dentener, F., Grassi, G., Meyer, C., Torseth, K., Edwards, D., Thompson, A. M., and Lohmann, U.: Fire in the air: biomass burning impacts in a changing climate, Critical Reviews in Environmental Science and Technology, 43, 40-83, 2013.

Keywood, M., Cope, M., Meyer, C. M., Iinuma, Y., and Emmerson, K.: When smoke comes to town: The impact of biomass burning smoke on air quality, Atmospheric Environment, 2015.

Keywood, M. D., Graham, B., Gillett, R. W., Gras, J. G., and Selleck, P. W.: High volume aerosol sampler. Baseline Atmospheric Program (Australia) 2001-200 edited by J. Cainey, N.Derek and P.Krummel. .Bureau of Meteorology CSIRO Atmospheric Research and, Melbourne, Australia: 74-77., 2004.

Keywood, M. D.: Aerosol composition at Cape Grim : an evaluation of PM10 sampling program and baseline event switches., Baseline Atmospheric Program Australia 2005-2006. 2005-2006 ed. J. M. Cainey, N. Derek, and P. B. Krummel (editors). Melbourne: Australian Bureau of Meteorology and CSIRO Marine and Atmospheric Research, 31-36, 2007.

Khalizov, A. F., Xue, H., Wang, L., Zheng, J., and Zhang, R.: Enhanced light absorption and scattering by carbon soot aerosol internally mixed with sulfuric acid, The Journal of Physical Chemistry A, 113, 1066-1074, 2009.

Knight, A. W., McTainsh, G., and Simpson, R.: Sediment loads in an Australian dust storm: implications for present and past dust processes, Catena, 24, 195-213, 1995.

Kobayashi, H., Hara, K., Shiobara, M., Yamanouchi, T., Osada, K., and Ohta, S.: Seasonal variation of carbonaceous and metal compositions of atmospheric aerosols at Syowa Station, Antarctica in 2001, Antarctic Record(Tokyo), 54, 554-561, 2010.

Koffman, B., Kreutz, K., Breton, D., Kane, E., Winski, D., Birkel, S., Kurbatov, A., and Handley, M.: Centennial-scale variability of the Southern Hemisphere westerly wind belt in the eastern Pacific over the past two millennia, Climate of the Past, 10, 1125-1144, 2014a.

Koffman, B. G., Handley, M. J., Osterberg, E. C., Wells, M. L., and Kreutz, K. J.: Dependence of ice-core relative trace-element concentration on acidification, Journal of Glaciology, 60, 103-112, 2014b.

Kohfeld, K. E., and Harrison, S. P.: DIRTMAP: the geological record of dust, Earth-Science Reviews, 54, 81-114, 2001.

Kok, J. F.: Does the size distribution of mineral dust aerosols depend on the wind speed at emission?, Atmospheric Chemistry and Physics, 11, 10149-10156, 2011a.

Kok, J. F.: A scaling theory for the size distribution of emitted dust aerosols suggests climate models underestimate the size of the global dust cycle, Proceedings of the National Academy of Sciences, 108, 1016-1021, 2011b.

Koppmann, R., Czapiewski, K. v., and Reid, J.: A review of biomass burning emissions, part I: gaseous emissions of carbon monoxide, methane, volatile organic compounds, and nitrogen containing compounds, Atmospheric Chemistry and Physics Discussions, 5, 10455-10516, 2005.

Kraemer, S.: Iron oxide dissolution and solubility in the presence of siderophores, Aquatic Sciences - Research Across Boundaries, 66, 3-18, 10.1007/s00027-003-0690-5, 2004.

Kraemer, S. M., Butler, A., Borer, P., and Cervini-Silva, J.: Siderophores and the Dissolution of Iron-Bearing Minerals in Marine Systems, Reviews in Mineralogy and Geochemistry, 59, 53-84, 10.2138/rmg.2005.59.4, 2005.

Krinner, G., and Genthon, C.: Tropospheric transport of continental tracers towards Antarctica under varying climatic conditions, Tellus B, 55, 54-70, 2003.

Krinner, G., Petit, J.-R., and Delmonte, B.: Altitude of atmospheric tracer transport towards Antarctica inpresent and glacial climate, Quaternary science reviews, 29, 274-284, 2010.

Kuma, K., and Matsunaga, K.: Availability of colloidal ferric oxides to coastal marine phytoplankton, Marine Biology, 122, 1-11, 1995.

Kumar, A., Sarin, M., and Srinivas, B.: Aerosol iron solubility over Bay of Bengal: Role of anthropogenic sources and chemical processing, Marine Chemistry, 121, 167-175, 2010.

Kustka, A. B., Sañudo-Wilhelmy, S. A., Carpenter, E. J., Capone, D., Burns, J., and Sunda, W. G.: Iron requirements for dinitrogen-and ammonium-supported growth in cultures of Trichodesmium (IMS 101): Comparison with nitrogen fixation rates and iron: Carbon ratios of field populations, Limnology and Oceanography, 48, 1869-1884, 2003.

Kustka, A. B., Kohut, J. T., White, A. E., Lam, P. J., Milligan, A. J., Dinniman, M. S., Mack, S., Hunter, E., Hiscock, M. R., Smith Jr, W. O., and Measures, C. I.: The roles of MCDW and deep water iron supply in sustaining a recurrent phytoplankton bloom on central Pennell Bank (Ross Sea), Deep Sea Research Part I: Oceanographic Research Papers, 105, 171-185, http://dx.doi.org/10.1016/j.dsr.2015.08.012, 2015.

Laborde, M., Mertes, P., Zieger, P., Dommen, J., Baltensperger, U., and Gysel, M.: Sensitivity of the Single Particle Soot Photometer to different black carbon types, Atmospheric Measurement Techniques, 5, 1031-1043, 2012.

Lamarque, J.-F., Bond, T. C., Eyring, V., Granier, C., Heil, A., Klimont, Z., Lee, D., Liousse, C., Mieville, A., and Owen, B.: Historical (1850–2000) gridded anthropogenic and biomass burning emissions of reactive gases and aerosols: methodology and application, Atmospheric Chemistry and Physics, 10, 7017-7039, 2010.

Lambert, F., Delmonte, B., Petit, J. R., Bigler, M., Kaufmann, P. R., Hutterli, M. A., Stocker, T. F., Ruth, U., Steffensen, J. P., and Maggi, V.: Dust-climate couplings over the past 800,000[thinsp]years from the EPICA Dome C ice core, Nature, 452, 616-619, http://www.nature.com/nature/journal/v452/n7187/suppinfo/nature06763_S1.html, 2008.

Lambert, F., Tagliabue, A., Shaffer, G., Lamy, F., Winckler, G., Farias, L., Gallardo, L., and De Pol-Holz, R.: Dust fluxes and iron fertilization in Holocene and Last Glacial Maximum climates, Geophysical Research Letters, n/a-n/a, 10.1002/2015GL064250, 2015.

Lancaster, N., Nickling, W. G., and Gillies, J. A.: Sand transport by wind on complex surfaces: Field studies in the McMurdo Dry Valleys, Antarctica, Journal of Geophysical Research: Earth Surface (2003–2012), 115, 2010.

Lanci, L., Delmonte, B., Maggi, V., Petit, J. R., and Kent, D. V.: Ice magnetization in the EPICA-Dome C ice core: Implication for dust sources during glacial and interglacial periods, J. Geophys. Res., 113, D14207, 10.1029/2007jd009678, 2008.

Lannuzel, D., Schoemann, V., de Jong, J., Tison, J., and Chou, L.: Distribution and biogeochemical behaviour of iron in the East Antarctic sea ice, Marine Chemistry, 106, 18-32, 2007.

Lannuzel, D., Schoemann, V., de Jong, J., Chou, L., Delille, B., Becquevort, S., and Tison, J.: Iron study during a time series in the western Weddell pack ice, Marine Chemistry, 108, 85-95, 2008.

Lannuzel, D., Schoemann, V., de Jong, J., Pasquer, B., van der Merwe, P., Masson, F., Tison, J.-L., and Bowie, A.: Distribution of dissolved iron in Antarctic sea ice: Spatial, seasonal, and inter-annual variability, J. Geophys. Res., 115, G03022, 10.1029/2009jg001031, 2010.

LaRoche, J., and Breitbarth, E.: Importance of the diazotrophs as a source of new nitrogen in the ocean, Journal of Sea Research, 53, 67-91, 2005.

Latimer, J. C., and Filippelli, G. M.: Terrigenous input and paleoproductivity in the Southern Ocean, Paleoceanography, 16, 627-643, 2001.

Latimer, J. C., Filippelli, G. M., Hendy, I. L., Gleason, J. D., and Blum, J. D.: Glacial-interglacial terrigenous provenance in the southeastern Atlantic Ocean: The importance of deep-water sources and surface currents, Geology, 34, 545-548, 2006.

Law, C., Woodward, E., Ellwood, M., Marriner, A., Bury, S., and Safi, K.: Response of surface nutrient inventories and nitrogen fixation to a tropical cyclone in the southwest Pacific, Limnology and Oceanography, 56, 1372-1385, 2011.

le Roux, J. P.: An alternative approach to the identification of net sediment transport paths based on grain-size trends, Sedimentary Geology, 94, 97-107, 1994.

Legrand, M., and Kirchner, S.: Polar atmospheric circulation and chemistry of recent (1957-1983) south polar precipitation, Geophysical research letters, 15, 879-882, 1988.

Lenes, J., Darrow, B., Walsh, J., Prospero, J., He, R., Weisberg, R., Vargo, G., and Heil, C.: Saharan dust and phosphatic fidelity: A three-dimensional biogeochemical model of Trichodesmium as a nutrient source for red tides on the West Florida Shelf, Continental Shelf Research, 28, 1091-1115, 2008.

Li, F., Ginoux, P., and Ramaswamy, V.: Distribution, transport, and deposition of mineral dust in the Southern Ocean and Antarctica: Contribution of major sources, J. Geophys. Res., 113, D10207, 10.1029/2007jd009190, 2008.

Lin, Y. C., Chen, J. P., Ho, T. Y., and Tsai, I.: Atmospheric iron deposition in the northwestern Pacific Ocean and its adjacent marginal seas: The importance of coal burning, Global Biogeochemical Cycles, 29, 138-159, 2015.

Lis, H., Shaked, Y., Kranzler, C., Keren, N., and Morel, F. M. M.: Iron bioavailability to phytoplankton: an empirical approach, ISME J, 9, 1003-1013, 10.1038/ismej.2014.199, 2015.

Liu, J., Mauzerall, D. L., Horowitz, L. W., Ginoux, P., and Fiore, A. M.: Evaluating inter-continental transport of fine aerosols:(1) Methodology, global aerosol distribution and optical depth, Atmospheric Environment, 43, 4327-4338, 2009.

Liu, J., Fan, S., Horowitz, L. W., and Levy, H.: Evaluation of factors controlling long-range transport of black carbon to the Arctic, Journal of Geophysical Research: Atmospheres (1984–2012), 116, 2011.

Lu, H., and Shao, Y.: Toward quantitative prediction of dust storms: an integrated wind erosion modelling system and its applications, Environmental Modelling & Software, 16, 233-249, 2001.

Luo, C., Mahowald, N. M., and del Corral, J.: Sensitivity study of meteorological parameters on mineral aerosol mobilization, transport, and distribution, J. Geophys. Res., 108, 4447, 10.1029/2003jd003483, 2003.

Luo, C., Mahowald, N. M., Meskhidze, N., Chen, Y., Siefert, R. L., Baker, A. R., and Johansen, A. M.: Estimation of iron solubility from observations and a global aerosol model, J. Geophys. Res., 110, D23307, 10.1029/2005jd006059, 2005.

Luo, C., Mahowald, N., Bond, T., Chuang, P. Y., Artaxo, P., Siefert, R., Chen, Y., and Schauer, J.: Combustion iron distribution and deposition, Global Biogeochem. Cycles, 22, GB1012, 10.1029/2007gb002964, 2008.

Mackie, D., Peat, J., McTainsh, G. H., Boyd, P., and Hunter, K.: Soil abrasion and eolian dust production: Implications for iron partitioning and solubility, Geochemistry, Geophysics, Geosystems, 7, 2006.

Mackie, D. S., Boyd, P. W., Hunter, K. A., and McTainsh, G. H.: Simulating the cloud processing of iron in Australian dust: pH and dust concentration, Geophys. Res. Lett., 32, L06809, 10.1029/2004gl022122, 2005.

Mackie, D. S., Boyd, P. W., McTainsh, G. H., Tindale, N. W., Westberry, T. K., and Hunter, K. A.: Biogeochemistry of iron in Australian dust: From eolian uplift to marine uptake, Geochem. Geophys. Geosyst., 9, Q03Q08, 10.1029/2007gc001813, 2008.

Macpherson, A.: The MacKay Glacier/Granite Harbour system (Ross Dependency, Antarctica). A study in nearshore glacial marine sedimentation, Victoria University of Wellington, Wellington, 85 pp., 1987.

Maenhaut, W., Salma, I., Cafmeyer, J., Annegarn, H. J., and Andreae, M. O.: Regional atmospheric aerosol composition and sources in the eastern Transvaal, South Africa, and impact of biomass burning, JOURNAL OF GEOPHYSICAL RESEARCH-ALL SERIES-, 101, 23,631-623,650, 1996.

Magee, J., Bowler, J., Miller, G., and Williams, D.: Stratigraphy, sedimentology, chronology and palaeohydrology of Quaternary lacustrine deposits at Madigan Gulf, Lake Eyre, South Australia, Palaeogeography, Palaeoclimatology, Palaeoecology, 113, 3-42, 1995.

Mahowald, N., Kohfeld, K., Hansson, M., Balkanski, Y., Harrison, S. P., Prentice, I. C., Schulz, M., and Rodhe, H.: Dust sources and deposition during the last glacial maximum and

current climate: A comparison of model results with paleodata from ice cores and marine sediments, J. Geophys. Res., 104, 15895-15916, 10.1029/1999jd900084, 1999.

Mahowald, N. M., Baker, A. R., Bergametti, G., Brooks, N., Duce, R. A., Jickells, T. D., Kubilay, N., Prospero, J. M., and Tegen, I.: Atmospheric global dust cycle and iron inputs to the ocean, Global Biogeochem. Cycles, 19, GB4025, 10.1029/2004gb002402, 2005.

Mahowald, N. M., Engelstaedter, S., Luo, C., Sealy, A., Artaxo, P., Benitez-Nelson, C., Bonnet, S., Chen, Y., Chuang, P. Y., and Cohen, D. D.: Atmospheric iron deposition: Global distribution, variability, and human perturbations*, Marine Science, 1, 2009.

Mahowald, N. M., Kloster, S., Engelstaedter, S., Moore, J. K., Mukhopadhyay, S., McConnell, J. R., Albani, S., Doney, S. C., Bhattacharya, A., Curran, M. A. J., Flanner, M. G., Hoffman, F. M., Lawrence, D. M., Lindsay, K., Mayewski, P. A., Neff, J., Rothenberg, D., Thomas, E., Thornton, P. E., and Zender, C. S.: Observed 20th century desert dust variability: impact on climate and biogeochemistry, Atmos. Chem. Phys., 10, 10875-10893, 10.5194/acp-10-10875-2010, 2010.

Marino, F., Castellano, E., Ceccato, D., De Deckker, P., Delmonte, B., Ghermandi, G., Maggi, V., Petit, J. R., Revel-Rolland, M., and Udisti, R.: Defining the geochemical composition of the EPICA Dome C ice core dust during the last glacial-interglacial cycle, Geochem. Geophys. Geosyst., 9, Q10018, 10.1029/2008gc002023, 2008.

Marsay, C., Sedwick, P. N., Dinniman, M., Barrett, P., Mack, S., and McGillicuddy, D. J.: Estimating the benthic efflux of dissolved iron on the Ross Sea continental shelf, Geophysical Research Letters, 41, 7576-7583, 2014.

Marticorena, B., and Bergametti, G.: Modeling the atmospheric dust cycle: 1. Design of a soil-derived dust emission scheme, J. Geophys. Res., 100, 16415-16430, 10.1029/95jd00690, 1995.

Martin, C. E., and McCulloch, M. T.: Nd-Sr isotopic and trace element geochemistry of river sediments and soils in a fertilized catchment, New South Wales, Australia, Geochimica et cosmochimica acta, 63, 287-305, 1999.

Martin, J. H.: Glacial-interglacial CO2 change: the iron hypothesis, Paleoceanography, 5, 1-11, 1990.

Martin, J. H., Gordon, R. M., and Fitzwater, S. E.: Iron in Antarctic waters, Nature, 345, 156-158, 1990.

Martin, J. H., Gordon, R. M., and Fitzwater, S. E.: The Case for Iron, Limnology and Oceanography, 36, 1793-1802, 1991.

Martínez-Garcia, A., Rosell-Melé, A., Geibert, W., Gersonde, R., Masqué, P., Gaspari, V., and Barbante, C.: Links between iron supply, marine productivity, sea surface temperature, and CO2 over the last 1.1 Ma, Paleoceanography, 24, PA1207, 10.1029/2008pa001657, 2009.

Martínez-García, A., Sigman, D. M., Ren, H., Anderson, R. F., Straub, M., Hodell, D. A., Jaccard, S. L., Eglinton, T. I., and Haug, G. H.: Iron Fertilization of the Subantarctic Ocean During the Last Ice Age, Science, 343, 1347-1350, 10.1126/science.1246848, 2014.

Marx, S. K., Kamber, B. S., and McGowan, H. A.: Estimates of Australian dust flux into New Zealand: Quantifying the eastern Australian dust plume pathway using trace element calibrated< sup> 210</sup> Pb as a monitor, Earth and Planetary Science Letters, 239, 336-351, 2005.

McConnell, J. R., Lamorey, G. W., and Hutterli, M. A.: A 250-year high-resolution record of Pb flux and crustal enrichment in central Greenland, Geophysical Research Letters, 29, 45-41-45-44, 2002.

McGillicuddy, D., Sedwick, P., Dinniman, M., Arrigo, K., Bibby, T., Greenan, B., Hofmann, E., Klinck, J., Smith, W., and Mack, S.: Iron supply and demand in an Antarctic shelf ecosystem, Geophysical Research Letters, 2015.

McGowan, H., and Clark, A.: Identification of dust transport pathways from Lake Eyre, Australia using Hysplit, Atmospheric Environment, 42, 6915-6925, 2008.

McGowan, H. A., Kamber, B., McTainsh, G. H., and Marx, S. K.: High resolution provenancing of long travelled dust deposited on the Southern Alps, New Zealand, Geomorphology, 69, 208-221, 2005.

McLaren, P.: An interpretation of trends in grain size measures, JOURNAL OF SEDIMENTARY RESEARCH, 51, 611-624, 10.1306/212f7cf2-2b24-11d7-8648000102c1865d, 1981.

McTainsh, G.: Quaternary aeolian dust processes and sediments in the Australian region, Quaternary Science Reviews, 8, 235-253, 1989.

McTainsh, G., and Leys, J.: Soil erosion by wind, Land Degradation Processes in Australia, 188-233, 1993.

McTainsh, G., and Lynch, A.: Quantitative estimates of the effect of climate change on dust storm activity in Australia during the Last Glacial Maximum, Geomorphology, 17, 263-271, 1996.

McTainsh, G., Leys, J., and Tews, E.: Wind erosion trends for the National State of the Environment Report: Data and Methods, Australia State of the Environment 2006, 2006.

Meskhidze, N., Chameides, W., Nenes, A., and Chen, G.: Iron mobilization in mineral dust: Can anthropogenic SO2 emissions affect ocean productivity?, Geophysical Research Letters, 30, 2003.

Meskhidze, N., and Nenes, A.: Phytoplankton and cloudiness in the Southern Ocean, Science, 314, 1419-1423, 2006.

Meyer, C. P., Luhar, A. K., and Mitchell, R. M.: Biomass burning emissions over northern Australia constrained by aerosol measurements: I—Modelling the distribution of hourly emissions, Atmospheric Environment, 42, 1629-1646, http://dx.doi.org/10.1016/j.atmosenv.2007.10.089, 2008.

Mills, M. M., Ridame, C., Davey, M., La Roche, J., and Geider, R. J.: Iron and phosphorus co-limit nitrogen fixation in the eastern tropical North Atlantic, Nature, 429, 292-294, 2004.

Mitchell, B. G., Brody, E. A., Holm-Hansen, O., McClain, C., and Bishop, J.: Light Limitation of Phytoplankton Biomass and Macronutrient Utilization in the Southern Ocean, Limnology and Oceanography, 36, 1662-1677, 1991.

Moore, J. K., Abbott, M. R., Richman, J. G., and Nelson, D. M.: The southern ocean at the Last Glacial Maximum: A strong sink for atmospheric carbon dioxide, Global Biogeochem. Cycles, 14, 455-475, 10.1029/1999gb900051, 2000.

Moore, J. K., Lindsay, K., Doney, S. C., Long, M. C., and Misumi, K.: Marine ecosystem dynamics and biogeochemical cycling in the Community Earth System Model [CESM1 (BGC)]: Comparison of the 1990s with the 2090s under the RCP4. 5 and RCP8. 5 scenarios, Journal of Climate, 26, 9291-9312, 2013.

Morton, P. L., Landing, W. M., Hsu, S.-C., Milne, A., Aguilar-Islas, A. M., Baker, A. R., Bowie, A. R., Buck, C. S., Gao, Y., and Gichuki, S.: Methods for the sampling and analysis of marine aerosols: results from the 2008 GEOTRACES aerosol intercalibration experiment, Limnology and Oceanography: Methods, 11, 62-78, 2013.

Moteki, N., and Kondo, Y.: Effects of mixing state on black carbon measurements by laser-induced incandescence, Aerosol Science and Technology, 41, 398-417, 2007.

Mouillot, F., and Field, C. B.: Fire history and the global carbon budget: a 1× 1 fire history reconstruction for the 20th century, Global Change Biology, 11, 398-420, 2005.

Narcisi, B., Petit, J.-R., Delmonte, B., Basile-Doelsch, I., and Maggi, V.: Characteristics and sources of tephra layers in the EPICA-Dome C ice record (East Antarctica): implications for past atmospheric circulation and ice core stratigraphic correlations, Earth and Planetary Science Letters, 239, 253-265, 2005.

Neff, P. D., and Bertler, N. A.: Trajectory modeling of modern dust transport to the Southern Ocean and Antarctica, Journal of Geophysical Research: Atmospheres, 120, 9303-9322, 2015a.

Neff, P. D., and Bertler, N. A.: Trajectory modeling of modern dust transport to the Southern Ocean and Antarctica, Journal of Geophysical Research: Atmospheres, 2015b.

Nicol, S., Bowie, A., Jarman, S., Lannuzel, D., Meiners, K. M., and Van Der Merwe, P.: Southern Ocean iron fertilization by baleen whales and Antarctic krill, Fish and Fisheries, 11, 203-209, 2010.

Nodwell, L. M., and Price, N. M.: Direct Use of Inorganic Colloidal Iron by Marine Mixotrophic Phytoplankton, Limnology and Oceanography, 46, 765-777, 2001.

Novakov, T.: Soot in the atmosphere, in: Particulate Carbon, Springer, 19-41, 1982.

Oshima, N., Koike, M., Zhang, Y., and Kondo, Y.: Aging of black carbon in outflow from anthropogenic sources using a mixing state resolved model: 2. Aerosol optical properties and cloud condensation nuclei activities, Journal of Geophysical Research: Atmospheres (1984–2012), 114, 2009.

Paerl, H. W., Crocker, K. M., and Prufert, L. E.: Limitation of N2 fixation in coastal marine waters: Relative importance of molybdenum, iron, phosphorus, and organic matter availability1, Limnology and Oceanography, 32, 525-536, 1987.

Paerl, H. W., Prufert-Bebout, L. E., and Guo, C.: Iron-stimulated N2 fixation and growth in natural and cultured populations of the planktonic marine cyanobacteria Trichodesmium spp, Applied and Environmental Microbiology, 60, 1044-1047, 1994.

Palmer, T. Y.: Large fire winds, gases and smoke, Atmospheric Environment (1967), 15, 2079-2090, 1981.

Paris, R., Desboeufs, K., Formenti, P., Nava, S., and Chou, C.: Chemical characterisation of iron in dust and biomass burning aerosols during AMMA-SOP0/DABEX: implication for iron solubility, Atmospheric Chemistry and Physics, 10, 4273-4282, 2010.

Paris, R., Desboeufs, K., and Journet, E.: Variability of dust iron solubility in atmospheric waters: Investigation of the role of oxalate organic complexation, Atmospheric Environment, 45, 6510-6517, 2011.

Paris, R., and Desboeufs, K.: Effect of atmospheric organic complexation on iron-bearing dust solubility, Atmospheric Chemistry and Physics, 13, 4895-4905, 2013.

Pereira, E., Setzer, A., Gerab, F., Artaxo, P., Pereira, M., and Monroe, G.: Airborne measurements of aerosols from burning biomass in Brazil related to the TRACE A experiment, Journal of Geophysical Research: Atmospheres (1984–2012), 101, 23983-23992, 1996.

Petit, J.-R., Briat, M., and Royer, A.: Ice age aerosol content from East Antarctic ice core samples and past wind strength, Nature, 293, 391-394, 1981.

Petit, J. R., Jouzel, J., Raynaud, D., Barkov, N. I., Barnola, J. M., Basile, I., Bender, M., Chappellaz, J., Davis, M., Delaygue, G., Delmotte, M., Kotlyakov, V. M., Legrand, M., Lipenkov, V. Y., Lorius, C., Pepin, L., Ritz, C., Saltzman, E., and Stievenard, M.: Climate and atmospheric history of the past 420,000 years from the Vostok ice core, Antarctica, Nature, 399, 429-436, 10.1038/20859, 1999.

Petters, M. D., Prenni, A. J., Kreidenweis, S. M., DeMott, P. J., Matsunaga, A., Lim, Y. B., and Ziemann, P. J.: Chemical aging and the hydrophobic-to-hydrophilic conversion of carbonaceous aerosol, Geophysical research letters, 33, 2006.

Pitman, A., Narisma, G., and McAneney, J.: The impact of climate change on the risk of forest and grassland fires in Australia, Climatic Change, 84, 383-401, 2007.

Planquette, H., Statham, P. J., Fones, G. R., Charette, M. A., Moore, C. M., Salter, I., Nedelec, F. H., Taylor, S. L., French, M., and Baker, A. R.: Dissolved iron in the vicinity of the Crozet Islands, Southern Ocean, Deep Sea Research Part II: Topical Studies in Oceanography, 54, 1999-2019, 2007.

Porstendorfer, J., Butterweck, G., and Reineking, A.: Daily variation of the radon concentration indoors and outdoors and the influence of meteorological parameters, Health physics, 67, 283-287, 1994.

Pósfai, M., Simonics, R., Li, J., Hobbs, P. V., and Buseck, P. R.: Individual aerosol particles from biomass burning in southern Africa: 1. Compositions and size distributions of carbonaceous particles, Journal of Geophysical Research: Atmospheres (1984–2012), 108, 2003.

Prospero, J. M., Ginoux, P., Torres, O., Nicholson, S. E., and Gill, T. E.: Environmental characterization of global sources of atmospheric soil dust identified with the Nimbus 7 Total Ozone Mapping Spectrometer (TOMS) absorbing aerosol product, Reviews of geophysics, 40, 2-1-2-31, 2002.

Pye, K.: Aeolian dust and dust deposits, Academic Press, Harcourt Brace Jovanovich, Publishers, 1989.

Radke, L. F., Hegg, D. A., Hobbs, P. V., Nance, J. D., Lyons, J. H., Laursen, K. K., Weiss, R. E., Riggan, P. J., and Ward, D. E.: Particulate and trace gas emissions from large biomass fires in North America, Global biomass burning: Atmospheric, climatic, and biospheric implications, 209-224, 1991.

Raiswell, R., Benning, L. G., Davidson, L., and Tranter, M.: Nanoparticulate bioavailable iron minerals in icebergs and glaciers, Mineral Mag, 72, 345-348, 10.1180/minmag.2008.072.1.345, 2008a.

Raiswell, R., Benning, L. G., Tranter, M., and Tulaczyk, S.: Bioavailable iron in the Southern Ocean: the significance of the iceberg conveyor belt, Geochemical Transactions, 9, 7, doi:10.1186/1467-4866-9-7, 2008b.

Ramanathan, V., and Carmichael, G.: Global and regional climate changes due to black carbon, Nature geoscience, 1, 221-227, 2008.

Reid, J., Koppmann, R., Eck, T., and Eleuterio, D.: A review of biomass burning emissions part II: intensive physical properties of biomass burning particles, Atmospheric Chemistry and Physics, 5, 799-825, 2005.

Reid, J. S., and Hobbs, P. V.: Physical and optical properties of young smoke from individual biomass fires in Brazil, Journal of Geophysical Research: Atmospheres (1984–2012), 103, 32013-32030, 1998.

Reid, J. S., Eck, T. F., Christopher, S. A., Hobbs, P. V., and Holben, B.: Use of the Angstrom exponent to estimate the variability of optical and physical properties of aging smoke particles in Brazil, Journal of Geophysical Research, 104, 27,473-427,489, 1999.

Resing, J. A., Sedwick, P. N., German, C. R., Jenkins, W. J., Moffett, J. W., Sohst, B. M., and Tagliabue, A.: Basin-scale transport of hydrothermal dissolved metals across the South Pacific Ocean, Nature, 523, 200-203, 10.1038/nature14577, 2015.

Revel-Rolland, M., De Deckker, P., Delmonte, B., Hesse, P. P., Magee, J. W., Basile-Doelsch, I., Grousset, F., and Bosch, D.: Eastern Australia: A possible source of dust in East Antarctica interglacial ice, Earth and Planetary Science Letters, 249, 1-13, 2006.

Reynolds, R. L., Cattle, S. R., Moskowitz, B. M., Goldstein, H. L., Yauk, K., Flagg, C. B., Berquó, T. S., Kokaly, R. F., Morman, S., and Breit, G. N.: Iron oxide minerals in dust of the Red Dawn event in eastern Australia, September 2009, Aeolian Research, 2014.

Rhodes, R. H., Bertler, N. A. N., Baker, J. A., Sneed, S. B., Oerter, H., and Arrigo, K. R.: Sea ice variability and primary productivity in the Ross Sea, Antarctica, from methylsulphonate snow record, Geophys. Res. Lett., 36, L10704, 10.1029/2009gl037311, 2009.

Rhodes, R. H., Baker, J. A., Millet, M.-A., and Bertler, N. A. N.: Experimental investigation of the effects of mineral dust on the reproducibility and accuracy of ice core trace element analysis, Chemical Geology, 286, 207-221, 2011.

Rich, H. W., and Morel, F. M. M.: Availability of Well-Defined Iron Colloids to the Marine Diatom Thalassiosira weissflogii, Limnology and Oceanography, 35, 652-662, 1990.

Riemer, N., Vogel, H., and Vogel, B.: Soot aging time scales in polluted regions during day and night, Atmospheric Chemistry and Physics, 4, 1885-1893, 2004.

Riemer, N., West, M., Zaveri, R., and Easter, R.: Estimating black carbon aging time-scales with a particle-resolved aerosol model, Journal of Aerosol Science, 41, 143-158, 2010.

Robinson, R. S., Brzezinski, M. A., Beucher, C. P., Horn, M. G., and Bedsole, P.: The changing roles of iron and vertical mixing in regulating nitrogen and silicon cycling in the Southern Ocean over the last glacial cycle, Paleoceanography, 2014.

Rubin, M., Berman-Frank, I., and Shaked, Y.: Dust-and mineral-iron utilization by the marine dinitrogen-fixer Trichodesmium, Nature Geoscience, 4, 529-534, 2011.

Ruellan, S., Cachier, H., Gaudichet, A., Masclet, P., and Lacaux, J. P.: Airborne aerosols over central Africa during the Experiment for Regional Sources and Sinks of Oxidants (EXPRESSO), Journal of Geophysical Research: Atmospheres (1984–2012), 104, 30673-30690, 1999.

Rueter, J. G.: IRON STIMULATION OF PHOTOSYNTHESIS AND NITROGEN FIXATION IN ANABAENA 7120 AND TRICHODESMIUM (CYANOPHYCEAE) 1, Journal of Phycology, 24, 249-254, 1988.

Rueter, J. G., Hutchins, D. A., Smith, R. W., and Unsworth, N. L.: Iron nutrition of Trichodesmium, in: Marine pelagic cyanobacteria: Trichodesmium and other Diazotrophs, Springer, 289-306, 1992.

Running, S. W.: Is global warming causing more, larger wildfires?, SCIENCE-NEW YORK THEN WASHINGTON-, 313, 927, 2006.

Ruth, U.: Concentration and size distribution of microparticles in the NGRIP Ice Core during the Last Glacial period, Dissertation, University Bremen, 2002.

Sato, M., Takeda, S., and Furuya, K.: Iron regeneration and organic iron(III)-binding ligand production during in situ zooplankton grazing experiment, Marine Chemistry, 106, 471-488, 2007.

Schroth, A. W., Crusius, J., Sholkovitz, E. R., and Bostick, B. C.: Iron solubility driven by speciation in dust sources to the ocean, Nature Geosci, 2, 337-340, http://www.nature.com/ngeo/journal/v2/n5/suppinfo/ngeo501_S1.html, 2009.

Schuck, I.: Mineralogical characterisation and geographic provenance of atmospheric particles in coastal Antarctic ice cores – indicators of past climatic variability, Diploma thesis, Universitat Karlsruhe, Karlsruhe, Germany, 2009.

Schulz, M., Prospero, J. M., Baker, A. R., Dentener, F., Ickes, L., Liss, P. S., Mahowald, N. M., Nickovic, S., García-Pando, C. P. r., and Rodríguez, S.: Atmospheric transport and deposition of mineral dust to the ocean: implications for research needs, Environmental science & technology, 46, 10390-10404, 2012.

Schüssler, U., Bröcker, M., Henjes-Kunst, F., and Will, T.: P–T–t evolution of the Wilson Terrane metamorphic basement at Oates Coast, Antarctica, Precambrian Research, 93, 235-258, http://dx.doi.org/10.1016/S0301-9268(98)00091-6, 1999.

Schwertmann, U.: Solubility and dissolution of iron oxides, in: Iron nutrition and interactions in plants, Springer, 3-27, 1991.

Sedwick, P. N., and DiTullio, G. R.: Regulation of algal blooms in Antarctic Shelf Waters by the release of iron from melting sea ice, Geophys. Res. Lett., 24, 2515-2518, 10.1029/97gl02596, 1997.

Sedwick, P. N., DiTullio, G. R., and Mackey, D. J.: Iron and manganese in the Ross Sea, Antarctica: Seasonal iron limitation in Antarctic shelf waters, J. Geophys. Res., 105, 11321-11336, 10.1029/2000jc000256, 2000.

Sedwick, P. N., Sholkovitz, E. R., and Church, T. M.: Impact of anthropogenic combustion emissions on the fractional solubility of aerosol iron: Evidence from the Sargasso Sea, Geochem. Geophys. Geosyst., 8, Q10Q06, 10.1029/2007gc001586, 2007.

Sedwick, P. N., Marsay, C. M., Sohst, B. M., Aguilar-Islas, A. M., Lohan, M. C., Long, M. C., Arrigo, K. R., Dunbar, R. B., Saito, M. A., Smith, W. O., and DiTullio, G. R.: Early season depletion of dissolved iron in the Ross Sea polynya: Implications for iron dynamics on the Antarctic continental shelf, J. Geophys. Res., 116, C12019, 10.1029/2010jc006553, 2011.

Seiler, W., and Crutzen, P. J.: Estimates of gross and net fluxes of carbon between the biosphere and the atmosphere from biomass burning, Climatic change, 2, 207-247, 1980.

Selby, M., Rains, J., and Palmer, R.: Eolian deposits of the ice free Victoria Valley, Southern Victoria Land, Antarctica, New Zealand Journal of Geology and Geophysics, 17, 543-562, 1974.

Shao, Y., and Leslie, L. M.: Wind erosion prediction over the Australian continent, JOURNAL OF GEOPHYSICAL RESEARCH-ALL SERIES-, 102, 30,091-030,105, 1997.

Shi, Z., Krom, M. D., Bonneville, S., and Benning, L. G.: Atmospheric Processing Outside Clouds Increases Soluble Iron in Mineral Dust, Environmental Science & Technology, 49, 1472-1477, 10.1021/es504623x, 2015.

Shiraiwa, M., Kondo, Y., Moteki, N., Takegawa, N., Miyazaki, Y., and Blake, D.: Evolution of mixing state of black carbon in polluted air from Tokyo, Geophysical Research Letters, 34, 2007.

Sholkovitz, E. R., Sedwick, P. N., and Church, T. M.: Influence of anthropogenic combustion emissions on the deposition of soluble aerosol iron to the ocean: Empirical estimates for island sites in the North Atlantic, Geochimica et Cosmochimica Acta, 73, 3981-4003, 2009.

Sholkovitz, E. R., Sedwick, P. N., Church, T. M., Baker, A. R., and Powell, C. F.: Fractional solubility of aerosol iron: Synthesis of a global-scale data set, Geochimica et cosmochimica acta, 89, 173-189, 2012.

Siefert, R. L., Johansen, A. M., and Hoffmann, M. R.: Chemical characterization of ambient aerosol collected during the southwest monsoon and intermonsoon seasons over the Arabian Sea: Labile-Fe(II) and other trace metals, J. Geophys. Res., 104, 3511-3526, 10.1029/1998jd100067, 1999.

Sinclair, K. E., Bertler, N. A. N., and Trompetter, W. J.: Synoptic controls on precipitation pathways and snow delivery to high-accumulation ice core sites in the Ross Sea region, Antarctica, J. Geophys. Res., 115, D22112, 10.1029/2010jd014383, 2010.

Slinn, S., and Slinn, W.: Predictions for particle deposition on natural waters, Atmospheric Environment (1967), 14, 1013-1016, 1980.

Smetacek, V., Assmy, P., and Henjes, J.: The role of grazing in structuring Southern Ocean pelagic ecosystems and biogeochemical cycles, Antarctic Science, 16, 541-558, 2004.

Smetacek, V., Klaas, C., Strass, V. H., Assmy, P., Montresor, M., Cisewski, B., Savoye, N., Webb, A., d'Ovidio, F., Arrieta, J. M., Bathmann, U., Bellerby, R., Berg, G. M., Croot, P., Gonzalez, S., Henjes, J., Herndl, G. J., Hoffmann, L. J., Leach, H., Losch, M., Mills, M. M., Neill, C., Peeken, I., Rottgers, R., Sachs, O., Sauter, E., Schmidt, M. M., Schwarz, J., Terbruggen, A., and Wolf-Gladrow, D.: Deep carbon export from a Southern Ocean iron-fertilized diatom bloom, Nature, 487, 313-319, http://www.nature.com/nature/journal/v487/n7407/abs/nature11229.html#supplementary-information, 2012.

Smith, W., and Nelson, D.: Importance of Ice Edge Phytoplankton Production in the Southern Ocean, BioScience, 36, 251-257, 1986.

Smith, W. O., and Gordon, L. I.: Hyperproductivity of the Ross Sea (Antarctica) polynya during austral spring, Geophys. Res. Lett., 24, 233-236, 10.1029/96gl03926, 1997.

Spokes, L. J., Jickells, T. D., and Lim, B.: Solubilisation of aerosol trace metals by cloud processing: A laboratory study, Geochimica et Cosmochimica Acta, 58, 3281-3287, 1994.

Spokes, L. J., and Jickells, T. D.: Factors controlling the solubility of aerosol trace metals in the atmosphere and on mixing into seawater, Aquatic Geochemistry, 1, 355-374, 10.1007/bf00702739, 1995.

Spolaor, A., Vallelonga, P., Gabrieli, J., Cozzi, G., Boutron, C., and Barbante, C.: Determination of Fe2+ and Fe3+ species by FIA-CRC-ICP-MS in Antarctic ice samples, Journal of Analytical Atomic Spectrometry, 27, 310-317, 2012.

Steffensen, J. P.: The size distribution of microparticles from selected segments of the Greenland Ice Core Project ice core representing different climatic periods, J. Geophys. Res., 102, 26755-26763, 10.1029/97jc01490, 1997.

Stephens, M., Turner, N., and Sandberg, J.: Particle identification by laser-induced incandescence in a solid-state laser cavity, Applied optics, 42, 3726-3736, 2003.

Sterle, K. M., McConnell, J. R., Dozier, J., Edwards, R., and Flanner, M.: Retention and radiative forcing of black carbon in eastern Sierra Nevada snow, The Cryosphere, 7, 365-374, 2013.

Tagliabue, A., and Arrigo, K. R.: Iron in the Ross Sea: 1. Impact on CO2 fluxes via variation in phytoplankton functional group and non-Redfield stoichiometry, J. Geophys. Res., 110, C03009, 10.1029/2004jc002531, 2005.

Tagliabue, A., and Arrigo, K. R.: Processes governing the supply of iron to phytoplankton in stratified seas, J. Geophys. Res., 111, C06019, 10.1029/2005jc003363, 2006.

Tagliabue, A., Bopp, L., Dutay, J.-C., Bowie, A. R., Chever, F., Jean-Baptiste, P., Bucciarelli, E., Lannuzel, D., Remenyi, T., Sarthou, G., Aumont, O., Gehlen, M., and Jeandel, C.: Hydrothermal contribution to the oceanic dissolved iron inventory, Nature Geosci, 3, 252-256, http://www.nature.com/ngeo/journal/v3/n4/suppinfo/ngeo818_S1.html, 2010.

Tagliabue, A., Sallee, J.-B., Bowie, A. R., Levy, M., Swart, S., and Boyd, P. W.: Surface-water iron supplies in the Southern Ocean sustained by deep winter mixing, Nature Geosci, 7, 314-320, 10.1038/ngeo2101

http://www.nature.com/ngeo/journal/v7/n4/abs/ngeo2101.html#supplementary-information, 2014.

Talarico, F., Borsi, L., and Lombardo, B.: Relict granulites in the Ross Orogen of northern Victoria Land (Antarctica), II. Geochemistry and palaeo-tectonic implications, Precambrian Research, 75, 157-174, 1995.

Textor, C., Schulz, M., Guibert, S., Kinne, S., Balkanski, Y., Bauer, S., Berntsen, T., Berglen, T., Boucher, O., and Chin, M.: Analysis and quantification of the diversities of aerosol life cycles within AeroCom, Atmospheric Chemistry and Physics, 6, 1777-1813, 2006.

Trapp, J. M., Millero, F. J., and Prospero, J. M.: Trends in the solubility of iron in dust-dominated aerosols in the equatorial Atlantic trade winds: Importance of iron speciation and sources, Geochem. Geophys. Geosyst., 11, Q03014, 10.1029/2009gc002651, 2010.

Tuohy, A., Bertler, N., Neff, P., Edwards, R., Emanuelsson, D., Beers, T., and Mayewski, P.: Transport and deposition of heavy metals in the Ross Sea Region, Antarctica, Journal of Geophysical Research: Atmospheres, 120, doi:110.1002/2015JD023293, 10.1002/2015JD023293, 2015.

Turn, S., Jenkins, B., Chow, J., Pritchett, L., Campbell, D., Cahill, T., and Whalen, S.: Elemental characterization of particulate matter emitted from biomass burning: Wind tunnel derived source profiles for herbaceous and wood fuels, Journal of Geophysical Research: Atmospheres (1984–2012), 102, 3683-3699, 1997.

Turns, S. R.: An introduction to combustion, McGraw-hill New York, 1996.

Uglietti, C., Gabrielli, P., Olesik, J. W., Lutton, A., and Thompson, L. G.: Large variability of trace element mass fractions determined by ICP-SFMS in ice core samples from worldwide high altitude glaciers, Applied Geochemistry, 47, 109-121, 2014.

Vallelonga, P., Gabrielli, P., Rosman, K. J. R., Barbante, C., and Boutron, C. F.: A 220 kyr record of Pb isotopes at Dome C Antarctica from analyses of the EPICA ice core, Geophys. Res. Lett., 32, L01706, 10.1029/2004gl021449, 2005.

Vallelonga, P., Gabrielli, P., Balliana, E., Wegner, A., Delmonte, B., Turetta, C., Burton, G., Vanhaecke, F., Rosman, K. J. R., Hong, S., Boutron, C. F., Cescon, P., and Barbante, C.: Lead isotopic compositions in the EPICA Dome C ice core and Southern Hemisphere Potential Source Areas, Quaternary Science Reviews, 29, 247-255, 2010.

Vallelonga, P., Barbante, C., Cozzi, G., Gabrieli, J., Schüpbach, S., Spolaor, A., and Turetta, C.: Iron fluxes to Talos Dome, Antarctica, over the past 200 kyr, Climate of the Past, 9, 597-604, 2013.

van der Werf, G. R., Randerson, J. T., Giglio, L., Collatz, G. J., Kasibhatla, P. S., and Arellano Jr, A. F.: Interannual variability in global biomass burning emissions from 1997 to 2004, Atmospheric Chemistry and Physics, 6, 3423-3441, 2006.

Wagener, T., Guieu, C., Losno, R., Bonnet, S., and Mahowald, N.: Revisiting atmospheric dust export to the Southern Hemisphere ocean: Biogeochemical implications, Global Biogeochem. Cycles, 22, GB2006, 10.1029/2007gb002984, 2008.

Walker, P., and Costin, A.: Atmospheric dust accession in South-Eastern Australia, Soil Research, 9, 1-5, 1971.

Walsh, J. J., and Steidinger, K. A.: Saharan dust and Florida red tides: the cyanophyte connection, Journal of Geophysical Research: Oceans (1978–2012), 106, 11597-11612, 2001.

Ward, D.: Factors influencing the emissions of gases and particulate matter from biomass burning, in: Fire in the Tropical Biota, Springer, 418-436, 1990.

Ward, D., Susott, R., Kauffman, J., Babbitt, R., Cummings, D., Dias, B., Holben, B., Kaufman, Y., Rasmussen, R., and Setzer, A.: Smoke and fire characteristics for cerrado and deforestation burns in Brazil: BASE-B experiment, Journal of Geophysical Research: Atmospheres (1984–2012), 97, 14601-14619, 1992.

Ward, D. E., Setzer, A. W., Kaufman, Y. J., and Rasmussen, R. A.: Characteristics of smoke emissions from biomass fires of the Amazon region-BASE-A experiment, Global Biomass Burning: Atmospheric, Climatic, and Biospheric Implications, 394-402, 1991.

Warneck, P.: In-cloud chemistry opens pathway to the formation of oxalic acid in the marine atmosphere, Atmospheric Environment, 37, 2423-2427, 2003.

Wasserburg, G., Jacousen, S., DePaolo, D., McCulloch, M., and Wen, T.: Precise determination of SmNd ratios, Sm and Nd isotopic abundances in standard solutions, Geochimica et Cosmochimica Acta, 45, 2311-2323, 1981.

Weller, R., Wöltjen, J., Piel, C., Resenberg, R., Wagenbach, D., KÖNIG-LANGLO, G., and Kriews, M.: Seasonal variability of crustal and marine trace elements in the aerosol at Neumayer station, Antarctica, Tellus B, 60, 742-752, 2008.

Wells, M., Zorkin, N., and Lewis, A.: The role of colloidal chemistry in providing a source of iron to phytoplankton, J Mar Res, 41, 731 - 746, 1983.

Windom, H. L.: Atmospheric Dust Records in Permanent Snowfields: Implications to Marine Sedimentation, Geological Society of America Bulletin, 80, 761-782, 10.1130/0016-7606(1969)80[761:adrips]2.0.co;2, 1969.

Winton, V. H. L., Dunbar, G. B., Bertler, N. A. N., Millet, M. A., Delmonte, B., Atkins, C. B., Chewings, J. M., and Andersson, P.: The contribution of aeolian sand and dust to iron fertilization of phytoplankton blooms in southwestern Ross Sea, Antarctica, Global Biogeochemical Cycles, 28, 2013GB004574, 10.1002/2013GB004574, 2014.

Winton, V. H. L., Bowie, A. R., Edwards, R., Keywood, M., Townsend, A. T., van der Merwe, P., and Bollhöfer, A.: Fractional iron solubility of atmospheric iron inputs to the Southern Ocean, Marine Chemistry, 177, Part 1, 20-32, http://dx.doi.org/10.1016/j.marchem.2015.06.006, 2015.

Wu, J., Boyle, E., Sunda, W., and Wen, L.-S.: Soluble and Colloidal Iron in the Oligotrophic North Atlantic and North Pacific, Science, 293, 847-849, 10.1126/science.1059251, 2001.

Wu, J., Rember, R., and Cahill, C.: Dissolution of aerosol iron in the surface waters of the North Pacific and North Atlantic oceans as determined by a semicontinuous flow-through reactor method, Global Biogeochem. Cycles, 21, GB4010, 10.1029/2006gb002851, 2007.

Wuttig, K., Wagener, T., Bressac, M., Dammshäuser, A., Streu, P., Guieu, C., and Croot, P.: Impacts of dust deposition on dissolved trace metal concentrations (Mn, Al and Fe) during a mesocosm experiment, Biogeosciences (BG), 10, 2583-2600, 2013.

Yamada, Y., Fukuda, H., Inoue, K., Kogure, K., and Nagata, T.: Effects of attached bacteria on organic aggregate settling velocity in seawater, Aquatic microbial ecology, 70, 261-272, 2013.

Yamasoe, M. A., Artaxo, P., Miguel, A. H., and Allen, A. G.: Chemical composition of aerosol particles from direct emissions of vegetation fires in the Amazon Basin: water-soluble species and trace elements, Atmospheric Environment, 34, 1641-1653, 2000.

Zahorowski, W., Chambers, S., and Henderson-Sellers, A.: Ground based radon-222 observations and their application to atmospheric studies, Journal of environmental radioactivity, 76, 3-33, 2004.

Zhang, R., Khalizov, A. F., Pagels, J., Zhang, D., Xue, H., and McMurry, P. H.: Variability in morphology, hygroscopicity, and optical properties of soot aerosols during atmospheric processing, Proceedings of the National Academy of Sciences, 105, 10291-10296, 2008.

Zhu, X., Prospero, J. M., Millero, F. J., Savoie, D. L., and Brass, G. W.: The solubility of ferric ion in marine mineral aerosol solutions at ambient relative humidities, Marine Chemistry, 38, 91-107, 1992.

Zhu, X., Prospero, J. M., Savoie, D. L., Millero, F. J., Zika, R. G., and Saltzman, E. S.: Photoreduction of Iron(III) in Marine Mineral Aerosol Solutions, J. Geophys. Res., 98, 9039-9046, 10.1029/93jd00202, 1993.

Zhuang, G., Duce, R. A., and Kester, D. R.: The Dissolution of Atmospheric Iron in Surface Seawater of the Open Ocean, J. Geophys. Res., 95, 16207-16216, 10.1029/JC095iC09p16207, 1990.

Zhuang, G., Yi, Z., Duce, R. A., and Brown, P. R.: Chemistry of iron in marine aerosols, Global Biogeochem. Cycles, 6, 161-173, 10.1029/92gb00756, 1992.

Zuberi, B., Johnson, K. S., Aleks, G. K., Molina, L. T., Molina, M. J., and Laskin, A.: Hydrophilic properties of aged soot, Geophysical research letters, 32, 2005.

Zuo, Y., and Zhan, J.: Effects of oxalate on Fe-catalyzed photooxidation of dissolved sulfur dioxide in atmospheric water, Atmospheric Environment, 39, 27-37, 2005.

Supplementary Information

S6.1 Methods

S6.1.1 Snow sampling at Roosevelt Island

Surface snow samples were collected from the southern summit of Roosevelt Island, Eastern Ross Sea, (Fig. 6.1) in November 2012 during the 2012/13 Roosevelt Island Climate Evolution (RICE) ice core drilling campaign. To prevent contamination by camp activities and skidoos, snow samples were collected from a designated snow sampling site located ~1 km from the RICE ice core drilling camp. Surface snow was collected 30 cm deep into the snow pack in 1000 mL pre-acid washed low-density polypropylene (LDPE) Nalgene wide mouth bottles. A total of three exposure blanks and 24 snow samples were collected from a designated grid (79.36645-79.36629 °S, 161.70053-161.6994 °W) to ensure collection of a sufficient amount of dust for Sr and Nd isotopic analysis.

Adjacent to the surface snow samples, snow was also sampled from a 1.5 m snow pit (samples RI1-51) using pre-washed centrifuge tubes. Sampling, at 3 cm resolution, was performed following ultra-clean protocols. Four parallel profiles were sampled for trace metal, stable isotope analysis, black carbon and Coulter Counter dust concentration and particle size analysis. Two exposure blanks (following the same method as the samples by opening the bottle at the field site but not filling the sample bottle with snow) were also collected for each type of sample. Snow density and temperature was measured every 5 cm (Fig. S6.2), and a visual log of snow pit stratigraphy were recorded. All samples were stored frozen in a snow trench kept below -20 ºC at Roosevelt Island.

S6.1.2 Dust concentration and particle size

Dust samples were transported frozen to the University of Milano-Bicocca, Italy where dust concentration and particle size were analysed using Beckman Coulter Multisizer 3 (MS3), following the method of *Delmonte et al.* [2002]. Three consecutive counts were performed, each on a volume of 0.5 mL, and the average value has been considered here. The instrument was set to measure particles in 300 individual size bins and having equivalent spherical diameter from 1 µm to 30 µm. Dust mass was calculated from the measured volume

assuming a particle density of 2.5 g cm^{-3}. Exposure blank concentrations average around 2 ng g^{-1} of dust (n=6).

The dust concentration and snow accumulation rates [*Conway et al.*, 1999] were used to calculate dust fluxes in the 1-5 µm and 1-30 µm (bulk) size bins. Particles >10 µm were detected by Coulter Counter measurements. For this reason, selected samples were filtered onto black polycarbonate membranes and particle micromorphology was observed using a BX51M reflected light optical microscope. Additionally, Scanning Electron Microscopy (SEM; Zeiss Neon 40EsB FIBSEM) methods with secondary (SE) and backscatter (BSD) electron detectors and a SiLi energy dispersive X-ray system (EDS) with Oxford Inca software were used to give a qualitative indication of the geochemistry of the particles. The conditions used (kV, spot size, WD and detector) are indicated in SEM images in Fig. S6.1. Filters were platinum-coated prior to SEM examination. These qualitative observations confirmed presence of large dust particles in the samples (Fig. S6.1). Two anomalous high particle concentrations were found in the 1-5 µm range (samples RI 38, 49-51 with dust concentrations of 52, 104, 413 ng g^{-1} respectively). These two sections were treated as outliers and excluded from the dust profile (Fig. 6.2g) because of possible contamination of the surface layers (samples RI49-51 were sampled 0-9 cm from the surface).

S6.1.3 Nd and Sr isotopic ratios and concentrations

S6.1.3.1 Sample processing

The minimum dust mass required for Sr and Nd isotopic composition analyses corresponds to about 100 µg of total dust [*Delmonte et al.*, 2008]. Therefore, 24 Roosevelt Island surface snow samples (1000 mL) were combined and filtered onto two separate 0.4 µm Nuclepore polycarbonate track-etched membranes (samples RI1-2). The filters were sonicated for 3 minutes with 5 mL of Milli-Q (MQ) water (resistivity of 18.2 MΩ-cm) in an acid-cleaned 15 mL Savillex beakers. The filter was removed, and liquid evaporated on a hotplate at 110 °C. The very tiny dry dust samples were then weighed a minimum of five times.

S6.1.3.2 Sample digestion

The chemical treatment of the samples including mineral dust digestion and an elemental separation (Rb-Sr and Sm-Nd) using ion exchange chromatography was performed at the

Swedish Museum of Natural History. Here, a line dedicated to the treatment of small dust samples (1-10 ng of Nd and 5-100 ng of Sr in dust for Antarctic ice core samples) was developed and described in *Delmonte et al.* [2008]. Briefly, the samples were spiked with mixed a $^{147}Sm/^{150}Nd$ spike and ^{84}Sr enriched spike for isotope dilution determination of the concentration and subsequently digested in a strong acid mixture.

S6.1.3.3 Ion exchange

To achieve separation of potential interfering elements (Fe, Ba, Rb, Sm, Ce, and Pr), and obtain high column yield and low blanks, the residue was subjected to chemical procedures described in *Delmonte et al.* [2008]. The total blank, including dissolution, chemical separation and mass spectrometry, was frequently monitored in each ion exchange batch, and blank concentrations were <5 pg for Nd and <130 pg for Sr.

S6.1.3.4 Mass spectrometry

Isotopic analysis of Nd and Sr ratios was performed with a Thermo Scientific TRITON Thermal Ionization Mass Spectrometer (TIMS). Neodymium was loaded mixed with colloidal graphite, Alfa Aesar, on double rhenium filaments and analysed as metal ions in static mode using rotating gain compensation. Concentrations and ratios were calculated assuming exponential fractionation. The calculated ratios were normalized to $^{146}Nd/^{144}Nd = 0.7219$. Epsilon units are calculated as follows:

$$\varepsilon Nd(0) = [(143_{Nd}/144_{Nd})_{sample}/(143_{Nd}/144_{Nd})_{CHUR} - 1]\, x\, 104;$$

CHUR, chondritic uniform reservoir with $(^{143}Nd/^{144}Nd)_{CHUR} = 0.512638$

The external precision of 43 ppm for $^{143}Nd/^{144}Nd$ was estimated by analysing a range (4-12 ng) of Ndß standard loads. The external precision becomes larger for smaller loads, with an estimated precision of about 40 ppm for small loads, for intermediate size about 30 ppm and about 20 ppm for larger loads. These values have been used to estimate the errors for the samples in Table 6.1. An accuracy correction was not applied since the mean $^{143}Nd/^{144}Nd$ ratio was 0.511895 ± 22 (n=20). Purified Sr samples were mixed with tantalum activator and loaded on a single rhenium filament. Two hundred 8 s integrations were recorded in multi-collector static mode, applying rotating gain compensation. Measured ^{87}Sr intensities were

corrected for Rb interference assuming $^{87}Rb/^{85}Rb = 0.38600$ and ratios were calculated using the exponential fractionation law and $^{88}Sr/^{86}Sr = 8.375209$.

We use the standard reference material (SRM) NBS 987 (pure Sr-carbonate) to determine the external precision of our $^{87}Sr/^{86}Sr$ measurements. Modern sea water is a complex natural chemical matrix with a constant $^{87}Sr/^{86}Sr$ value, which makes it an excellent natural standard for tracking long term laboratory reproducibility in this type of matrix. By analyzing several CIT#39 sea water during the course of the project the reproducibility for $^{87}Sr/^{86}Sr$ in natural samples can be estimated. External precision for $^{87}Sr/^{86}Sr$ estimated from analyzing NBS SRM 987 gave a mean ratio of 0.710217 with a reproducibility of 0.000016 or 22 ppm (2 SD, n=12). Repeated measurements of prepared CIT #39 sea water gave a mean ratio of 0.709138 with a reproducibility of 0.0000082 or 12 ppm (2 SD, n=21), which was taken to be the best estimate of the external precision. An accuracy correction was applied to the $^{87}Sr/^{86}Sr$ ratios corresponding to a $^{87}Sr/^{86}Sr$ ratio of 0.710245 for NBS SRM 987 standard (NBS 987: literature value 0.710245, Department of Geosciences value 0.710217±0.000016; difference: 0.000028).

The accuracy of the Nd and Sr isotopic composition of small dust samples was determined using the Basalt Columbia River (BCR-2) certified reference material [*Jochum et al.*, 2005]. Preparation and analysis of 150 to 600 µg aliquots of BCR-2 in each batch of ion exchange resulted in an accuracy of >79 % (n=6) for concentration and >99 % (n=6) for isotopic composition. Due to the small dust samples and the difficulty of weighing such small masses we estimate a Sr and Nd concentration error of ±10 % estimated by repeated weighing of BCR-2 standards (~0.3 mg).

S6.1.4 Stable isotope analysis

Melted water stable isotope samples were measured for stable $\delta^{18}O$ and δD isotopes using high resolution laser absorption spectroscopy (Los Gatos Research Liquid-Water Isotope Analyser) at the Stable Isotope Laboratory, GNS Science, New Zealand. The $\delta^{18}O$ and δD results are reported with respect to Vienna Mean Standard Ocean Water (VSMOW2) and normalized to two internal standards: SM1 with reported values of -29.12 ‰ for $\delta 1^{8}O$, -227.4 ‰ for δD, and INS11 with reported values of -0.36 ‰ for $\delta^{18}O$, -3.8 ‰ for δD. The analytical precision of this instrument is <0.2 ‰ for $\delta^{18}O$ and 1.0 ‰ for δD.

S6.1.5 Trace metal sample preparation and ICP-MS analysis

All sample preparation and analysis was conducted in a trace metal clean laboratory (class 100 metal-free environment with HEPA-filtered air) at Curtin University following ultra-clean methodology. Nitric and hydrochloric acid used throughout the study was high purity (<10 pg g^{-1} Fe), double distilled in-house from Seastar® Instrument Quality (IQ) grade acids (Choice Analytical Pty Ltd, Australia) using an all polytetrafluoroethylene (PFA) acid purification system (DST-1000, Savillex®). These acids are herein, described as ultra-pure acid. Ultra-pure water (resistivity of 18.2 MΩ-cm, Purelab Classic, ELGA, Germany) was used throughout. All bottles, syringes, filters and laboratory wear were rigorously acid washed following the procedure: one week 20 % IQ grade HNO_3, one week 10% ultra-pure HCl, one week, 1 % ultra-pure HCl, one week 1 % ultra-pure HNO_3, one week ultra-pure water and rinsed with copious qualities of ultra-pure water between acid baths.

Immediately after melting (within minutes), 10 mL of each snow sample was filtered through 0.2 µm acid-cleaned PDVF syringe filters and acidified to 1 % with ultra-pure HCl, to stabilize the dissolved trace metal fraction. High-resolution inductively coupled plasma mass spectrometry (HR-ICPMS, Element XR ThermoFisher) analysis of the dissolved samples was performed within an hour of acidification. Remaining unfiltered samples were acidified to 1 % with ultra-pure HCl and left to sit for six months [*Edwards and Sedwick*, 2001; *Koffman et al.*, 2014a; *Rhodes et al.*, 2011; *Uglietti et al.*, 2014] at room temperature for total dissolvable metal analysis following the method for TDFe in Antarctic sea ice and snow samples of Lannuzel et al. (2008). Dissolved trace metals are operationally defined as the trace metal passing through a 0.2 µm filter. Total dissolvable trace metals are the unfiltered bulk fraction acidified to 1 % ultra-pure HCl for six months [*Cutter et al.*, 2010].

Both the dissolved leachates and total dissolvable sample solutions were analysed by HR-ICP-MS. Measured isotopes and the spectral resolutions, along with typical operating conditions, are reported in Table S6.1. An auto sampler was used to introduce the sample to the HR-ICP-MS. The HR-ICP-MS was operated with a jet interface using jet cones, and an Apex desolvation unit (Elemental Scientific Inc, ESI) pumped with a Seafast II system syringe pumps (ESI). During the course of the sample sequence, standards were regularly measured as quality control (QC) samples. Instrumental blank solutions were also regularly measured during the course of the sample sequence determined by carrying out identical analytical procedures as the leachates (Table S6.2), but vials were filled with ultra-pure water

rather than the snow melt. Two exposure blanks and five procedural blanks were also measured following the same method above. Blank concentrations and detection limits are reported in Table S6.2. Reported concentrations for samples are corrected for exposure blank concentrations. The sample introduction line was rinsed with 3 % ultra-pure HCl between samples for 1.5 minutes.

Standard solutions were prepared by serial dilution from 100 µg mL^{-1} stock solutions using ultra clean water, with a final HCl concentration of 1 %. Preparation of standards in 1 % HCl matrix matched the leachates. Ten-point multiple calibration solutions were measured. Indium, at a concentration of 1.5 ppb, was used as an internal standard.

S6.1.6 Refractory black carbon analysis

Black carbon samples were analysed for refractory black carbon (rBC) using a single particle intracavity laser-induced incandescence photometer (SP2, Droplet Measurement Technologies, Boulder, Colorado) following a similar method to *Sterle et al.* [2013]. Briefly, snow pit samples were melted and immediately analysed by a SP2 connected to an ultrasonic nebulizer (USN; CETAC UT5000) by conductive rubber tubing and an over-supplied open-split (stainless steel tee). The USN conditions were: nebuliser gas (ultra-pure air) flow rate = 400 sccm, sample flow rate = 1 mL min^{-1}, heater temp = 120 °C and chiller temp = 3 °C. Other studies have found size selective mass transport through the USN with the transport efficiency of rBC decreasing for rBC particles with mobility equivalent diameters (MED) >500 nm. We confirmed the decreased mass transport for MED > 500 nm. However, because of the remoteness of the study site we do not expect a significant proportion of the rBC particles to have MED >500 nm. We have also confirmed this assumption by studying single rBC particles in Antarctic snow meltwater by transmission electron microscopy. The SP2 instrument single rBC response was calibrated using Aquadag graphite particles size separated using a differential mobility analyser (DMA). For the calibration we used an Aquadag effective density from *Gysel et al.* [2011]. Recent studies have found that the single particle emissivity of Aquadag graphite is greater than that of biomass burning soot [*Laborde et al.*, 2012]. To correct for the emissivity difference between Aquadag and biomass burning soot we used a correction factor of 1.5 [*R. Subramanium*, unpublished data, 2015]. External rBC concentration calibrations were performed using colloidal rBC standards prepared gravimetrically from Eb6 100% carbon pigment (Inksupply, EB-6-K) and fullerene soot (Sigma Aldrich, #572497), both standards gave comparable linear calibration curves.

Table S6.1:HR-ICP-MS instrument conditions.

Instrument	HR-ICPMS, Element XR (Thermo Fisher, Germany)
Torch	Precision type, quartz o-ring free, PFA injector (Element Scientific Inc.)
Spray chamber	APEX with quartz spray chamber (ESI)
Nebuliser	ST micro centric PFA (ESI)
RF power (W)	~1350
Cool gas flow (L min^{-1})	~16
Auxiliary gas flow (L min^{-1})	~0.7
Sample gas flow (L min^{-1})	~0.7
Additional gas (L min^{-1})	~0.2 N_2
Additional gas (L min^{-1})	~~0.4 Ar
Guard electrode	Activated
Sample uptake	90 s (Seafast II pump auto-sampler with fast 3 sample injection valve)
Sample rinse	30 s, 3 % HCl
Scan type	E-scan
Elements measured in medium resolution ($m/\Delta m$ ~4000)	Al, S, Fe

Table S6.2: Average exposure (n=2), procedure (n=5) and instrumental (n=5) blank concentrations and detection limits of measured elements. Concentrations were determined by ten-point calibration standards. DL: detection limit, SD: standard deviation, EB: exposure blank, PB: procedural blank, IB: instrumental blank.

	Dissolved							Total dissolvable						
	EB conc.	**SD**	**PB conc.**	**SD**	**IB conc.**	**SD**	**DL (3σ)**	**EB conc.**	**SD**	**PB conc.**	**SD**	**IB conc.**	**SD.**	**DL (3σ)**
Al (pg g^{-1})	6.5	2.8	6.0	1.1	7.8	4.4	1.1	67	45	72	15	20	14	12
S (ng g^{-1})	4.5	0.3	6.5	0.7	7.2	1.1	2.5	<DL		<DL		0.7	1.6	4.7
Fe (pg g^{-1})	1.4	0.6	1.5	1.0	0.6	0.4	0.57	19	6.0	39	39	6.6	1.9	5.7

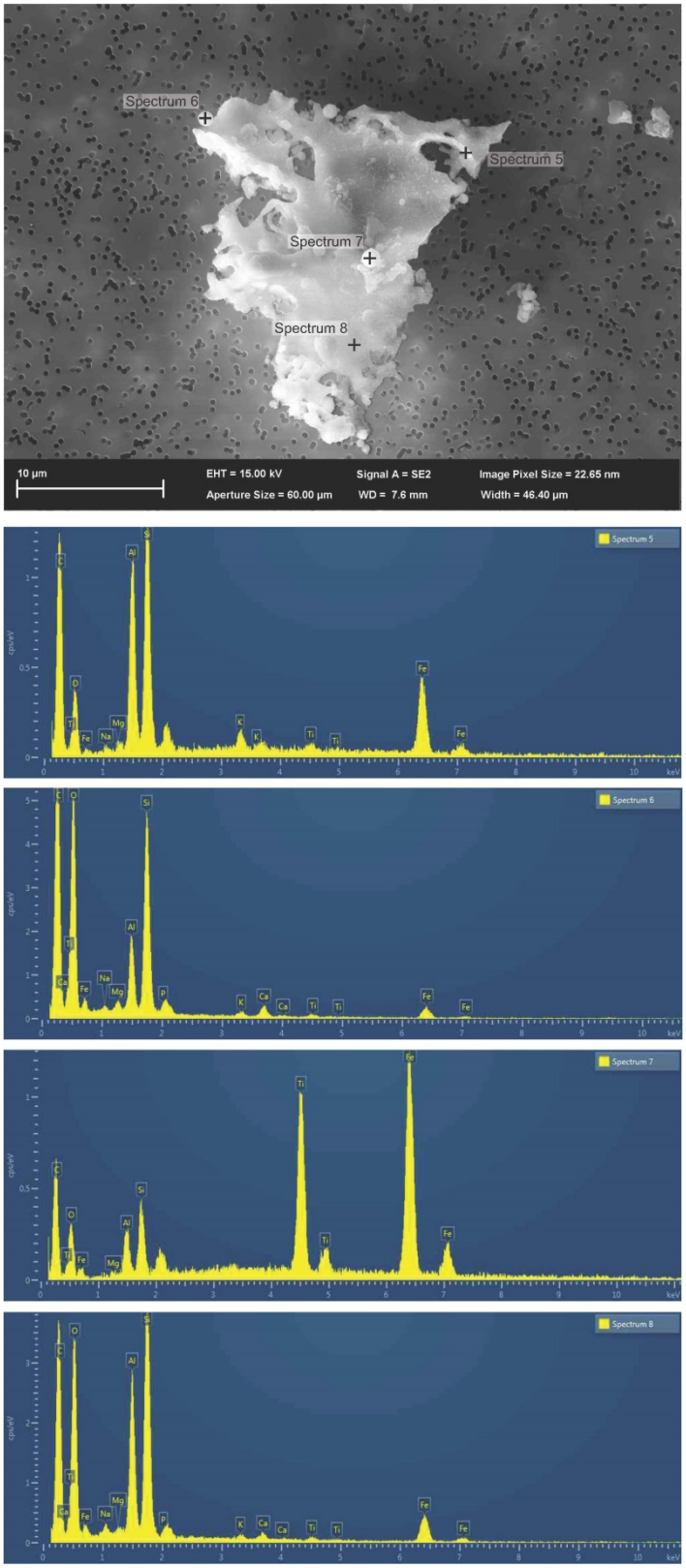

Fig. S6.1: Scanning electron microscope image of coarse particles in a snow pit from Roosevelt Island (RI24).

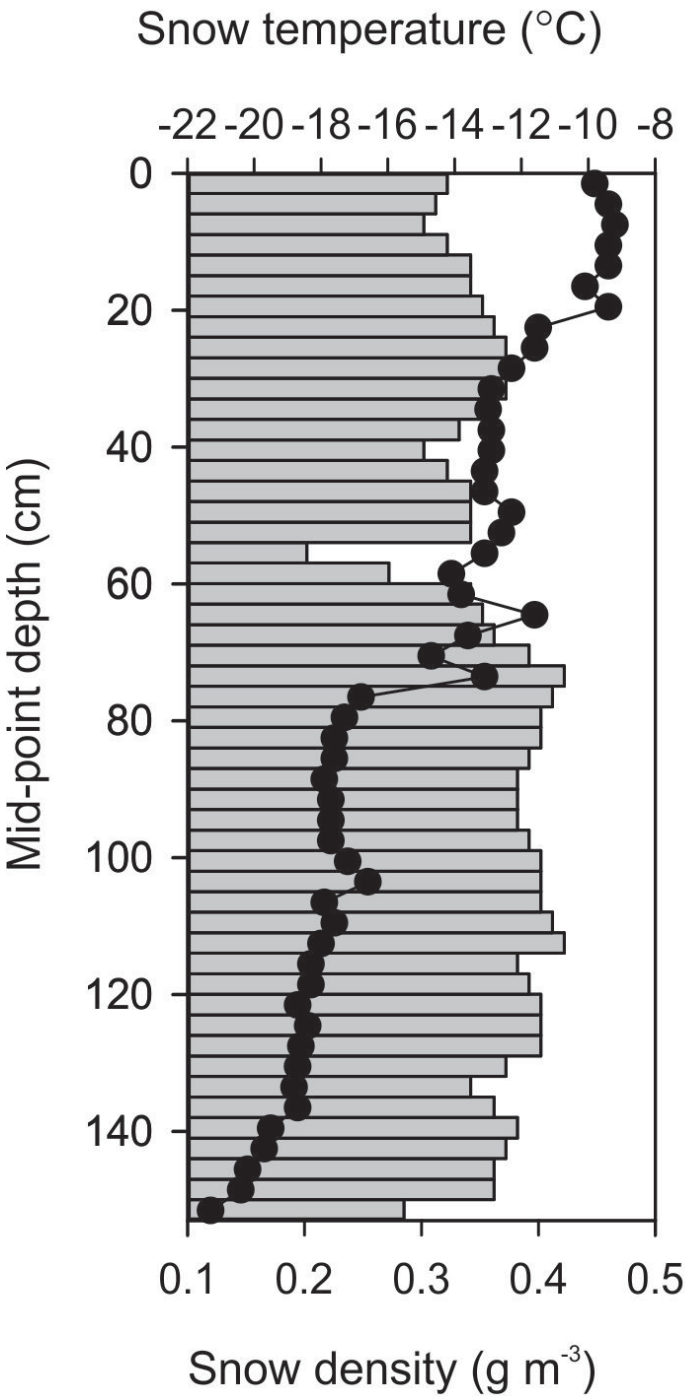

Fig. S6.2: Roosevelt Island 2012/2013 1.5 m snow pit temperature and snow density profile.

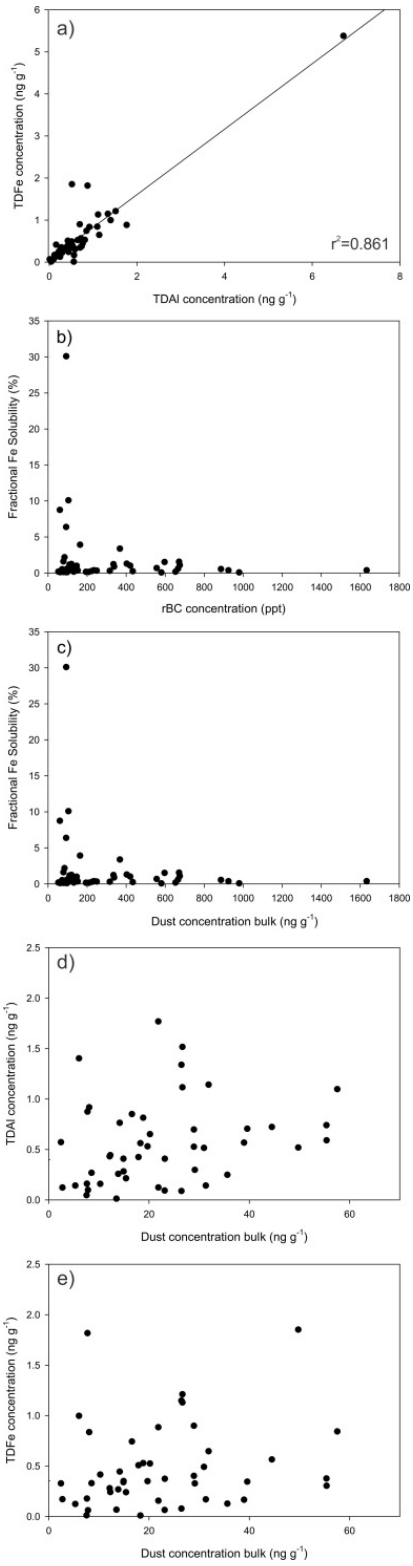

Fig. S6.3: Relationships between variables in the snow pit. a) Correlation between TDAl concentrations and TDFe concentrations, b) inverse hyperbolic relationship between fractional Fe solubility and rBC concentrations, c) inverse hyperbolic relationship between fractional Fe solubility and dust concentrations, d) scatterplots of dust concentrations and TDAl concentrations, e) scatterplots of dust concentrations and TDFe concentrations.

References

Conway, H., B. L. Hall, G. H. Denton, A. M. Gades, and E. D. Waddington (1999), Past and Future Grounding-Line Retreat of the West Antarctic Ice Sheet, *Science*, *286*(5438), 280-283.

Cutter, G., P. Andersson, L. Codispoti, P. Croot, R. Francois, M. Lohan, H. Obata, and M. Rutgers vd Loeff (2010), Sampling and sample-handling protocols for GEOTRACES Cruises.

Delmonte, B., J. R. Petit, and V. Maggi (2002), Glacial to Holocene implications of the new 27000-year dust record from the EPICA Dome C (East Antarctica) ice core, *Climate Dynamics*, *18*(8), 647-660.

Delmonte, B., P. S. Andersson, M. Hansson, H. Schöberg, J. R. Petit, I. Basile-Doelsch, and V. Maggi (2008), Aeolian dust in East Antarctica (EPICA-Dome C and Vostok): Provenance during glacial ages over the last 800 kyr, *Geophys. Res. Lett.*, *35*(7), L07703.

Edwards, R., and P. Sedwick (2001), Iron in East Antarctic snow: Implications for atmospheric iron deposition and algal production in Antarctic waters, *Geophys. Res. Lett.*, *28*(20), 3907-3910.

Gysel, M., M. Laborde, J. Olfert, R. Subramanian, and A. Gröhn (2011), Effective density of Aquadag and fullerene soot black carbon reference materials used for SP2 calibration, *Atmospheric Measurement Techniques*, *4*(12), 2851-2858.

Jochum, K. P., U. Nohl, K. Herwig, E. Lammel, B. Stoll, and A. W. Hofmann (2005), GeoReM: A New Geochemical Database for Reference Materials and Isotopic Standards, *Geostandards and Geoanalytical Research*, *29*(3), 333-338.

Koffman, B. G., M. J. Handley, E. C. Osterberg, M. L. Wells, and K. J. Kreutz (2014), Dependence of ice-core relative trace-element concentration on acidification, *Journal of Glaciology*, *60*(219), 103-112.

Laborde, M., P. Mertes, P. Zieger, J. Dommen, U. Baltensperger, and M. Gysel (2012), Sensitivity of the Single Particle Soot Photometer to different black carbon types, *Atmospheric Measurement Techniques*, *5*(5), 1031-1043.

Rhodes, R. H., J. A. Baker, M.-A. Millet, and N. A. N. Bertler (2011), Experimental investigation of the effects of mineral dust on the reproducibility and accuracy of ice core trace element analysis, *Chemical Geology*, *286*(3), 207-221.

Sterle, K. M., J. R. McConnell, J. Dozier, R. Edwards, and M. Flanner (2013), Retention and radiative forcing of black carbon in eastern Sierra Nevada snow, *The Cryosphere*, *7*(1), 365-374.

Uglietti, C., P. Gabrielli, J. W. Olesik, A. Lutton, and L. G. Thompson (2014), Large variability of trace element mass fractions determined by ICP-SFMS in ice core samples from worldwide high altitude glaciers, *Applied Geochemistry*, *47*, 109-121.

Chapter 7. The origin of lithogenic sediment in the southwestern Ross Sea and implications for iron fertilisation

This chapter is published in *Antarctic Science*. The data has been published in the *Curtin University Research Data Repository*. Co-author contributions can be found in Appendix A4.

V.H.L. Winton, G.B. Dunbar, C.B. Atkins, N.A.N. Bertler, B. Delmonte, P. S. Andersson, A. Bowie, R. Edwards, 2016. The origin of lithogenic sediment in the south western Ross Sea and implications for iron fertilization. *Antarctic Science*, available on CJO2016. doi:10.1017/S095410201600002X.

V.H.L Winton, G.B. Dunbar, C. Atkins, N.A.N. Bertler, B. Delmonte, P. Andersson, A. Bowie, and R. Edwards, 2015. McMurdo Sound dust Sr and Nd isotopic data, *Curtin University Research Data*, http://doi.org/10.4225/06/5643EBA1C8473.

Abstract

Austral summer iron (Fe) fertilisation in the Ross Sea has previously been observed in association with diatom productivity, lithogenic particles and excess Fe in the water column [*Collier et al.*, 2000]. This productivity event occurred during an early break out of sea ice via katabatic winds, suggesting that aeolian dust could be an important source of lithogenic Fe required for diatom growth in the Ross Sea. Here we investigate the provenance of size-selected dust deposited on sea ice in McMurdo Sound, southwestern (SW) Ross Sea. The isotopic signature of McMurdo Sound dust ($0.70533 < {}^{87}Sr/{}^{86}Sr < 0.70915$ and $-1.1 < \varepsilon_{Nd}(0) < 3.45$) confirms that dust is locally sourced from the McMurdo Sound debris bands and comprises a two-component mixture of McMurdo Volcanic Group and Southern Victoria Land lithologies. In addition, we investigate the provenance of lithogenic sediment trapped in the water column: the isotopic signature ($\varepsilon_{Nd}(0)=3.9$, ${}^{87}Sr/{}^{86}Sr=0.70434$) is differentiated from long-range transport dust originating from South America and Australia. Elevated lithogenic accumulation rates in deeper sediment traps in the Ross Sea, suggest that sinking particles in the water column cannot simply result from dust input at the surface. This discrepancy can

best be explained by significant upwelling and remobilisation of lithogenic Fe from the sea floor.

7.1 Introduction

Atmospheric dust is potentially an important source of dissolved iron (DFe) which is the limiting nutrient required for primary production in vast regions of the remote Southern Ocean, including Antarctica's marginal seas [*Boyd et al.*, 2010; *Sedwick et al.*, 2000]. Despite being seasonally iron (Fe) limited, the high-nutrient, high chlorophyll (HNHC) regime of the Ross Sea is the most biologically productive continental shelf region in Antarctica, and supports intense phytoplankton blooms in the austral summer [*Arrigo et al.*, 2008b]. Although the flux of Fe into the Ross Sea plays a critical role in determining its productivity, the origin(s) of this Fe remains poorly constrained [*Sedwick et al.*, 2011].

7.1.1 Dust deposition in Antarctica

Global 'background' dust is characterized by fine particles having a mass modal diameter <5 μm, long atmospheric residence time and modern mass deposition rates in the order of 0.001-0.02 g m^{-2} yr^{-1} in the Southern Ocean [*Wagener et al.*, 2008; and references therein]. The isolated, snow and ice-covered central East Antarctic Plateau (EAP) has proven to be an excellent location for investigating long-range transport of dust representative of the broader Southern Hemisphere, both at present and in the past [*Delmonte et al.*, 2007; *Delmonte et al.*, 2008]. Moreover, the high East Antarctic Plateau (EAP) has much lower accumulation rates of around 0.0002-0.0006 g m^{-2} yr^{-1} during the Holocene [*Albani et al.*, 2012b]. Recently, it has become apparent that peripheral areas of the Antarctic ice sheet, close to high-elevation ice-free mountain ranges, such as the Transantarctic Mountains (TAM), can receive significant additional dust inputs from exposed Antarctic sources, some of which have been ice-free for millions of years [*Delmonte et al.*, 2013 and references therein].

The relative contribution of much smaller, patchy but proximal dust sources to the atmospheric dust load over Antarctica and the Southern Ocean is not well known. The largest expanse of contiguous ice-free ground in Antarctica is found in the McMurdo Dry Valleys - a series of west-to-east-oriented, glacially carved valleys located between the high EAP and the Ross Sea in Southern Victoria Land. However, the dustiest known place in Antarctica is located in the southwestern (SW) Ross Sea, associated with the so-called 'debris bands' area on the McMurdo Ice Shelf [*Kellogg et al.*, 1990] (Fig. 7.1). In this region, dust deposition flux (~1 g m^{-2} yr^{-1}) is at least two orders of magnitude greater than fallout of long-range

transport dust measured in ice cores from the EAP [*Atkins and Dunbar*, 2009; *Chewings et al.*, 2014; *Delmonte et al.*, 2013] and is, potentially, an important source of bioavailable Fe to the Ross Sea [*Winton et al.*, 2014].

Dust provenance in Antarctica can be determined from the $^{87}Sr/^{86}Sr$ and $^{143}Nd/^{144}Nd$ radiogenic isotope composition of dust in snow and ice by comparison with potential source areas (PSAs) [e.g. *Delmonte et al.*, 2010b]. This geochemical method allows mantle-derived (basaltic rocks, tephra and soils derived from them, weathered and eroded mafic rocks) and crustal-derived sediments and soils to be identified. Both the geochemical fingerprint and particle size of dust deposited on the EAP suggests it originates from arid regions in southern South America during glacial periods [*Delmonte et al.*, 2008; *Gaiero et al.*, 2007]. However, for dust deposited during interglacial periods, that is when dust input to inner Antarctica was extremely low, the source is less certain [*Delmonte et al.*, 2007], and an Australian contribution is likely [*Delmonte et al.*, 2007; *Delmonte et al.*, 2008; *Revel-Rolland et al.*, 2006]. In addition to atmospheric circulation, dust transport efficiency is dependent on particle size; for example, long-range dust deposited on the EAP has a mass-modal size of ~2-3 μm [*Delmonte et al.*, 2002]. When investigating the provenance of dust, the fractionation of Sr isotopes into different grain size fractions needs to be considered, as there is a correlation between grain size and $^{87}Rb/^{86}Sr$ ratios and thus $^{87}Sr/^{86}Sr$ ratios. In coarse (fine) grained suspended particulate matter Sr is enriched (depleted) in less radiogenic Sr isotopic ratios [e.g. *Andersson et al.*, 1994]. In contrast, Nd isotopic ratios are not influenced to the same extent by particle size [e.g. *Andersson et al.*, 1994].

7.1.2 Iron-fertilisation in the Ross Sea

The Ross Sea is one of the most productive regions in the Southern Ocean and an important oceanic sink for atmospheric carbon dioxide (CO_2) [e.g. *Arrigo et al.*, 2008b]. The environmental factors responsible for controlling the rates of phytoplankton production and incomplete utilisation of inorganic macronutrients include: grazing [*Banse*, 1991], temperature [*Bunt and Wood*, 1963], light availability [e.g. *Mitchell et al.*, 1991], micro-nutrient availability (e.g. Fe and Mn) [*Sedwick and DiTullio*, 1997; *Sedwick et al.*, 2000], or a combination of these [e.g. *Arrigo et al.*, 2000]. *Collier et al.* [2000] show that a Ross Sea diatom productivity event, captured during the 1996-1997 deployment of moored Antarctic Environment and Southern Ocean Process Study (AESOPS) sediment traps, is correlated with elevated lithogenic particle accumulation rates, excess Fe (determined from high Fe/Al

ratios), and with an early breakout of sea ice caused by katabatic winds. They go on to suggest that there may be a causal relationship between the retreat of sea ice, the supply of particulate Fe and diatom production and export. The source of this lithogenic Fe to the Ross Sea is unknown but could be derived from either dust released into the ocean from melting sea ice from local and/or from distal sources, or new particulate Fe derived from ice shelves, icebergs, upwelling of resuspended continental sediments from the sea floor, circumpolar deep water or some combination thereof.

Multiple sources of new Fe to the Ross Sea region have been identified, which include local dust sourced mainly from the McMurdo Ice Shelf [*Atkins and Dunbar*, 2009; *Chewings et al.*, 2014; *de Jong et al.*, 2013; *Winton et al.*, 2014], sea ice melt [*de Jong et al.*, 2013; *Sedwick and DiTullio*, 1997], and lithogenic sediments resuspended from the sea floor [*de Jong et al.*, 2013; *Gerringa et al.*, 2015; *Marsay et al.*, 2014; *Sedwick et al.*, 2011]. However, the relative importance of these sources for stimulating primary production remains an open question. *Winton et al.* [2014] estimate that the supply of soluble aeolian Fe in dust from the debris bands, southern McMurdo Sound to the adjacent ocean could support up to ~15 % of primary production in the area. The implication being that Fe supporting the remaining 85 % of productivity was derived largely from other sources, such as lithogenic sediment resuspended from the sea floor [*de Jong et al.*, 2013; *Gerringa et al.*, 2015; *Kustka et al.*, 2015; *Marsay et al.*, 2014; *McGillicuddy et al.*, 2015; *Sedwick et al.*, 2011].

As Fe is critical for seasonal phytoplankton growth in the Ross Sea, this study aims to further investigate the source(s) of lithogenic Fe as a driver of the vast austral summer phytoplankton blooms in the SW Ross Sea. We do this by examining the provenance of lithogenic material sinking in the upper 200 meters below sea level (mbsl) of the water column and compare its origin to both known local and global sources. Here we report the Sr-Nd isotopic composition of i) size-selected dust from snow samples on sea ice from McMurdo Sound, and ii) sediment trap material from the Research on Ocean - Atmosphere Variability and Ecosystem Response in the Ross Sea (ROAVERRS) moorings program (1996-98) that represents accumulation of sediment settling out of the water column. When investigating PSAs to Antarctica, previous studies have size-selected the PSA samples prior to Sr analysis to be comparable to that of the fine size range of dust deposited in Antarctica [*Delmonte et al.*, 2008], and a similar approach is used here.

7.2 Methods

7.2.1 Samples used in this study

Previous studies have focused on dust flux and particle size distribution patterns in McMurdo Sound [*Atkins and Dunbar*, 2009; *Chewings et al.*, 2014; *Dunbar et al.*, 2009]. This study is based on the following samples:

- Samples of dust-laden snow collected from sea ice along a south-north X-Y transect in McMurdo Sound, collected in November 2010 and described in [*Chewings et al.*, 2014] and in *Winton et al.* [2014] (Fig. 7.1b).

- A Ross Sea sediment trap sample from 200 mbsl, collected between 25 Dec. 1997 and 3 Jan. 1998 from the ROAVERRS program Chinstrap site (76° 20.5'S, 165° 1.78'E) in the SW Ross Sea. This site was anchored in 830 m water depth in the southern extension of the Drygalski Basin (Fig. 7.1a).

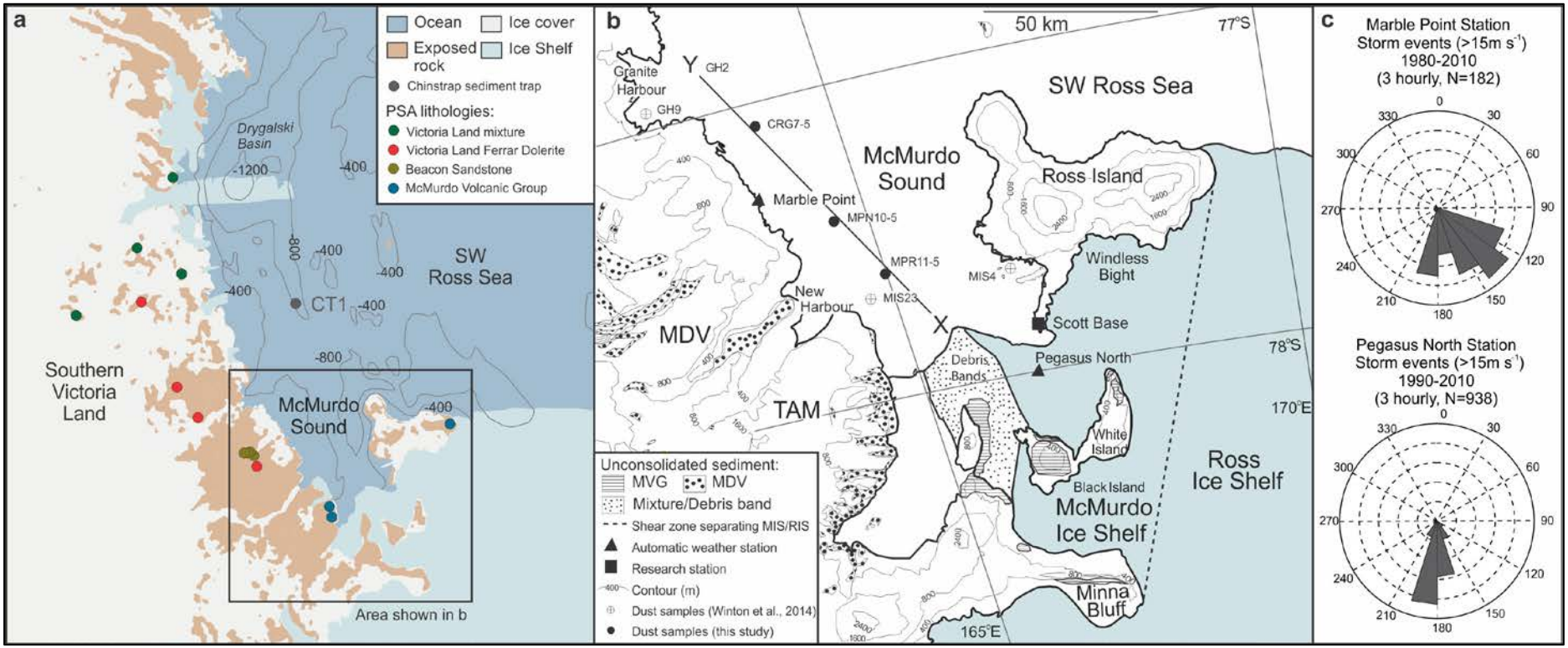

Fig. 7.1: a) Map of the SW Ross Sea showing the location of SW Ross Sea Chinstrap sediment trap (CT1). b) Insert of McMurdo Sound within the SW Ross Sea showing location of McMurdo Sound snow on sea ice samples (solid: this study, cross: *Winton et al.* [2014] and shaded: exposed areas of unconsolidated sediment. Samples are named based on their location i.e. MP: Marble Point; CR: Cape Robert; GH: Granite Harbour; MIS: McMurdo Sea Ice. EAIS: East Antarctic Ice Sheet, MDV: McMurdo Dry Valleys, TAM: Transantarctic Mountains. Transect X-Y shown in red. c) Wind roses illustrating the direction of storm events at Pegasus North and Marble Point automatic weather stations (AWS). Locations of AWS shown in Fig. 7.1c). Modified from *Winton et al.* [2014].

7.2.2 Nd and Sr isotopic ratios and concentrations

7.2.2.1 Sample processing

McMurdo Sound surface snow on sea ice samples

The samples analysed in this work were size-selected in order to be comparable to provenance measurements made on dust from ice core PSAs and with similar studies on dust in Antarctica [e.g. *Delmonte et al.*, 2008; *Delmonte et al.*, 2004b; *Delmonte et al.*, 2010b]. We analysed both the bulk (all particle sizes) and fine (<10 µm) fraction of McMurdo Sound dust to check for particle size induced bias in the isotopic fractionation of samples. The coarse fraction was removed from bulk samples by using a pre-washed 10 µm SEFAR Nitex® open mesh while the fraction 0.4µm<∅<10µm was collected on 0.4 µm Isopore™ polycarbonate membranes. After filtration, the membranes were put into pre-cleaned Corning® tubes filled with ~10 ml of ultra-pure water, and micro-particles were removed from the filter by sonication. Samples were transported to the Department of Geosciences, Swedish Museum of Natural History, Sweden where the liquid was evaporated in acid-cleaned 15 ml Savillex® beakers. Dry dust samples, ranging between 0.1 and 1.2 mg, were weighed a minimum of five times to obtain a mean weight, which was used for subsequent calculations.

Sediment trap samples

Isotopic analysis of bulk sediment revealed that the biogenic fraction of the sediment (~up to 70 % total mass estimated from AESOPS sediment trap data reported in *Collier et al.* [2000]) incorporated marine Sr and thus the isotopic signature could not be distinguished from that of seawater (Table 7.1). To remove the biogenic silica and calcium carbonate fraction of the sediment we leached the sediment with 6 M HCl in Savillex® beakers and centrifuged following the method of *Freydier et al.* [2001]. The lithogenic residue was then rinsed three times with ultra-pure water and dried.

Table 7.1: Nd and Sr concentrations and isotopic composition of McMurdo Sound and Chinstrap sediment trap samples analysed in this study.

Sample	Size (µm)	Location	Date sampled	$^{143}Nd/^{144}Nd$	a) $\pm 2\sigma_{mean}$ *10^6	b) $\varepsilon_{Nd}(0)$	c) $\pm 2\sigma$	C_{Nd} (ppm)	$^{87}Sr/^{86}Sr$	d) $\pm 2\sigma_{mean}$ *10^6	e) $^{87}Sr/^{86}Sr$ corrected	f) $\pm 2\sigma$ *10^6	C_{Sr} (ppm)	Reference
McMurdo Sound														
MPR11-5	Bulk	77° 35.44 S 164° 31.36 E	Nov 2011	0.512580	12	-1.1	0.2	110	0.708158	6.0	0.708186	8	140	g)
MPR11-5	<10	77° 35.44 S 164° 31.36 E	Nov 2011	0.512590	7	-0.94	0.2	220	0.709119	5.3	0.709147	8	320	g)
CRG7-5	Bulk	77° 05.44 S 163° 41.86 E	Nov 2011	0.512633	11	-0.10	0.3	38	0.707607	4.2	0.707635	8	510	g)
CRG7-5	<10	77° 05.44 S 163° 41.86 E	Nov 2011	0.512632	8	-0.12	0.3	68	0.708943	8.0	0.708971	8	570	g)
MPN10-5	Bulk	77° 24.52 S 164° 18.60 E	Nov 2011	0.512735	6	1.9	0.4	40	0.706705	13	0.706733	13	6600	g)
MPN10-5	<10	77° 24.52 S 164° 18.60 E	Nov 2011	0.512682	8	0.86	0.4	20	0.708188	6.4	0.708216	8	910	g)
GH2	Bulk	76° 55.33 S 163° 6.17 E	Nov 2009	0.512650	11	0.23	0.3	76	0.707299	12	0.707327	12	890	g)
GH2	<10	76° 55. 33 S 163° 6.17 E	Nov 2009	0.512654	6	0.31	0.3	72	0.708045	5.8	0.708073	8	620	g)
GH9	Bulk	76° 58.36 S 162° 52.80 E	Nov 2009	0.512321	5	-6.18	0.3	37	0.712260	5.0	0.712288	8	290	h)

MIS4	Bulk	77° 40.03 S 166° 35.97 E	Nov 2009	0.512815	4	3.45	0.3	56	0.705303	5.0	0.705331	8	800	h)
MIS23	Bulk	77° 40.03 S 164° 35.79 E	Nov 2009	0.51276	6	2.38	0.3	51	0.705608	5.0	0.705636	8	520	h)
Ross Sea Sediment														
CT1	Bulk	76° 20.5 S 165° 1.78 E	1997	0.512715	7	1.5	0.3	0.4	0.709008	5.1	0.709036	8	110	g)
CT1-leach	Bulk	76° 20.5 S 165° 1.78 E	1997	0.512836	8	3.9	0.3	0.5	0.704314	4.4	0.704342	8	20	g)

[a)]Internal precision, 2 standard errors of the mean.
[b)]Nd isotopic ratios expressed as epsilon units $\varepsilon_{Nd}(0) = [(^{143}Nd/^{144}Nd)_{sample}/(^{143}Nd/^{144}Nd)_{CHUR}-1]x10^4$; CHUR, chondritic uniform reservoir.
[c)]Uncertainty estimates based upon external precision for standard runs. Internal precision is used if it exceeds the external.
[d)]Internal precision, 2 standard errors of the mean.
[e)]Corrected to a NBS987 $^{87}Sr/^{86}Sr$ ratio of 0.710245.
[f)]Uncertainty estimates based upon external precision for standard runs. Internal precision is used if it exceeds the external.
[g)]This study.
[h)]Winton et al. (2014).

7.2.2.2 Sample digestion

The chemical treatment of the dust samples and leached sediment, including digestion and elemental separation (Rb-Sr and Sm-Nd) using ion exchange chromatography, was performed at the Swedish Museum of Natural History following the established method *Delmonte et al.* [2008]. The samples were spiked with a mixed $^{147}Sm/^{150}Nd$ spike and ^{84}Sr-enriched spike for the isotope dilution determination of the concentrations. Samples were digested in an acid mixture of 1.5 ml, of HNO_3, HF and $HClO_4$ heated to 90 ºC in closed Savillex® beakers for 24 h. The solution was evaporated to complete dryness on a hot plate, and the residue re-dissolved in 4 ml 6 M HCl.

7.2.2.3 Ion exchange

To achieve separation of potential interfering elements (Fe, Ba, Rb, Sm, Ce, and Pr), and obtain high column yield and low blanks, the residue was subjected to chemical procedures described in *Delmonte et al.* [2008]. The total blank, including dissolution, chemical separation and mass spectrometry, was frequently monitored in each ion exchange batch and blank concentrations were <5 pg for Nd and <130 pg for Sr.

7.2.2.4 Mass spectrometry

Isotopic analysis of Nd and Sr was performed with a Thermo Scientific TRITON Thermal Ionisation Mass Spectrometer (TIMS). Neodymium was loaded mixed with colloidal graphite, Alfa Aesar, on double rhenium filaments and analysed as metal ions in static mode using rotating gain compensation. Concentrations and ratios were calculated assuming exponential fractionation. The calculated ratios were normalised to $^{146}Nd/^{144}Nd = 0.7219$. Epsilon units are calculated as follows:

$$\varepsilon_{Nd}(0) = [(143_{Nd}/144_{Nd})_{sample}/(143_{Nd}/144_{Nd})_{CHUR} - 1]\, x\, 104;$$

CHUR, chondritic uniform reservoir with $(^{143}Nd/^{144}Nd)_{CHUR} = 0.512638$

The external precision for $^{143}Nd/^{144}Nd$ is estimated from analysis of the nNdß standard [*Wasserburg et al.*, 1981] by analysing a range, 4-12 ng loads, of nNdß standard. The external precision becomes larger for smaller loads, with an estimated precision of about 40 ppm for small loads, for intermediate size about 30 ppm and about 20 ppm for larger loads.

These values have been used to estimate the errors for the samples in Table 7.1. The mean $^{143}Nd/^{144}Nd$ ratio for the nNdß was 0.511895±22 (n=20). Literature values for repeated analysis of standard nNdβ [*Andreasen and Sharma*, 2006] yielded $^{143}Nd/^{144}Nd$ = 0.511892±3 (2σ, n = 23) and thus no accuracy correction was applied.

Purified Sr samples were mixed with tantalum activator and loaded on a single rhenium filament. Two hundred 8 s integrations were recorded in multi-collector static mode, applying a rotating gain compensation. Measured ^{87}Sr intensities were corrected for Rb interference assuming $^{87}Rb/^{85}Rb$=0.38600 and ratios were calculated using the exponential fractionation law and $^{88}Sr/^{86}Sr$=8.375209. External precision for $^{87}Sr/^{86}Sr$, estimated from analysing NBS SRM987 standard, was calculated as ±0.000016 (n=12) while repeated measurements of prepared CIT #39 sea water gave a reproducibility of ±0.0000082 or 12 ppm (n=21) which was taken to be the best estimate of the external precision. Accuracy correction was applied to the $^{87}Sr/^{86}Sr$ ratios corresponding to a $^{87}Sr/^{86}Sr$ ratio of 0.710245 for NBS SRM 987 standard (NBS 987: literature value 0.710245, Department of Geosciences value 0.710217 ±16 (n=12); difference: 0.000028).

The accuracy of the Nd and Sr isotopic composition of small dust samples was determined using the Basalt Columbia River rock standard (BCR-2), a certified reference material. Preparation and analysis of 150 to 600 µg aliquots of BCR-2 in each batch of ion exchange resulted in a recovery of >79 % (n=6) for concentration and >99 % (n=6) for isotopic composition. Due to the small dust samples and the difficulty of weighing such small masses we estimate a Sr and Nd concentration error of ±10 % estimated by repeated weighing of BCR-2 standards (~0.3 mg).

7.3 Results

The Sr and Nd isotopic composition of dust are primarily related to lithology and geologic age of parent materials, although the Sr isotopic composition, for particles between 2-50 µm can also be influenced by their size. The Sr and Nd isotopic composition of the fine (<10 µm) and bulk (all sizes included) dust samples collected in this study are well characterised and reported in Table 7.1 and Fig. 7.2 along with additional isotopic data from McMurdo Sound measured in an earlier study [*Winton et al.*, 2014]. Samples in Fig. 7.2 are grouped by geographic location. The samples collected from the snow on sea ice in McMurdo Sound

display a narrow isotopic composition ($0.70533 < {}^{87}Sr/{}^{86}Sr < 0.70915$ and $-1.1 < \varepsilon_{Nd}(0) < 3.45$). Our fine dust (<10 μm) samples have relatively higher $^{87}Sr/^{86}Sr$ ratios compared to the bulk samples (Fig. 7.2), consistent with previous studies of size-dependent fractionation [*Andersson et al.*, 1994]. The Nd isotopes do not fractionate with the particle size (with the exception of MPN10-5 which could be related to the different size fractions originating from different sources; Fig. 7.2), also consistent with previous studies. The $\Delta^{87}Sr/^{86}Sr$ is about 0.00115, that is slightly smaller than the $^{87}Sr/^{86}Sr$ increase of ~0.0028 units observed between 63 μm and 2 μm dust particles by *Gaiero et al.* [2007]. The isotopic ratios of leached (lithogenic sediment fraction) and unleached (lithogenic and biogenic sediment fraction) Ross Sea sediment obtained from the upper Chinstrap sediment trap (200 mbsl) are reported in Table 7.1. Leaching had a significant effect on the Sr isotopic ratio of this sample and removed a Sr seawater overprint from the sediment. After leaching, the remaining lithogenic sediment has an isotopic signature between the McMurdo Volcanic Group and Southern Victoria Land PSAs (Fig. 7.2).

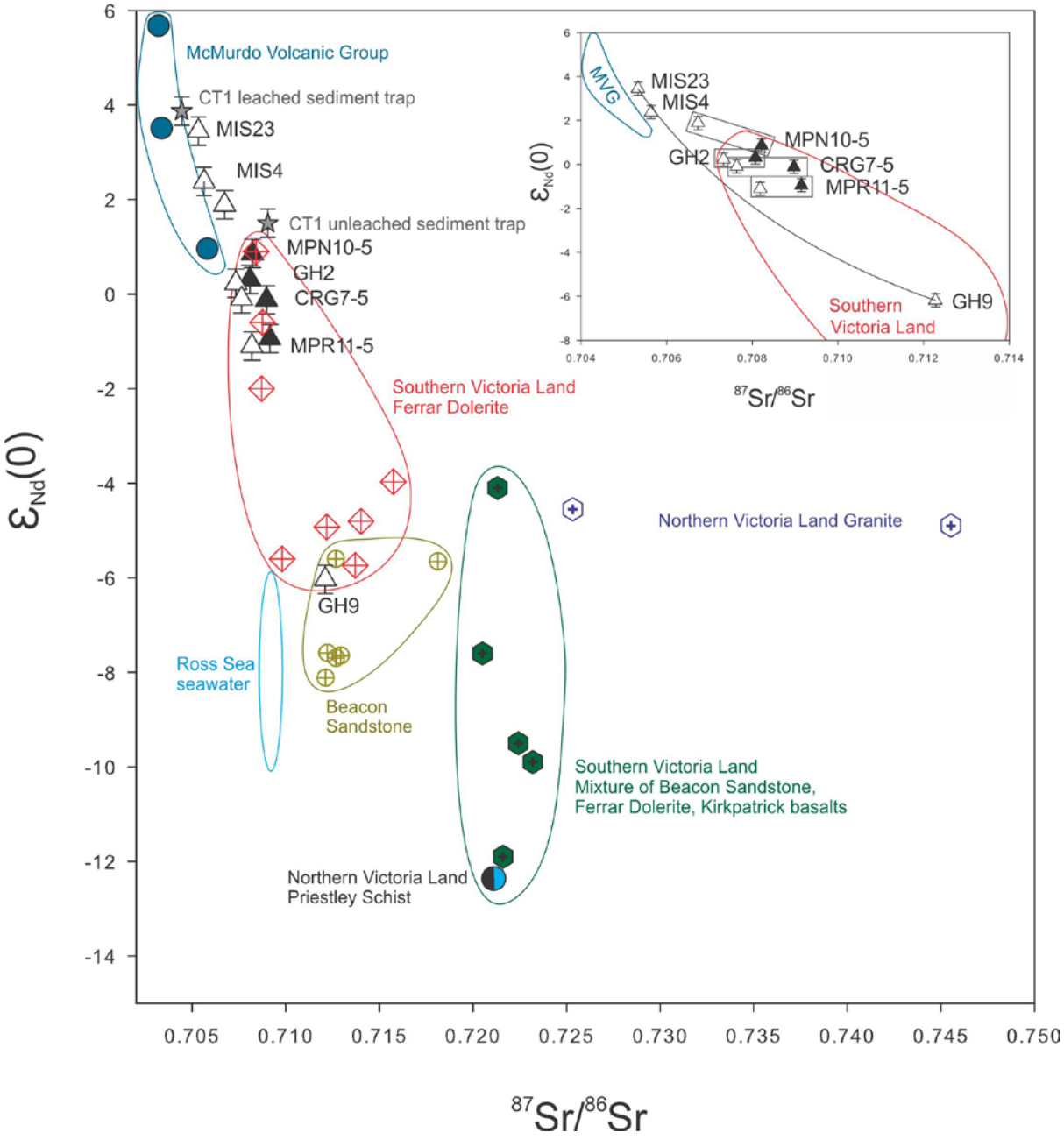

Fig. 7.2: Nd and Sr isotope signature of fine (black triangles) and bulk (white triangles) McMurdo Sound dust, including bulk McMurdo Sound data (GH9, MIS4 and MIS23; *Winton et al.* [2014]) and leached and unleached Chinstrap sediment trap material. Also plotted are data from Victoria Land potential dust sources that include different parent lithologies located in Fig. 1. [*Delmonte et al.*, 2004b; *Delmonte et al.*, 2013; *Delmonte et al.*, 2010b] and the isotopic composition of Ross Sea seawater [*Basak et al.*, 2015; *Elderfield*, 1986]. Insert top right: McMurdo Sound dust highlighting the fractionation between fine and coarse particle sizes and a hypothetical mixing line between the two end members MVG and Southern Victoria Land, TAM.

7.4 Discussion

7.4.1 Dust provenance

7.4.1.1 McMurdo Sound

The overwhelming majority of dust deposited in snow on sea ice in McMurdo Sound is locally sourced. It is not possible to detect any contribution from South American or Australian sources with our approach. Sedimentological, meteorological and geochemical evidence consistently points to the debris bands on the McMurdo Ice Shelf [*Kellogg et al.*, 1990] as the dominant local dust source in the McMurdo Sound region (Fig. 7.1) [*Atkins and Dunbar*, 2009; *Chewings et al.*, 2014; *Winton et al.*, 2014]. Studies of spatial variability of dust and particle size for the greater McMurdo Sound region show a distinct decrease in particle size and dust flux along transect X-Y (Fig. 7.1b) as part of a dust plume extending northwards from the debris bands [*Atkins and Dunbar*, 2009; *Chewings et al.*, 2014]. As the plume extends northwards away from the debris bands the particle size and dust accumulation rate decrease, although secondary elevated patches of both occur near coastal headlands. Overall dust accumulation declines exponentially from 55 g m^{-2} yr^{-1} near the debris bands to ~0.2 g m^{-2} yr^{-1} 120 km north of the debris bands [*Atkins and Dunbar*, 2009; *Chewings et al.*, 2014]. This northward dust dispersal is consistent with the local meteorology whereby the highest wind speeds, i.e. those most competent with respect to entraining silt and fine sand, are predominately from the south (Fig. 7.1c), dispersing dust from the debris bands north along the Southern Victoria Land coastline.

In addition to sedimentological considerations, geochemical evidence also points to dust being locally sourced. The Sr isotopic of modern seawater is homogenous ($^{87}Sr/^{86}Sr$=0.70924; *Elderfield* [1986]), and has a similar Sr isotopic composition to the geology in McMurdo Sound (Fig. 7.2). However, the Nd isotopic composition of the local geology and Ross Sea seawater ($-10<\varepsilon_{Nd}(0)<-6$; *Basak et al.* [2015]) is distinguished in Fig. 7.2, and combined with other provenance indicators (coarse particle size, high dust flux and Fe/Al elemental ratios [*Atkins and Dunbar*, 2009; *de Jong et al.*, 2013]; see below, allows tracing of dust to local PSAs. *Winton et al.* [2014] report two Sr and Nd isotopic ratios of the bulk sediment from snow on sea ice in southern McMurdo Sound and one from Granite Harbour (Fig. 7.1). The values are consistent with dust originating from McMurdo Volcanic Group (MVG), although within the Granite Harbour embayment there is also evidence for

dust-derived from TAM lithologies. We rule out the possibility that the volcanic signature of McMurdo Sound dust on sea ice is derived from volcanic rocks in Marie Byrd Land ($0.7026< {}^{87}Sr/{}^{86}Sr <0.7032$ and $1.99< \varepsilon_{Nd}(0) <6.87$) [*Futa and Le Masurier*, 1983; *Hole and LeMasurier*, 1994] due to the northerly direction of the prevailing winds [*Chewings et al.*, 2014].

Consequently, only local potential source areas (PSAs) are considered for comparison to the new isotopic dataset. Overall, the Sr isotopic ratios for McMurdo Sound samples analysed in this study and in *Winton et al.* [2014] are tightly grouped and range between $0.705< {}^{87}Sr/{}^{86}Sr <0.709$ while $\varepsilon_{Nd}(0)$ ranges between $3.45<\varepsilon_{Nd}(0)<-1.1$. These new isotopic data form a linear array in Fig. 7.2. McMurdo Sound dust can be considered the result of a two-component mixture derived from isotopically distinct end-members: i) the MVG volcanic rocks and ii) Southern Victoria Land lithologies found in the TAM such as Ferrar Dolerites and Beacon sandstone (Fig. 7.2). The narrow range of isotopic ratios of McMurdo Sound dust along the south-north transect X-Y represents northwards dust dispersal downwind from the debris bands, that is a mixture of TAM and MVG sources, with minor localised additions of TAM dust input from coastal outcrops from New Harbour and Marble Point that contribute to the dominant south to north dust plume (Fig. 7.1). This is consistent with field observations showing sediment on the McMurdo Ice Shelf debris bands is itself a mixture of MVG and TAM lithologies [*Kellogg et al.*, 1990].

Previous studies have shown dust deposited within embayments or adjacent to headlands along the Southern Victoria Land coastline is not widely dispersed [*Barrett et al.*, 1983; *Chewings et al.*, 2014; *de Jong et al.*, 2013]. Within the narrow range of isotopic ratios of McMurdo Sound dust, GH9 is isotopically distinct and displays a dominant TAM signature (Fig. 7.2). This sample is not situated under the main northward-directed dust plume and hence represents localised dust accumulation within the Granite Harbour embayment (Fig. 7.1). In contrast, the isotopic composition of GH2 lies within the tight cluster of McMurdo Sound dust and thus highlights that the mass of dust on the sea ice immediately seawards of Granite Harbour originates from the south. A single-source from the debris bands is also consistent with Fe concentrations within dust samples that were uniform along the transport pathway [*Winton et al.*, 2014].

7.4.1.2 Southwestern Ross Sea

The isotopic signature of the lithogenic fraction of sediment from the upper 200 mbsl Chinstrap sediment trap, located ~170 km north of the debris bands ($^{87}Sr/^{86}Sr$=0.704, $\varepsilon_{Nd}(0)$=3.9), falls outside of the isotopic range of dust originating in Australia (0.709<$^{87}Sr/^{86}Sr$<0.763, -2.9<$\varepsilon_{Nd}(0)$<-15.4; *Delmonte et al.* [2004b]; *Revel-Rolland et al.* [2006]) and South America (0.704<$^{87}Sr/^{86}Sr$<0.713, -8.9<$\varepsilon_{Nd}(0)$<-8.3; *Delmonte et al.* [2004b]). These two potential Southern Hemisphere sources supply dust to the high elevation EAP at very low deposition rates [e.g. *Delmonte et al.*, 2008]. The signature of the lithogenic fraction of sediment from SW Ross Sea (Chinstrap) matches that of the local geology and dust on sea ice in McMurdo Sound. Thus, the lithogenic particles, and their associated Fe, collected here are 'locally' sourced from the Ross Sea region (Fig. 7.2).

7.4.1.3 Dust transport and deposition in the southwestern Ross Sea

Deposition of local dust into the SW Ross Sea can occur by direct atmospheric fallout into ice-free surface waters, and released into surface waters by sea ice melt associated with subsequent northwards advection [*Atkins and Dunbar*, 2009; *Chewings et al.*, 2014; *de Jong et al.*, 2013]. The geographical area over which local dust is transported into the Ross Sea and hence contributes to Fe-fertilisation is potentially large. Although dust accumulation measurements only exist up to 120 km from the debris bands and decrease exponentially from the source, local dust deposition likely extends far beyond this point. Extrapolating the dust flux trend observed by *Chewings et al.* [2014] suggests that the Chinstrap site may represent a northern extension of the dust and DFe dispersal pattern reported by *Winton et al.* [2014]. We estimate an annual accumulation rate of ~0.01 g m^{-2} yr^{-1} at the Chinstrap site from aeolian dust, although we do not have accumulation rate data from the Chinstrap sediment trap with which to compare this estimate. Whether or not locally sourced aeolian sediment this is the main source of the lithogenic sediment in the Chinstrap site remains somewhat of an open question. However, when the relationship between DFe and phytoplankton productivity in McMurdo Sound is considered we suggest this is unlikely to be the case (Fig. 7.3; Section 7.4.2).

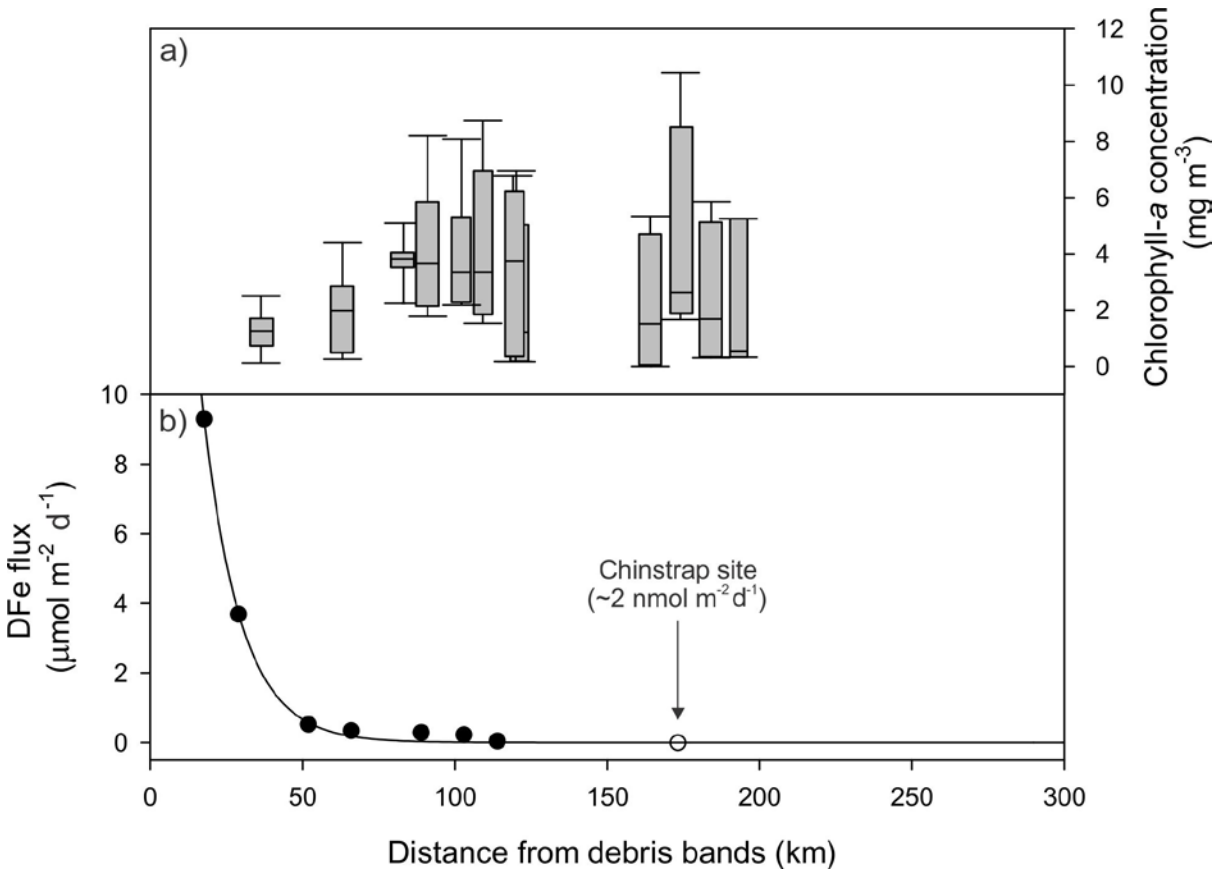

Fig. 7.3: a) Extrapolation of the annual DFe flux from McMurdo Sound into the SW Ross Sea. DFe data sourced from: *Winton et al.* [2014]. The predicted dust flux at the Chinstrap site is estimated at ~0.01 g m^{-2} yr^{-1} with a corresponding DFe flux of ~2 nmol m^{-2} d^{-1}. b) Also shown is the rate of primary production with distance from McMurdo Sound. As the dust flux exponentially decreases, the rate of primary production increases. Primary production inferred from the annual mean chlorophyll-*a* concentration (2000-2009) in the McMurdo Sound polynya (72.0 °S - 78.083 °S, 160.916 °E - 179.040 °W) from SeaWiFS satellite data (http://giovanni.gsfc.nasa.gov).

7.4.2 4.2. Implications for iron-fertilisation

7.4.2.1 Contribution of local dust to lithogenic iron

By extrapolating the dust flux trend observed by *Chewings et al.* [2014] and its associated contribution to DFe (*Winton et al.* [2014] into the SW Ross Sea, we can estimate the upper bound of the DFe at the Chinstrap site from the debris bands (Fig. 7.3). Assuming a lithogenic dust flux of ~0.01 g m^{-2} yr^{-1} and an associated total Fe content of 4 % and 11 % of this Fe is soluble [*Winton et al.*, 2014], we estimate a maximum DFe flux of ~2 nmol m^{-2} d^{-1} to the Chinstrap site (Fig. 7.3). However, when this is considered relative to the spatial distribution of primary production in the SW Ross Sea, using averaged annual Sea-Viewing

Wide Field-of-View Sensor (SeaWiFS) satellite chlorophyll-*a* data, we find that the gradient in increasing chlorophyll-*a* concentration with distance from the debris bands within the McMurdo Sound polynya does not match the pattern of decreasing dust accumulation (Fig. 7.3). This pattern suggests that DFe from dust not regulate growth in the SW Ross Sea. A seasonal phytoplankton bloom occurs in the McMurdo Sound polynya, SW Ross Sea each summer and is dominated by diatoms. The rate of primary production is greatest in the centre of the McMurdo Sound Polynya. As the dust flux decreases and primary production increases with distance from McMurdo Sound, it is difficult to reconcile these patterns at the Chinstrap site assuming only a local dust source (Fig. 7.3).

7.4.2.2 Supporting evidence from the wider Ross Sea

Some further insight into the origin of sediment in the water column in the SW Ross see may be inferred from the data published by *Collier et al.* [2000]. They show a significantly elevated lithogenic accumulation rate in deep AESOPS sediment traps compared to accumulation rates measured in the upper AESOPS sediment traps at other sites in the Ross Sea (e.g. MS-7; 76°30'S, 178°1'W). In addition, lithogenic Fe fluxes between 1-90 µg m^{-2} d^{-1} have been measured for the upper 200 mbsl AESOPS trap (MIS-7b) and 40-850 µg m^{-2} d^{-1} for the deep trap (MS-7a). The greater mass of sediment and lithogenic Fe flux in the deep traps in the Ross Sea highlight that concentrations of suspended sediment in the water column at these sites cannot simply result from sediment input at the surface (whereby the accumulation in each trap would be the same regardless of depth). Instead, the increase in accumulation with depth likely reflects resuspension and horizontal near-bottom transport processes. Whilst we do not have the data to constraint these processes at Chinstrap we infer, based on the provenance of the lithogenic sediment and distance from known local sources, that the lithogenic sediment accumulating there is most likely dominated by resuspended bottom sediments, potentially from sills either side of the Drygalski Basin but also locally sourced material falling through the water column sourced from atmospheric deposition or ice rafting. Although, no Fe flux data for the Chinstrap site are available, future work could examine the relationship between Fe fluxes in the Chinstrap sediment trap and those DFe fluxes reported for locally derived dust at McMurdo Sound.

Despite McMurdo Sound representing the upper bound of locally derived dust and associated DFe to Antarctic waters, previous studies have ruled out local dust as the major source of DFe supply for phytoplankton blooms in the Ross Sea. Dissolved Fe in McMurdo Sound dust

can only support up to 15 % of primary production in the region [*Winton et al.*, 2014]. Furthermore, based on regional scale estimates of dust deposition to the Southern Ocean, primary production triggered by long-range transport dust is likely to be less significant than local dust [e.g. *Edwards and Sedwick*, 2001]. Evidence from the extrapolation of the mass accumulation rate to the upper 200 mbsl Chinstrap trap, the sedimentological study of *Chewings et al.* [2014], sedimentation in the water column, and the low contribution of local aeolian DFe to phytoplankton blooms, suggest that it is unlikely that aeolian dust deposition is the dominant process by which lithogenic Fe is supplied to the water column in the SW Ross Sea. Considered together, these lines of evidence point to a combination of resuspended bottom sediments with smaller additions of local dust sourced from atmospheric deposition or ice rafting as the sources of Fe-bearing sediment to the water column in the SW Ross Sea.

7.4.2.3 Implications for iron-fertilisation

More broadly, *Sedwick et al.* [2011] noted that the phytoplankton-Fe limitation must be overcome by continuous replenishment from new sources to sustain the significant biomass observed over summer. They considered the following as potential sources of new DFe: vertical mixing, lateral advection, aerosol input, and dissolution of particulate Fe from any or all of these sources. Consistent with upwelling of DFe as a major source of DFe in the Ross Sea, *Marsay et al.* [2014] reported the highest DFe concentrations are found within 50 m of the seafloor in the austral summer 2012. Most recently, *Gerringa et al.* [2015] measured seawater DFe concentrations in the 2013-2014 austral summer, and concluded that DFe from the seafloor and land mass sediments are the main sources of DFe which support phytoplankton in the upper mixed layer of the Ross Sea Polynya in the early summer. Similarly, phytoplankton blooms in the Pennell Bank region of the Ross Sea are supported by upwelling of DFe [*Kustka et al.*, 2015]. However, *Kustka et al.* [2015] also highlight the spatial variability of processes supplying DFe in the Ross Sea. For example, circulation patterns around bathymetric features can alter the input of DFe from increased upwelling rates and higher concentrations of DFe. Numerical modelling of DFe supply by *McGillicuddy et al.* [2015] suggests that the largest sources to the euphotic zone are wintertime mixing and melting sea ice [e.g. *de Jong et al.*, 2013; *Sedwick and DiTullio*, 1997] with smaller inputs from Circumpolar Deep Water and from melting glacial ice.

7.5 Conclusions

Dust extracted from surface snow on McMurdo Sound sea ice enables us to document the present day provenance of dust reaching the SW Ross Sea. Based on our measurements of Sr and Nd isotopic ratios of dust deposited in surface snow on sea ice at McMurdo Sound and in the Chinstrap sediment trap in the SW Ross Sea we conclude the following:

1. The Sr and Nd isotopic signature of lithogenic sediment from the upper Chinstrap sediment trap in the SW Ross Sea ($\varepsilon_{Nd}(0)$=3.9, $^{87}Sr/^{86}Sr$=0.70434) matches local dust sources.

2. McMurdo Sound has been well characterised in terms of the Sr and Nd isotopic composition of locally derived dust deposited on sea ice. Dust found there displays a narrow isotopic field between 0.70533< $^{87}Sr/^{86}Sr$ <0.70819 and -1.1< $\varepsilon_{Nd}(0)$ <3.45 for the bulk fraction and 0.70807< $^{87}Sr/^{86}Sr$ <0.70915 and -0.94< $\varepsilon_{Nd}(0)$ <0.86 for the fine fraction. Due to Sr isotopic fractionation with particle size, the signature of the fine fraction reference adds to the PSA database for comparison to Antarctic ice core dust provenance studies.

3. Locally derived dust from McMurdo Sound is unlikely to be the major source of DFe for seasonal phytoplankton blooms in the SW Ross Sea. Although, Sr and Nd isotopic ratios of local dust on sea ice show similarities to lithogenic marine sediment, we acknowledge the limited transport distance of coarse-sized dust in this region. As dust transport varies from year to year, we cannot completely exclude the possibility that local dust can contribute to DFe to the greater Ross Sea region although this is not the dominant source of lithogenic Fe.

4. We surmise that there is significant remobilisation and upwelling of Fe from the sea floor that contributes to Fe-fertilisation of phytoplankton during the austral summer in the SW Ross Sea.

5. Source information of dust inputs to regions, such as the Ross Sea, improves the ability to predict how such supply will change as the climate changes. As local sources are important to the SW Ross Sea, this data could be included in models that predict changes in snow and ice cover in the region.

Acknowledgements

We would like to thank Antarctica New Zealand and Scott Base personnel for logistics support. Thank you to Jane Chewings, Assoc. Prof. Brent Alloway and Assistant Prof. Ana Aguilar-Islas for the collection of McMurdo Sound and Granite Harbour dust samples. Additional thanks to Prof. Robert Dunbar for Chinstrap sediment trap samples from the ROAVERRS mooring program. V.H.L.W. would like to thank the following organizations for scholarship and other funding support: Curtin University (Australian Postgraduate Award and Curtin Research Scholarship) and Antarctic Science (Antarctic Science Bursary). This project was funded by Curtin University (Curtin Research Fellowship to R.E.: RES-SE-DAP-AW-47679-1), and New Zealand Ministry of Science and Innovation through contracts to Victoria University of Wellington (Contracts: VUW0704; RDF-VUW1103) and GNS Science (Contracts: 540GCT32; C05X1001). Isotopic analyses for provenance characterization were carried out at the Swedish Museum of Natural History and were supported by the Department of Geosciences, Swedish Museum of Natural History. Thank you to Karin Wallner and Hans Schöberg for technical support. The isotopic dataset for this paper is freely available from the Curtin University Research Data repository http://doi.org/10.4225/06/5643EBA1C8473. The chlorophyll-a data was obtained freely from the Sea-Viewing Wide Field-of-View Sensor (http://giovanni.gsfc.nasa.gov/). Additional thanks for the helpful comments and suggestions of Jeroen de Jong and an anonymous reviewer that aided in revision of this manuscript.

Author contributions

V.H.L.W, G.B.D, C.B.A and N.A.N.B designed the research; G.B.D and C.B.A collected the samples; V.H.L.W, B.D and P.S.A prepared the samples and analysed the data; V.H.L.W, G.B.D, C.B.A, B.D and P.S.A evaluated the data; all authors contributed to the interpretation of the data and the writing of the manuscript

References

Abram, N. J., M. K. Gagan, M. T. McCulloch, J. Chappell, and W. S. Hantoro (2003), Coral reef death during the 1997 Indian Ocean dipole linked to Indonesian wildfires, *Science*, *301*(5635), 952-955.

Adams, C., D. Seward, and S. Weaver (1995), Geochronology of Cretaceous granites and metasedimentary basement on Edward VII Peninsula, Marie Byrd Land, West Antarctica, *Antarctic science*, *7*(03), 265-276.

Aguilar-Islas, A. M., J. Wu, R. Rember, A. M. Johansen, and L. M. Shank (2010), Dissolution of aerosol-derived iron in seawater: Leach solution chemistry, aerosol type, and colloidal iron fraction, *Marine Chemistry*, *120*(1-4), 25-33.

Albani, S., N. Mahowald, B. Delmonte, V. Maggi, and G. Winckler (2012), Comparing modeled and observed changes in mineral dust transport and deposition to Antarctica between the Last Glacial Maximum and current climates, *Climate Dynamics*, *38*(9-10), 1731-1755.

Albani, S., B. Delmonte, V. Maggi, C. Baroni, J. R. Petit, B. Stenni, C. Mazzola, and M. Frezzotti (2012), Interpreting last glacial to Holocene dust changes at Talos Dome (East Antarctica): implications for atmospheric variations from regional to hemispheric scales, *Clim. Past Discuss.*, *8*(1), 145-168.

Albani, S., et al. (2015), Twelve thousand years of dust: the Holocene global dust cycle constrained by natural archives, *Clim. Past*, *11*(6), 869-903.

Alexander, J. M., V. H. Grassian, M. A. Young, and P. D. Kleiber (2015), Optical properties of selected components of mineral dust aerosol processed with organic acids and humic material, *Journal of Geophysical Research: Atmospheres*, *120*(6), 2437-2452.

Alying, B. (2001), Dust accumulation on the Victoria Lower Glacier and Wilson Piedmont, coastal South Victoria Land, Antarctica, and its potential as a paleowind indicator, Victoria University of Wellington, Wellington.

Anderson, R. F., S. Barker, M. Fleisher, R. Gersonde, S. L. Goldstein, G. Kuhn, P. G. Mortyn, K. Pahnke, and J. P. Sachs (2014), Biological response to millennial variability of dust and nutrient supply in the Subantarctic South Atlantic Ocean, *Philosophical Transactions of the Royal Society of London A: Mathematical, Physical and Engineering Sciences*, *372*(2019).

Andersson, P. S., G. Wasserburg, J. Ingri, and M. C. Stordal (1994), Strontium, dissolved and particulate loads in fresh and brackish waters: the Baltic Sea and Mississippi Delta, *Earth and Planetary Science Letters*, *124*(1), 195-210.

Andreae, M., and A. Gelencsér (2006), Black carbon or brown carbon? The nature of light-absorbing carbonaceous aerosols, *Atmospheric Chemistry and Physics*, *6*(10), 3131-3148.

Andreae, M. O. (1991), Biomass burning: Its history, use and distribution and its impact on environmental quality and global climate, *Global Biomass Burning: Atmospheric, Climatic, and Biospheric Implications, edited by J. S. Levine, pp. 3-21, MIT Press, Cambridge, Mass.*

Andreae, M. O. (1993), The influence of tropical biomass burning on climate and the atmospheric environment, in *Biogeochemistry of Global Change*, edited, pp. 113-150, Springer.

Andreasen, R., and M. Sharma (2006), Solar nebula heterogeneity in p-process samarium and neodymium isotopes, *Science*, *314*(5800), 806-809.

Antonini, P., E. Piccirillo, R. Petrini, L. Civetta, M. D'Antonio, and G. Orsi (1999), Enriched mantle–Dupal signature in the genesis of the Jurassic Ferrar tholeiites from Prince Albert Mountains (Victoria Land, Antarctica), *Contributions to Mineralogy and Petrology*, *136*(1-2), 1-19.

Arimoto, R., and R. A. Duce (1986), DRY DEPOSITION MODELS AND THE AIR/SEA EXCHANGE OF TRACE ELEMENTS, *J. Geophys. Res.*, *91*(D2), 2787-2792.

Arimoto, R., R. Duce, B. Ray, and C. Unni (1985), Atmospheric trace elements at Enewetak Atoll: 2. Transport to the ocean by wet and dry deposition, *Journal of Geophysical Research: Atmospheres (1984–2012)*, *90*(D1), 2391-2408.

Arrigo, K. R., and C. R. McClain (1994), Spring Phytoplankton Production in the Western Ross Sea, *Science*, *266*(5183), 261-263.

Arrigo, K. R., and G. L. van Dijken (2004), Annual changes in sea-ice, chlorophyll a, and primary production in the Ross Sea, Antarctica, *Deep Sea Research Part II: Topical Studies in Oceanography*, *51*(1-3), 117-138.

Arrigo, K. R., and G. L. Van Dijken (2007), Interannual variation in air-sea CO2 flux in the Ross Sea, Antarctica: A model analysis, *J. Geophys. Res.*, *112*(C3), C03020.

Arrigo, K. R., A. M. Weiss, and W. O. Smith, Jr. (1998), Physical forcing of phytoplankton dynamics in the southwestern Ross Sea, *J. Geophys. Res.*, *103*(C1), 1007-1021.

Arrigo, K. R., G. L. van Dijken, and S. Bushinsky (2008a), Primary production in the Southern Ocean, 1997-2006, *J. Geophys. Res.*, *113*(C8), C08004.

Arrigo, K. R., G. van Dijken, and M. Long (2008b), Coastal Southern Ocean: A strong anthropogenic CO2 sink, *Geophys. Res. Lett.*, *35*(21), L21602.

Arrigo, K. R., G. R. DiTullio, R. B. Dunbar, D. H. Robinson, M. VanWoert, D. L. Worthen, and M. P. Lizotte (2000), Phytoplankton taxonomic variability in nutrient utilization and primary production in the Ross Sea, *J. Geophys. Res.*, *105*(C4), 8827-8846.

Artaxo, P., F. Gerab, M. A. Yamasoe, and J. V. Martins (1994), Fine mode aerosol composition at three long-term atmospheric monitoring sites in the Amazon Basin, *Journal of Geophysical Research: Atmospheres (1984–2012)*, *99*(D11), 22857-22868.

Artaxo, P., E. T. Fernandas, J. V. Martins, M. A. Yamasoe, P. V. Hobbs, W. Maenhaut, K. M. Longo, and A. Castanho (1998), Large-scale aerosol source apportionment in Amazonia, *Journal of Geophysical Research: Atmospheres (1984–2012)*, *103*(D24), 31837-31847.

Atkins, C. B., and G. B. Dunbar (2009), Aeolian sediment flux from sea ice into Southern McMurdo Sound, Antarctica, *Global and Planetary Change*, *69*(3), 133-141.

Augustinus, P., and G. Duller (2002), Luminescence and radiocarbon dating of raised beach sediments, Bunger Hills, East Antarctica, paper presented at Antarctica at the close of a millennium: proceedings of the 8th International Symposium on Antarctic Earth Sciences, Wellington 1999.

Ayers, G., J. Ivey, and H. Goodman (1987), Sulfate and Methanesulfonnate in the Maritime Aerosol at Cape Grim, Tasmania, in *Scientific Application of Baseline Observations of Atmospheric Composition (SABOAC)*, edited, pp. 371-383, Springer.

Ayers, G., J. Cainey, R. Gillett, and J. Ivey (1997), Atmospheric sulphur and cloud condensation nuclei in marine air in the Southern Hemisphere, *Philosophical Transactions of the Royal Society of London B: Biological Sciences*, *352*(1350), 203-211.

Ayers, G. P., J. Ivey, and R. Gillett (1990), High Volume Samplers in Baseline Atmospheric Program (Australia) 1988, edited by S.R. Wilson and G.P. Ayers, CSIRO Atmospheric Research, Melbourne, Australia, 45.

Ayling, B., and H. McGowan (2006), Niveo-eolian Sediment Deposits in Coastal South Victoria Land, Antarctica: Indicators of Regional Variability in Weather and Climate, *Arctic, Antarctic, and Alpine Research*, *38*(3), 313-324.

Bagnold, R. (1941), *The physics of blown sand and desert dunes*, Methuen, London.

Baker, A., S. Kelly, K. Biswas, M. Witt, and T. Jickells (2003), Atmospheric deposition of nutrients to the Atlantic Ocean, *Geophysical Research Letters*, *30*(24).

Baker, A., C. Adams, T. Bell, T. Jickells, and L. Ganzeveld (2013), Estimation of atmospheric nutrient inputs to the Atlantic Ocean from 50° N to 50° S based on large-scale field sampling: Iron and other dust-associated elements, *Global Biogeochemical Cycles*, *27*(3), 755-767.

Baker, A., K. Weston, S. Kelly, M. Voss, P. Streu, and J. Cape (2007), Dry and wet deposition of nutrients from the tropical Atlantic atmosphere: Links to primary productivity and nitrogen fixation, *Deep Sea Research Part I: Oceanographic Research Papers*, *54*(10), 1704-1720.

Baker, A. R., and T. D. Jickells (2006), Mineral particle size as a control on aerosol iron solubility, *Geophys. Res. Lett.*, *33*(17), L17608.

Baker, A. R., and P. L. Croot (2010), Atmospheric and marine controls on aerosol iron solubility in seawater, *Marine Chemistry*, *120*(1-4), 4-13.

Baker, A. R., T. D. Jickells, M. Witt, and K. L. Linge (2006), Trends in the solubility of iron, aluminium, manganese and phosphorus in aerosol collected over the Atlantic Ocean, *Marine Chemistry*, *98*(1), 43-58.

Banerjee, P., and S. Prasanna Kumar (2014), Dust-induced episodic phytoplankton blooms in the Arabian Sea during winter monsoon, *Journal of Geophysical Research: Oceans*, *119*(10), 7123-7138.

Banse, K. (1991), Rates of Phytoplankton Cell Division in the Field and in Iron Enrichment Experiments, *Limnology and Oceanography*, *36*(8), 1886-1898.

Barbeau, K., J. W. Moffett, D. A. Caron, P. L. Croot, and D. L. Erdner (1996), Role of protozoan grazing in relieving iron limitation of phytoplankton, *Nature*, *380*(6569), 61-64.

Barbeau, K. A., and J. W. Moffett (1998), Dissolution of Iron Oxides by Phagotrophic Protists: Using a Novel Method To Quantify Reaction Rates, *Environmental Science & Technology*, *32*(19), 2969-2975.

Barrett, P., A. Pyne, and B. Ward (1983), Modern sedimentation in McMurdo Sound, Antarctica In: Oliver, R.L., James, P.R., Jago, J.B. (Eds.), *Antarctic Earth Science*, 550-554.

Basak, C., K. Pahnke, M. Frank, F. Lamy, and R. Gersonde (2015), Neodymium isotopic characterization of Ross Sea Bottom Water and its advection through the southern South Pacific, *Earth and Planetary Science Letters*, *419*, 211-221.

Basile, I., J. R. Petit, S. Touron, F. E. Grousset, and N. Barkov (2001), Volcanic layers in Antarctic (Vostok) ice cores: Source identification and atmospheric implications, *Journal of Geophysical Research: Atmospheres (1984–2012)*, *106*(D23), 31915-31931.

Basile, I., F. E. Grousset, M. Revel, J. R. Petit, P. E. Biscaye, and N. I. Barkov (1997), Patagonian origin of glacial dust deposited in East Antarctica (Vostok and Dome C) during glacial stages 2, 4 and 6, *Earth and Planetary Science Letters*, *146*(3-4), 573-589.

Berger, C. J., S. M. Lippiatt, M. G. Lawrence, and K. W. Bruland (2008), Application of a chemical leach technique for estimating labile particulate aluminum, iron, and manganese in the Columbia River plume and coastal waters off Oregon and Washington, *Journal of Geophysical Research: Oceans (1978–2012)*, *113*(C2).

Berman-Frank, I., J. T. Cullen, Y. Shaked, R. M. Sherrell, and P. G. Falkowski (2001), Iron availability, cellular iron quotas, and nitrogen fixation in Trichodesmium, *Limnology and Oceanography*, *46*(6), 1249-1260.

Bhattachan, A., and P. D'Odorico (2014), Can land use intensification in the Mallee, Australia increase the supply of soluble iron to the Southern Ocean?, *Scientific reports*, *4*.

Bhattachan, A., L. Wang, M. F. Miller, K. J. Licht, and P. D'Odorico (2015), Antarctica's Dry Valleys: A potential source of soluble iron to the Southern Ocean?, *Geophysical Research Letters*, *42*(6), 1912-1918.

Biscaye, P. E., F. E. Grousset, M. Revel, S. Van der Gaast, G. A. Zielinski, A. Vaars, and G. Kukla (1997), Asian provenance of glacial dust (stage 2) in the Greenland Ice Sheet Project 2 Ice Core, Summit, Greenland, *J. Geophys. Res.*, *102*(C12), 26765-26781.

Bisiaux, M., R. Edwards, J. McConnell, M. Albert, H. Anschütz, T. Neumann, E. Isaksson, and J. Penner (2012a), Variability of black carbon deposition to the East Antarctic Plateau, 1800–2000 AD, *Atmospheric Chemistry and Physics*, *12*(8), 3799-3808.

Bisiaux, M., R. Edwards, J. McConnell, M. Curran, T. Van Ommen, A. Smith, T. Neumann, D. Pasteris, J. Penner, and K. Taylor (2012b), Changes in black carbon deposition to Antarctica from two high-resolution ice core records, 1850–2000 AD, *Atmospheric Chemistry and Physics*, *12*(9), 4107-4115.

Blain, S., et al. (2007), Effect of natural iron fertilization on carbon sequestration in the Southern Ocean, *Nature*, *446*(7139), 1070-1074.

Bollhöfer, A., and K. Rosman (2000), Isotopic source signatures for atmospheric lead: the Southern Hemisphere, *Geochimica et Cosmochimica Acta*, *64*(19), 3251-3262.

Bollhöfer, A., and K. Rosman (2001), Isotopic source signatures for atmospheric lead: the Northern Hemisphere, *Geochimica et Cosmochimica Acta*, *65*(11), 1727-1740.

Bollhöfer, A., W. Chisholm, and K. Rosman (1999), Sampling aerosols for lead isotopes on a global scale, *Analytica chimica acta*, *390*(1), 227-235.

Bollhöfer, A., W. Chisholm, and K. J. R. Rosman (1999), Sampling aerosols for lead isotopes on a global scale, *Analytica Chimica Acta*, *390*(1–3), 227-235.

Bollhöfer, A. F., K. J. R. Rosman, A. L. Dick, W. Chisholm, G. R. Burton, R. D. Loss, and W. Zahorowski (2005), Concentration, isotopic composition, and sources of lead in Southern Ocean air during 1999/2000, measured at the Cape Grim Baseline Air Pollution Station, Tasmania, *Geochimica et Cosmochimica Acta*, *69*(20), 4747-4757.

Bonnet, S., and C. Guieu (2004), Dissolution of atmospheric iron in seawater, *Geophys. Res. Lett.*, *31*(3), L03303.

Bory, A., E. Wolff, R. Mulvaney, E. Jagoutz, A. Wegner, U. Ruth, and H. Elderfield (2010), Multiple sources supply eolian mineral dust to the Atlantic sector of coastal Antarctica: Evidence from recent snow layers at the top of Berkner Island ice sheet, *Earth and Planetary Science Letters*, *291*(1-4), 138-148.

Bory, A. J. M., P. E. Biscaye, A. Svensson, and F. E. Grousset (2002), Seasonal variability in the origin of recent atmospheric mineral dust at NorthGRIP, Greenland, *Earth and Planetary Science Letters*, *196*(3-4), 123-134.

Bowie, A., P. van der Merwe, F. Quéroué, T. Trull, M. Fourquez, F. Planchon, G. Sarthou, F. Chever, A. Townsend, and I. Obernosterer (2014), Iron budgets for three distinct biogeochemical sites around the Kerguelen archipelago (Southern Ocean) during the natural fertilisation experiment KEOPS-2, *Biogeosciences Discussions*, *11*(12), 17861-17923.

Bowie, A. R., F. B. Griffiths, F. Dehairs, and T. W. Trull (2011), Oceanography of the subantarctic and polar frontal zones south of Australia during summer: setting for the SAZ-Sense study, *Deep Sea Research Part II: Topical Studies in Oceanography*, *58*(21), 2059-2070.

Bowie, A. R., A. T. Townsend, D. Lannuzel, T. A. Remenyi, and P. Van der Merwe (2010), Modern sampling and analytical methods for the determination of trace elements in marine particulate material using magnetic sector inductively coupled plasma–mass spectrometry, *Analytica chimica acta*, *676*(1), 15-27.

Bowie, A. R., D. Lannuzel, T. A. Remenyi, T. Wagener, P. J. Lam, P. W. Boyd, C. Guieu, A. T. Townsend, and T. W. Trull (2009), Biogeochemical iron budgets of the Southern Ocean south of Australia: Decoupling of iron and nutrient cycles in the subantarctic zone by the summertime supply, *Global Biogeochem. Cycles*, *23*(4), GB4034.

Bowler, J. (1976), Aridity in Australia: age, origins and expression in aeolian landforms and sediments, *Earth-Science Reviews*, *12*(2), 279-310.

Boyd, P., P. Dillingham, C. McGraw, E. Armstrong, C. Cornwall, Y.-y. Feng, C. Hurd, M. Gault-Ringold, M. Roleda, and E. Timmins-Schiffman (2015), Physiological responses of a Southern Ocean diatom to complex future ocean conditions, *Nature Climate Change*.

Boyd, P. W., and D. S. Mackie (2008), Comment on 'The Southern Ocean biological response to aeolian iron deposition', *Science*, *319*, 159.

Boyd, P. W., and M. J. Ellwood (2010), The biogeochemical cycle of iron in the ocean, *Nature Geosci*, *3*(10), 675-682.

Boyd, P. W., D. S. Mackie, and K. A. Hunter (2010), Aerosol iron deposition to the surface ocean - Modes of iron supply and biological responses, *Marine Chemistry*, *120*(1-4), 128-143.

Boyd, P. W., S. C. Doney, R. Strzepek, J. Dusenberry, K. Lindsay, and I. Fung (2008), Climate-mediated changes to mixed-layer properties in the Southern Ocean: assessing the phytoplankton response, *Biogeosciences*, *5*(3), 847-864.

Boyd, P. W., G. McTainsh, V. Sherlock, K. Richardson, S. Nichol, M. Ellwood, and R. Frew (2004), Episodic enhancement of phytoplankton stocks in New Zealand subantarctic waters: Contribution of atmospheric and oceanic iron supply, *Global Biogeochem. Cycles*, *18*(1), GB1029.

Boyd, P. W., et al. (2007), Mesoscale Iron Enrichment Experiments 1993-2005: Synthesis and Future Directions, *Science*, *315*(5812), 612-617.

Boyd, P. W., et al. (2005), FeCycle: Attempting an iron biogeochemical budget from a mesoscale SF6 tracer experiment in unperturbed low iron waters, *Global Biogeochem. Cycles*, *19*(4), GB4S20.

Boyd, P. W., et al. (2000), A mesoscale phytoplankton bloom in the polar Southern Ocean stimulated by iron fertilization, *Nature*, *407*(6805), 695-702.

Buck, C. S., W. M. Landing, J. A. Resing, and G. T. Lebon (2006), Aerosol iron and aluminum solubility in the northwest Pacific Ocean: Results from the 2002 IOC cruise, *Geochem. Geophys. Geosyst.*, *7*(4), Q04M07.

Bunt, J. S. (1963), Microbiology of Antarctic Sea-ice: Diatoms of Antarctic Sea-ice as Agents of Primary Production, *Nature*, *199*(4900), 1255-1257.

Bunt, J. S., and E. J. F. Wood (1963), Microbiology of Antarctic Sea-ice: Microalgae and Antarctic Sea-ice, *Nature*, *199*(4900), 1254-1255.

Butler, H., W. L. Hogarth, and G. H. McTainsh (2001), Effects of spatial variations in source areas upon dust concentration profiles during three wind erosion events in Australia, *Earth Surface Processes and Landforms*, *26*(10), 1039-1048.

Calloway, C., S. Li, J. Buchanan, and R. Stevens (1989), A refinement of the potassium tracer method for residential wood smoke, *Atmospheric Environment (1967)*, *23*(1), 67-69.

Cammas, J.-P., J. Brioude, J.-P. Chaboureau, J. Duron, C. Mari, P. Mascart, P. Nédélec, H. Smit, H.-W. Pätz, and A. Volz-Thomas (2009), Injection in the lower stratosphere of biomass fire emissions followed by long-range transport: a MOZAIC case study, *Atmospheric Chemistry and Physics*, *9*(15), 5829-5846.

Carslaw, D. C. (2014), The openair manual - open-source tools for analysing air pollution data., *Manual for version 1.0, King's College London.*

Carslaw, D. C., and K. Ropkins (2012), Openair - An R package for air quality data analysis, *Environmental Modelling & Software*, *27*, 52-61.

Chakrabarty, R. K., H. Moosmüller, W. P. Arnott, M. A. Garro, J. G. Slowik, E. S. Cross, J.-H. Han, P. Davidovits, T. B. Onasch, and D. R. Worsnop (2007), Light scattering and absorption by fractal-like carbonaceous chain aggregates: Comparison of theories and experiment, *Applied optics*, *46*(28), 6990-7006.

Chambers, S., A. Williams, J. Crawford, and A. Griffiths (2014), On the use of radon for quantifying the effects of atmospheric stability on urban emissions, *Atmos. Chem. Phys. Discuss*, *14*, 25,411-425,452.

Chance, R., T. D. Jickells, and A. R. Baker (2015), Atmospheric trace metal concentrations, solubility and deposition fluxes in remote marine air over the south-east Atlantic, *Marine Chemistry*.

Chandler, C., P. Cheney, P. Thomas, L. Trabaud, and D. Williams (1983), Fire in forestry. Forest fire behaviour and effects, *Ed. John Wiley & Sons*, *1*.

Chang-Graham, A. L., L. T. Profeta, T. J. Johnson, R. J. Yokelson, A. Laskin, and J. Laskin (2011), Case study of water-soluble metal containing organic constituents of biomass burning aerosol, *Environmental science & technology*, *45*(4), 1257-1263.

Chen, Y., and R. L. Siefert (2003), Determination of various types of labile atmospheric iron over remote oceans, *J. Geophys. Res.*, *108*(D24), 4774.

Chen, Y., and R. L. Siefert (2004), Seasonal and spatial distributions and dry deposition fluxes of atmospheric total and labile iron over the tropical and subtropical North Atlantic Ocean, *J. Geophys. Res.*, *109*(D9), D09305.

Chewings, J. M., C. B. Atkins, G. B. Dunbar, and N. R. Golledge (2014), Aeolian sediment transport and deposition in a modern high-latitude glacial marine environment, *Sedimentology*, n/a-n/a.

Chewings, J. M., C. B. Atkins, G. B. Dunbar, and N. R. Golledge (2014), Aeolian sediment transport and deposition in a modern high latitude glacial marine environment, *Sedimentology*.

Chow, J. C., J. G. Watson, L.-W. A. Chen, M. O. Chang, N. F. Robinson, D. Trimble, and S. Kohl (2007), The IMPROVE_A temperature protocol for thermal/optical carbon analysis: maintaining consistency with a long-term database, *Journal of the Air & Waste Management Association*, *57*(9), 1014-1023.

Chuang, P. Y., R. M. Duvall, M. M. Shafer, and J. J. Schauer (2005), The origin of water soluble particulate iron in the Asian atmospheric outflow, *Geophys. Res. Lett.*, *32*(7), L07813.

Chughtai, A., M. Brooks, and D. Smith (1996), Hydration of black carbon, *Journal of Geophysical Research: Atmospheres (1984–2012)*, *101*(D14), 19505-19514.

Chughtai, A., J. Jassim, J. Peterson, D. Stedman, and D. Smith (1991), Spectroscopic and solubility characteristics of oxidized soots, *Aerosol Science and Technology*, *15*(2), 112-126.

Cleveland, W. S., and S. J. Devlin (1988), Locally weighted regression: an approach to regression analysis by local fitting, *Journal of the American Statistical Association*, *83*(403), 596-610.

Coale, K. H., X. Wang, S. J. Tanner, and K. S. Johnson (2003), Phytoplankton growth and biological response to iron and zinc addition in the Ross Sea and Antarctic Circumpolar Current along 170 W, *Deep Sea Research Part II: Topical Studies in Oceanography*, *50*(3), 635-653.

Coale, K. H., et al. (2004), Southern Ocean Iron Enrichment Experiment: Carbon Cycling in High- and Low-Si Waters, *Science*, *304*(5669), 408-414.

Cohen, L. (2013), Atmospheric Variability and Precipitation in the Ross Sea Region, Antarctica, *PhD thesis, Victoria University of Wellington, Wellington*.

Collier, R., J. Dymond, S. Honjo, S. Manganini, R. Francois, and R. Dunbar (2000), The vertical flux of biogenic and lithogenic material in the Ross Sea: moored sediment trap observations 1996-1998, *Deep Sea Research Part II: Topical Studies in Oceanography*, *47*(15-16), 3491-3520.

Conway, H., B. L. Hall, G. H. Denton, A. M. Gades, and E. D. Waddington (1999), Past and Future Grounding-Line Retreat of the West Antarctic Ice Sheet, *Science*, *286*(5438), 280-283.

Conway, T., E. Wolff, R. Röthlisberger, R. Mulvaney, and H. Elderfield (2015), Constraints on soluble aerosol iron flux to the Southern Ocean at the Last Glacial Maximum, *Nature Communications*, *6*.

Cook, C. P., et al. (2013), Dynamic behaviour of the East Antarctic ice sheet during Pliocene warmth, *Nature Geosci*, *6*(9), 765-769.

Cooke, W., V. Ramaswamy, and P. Kasibhatla (2002), A general circulation model study of the global carbonaceous aerosol distribution, *Journal of Geophysical Research: Atmospheres (1984–2012)*, *107*(D16), ACH 2-1-ACH 2-32.

Cox, S. C., D. L. Parkinson, A. H. Allibone, and A. F. Cooper (2000), Isotopic character of Cambro-Ordovician plutonism, southern Victoria Land, Antarctica, *New Zealand Journal of Geology and Geophysics*, *43*(4), 501-520.

Croot, P., K. Bluhm, C. Schlosser, P. Streu, E. Breitbarth, R. Frew, and M. Van Ardelan (2008), Regeneration of Fe (II) during EIFeX and SOFeX, *Geophysical Research Letters*, *35*(19).

Croot, P. L., A. R. Bowie, R. D. Frew, M. T. Maldonado, J. A. Hall, K. A. Safi, J. La Roche, P. W. Boyd, and C. S. Law (2001), Retention of dissolved iron and Fe II in an iron induced Southern Ocean phytoplankton bloom, *Geophys. Res. Lett.*, *28*(18), 3425-3428.

Croot, P. L., et al. (2005), Spatial and temporal distribution of Fe(II) and H2O2 during EisenEx, an open ocean mescoscale iron enrichment, *Marine Chemistry*, *95*(1-2), 65-88.

Cropp, R. A., A. J. Gabric, M. Levasseur, G. H. McTainsh, A. Bowie, C. S. Hassler, C. S. Law, H. McGowan, N. Tindale, and R. Viscarra Rossel (2013), The likelihood of observing dust-stimulated phytoplankton growth in waters proximal to the Australian continent, *Journal of Marine Systems*, *117–118*, 43-52.

Crutzen, P. J., and M. O. Andreae (1990), Biomass burning in the tropics: Impact on atmospheric chemistry and biogeochemical cycles, *Science*, *250*(4988), 1669-1678.

Cruz, M., A. Sullivan, J. Gould, N. Sims, A. Bannister, J. Hollis, and R. Hurley (2012), Anatomy of a catastrophic wildfire: the Black Saturday Kilmore East fire in Victoria, Australia, *Forest Ecology and Management*, *284*, 269-285.

Cutter, G., P. Andersson, L. Codispoti, P. Croot, R. Francois, M. Lohan, H. Obata, and M. Rutgers vd Loeff (2010), Sampling and sample-handling protocols for GEOTRACES Cruises.

Dansgaard, W. (1954), The O18- abundance in fresh water, *Geochimica et Cosmochimica Acta 6*, 241-260.

de Baar, H. J. W., and J. T. M. de Jong (2001), Distribution, sources and sinks of iron in seawater, *The Biogeochemistry of Iron in Seawater*, 123 - 253.

de Baar, H. J. W., J. T. M. de Jong, D. C. E. Bakker, B. M. Loscher, C. Veth, U. Bathmann, and V. Smetacek (1995), Importance of iron for plankton blooms and carbon dioxide drawdown in the Southern Ocean, *Nature*, *373*(6513), 412-415.

de Baar, H. J. W., et al. (2005), Synthesis of iron fertilization experiments: From the Iron Age in the Age of Enlightenment, *J. Geophys. Res.*, *110*(C9), C09S16.

De Deckker, P., M. Norman, I. D. Goodwin, A. Wain, and F. X. Gingele (2010), Lead isotopic evidence for an Australian source of aeolian dust to Antarctica at times over the last 170,000 years, *Palaeogeography, Palaeoclimatology, Palaeoecology*, *285*(3-4), 205-223.

de Jong, J., V. Schoemann, N. Maricq, N. Mattielli, P. Langhorne, T. Haskell, and J.-L. Tison (2013), Iron in land-fast sea ice of McMurdo Sound derived from sediment resuspension and wind-blown dust attributes to primary productivity in the Ross Sea, Antarctica, *Marine Chemistry*, *157*(0), 24-40.

Decesari, S., M. Facchini, E. Matta, M. Mircea, S. Fuzzi, A. Chughtai, and D. Smith (2002), Water soluble organic compounds formed by oxidation of soot, *Atmospheric Environment*, *36*(11), 1827-1832.

Delmonte, B., J. R. Petit, and V. Maggi (2002), Glacial to Holocene implications of the new 27000-year dust record from the EPICA Dome C (East Antarctica) ice core, *Climate Dynamics*, *18*(8), 647-660.

Delmonte, B., J. Robert Petit, I. Basile-Doelsch, E. Jagoutz, and V. Maggi (2007), 6. Late quaternary interglacials in East Antarctica from ice-core dust records, in *Developments in Quaternary Sciences*, edited by M. C. M. F. S. G. Frank Sirocko and L. Thomas, pp. 53-73, Elsevier.

Delmonte, B., J. R. Petit, K. K. Andersen, I. Basile-Doelsch, V. Maggi, and V. Ya Lipenkov (2004a), Dust size evidence for opposite regional atmospheric circulation changes over east Antarctica during the last climatic transition, *Climate Dynamics*, *23*(3), 427-438.

Delmonte, B., J. R. Petit, G. Krinner, V. Maggi, J. Jouzel, and R. Udisti (2005), Ice core evidence for secular variability and 200-year dipolar oscillations in atmospheric circulation over East Antarctica during the Holocene, *Climate Dynamics*, *24*(6), 641-654.

Delmonte, B., P. S. Andersson, M. Hansson, H. Schöberg, J. R. Petit, I. Basile-Doelsch, and V. Maggi (2008), Aeolian dust in East Antarctica (EPICA-Dome C and Vostok): Provenance during glacial ages over the last 800 kyr, *Geophys. Res. Lett.*, *35*(7), L07703.

Delmonte, B., I. Basile-Doelsch, J. R. Petit, V. Maggi, M. Revel-Rolland, A. Michard, E. Jagoutz, and F. Grousset (2004b), Comparing the Epica and Vostok dust records during the last 220,000 years: stratigraphical correlation and provenance in glacial periods, *Earth-Science Reviews*, *66*(1-2), 63-87.

Delmonte, B., P. S. Andersson, H. Schöberg, M. Hansson, J. R. Petit, R. Delmas, D. M. Gaiero, V. Maggi, and M. Frezzotti (2010a), Geographic provenance of aeolian dust in East Antarctica during Pleistocene glaciations: preliminary results from Talos Dome and comparison with East Antarctic and new Andean ice core data, *Quaternary Science Reviews*, *29*(1-2), 256-264.

Delmonte, B., C. Baroni, P. Andersson, B. Narcisi, M. Salvatore, J. Petit, C. Scarchilli, M. Frezzotti, S. Albani, and V. Maggi (2013), Modern and Holocene aeolian dust variability from Talos Dome (Northern Victoria Land) to the interior of the Antarctic ice sheet, *Quaternary Science Reviews*, *64*, 76-89.

Delmonte, B., et al. (2010b), Aeolian dust in the Talos Dome ice core (East Antarctica, Pacific/Ross Sea sector): Victoria Land versus remote sources over the last two climate cycles, *Journal of Quaternary Science*, *25*(8), 1327-1337.

Denton, G. H., and D. R. Marchant (2000), The Geologic Basis for a Reconstruction of a Grounded Ice Sheet in McMurdo Sound, Antarctica, at the Last Glacial Maximum, *Geografiska Annaler: Series A, Physical Geography*, *82*(2-3), 167-211.

Denton, G. H., and T. J. Hughes (2002), Reconstructing the Antarctic Ice Sheet at the Last Glacial Maximum, *Quaternary Science Reviews*, *21*(1-3), 193-202.

DePaolo, D. J., and G. J. Wasserburg (1976), Inferences about magma sources and mantle structure from variations of 143Nd/144Nd, *Geophys. Res. Lett.*, *3*(12), 743-746.

Desboeufs, K., A. Sofikitis, R. Losno, J. Colin, and P. Ausset (2005), Dissolution and solubility of trace metals from natural and anthropogenic aerosol particulate matter, *Chemosphere*, *58*(2), 195-203.

Desboeufs, K. V., R. Losno, F. Vimeux, and S. Cholbi (1999), The pH-dependent dissolution of wind-transported Saharan dust, *Journal of Geophysical Research: Atmospheres (1984–2012)*, *104*(D17), 21287-21299.

Desboeufs, K. V., A. Sofikitis, R. Losno, J. L. Colin, and P. Ausset (2005), Dissolution and solubility of trace metals from natural and anthropogenic aerosol particulate matter, *Chemosphere*, *58*(2), 195-203.

Dirksen, R. J., K. Folkert Boersma, J. De Laat, P. Stammes, G. R. Van Der Werf, M. Val Martin, and H. M. Kelder (2009), An aerosol boomerang: Rapid around-the-world transport of smoke from the December 2006 Australian forest fires observed from space, *Journal of Geophysical Research: Atmospheres (1984–2012)*, *114*(D21).

Donaghay, P., P. Liss, R. A. Duce, D. Kester, A. Hanson, T. Villareal, N. W. Tindale, and D. Gifford (1991), The role of episodic atmospheric nutrient input in the chemical and biological dynamics of ocean ice ecosystems, *Oceanography*, *4*, 62-70.

Dörr, H., B. Kromer, I. Levin, K. Münnich, and H. J. Volpp (1983), CO2 and Radon 222 as tracers for atmospheric transport, *Journal of Geophysical Research: Oceans (1978–2012)*, *88*(C2), 1309-1313.

Draxler, R. R., and G. D. Rolph (2003), Hybrid Single-Particle Lagrangian Integrated Trajectory (HYSPLIT), model, http://www.arl.noaa.gov/ready/hysplit4.html.

Duan, F., X. Liu, T. Yu, and H. Cachier (2004), Identification and estimate of biomass burning contribution to the urban aerosol organic carbon concentrations in Beijing, *Atmospheric Environment*, *38*(9), 1275-1282.

Duce, R. A., et al. (1991), The atmospheric input of trace species to the world ocean, *Global Biogeochem. Cycles*, *5*(3), 193-259.

Dulac, F., P. BUAT-MÉNARD, U. Ezat, S. Melki, and G. Bergametti (1989), Atmospheric input of trace metals to the western Mediterranean: uncertainties in modelling dry deposition from cascade impactor data, *Tellus B*, *41*(3), 362-378.

Dulaiova, H., M. Ardelan, P. B. Henderson, and M. A. Charette (2009), Shelf-derived iron inputs drive biological productivity in the southern Drake Passage, *Global Biogeochemical Cycles*, *23*(4).

Dunbar, G. B., N. A. N. Bertler, and R. M. McKay (2009), Sediment flux through the McMurdo Ice Shelf in Windless Bight, Antarctica, *Global and Planetary Change*, *69*(3), 87-93.

Duncan, B. N., R. V. Martin, A. C. Staudt, R. Yevich, and J. A. Logan (2003), Interannual and seasonal variability of biomass burning emissions constrained by satellite observations, *Journal of Geophysical Research: Atmospheres (1984–2012)*, *108*(D2), ACH 1-1-ACH 1-22.

Echalar, F., A. Gaudichet, H. Cachier, and P. Artaxo (1995), Aerosol emissions by tropical forest and savanna biomass burning: characteristic trace elements and fluxes, *Geophysical research letters*, *22*(22), 3039-3042.

Echalar, F., P. Artaxo, J. V. Martins, M. Yamasoe, F. Gerab, W. Maenhaut, and B. Holben (1998), Long-term monitoring of atmospheric aerosols in the Amazon Basin: Source identification and apportionment, *Journal of Geophysical Research: Atmospheres (1984–2012)*, *103*(D24), 31849-31864.

Edwards, P., P. Sedwick, V. Morgan, C. Boutron, and S. Hong (1998), Iron in ice cores from Law Dome, East Antarctica: implications for past deposition of aerosol iron, *Annals of Glaciology*, *27*, 365-370.

Edwards, R., and P. Sedwick (2001), Iron in East Antarctic snow: Implications for atmospheric iron deposition and algal production in Antarctic waters, *Geophys. Res. Lett.*, *28*(20), 3907-3910.

Edwards, R., P. Sedwick, V. Morgan, and C. Boutron (2006), Iron in ice cores from Law Dome: A record of atmospheric iron deposition for maritime East Antarctica during the Holocene and Last Glacial Maximum, *Geochemistry, Geophysics, Geosystems*, *7*(12), Q12Q01.

Elderfield, H. (1986), Strontium isotope stratigraphy, *Palaeogeography, Palaeoclimatology, Palaeoecology*, *57*(1), 71-90.

Elliot, D. H., T. H. Fleming, P. R. Kyle, and K. A. Foland (1999), Long-distance transport of magmas in the Jurassic Ferrar Large Igneous Province, Antarctica, *Earth and Planetary Science Letters*, *167*(1–2), 89-104.

Ellis, A., R. Edwards, M. Saunders, R. Chakrabarty, R. Subramanian, A. van Riessen, A. Smith, D. Lambrinidis, L. Nunes, and P. Vallelonga (2015), Characterizing black carbon in rain and ice cores using coupled tangential flow filtration and transmission electron microscopy.

Ellis, A., et al. (2015), Characterizing black carbon in rain and ice cores using coupled tangential flow filtration and transmission electron microscopy, *Atmos. Meas. Tech.*, *8*(9), 3959-3969.

Ellwood, M. J., D. A. Hutchins, M. C. Lohan, A. Milne, P. Nasemann, S. D. Nodder, S. G. Sander, R. Strzepek, S. W. Wilhelm, and P. W. Boyd (2015), Iron stable isotopes track pelagic iron cycling during a subtropical phytoplankton bloom, *Proceedings of the National Academy of Sciences*, *112*(1), E15-E20.

Elrod, V., W. Berelson, K. Coale, and K. Johnson (2004), The flux of iron from continental shelf sediments: a missing source for global budgets, *Geophys Res Lett*, *31*, L12307.

Ezat, U., and F. Dulac (1995), Size distribution of mineral aerosols at Amsterdam-island and dry deposition rates in the Southern Indian Ocean, *Comptes Rendus De L Acadmie Des Sciences Serie II*, *320*(1), 9-14.

Falkowski, P. G. (1997), Evolution of the nitrogen cycle and its influence on the biological sequestration of CO 2 in the ocean, *Nature*, *387*(6630), 272-275.

Faure, G. (1986), *Principles of Isotope Geology (2nd ed.)Wiley, New York (1986), p. 589*.

Ferek, R. J., J. S. Reid, P. V. Hobbs, D. R. Blake, and C. Liousse (1998), Emission factors of hydrocarbons, halocarbons, trace gases and particles from biomass burning in Brazil, *Journal of Geophysical Research: Atmospheres (1984–2012)*, *103*(D24), 32107-32118.

Field, R. D., G. R. van der Werf, and S. S. Shen (2009), Human amplification of drought-induced biomass burning in Indonesia since 1960, *Nature Geoscience*, *2*(3), 185-188.

Fishwick, M. P., P. N. Sedwick, M. C. Lohan, P. J. Worsfold, K. N. Buck, T. M. Church, and S. J. Ussher (2014), The impact of changing surface ocean conditions on the dissolution of aerosol iron, *Global Biogeochemical Cycles*, 2014GB004921.

Fitzwater, S. E., K. S. Johnson, R. M. Gordon, K. H. Coale, and W. O. Smith (2000), Trace metal concentrations in the Ross Sea and their relationship with nutrients and phytoplankton growth, *Deep Sea Research Part II: Topical Studies in Oceanography*, *47*(15-16), 3159-3179.

Fleming, T., K. Foland, and D. Elliot (1995), Isotopic and chemical constraints on the crustal evolution and source signature of Ferrar magmas, north Victoria Land, Antarctica, *Contributions to Mineralogy and Petrology*, *121*(3), 217-236.

Fomba, K., K. Müller, D. v. Pinxteren, and H. Herrmann (2012), Aerosol size-resolved trace metal composition in remote northern tropical Atlantic marine environment: case study Cape Verde Islands, *Atmospheric Chemistry and Physics Discussions*, *12*(11), 29535-29569.

Formenti, P., W. Elbert, W. Maenhaut, J. Haywood, S. Osborne, and M. Andreae (2003), Inorganic and carbonaceous aerosols during the Southern African Regional Science Initiative (SAFARI 2000) experiment: Chemical characteristics, physical properties, and emission data for smoke from African biomass burning, *Journal of Geophysical Research: Atmospheres (1984–2012)*, *108*(D13).

Frenklach, M. (2002), Reaction mechanism of soot formation in flames, *Physical Chemistry Chemical Physics*, *4*(11), 2028-2037.

Freydier, R., A. Michard, G. De Lange, and J. Thomson (2001), Nd isotopic compositions of Eastern Mediterranean sediments: tracers of the Nile influence during sapropel S1 formation?, *Marine Geology*, *177*(1), 45-62.

Friedman, B., H. Herich, L. Kammermann, D. S. Gross, A. Arneth, T. Holst, and D. J. Cziczo (2009), Subarctic atmospheric aerosol composition: 1. Ambient aerosol characterization, *Journal of Geophysical Research: Atmospheres (1984–2012)*, *114*(D13).

Fu, H., G. Shang, J. Lin, Y. Hu, Q. Hu, L. Guo, Y. Zhang, and J. Chen (2014), Fractional iron solubility of aerosol particles enhanced by biomass burning and ship emission in Shanghai, East China, *Science of The Total Environment*, *481*, 377-391.

Futa, K., and W. Le Masurier (1983), Nd and Sr isotopic studies on Cenozoic mafic lavas from West Antarctica: Another source for continental alkali basalts, *Contributions to Mineralogy and Petrology*, *83*(1-2), 38-44.

Gabric, A. J., R. A. Cropp, G. H. McTainsh, B. M. Johnston, H. Butler, B. Tilbrook, and M. Keywood (2010), Australian dust storms in 2002–2003 and their impact on Southern Ocean biogeochemistry, *Global Biogeochemical Cycles*, *24*(2).

Gabrielli, P., A. Wegner, J. R. Petit, B. Delmonte, P. De Deckker, V. Gaspari, H. Fischer, U. Ruth, M. Kriews, and C. Boutron (2010a), A major glacial-interglacial change in aeolian dust composition inferred from Rare Earth Elements in Antarctic ice, *Quaternary Science Reviews*, *29*(1), 265-273.

Gabrielli, P., et al. (2010b), A major glacial-interglacial change in aeolian dust composition inferred from Rare Earth Elements in Antarctic ice, *Quaternary Science Reviews*, *29*(1-2), 265-273.

Gaiero, D. M. (2008), Reply to comment by B. Delmonte et al. on "Dust provenance in Antarctic ice during glacial periods: From where in southern South America?", *Geophysical Research Letters*, *35*(8).

Gaiero, D. M., F. Brunet, J.-L. Probst, and P. J. Depetris (2007), A uniform isotopic and chemical signature of dust exported from Patagonia: Rock sources and occurrence in southern environments, *Chemical Geology*, *238*(1), 107-120.

Gaiero, D. M., J.-L. Probst, P. J. Depetris, S. M. Bidart, and L. Leleyter (2003), Iron and other transition metals in Patagonian riverborne and windborne materials: geochemical control and transport to the southern South Atlantic Ocean, *Geochimica et Cosmochimica Acta*, *67*(19), 3603-3623.

Gao, S., D. A. Hegg, and H. Jonsson (2003), Aerosol chemistry, and light-scattering and hygroscopicity budgets during outflow from East Asia, *Journal of Atmospheric Chemistry*, *46*(1), 55-88.

Gao, Y., Y. J. Kaufman, D. Tanré, D. Kolber, and P. G. Falkowski (2001), Seasonal distributions of aeolian iron fluxes to the global ocean, *Geophys. Res. Lett.*, *28*(1), 29-32.

Gao, Y., G. Xu, J. Zhan, J. Zhang, W. Li, Q. Lin, L. Chen, and H. Lin (2013), Spatial and particle size distributions of atmospheric dissolvable iron in aerosols and its input to the Southern Ocean and coastal East Antarctica, *Journal of Geophysical Research: Atmospheres*, *118*(22), 12,634-612,648.

Gaspari, V., C. Barbante, G. Cozzi, P. Cescon, C. F. Boutron, P. Gabrielli, G. Capodaglio, C. Ferrari, J. R. Petit, and B. Delmonte (2006), Atmospheric iron fluxes over the last deglaciation: Climatic implications, *Geophys. Res. Lett.*, *33*(3), L03704.

Gatehouse, R. D., I. Williams, and B. Pillans (2001), Fingerprinting windblown dust in south-eastern Australian soils by uranium-lead dating of detrital zircon, *Soil Research*, *39*(1), 7-12.

Gaudichel, A., M. De Angelis, S. Joussaume, J. Petit, Y. Korotkevitch, and V. Petrov (1992), Comments on the origin of dust in East Antarctica for present and ice age conditions, *Journal of atmospheric chemistry*, *14*(1-4), 129-142.

Gerringa, L. J. A., P. Laan, G. L. van Dijken, H. van Haren, H. J. W. De Baar, K. R. Arrigo, and A. C. Alderkamp (2015), Sources of iron in the Ross Sea Polynya in early summer, *Marine Chemistry*, *177, Part 3*, 447-459.

Gerringa, L. J. A., P. Laan, G. L. van Dijken, H. van Haren, H. J. W. De Baar, K. R. Arrigo, and A. C. Alderkamp (in press), Sources of iron in the Ross Sea polynya in early summer, *Marine Chemistry*, http://dx.doi.org/10.1016/j.marchem.2015.06.002.

Gerringa, L. J. A., A.-C. Alderkamp, P. Laan, C.-E. Thuróczy, H. J. W. De Baar, M. M. Mills, G. L. van Dijken, H. v. Haren, and K. R. Arrigo (2012), Iron from melting glaciers fuels the phytoplankton blooms in Amundsen Sea (Southern Ocean): Iron biogeochemistry, *Deep Sea Research Part II: Topical Studies in Oceanography*, *71–76*(0), 16-31.

Gibbs, R., M. Mathews, and D. Unk (1971), The relationship between sphere size and settling velocity, *Journal of Sedimentary Petrology*, *41*(1), 7-18.

Giglio, L., J. T. Randerson, and G. R. Werf (2013), Analysis of daily, monthly, and annual burned area using the fourth-generation global fire emissions database (GFED4), *Journal of Geophysical Research: Biogeosciences*, *118*(1), 317-328.

Gillies, J. A., W. G. Nickling, and M. Tilson (2013), Frequency, magnitude, and characteristics of aeolian sediment transport: McMurdo Dry Valleys, Antarctica, *Journal of Geophysical Research: Earth Surface*, *118*(2), 461-479.

Gingele, F., and P. De Deckker (2005), Clay mineral, geochemical and Sr–Nd isotopic fingerprinting of sediments in the Murray–Darling fluvial system, southeast Australia, *Australian Journal of Earth Sciences*, *52*(6), 965-974.

Glassman, I. (1989), Soot formation in combustion processes, paper presented at Symposium (international) on combustion, Elsevier.

Gore, D., E. Rhodes, P. Augustinus, M. Leishman, E. Colhoun, and J. Rees-Jones (2001), Bunger Hills, East Antarctica: ice free at the last glacial maximum, *Geology*, *29*(12), 1103-1106.

Grand, M. M., C. I. Measures, M. Hatta, W. T. Hiscock, C. S. Buck, and W. M. Landing (2015a), Dust deposition in the eastern Indian Ocean: The ocean perspective from Antarctica to the Bay of Bengal, *Global Biogeochemical Cycles*.

Grand, M. M., C. I. Measures, M. Hatta, P. L. Morton, P. Barrett, A. Milne, J. A. Resing, and W. M. Landing (2015b), The impact of circulation and dust deposition in controlling the distributions of dissolved Fe and Al in the south Indian subtropical gyre, *Marine Chemistry*, *176*, 110-125.

Grand, M. M., C. I. Measures, M. Hatta, W. T. Hiscock, W. M. Landing, P. L. Morton, C. S. Buck, P. M. Barrett, and J. A. Resing (2015), Dissolved Fe and Al in the upper 1000 m of the eastern Indian Ocean: A high-resolution transect along 95°E from the Antarctic margin to the Bay of Bengal, *Global Biogeochemical Cycles*, *29*(3), 375-396.

Greeley, R., and J. Iversen (1985), Wind as a geological process, no. 4 in Cambridge Planetary Science Series, *Cambridge Univ. Press, New York, NY*, *3*(3), 3.2.

Grousset, F., P. Rognon, G. Coudé-Gaussen, and P. Pédemay (1992), Origins of peri-Saharan dust deposits traced by their Nd and Sr isotopic composition, *Palaeogeography, Palaeoclimatology, Palaeoecology*, *93*(3), 203-212.

Grousset, F. E., and P. E. Biscaye (2005), Tracing dust sources and transport patterns using Sr, Nd and Pb isotopes, *Chemical Geology*, *222*(3-4), 149-167.

Grousset, F. E., P. E. Biscaye, A. Zindler, J. Prospero, and R. Chester (1988), Neodymium isotopes as tracers in marine sediments and aerosols: North Atlantic, *Earth and Planetary Science Letters*, *87*(4), 367-378.

Grousset, F. E., P. E. Biscaye, M. Revel, J.-R. Petit, K. Pye, S. Joussaume, and J. Jouzel (1992), Antarctic (Dome C) ice-core dust at 18 ky BP: Isotopic constraints on origins, *Earth and Planetary Science Letters*, *111*(1), 175-182.

Grousset, F. E., P. E. Biscaye, M. Revel, J.-R. Petit, K. Pye, S. Joussaume, and J. Jouzel (1992), Antarctic (Dome C) ice-core dust at 18 k.y. B.P.: Isotopic constraints on origins, *Earth and Planetary Science Letters*, *111*(1), 175-182.

Guieu, C., S. Bonnet, T. Wagener, and M. D. Loÿe-Pilot (2005), Biomass burning as a source of dissolved iron to the open ocean?, *Geophysical Research Letters*, *32*(19).

Guieu, C., et al. (2014), The significance of the episodic nature of atmospheric deposition to Low Nutrient Low Chlorophyll regions, *Global Biogeochemical Cycles*, 2014GB004852.

Gysel, M., M. Laborde, J. Olfert, R. Subramanian, and A. Gröhn (2011), Effective density of Aquadag and fullerene soot black carbon reference materials used for SP2 calibration, *Atmospheric Measurement Techniques*, *4*(12), 2851-2858.

Halstead, M. J., R. G. Cunninghame, and K. A. Hunter (2000), Wet deposition of trace metals to a remote site in Fiordland, New Zealand, *Atmospheric Environment*, *34*(4), 665-676.

Hand, J. L., N. M. Mahowald, Y. Chen, R. L. Siefert, C. Luo, A. Subramaniam, and I. Fung (2004), Estimates of atmospheric-processed soluble iron from observations and a global mineral aerosol model: Biogeochemical implications, *J. Geophys. Res.*, *109*(D17), D17205.

Hao, W. M., and M. H. Liu (1994), Spatial and temporal distribution of tropical biomass burning, *Global biogeochemical cycles*, *8*(4), 495-503.

Hasegawa, S., and S. Ohta (2002), Some measurements of the mixing state of soot-containing particles at urban and non-urban sites, *Atmospheric Environment*, *36*(24), 3899-3908.

Hayes, C. T., J. N. Fitzsimmons, E. A. Boyle, D. McGee, R. F. Anderson, R. Weisend, and P. L. Morton (2015), Thorium isotopes tracing the iron cycle at the Hawaii Ocean Time-series Station ALOHA, *Geochimica et Cosmochimica Acta*, *169*, 1-16.

Heimburger, A., R. Losno, and S. Triquet (2013), Solubility of iron and other trace elements in rainwater collected on the Kerguelen Islands (South Indian Ocean), *Biogeosciences*, *10*(10).

Heimburger, A., R. Losno, S. Triquet, and E. B. Nguyen (2013), Atmospheric deposition fluxes of 26 elements over the Southern Indian Ocean: Time series on Kerguelen and Crozet Islands, *Global Biogeochemical Cycles*, *27*(2), 440-449.

Heimburger, A., R. Losno, S. Triquet, F. Dulac, and N. Mahowald (2012), Direct measurements of atmospheric iron, cobalt, and aluminum-derived dust deposition at Kerguelen Islands, *Global Biogeochemical Cycles*, *26*(4).

Hesse, P. P. (1994), The record of continental dust from Australia in Tasman Sea sediments, *Quaternary Science Reviews*, *13*(3), 257-272.

Hesse, P. P. (1997), Mineral magnetic 'tracing'of aeolian dust in southwest Pacific sediments, *Palaeogeography, Palaeoclimatology, Palaeoecology*, *131*(3), 327-353.

Hesse, P. P., and G. H. McTainsh (2003), Australian dust deposits: modern processes and the Quaternary record, *Quaternary Science Reviews*, *22*(18), 2007-2035.

Hinkley, T. K., and A. Matsumoto (2001), Atmospheric regime of dust and salt through 75,000 years of Taylor Dome ice core: Refinement by measurement of major, minor, and trace metal suites, *J. Geophys. Res.*, *106*(D16), 18487-18493.

Hoelzemann, J. J., M. G. Schultz, G. P. Brasseur, C. Granier, and M. Simon (2004), Global Wildland Fire Emission Model (GWEM): Evaluating the use of global area burnt satellite data, *Journal of Geophysical Research: Atmospheres (1984–2012)*, *109*(D14).

Hoffer, A., A. Gelencsér, P. Guyon, G. Kiss, O. Schmid, G. Frank, P. Artaxo, and M. Andreae (2005), Optical properties of humiclike substances (HULIS) in biomass-burning aerosols, *Atmos. Chem. Phys. Discuss*, *5*(4), 7341-7360.

Hole, M., and W. LeMasurier (1994), Tectonic controls on the geochemical composition of Cenozoic, mafic alkaline volcanic rocks from West Antarctica, *Contributions to Mineralogy and Petrology*, *117*(2), 187-202.

Hope, B. K. (2008), A dynamic model for the global cycling of anthropogenic vanadium, *Global Biogeochemical Cycles*, *22*(4).

Huang, X., T. Gordon, W. N. Rom, and R. B. Finkelman (2006), Interaction of iron and calcium minerals in coals and their roles in coal dust-induced health and environmental problems, *Reviews in mineralogy and geochemistry*, *64*(1), 153-178.

Huang, X., Y. Song, C. Zhao, M. Li, T. Zhu, Q. Zhang, and X. Zhang (2014), Pathways of sulfate enhancement by natural and anthropogenic mineral aerosols in China, *Journal of Geophysical Research: Atmospheres*.

Hurst, M. P., and K. W. Bruland (2007), An investigation into the exchange of iron and zinc between soluble, colloidal, and particulate size-fractions in shelf waters using low-abundance isotopes as tracers in shipboard incubation experiments, *Marine chemistry*, *103*(3), 211-226.

Hutchins, D. A., G. R. DiTullio, and K. W. Bruland (1993), Iron and Regenerated Production: Evidence for Biological Iron Recycling in Two Marine Environments, *Limnology and Oceanography*, *38*(6), 1242-1255.

Ito, A. (2011), Mega fire emissions in Siberia: potential supply of bioavailable iron from forests to the ocean, *Biogeosciences*, *8*(6).

Ito, A. (2012), Contrasting the effect of iron mobilization on soluble iron deposition to the ocean in the Northern and Southern Hemispheres, *Meteorol. Soc. Japan*, *90*(0), 167-188.

Ito, A. (2013), Global modeling study of potentially bioavailable iron input from shipboard aerosol sources to the ocean, *Global Biogeochemical Cycles*, *27*(1), 1-10.

Ito, A. (2015), Atmospheric Processing of Combustion Aerosols as a Source of Bioavailable Iron, *Environmental Science & Technology Letters*, *2*(3), 70-75.

Ito, A., and J. E. Penner (2004), Global estimates of biomass burning emissions based on satellite imagery for the year 2000, *Journal of Geophysical Research: Atmospheres (1984–2012)*, *109*(D14).

Ito, A., and Z. Shi (2015), Delivery of anthropogenic bioavailable iron from mineral dust and combustion aerosols to the ocean, *Atmospheric Chemistry and Physics Discussions*, *15*(16), 23051-23088.

Jacobs, S. S., A. F. Amos, and P. M. Bruchhausen (1970), Ross sea oceanography and antarctic bottom water formation, *Deep Sea Research and Oceanographic Abstracts*, *17*(6), 935-962.

Jacobsen, S. B., and G. J. Wasserburg (1980), Sm-Nd isotopic evolution of chondrites, *Earth and Planetary Science Letters*, *50*(1), 139-155.

Jacobson, M. Z. (2003), Development of mixed-phase clouds from multiple aerosol size distributions and the effect of the clouds on aerosol removal, *Journal of Geophysical Research: Atmospheres (1984–2012)*, *108*(D8).

Jang, H.-N., Y.-C. Seo, J.-H. Lee, K.-W. Hwang, J.-I. Yoo, C.-H. Sok, and S.-H. Kim (2007), Formation of fine particles enriched by V and Ni from heavy oil combustion: Anthropogenic sources and drop-tube furnace experiments, *Atmospheric Environment*, *41*(5), 1053-1063.

Jeong, D., K. Kim, and W. Choi (2012), Accelerated dissolution of iron oxides in ice, *Atmospheric Chemistry and Physics*, *12*(22), 11125-11133.

Jickells, T., et al. (2005), Global iron connections between desert dust, ocean biogeochemistry, and climate, *Science*, *308*, 67 - 73.

Jochum, K. P., U. Nohl, K. Herwig, E. Lammel, B. Stoll, and A. W. Hofmann (2005), GeoReM: A New Geochemical Database for Reference Materials and Isotopic Standards, *Geostandards and Geoanalytical Research*, *29*(3), 333-338.

Johnsen, S. J., W. Dansgaard, H. B. Clausen, and C. C. Langway (1972), Oxygen Isotope Profiles through the Antarctic and Greenland Ice Sheets, *Nature*, *235*(5339), 429-434.

Johnson, B., B. Heese, S. McFarlane, P. Chazette, A. Jones, and N. Bellouin (2008), Vertical distribution and radiative effects of mineral dust and biomass burning aerosol over West Africa during DABEX, *Journal of Geophysical Research: Atmospheres (1984–2012)*, *113*(D23).

Johnson, K., F. Chavez, and G. Friederich (1999), Continental-shelf sediment as a primary source of iron for coastal phytoplankton, *Nature*, *398*, 697 - 700.

Johnson, K., K. Coale, V. Elrod, and W. Tindale (1994), Iron photochemistry in seawater from the equatorial Pacific, *Mar Chem*, *46*, 319 - 334.

Johnson, K. S., R. M. Gordon, and K. H. Coale (1997), What controls dissolved iron concentrations in the world ocean?, *Marine Chemistry*, *57*(3), 137-161.

Johnson, M. S., N. Meskhidze, V. P. Kiliyanpilakkil, and S. Gassó (2010), Understanding the transport of Patagonian dust and its influence on marine biological activity in the South Atlantic Ocean, *Atmos. Chem. Phys. Discuss.*, *10*(11), 27283-27320.

Johnston, S. W. (2001), The influence of aeolian dust deposits on alpine soils in south-eastern Australia, *Soil Research*, *39*(1), 81-88.

Jong, J., V. Schoemann, D. Lannuzel, P. Croot, H. Baar, and J. L. Tison (2012), Natural iron fertilization of the Atlantic sector of the Southern Ocean by continental shelf sources of the Antarctic Peninsula, *Journal of Geophysical Research: Biogeosciences (2005–2012)*, *117*(G1).

Kadko, D., W. M. Landing, and R. U. Shelley (2015), A novel tracer technique to quantify the atmospheric flux of trace elements to remote ocean regions, *Journal of Geophysical Research: Oceans*.

Kalinske, A. A. (1943), Turbulence and the transport of sand and silt by wind, *Annals of the New York Academy of Sciences*, *44*(1), 41-54.

Kasischke, E. S., and J. E. Penner (2004), Improving global estimates of atmospheric emissions from biomass burning, *Journal of Geophysical Research: Atmospheres (1984–2012)*, *109*(D14).

Kellogg, T. B., D. Kellogg, and M. Stuiver (1990), Late Quaternary History of the Southwestern Ross Sea: Evidence from Debris Bands on the McMurdo Ice Shelf, Antarctica, *Antarctic Res. Ser. (AGU)*, *50*, 25-56.

Keywood, M., M. Cope, C. M. Meyer, Y. Iinuma, and K. Emmerson (2015), When smoke comes to town: The impact of biomass burning smoke on air quality, *Atmospheric Environment*.

Keywood, M., M. Kanakidou, A. Stohl, F. Dentener, G. Grassi, C. Meyer, K. Torseth, D. Edwards, A. M. Thompson, and U. Lohmann (2013), Fire in the air: biomass burning impacts in a changing climate, *Critical Reviews in Environmental Science and Technology*, *43*(1), 40-83.

Keywood, M. D. (2007), Aerosol composition at Cape Grim : an evaluation of PM10 sampling program and baseline event switches., *Baseline Atmospheric Program Australia 2005-2006. 2005-2006 ed. J. M. Cainey, N. Derek, and P. B. Krummel (editors). Melbourne: Australian Bureau of Meteorology and CSIRO Marine and Atmospheric Research*, 31-36.

Keywood, M. D., B. Graham, R. W. Gillett, J. G. Gras, and P. W. Selleck (2004), High volume aerosol sampler. Baseline Atmospheric Program (Australia) 2001-200 edited by J. Cainey, N.Derek and P.Krummel. .Bureau of Meteorology CSIRO Atmospheric Research and, Melbourne, Australia: 74-77.

Khalizov, A. F., H. Xue, L. Wang, J. Zheng, and R. Zhang (2009), Enhanced light absorption and scattering by carbon soot aerosol internally mixed with sulfuric acid, *The Journal of Physical Chemistry A*, *113*(6), 1066-1074.

Kipling, Z., P. Stier, J. Schwarz, A. Perring, J. Spackman, G. Mann, C. Johnson, and P. Telford (2013), Constraints on aerosol processes in climate models from vertically-resolved aircraft observations of black carbon, *Atmospheric Chemistry and Physics*, *13*(12), 5969.

Knight, A. W., G. McTainsh, and R. Simpson (1995), Sediment loads in an Australian dust storm: implications for present and past dust processes, *Catena*, *24*(3), 195-213.

Kobayashi, H., K. Hara, M. Shiobara, T. Yamanouchi, K. Osada, and S. Ohta (2010), Seasonal variation of carbonaceous and metal compositions of atmospheric aerosols at Syowa Station, Antarctica in 2001, *Antarctic Record(Tokyo)*, *54*, 554-561.

Koffman, B., K. Kreutz, D. Breton, E. Kane, D. Winski, S. Birkel, A. Kurbatov, and M. Handley (2014), Centennial-scale variability of the Southern Hemisphere westerly wind belt in the eastern Pacific over the past two millennia, *Climate of the Past*, *10*(3), 1125-1144.

Koffman, B. G., M. J. Handley, E. C. Osterberg, M. L. Wells, and K. J. Kreutz (2014), Dependence of ice-core relative trace-element concentration on acidification, *Journal of Glaciology*, *60*(219), 103-112.

Kohfeld, K. E., and S. P. Harrison (2001), DIRTMAP: the geological record of dust, *Earth-Science Reviews*, *54*(1-3), 81-114.

Kok, J. F. (2011a), Does the size distribution of mineral dust aerosols depend on the wind speed at emission?, *Atmospheric Chemistry and Physics*, *11*(19), 10149-10156.

Kok, J. F. (2011b), A scaling theory for the size distribution of emitted dust aerosols suggests climate models underestimate the size of the global dust cycle, *Proceedings of the National Academy of Sciences*, *108*(3), 1016-1021.

Koppmann, R., K. v. Czapiewski, and J. Reid (2005), A review of biomass burning emissions, part I: gaseous emissions of carbon monoxide, methane, volatile organic compounds, and nitrogen containing compounds, *Atmospheric Chemistry and Physics Discussions*, *5*(5), 10455-10516.

Kraemer, S. (2004), Iron oxide dissolution and solubility in the presence of siderophores, *Aquatic Sciences - Research Across Boundaries*, *66*(1), 3-18.

Kraemer, S. M., A. Butler, P. Borer, and J. Cervini-Silva (2005), Siderophores and the Dissolution of Iron-Bearing Minerals in Marine Systems, *Reviews in Mineralogy and Geochemistry*, *59*(1), 53-84.

Krinner, G., and C. Genthon (2003), Tropospheric transport of continental tracers towards Antarctica under varying climatic conditions, *Tellus B*, *55*(1), 54-70.

Krinner, G., J.-R. Petit, and B. Delmonte (2010), Altitude of atmospheric tracer transport towards Antarctica inpresent and glacial climate, *Quaternary science reviews*, *29*(1), 274-284.

Kuma, K., and K. Matsunaga (1995), Availability of colloidal ferric oxides to coastal marine phytoplankton, *Marine Biology*, *122*(1), 1-11.

Kumar, A., M. Sarin, and B. Srinivas (2010), Aerosol iron solubility over Bay of Bengal: Role of anthropogenic sources and chemical processing, *Marine Chemistry*, *121*(1), 167-175.

Kustka, A. B., S. A. Sañudo-Wilhelmy, E. J. Carpenter, D. Capone, J. Burns, and W. G. Sunda (2003), Iron requirements for dinitrogen-and ammonium-supported growth in cultures of Trichodesmium (IMS 101): Comparison with nitrogen fixation rates and iron: Carbon ratios of field populations, *Limnology and Oceanography*, *48*(5), 1869-1884.

Kustka, A. B., et al. (2015), The roles of MCDW and deep water iron supply in sustaining a recurrent phytoplankton bloom on central Pennell Bank (Ross Sea), *Deep Sea Research Part I: Oceanographic Research Papers*, *105*, 171-185.

Laborde, M., P. Mertes, P. Zieger, J. Dommen, U. Baltensperger, and M. Gysel (2012), Sensitivity of the Single Particle Soot Photometer to different black carbon types, *Atmospheric Measurement Techniques*, *5*(5), 1031-1043.

Lamarque, J.-F., T. C. Bond, V. Eyring, C. Granier, A. Heil, Z. Klimont, D. Lee, C. Liousse, A. Mieville, and B. Owen (2010), Historical (1850–2000) gridded anthropogenic and biomass burning emissions of reactive gases and aerosols: methodology and application, *Atmospheric Chemistry and Physics*, *10*(15), 7017-7039.

Lambert, F., A. Tagliabue, G. Shaffer, F. Lamy, G. Winckler, L. Farias, L. Gallardo, and R. De Pol-Holz (2015), Dust fluxes and iron fertilization in Holocene and Last Glacial Maximum climates, *Geophysical Research Letters*, n/a-n/a.

Lambert, F., B. Delmonte, J. R. Petit, M. Bigler, P. R. Kaufmann, M. A. Hutterli, T. F. Stocker, U. Ruth, J. P. Steffensen, and V. Maggi (2008), Dust-climate couplings over the past 800,000[thinsp]years from the EPICA Dome C ice core, *Nature*, *452*(7187), 616-619.

Lancaster, N., W. G. Nickling, and J. A. Gillies (2010), Sand transport by wind on complex surfaces: Field studies in the McMurdo Dry Valleys, Antarctica, *Journal of Geophysical Research: Earth Surface (2003–2012)*, *115*(F3).

Lanci, L., B. Delmonte, V. Maggi, J. R. Petit, and D. V. Kent (2008), Ice magnetization in the EPICA-Dome C ice core: Implication for dust sources during glacial and interglacial periods, *J. Geophys. Res.*, *113*(D14), D14207.

Lane, S., B. C. Proemse, A. Tennant, and M. E. Wieser (2013), Concentration measurements and isotopic composition of airborne molybdenum collected in an urban environment, *Analytical and bioanalytical chemistry*, *405*(9), 2957-2963.

Lannuzel, D., V. Schoemann, J. de Jong, J.-L. Tison, and L. Chou (2007), Distribution and biogeochemical behaviour of iron in the East Antarctic sea ice, *Marine Chemistry*, *106*(1-2), 18-32.

Lannuzel, D., V. Schoemann, J. de Jong, J. Tison, and L. Chou (2007), Distribution and biogeochemical behaviour of iron in the East Antarctic sea ice, *Marine Chemistry*, *106*(1-2), 18-32.

Lannuzel, D., V. Schoemann, J. de Jong, L. Chou, B. Delille, S. Becquevort, and J. Tison (2008), Iron study during a time series in the western Weddell pack ice, *Marine Chemistry*, *108*(1-2), 85-95.

Lannuzel, D., V. Schoemann, J. de Jong, B. Pasquer, P. van der Merwe, F. Masson, J.-L. Tison, and A. Bowie (2010), Distribution of dissolved iron in Antarctic sea ice: Spatial, seasonal, and inter-annual variability, *J. Geophys. Res.*, *115*(G3), G03022.

LaRoche, J., and E. Breitbarth (2005), Importance of the diazotrophs as a source of new nitrogen in the ocean, *Journal of Sea Research*, *53*(1), 67-91.

Latimer, J. C., and G. M. Filippelli (2001), Terrigenous input and paleoproductivity in the Southern Ocean, *Paleoceanography*, *16*(6), 627-643.

Latimer, J. C., G. M. Filippelli, I. L. Hendy, J. D. Gleason, and J. D. Blum (2006), Glacial-interglacial terrigenous provenance in the southeastern Atlantic Ocean: The importance of deep-water sources and surface currents, *Geology*, *34*(7), 545-548.

Law, C., E. Woodward, M. Ellwood, A. Marriner, S. Bury, and K. Safi (2011), Response of surface nutrient inventories and nitrogen fixation to a tropical cyclone in the southwest Pacific, *Limnology and Oceanography*, *56*(4), 1372-1385.

le Roux, J. P. (1994), An alternative approach to the identification of net sediment transport paths based on grain-size trends, *Sedimentary Geology*, *94*(1-2), 97-107.

Legrand, M., and S. Kirchner (1988), Polar atmospheric circulation and chemistry of recent (1957-1983) south polar precipitation, *Geophysical research letters*, *15*(8), 879-882.

Lenes, J., B. Darrow, J. Walsh, J. Prospero, R. He, R. Weisberg, G. Vargo, and C. Heil (2008), Saharan dust and phosphatic fidelity: A three-dimensional biogeochemical model of Trichodesmium as a nutrient source for red tides on the West Florida Shelf, *Continental Shelf Research*, *28*(9), 1091-1115.

Li, F., P. Ginoux, and V. Ramaswamy (2008), Distribution, transport, and deposition of mineral dust in the Southern Ocean and Antarctica: Contribution of major sources, *J. Geophys. Res.*, *113*(D10), D10207.

Lin, Y. C., J. P. Chen, T. Y. Ho, and I. Tsai (2015), Atmospheric iron deposition in the northwestern Pacific Ocean and its adjacent marginal seas: The importance of coal burning, *Global Biogeochemical Cycles*, *29*(2), 138-159.

Lis, H., Y. Shaked, C. Kranzler, N. Keren, and F. M. M. Morel (2015), Iron bioavailability to phytoplankton: an empirical approach, *ISME J*, *9*(4), 1003-1013.

Liu, J., S. Fan, L. W. Horowitz, and H. Levy (2011), Evaluation of factors controlling long-range transport of black carbon to the Arctic, *Journal of Geophysical Research: Atmospheres (1984–2012)*, *116*(D4).

Liu, J., D. L. Mauzerall, L. W. Horowitz, P. Ginoux, and A. M. Fiore (2009), Evaluating inter-continental transport of fine aerosols:(1) Methodology, global aerosol distribution and optical depth, *Atmospheric Environment*, *43*(28), 4327-4338.

Lohmann, U., J. Feichter, J. Penner, and R. Leaitch (2000), Indirect effect of sulfate and carbonaceous aerosols- A mechanistic treatment, *Journal of Geophysical Research*, *105*(D10), 12193-12206.

Lu, H., and Y. Shao (2001), Toward quantitative prediction of dust storms: an integrated wind erosion modelling system and its applications, *Environmental Modelling & Software*, *16*(3), 233-249.

Luo, C., N. M. Mahowald, and J. del Corral (2003), Sensitivity study of meteorological parameters on mineral aerosol mobilization, transport, and distribution, *J. Geophys. Res.*, *108*(D15), 4447.

Luo, C., N. M. Mahowald, N. Meskhidze, Y. Chen, R. L. Siefert, A. R. Baker, and A. M. Johansen (2005), Estimation of iron solubility from observations and a global aerosol model, *J. Geophys. Res.*, *110*(D23), D23307.

Luo, C., N. Mahowald, T. Bond, P. Y. Chuang, P. Artaxo, R. Siefert, Y. Chen, and J. Schauer (2008), Combustion iron distribution and deposition, *Global Biogeochem. Cycles*, *22*(1), GB1012.

Mackie, D., J. Peat, G. H. McTainsh, P. Boyd, and K. Hunter (2006), Soil abrasion and eolian dust production: Implications for iron partitioning and solubility, *Geochemistry, Geophysics, Geosystems*, *7*(12).

Mackie, D. S., P. W. Boyd, K. A. Hunter, and G. H. McTainsh (2005), Simulating the cloud processing of iron in Australian dust: pH and dust concentration, *Geophys. Res. Lett.*, *32*(6), L06809.

Mackie, D. S., P. W. Boyd, G. H. McTainsh, N. W. Tindale, T. K. Westberry, and K. A. Hunter (2008), Biogeochemistry of iron in Australian dust: From eolian uplift to marine uptake, *Geochem. Geophys. Geosyst.*, *9*(3), Q03Q08.

Macpherson, A. (1987), The MacKay Glacier/Granite Harbour system (Ross Dependency, Antarctica). A study in nearshore glacial marine sedimentation, 85 pp, Victoria University of Wellington, Wellington.

Maenhaut, W., M.-T. Fernández-Jiménez, I. Rajta, and P. Artaxo (2002), Two-year study of atmospheric aerosols in Alta Floresta, Brazil: Multielemental composition and source apportionment, *Nuclear Instruments and Methods in Physics Research Section B: Beam Interactions with Materials and Atoms*, *189*(1), 243-248.

Maenhaut, W., I. Salma, J. Cafmeyer, H. J. Annegarn, and M. O. Andreae (1996), Regional atmospheric aerosol composition and sources in the eastern Transvaal, South Africa, and impact of biomass burning, *JOURNAL OF GEOPHYSICAL RESEARCH-ALL SERIES-*, *101*, 23,631-623,650.

Magee, J., J. Bowler, G. Miller, and D. Williams (1995), Stratigraphy, sedimentology, chronology and palaeohydrology of Quaternary lacustrine deposits at Madigan Gulf, Lake Eyre, South Australia, *Palaeogeography, Palaeoclimatology, Palaeoecology*, *113*(1), 3-42.

Mahowald, N., K. Kohfeld, M. Hansson, Y. Balkanski, S. P. Harrison, I. C. Prentice, M. Schulz, and H. Rodhe (1999), Dust sources and deposition during the last glacial maximum

and current climate: A comparison of model results with paleodata from ice cores and marine sediments, *J. Geophys. Res.*, *104*(D13), 15895-15916.

Mahowald, N. M., A. R. Baker, G. Bergametti, N. Brooks, R. A. Duce, T. D. Jickells, N. Kubilay, J. M. Prospero, and I. Tegen (2005), Atmospheric global dust cycle and iron inputs to the ocean, *Global Biogeochem. Cycles*, *19*(4), GB4025.

Mahowald, N. M., S. Engelstaedter, C. Luo, A. Sealy, P. Artaxo, C. Benitez-Nelson, S. Bonnet, Y. Chen, P. Y. Chuang, and D. D. Cohen (2009), Atmospheric iron deposition: Global distribution, variability, and human perturbations*, *Marine Science*, *1*.

Mahowald, N. M., et al. (2010), Observed 20th century desert dust variability: impact on climate and biogeochemistry, *Atmos. Chem. Phys.*, *10*(22), 10875-10893.

Marino, F., E. Castellano, D. Ceccato, P. De Deckker, B. Delmonte, G. Ghermandi, V. Maggi, J. R. Petit, M. Revel-Rolland, and R. Udisti (2008), Defining the geochemical composition of the EPICA Dome C ice core dust during the last glacial-interglacial cycle, *Geochem. Geophys. Geosyst.*, *9*(10), Q10018.

Marsay, C., P. N. Sedwick, M. Dinniman, P. Barrett, S. Mack, and D. J. McGillicuddy (2014), Estimating the benthic efflux of dissolved iron on the Ross Sea continental shelf, *Geophysical Research Letters*, *41*(21), 7576-7583.

Marticorena, B., and G. Bergametti (1995), Modeling the atmospheric dust cycle: 1. Design of a soil-derived dust emission scheme, *J. Geophys. Res.*, *100*(D8), 16415-16430.

Martin, C. E., and M. T. McCulloch (1999), Nd-Sr isotopic and trace element geochemistry of river sediments and soils in a fertilized catchment, New South Wales, Australia, *Geochimica et cosmochimica acta*, *63*(2), 287-305.

Martin, J. H. (1990), Glacial-interglacial CO2 change: the iron hypothesis, *Paleoceanography*, *5*, 1-11.

Martin, J. H., R. M. Gordon, and S. E. Fitzwater (1990), Iron in Antarctic waters, *Nature*, *345*(6271), 156-158.

Martin, J. H., R. M. Gordon, and S. E. Fitzwater (1991), The Case for Iron, *Limnology and Oceanography*, *36*(8), 1793-1802.

Martínez-Garcia, A., A. Rosell-Melé, W. Geibert, R. Gersonde, P. Masqué, V. Gaspari, and C. Barbante (2009), Links between iron supply, marine productivity, sea surface temperature, and CO2 over the last 1.1 Ma, *Paleoceanography*, *24*(1), PA1207.

Martínez-García, A., D. M. Sigman, H. Ren, R. F. Anderson, M. Straub, D. A. Hodell, S. L. Jaccard, T. I. Eglinton, and G. H. Haug (2014), Iron Fertilization of the Subantarctic Ocean During the Last Ice Age, *Science*, *343*(6177), 1347-1350.

Marx, S. K., B. S. Kamber, and H. A. McGowan (2005), Estimates of Australian dust flux into New Zealand: Quantifying the eastern Australian dust plume pathway using trace element calibrated< sup> 210</sup> Pb as a monitor, *Earth and Planetary Science Letters*, *239*(3), 336-351.

McConnell, J. R., G. W. Lamorey, and M. A. Hutterli (2002), A 250-year high-resolution record of Pb flux and crustal enrichment in central Greenland, *Geophysical Research Letters*, *29*(23), 45-41-45-44.

McGillicuddy, D., P. Sedwick, M. Dinniman, K. Arrigo, T. Bibby, B. Greenan, E. Hofmann, J. Klinck, W. Smith, and S. Mack (2015), Iron supply and demand in an Antarctic shelf ecosystem, *Geophysical Research Letters*.

McGowan, H., and A. Clark (2008), Identification of dust transport pathways from Lake Eyre, Australia using Hysplit, *Atmospheric Environment*, *42*(29), 6915-6925.

McGowan, H. A., B. Kamber, G. H. McTainsh, and S. K. Marx (2005), High resolution provenancing of long travelled dust deposited on the Southern Alps, New Zealand, *Geomorphology*, *69*(1), 208-221.

McLaren, P. (1981), An interpretation of trends in grain size measures, *JOURNAL OF SEDIMENTARY RESEARCH*, *51*(2), 611-624.

McTainsh, G. (1989), Quaternary aeolian dust processes and sediments in the Australian region, *Quaternary Science Reviews*, *8*(3), 235-253.

McTainsh, G., and J. Leys (1993), Soil erosion by wind, *Land Degradation Processes in Australia*, 188-233.

McTainsh, G., and A. Lynch (1996), Quantitative estimates of the effect of climate change on dust storm activity in Australia during the Last Glacial Maximum, *Geomorphology*, *17*(1), 263-271.

McTainsh, G., J. Leys, and E. Tews (2006), Wind erosion trends for the National State of the Environment Report: Data and Methods, *Australia State of the Environment 2006*.

McTainsh, G., Y.-c. Chan, H. McGowan, J. Leys, and K. Tews (2005), The 23rd October 2002 dust storm in eastern Australia: characteristics and meteorological conditions, *Atmospheric Environment*, *39*(7), 1227-1236.

Meskhidze, N., and A. Nenes (2006), Phytoplankton and cloudiness in the Southern Ocean, *Science*, *314*(5804), 1419-1423.

Meskhidze, N., W. Chameides, A. Nenes, and G. Chen (2003), Iron mobilization in mineral dust: Can anthropogenic SO2 emissions affect ocean productivity?, *Geophysical Research Letters*, *30*(21).

Meyer, C. P., A. K. Luhar, and R. M. Mitchell (2008), Biomass burning emissions over northern Australia constrained by aerosol measurements: I—Modelling the distribution of hourly emissions, *Atmospheric Environment*, *42*(7), 1629-1646.

Mills, M. M., C. Ridame, M. Davey, J. La Roche, and R. J. Geider (2004), Iron and phosphorus co-limit nitrogen fixation in the eastern tropical North Atlantic, *Nature*, *429*(6989), 292-294.

Mitchell, B. G., E. A. Brody, O. Holm-Hansen, C. McClain, and J. Bishop (1991), Light Limitation of Phytoplankton Biomass and Macronutrient Utilization in the Southern Ocean, *Limnology and Oceanography*, *36*(8), 1662-1677.

Moore, J. K., M. R. Abbott, J. G. Richman, and D. M. Nelson (2000), The southern ocean at the Last Glacial Maximum: A strong sink for atmospheric carbon dioxide, *Global Biogeochem. Cycles*, *14*(1), 455-475.

Moore, J. K., K. Lindsay, S. C. Doney, M. C. Long, and K. Misumi (2013), Marine ecosystem dynamics and biogeochemical cycling in the Community Earth System Model [CESM1 (BGC)]: Comparison of the 1990s with the 2090s under the RCP4. 5 and RCP8. 5 scenarios, *Journal of Climate*, *26*(23), 9291-9312.

Morton, P. L., W. M. Landing, S.-C. Hsu, A. Milne, A. M. Aguilar-Islas, A. R. Baker, A. R. Bowie, C. S. Buck, Y. Gao, and S. Gichuki (2013), Methods for the sampling and analysis of marine aerosols: results from the 2008 GEOTRACES aerosol intercalibration experiment, *Limnology and Oceanography: Methods*, *11*(FEB), 62-78.

Moteki, N., and Y. Kondo (2007), Effects of mixing state on black carbon measurements by laser-induced incandescence, *Aerosol Science and Technology*, *41*(4), 398-417.

Mouillot, F., and C. B. Field (2005), Fire history and the global carbon budget: a 1× 1 fire history reconstruction for the 20th century, *Global Change Biology*, *11*(3), 398-420.

Narcisi, B., J.-R. Petit, B. Delmonte, I. Basile-Doelsch, and V. Maggi (2005), Characteristics and sources of tephra layers in the EPICA-Dome C ice record (East Antarctica): implications for past atmospheric circulation and ice core stratigraphic correlations, *Earth and Planetary Science Letters*, *239*(3), 253-265.

Neff, P. D., and N. A. Bertler (2015a), Trajectory modeling of modern dust transport to the Southern Ocean and Antarctica, *Journal of Geophysical Research: Atmospheres*.

Neff, P. D., and N. A. Bertler (2015b), Trajectory modeling of modern dust transport to the Southern Ocean and Antarctica, *Journal of Geophysical Research: Atmospheres*, *120*(18), 9303-9322.

Nicol, S., A. Bowie, S. Jarman, D. Lannuzel, K. M. Meiners, and P. Van Der Merwe (2010), Southern Ocean iron fertilization by baleen whales and Antarctic krill, *Fish and Fisheries*, *11*(2), 203-209.

Nodwell, L. M., and N. M. Price (2001), Direct Use of Inorganic Colloidal Iron by Marine Mixotrophic Phytoplankton, *Limnology and Oceanography*, *46*(4), 765-777.

Novakov, T. (1982), Soot in the atmosphere, in *Particulate Carbon*, edited, pp. 19-41, Springer.

Oberholzer, P., C. Baroni, M. Salvatore, H. Baur, and R. Wieler (2008), Dating late Cenozoic erosional surfaces in Victoria Land, Antarctica, with cosmogenic neon in pyroxenes, *Antarctic Science*, *20*(01), 89-98.

Oberholzer, P., C. Baroni, J. M. Schaefer, G. Orombelli, S. I. Ochs, P. W. Kubik, H. Baur, and R. Wieler (2003), Limited Pliocene/Pleistocene glaciation in Deep Freeze Range,

northern Victoria Land, Antarctica, derived from in situ cosmogenic nuclides, *Antarctic science*, *15*(04), 493-502.

Oshima, N., M. Koike, Y. Zhang, and Y. Kondo (2009), Aging of black carbon in outflow from anthropogenic sources using a mixing state resolved model: 2. Aerosol optical properties and cloud condensation nuclei activities, *Journal of Geophysical Research: Atmospheres (1984–2012)*, *114*(D18).

Pacyna, J., and J. Nriagu (1988), Atmospheric emissions of chromium from natural and anthropogenic sources, *Chromium in the Natural and Human Environments*, 105-123.

Paerl, H. W., K. M. Crocker, and L. E. Prufert (1987), Limitation of N2 fixation in coastal marine waters: Relative importance of molybdenum, iron, phosphorus, and organic matter availability1, *Limnology and Oceanography*, *32*(3), 525-536.

Paerl, H. W., L. E. Prufert-Bebout, and C. Guo (1994), Iron-stimulated N2 fixation and growth in natural and cultured populations of the planktonic marine cyanobacteria Trichodesmium spp, *Applied and Environmental Microbiology*, *60*(3), 1044-1047.

Palmer, T. Y. (1981), Large fire winds, gases and smoke, *Atmospheric Environment (1967)*, *15*(10), 2079-2090.

Parekh, P. (1990), A study of manganese from anthropogenic emissions at a rural site in the eastern United States, *Atmospheric Environment. Part A. General Topics*, *24*(2), 415-421.

Paris, R., and K. Desboeufs (2013), Effect of atmospheric organic complexation on iron-bearing dust solubility, *Atmospheric Chemistry and Physics*, *13*(9), 4895-4905.

Paris, R., K. Desboeufs, and E. Journet (2011), Variability of dust iron solubility in atmospheric waters: Investigation of the role of oxalate organic complexation, *Atmospheric Environment*, *45*(36), 6510-6517.

Paris, R., K. Desboeufs, P. Formenti, S. Nava, and C. Chou (2010), Chemical characterisation of iron in dust and biomass burning aerosols during AMMA-SOP0/DABEX: implication for iron solubility, *Atmospheric Chemistry and Physics*, *10*(9), 4273-4282.

Pereira, E., A. Setzer, F. Gerab, P. Artaxo, M. Pereira, and G. Monroe (1996), Airborne measurements of aerosols from burning biomass in Brazil related to the TRACE A experiment, *Journal of Geophysical Research: Atmospheres (1984–2012)*, *101*(D19), 23983-23992.

Petit, J.-R., M. Briat, and A. Royer (1981), Ice age aerosol content from East Antarctic ice core samples and past wind strength, *Nature*, *293*(5831), 391-394.

Petit, J. R., et al. (1999), Climate and atmospheric history of the past 420,000 years from the Vostok ice core, Antarctica, *Nature*, *399*(6735), 429-436.

Petters, M. D., A. J. Prenni, S. M. Kreidenweis, P. J. DeMott, A. Matsunaga, Y. B. Lim, and P. J. Ziemann (2006), Chemical aging and the hydrophobic-to-hydrophilic conversion of carbonaceous aerosol, *Geophysical research letters*, *33*(24).

Pitman, A., G. Narisma, and J. McAneney (2007), The impact of climate change on the risk of forest and grassland fires in Australia, *Climatic Change*, *84*(3-4), 383-401.

Planquette, H., P. J. Statham, G. R. Fones, M. A. Charette, C. M. Moore, I. Salter, F. H. Nedelec, S. L. Taylor, M. French, and A. R. Baker (2007), Dissolved iron in the vicinity of the Crozet Islands, Southern Ocean, *Deep Sea Research Part II: Topical Studies in Oceanography*, *54*(18), 1999-2019.

Porstendorfer, J., G. Butterweck, and A. Reineking (1994), Daily variation of the radon concentration indoors and outdoors and the influence of meteorological parameters, *Health physics*, *67*(3), 283-287.

Pósfai, M., R. Simonics, J. Li, P. V. Hobbs, and P. R. Buseck (2003), Individual aerosol particles from biomass burning in southern Africa: 1. Compositions and size distributions of carbonaceous particles, *Journal of Geophysical Research: Atmospheres (1984–2012)*, *108*(D13).

Prospero, J. M., P. Ginoux, O. Torres, S. E. Nicholson, and T. E. Gill (2002), Environmental characterization of global sources of atmospheric soil dust identified with the Nimbus 7 Total Ozone Mapping Spectrometer (TOMS) absorbing aerosol product, *Reviews of geophysics*, *40*(1), 2-1-2-31.

Pye, K. (1989), *Aeolian dust and dust deposits*, Academic Press, Harcourt Brace Jovanovich, Publishers.

Radke, L. F., D. A. Hegg, P. V. Hobbs, J. D. Nance, J. H. Lyons, K. K. Laursen, R. E. Weiss, P. J. Riggan, and D. E. Ward (1991), Particulate and trace gas emissions from large biomass fires in North America, *Global biomass burning: Atmospheric, climatic, and biospheric implications*, 209-224.

Raiswell, R., L. G. Benning, M. Tranter, and S. Tulaczyk (2008a), Bioavailable iron in the Southern Ocean: the significance of the iceberg conveyor belt, *Geochemical Transactions*, *9*(1), 7.

Raiswell, R., L. G. Benning, L. Davidson, and M. Tranter (2008b), Nanoparticulate bioavailable iron minerals in icebergs and glaciers, *Mineral Mag*, *72*(1), 345-348.

Ramanathan, V., and G. Carmichael (2008), Global and regional climate changes due to black carbon, *Nature geoscience*, *1*(4), 221-227.

Reid, J., R. Koppmann, T. Eck, and D. Eleuterio (2005), A review of biomass burning emissions part II: intensive physical properties of biomass burning particles, *Atmospheric Chemistry and Physics*, *5*(3), 799-825.

Reid, J. S., and P. V. Hobbs (1998), Physical and optical properties of young smoke from individual biomass fires in Brazil, *Journal of Geophysical Research: Atmospheres (1984–2012)*, *103*(D24), 32013-32030.

Reid, J. S., T. F. Eck, S. A. Christopher, P. V. Hobbs, and B. Holben (1999), Use of the Angstrom exponent to estimate the variability of optical and physical properties of aging smoke particles in Brazil, *Journal of Geophysical Research*, *104*(D22), 27,473-427,489.

Resing, J. A., P. N. Sedwick, C. R. German, W. J. Jenkins, J. W. Moffett, B. M. Sohst, and A. Tagliabue (2015), Basin-scale transport of hydrothermal dissolved metals across the South Pacific Ocean, *Nature*, *523*(7559), 200-203.

Revel-Rolland, M., P. De Deckker, B. Delmonte, P. P. Hesse, J. W. Magee, I. Basile-Doelsch, F. Grousset, and D. Bosch (2006), Eastern Australia: A possible source of dust in East Antarctica interglacial ice, *Earth and Planetary Science Letters*, *249*(1-2), 1-13.

Reynolds, R. L., S. R. Cattle, B. M. Moskowitz, H. L. Goldstein, K. Yauk, C. B. Flagg, T. S. Berquó, R. F. Kokaly, S. Morman, and G. N. Breit (2014), Iron oxide minerals in dust of the Red Dawn event in eastern Australia, September 2009, *Aeolian Research*.

Rhodes, R. H., J. A. Baker, M.-A. Millet, and N. A. N. Bertler (2011), Experimental investigation of the effects of mineral dust on the reproducibility and accuracy of ice core trace element analysis, *Chemical Geology*, *286*(3), 207-221.

Rhodes, R. H., N. A. N. Bertler, J. A. Baker, S. B. Sneed, H. Oerter, and K. R. Arrigo (2009), Sea ice variability and primary productivity in the Ross Sea, Antarctica, from methylsulphonate snow record, *Geophys. Res. Lett.*, *36*(10), L10704.

Rich, H. W., and F. M. M. Morel (1990), Availability of Well-Defined Iron Colloids to the Marine Diatom Thalassiosira weissflogii, *Limnology and Oceanography*, *35*(3), 652-662.

Riemer, N., H. Vogel, and B. Vogel (2004), Soot aging time scales in polluted regions during day and night, *Atmospheric Chemistry and Physics*, *4*(7), 1885-1893.

Riemer, N., M. West, R. Zaveri, and R. Easter (2010), Estimating black carbon aging time-scales with a particle-resolved aerosol model, *Journal of Aerosol Science*, *41*(1), 143-158.

Robinson, R. S., M. A. Brzezinski, C. P. Beucher, M. G. Horn, and P. Bedsole (2014), The changing roles of iron and vertical mixing in regulating nitrogen and silicon cycling in the Southern Ocean over the last glacial cycle, *Paleoceanography*.

Rubin, M., I. Berman-Frank, and Y. Shaked (2011), Dust-and mineral-iron utilization by the marine dinitrogen-fixer Trichodesmium, *Nature Geoscience*, *4*(8), 529-534.

Ruellan, S., H. Cachier, A. Gaudichet, P. Masclet, and J. P. Lacaux (1999), Airborne aerosols over central Africa during the Experiment for Regional Sources and Sinks of Oxidants (EXPRESSO), *Journal of Geophysical Research: Atmospheres (1984–2012)*, *104*(D23), 30673-30690.

Rueter, J. G. (1988), IRON STIMULATION OF PHOTOSYNTHESIS AND NITROGEN FIXATION IN ANABAENA 7120 AND TRICHODESMIUM (CYANOPHYCEAE) 1, *Journal of Phycology*, *24*(2), 249-254.

Rueter, J. G., D. A. Hutchins, R. W. Smith, and N. L. Unsworth (1992), Iron nutrition of Trichodesmium, in *Marine pelagic cyanobacteria: Trichodesmium and other Diazotrophs*, edited, pp. 289-306, Springer.

Running, S. W. (2006), Is global warming causing more, larger wildfires?, *SCIENCE-NEW YORK THEN WASHINGTON-*, *313*(5789), 927.

Ruth, U. (2002), Concentration and size distribution of microparticles in the NGRIP Ice Core during the Last Glacial period, University Bremen.

Sato, M., S. Takeda, and K. Furuya (2007), Iron regeneration and organic iron(III)-binding ligand production during in situ zooplankton grazing experiment, *Marine Chemistry, 106*(3-4), 471-488.

Schroth, A. W., J. Crusius, E. R. Sholkovitz, and B. C. Bostick (2009), Iron solubility driven by speciation in dust sources to the ocean, *Nature Geosci, 2*(5), 337-340.

Schuck, I. (2009), Mineralogical characterisation and geographic provenance of atmospheric particles in coastal Antarctic ice cores – indicators of past climatic variability, *Diploma thesis, Universitat Karlsruhe, Karlsruhe, Germany*.

Schulz, M., J. M. Prospero, A. R. Baker, F. Dentener, L. Ickes, P. S. Liss, N. M. Mahowald, S. Nickovic, C. P. r. García-Pando, and S. Rodríguez (2012), Atmospheric transport and deposition of mineral dust to the ocean: implications for research needs, *Environmental science & technology, 46*(19), 10390-10404.

Schüssler, U., M. Bröcker, F. Henjes-Kunst, and T. Will (1999), P–T–t evolution of the Wilson Terrane metamorphic basement at Oates Coast, Antarctica, *Precambrian Research, 93*(2–3), 235-258.

Schwertmann, U. (1991), Solubility and dissolution of iron oxides, in *Iron nutrition and interactions in plants*, edited, pp. 3-27, Springer.

Sedwick, P. N., and G. R. DiTullio (1997), Regulation of algal blooms in Antarctic Shelf Waters by the release of iron from melting sea ice, *Geophys. Res. Lett., 24*(20), 2515-2518.

Sedwick, P. N., G. R. DiTullio, and D. J. Mackey (2000), Iron and manganese in the Ross Sea, Antarctica: Seasonal iron limitation in Antarctic shelf waters, *J. Geophys. Res., 105*(C5), 11321-11336.

Sedwick, P. N., E. R. Sholkovitz, and T. M. Church (2007), Impact of anthropogenic combustion emissions on the fractional solubility of aerosol iron: Evidence from the Sargasso Sea, *Geochem. Geophys. Geosyst., 8*(10), Q10Q06.

Sedwick, P. N., et al. (2011), Early season depletion of dissolved iron in the Ross Sea polynya: Implications for iron dynamics on the Antarctic continental shelf, *J. Geophys. Res., 116*(C12), C12019.

Seiler, W., and P. J. Crutzen (1980), Estimates of gross and net fluxes of carbon between the biosphere and the atmosphere from biomass burning, *Climatic change, 2*(3), 207-247.

Selby, M., J. Rains, and R. Palmer (1974), Eolian deposits of the ice free Victoria Valley, Southern Victoria Land, Antarctica, *New Zealand Journal of Geology and Geophysics, 17*, 543-562.

Shao, Y., and L. M. Leslie (1997), Wind erosion prediction over the Australian continent, *JOURNAL OF GEOPHYSICAL RESEARCH-ALL SERIES-, 102*, 30,091-030,105.

Shaw, E. C., A. J. Gabric, and G. H. McTainsh (2008), Impacts of aeolian dust deposition on phytoplankton dynamics in Queensland coastal waters, *Marine and Freshwater Research*, *59*(11), 951-962.

Shi, Z., M. D. Krom, S. Bonneville, and L. G. Benning (2015), Atmospheric Processing Outside Clouds Increases Soluble Iron in Mineral Dust, *Environmental Science & Technology*, *49*(3), 1472-1477.

Shiraiwa, M., Y. Kondo, N. Moteki, N. Takegawa, Y. Miyazaki, and D. Blake (2007), Evolution of mixing state of black carbon in polluted air from Tokyo, *Geophysical Research Letters*, *34*(16).

Sholkovitz, E. R., P. N. Sedwick, and T. M. Church (2009), Influence of anthropogenic combustion emissions on the deposition of soluble aerosol iron to the ocean: Empirical estimates for island sites in the North Atlantic, *Geochimica et Cosmochimica Acta*, *73*(14), 3981-4003.

Sholkovitz, E. R., P. N. Sedwick, T. M. Church, A. R. Baker, and C. F. Powell (2012), Fractional solubility of aerosol iron: Synthesis of a global-scale data set, *Geochimica et cosmochimica acta*, *89*, 173-189.

Siefert, R. L., A. M. Johansen, and M. R. Hoffmann (1999), Chemical characterization of ambient aerosol collected during the southwest monsoon and intermonsoon seasons over the Arabian Sea: Labile-Fe(II) and other trace metals, *J. Geophys. Res.*, *104*(D3), 3511-3526.

Sinclair, K. E., N. A. N. Bertler, and W. J. Trompetter (2010), Synoptic controls on precipitation pathways and snow delivery to high-accumulation ice core sites in the Ross Sea region, Antarctica, *J. Geophys. Res.*, *115*(D22), D22112.

Slinn, S., and W. Slinn (1980), Predictions for particle deposition on natural waters, *Atmospheric Environment (1967)*, *14*(9), 1013-1016.

Smetacek, V., P. Assmy, and J. Henjes (2004), The role of grazing in structuring Southern Ocean pelagic ecosystems and biogeochemical cycles, *Antarctic Science*, *16*(04), 541-558.

Smetacek, V., et al. (2012), Deep carbon export from a Southern Ocean iron-fertilized diatom bloom, *Nature*, *487*(7407), 313-319.

Smith, W., and D. Nelson (1986), Importance of Ice Edge Phytoplankton Production in the Southern Ocean, *BioScience*, *36*(4), 251-257.

Smith, W. O., and L. I. Gordon (1997), Hyperproductivity of the Ross Sea (Antarctica) polynya during austral spring, *Geophys. Res. Lett.*, *24*(3), 233-236.

Spokes, L. J., and T. D. Jickells (1995), Factors controlling the solubility of aerosol trace metals in the atmosphere and on mixing into seawater, *Aquatic Geochemistry*, *1*(4), 355-374.

Spokes, L. J., T. D. Jickells, and B. Lim (1994), Solubilisation of aerosol trace metals by cloud processing: A laboratory study, *Geochimica et Cosmochimica Acta*, *58*(15), 3281-3287.

Spolaor, A., P. Vallelonga, J. Gabrieli, G. Cozzi, C. Boutron, and C. Barbante (2012), Determination of Fe2+ and Fe3+ species by FIA-CRC-ICP-MS in Antarctic ice samples, *Journal of Analytical Atomic Spectrometry*, *27*(2), 310-317.

Steffensen, J. P. (1997), The size distribution of microparticles from selected segments of the Greenland Ice Core Project ice core representing different climatic periods, *J. Geophys. Res.*, *102*(C12), 26755-26763.

Stephens, M., N. Turner, and J. Sandberg (2003), Particle identification by laser-induced incandescence in a solid-state laser cavity, *Applied optics*, *42*(19), 3726-3736.

Sterle, K. M., J. R. McConnell, J. Dozier, R. Edwards, and M. Flanner (2013), Retention and radiative forcing of black carbon in eastern Sierra Nevada snow, *The Cryosphere*, *7*(1), 365-374.

Stohl, A. (1998), Computation, accuracy and applications of trajectories—a review and bibliography, *Atmospheric Environment*, *32*(6), 947-966.

Tagliabue, A., and K. R. Arrigo (2005), Iron in the Ross Sea: 1. Impact on CO2 fluxes via variation in phytoplankton functional group and non-Redfield stoichiometry, *J. Geophys. Res.*, *110*(C3), C03009.

Tagliabue, A., and K. R. Arrigo (2006), Processes governing the supply of iron to phytoplankton in stratified seas, *J. Geophys. Res.*, *111*(C6), C06019.

Tagliabue, A., J.-B. Sallee, A. R. Bowie, M. Levy, S. Swart, and P. W. Boyd (2014), Surface-water iron supplies in the Southern Ocean sustained by deep winter mixing, *Nature Geosci*, *7*(4), 314-320.

Tagliabue, A., et al. (2010), Hydrothermal contribution to the oceanic dissolved iron inventory, *Nature Geosci*, *3*(4), 252-256.

Talarico, F., L. Borsi, and B. Lombardo (1995), Relict granulites in the Ross Orogen of northern Victoria Land (Antarctica), II. Geochemistry and palaeo-tectonic implications, *Precambrian Research*, *75*(3), 157-174.

Taylor, S. R., and S. M. McLennan (1995), The geochemical evolution of the continental crust, *Rev. Geophys.*, *33*(2), 241-265.

Textor, C., M. Schulz, S. Guibert, S. Kinne, Y. Balkanski, S. Bauer, T. Berntsen, T. Berglen, O. Boucher, and M. Chin (2006), Analysis and quantification of the diversities of aerosol life cycles within AeroCom, *Atmospheric Chemistry and Physics*, *6*(7), 1777-1813.

Trapp, J. M., F. J. Millero, and J. M. Prospero (2010), Trends in the solubility of iron in dust-dominated aerosols in the equatorial Atlantic trade winds: Importance of iron speciation and sources, *Geochem. Geophys. Geosyst.*, *11*(3), Q03014.

Tuohy, A., N. Bertler, P. Neff, R. Edwards, D. Emanuelsson, T. Beers, and P. Mayewski (2015), Transport and deposition of heavy metals in the Ross Sea Region, Antarctica, *Journal of Geophysical Research: Atmospheres*, 120, doi:110.1002/2015JD023293.

Turn, S., B. Jenkins, J. Chow, L. Pritchett, D. Campbell, T. Cahill, and S. Whalen (1997), Elemental characterization of particulate matter emitted from biomass burning: Wind tunnel derived source profiles for herbaceous and wood fuels, *Journal of Geophysical Research: Atmospheres (1984–2012)*, *102*(D3), 3683-3699.

Turns, S. R. (1996), *An introduction to combustion*, McGraw-hill New York.

Uglietti, C., P. Gabrielli, J. W. Olesik, A. Lutton, and L. G. Thompson (2014), Large variability of trace element mass fractions determined by ICP-SFMS in ice core samples from worldwide high altitude glaciers, *Applied Geochemistry*, *47*, 109-121.

Vallelonga, P., P. Gabrielli, K. J. R. Rosman, C. Barbante, and C. F. Boutron (2005), A 220 kyr record of Pb isotopes at Dome C Antarctica from analyses of the EPICA ice core, *Geophys. Res. Lett.*, *32*(1), L01706.

Vallelonga, P., C. Barbante, G. Cozzi, J. Gabrieli, S. Schüpbach, A. Spolaor, and C. Turetta (2013), Iron fluxes to Talos Dome, Antarctica, over the past 200 kyr, *Climate of the Past*, *9*(2), 597-604.

Vallelonga, P., et al. (2010), Lead isotopic compositions in the EPICA Dome C ice core and Southern Hemisphere Potential Source Areas, *Quaternary Science Reviews*, *29*(1-2), 247-255.

Van Der Merwe, P., D. Lannuzel, A. Bowie, and K. Meiners (2011a), High temporal resolution observations of spring fast ice melt and seawater iron enrichment in East Antarctica, *Journal of Geophysical Research: Biogeosciences (2005–2012)*, *116*(G3).

van der Merwe, P., D. Lannuzel, A. R. Bowie, C. A. Mancuso Nichols, and K. M. Meiners (2011b), Iron fractionation in pack and fast ice in East Antarctica: Temporal decoupling between the release of dissolved and particulate iron during spring melt, *Deep Sea Research Part II: Topical Studies in Oceanography*, *58*(9-10), 1222-1236.

van der Werf, G. R., J. T. Randerson, L. Giglio, G. J. Collatz, P. S. Kasibhatla, and A. F. Arellano Jr (2006), Interannual variability in global biomass burning emissions from 1997 to 2004, *Atmospheric Chemistry and Physics*, *6*(11), 3423-3441.

Wagener, T., C. Guieu, R. Losno, S. Bonnet, and N. Mahowald (2008), Revisiting atmospheric dust export to the Southern Hemisphere ocean: Biogeochemical implications, *Global Biogeochem. Cycles*, *22*(2), GB2006.

Walker, P., and A. Costin (1971), Atmospheric dust accession in South-Eastern Australia, *Soil Research*, *9*(1), 1-5.

Walsh, J. J., and K. A. Steidinger (2001), Saharan dust and Florida red tides: the cyanophyte connection, *Journal of Geophysical Research: Oceans (1978–2012)*, *106*(C6), 11597-11612.

Ward, D. (1990), Factors influencing the emissions of gases and particulate matter from biomass burning, in *Fire in the Tropical Biota*, edited, pp. 418-436, Springer.

Ward, D., R. Susott, J. Kauffman, R. Babbitt, D. Cummings, B. Dias, B. Holben, Y. Kaufman, R. Rasmussen, and A. Setzer (1992), Smoke and fire characteristics for cerrado

and deforestation burns in Brazil: BASE-B experiment, *Journal of Geophysical Research: Atmospheres (1984–2012)*, *97*(D13), 14601-14619.

Ward, D. E., and C. C. Hardy (1991), Smoke emissions from wildland fires, *Environment International*, *17*(2), 117-134.

Ward, D. E., A. W. Setzer, Y. J. Kaufman, and R. A. Rasmussen (1991), Characteristics of smoke emissions from biomass fires of the Amazon region-BASE-A experiment, *Global Biomass Burning: Atmospheric, Climatic, and Biospheric Implications*, 394-402.

Warneck, P. (2003), In-cloud chemistry opens pathway to the formation of oxalic acid in the marine atmosphere, *Atmospheric Environment*, *37*(17), 2423-2427.

Wasserburg, G., S. Jacousen, D. DePaolo, M. McCulloch, and T. Wen (1981), Precise determination of SmNd ratios, Sm and Nd isotopic abundances in standard solutions, *Geochimica et Cosmochimica Acta*, *45*(12), 2311-2323.

Wedepohl, K. H. (1995), The composition of the continental crust, *Geochimica et Cosmochimica Acta*, *59*(7), 1217-1232.

Weller, R., J. Wöltjen, C. Piel, R. Resenberg, D. Wagenbach, G. KÖNIG-LANGLO, and M. Kriews (2008), Seasonal variability of crustal and marine trace elements in the aerosol at Neumayer station, Antarctica, *Tellus B*, *60*(5), 742-752.

Wells, M., N. Zorkin, and A. Lewis (1983), The role of colloidal chemistry in providing a source of iron to phytoplankton, *J Mar Res*, *41*, 731 - 746.

Windom, H. L. (1969), Atmospheric Dust Records in Permanent Snowfields: Implications to Marine Sedimentation, *Geological Society of America Bulletin*, *80*(5), 761-782.

Winton, V. H. L., A. R. Bowie, R. Edwards, M. Keywood, A. T. Townsend, P. van der Merwe, and A. Bollhöfer (2015), Fractional iron solubility of atmospheric iron inputs to the Southern Ocean, *Marine Chemistry*, *177*, *Part 1*, 20-32.

Winton, V. H. L., G. B. Dunbar, N. A. N. Bertler, M. A. Millet, B. Delmonte, C. B. Atkins, J. M. Chewings, and P. Andersson (2014), The contribution of aeolian sand and dust to iron fertilization of phytoplankton blooms in southwestern Ross Sea, Antarctica, *Global Biogeochemical Cycles*, *28*(4), 2013GB004574.

Wolff, E. W., et al. (2006), Southern Ocean sea-ice extent, productivity and iron flux over the past eight glacial cycles, *Nature*, *440*(7083), 491-496.

Wu, J., R. Rember, and C. Cahill (2007), Dissolution of aerosol iron in the surface waters of the North Pacific and North Atlantic oceans as determined by a semicontinuous flow-through reactor method, *Global Biogeochem. Cycles*, *21*(4), GB4010.

Wu, J., E. Boyle, W. Sunda, and L.-S. Wen (2001), Soluble and Colloidal Iron in the Oligotrophic North Atlantic and North Pacific, *Science*, *293*(5531), 847-849.

Wuttig, K., T. Wagener, M. Bressac, A. Dammshäuser, P. Streu, C. Guieu, and P. Croot (2013), Impacts of dust deposition on dissolved trace metal concentrations (Mn, Al and Fe) during a mesocosm experiment, *Biogeosciences (BG)*, *10*(4), 2583-2600.

Yamada, Y., H. Fukuda, K. Inoue, K. Kogure, and T. Nagata (2013), Effects of attached bacteria on organic aggregate settling velocity in seawater, *Aquatic microbial ecology*, *70*(3), 261-272.

Yamasoe, M. A., P. Artaxo, A. H. Miguel, and A. G. Allen (2000), Chemical composition of aerosol particles from direct emissions of vegetation fires in the Amazon Basin: water-soluble species and trace elements, *Atmospheric Environment*, *34*(10), 1641-1653.

Zahorowski, W., S. Chambers, and A. Henderson-Sellers (2004), Ground based radon-222 observations and their application to atmospheric studies, *Journal of environmental radioactivity*, *76*(1), 3-33.

Zhang, R., A. F. Khalizov, J. Pagels, D. Zhang, H. Xue, and P. H. McMurry (2008), Variability in morphology, hygroscopicity, and optical properties of soot aerosols during atmospheric processing, *Proceedings of the National Academy of Sciences*, *105*(30), 10291-10296.

Zhu, X., J. M. Prospero, F. J. Millero, D. L. Savoie, and G. W. Brass (1992), The solubility of ferric ion in marine mineral aerosol solutions at ambient relative humidities, *Marine Chemistry*, *38*(1-2), 91-107.

Zhu, X., J. M. Prospero, D. L. Savoie, F. J. Millero, R. G. Zika, and E. S. Saltzman (1993), Photoreduction of Iron(III) in Marine Mineral Aerosol Solutions, *J. Geophys. Res.*, *98*(D5), 9039-9046.

Zhuang, G., R. A. Duce, and D. R. Kester (1990), The Dissolution of Atmospheric Iron in Surface Seawater of the Open Ocean, *J. Geophys. Res.*, *95*(C9), 16207-16216.

Zhuang, G., Z. Yi, R. A. Duce, and P. R. Brown (1992), Chemistry of iron in marine aerosols, *Global Biogeochem. Cycles*, *6*(2), 161-173.

Zuberi, B., K. S. Johnson, G. K. Aleks, L. T. Molina, M. J. Molina, and A. Laskin (2005), Hydrophilic properties of aged soot, *Geophysical research letters*, *32*(1).

Zuo, Y., and J. Zhan (2005), Effects of oxalate on Fe-catalyzed photooxidation of dissolved sulfur dioxide in atmospheric water, *Atmospheric Environment*, *39*(1), 27-37.

Chapter 8. Exegesis review: The impact of dust and biomass burning on deposition of soluble iron to Australian and Antarctic waters

8.1 Introduction

This exegesis review, discusses the impact of dust and biomass burring aerosol (elemental carbon and refractory black carbon (rBC) as fire tracers) on the deposition of soluble iron (Fe) to Australian and Antarctic waters through the following objectives. Conclusions are contained in individual chapters. Here, I discuss the overall conclusions related to the exegesis introduction by bringing together individual chapters as a whole body of work. Future work and recommendations are also discussed.

1. *Do latitudinal gradients in soluble iron exist in the Australian sector of the Southern Hemisphere?*

   Soluble iron concentrations and fractional iron solubility of aerosols are compared at a number of sites (Gunn Point, Cape Grim, McMurdo Sound, and Roosevelt Island) along a latitudinal gradient from northern tropical Australia to the polar plateau.

2. *Can the variability in fractional iron solubility be explained by biomass burning emissions?*

   The large range of fractional iron solubility (1-90 %) observed on a global scale is investigated by comparing black/elemental carbon, dust and soluble iron in time series in the Australian sector of the Southern Hemisphere. The relationship between soluble iron and black/elemental carbon with respect to aeolian iron transport and deposition to the surface ocean are investigated.

3. *What are the potential impacts of changes in fractional iron solubility on glacial to interglacial climate regimes?*

   A simple two-component mixing model with “mineral dust” and “combustion aerosol” end members is applied to a dust record from an Antarctic ice core to

investigate how soluble iron deposition may have changed in relation to iron sources during glacial-interglacial transitions.

8.2 Latitudinal gradients of soluble iron in the Australian sector of the Southern Hemisphere

The mean global distribution of atmospheric iron deposition is well known [e.g. *Mahowald et al.*, 2005; *Mahowald et al.*, 2009], but its solubility and bioavailability is not. Soluble iron fluxes were investigated at a number of sites in Australia (Gunn Point, Cape Grim Baseline Air Pollution Station; CGBAPS) and Antarctica (McMurdo Sound and Roosevelt Island) (Chapters 4-7). In addition, preliminary snow pit data from Aurora Basin North (ABN), East Antarctica (see section 8.5.2.) is also discussed in this review. Soluble iron data from this study and the literature, concerning the Australian sector of the Southern Hemisphere, are compiled in Fig. 8.1. As a general trend, soluble iron fluxes are highest in the Southern Hemisphere tropics and decrease with increasing latitude southward. Soluble iron fluxes decreased by orders of magnitude from an estimated 1.9×10^{-2} g m^{-2} y^{-1} at Gunn Point to 4.1×10^{-5} g m^{-2} y^{-1} at Cape Grim to 1.2×10^{-6} g m^{-2} y^{-1} at Roosevelt Island to 2.5×10^{-7} g m^{-2} y^{-1} at ABN. It should be noted that the soluble iron fluxes presented here are a combination of dry deposition fluxes from continental Australia (Gunn Point and CGBAPS) and total (wet and dry) deposition fluxes from Antarctica (McMurdo Sound, Roosevelt Island and ABN). Regardless, the dry deposition fluxes over continental Australia are still order of magnitude greater than the total fluxes in Antarctica. The decreasing latitudinal trend is consistent with soluble iron deposition models that estimate low soluble iron fluxes in the Southern Ocean [*Mahowald et al.*, 2009], and high soluble iron fluxes derived from combustion over land masses in the tropics [*Ito*, 2015], consistent with a biomass burning source at the equator.

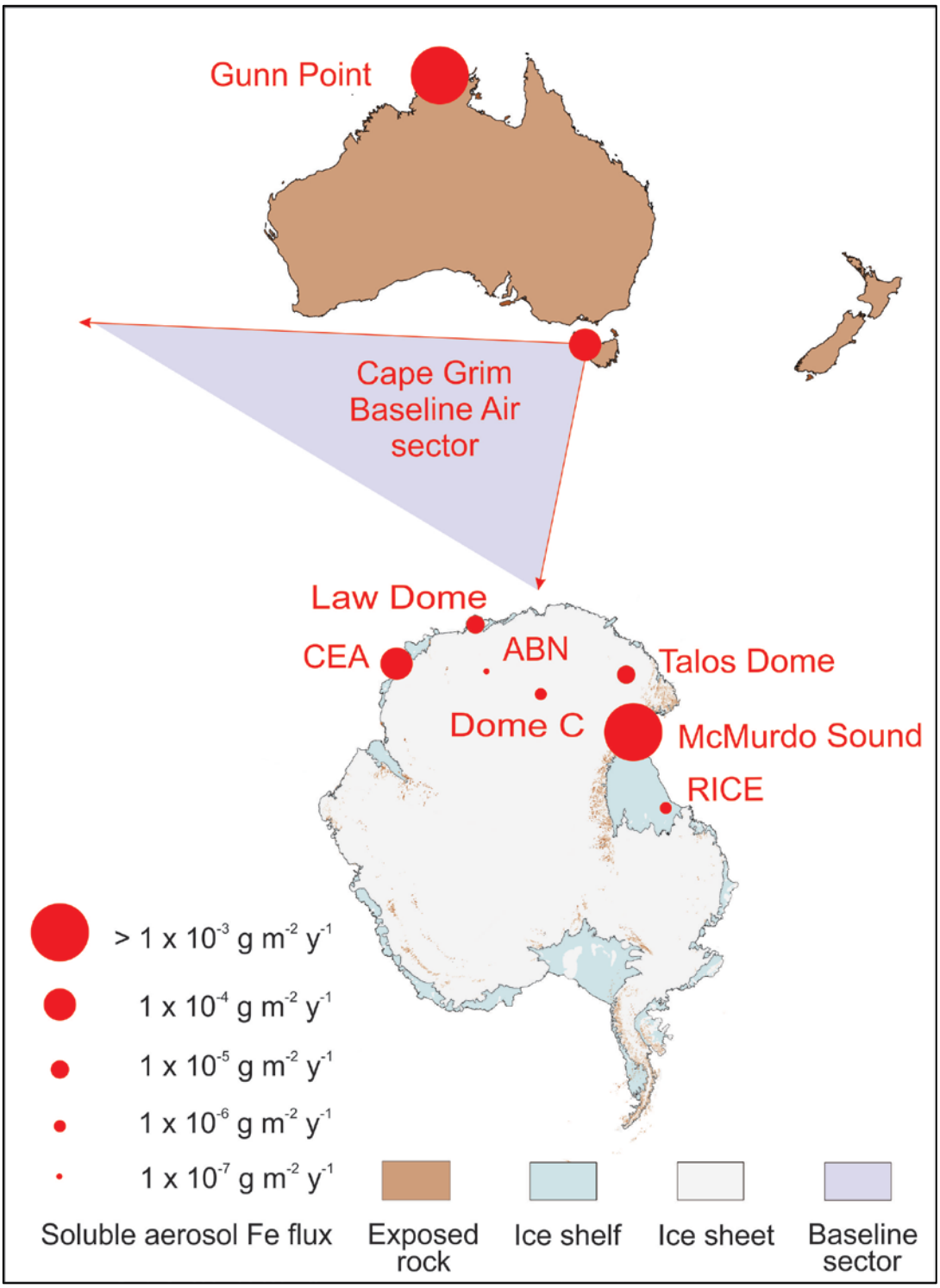

Fig. 8.1: Soluble iron flux in the Australian sector of the Southern Hemisphere. Soluble iron fluxes from continental Australia are dry deposition fluxes while soluble iron fluxes from Antarctica are total (wet and dry) deposition fluxes. Note that the data from ice core sites are from Holocene ice and assume no large Holocene changes in deposition (Law Dome; Edwards et al. [1998], Talos Dome; Vallelonga et al. [2013], Dome C; Gaspari et al. [2006]). McMurdo Sound dust data is from Winton et al. [2014] and coastal East Antarctica (CEA) aerosol data is from Gao et al. [2013].

Two exceptions to this trend have been reported. Firstly, soluble iron fluxes of Last Glacial Maximum (LGM) dust are higher by an order of magnitude. In the Dome C ice core, soluble iron fluxes of 8.4×10^{-4} to 1.0×10^{-5} g m^{-2} y^{-1} [*Conway et al.*, 2015] are considerably higher than present day Holocene fluxes on the East Antarctic Plateau (EAP) (Fig. 8.2). Secondly, the occurrence of sparse ice-free rock outcrops around the low-elevation margins of Antarctica (Fig. 8.1) represents a non-negligible dust source to the local atmosphere. Some of these potential source areas (PSA) have been ice-free for millions of years [*Delmonte et al.*, 2013; and references therein; *Oberholzer et al.*, 2008; *Oberholzer et al.*, 2003]. The local dust cycle in these coastal regions is widely different from the high-elevation polar plateau, in terms of dust abundance and origin [*Delmonte et al.*, 2002; *Delmonte et al.*, 2004b; *Lambert et al.*, 2008]. Here, mesoscale dust entrainment, advection and deposition is driven by regional atmospheric circulation. In the coastal Ross Sea region, two PSA have been identified: unconsolidated sediment on the debris bands in southern McMurdo Sound (Chapter 7), and ice-free mountains in Marie Byrd Land (Chapter 6), both of which supply new soluble iron to the Ross Sea. The Messa Range, Northern Victoria Land is a PSA for dust, and most likely iron, to the Talos Dome ice core site [*Delmonte et al.*, 2010b; *Vallelonga et al.*, 2013]. Exposed outcrops in coastal East Antarctica have also been suggested as a source of dissolved iron (DFe) to proximal Antarctic waters [*Gao et al.*, 2013]. Other PSA exist on the margins of Antarctica (e.g. McMurdo Dry Valleys, Terra Nova Bay, Bunger Hills, and the Antarctic Peninsula), however these are not quantified in terms of dust composition and abundance or the soluble iron content. An important conclusion from this research is that the DFe supply from the largest local dust source in Antarctica [*Winton et al.*, 2014] (Chapter 7) does not appear to be the dominant source of DFe to the SW Ross Sea or Antarctic waters in general. The SW Ross Sea region represents the dustiest known area in Antarctica [*Chewings et al.*, 2014], and previous estimates suggest that local dust contributes up to 15 % of the DFe supply to the SW Ross Sea [*Winton et al.*, 2014]. In the case of the Ross Sea, resuspension and upwelling of iron rich sediments is likely the major source of DFe to surface waters (as identified in Chapter 7 in agreement with *Marsay et al.* [2014]; *Sedwick et al.* [2011]). Nevertheless, local PSA around the margins of Antarctica contribute an important source of iron to biogeochemical iron budgets in snow on sea ice [*de Jong et al.*, 2013]. Sea ice also plays an important role in the storage of DFe through the austral winter, and acts as a transport vector and redistributes of DFe into the Southern Ocean during austral spring-summer sea ice melt [*Lannuzel et al.*, 2007; *Lannuzel et al.*, 2010; *Van Der Merwe et al.*, 2011a; *van der Merwe et al.*, 2011b] (Chapter 7).

A large range in fractional iron solubility was observed between sites and also between samples at sites (Table 8.1). Unlike soluble iron fluxes, fractional iron solubility did not display a clear latitudinal gradient. However, the fractional iron solubility minimum decreased by orders of magnitude with increased latitude from 2 % at Gunn Point to 0.003 % at ABN (Table 8.1). The fractional iron solubility was highest in pristine baseline air over the Southern Ocean, and lowest in remote locations in Antarctica. Values of fractional iron solubility in mixed dust and fresh smoke at Gunn Point (2-11 %) lie between these values, and are consistent with modelling studies that suggest a relatively low fractional iron solubility near sources of biomass burning and coal combustion [*Ito*, 2015]. It is thought that fractional iron solubility increases as aerosols age during transport and are exposed to organic acids (e.g. sulfuric and oxalic acid; determined by oxalate as the conjugate base) in the atmosphere [*Ito*, 2015]. No relationship between these acid species and solubility was observed at Cape Grim (Chapter 5). The large range in fractional iron solubility for these samples was attributed to a mixture of aerosol iron sources. The ~1 year time series at Cape Grim was too short to rule out the possibility that atmosphere processing with oxalic and sulfuric acid in baseline can enhance iron solubility. Little is known about the enhancement of oxalic acid and sulfuric acid on the fractional iron solubility in pristine air over the Southern Ocean. Unlike polluted air masses over mega cities [*Chuang et al.*, 2005; *Kumar et al.*, 2010; *Sedwick et al.*, 2007; *Sholkovitz et al.*, 2009], where concentrations of organic acids are high, the lack of correlation between soluble iron and oxalic acid at Cape Grim could be related to the extremely clean air over the Southern Ocean and Antarctica. In the absence, or trace concentrations, of organic acids in the atmosphere over the Southern Ocean [*Keywood*, 2007], the enhancement of iron solubility would not take place. Furthermore, Roosevelt Island is influenced by local dust sources from Marie Byrd Land (Chapter 6) and the mean fractional iron solubility of 1.8 % is similar to that of mineral dust (0.5-2 %). However, the fractional iron solubility at the site episodically rose up to 30 % but was unrelated to refractory black carbon (rBC), a proxy for biomass burning. There is considerable spatial variability in the fractional iron solubility in the Australian sector of the Southern Hemisphere. The time series in this study were too short to investigate seasonality in fractional iron solubility; however episodic variability at sites was related to changes in aerosol source.

Table 8.1: Fractional iron solubility at various sites in this research. Site locations are shown in Fig. 8.1.

	Latitude	Fractional Fe solubility minimum (%)	Fractional Fe solubility maximum (%)	Fractional Fe solubility mean (%)
Gunn Point	12.25 °S	2	11	6
Cape Grim	40.68 °S	0.5	56	15
Roosevelt Island	79.36 ºS	0.07	30	1.8
Aurora Basin North	71.17 °S	0.003	6	0.4

8.3 Can the variability in fractional iron solubility be explained by biomass burning emissions?

8.3.1 Two component mixing of aerosol iron sources

To date most studies have assumed that mineral dust represents the primary source of soluble iron in the atmosphere [e.g. *Jickells et al.*, 2005]. However, fire emissions, oil combustion and extra-terrestrial iron are other potential sources. This study tested the hypothesis that the variability in fractional iron solubility can be explained by biomass burning emissions. The variation in the fractional iron solubility as a function of total aerosol iron loading is illustrated by scatter plots of fractional iron solubility versus total aerosol iron loading (Fig 8.2). The data in this research and other studies [*Bowie et al.*, 2009; *Gao et al.*, 2013; *Sholkovitz et al.*, 2012; and references within] are separated into three main regions: a) global, b) Southern Hemisphere, and c) Antarctica in Fig. 8.2. *Sholkovitz et al.* [2012] complied a global dataset of fractional iron solubility, and found that the large variability in fractional iron solubility observed is related to a mixing of aerosols sources, i.e. mineral dust with a low fractional iron solubility (0.5-2 %) and combustion aerosol with a high fractional iron solubility (up to 60 %; Fig. 8.2a). On a global scale, the range in fractional iron solubility is large (Fig. 8.2a). The total aerosol iron loading in the Southern Hemisphere (Fig. 8.2b) is less than the Northern Hemisphere (Fig. 8.2a). The relationship between total iron and fractional iron solubility is also consistent with Antarctic data from this study (Fig. 8.2c). Total aerosol iron loading in Antarctica (Fig. 8.2c) is even lower that the Southern Ocean, but the range in fractional iron solubility is still comparable to the Southern Hemisphere.

The Southern Hemisphere is characterised by low aerosol iron loading ranges between 5-150 ng m^{-3} and fractional iron solubility ranges between 0.5-22 % [*Sholkovitz et al.*, 2012]. The study reported here doubles the number of data points used to characterise the Southern

Ocean (i.e. in a different sector to the South Atlantic Ocean previously investigated) and Antarctica (Fig. 8.2b-c). Incorporating these new estimates, total aerosol iron in the Southern Hemisphere is characterised by concentrations ranging between 0.01-1200 ng m^{-3} and fractional iron solubility between 0.5-60 %. This range is wider than previous estimates as the latitudinal distribution of Southern Hemispheric aerosol iron sampling was extended from the pole to the equator, thereby capturing a larger range of aerosol iron PSA. *Sholkovitz et al.* [2012] found that around a quarter of the Southern Hemispheric samples had a fractional iron solubility of <2 %, similar to the fractional iron solubility of mineral dust (0.5-2 %). While only one known value is reported for the fractional iron solubility of Australian mineral dust, i.e. 0.9 % in soil from Thargomindah, SW Queensland [*Mackie et al.*, 2006], the low fractional iron solubility of Australian mineral dust is consistent with global estimates of mineral dust. The only other known study of iron solubility in Australia examined soil from Mallee, Murray River region [*Bhattachan and D'Odorico*, 2014]. However, different fractions of soluble iron were analysed than in this research, which is problematic as the fractional iron solubility of the long-range transportable size fraction (i.e. <5 µm) could be different to the bulk fraction. Furthermore, no measurements of total iron concentration or fractional iron solubility were reported. Soluble ferrous iron, Fe(II) in Mallee soil particles <45 µm ranged from 0.05 to 0.24 mg g^{-1} and acid-leachable iron (determined using a similar labile iron method described in Chapter 5) ranged from 0.17-0.19 mg g^{-1}. The acid leachable or labile fraction of iron in the unprocessed soil is unsurprisingly orders of magnitude higher than estimates of labile iron in baseline air over the Southern Ocean (Chapter 5).

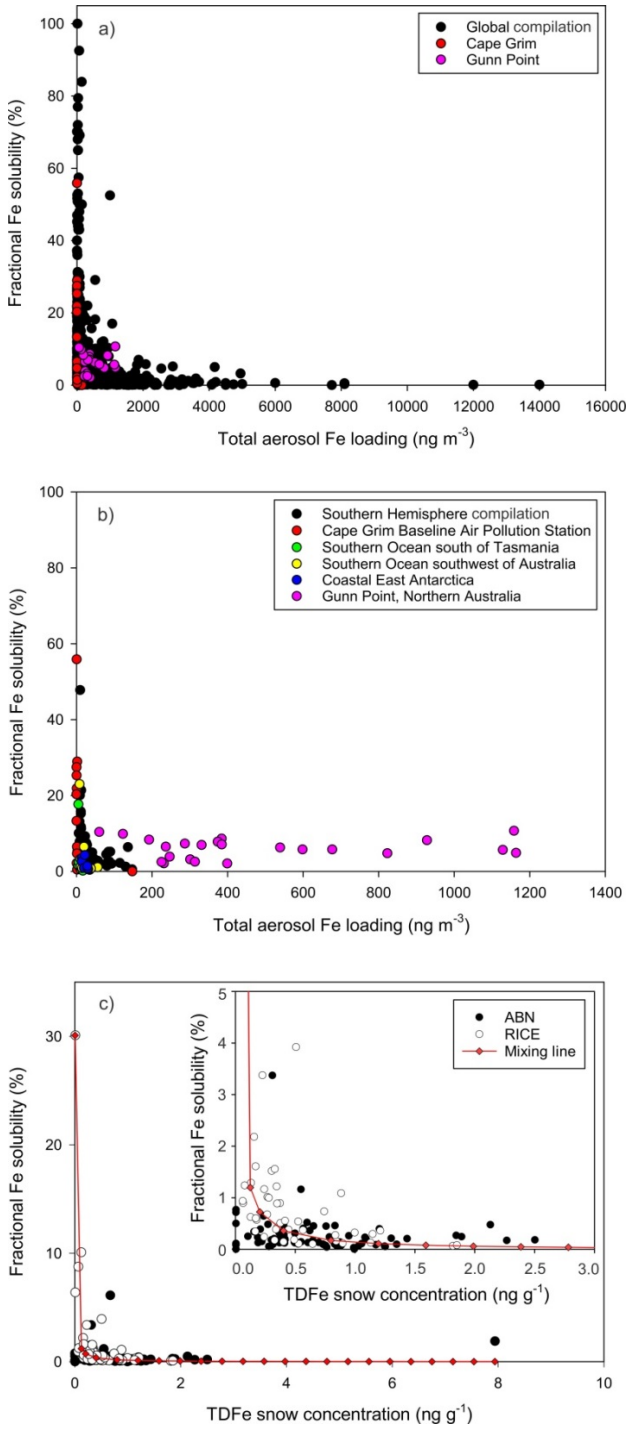

Fig. 8.2: Compilation of fractional iron solubility. a) Global compilation of aerosol iron solubility (*Sholkovitz et al.* [2012; and references therein], Cape Grim: Chapter 5, Gunn Point: Chapter 4). b) Aerosol iron solubility data from the Australian sector of the Southern Hemisphere (Southern Hemisphere compilation: *Sholkovitz et al.* [2012; and references therein], Cape Grim Baseline Air Pollution Station: Chapter 5, Southern Ocean south of Tasmania: *Bowie et al.* [2009], Southern Ocean southwest of Australia and coastal East Antarctica: *Gao et al.* [2013], Gunn Point: Chapter 4). c) Fractional iron solubility from Antarctic snow (Roosevelt Island; Chapter 6, ABN; see section 8.5.1) and the results of two end-member (mineral dust and combustion aerosol) conservative mixing model.

The Antarctic snow fractional iron solubility data fall along a simple two component mixing line in Fig. 8.2c. The mixing line was calculated assuming the conservative mixing of two aerosol end-members each characterised by distinct atmospheric loadings of total aerosol iron and fractional iron solubility, following *Sedwick et al.* [2007] and *Sholkovitz et al.* [2012]. The first end member "mineral dust" is characterised by relatively high aerosol iron loading and relatively low fractional iron solubility. The second end member "combustion aerosol" is characterised by relatively low total aerosol iron loading and relatively high fractional iron solubility. Fractional iron solubility from oil and coal combustion is high and estimates vary around 1-50 % [*Kumar et al.*, 2010; *Sedwick et al.*, 2007; *Sholkovitz et al.*, 2009]. However, relatively little is known about fractional iron solubility of biomass burning emissions. Of the few estimates, there is a large range (1-60 %), and these may vary in relationship to biomass and fire characteristics as well as that of the underlying terrain [*Guieu et al.*, 2005; *Ito*, 2011; *Paris et al.*, 2010]. To investigate whether the high values of fractional iron solubility can be explained by biomass sources, Roosevelt Island and Gunn Point records of soluble iron and black/elemental carbon, a proxy for biomass burning, were investigated.

8.3.2 Biomass burning and soluble iron at Roosevelt Island

Mixed dust and rBC sources of soluble iron were identified at Roosevelt Island (Chapter 6). Exceptionally high rBC concentrations (up to 2 ppb comparable to Greenland levels) during an event in austral summer 2012 paralleled dust concentrations and soluble iron deposition. However, the fractional iron solubility at this time was low (0.7 %) but rose up to 10 % and 30 % during the austral winter in 2011 and 2012 respectively when rBC and dust concentrations were low (Fig. 8.2c). It is important to note that local dust sources from Marie Byrd Land contribute to the soluble iron input to the site. In this short record, it is not possible to separate out dust and rBC sources of soluble iron to Roosevelt Island. Refractory black carbon deposition to West Antarctica is seasonal, occurring in late winter to early spring [*Bisiaux et al.*, 2012b]. While the long term seasonally of dust deposition at Roosevelt Island are currently unconstrained but under investigation [*B. Delmonte Pers. Comm.*, 2015], the snow pit data suggested that dust input to the site was episodic. Longer records of soluble iron deposition are required to determine whether rBC and dust deposition occur in different seasons. A seasonal separation of these soluble iron sources would help assess whether the large spikes in fractional iron solubility are related to biomass burning.

8.3.3 Biomass burning and soluble iron at Gunn Point

To investigate whether these large peaks in fractional iron solubility at Roosevelt Island displayed characteristics related to biomass burning, aerosol iron from a source region of annual savannah biomass burning in the Australian tropics (Gunn Point) was analysed (Chapter 4). Similar to Roosevelt Island, aerosol iron sources were mixed and included mineral dust and biomass burning. Mineral dust from central Australia was determined by a combination of tracers, elemental ratios, enrichment factor analysis, and air mass back trajectories. These tracers showed that mineral dust was present in all samples. In particular, two major dust events were identified with high soluble and total iron concentrations. Biomass burning was identified continuously throughout the campaign and two major fire events occurred on different days that the mineral dust events. Although the aerosols were a mixture of these two end member sources, they peaked at different times throughout the record in contrast to Roosevelt Island where the largest rBC peak occurred simultaneously with dust deposition. Fractional iron solubility was relatively high (8 %) during the dust events but dropped to ~2 % during the largest and most proximal fire event. Soluble iron concentrations also dropped during the largest and most proximal fire event. For the majority of the time series, elemental carbon concentrations were greater when fractional iron solubility was lower, and vice versa, suggesting that fresh elemental was not a direct source of soluble iron at the biomass burning source. Furthermore, no relationship between rBC and soluble iron was found at Roosevelt Island. Estimates of the fractional iron solubility in aerosols produced from natural biomass burning were relatively low in studies by Guieu et al. [2005] and Paris et al. [2010] who report fractional iron solubility of 2 % for samples collected off Africa and southern France, respectively. While more studies are required, results from Roosevelt Island and Gunn Point question whether black/elemental carbon is a direct source of soluble iron.

8.3.4 Global chemical transport model of soluble iron and implications for biomass burning sources of soluble aerosol iron

In order to explain the unexpected low soluble iron concentrations and fractional iron solubility during fire events at Gunn Point, the Gunn Point aerosol data was compared to the global chemical transport model of soluble iron models [*A. Ito, Pers. Comm.*, 2015]. The range of fractional iron solubility at Gunn Point (2-10 %) fits well with model predictions of 1-8 % fractional iron solubility for June at the Gunn Point site from the global atmospheric

chemistry model of *Ito and Shi* [2015]. The model uses an empirical scheme to estimate the release of iron from mineral dust by inorganic and organic acids in water (Fig. 8.3). It is important to note that the input data used in the model was from June 2010, described in *Ito and Shi* [2015], and therefore is not directly comparable. Future works will focus on using input data for June 2014. According to the global chemical transport model, biomass burning indirectly contributed to soluble iron deposition at the Gunn Point site. The model can reproduce relatively low fractional iron solubility near Australian biomass burning source regions (1-8 %), compared to the open ocean [*Ito*, 2015], although the model underestimated fractional iron solubility under the dust event.

Ito and Shi [2015] found that iron dissolution of mineral dust is substantially enhanced in the presence of excess oxalic acid under low acidity. Oxalic acid, determined as oxalate as the conjugate base in this research, is an organic acid in fresh smoke which makes up <1% of the total particle mass of biomass burning [*Ferek et al.*, 1998; *Yamasoe et al.*, 2000]. During the Gunn Point Savannah Fires in the Early Dry Season (SAFIRED) campaign in June 2014, elemental ratios and enrichment factors were consistent with a mineral dust source. Furthermore, air mass back trajectories suggest central Australia as the general fetch area. The source of soluble iron at Gunn point was attributed to the background composition of Australian aeolian dust transported to the Australian tropics, and subsequently mixing with biomass burning emissions from north Australian savannahs. Iron from biomass burning can originate from ash and/or local soil entrained by pyro-convection. Local soil at the combustion site can thus contribute to the mineral dust component in the sample. Even if iron is mainly transported from the southeast over inland, low population regions of Australia with a low fractional iron solubility (e.g. 0.9 %) [*Mackie et al.*, 2006], soluble iron can also originate from soil at the savannah combustion source (Fig. 8.3). In this research, it is not possible to discriminate between the composition of 'background Australian dust' and the local soil entrained by pyro-convection as there is little geochemical data for savannah soils in the Northern Territory. During the mixing of dust and biomass burning emissions, soluble iron contained in dust could be enhanced by oxalic acid derived from the fire combustion. The relatively low values of fractional iron solubility at Gunn Point are comparable to the model predictions of relatively low fractional iron solubility at the biomass burning source region which increase during transport and atmospheric processing to the open ocean [*Ito*, 2015]. It is interesting to note that the fractional iron solubility was lowest during proximal fires compared to more distally sourced fires. In this case, mineral dust is the major source of

soluble iron to proximal tropical waters. Fresh rBC/elemental carbon is likely to have a low total iron content (e.g. iron estimates for fresh smoke range between 0.02-1.2 % [*Ferek et al.*, 1998; *Turn et al.*, 1997; *Ward et al.*, 1992; *Ward and Hardy*, 1991; *Ward et al.*, 1991; *Yamasoe et al.*, 2000]) and although some fresh rBC/elemental carbon may not pass through a 0.2 µm filter, due to the hydrophobic surface of fresh rBC/elemental carbon, any iron associated with the rBC/elemental carbon is not likely to be dispersed into solution (Chapter 4). By characterising the biomass burning end member at the source, this research found that fresh rBC/elemental carbon does not necessarily result in high fractional iron solubility as hypothesised. This same conclusion was found with aged and long range transported rBC to Roosevelt Island. Nevertheless, biomass burning emissions of organic and inorganic acid species could enhance the fractional iron solubility of mineral dust. The relationship between soluble iron, dust and biomass burning is complex and a number of interacting processes from dust advection and biomass combustion to aeolian transport to deposition in the ocean are likely to explain the variability in fractional iron solubility (Fig. 8.4).

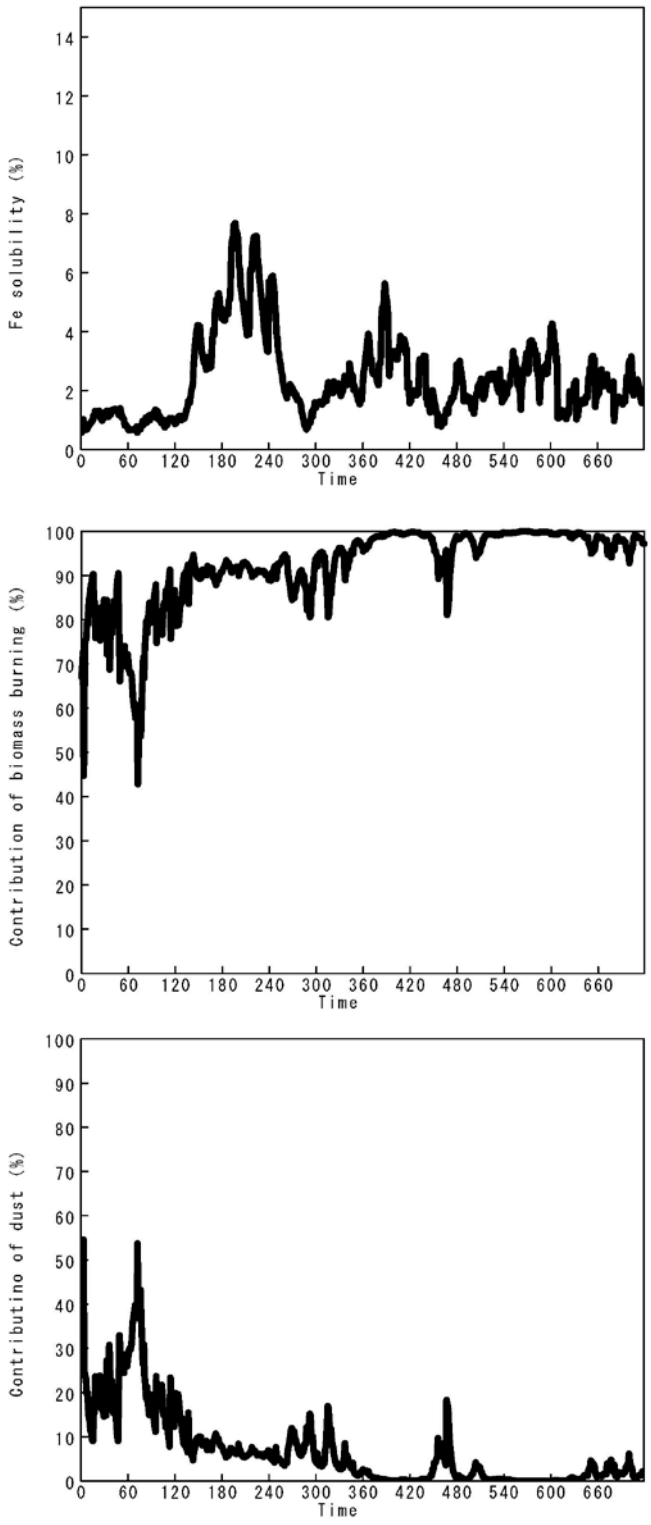

Fig. 8.3: Soluble iron model results for Gunn Point in June 2010. Input data are taken from Ito and Shi [2015]. a) Fractional iron solubility. b) The contribution of biomass burning to the total soluble iron. c) The contribution of dust to the total soluble iron. Source: *A. Ito Pers. Comm.* [2015].

8.3.5 Processes by which biomass burning can influence soluble aerosol iron

The latitudinal gradients in soluble iron fluxes and the episodic high fractional iron solubility in baseline air over the Southern Ocean and Antarctica can be explained by two processes illustrated in Fig.8.4:

1. Enhancement of iron solubility in mineral dust by organic and inorganic species in smoke plumes from biomass burning regions.

2. Iron binding to elemental/black carbon aerosols or chemical absorption of iron onto the surface of elemental/black carbon aerosols with subsequent release to the remote open ocean. The transport and aging of nano-sized, fresh elemental/black carbon can occur through a number of processes including the coating of elemental/black carbon particles with sulfate, oxalate and other organic species (Chapter 4). Although the total iron content in biomass is low, elemental/black carbon can bind to inorganic species and vice versa, e.g. mineral dust and nano-iron particles, during long range transport [*Ellis et al.,* 2015]. These processes can result in the elemental/black carbon becoming hydrophilic, dispersing in water and forming a colloid, and thus operationally defined as soluble iron when it passes through a 0.2 μm filter.

Upon deposition to the ocean, iron from mineral dust and coated and aged elemental/black carbon can be released into the surface water (Fig. 8.4). Even, if elemental/black carbon does not become hydrophilic during atmospheric transport, processes in the ocean or atmosphere-ocean interface could coat and functionalize the particles making them a potential bioavailable iron source. Elemental/black carbon is ubiquitous, and likely elemental/black carbon floats on surface waters for long periods of time (Fig. 8.4). Elemental/black carbon itself may not be a direct source of soluble iron, unless it can become bound to iron nano-particles and coated to make it hydrophilic during transport. In addition, other species emitted during fire combustion (e.g. oxalate, sulfate) could enhance the fractional iron solubility of mineral dust. Australia is a large PSA of both dust and biomass burning emissions for the Southern Hemisphere and the mixing of the two aerosols sources could be an important source of bioavailable iron for both tropical and Southern Ocean waters (Fig. 8.2b).

Higher soluble iron fluxes at lower latitudes and lower soluble iron fluxes at higher latitudes are related to a mixture of aerosol iron sources with greater biomass burning near the tropics

enhancing the dissolution of mineral dust. As dust and biomass burning emissions are transported over the open ocean, a number of interactions take place which can either continue to enhance the solubility of mineral dust and/or make elemental/black carbon soluble (Fig. 8.4). Dust events are episodic and not all dust events will coincide with the mixing of a biomass burning plume. This could explain the episodic high fractional iron solubility observed in aged/long-range transported aerosols to Cape Grim and Antarctica. The mixing of these two sources could also explain why not all major Australian dust events result in a biotic response [*Boyd and Mackie*, 2008; *Boyd et al.*, 2010; *Boyd et al.*, 2004; *Gabric et al.*, 2010]; that is, in the absence of biomass burning, the fractional iron solubility of mineral dust may be too low stimulate productivity. The onset of toxic *Trichodeium* blooms were linked to iron-fertilisation by Indonesian wild fires [*Abram et al.*, 2003]. In this case, the wildfire could have enhanced the solubility of aerosol iron in that region. This unusual type of event could become more frequent as biomass burning emissions are predicted to rise over the next century [*Keywood et al.*, 2013]. More frequent and larger biomass burning events could have implications on the bioavailability of atmospheric iron to ocean waters and the heath of the marine ecosystem in tropical waters.

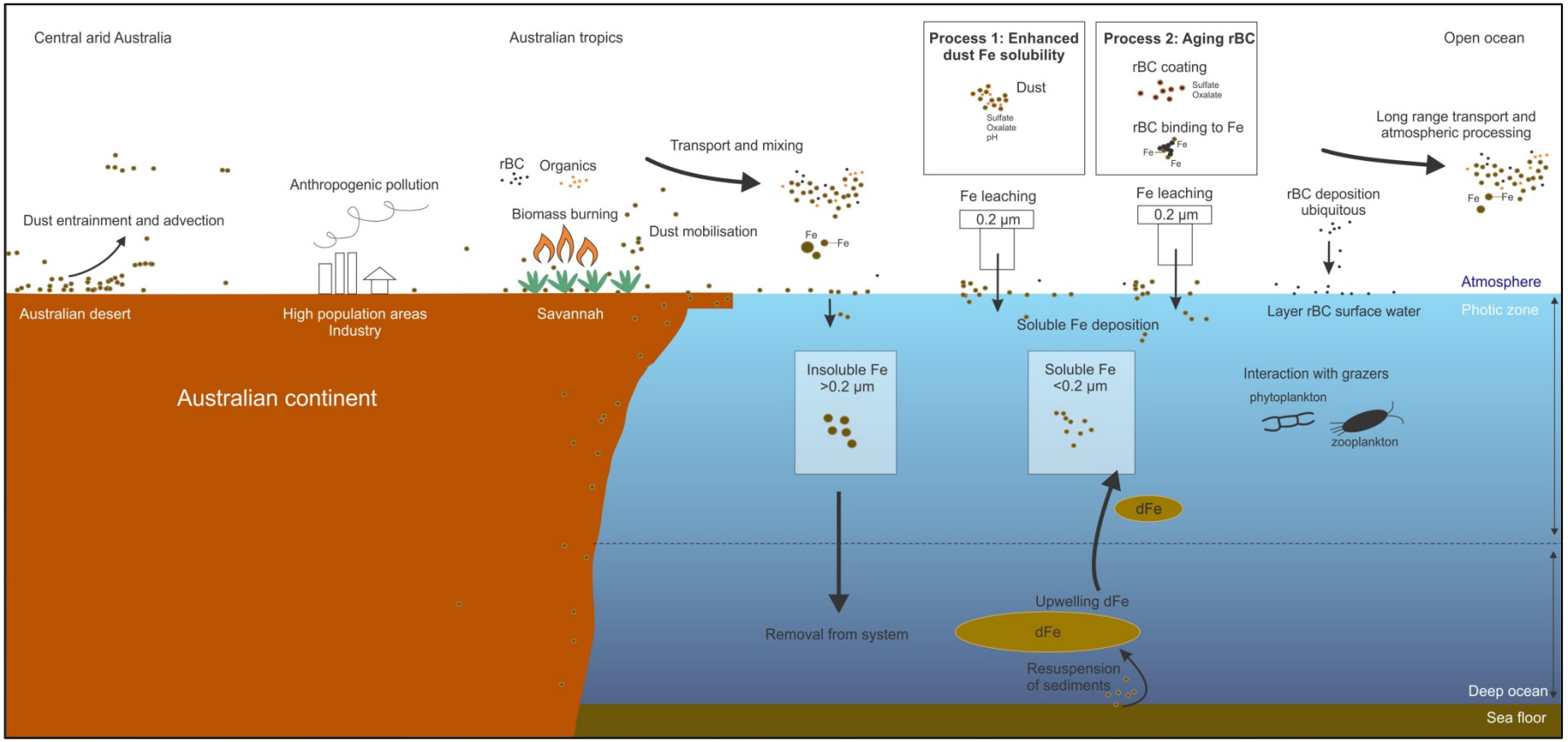

Fig. 8.4: Schematic indicating the processes by which dust and biomass burning supply soluble iron to Australian and Antarctic waters.

8.4 What are the potential impacts of changes in fractional iron solubility on glacial to interglacial climate regimes?

It is well recognised in paleoclimate records that dust fluxes rose dramatically, up to an order of magnitude, during glacial periods [e.g. *Lambert et al.*, 2008; *Martínez-Garcia et al.*, 2009]. The inverse relationship between dust fluxes, iron fluxes, atmospheric CO_2 concentrations and temperature in Antarctic ice cores suggested that iron-fertilisation from dust might stimulate phytoplankton growth in high nutrient, low chlorophyll (HNLC) waters and hence increase the vigour of the ocean's "biological carbon pump" during glacial periods, drawing down atmospheric CO_2 into the ocean and initiating global temperature changes. Aspects of the "iron hypothesis" [*Martin*, 1990] have now been confirmed by *in situ* iron-fertilisation experiments [e.g. *Boyd et al.*, 2000] resulting in carbon sequestration to deep sediments [*Smetacek et al.*, 2012]. Subantarctic marine sediment records characterise glacial periods by increases in nitrate consumption in correspondence with higher dust fluxes, burial fluxes of iron and primary productivity [*Martínez-García et al.*, 2014]. However, the lag between dust and CO_2 records has become apparent in new high-resolution records and this questions the validity of the "iron hypothesis."

In terms of iron bioavailability, it is not the total amount of iron that is important to phytoplankton but the fraction that is available for biological uptake; soluble iron is often used as a proxy for bioavailable iron. Previous studies using Antarctic ice core records either have not measured the soluble fraction of iron (i.e., <0.2 µm), or they assumed a constant fractional iron solubility derived solely from dust and total iron sources [*Edwards et al.*, 2006; *Gaspari et al.*, 2006; *Wolff et al.*, 2006]. This assumption was also made for the Talos Dome ice core which is influenced by local dust sources in the current climate [*Delmonte et al.*, 2010b; *Vallelonga et al.*, 2013]. However, in this research, a high-resolution snow pit record from Roosevelt Island, also influenced by local dust sources and where the TDFe and TDAl concentrations co-vary, soluble iron and fractional iron solubility do not parallel dust, TDAl or TDFe concentrations (Chapter 6). Here, fractional iron solubility is episodic, and soluble iron concentrations reflect multiple sources. The non-linear relationship between total iron and fractional iron solubility (Fig. 8.2) is even more apparent at the inland location of ABN, where there is a very weak correlation between soluble iron and TDAl or TDFe concentrations. Figure 8.2c and section 8.5.2 show that fractional iron solubility is a function

of total aerosol iron, and that the inverse hyperbolic relationship can be explained by a simple two component mixture of mineral dust and combustion iron sources. Therefore, the assumption made in ice core records that fractional iron solubility is constant with total iron is incorrect.

To advance the understanding of how the variability in mineral dust sources relates to changes in soluble iron deposition during glacial-interglacial transitions, the equation of the mixing line in Fig 8.2c was applied to the 800 kyr Antarctic dust record at EPICA Dome C [*Lambert et al.*, 2008]. In doing this simple thought experiment, the assumption is made that the total iron content in dust is constant at 3.5 wt % over the last 800 kyr [*Taylor and McLennan*, 1995]. It is acknowledged that the relationship between dust and total iron in Antarctic snow and ice is not always linear, especially for sites influenced by long-range transported dust, however no high resolution direct measurements of total iron are reported for the Dome C ice core. Figure 8.5 illustrates the estimated soluble iron concentration and fractional iron solubility over the last 800 kyr at Dome C. These estimates do not capture the exceptionally high fractional iron solubility observed at Roosevelt Island (up to 30 %), ABN (up to 6 %) or Cape Grim (up to 60 %). The estimated fractional iron solubility in Fig. 8.5 only ranges between 0.001-1.4 %. Similar to Roosevelt Island, actual measurements of fractional iron solubility in discrete samples of LGM dust from Dome C were variable and ranged between 1-42 % [*Conway et al.*, 2015]. The estimates here do not capture the higher fractional iron solubility end member because total iron is assumed to be constant over the past 800 kyr. Total iron concentrations may have varied due to changes in PSA of dust [*Delmonte et al.*, 2002; *Delmonte et al.*, 2004a; *Gabrielli et al.*, 2010b], or to changes in the aerosol source e.g. combustion aerosol with a lower total iron content. Therefore, the upper values of estimated fractional iron solubility are likely to be underestimated. Nevertheless, fractional iron solubility is higher during the Holocene and drops off during the LGM. According to the mixing model, the increase in fractional iron solubility could be related to changes in mineral dust and combustion sources during the LGM [*Delmonte et al.*, 2002]. Biomass burning records from the WAIS Divide ice core [*Bisiaux et al.*, 2012b] and the Roosevelt Island ice core [*unpublished data, R. Edwards*, 2015] show an increase in rBC around 8-10 kyr. Fire emissions were lower during the LGM when fractional iron solubility is low. Increased soluble iron concentrations during the Holocene could have been enhanced by biomass burning-derived oxalate (see section 8.3.4).

Estimated soluble iron concentrations for the past 800 kyr at Dome C are on the same order of magnitude as observed in present day snow at Roosevelt Island and ABN, i.e., concentrations range between 0.001-0.004 ng g^{-1} of soluble iron. However, applying the mixing model to the Dome C dust record demonstrates that there is only an increase in about half of the soluble iron concentration between glacial and interglacial periods, compared to the total iron or dust variability which is an order of magnitude. Therefore, soluble or bioavailable iron deposition to the Southern Ocean over the last glacial may have been minimal, and a change in thinking of the importance of dust medicated primary productivity may be in order. New inputs of DFe from upwelling in the modern and paleo-Southern Ocean have been shown to be a key driver of primary production [e.g. *Dulaiova et al.*, 2009; *Jong et al.*, 2012; *Latimer and Filippelli*, 2001; *Latimer et al.*, 2006; *Marsay et al.*, 2014]. Even if past natural iron-fertilisation was low, future inputs of soluble iron could be higher with combustion sources predicted to rise over the next century, e.g. coal combustion [*Lin et al.*, 2015] and biomass burning [*Scheiter et al.*, 2015], and hence the potential of biomass burning derived oxalate to enhance the fractional iron solubility of mineral dust. Furthermore, ice core records show that dust leads CO_2 concentrations during glacial-interglacial transitions and that there is a ~1000-2000 year difference between dust and CO_2 concentrations [*Ridgwell and Watson*, 2002]. One hypothesis which could explain the shift during glacial-interglacial transitions is that changes in vegetation growth and increased biomass burning enhanced the fractional iron solubility of mineral dust and increased soluble iron inputs to the ocean. This simple thought experiment highlights that the relationship between soluble iron and dust is complex and a simple scaling of dust/total iron to soluble iron is not a good estimation of bioavailable iron inputs to the Southern Ocean.

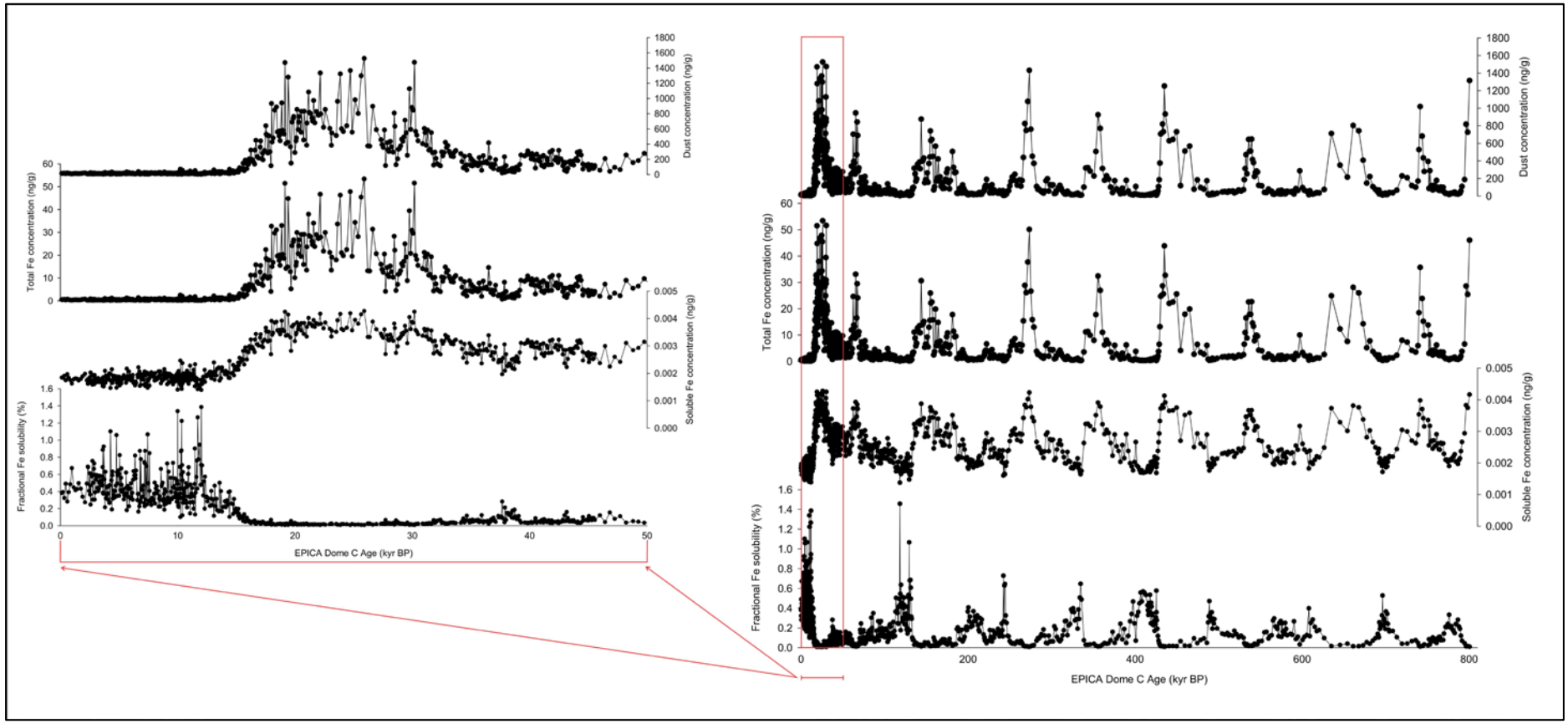

Fig. 8.5: Estimated soluble iron concentrations and fractional iron solubility in the EPICA Dome C ice core (location in Fig 8.1) using a simple two component mixing model and assuming the total iron concentration in dust is constant at 3.5 % [Taylor and McLennan, 1995] throughout the last 800 kyr. Right: 800 kyr ice core record. a) Dust concentration (data source: Lambert et al. [2008]). b) Estimated total iron concentration. c) Estimated soluble iron concentration. d) Estimated fractional iron solubility. Left: insert of the Holocene and LGM transition.

8.5 Future work and recommendations

8.5.1 Future work

In addition to longer high-resolution records of soluble iron, oxalic acid and elemental/black carbon concentrations for the Australian section of the Southern Hemisphere, the following future work is suggested to better understand the impact of dust and biomass burning on soluble iron deposition.

8.5.1.1 New study sites in the Australian section of the Southern Hemisphere

More study sites in the Australian section of the Southern Hemisphere are required for better spatial coverage to investigate latitudinal gradients of soluble iron deposition. Additional sites could also highlight contributions of local versus remote dust sources. Figure 8.6 illustrates the spatial distribution of sampling sites, using various platforms, investigated in this research and those proposed and/or commenced for future work.

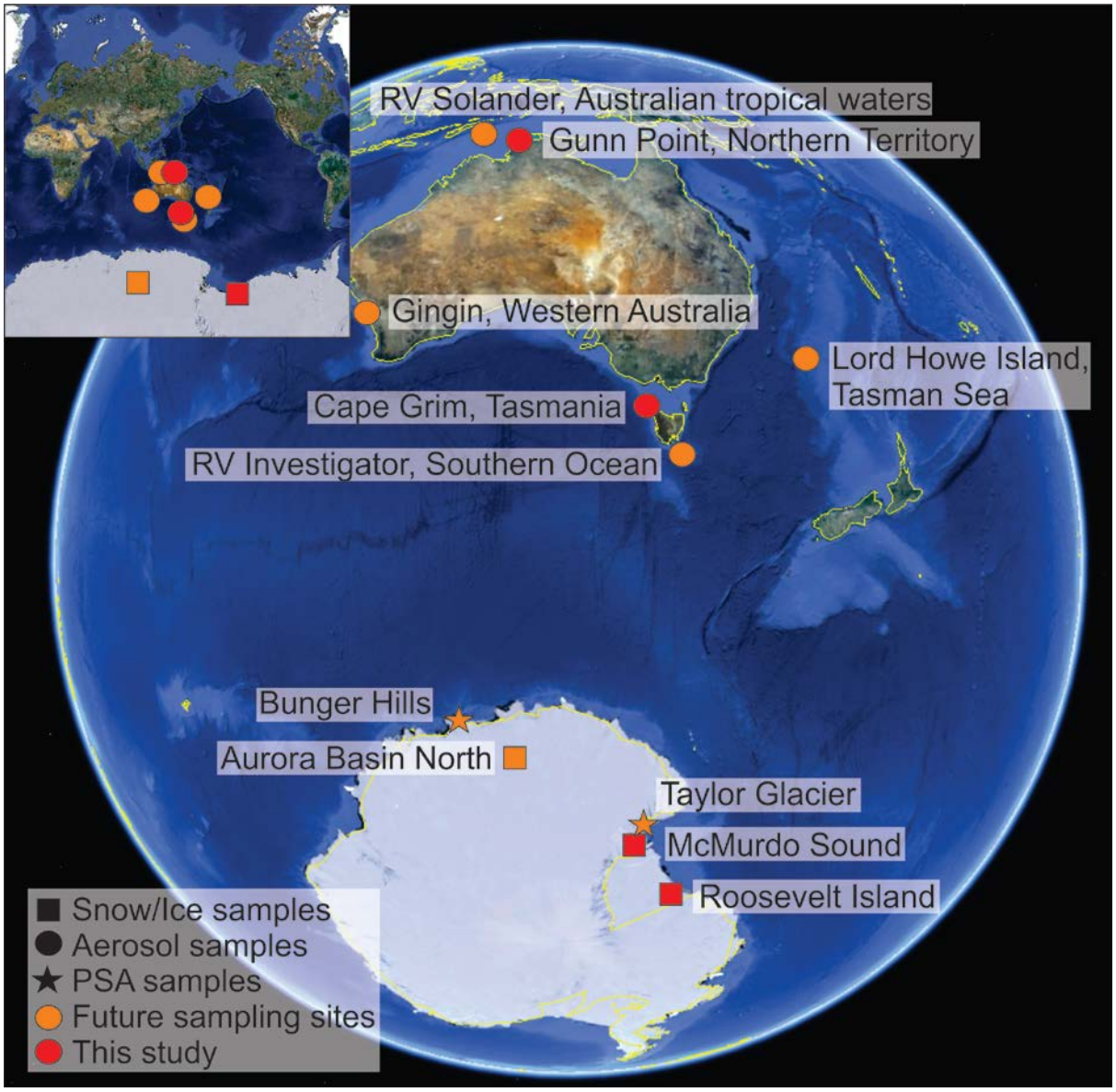

Fig. 8.6: Current (red) and future (orange) sample sites for aerosols (circle), snow/ice (square) and potential source area (PSA; star) samples.

Land-based sampling sites

In terms of land-based aerosol sampling around coastal Australia, two additional sites have been identified for long-term monitoring of marine trace metal aerosols. A high-volume aerosol sampler (Lear Siegler) has been installed at the Gingin Gravity Discovery Center in Western Australia (31.36 °S, 115.71 °E) (Figs. 8.6 and 8.7a-b). The sampler was installed on the 50 m Gingin tower to minimize local soil contamination following recommendations for low level aerosol sampling in Chapter 3. The Bureau of Meteorology wind data for 9 am and 3 pm (AWST) at the Gingin airport show a switch from easterlies in the morning to south

easterlies in the afternoon associated with a sea breeze (http://www.bom.gov.au/climate/averages/tables/cw_009178.shtml). Ten-day air mass back trajectories were generated for the Gingin site, based on an air mass trajectory finishing elevation of 50 m a.g.l., and using the HYSPLIT model and reanalysis data downloaded from the NOAA website (https://ready.arl.noaa.gov/HYSPLIT.php). Examples of air mass back trajectories are illustrated in Fig. 8.7c. Based on the preliminary air mass back trajectories, this is an ideal site to investigate trace metal aerosols from a different section of the Southern Hemisphere than Cape Grim. By setting up a baseline switch, similar to Cape Grim, sector controlled marine air can be sampled from the Southern Indian Ocean. This site has the potential to capture African biomass burning events transported into the Southern Ocean, for example the GOCART model (Fig. 2.10) indicates that the migration of African rBC plumes over the Southern Ocean is common and some plumes sweep back up to southwestern Australia (rBC model animation: https://svs.gsfc.nasa.gov/cgi-bin/details.cgi?aid=3668). Lord Howe Island, in the Tasman Sea has also been identified as a possible location to set up a long-term monitoring campaign for trace metal aerosols (Fig. 8.6). In addition, sampling at Cape Grim will continue with the intention to minimise local soil contamination by sealing the sampler's air inlet during non-baseline conditions following recommendations in Chapter 3 for low level soluble iron sampling.

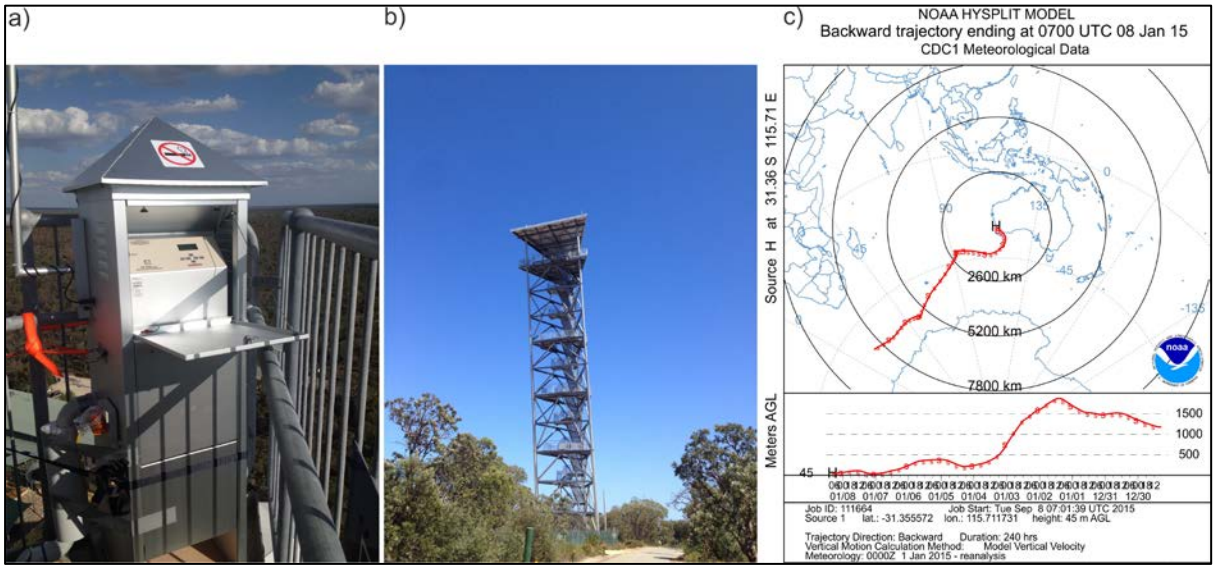

Fig. 8.7: Aerosol sampling at Gingin, Western Australia. a) High-volume aerosol sampler. b) The 50 m Gingin tower. c) Example of ten-day air mass back trajectory arriving at Gingin.

Ship-based sampling platforms

Two future opportunities exist for ship-based trace metal aerosol sampling. Firstly, a purpose built sampling system for low level trace metal aerosol loading over the Southern Ocean was tested on Australia's new research vessel the "RV Investigator" during sea trials in March 2015. Due to the low concentrations of aerosol iron over the Southern Ocean (Chapter 5), large volumes of air are required for analysis of soluble iron. The sampler design followed recommendations from Chapter 3 to minimise contamination. The trace metal aerosol sampling design took advantage of the ship's 10 m aerosol mast and air intake to the aerosol lab located at the bow of the ship. Here, an ultra-clean in-line aerosol filtration sampling system was tested. The sampler consisted of marine air being filtered through acid-washed Whatman 41 filters housed in all PFA acid-washed filter holders (Fig. 8.8). During the three day cruise, five samples were collected (Table 8.2) and 24 hour exposure blanks were run (n=3). Future work will focus on measuring the total and soluble iron concentrations of the blank filters and conducting microscope observations (following recommendations in Chapter 3) to test the cleanliness of this system for future voyages. In addition, a "baseline switch" will be set up to avoid sampling the ship exhaust. This will allow semi-permanent sampling during voyages with minimal personal requirements to change over filters. Secondly, future opportunities exist to collect trace metal aerosol samples over the Australian tropical waters on-board the RV Solander in collaboration with Australian Institute of Marine Science (AIMS).

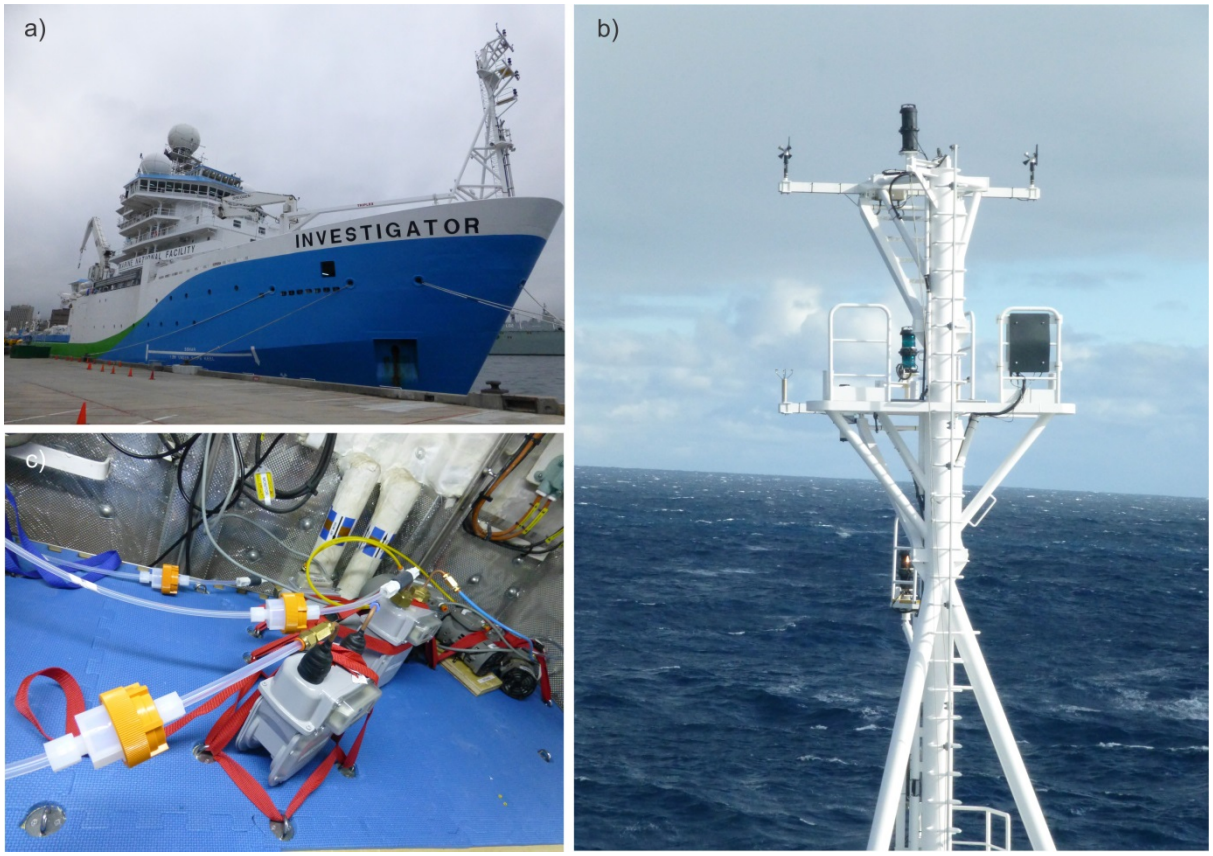

Fig. 8.8: Trace metal aerosol sampling on board the RV Investigator. a) RV Investigator, b) The 10 m aerosol mast and air intake. c) Aerosol in-line filtration sampling system.

Table 8.2: RV Investigator trace metal aerosol samples. Pumps were turned on only when the wind direction was in the clean air sector i.e. 45 ° either side of the bow. Location of station 1: 43° 29.635 S, 148°24.653 E.

Sample name	Start date (EAST)	Finish date (EAST)	Total sampling time (hours)	Total sampling volume (m^3)	Location
RVI15TM_ Line1_01	25/04/2015 22:10 26/04/2015 5:22	26/04/2015 1:41 26/04/2015 6:23	4:32	0	Hobart to Station 1
RVI15TM_ Line2_01	25/04/2015 22:10 26/04/2015 5:22	26/04/2015 1:41 26/04/2015 6:23	4:32	4612	Hobart to Station 1
RVI15TM_ Line3_01	25/04/2015 22:10 26/04/2015 5:22	26/04/2015 1:41 26/04/2015 6:23	4:32	4715	Hobart to Station 1
RVI15TM_ Line1_02	26/04/2015 10:40 27/04/2015 8:25	27/04/2015 4:52 27/04/2015 23:51	33.38	32792	Station 1
RVI15TM_ Line2_02	26/04/2015 10:40 27/04/2015 8:25	27/04/2015 4:52 27/04/2015 23:51	33.38	33174	Station 1

Antarctic ice core sites

The spatial coverage of soluble iron measurements over the Antarctic continent should be increased; as local dust sources (observed at Roosevelt Island, McMurdo Sound, Talos Dome, Berkner Island) can mask a long-range transport signal. Higher-resolution and longer ice core records are thus needed from inland sites located well away from exposed rock. One such site is ABN, located in East Antarctica half way between coastal Law Dome and high elevation Dome C ice core sites (Fig. 8.6). Preliminary data from an eight year snow pit from the ABN site are shown in Fig. 8.9 and were acquired following the same method as at Roosevelt Island (Chapter 6). The snow pit was dated using annual layer counting of non-sea-salt (nss) S concentrations, assuming the maximum annual concentration occurs in January (Chapter 6). Due to the high surface roughness at the site and consequently uneven annual snow layers (indicated by the back lit stratigraphy of the snow pit), spatial variability between parallel profiles was observed. Thus, the peaks and troughs in the water stable isotope record (measured on a different set of samples to the glacio-chemical sample profile) were pinned to the nss-S concentration peaks and troughs using Analy Series. The dating error is assumed to be ± one year and 5 cm w.e. depth. Refractory black carbon displayed seasonal variability, with maximum concentrations in late winter early spring consistent with the WAIS Divide ice core [*Bisiaux et al.*, 2012b]. The rBC concentrations were extremely low and ranged between 3-63 pg g^{-1} of rBC. Exceptionally high rBC was observed in the top 10 cm of the snow pack. Although the snow pit was sampled in a designed clean zone, a few days before sampling issues with the kerosene heater operating at high elevation caused an explosion of soot within a >10 m radius of the camp. The kerosene heater may have contaminated the upper four samples in the snow pit. Concentrations of DFe in the ABN snow pit were even lower than Roosevelt Island, and often below the detection limit. However, there were three peaks in DFe concentrations; one occurring simultaneously with the high rBC concentrations at the surface and thus this peak is related to soot contamination. Of the other two peaks, one occurred at the same time as high TDFe, TDAl and rBC concentrations, while the other was not associated with TDFe or TDAl and only relatively low concentrations of rBC. At ABN, there are episodic changes in DFe, with a complex relation between TDFe inputs and rBC. Fractional iron solubility was not linearly correlated to TDFe. Even away from local dust sources, the fractional iron solubility was <1 %, similar to Roosevelt Island (Fig. 8.2), suggesting that the long-range transport of soluble iron is not enhanced in the pristine

atmosphere over the Southern Ocean. Clearly, longer ice core records of soluble iron and rBC are required to resolve the seasonality of soluble iron deposition to central Antarctica, and investigate the processing of soluble iron in a baseline air.

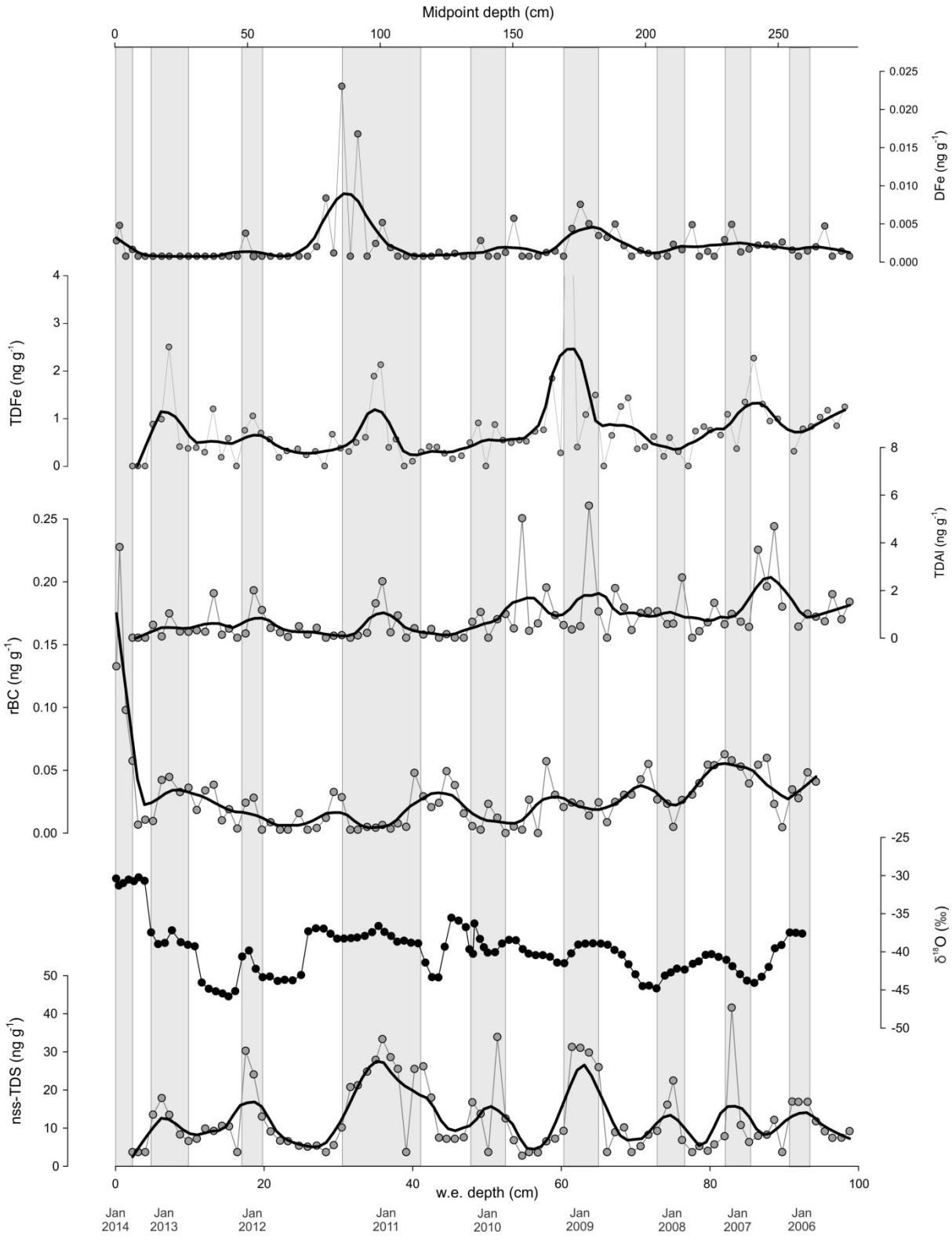

Fig. 8.9: Preliminary data from the Aurora Basin North snow pit. a) Dissolved iron concentration. b) Total dissolvable iron concentration. c) Total dissolvable aluminium concentration. d) Refractory black carbon concentration. e) Water isotope ratio (data source: *A. Moy*, 2015). f) Non sea salt-sulfer concentration.

8.5.1.2 Implications of biomass burning emissions to soluble iron deposition

This research has shown that biomass burring could influence soluble iron by a number of processes either; i) by iron binding to elemental/black carbon aerosols or chemical absorption of iron onto the surface of elemental/black carbon aerosols, ii) by the enhancement of fractional iron solubility in dust by interaction of biomass burring derived organic acids, or iii) by the suspension of local soil into the smoke plume via pyro-convection. Future work could investigate the process by which soluble iron is incorporated into aerosol populations and how biomass burning emissions can interact with dust to enhance the fractional iron solubility. It would be interesting to sample aerosols downwind from biomass burning sites and to follow a smoke plume at sea using ultra-trace sampling protocols (Chapter 3), such as an aerosol inline-filtration device (see section 8.5.1). This would provide information on soluble iron as it ages and is transported from the source to the open ocean. Single particle analysis of rBC could shed light about mixed iron sources at various latitudes. In order to determine if oxalate enhances the fractional iron solubility in dust in pristine air over the Southern Ocean, longer high-resolution Antarctic ice core records of soluble iron, pH and oxalate are required. As rBC may not be a direct source of soluble iron to surface waters, other fire proxies such as levoglucosan should be measured in conjunction with soluble iron in ice cores.

8.5.1.3 Antarctic potential source areas

Little is known about the importance of local dust sources to Antarctic ice core sites [*Bory et al.*, 2010; *Delmonte et al.*, 2010b] and proximal Antarctic waters (Chapters 6 and 7). Antarctic potential source areas (PSA) need to be identified and characterised to assess their influence on soluble iron inputs to Antarctic waters and the Southern Ocean (section 8.2). Chapters 6 and 7 identified and characterised PSA around the Ross Sea. At Roosevelt Island, local dust sources from Marie Byrd Land contributed to the dust flux and soluble iron supply. Here, the mean fractional iron solubility was <1 %, excluding two large peaks. The low fractional iron solubility was interpreted to reflect local mineral dust sources. However, at ABN located 550 km inland from the coast, the fractional iron solubility was also <1 %. It is currently unknown if local or long-range transported dust influence the low fractional iron solubility. Preliminary Sr isotopic composition of ABN dust is reported in Fig. 8.10 and compared to Antarctica and remote PSA. The Sr isotopic composition of ABN dust lies between Roosevelt Island and EAIS pre-industrial dust. Both of these sites receive

contributions from local and remote sources. However, there is currently insufficient data to determine the provenance of the ABN dust. In addition to more Sr-Nd isotopic analyses of dust from the ABN site, particles counts, particle size distribution and microscope observations of particles are required to assess the provenance of dust deposited at ABN. The difficulty with making Sr and Nd isotopic measurements of dust contained in Antarctic snow and ice is the low concentration of dust. This means that large volumes of snow and ice are required to concentrate enough dust for isotopic analysis. For efficiency, future ice core fieldwork could consider melting and filtering large volumes of snow and ice in the field [*Bory et al.*, 2010].

Other Antarctica PSA are yet to be sampled and characterised in terms of their isotopic composition, for example Terra Nova Bay in Southern Victoria Land, the Antarctic Peninsula, Vestfold Hills and Bunger Hills in coastal East Antarctica, other mountain ranges and valley glaciers in the Transantarctic Mountains such as Taylor Glacier Valley, and nunataks proximal to ice core sites and coastal regions. New size selected Sr and Nd isotopic data from Bunger Hills (exposed during the LGM; *Augustinus and Duller* [2002]; *Gore et al.* [2001]) and Taylor Glacier Valley are reported in Fig. 8.10. This isotopic data will be valuable for future studies investigating the provenance of dust in ice cores. Furthermore, Antarctic PSA can change in terms of their extent and ice coverage between glacial and interglacial periods [e.g. *Denton and Marchant*, 2000; *Denton and Hughes*, 2002]. It is therefore important to select PSA that were exposed during the LGM for comparison to LGM ice core dust and soluble iron concentrations. Furthermore, as Antarctic ice shelves are predicted to melt during the next century, new and greater aerial extent of existing PSA may emerge.

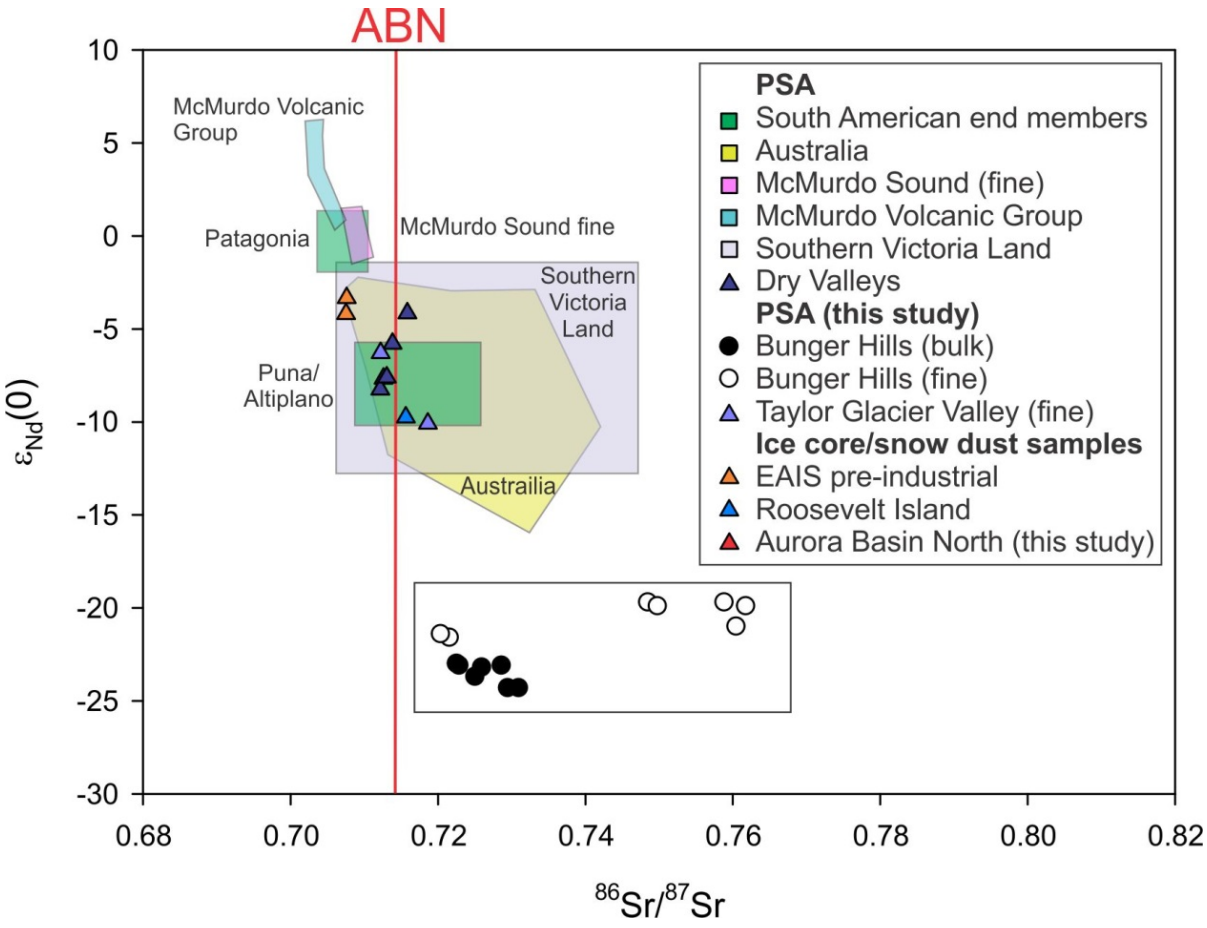

Fig. 8.10: Sr and Nd isotopic composition of Aurora Basin North dust and Antarctic PSA samples from Taylor Glacier Valley and Bunger Hills. Locations of samples are shown in Fig. 8.6. Also plotted are PSA data for South America [Delmonte et al., 2004b], Australia [*Delmonte et al.*, 2004b; *Grousset et al.*, 1992c; *Revel-Rolland et al.*, 2006], southern Victoria Land [Delmonte et al., 2004b; Delmonte et al., 2013], McMurdo Sound (Chapter 7), the Dry Valleys [Delmonte et al., 2004b; Delmonte et al., 2013] and McMurdo Volcanic Group [Delmonte et al., 2004b]. The composition of ice core/snow dust other Antarctic ice core sites are plotted (pre-industrial dust from the East Antarctic Ice Sheet (EAIS) [Delmonte et al., 2013]; Roosevelt Island (Chapter 6)).

8.5.2 Recommendations

8.5.2.1 Future sampling for low level aerosol iron

Recommendations for future aerosol sampling for soluble iron analysis in pristine air include:

1. Microscope observations of blank filters

Contamination of exposure blanks filters in Chapter 3 was invisible to the naked eye. However, local soil contamination constituted a substantial source of the iron blank

budget compared to the expected iron aerosol loading in marine at Cape Grim in uncontaminated samples (Chapter 5).

2. Location of high-volume aerosol sampler

High-volume aerosol samplers at low aerosol iron loading locations, such as Southern Ocean sites and Subantarctic Islands, should be located above the boundary layer to avoid local soil contamination e.g. 50 m tower at Gingin Gravity Discovery Centre (section 8.5.1).

3. Closure of aerosol sampler during non-baseline/out of sector winds

The contamination at Cape Grim in Chapter 3 was primarily due to the lack of an air-tight closure at the sample intake when the sampler was turned off. A hermetic closure is desirable to minimise contamination when the wind direction is out of sector.

4. Ship-based high-volume aerosol samplers

Ship-based high-volume aerosol samplers are exposed to contaminates from ship exhaust (Edwards, 1999) for similar reasons to land based aerosol samplers (Chapter 3), and should also be fitted with a hermetic closure to completely seal the sampler when the wind direction is out of sector or the wind speed is too low. An in-line filtration system, such as that tested on the RV Investigator (section 8.5.1; Fig. 8.8) is also recommended.

5. Antarctic ice core sites

Energy generation and transport (e.g. skidoos, kerosene heaters) at ice core sites can contaminate the surface snow, as seen in the top 10 cm at ABN (see section 8.5.1). Ice core drilling sites and snow pits should be situated in a designated ‘clean zone’ well away from camp activities.

8.5.2.2 Caution using dust or total iron to estimate soluble iron

As a whole, the results of this research revealed that iron solubility cannot be directly compared to total iron inputs, and that considerable spatial and temporal variations exist.

Thus, previous total iron flux estimates from Antarctic ice cores may not be translated into bioavailable iron estimates (see section 8.4). Caution is advised in ice core and model interpretations of dust or total iron to estimate soluble iron, as the fractional iron solubility is not always linear (Fig. 8.2c). New high-resolution soluble iron measurements from ice cores are needed over the glacial transition to understand the impact of past iron deposition on Southern Ocean primary productivity.

8.5.2.3 Future analytical advances and a standardised method for determining aerosol iron solubility

This research used ultra-pure water and Antarctic snow leaches to estimate soluble iron concentrations in aerosols and Antarctic snowfall. Soluble iron, while it principally influences iron bioavailability, can be absorbed and thus only a fraction of the iron is potentially bioavailable. There are advantages and disadvantages of using soluble iron as a measure of bioavailability and thus the *Berger et al.* [2008] acetic acid leach is recommended as a standardised method for determining aerosol iron solubility rather than the instantaneous ultra-pure water leach method. While iron solubility experiments do not determine if the iron is taken up by phytoplankton, they are comparatively fast, inexpensive and reproducible when compared to more complex ecosystem studies. Experimental artefacts arising from the numerous leaching scheme employed in the literature, such as the organic complexing capacity of the leaching solution [*Wu et al.*, 2007] and the pH of the leaching solution [*Buck et al.*, 2006; *Mackie et al.*, 2005; *Spokes and Jickells*, 1995] can make comparisons of iron solubility challenging. The successive ultra-pure water leach used in this research may underestimate the fractional iron solubility. For example, iron continued to leach out of the Gunn Point aerosols even after 20 passes of ultra-pure water. Although seawater is the obvious choice of leaching solution, seawater is heterogeneous in time and space. In addition, ligands in seawater are not present in ultra-pure water. Recently, it has been observed that organic ligands control the concentrations of DFe in Antarctic sea ice [*Lannuzel et al.*, 2015]. Moreover, bioavailability can be dependent on the oxidation state of iron. Fe(II) has been shown to be more soluble and therefore more bioavailable. Some researchers use Fe(II) as a proxy for labile iron [*Chen and Siefert*, 2004]. Due to the limitations of using an ultra-pure water leach to estimate soluble iron (bioavailable Fe), future analytical advances in iron leaching schemes could focus on; i) measuring Fe(II) in aerosols [e.g. *Chen and Siefert*,

2004] and snow/ice core samples [*Spolaor et al.*, 2012], and ii) conducting iron leaching experiments with ligands to evaluate iron bioavailability.

References

Abram, N. J., M. K. Gagan, M. T. McCulloch, J. Chappell, and W. S. Hantoro (2003), Coral reef death during the 1997 Indian Ocean dipole linked to Indonesian wildfires, *Science*, *301*(5635), 952-955.

Augustinus, P., and G. Duller (2002), Luminescence and radiocarbon dating of raised beach sediments, Bunger Hills, East Antarctica, paper presented at Antarctica at the close of a millennium: proceedings of the 8th International Symposium on Antarctic Earth Sciences, Wellington 1999.

Bhattachan, A., and P. D'Odorico (2014), Can land use intensification in the Mallee, Australia increase the supply of soluble iron to the Southern Ocean?, *Scientific reports*, *4*.

Bisiaux, M., R. Edwards, J. McConnell, M. Curran, T. Van Ommen, A. Smith, T. Neumann, D. Pasteris, J. Penner, and K. Taylor (2012), Changes in black carbon deposition to Antarctica from two high-resolution ice core records, 1850–2000 AD, *Atmospheric Chemistry and Physics*, *12*(9), 4107-4115.

Bory, A., E. Wolff, R. Mulvaney, E. Jagoutz, A. Wegner, U. Ruth, and H. Elderfield (2010), Multiple sources supply eolian mineral dust to the Atlantic sector of coastal Antarctica: Evidence from recent snow layers at the top of Berkner Island ice sheet, *Earth and Planetary Science Letters*, *291*(1-4), 138-148.

Bowie, A. R., D. Lannuzel, T. A. Remenyi, T. Wagener, P. J. Lam, P. W. Boyd, C. Guieu, A. T. Townsend, and T. W. Trull (2009), Biogeochemical iron budgets of the Southern Ocean south of Australia: Decoupling of iron and nutrient cycles in the subantarctic zone by the summertime supply, *Global Biogeochem. Cycles*, *23*(4), GB4034.

Boyd, P. W., and D. S. Mackie (2008), Comment on 'The Southern Ocean biological response to aeolian iron deposition', *Science*, *319*, 159.

Boyd, P. W., D. S. Mackie, and K. A. Hunter (2010), Aerosol iron deposition to the surface ocean - Modes of iron supply and biological responses, *Marine Chemistry*, *120*(1-4), 128-143.

Boyd, P. W., G. McTainsh, V. Sherlock, K. Richardson, S. Nichol, M. Ellwood, and R. Frew (2004), Episodic enhancement of phytoplankton stocks in New Zealand subantarctic waters: Contribution of atmospheric and oceanic iron supply, *Global Biogeochem. Cycles*, *18*(1), GB1029.

Boyd, P. W., et al. (2000), A mesoscale phytoplankton bloom in the polar Southern Ocean stimulated by iron fertilization, *Nature*, *407*(6805), 695-702.

Chewings, J. M., C. B. Atkins, G. B. Dunbar, and N. R. Golledge (2014), Aeolian sediment transport and deposition in a modern high latitude glacial marine environment, *Sedimentology*.

Chuang, P. Y., R. M. Duvall, M. M. Shafer, and J. J. Schauer (2005), The origin of water soluble particulate iron in the Asian atmospheric outflow, *Geophys. Res. Lett.*, *32*(7), L07813.

Conway, T., E. Wolff, R. Röthlisberger, R. Mulvaney, and H. Elderfield (2015), Constraints on soluble aerosol iron flux to the Southern Ocean at the Last Glacial Maximum, *Nature Communications*, *6*.

de Jong, J., V. Schoemann, N. Maricq, N. Mattielli, P. Langhorne, T. Haskell, and J.-L. Tison (2013), Iron in land-fast sea ice of McMurdo Sound derived from sediment resuspension and wind-blown dust attributes to primary productivity in the Ross Sea, Antarctica, *Marine Chemistry*, *157*(0), 24-40.

Delmonte, B., J. R. Petit, and V. Maggi (2002), Glacial to Holocene implications of the new 27000-year dust record from the EPICA Dome C (East Antarctica) ice core, *Climate Dynamics*, *18*(8), 647-660.

Delmonte, B., J. R. Petit, K. K. Andersen, I. Basile-Doelsch, V. Maggi, and V. Ya Lipenkov (2004a), Dust size evidence for opposite regional atmospheric circulation changes over east Antarctica during the last climatic transition, *Climate Dynamics*, *23*(3), 427-438.

Delmonte, B., I. Basile-Doelsch, J. R. Petit, V. Maggi, M. Revel-Rolland, A. Michard, E. Jagoutz, and F. Grousset (2004b), Comparing the Epica and Vostok dust records during the last 220,000 years: stratigraphical correlation and provenance in glacial periods, *Earth-Science Reviews*, *66*(1-2), 63-87.

Delmonte, B., C. Baroni, P. Andersson, B. Narcisi, M. Salvatore, J. Petit, C. Scarchilli, M. Frezzotti, S. Albani, and V. Maggi (2013), Modern and Holocene aeolian dust variability from Talos Dome (Northern Victoria Land) to the interior of the Antarctic ice sheet, *Quaternary Science Reviews*, *64*, 76-89.

Delmonte, B., et al. (2010), Aeolian dust in the Talos Dome ice core (East Antarctica, Pacific/Ross Sea sector): Victoria Land versus remote sources over the last two climate cycles, *Journal of Quaternary Science*, *25*(8), 1327-1337.

Denton, G. H., and D. R. Marchant (2000), The Geologic Basis for a Reconstruction of a Grounded Ice Sheet in McMurdo Sound, Antarctica, at the Last Glacial Maximum, *Geografiska Annaler: Series A, Physical Geography*, *82*(2-3), 167-211.

Denton, G. H., and T. J. Hughes (2002), Reconstructing the Antarctic Ice Sheet at the Last Glacial Maximum, *Quaternary Science Reviews*, *21*(1-3), 193-202.

Draxler, R. R., and G. D. Rolph (2003), Hybrid Single-Particle Lagrangian Integrated Trajectory (HYSPLIT), model, http://www.arl.noaa.gov/ready/hysplit4.html.

Dulaiova, H., M. Ardelan, P. B. Henderson, and M. A. Charette (2009), Shelf-derived iron inputs drive biological productivity in the southern Drake Passage, *Global Biogeochemical Cycles*, *23*(4).

Edwards, P., P. Sedwick, V. Morgan, C. Boutron, and S. Hong (1998), Iron in ice cores from Law Dome, East Antarctica: implications for past deposition of aerosol iron, *Annals of Glaciology*, *27*, 365-370.

Edwards, R., P. Sedwick, V. Morgan, and C. Boutron (2006), Iron in ice cores from Law Dome: A record of atmospheric iron deposition for maritime East Antarctica during the Holocene and Last Glacial Maximum, *Geochemistry, Geophysics, Geosystems*, *7*(12), Q12Q01.

Ellis, A., R. Edwards, M. Saunders, R. Chakrabarty, R. Subramanian, A. van Riessen, A. Smith, D. Lambrinidis, L. Nunes, and P. Vallelonga (2015), Characterizing black carbon in rain and ice cores using coupled tangential flow filtration and transmission electron microscopy.

Ferek, R. J., J. S. Reid, P. V. Hobbs, D. R. Blake, and C. Liousse (1998), Emission factors of hydrocarbons, halocarbons, trace gases and particles from biomass burning in Brazil, *Journal of Geophysical Research: Atmospheres (1984–2012)*, *103*(D24), 32107-32118.

Gabric, A. J., R. A. Cropp, G. H. McTainsh, B. M. Johnston, H. Butler, B. Tilbrook, and M. Keywood (2010), Australian dust storms in 2002–2003 and their impact on Southern Ocean biogeochemistry, *Global Biogeochemical Cycles*, *24*(2).

Gabrielli, P., et al. (2010), A major glacial-interglacial change in aeolian dust composition inferred from Rare Earth Elements in Antarctic ice, *Quaternary Science Reviews*, *29*(1-2), 265-273.

Gao, Y., G. Xu, J. Zhan, J. Zhang, W. Li, Q. Lin, L. Chen, and H. Lin (2013), Spatial and particle size distributions of atmospheric dissolvable iron in aerosols and its input to the Southern Ocean and coastal East Antarctica, *Journal of Geophysical Research: Atmospheres*, *118*(22), 12,634-612,648.

Gaspari, V., C. Barbante, G. Cozzi, P. Cescon, C. F. Boutron, P. Gabrielli, G. Capodaglio, C. Ferrari, J. R. Petit, and B. Delmonte (2006), Atmospheric iron fluxes over the last deglaciation: Climatic implications, *Geophys. Res. Lett.*, *33*(3), L03704.

Gore, D., E. Rhodes, P. Augustinus, M. Leishman, E. Colhoun, and J. Rees-Jones (2001), Bunger Hills, East Antarctica: ice free at the last glacial maximum, *Geology*, *29*(12), 1103-1106.

Grousset, F. E., P. E. Biscaye, M. Revel, J.-R. Petit, K. Pye, S. Joussaume, and J. Jouzel (1992), Antarctic (Dome C) ice-core dust at 18 k.y. B.P.: Isotopic constraints on origins, *Earth and Planetary Science Letters*, *111*(1), 175-182.

Guieu, C., S. Bonnet, T. Wagener, and M. D. Loÿe-Pilot (2005), Biomass burning as a source of dissolved iron to the open ocean?, *Geophysical Research Letters*, *32*(19).

Ito, A. (2011), Mega fire emissions in Siberia: potential supply of bioavailable iron from forests to the ocean, *Biogeosciences*, *8*(6).

Ito, A. (2015), Atmospheric Processing of Combustion Aerosols as a Source of Bioavailable Iron, *Environmental Science & Technology Letters*, *2*(3), 70-75.

Ito, A., and Z. Shi (2015), Delivery of anthropogenic bioavailable iron from mineral dust and combustion aerosols to the ocean, *Atmospheric Chemistry and Physics Discussions*, *15*(16), 23051-23088.

Jickells, T., et al. (2005), Global iron connections between desert dust, ocean biogeochemistry, and climate, *Science*, *308*, 67 - 73.

Jong, J., V. Schoemann, D. Lannuzel, P. Croot, H. Baar, and J. L. Tison (2012), Natural iron fertilization of the Atlantic sector of the Southern Ocean by continental shelf sources of the Antarctic Peninsula, *Journal of Geophysical Research: Biogeosciences (2005–2012)*, *117*(G1).

Keywood, M. D. (2007), Aerosol composition at Cape Grim : an evaluation of PM10 sampling program and baseline event switches., *Baseline Atmospheric Program Australia 2005-2006. 2005-2006 ed. J. M. Cainey, N. Derek, and P. B. Krummel (editors). Melbourne: Australian Bureau of Meteorology and CSIRO Marine and Atmospheric Research*, 31-36.

Kumar, A., M. Sarin, and B. Srinivas (2010), Aerosol iron solubility over Bay of Bengal: Role of anthropogenic sources and chemical processing, *Marine Chemistry*, *121*(1), 167-175.

Lambert, F., B. Delmonte, J. R. Petit, M. Bigler, P. R. Kaufmann, M. A. Hutterli, T. F. Stocker, U. Ruth, J. P. Steffensen, and V. Maggi (2008), Dust-climate couplings over the past 800,000[thinsp]years from the EPICA Dome C ice core, *Nature*, *452*(7187), 616-619.

Lannuzel, D., V. Schoemann, J. de Jong, J.-L. Tison, and L. Chou (2007), Distribution and biogeochemical behaviour of iron in the East Antarctic sea ice, *Marine Chemistry*, *106*(1-2), 18-32.

Lannuzel, D., V. Schoemann, J. de Jong, B. Pasquer, P. van der Merwe, F. Masson, J.-L. Tison, and A. Bowie (2010), Distribution of dissolved iron in Antarctic sea ice: Spatial, seasonal, and inter-annual variability, *J. Geophys. Res.*, *115*(G3), G03022.

Latimer, J. C., and G. M. Filippelli (2001), Terrigenous input and paleoproductivity in the Southern Ocean, *Paleoceanography*, *16*(6), 627-643.

Latimer, J. C., G. M. Filippelli, I. L. Hendy, J. D. Gleason, and J. D. Blum (2006), Glacial-interglacial terrigenous provenance in the southeastern Atlantic Ocean: The importance of deep-water sources and surface currents, *Geology*, *34*(7), 545-548.

Lin, Y. C., J. P. Chen, T. Y. Ho, and I. Tsai (2015), Atmospheric iron deposition in the northwestern Pacific Ocean and its adjacent marginal seas: The importance of coal burning, *Global Biogeochemical Cycles*, *29*(2), 138-159.

Mackie, D., J. Peat, G. H. McTainsh, P. Boyd, and K. Hunter (2006), Soil abrasion and eolian dust production: Implications for iron partitioning and solubility, *Geochemistry, Geophysics, Geosystems*, *7*(12).

Mahowald, N. M., A. R. Baker, G. Bergametti, N. Brooks, R. A. Duce, T. D. Jickells, N. Kubilay, J. M. Prospero, and I. Tegen (2005), Atmospheric global dust cycle and iron inputs to the ocean, *Global Biogeochem. Cycles*, *19*(4), GB4025.

Mahowald, N. M., S. Engelstaedter, C. Luo, A. Sealy, P. Artaxo, C. Benitez-Nelson, S. Bonnet, Y. Chen, P. Y. Chuang, and D. D. Cohen (2009), Atmospheric iron deposition: Global distribution, variability, and human perturbations*, *Marine Science*, *1*.

Marsay, C., P. N. Sedwick, M. Dinniman, P. Barrett, S. Mack, and D. J. McGillicuddy (2014), Estimating the benthic efflux of dissolved iron on the Ross Sea continental shelf, *Geophysical Research Letters*, *41*(21), 7576-7583.

Martin, J. H. (1990), Glacial-interglacial CO2 change: the iron hypothesis, *Paleoceanography*, *5*, 1-11.

Martínez-Garcia, A., A. Rosell-Melé, W. Geibert, R. Gersonde, P. Masqué, V. Gaspari, and C. Barbante (2009), Links between iron supply, marine productivity, sea surface temperature, and CO2 over the last 1.1 Ma, *Paleoceanography*, *24*(1), PA1207.

Martínez-García, A., D. M. Sigman, H. Ren, R. F. Anderson, M. Straub, D. A. Hodell, S. L. Jaccard, T. I. Eglinton, and G. H. Haug (2014), Iron Fertilization of the Subantarctic Ocean During the Last Ice Age, *Science*, *343*(6177), 1347-1350.

Oberholzer, P., C. Baroni, M. Salvatore, H. Baur, and R. Wieler (2008), Dating late Cenozoic erosional surfaces in Victoria Land, Antarctica, with cosmogenic neon in pyroxenes, *Antarctic Science*, *20*(01), 89-98.

Oberholzer, P., C. Baroni, J. M. Schaefer, G. Orombelli, S. I. Ochs, P. W. Kubik, H. Baur, and R. Wieler (2003), Limited Pliocene/Pleistocene glaciation in Deep Freeze Range, northern Victoria Land, Antarctica, derived from in situ cosmogenic nuclides, *Antarctic science*, *15*(04), 493-502.

Paris, R., K. Desboeufs, P. Formenti, S. Nava, and C. Chou (2010), Chemical characterisation of iron in dust and biomass burning aerosols during AMMA-SOP0/DABEX: implication for iron solubility, *Atmospheric Chemistry and Physics*, *10*(9), 4273-4282.

Revel-Rolland, M., P. De Deckker, B. Delmonte, P. P. Hesse, J. W. Magee, I. Basile-Doelsch, F. Grousset, and D. Bosch (2006), Eastern Australia: A possible source of dust in East Antarctica interglacial ice, *Earth and Planetary Science Letters*, *249*(1-2), 1-13.

Sedwick, P. N., E. R. Sholkovitz, and T. M. Church (2007), Impact of anthropogenic combustion emissions on the fractional solubility of aerosol iron: Evidence from the Sargasso Sea, *Geochem. Geophys. Geosyst.*, *8*(10), Q10Q06.

Sedwick, P. N., et al. (2011), Early season depletion of dissolved iron in the Ross Sea polynya: Implications for iron dynamics on the Antarctic continental shelf, *J. Geophys. Res.*, *116*(C12), C12019.

Sholkovitz, E. R., P. N. Sedwick, and T. M. Church (2009), Influence of anthropogenic combustion emissions on the deposition of soluble aerosol iron to the ocean: Empirical estimates for island sites in the North Atlantic, *Geochimica et Cosmochimica Acta*, *73*(14), 3981-4003.

Sholkovitz, E. R., P. N. Sedwick, T. M. Church, A. R. Baker, and C. F. Powell (2012), Fractional solubility of aerosol iron: Synthesis of a global-scale data set, *Geochimica et cosmochimica acta*, *89*, 173-189.

Smetacek, V., et al. (2012), Deep carbon export from a Southern Ocean iron-fertilized diatom bloom, *Nature*, *487*(7407), 313-319.

Taylor, S. R., and S. M. McLennan (1995), The geochemical evolution of the continental crust, *Rev. Geophys.*, *33*(2), 241-265.

Turn, S., B. Jenkins, J. Chow, L. Pritchett, D. Campbell, T. Cahill, and S. Whalen (1997), Elemental characterization of particulate matter emitted from biomass burning: Wind tunnel derived source profiles for herbaceous and wood fuels, *Journal of Geophysical Research: Atmospheres (1984–2012)*, *102*(D3), 3683-3699.

Vallelonga, P., C. Barbante, G. Cozzi, J. Gabrieli, S. Schüpbach, A. Spolaor, and C. Turetta (2013), Iron fluxes to Talos Dome, Antarctica, over the past 200 kyr, *Climate of the Past*, *9*(2), 597-604.

Van Der Merwe, P., D. Lannuzel, A. Bowie, and K. Meiners (2011a), High temporal resolution observations of spring fast ice melt and seawater iron enrichment in East Antarctica, *Journal of Geophysical Research: Biogeosciences (2005–2012)*, *116*(G3).

van der Merwe, P., D. Lannuzel, A. R. Bowie, C. A. Mancuso Nichols, and K. M. Meiners (2011b), Iron fractionation in pack and fast ice in East Antarctica: Temporal decoupling between the release of dissolved and particulate iron during spring melt, *Deep Sea Research Part II: Topical Studies in Oceanography*, *58*(9-10), 1222-1236.

Ward, D., R. Susott, J. Kauffman, R. Babbitt, D. Cummings, B. Dias, B. Holben, Y. Kaufman, R. Rasmussen, and A. Setzer (1992), Smoke and fire characteristics for cerrado and deforestation burns in Brazil: BASE-B experiment, *Journal of Geophysical Research: Atmospheres (1984–2012)*, *97*(D13), 14601-14619.

Ward, D. E., and C. C. Hardy (1991), Smoke emissions from wildland fires, *Environment International*, *17*(2), 117-134.

Ward, D. E., A. W. Setzer, Y. J. Kaufman, and R. A. Rasmussen (1991), Characteristics of smoke emissions from biomass fires of the Amazon region-BASE-A experiment, *Global Biomass Burning: Atmospheric, Climatic, and Biospheric Implications*, 394-402.

Winton, V. H. L., G. B. Dunbar, N. A. N. Bertler, M. A. Millet, B. Delmonte, C. B. Atkins, J. M. Chewings, and P. Andersson (2014), The contribution of aeolian sand and dust to iron fertilization of phytoplankton blooms in southwestern Ross Sea, Antarctica, *Global Biogeochemical Cycles*, *28*(4), 2013GB004574.

Wolff, E. W., et al. (2006), Southern Ocean sea-ice extent, productivity and iron flux over the past eight glacial cycles, *Nature*, *440*(7083), 491-496.

Yamasoe, M. A., P. Artaxo, A. H. Miguel, and A. G. Allen (2000), Chemical composition of aerosol particles from direct emissions of vegetation fires in the Amazon Basin: water-soluble species and trace elements, *Atmospheric Environment*, *34*(10), 1641-1653.

Bibliography

Abram, N. J., M. K. Gagan, M. T. McCulloch, J. Chappell, and W. S. Hantoro (2003), Coral reef death during the 1997 Indian Ocean dipole linked to Indonesian wildfires, Science, 301(5635), 952-955.

Adams, C., D. Seward, and S. Weaver (1995), Geochronology of Cretaceous granites and metasedimentary basement on Edward VII Peninsula, Marie Byrd Land, West Antarctica, Antarctic science, 7(03), 265-276.

Aguilar-Islas, A. M., J. Wu, R. Rember, A. M. Johansen, and L. M. Shank (2010), Dissolution of aerosol-derived iron in seawater: Leach solution chemistry, aerosol type, and colloidal iron fraction, Marine Chemistry, 120(1-4), 25-33.

Albani, S., N. Mahowald, B. Delmonte, V. Maggi, and G. Winckler (2012), Comparing modeled and observed changes in mineral dust transport and deposition to Antarctica between the Last Glacial Maximum and current climates, Climate Dynamics, 38(9-10), 1731-1755.

Albani, S., B. Delmonte, V. Maggi, C. Baroni, J. R. Petit, B. Stenni, C. Mazzola, and M. Frezzotti (2012), Interpreting last glacial to Holocene dust changes at Talos Dome (East Antarctica): implications for atmospheric variations from regional to hemispheric scales, Clim. Past Discuss., 8(1), 145-168.

Albani, S., et al. (2015), Twelve thousand years of dust: the Holocene global dust cycle constrained by natural archives, Clim. Past, 11(6), 869-903.

Alexander, J. M., V. H. Grassian, M. A. Young, and P. D. Kleiber (2015), Optical properties of selected components of mineral dust aerosol processed with organic acids and humic material, Journal of Geophysical Research: Atmospheres, 120(6), 2437-2452.

Alying, B. (2001), Dust accumulation on the Victoria Lower Glacier and Wilson Piedmont, coastal South Victoria Land, Antarctica, and its potential as a paleowind indicator, Victoria University of Wellington, Wellington.

Anderson, R. F., S. Barker, M. Fleisher, R. Gersonde, S. L. Goldstein, G. Kuhn, P. G. Mortyn, K. Pahnke, and J. P. Sachs (2014), Biological response to millennial variability of dust and nutrient supply in the Subantarctic South Atlantic Ocean, Philosophical Transactions of the Royal Society of London A: Mathematical, Physical and Engineering Sciences, 372(2019).

Andersson, P. S., G. Wasserburg, J. Ingri, and M. C. Stordal (1994), Strontium, dissolved and particulate loads in fresh and brackish waters: the Baltic Sea and Mississippi Delta, Earth and Planetary Science Letters, 124(1), 195-210.

Andreae, M. O. (1991), Biomass burning: Its history, use and distribution and its impact on environmental quality and global climate, Global Biomass Burning: Atmospheric, Climatic, and Biospheric Implications, edited by J. S. Levine, pp. 3-21, MIT Press, Cambridge, Mass.

Andreae, M. O. (1993), The influence of tropical biomass burning on climate and the atmospheric environment, in Biogeochemistry of Global Change, edited, pp. 113-150, Springer.

Andreae, M., and A. Gelencsér (2006), Black carbon or brown carbon? The nature of light-absorbing carbonaceous aerosols, Atmospheric Chemistry and Physics, 6(10), 3131-3148.

Andreasen, R., and M. Sharma (2006), Solar nebula heterogeneity in p-process samarium and neodymium isotopes, Science, 314(5800), 806-809.

Antonini, P., E. Piccirillo, R. Petrini, L. Civetta, M. D'Antonio, and G. Orsi (1999), Enriched mantle–Dupal signature in the genesis of the Jurassic Ferrar tholeiites from Prince Albert Mountains (Victoria Land, Antarctica), Contributions to Mineralogy and Petrology, 136(1-2), 1-19.

Arimoto, R., and R. A. Duce (1986), DRY DEPOSITION MODELS AND THE AIR/SEA EXCHANGE OF TRACE ELEMENTS, J. Geophys. Res., 91(D2), 2787-2792.

Arrigo, K. R., and C. R. McClain (1994), Spring Phytoplankton Production in the Western Ross Sea, Science, 266(5183), 261-263.

Arrigo, K. R., and G. L. van Dijken (2004), Annual changes in sea-ice, chlorophyll a, and primary production in the Ross Sea, Antarctica, Deep Sea Research Part II: Topical Studies in Oceanography, 51(1-3), 117-138.

Arrigo, K. R., and G. L. Van Dijken (2007), Interannual variation in air-sea CO2 flux in the Ross Sea, Antarctica: A model analysis, J. Geophys. Res., 112(C3), C03020.

Arrigo, K. R., A. M. Weiss, and W. O. Smith, Jr. (1998), Physical forcing of phytoplankton dynamics in the southwestern Ross Sea, J. Geophys. Res., 103(C1), 1007-1021.

Arrigo, K. R., G. van Dijken, and M. Long (2008), Coastal Southern Ocean: A strong anthropogenic CO2 sink, Geophys. Res. Lett., 35(21), L21602.

Arrigo, K. R., G. L. van Dijken, and S. Bushinsky (2008), Primary production in the Southern Ocean, 1997-2006, J. Geophys. Res., 113(C8), C08004.

Arrigo, K. R., G. R. DiTullio, R. B. Dunbar, D. H. Robinson, M. VanWoert, D. L. Worthen, and M. P. Lizotte (2000), Phytoplankton taxonomic variability in nutrient utilization and primary production in the Ross Sea, J. Geophys. Res., 105(C4), 8827-8846.

Arrigo, K. R., G. R. DiTullio, R. B. Dunbar, D. H. Robinson, M. VanWoert, D. L. Worthen, and M. P. Lizotte (2000), Phytoplankton taxonomic variability in nutrient utilization and primary production in the Ross Sea, J. Geophys. Res., 105(C4), 8827-8846.

Artaxo, P., F. Gerab, M. A. Yamasoe, and J. V. Martins (1994), Fine mode aerosol composition at three long-term atmospheric monitoring sites in the Amazon Basin, Journal of Geophysical Research: Atmospheres (1984–2012), 99(D11), 22857-22868.

Artaxo, P., E. T. Fernandas, J. V. Martins, M. A. Yamasoe, P. V. Hobbs, W. Maenhaut, K. M. Longo, and A. Castanho (1998), Large-scale aerosol source apportionment in Amazonia, Journal of Geophysical Research: Atmospheres (1984–2012), 103(D24), 31837-31847.

Atkins, C. B., and G. B. Dunbar (2009), Aeolian sediment flux from sea ice into Southern McMurdo Sound, Antarctica, Global and Planetary Change, 69(3), 133-141.

Augustinus, P., and G. Duller (2002), Luminescence and radiocarbon dating of raised beach sediments, Bunger Hills, East Antarctica, paper presented at Antarctica at the close of a millennium: proceedings of the 8th International Symposium on Antarctic Earth Sciences, Wellington 1999.

Ayers, G., J. Ivey, and H. Goodman (1987), Sulfate and Methanesulfonnate in the Maritime Aerosol at Cape Grim, Tasmania, in Scientific Application of Baseline Observations of Atmospheric Composition (SABOAC), edited, pp. 371-383, Springer.

Ayers, G. P., J. Ivey, and R. Gillett (1990), High Volume Samplers in Baseline Atmospheric Program (Australia) 1988, edited by S.R. Wilson and G.P. Ayers, CSIRO Atmospheric Research, Melbourne, Australia, 45.

Ayers, G., J. Cainey, R. Gillett, and J. Ivey (1997), Atmospheric sulphur and cloud condensation nuclei in marine air in the Southern Hemisphere, Philosophical Transactions of the Royal Society of London B: Biological Sciences, 352(1350), 203-211.

Ayling, B., and H. McGowan (2006), Niveo-eolian Sediment Deposits in Coastal South Victoria Land, Antarctica: Indicators of Regional Variability in Weather and Climate, Arctic, Antarctic, and Alpine Research, 38(3), 313-324.

Bagnold, R. (1941), The physics of blown sand and desert dunes, Methuen, London.

Baker, A. R., and T. D. Jickells (2006), Mineral particle size as a control on aerosol iron solubility, Geophys. Res. Lett., 33(17), L17608.

Baker, A. R., and T. D. Jickells (2006), Mineral particle size as a control on aerosol iron solubility, Geophys. Res. Lett., 33(17), L17608.

Baker, A. R., and P. L. Croot (2010), Atmospheric and marine controls on aerosol iron solubility in seawater, Marine Chemistry, 120(1-4), 4-13.

Baker, A. R., and P. L. Croot (2010), Atmospheric and marine controls on aerosol iron solubility in seawater, Marine Chemistry, 120(1-4), 4-13.

Baker, A. R., T. D. Jickells, M. Witt, and K. L. Linge (2006), Trends in the solubility of iron, aluminium, manganese and phosphorus in aerosol collected over the Atlantic Ocean, Marine Chemistry, 98(1), 43-58.

Baker, A. R., T. D. Jickells, M. Witt, and K. L. Linge (2006), Trends in the solubility of iron, aluminium, manganese and phosphorus in aerosol collected over the Atlantic Ocean, Marine Chemistry, 98(1), 43-58.

Baker, A., S. Kelly, K. Biswas, M. Witt, and T. Jickells (2003), Atmospheric deposition of nutrients to the Atlantic Ocean, Geophysical Research Letters, 30(24).

Baker, A., C. Adams, T. Bell, T. Jickells, and L. Ganzeveld (2013), Estimation of atmospheric nutrient inputs to the Atlantic Ocean from 50° N to 50° S based on large-scale

field sampling: Iron and other dust-associated elements, Global Biogeochemical Cycles, 27(3), 755-767.

Baker, A., K. Weston, S. Kelly, M. Voss, P. Streu, and J. Cape (2007), Dry and wet deposition of nutrients from the tropical Atlantic atmosphere: Links to primary productivity and nitrogen fixation, Deep Sea Research Part I: Oceanographic Research Papers, 54(10), 1704-1720.

Banerjee, P., and S. Prasanna Kumar (2014), Dust-induced episodic phytoplankton blooms in the Arabian Sea during winter monsoon, Journal of Geophysical Research: Oceans, 119(10), 7123-7138.

Banse, K. (1991), Rates of Phytoplankton Cell Division in the Field and in Iron Enrichment Experiments, Limnology and Oceanography, 36(8), 1886-1898.

Barbeau, K. A., and J. W. Moffett (1998), Dissolution of Iron Oxides by Phagotrophic Protists: Using a Novel Method To Quantify Reaction Rates, Environmental Science & Technology, 32(19), 2969-2975.

Barbeau, K., J. W. Moffett, D. A. Caron, P. L. Croot, and D. L. Erdner (1996), Role of protozoan grazing in relieving iron limitation of phytoplankton, Nature, 380(6569), 61-64.

Barrett, P., A. Pyne, and B. Ward (1983), Modern sedimentation in McMurdo Sound, Antarctica In: Oliver, R.L., James, P.R., Jago, J.B. (Eds.), Antarctic Earth Science, 550-554.

Basak, C., K. Pahnke, M. Frank, F. Lamy, and R. Gersonde (2015), Neodymium isotopic characterization of Ross Sea Bottom Water and its advection through the southern South Pacific, Earth and Planetary Science Letters, 419, 211-221.

Baseline (2014), Baseline Atmospheric Program Australia 2009-2010. Edited by Derek. N, Krummel. P. B, Cleland. S. J. Australian Bureau of Meteorology and CSIRO Marine and Atmospheric ResearchRep.

Basile, I., J. R. Petit, S. Touron, F. E. Grousset, and N. Barkov (2001), Volcanic layers in Antarctic (Vostok) ice cores: Source identification and atmospheric implications, Journal of Geophysical Research: Atmospheres (1984–2012), 106(D23), 31915-31931.

Basile, I., F. E. Grousset, M. Revel, J. R. Petit, P. E. Biscaye, and N. I. Barkov (1997), Patagonian origin of glacial dust deposited in East Antarctica (Vostok and Dome C) during glacial stages 2, 4 and 6, Earth and Planetary Science Letters, 146(3-4), 573-589.

Bentley, P. (1979), Characteristics and distribution of wind blown sediments, Western McMurdo Sound, Antarctica, Victoria University of Wellington, Wellington.

Berger, C. J., S. M. Lippiatt, M. G. Lawrence, and K. W. Bruland (2008), Application of a chemical leach technique for estimating labile particulate aluminum, iron, and manganese in the Columbia River plume and coastal waters off Oregon and Washington, Journal of Geophysical Research: Oceans (1978–2012), 113(C2).

Berman-Frank, I., J. T. Cullen, Y. Shaked, R. M. Sherrell, and P. G. Falkowski (2001), Iron availability, cellular iron quotas, and nitrogen fixation in Trichodesmium, Limnology and Oceanography, 46(6), 1249-1260.

Bhattachan, A., and P. D'Odorico (2014), Can land use intensification in the Mallee, Australia increase the supply of soluble iron to the Southern Ocean?, Scientific reports, 4.

Bhattachan, A., L. Wang, M. F. Miller, K. J. Licht, and P. D'Odorico (2015), Antarctica's Dry Valleys: A potential source of soluble iron to the Southern Ocean?, Geophysical Research Letters, 42(6), 1912-1918.

Biscaye, P. E., F. E. Grousset, M. Revel, S. Van der Gaast, G. A. Zielinski, A. Vaars, and G. Kukla (1997), Asian provenance of glacial dust (stage 2) in the Greenland Ice Sheet Project 2 Ice Core, Summit, Greenland, J. Geophys. Res., 102(C12), 26765-26781.

Bisiaux, M., R. Edwards, J. McConnell, M. Albert, H. Anschütz, T. Neumann, E. Isaksson, and J. Penner (2012), Variability of black carbon deposition to the East Antarctic Plateau, 1800–2000 AD, Atmospheric Chemistry and Physics, 12(8), 3799-3808.

Bisiaux, M., R. Edwards, J. McConnell, M. Curran, T. Van Ommen, A. Smith, T. Neumann, D. Pasteris, J. Penner, and K. Taylor (2012), Changes in black carbon deposition to Antarctica from two high-resolution ice core records, 1850–2000 AD, Atmospheric Chemistry and Physics, 12(9), 4107-4115.

Blain, S., et al. (2007), Effect of natural iron fertilization on carbon sequestration in the Southern Ocean, Nature, 446(7139), 1070-1074.

Blain, S., et al. (2007), Effect of natural iron fertilization on carbon sequestration in the Southern Ocean, Nature, 446(7139), 1070-1074.

Bollhöfer, A., and K. Rosman (2000), Isotopic source signatures for atmospheric lead: the Southern Hemisphere, Geochimica et Cosmochimica Acta, 64(19), 3251-3262.

Bollhöfer, A., and K. Rosman (2001), Isotopic source signatures for atmospheric lead: the Northern Hemisphere, Geochimica et Cosmochimica Acta, 65(11), 1727-1740.

Bollhöfer, A., W. Chisholm, and K. J. R. Rosman (1999), Sampling aerosols for lead isotopes on a global scale, Analytica Chimica Acta, 390(1–3), 227-235.

Bollhöfer, A., K. J. R. Rosman, A. L. Dick, W. Chisholm, G. R. Burton, R. D. Loss, and W. Zahorowski (2005), Concentration, isotopic composition, and sources of lead in Southern Ocean air during 1999/2000, measured at the Cape Grim Baseline Air Pollution Station, Tasmania, Geochimica et Cosmochimica Acta, 69(20), 4747-4757.

Bond, T. C., et al. (2013), Bounding the role of black carbon in the climate system: A scientific assessment, Journal of Geophysical Research: Atmospheres, 118(11), 5380-5552.

Bonnet, S., and C. Guieu (2004), Dissolution of atmospheric iron in seawater, Geophys. Res. Lett., 31(3), L03303.

Bory, A. J. M., P. E. Biscaye, A. Svensson, and F. E. Grousset (2002), Seasonal variability in the origin of recent atmospheric mineral dust at NorthGRIP, Greenland, Earth and Planetary Science Letters, 196(3-4), 123-134.

Bory, A., E. Wolff, R. Mulvaney, E. Jagoutz, A. Wegner, U. Ruth, and H. Elderfield (2010), Multiple sources supply eolian mineral dust to the Atlantic sector of coastal Antarctica:

Evidence from recent snow layers at the top of Berkner Island ice sheet, Earth and Planetary Science Letters, 291(1-4), 138-148.

Bowie, A. R., F. B. Griffiths, F. Dehairs, and T. W. Trull (2011), Oceanography of the subantarctic and polar frontal zones south of Australia during summer: setting for the SAZ-Sense study, Deep Sea Research Part II: Topical Studies in Oceanography, 58(21), 2059-2070.

Bowie, A. R., A. T. Townsend, D. Lannuzel, T. A. Remenyi, and P. Van der Merwe (2010), Modern sampling and analytical methods for the determination of trace elements in marine particulate material using magnetic sector inductively coupled plasma–mass spectrometry, Analytica chimica acta, 676(1), 15-27.

Bowie, A. R., D. Lannuzel, T. A. Remenyi, T. Wagener, P. J. Lam, P. W. Boyd, C. Guieu, A. T. Townsend, and T. W. Trull (2009), Biogeochemical iron budgets of the Southern Ocean south of Australia: Decoupling of iron and nutrient cycles in the subantarctic zone by the summertime supply, Global Biogeochem. Cycles, 23(4), GB4034.

Bowie, A. R., D. Lannuzel, T. A. Remenyi, T. Wagener, P. J. Lam, P. W. Boyd, C. Guieu, A. T. Townsend, and T. W. Trull (2009), Biogeochemical iron budgets of the Southern Ocean south of Australia: Decoupling of iron and nutrient cycles in the subantarctic zone by the summertime supply, Global Biogeochem. Cycles, 23(4), GB4034.

Bowie, A., P. van der Merwe, F. Quéroué, T. Trull, M. Fourquez, F. Planchon, G. Sarthou, F. Chever, A. Townsend, and I. Obernosterer (2014), Iron budgets for three distinct biogeochemical sites around the Kerguelen archipelago (Southern Ocean) during the natural fertilisation experiment KEOPS-2, Biogeosciences Discussions, 11(12), 17861-17923.

Bowler, J. (1976), Aridity in Australia: age, origins and expression in aeolian landforms and sediments, Earth-Science Reviews, 12(2), 279-310.

Boyd, P. W., and D. S. Mackie (2008), Comment on 'The Southern Ocean biological response to aeolian iron deposition', Science, 319, 159.

Boyd, P. W., and M. J. Ellwood (2010), The biogeochemical cycle of iron in the ocean, Nature Geosci, 3(10), 675-682.

Boyd, P. W., D. S. Mackie, and K. A. Hunter (2010), Aerosol iron deposition to the surface ocean - Modes of iron supply and biological responses, Marine Chemistry, 120(1-4), 128-143.

Boyd, P. W., S. C. Doney, R. Strzepek, J. Dusenberry, K. Lindsay, and I. Fung (2008), Climate-mediated changes to mixed-layer properties in the Southern Ocean: assessing the phytoplankton response, Biogeosciences, 5(3), 847-864.

Boyd, P. W., G. McTainsh, V. Sherlock, K. Richardson, S. Nichol, M. Ellwood, and R. Frew (2004), Episodic enhancement of phytoplankton stocks in New Zealand subantarctic waters: Contribution of atmospheric and oceanic iron supply, Global Biogeochem. Cycles, 18(1), GB1029.

Boyd, P., P. Dillingham, C. McGraw, E. Armstrong, C. Cornwall, Y.-y. Feng, C. Hurd, M. Gault-Ringold, M. Roleda, and E. Timmins-Schiffman (2015), Physiological responses of a Southern Ocean diatom to complex future ocean conditions, Nature Climate Change.

Boyd, P. W., et al. (2007), Mesoscale Iron Enrichment Experiments 1993-2005: Synthesis and Future Directions, Science, 315(5812), 612-617.

Boyd, P. W., et al. (2005), FeCycle: Attempting an iron biogeochemical budget from a mesoscale SF6 tracer experiment in unperturbed low iron waters, Global Biogeochem. Cycles, 19(4), GB4S20.

Boyd, P. W., et al. (2000), A mesoscale phytoplankton bloom in the polar Southern Ocean stimulated by iron fertilization, Nature, 407(6805), 695-702.

Boyd, P. W., et al. (2000), A mesoscale phytoplankton bloom in the polar Southern Ocean stimulated by iron fertilization, Nature, 407(6805), 695-702.

Buck, C. S., W. M. Landing, J. A. Resing, and G. T. Lebon (2006), Aerosol iron and aluminum solubility in the northwest Pacific Ocean: Results from the 2002 IOC cruise, Geochem. Geophys. Geosyst., 7(4), Q04M07.

Buck, C. S., W. M. Landing, J. A. Resing, and G. T. Lebon (2006), Aerosol iron and aluminum solubility in the northwest Pacific Ocean: Results from the 2002 IOC cruise, Geochem. Geophys. Geosyst., 7(4), Q04M07.

Bunt, J. S. (1963), Microbiology of Antarctic Sea-ice: Diatoms of Antarctic Sea-ice as Agents of Primary Production, Nature, 199(4900), 1255-1257.

Bunt, J. S., and E. J. F. Wood (1963), Microbiology of Antarctic Sea-ice: Microalgae and Antarctic Sea-ice, Nature, 199(4900), 1254-1255.

Butler, H., W. L. Hogarth, and G. H. McTainsh (2001), Effects of spatial variations in source areas upon dust concentration profiles during three wind erosion events in Australia, Earth Surface Processes and Landforms, 26(10), 1039-1048.

Calloway, C., S. Li, J. Buchanan, and R. Stevens (1989), A refinement of the potassium tracer method for residential wood smoke, Atmospheric Environment (1967), 23(1), 67-69.

Cammas, J.-P., J. Brioude, J.-P. Chaboureau, J. Duron, C. Mari, P. Mascart, P. Nédélec, H. Smit, H.-W. Pätz, and A. Volz-Thomas (2009), Injection in the lower stratosphere of biomass fire emissions followed by long-range transport: a MOZAIC case study, Atmospheric Chemistry and Physics, 9(15), 5829-5846.

Carslaw, D. C. (2014), The openair manual - open-source tools for analysing air pollution data., Manual for version 1.0, King’s College London.

Carslaw, D. C., and K. Ropkins (2012), Openair - An R package for air quality data analysis, Environmental Modelling & Software, 27, 52-61.

Chakrabarty, R. K., H. Moosmüller, W. P. Arnott, M. A. Garro, J. G. Slowik, E. S. Cross, J.-H. Han, P. Davidovits, T. B. Onasch, and D. R. Worsnop (2007), Light scattering and

absorption by fractal-like carbonaceous chain aggregates: Comparison of theories and experiment, Applied optics, 46(28), 6990-7006.

Chambers, S., A. Williams, J. Crawford, and A. Griffiths (2014), On the use of radon for quantifying the effects of atmospheric stability on urban emissions, Atmos. Chem. Phys. Discuss, 14, 25,411-425,452.

Chambers, S., S.-B. Hong, A. Williams, J. Crawford, A. Griffiths, and S.-J. Park (2014), Characterising terrestrial influences on Antarctic air masses using Radon-222 measurements at King George Island, Atmospheric Chemistry and Physics, 14(18), 9903-9916.

Chance, R., T. D. Jickells, and A. R. Baker (2015), Atmospheric trace metal concentrations, solubility and deposition fluxes in remote marine air over the south-east Atlantic, Marine Chemistry.

Chandler, C., P. Cheney, P. Thomas, L. Trabaud, and D. Williams (1983), Fire in forestry. Forest fire behaviour and effects, Ed. John Wiley & Sons, 1.

Chang-Graham, A. L., L. T. Profeta, T. J. Johnson, R. J. Yokelson, A. Laskin, and J. Laskin (2011), Case study of water-soluble metal containing organic constituents of biomass burning aerosol, Environmental science & technology, 45(4), 1257-1263.

Chen, Y., and R. L. Siefert (2003), Determination of various types of labile atmospheric iron over remote oceans, J. Geophys. Res., 108(D24), 4774.

Chen, Y., and R. L. Siefert (2004), Seasonal and spatial distributions and dry deposition fluxes of atmospheric total and labile iron over the tropical and subtropical North Atlantic Ocean, J. Geophys. Res., 109(D9), D09305.

Chen, Y., and R. L. Siefert (2004), Seasonal and spatial distributions and dry deposition fluxes of atmospheric total and labile iron over the tropical and subtropical North Atlantic Ocean, J. Geophys. Res., 109(D9), D09305.

Chow, J. C. (1995), Measurement methods to determine compliance with ambient air quality standards for suspended particles, Journal of the Air & Waste Management Association, 45(5), 320-382.

Chow, J. C., J. G. Watson, L.-W. A. Chen, M. O. Chang, N. F. Robinson, D. Trimble, and S. Kohl (2007), The IMPROVE_A temperature protocol for thermal/optical carbon analysis: maintaining consistency with a long-term database, Journal of the Air & Waste Management Association, 57(9), 1014-1023.

Chuang, P. Y., R. M. Duvall, M. M. Shafer, and J. J. Schauer (2005), The origin of water soluble particulate iron in the Asian atmospheric outflow, Geophys. Res. Lett., 32(7), L07813.

Chughtai, A., M. Brooks, and D. Smith (1996), Hydration of black carbon, Journal of Geophysical Research: Atmospheres (1984–2012), 101(D14), 19505-19514.

Chughtai, A., J. Jassim, J. Peterson, D. Stedman, and D. Smith (1991), Spectroscopic and solubility characteristics of oxidized soots, Aerosol Science and Technology, 15(2), 112-126.

Cleveland, W. S., and S. J. Devlin (1988), Locally weighted regression: an approach to regression analysis by local fitting, Journal of the American Statistical Association, 83(403), 596-610.

Coale, K. H., X. Wang, S. J. Tanner, and K. S. Johnson (2003), Phytoplankton growth and biological response to iron and zinc addition in the Ross Sea and Antarctic Circumpolar Current along 170 W, Deep Sea Research Part II: Topical Studies in Oceanography, 50(3), 635-653.

Coale, K. H., et al. (2004), Southern Ocean Iron Enrichment Experiment: Carbon Cycling in High- and Low-Si Waters, Science, 304(5669), 408-414.

Cohen, L. (2013), Atmospheric Variability and Precipitation in the Ross Sea Region, Antarctica, PhD thesis, Victoria University of Wellington, Wellington.

Cohen, D. D., and E. Stelcer (2014), Fine particle sampling at Cape Grim, 2009-2010 Baseline report, 75.

Cohen, D. D., D. Garton, and E. Stelcer (2000), Multi-elemental methods for fine particle source apportionment at the global baseline station at Cape Grim, Tasmania, Nuclear Instruments and Methods in Physics Research Section B: Beam Interactions with Materials and Atoms, 161, 775-779.

Collier, R., J. Dymond, S. Honjo, S. Manganini, R. Francois, and R. Dunbar (2000), The vertical flux of biogenic and lithogenic material in the Ross Sea: moored sediment trap observations 1996-1998, Deep Sea Research Part II: Topical Studies in Oceanography, 47(15-16), 3491-3520.

Conway, H., B. L. Hall, G. H. Denton, A. M. Gades, and E. D. Waddington (1999), Past and Future Grounding-Line Retreat of the West Antarctic Ice Sheet, Science, 286(5438), 280-283.

Conway, T., E. Wolff, R. Röthlisberger, R. Mulvaney, and H. Elderfield (2015), Constraints on soluble aerosol iron flux to the Southern Ocean at the Last Glacial Maximum, Nature Communications, 6.

Cook, C. P., et al. (2013), Dynamic behaviour of the East Antarctic ice sheet during Pliocene warmth, Nature Geosci, 6(9), 765-769.

Cooke, W., V. Ramaswamy, and P. Kasibhatla (2002), A general circulation model study of the global carbonaceous aerosol distribution, Journal of Geophysical Research: Atmospheres (1984–2012), 107(D16), ACH 2-1-ACH 2-32.

Cox, S. C., D. L. Parkinson, A. H. Allibone, and A. F. Cooper (2000), Isotopic character of Cambro-Ordovician plutonism, southern Victoria Land, Antarctica, New Zealand Journal of Geology and Geophysics, 43(4), 501-520.

Croot, P., K. Bluhm, C. Schlosser, P. Streu, E. Breitbarth, R. Frew, and M. Van Ardelan (2008), Regeneration of Fe (II) during EIFeX and SOFeX, Geophysical Research Letters, 35(19).

Croot, P. L., A. R. Bowie, R. D. Frew, M. T. Maldonado, J. A. Hall, K. A. Safi, J. La Roche, P. W. Boyd, and C. S. Law (2001), Retention of dissolved iron and Fe II in an iron induced Southern Ocean phytoplankton bloom, Geophys. Res. Lett., 28(18), 3425-3428.

Croot, P. L., et al. (2005), Spatial and temporal distribution of Fe(II) and H2O2 during EisenEx, an open ocean mescoscale iron enrichment, Marine Chemistry, 95(1-2), 65-88.

Cropp, R. A., A. J. Gabric, M. Levasseur, G. H. McTainsh, A. Bowie, C. S. Hassler, C. S. Law, H. McGowan, N. Tindale, and R. Viscarra Rossel (2013), The likelihood of observing dust-stimulated phytoplankton growth in waters proximal to the Australian continent, Journal of Marine Systems, 117–118, 43-52.

Crutzen, P. J., and M. O. Andreae (1990), Biomass burning in the tropics: Impact on atmospheric chemistry and biogeochemical cycles, Science, 250(4988), 1669-1678.

Cruz, M., A. Sullivan, J. Gould, N. Sims, A. Bannister, J. Hollis, and R. Hurley (2012), Anatomy of a catastrophic wildfire: the Black Saturday Kilmore East fire in Victoria, Australia, Forest Ecology and Management, 284, 269-285.

Cutter, G., P. Andersson, L. Codispoti, P. Croot, R. Francois, M. Lohan, H. Obata, and M. Rutgers vd Loeff (2010), Sampling and sample-handling protocols for GEOTRACES Cruises.

Dansgaard, W. (1954), The O18- abundance in fresh water, Geochimica et Cosmochimica Acta 6, 241-260.

de Baar, H. J. W., and J. T. M. de Jong (2001), Distribution, sources and sinks of iron in seawater, The Biogeochemistry of Iron in Seawater, 123 - 253.

de Baar, H. J. W., J. T. M. de Jong, D. C. E. Bakker, B. M. Loscher, C. Veth, U. Bathmann, and V. Smetacek (1995), Importance of iron for plankton blooms and carbon dioxide drawdown in the Southern Ocean, Nature, 373(6513), 412-415.

de Baar, H. J. W., J. T. M. de Jong, D. C. E. Bakker, B. M. Loscher, C. Veth, U. Bathmann, and V. Smetacek (1995), Importance of iron for plankton blooms and carbon dioxide drawdown in the Southern Ocean, Nature, 373(6513), 412-415.

de Baar, H. J. W., et al. (2005), Synthesis of iron fertilization experiments: From the Iron Age in the Age of Enlightenment, J. Geophys. Res., 110(C9), C09S16.

De Deckker, P., M. Norman, I. D. Goodwin, A. Wain, and F. X. Gingele (2010), Lead isotopic evidence for an Australian source of aeolian dust to Antarctica at times over the last 170,000 years, Palaeogeography, Palaeoclimatology, Palaeoecology, 285(3-4), 205-223.

de Jong, J., V. Schoemann, N. Maricq, N. Mattielli, P. Langhorne, T. Haskell, and J.-L. Tison (2013), Iron in land-fast sea ice of McMurdo Sound derived from sediment resuspension and wind-blown dust attributes to primary productivity in the Ross Sea, Antarctica, Marine Chemistry, 157(0), 24-40.

Decesari, S., M. Facchini, E. Matta, M. Mircea, S. Fuzzi, A. Chughtai, and D. Smith (2002), Water soluble organic compounds formed by oxidation of soot, Atmospheric Environment, 36(11), 1827-1832.

Delmonte, B., J. R. Petit, and V. Maggi (2002), Glacial to Holocene implications of the new 27000-year dust record from the EPICA Dome C (East Antarctica) ice core, Climate Dynamics, 18(8), 647-660.

Delmonte, B., J. R. Petit, and V. Maggi (2002), Glacial to Holocene implications of the new 27000-year dust record from the EPICA Dome C (East Antarctica) ice core, Climate Dynamics, 18(8), 647-660.

Delmonte, B., J. Robert Petit, I. Basile-Doelsch, E. Jagoutz, and V. Maggi (2007), 6. Late quaternary interglacials in East Antarctica from ice-core dust records, in Developments in Quaternary Sciences, edited by M. C. M. F. S. G. Frank Sirocko and L. Thomas, pp. 53-73, Elsevier.

Delmonte, B., J. R. Petit, K. K. Andersen, I. Basile-Doelsch, V. Maggi, and V. Ya Lipenkov (2004), Dust size evidence for opposite regional atmospheric circulation changes over east Antarctica during the last climatic transition, Climate Dynamics, 23(3), 427-438.

Delmonte, B., J. R. Petit, G. Krinner, V. Maggi, J. Jouzel, and R. Udisti (2005), Ice core evidence for secular variability and 200-year dipolar oscillations in atmospheric circulation over East Antarctica during the Holocene, Climate Dynamics, 24(6), 641-654.

Delmonte, B., P. S. Andersson, M. Hansson, H. Schöberg, J. R. Petit, I. Basile-Doelsch, and V. Maggi (2008), Aeolian dust in East Antarctica (EPICA-Dome C and Vostok): Provenance during glacial ages over the last 800 kyr, Geophys. Res. Lett., 35(7), L07703.

Delmonte, B., P. S. Andersson, M. Hansson, H. Schöberg, J. R. Petit, I. Basile-Doelsch, and V. Maggi (2008), Aeolian dust in East Antarctica (EPICA-Dome C and Vostok): Provenance during glacial ages over the last 800 kyr, Geophys. Res. Lett., 35(7), L07703.

Delmonte, B., I. Basile-Doelsch, J. R. Petit, V. Maggi, M. Revel-Rolland, A. Michard, E. Jagoutz, and F. Grousset (2004), Comparing the Epica and Vostok dust records during the last 220,000 years: stratigraphical correlation and provenance in glacial periods, Earth-Science Reviews, 66(1-2), 63-87.

Delmonte, B., P. S. Andersson, H. Schöberg, M. Hansson, J. R. Petit, R. Delmas, D. M. Gaiero, V. Maggi, and M. Frezzotti (2010), Geographic provenance of aeolian dust in East Antarctica during Pleistocene glaciations: preliminary results from Talos Dome and comparison with East Antarctic and new Andean ice core data, Quaternary Science Reviews, 29(1-2), 256-264.

Delmonte, B., C. Baroni, P. Andersson, B. Narcisi, M. Salvatore, J. Petit, C. Scarchilli, M. Frezzotti, S. Albani, and V. Maggi (2013), Modern and Holocene aeolian dust variability from Talos Dome (Northern Victoria Land) to the interior of the Antarctic ice sheet, Quaternary Science Reviews, 64, 76-89.

Delmonte, B., et al. (2010), Aeolian dust in the Talos Dome ice core (East Antarctica, Pacific/Ross Sea sector): Victoria Land versus remote sources over the last two climate cycles, Journal of Quaternary Science, 25(8), 1327-1337.

Denton, G. H., and D. R. Marchant (2000), The Geologic Basis for a Reconstruction of a Grounded Ice Sheet in McMurdo Sound, Antarctica, at the Last Glacial Maximum, Geografiska Annaler: Series A, Physical Geography, 82(2-3), 167-211.

Denton, G. H., and T. J. Hughes (2002), Reconstructing the Antarctic Ice Sheet at the Last Glacial Maximum, Quaternary Science Reviews, 21(1-3), 193-202.

DePaolo, D. J., and G. J. Wasserburg (1976), Inferences about magma sources and mantle structure from variations of 143Nd/144Nd, Geophys. Res. Lett., 3(12), 743-746.

Desboeufs, K., R. Losno, F. Vimeux, and S. Cholbi (1999), The pH-dependent dissolution of wind-transported Saharan dust, Journal of Geophysical Research: Atmospheres (1984–2012), 104(D17), 21287-21299.

Desboeufs, K., A. Sofikitis, R. Losno, J. L. Colin, and P. Ausset (2005), Dissolution and solubility of trace metals from natural and anthropogenic aerosol particulate matter, Chemosphere, 58(2), 195-203.

Desboeufs, K., A. Sofikitis, R. Losno, J. Colin, and P. Ausset (2005), Dissolution and solubility of trace metals from natural and anthropogenic aerosol particulate matter, Chemosphere, 58(2), 195-203.

Dirksen, R. J., K. Folkert Boersma, J. De Laat, P. Stammes, G. R. Van Der Werf, M. Val Martin, and H. M. Kelder (2009), An aerosol boomerang: Rapid around-the-world transport of smoke from the December 2006 Australian forest fires observed from space, Journal of Geophysical Research: Atmospheres (1984–2012), 114(D21).

Donaghay, P., P. Liss, R. A. Duce, D. Kester, A. Hanson, T. Villareal, N. W. Tindale, and D. Gifford (1991), The role of episodic atmospheric nutrient input in the chemical and biological dynamics of ocean ice ecosystems, Oceanography, 4, 62-70.

Dörr, H., B. Kromer, I. Levin, K. Münnich, and H. J. Volpp (1983), CO2 and Radon 222 as tracers for atmospheric transport, Journal of Geophysical Research: Oceans (1978–2012), 88(C2), 1309-1313.

Draxler, R. R., and G. D. Rolph (2003), Hybrid Single-Particle Lagrangian Integrated Trajectory (HYSPLIT), model, http://www.arl.noaa.gov/ready/hysplit4.html.

Duan, F., X. Liu, T. Yu, and H. Cachier (2004), Identification and estimate of biomass burning contribution to the urban aerosol organic carbon concentrations in Beijing, Atmospheric Environment, 38(9), 1275-1282.

Duce, R. A., et al. (1991), The atmospheric input of trace species to the world ocean, Global Biogeochem. Cycles, 5(3), 193-259.

Duce, R. A., et al. (1991), The atmospheric input of trace species to the world ocean, Global Biogeochem. Cycles, 5(3), 193-259.

Dulac, F., P. BUAT-MÉNARD, U. Ezat, S. Melki, and G. Bergametti (1989), Atmospheric input of trace metals to the western Mediterranean: uncertainties in modelling dry deposition from cascade impactor data, Tellus B, 41(3), 362-378.

Dulaiova, H., M. Ardelan, P. B. Henderson, and M. A. Charette (2009), Shelf-derived iron inputs drive biological productivity in the southern Drake Passage, Global Biogeochemical Cycles, 23(4).

Dunbar, G. B., N. A. N. Bertler, and R. M. McKay (2009), Sediment flux through the McMurdo Ice Shelf in Windless Bight, Antarctica, Global and Planetary Change, 69(3), 87-93.

Duncan, B. N., R. V. Martin, A. C. Staudt, R. Yevich, and J. A. Logan (2003), Interannual and seasonal variability of biomass burning emissions constrained by satellite observations, Journal of Geophysical Research: Atmospheres (1984–2012), 108(D2), ACH 1-1-ACH 1-22.

Echalar, F., A. Gaudichet, H. Cachier, and P. Artaxo (1995), Aerosol emissions by tropical forest and savanna biomass burning: characteristic trace elements and fluxes, Geophysical research letters, 22(22), 3039-3042.

Echalar, F., P. Artaxo, J. V. Martins, M. Yamasoe, F. Gerab, W. Maenhaut, and B. Holben (1998), Long-term monitoring of atmospheric aerosols in the Amazon Basin: Source identification and apportionment, Journal of Geophysical Research: Atmospheres (1984–2012), 103(D24), 31849-31864.

Edwards, R. (1999), Iron in modern and ancient East Antarctic snow: implications for phytoplankton production in the Southern Ocean, PhD thesis, University of Tasmania, Hobart.

Edwards, R., and P. Sedwick (2001), Iron in East Antarctic snow: Implications for atmospheric iron deposition and algal production in Antarctic waters, Geophys. Res. Lett., 28(20), 3907-3910.

Edwards, A., J. Russell-Smith, and M. Meyer (2015), Contemporary fire regime risks to key ecological assets and processes in north Australian savannas, International Journal of Wildland Fire, 24(6), 857-870.

Edwards, R., P. Sedwick, V. Morgan, and C. Boutron (2006), Iron in ice cores from Law Dome: A record of atmospheric iron deposition for maritime East Antarctica during the Holocene and Last Glacial Maximum, Geochemistry, Geophysics, Geosystems, 7(12), Q12Q01.

Edwards, P., P. Sedwick, V. Morgan, C. Boutron, and S. Hong (1998), Iron in ice cores from Law Dome, East Antarctica: implications for past deposition of aerosol iron, Annals of Glaciology, 27, 365-370.

Elderfield, H. (1986), Strontium isotope stratigraphy, Palaeogeography, Palaeoclimatology, Palaeoecology, 57(1), 71-90.

Elliot, D. H., T. H. Fleming, P. R. Kyle, and K. A. Foland (1999), Long-distance transport of magmas in the Jurassic Ferrar Large Igneous Province, Antarctica, Earth and Planetary Science Letters, 167(1–2), 89-104.

Ellis, A., et al. (2015), Characterizing black carbon in rain and ice cores using coupled tangential flow filtration and transmission electron microscopy, Atmos. Meas. Tech., 8(9), 3959-3969.

Ellwood, M. J., D. A. Hutchins, M. C. Lohan, A. Milne, P. Nasemann, S. D. Nodder, S. G. Sander, R. Strzepek, S. W. Wilhelm, and P. W. Boyd (2015), Iron stable isotopes track

pelagic iron cycling during a subtropical phytoplankton bloom, Proceedings of the National Academy of Sciences, 112(1), E15-E20.

Elrod, V., W. Berelson, K. Coale, and K. Johnson (2004), The flux of iron from continental shelf sediments: a missing source for global budgets, Geophys Res Lett, 31, L12307.

Ezat, U., and F. Dulac (1995), Size distribution of mineral aerosols at Amsterdam-island and dry deposition rates in the Southern Indian Ocean, Comptes Rendus De L Acadmie Des Sciences Serie II, 320(1), 9-14.

Falkowski, P. G. (1997), Evolution of the nitrogen cycle and its influence on the biological sequestration of CO 2 in the ocean, Nature, 387(6630), 272-275.

Faure, G. (1986), Principles of Isotope Geology (2nd ed.)Wiley, New York (1986), p. 589.

Ferek, R. J., J. S. Reid, P. V. Hobbs, D. R. Blake, and C. Liousse (1998), Emission factors of hydrocarbons, halocarbons, trace gases and particles from biomass burning in Brazil, Journal of Geophysical Research: Atmospheres (1984–2012), 103(D24), 32107-32118.

Field, R. D., G. R. van der Werf, and S. S. Shen (2009), Human amplification of drought-induced biomass burning in Indonesia since 1960, Nature Geoscience, 2(3), 185-188.

Fishwick, M. P., P. N. Sedwick, M. C. Lohan, P. J. Worsfold, K. N. Buck, T. M. Church, and S. J. Ussher (2014), The impact of changing surface ocean conditions on the dissolution of aerosol iron, Global Biogeochemical Cycles, 2014GB004921.

Fitzwater, S. E., K. S. Johnson, R. M. Gordon, K. H. Coale, and W. O. Smith (2000), Trace metal concentrations in the Ross Sea and their relationship with nutrients and phytoplankton growth, Deep Sea Research Part II: Topical Studies in Oceanography, 47(15-16), 3159-3179.

Fleming, T., K. Foland, and D. Elliot (1995), Isotopic and chemical constraints on the crustal evolution and source signature of Ferrar magmas, north Victoria Land, Antarctica, Contributions to Mineralogy and Petrology, 121(3), 217-236.

Fomba, K., K. Müller, D. v. Pinxteren, and H. Herrmann (2012), Aerosol size-resolved trace metal composition in remote northern tropical Atlantic marine environment: case study Cape Verde Islands, Atmospheric Chemistry and Physics Discussions, 12(11), 29535-29569.

Formenti, P., W. Elbert, W. Maenhaut, J. Haywood, S. Osborne, and M. Andreae (2003), Inorganic and carbonaceous aerosols during the Southern African Regional Science Initiative (SAFARI 2000) experiment: Chemical characteristics, physical properties, and emission data for smoke from African biomass burning, Journal of Geophysical Research: Atmospheres (1984–2012), 108(D13).

Frants, M., M. Holzer, T. DeVries, and R. Matear (2016), Constraints on the global marine iron cycle from a simple inverse model, Journal of Geophysical Research: Biogeosciences, n/a-n/a.

Frenklach, M. (2002), Reaction mechanism of soot formation in flames, Physical Chemistry Chemical Physics, 4(11), 2028-2037.

Freydier, R., A. Michard, G. De Lange, and J. Thomson (2001), Nd isotopic compositions of Eastern Mediterranean sediments: tracers of the Nile influence during sapropel S1 formation?, Marine Geology, 177(1), 45-62.

Friedman, B., H. Herich, L. Kammermann, D. S. Gross, A. Arneth, T. Holst, and D. J. Cziczo (2009), Subarctic atmospheric aerosol composition: 1. Ambient aerosol characterization, Journal of Geophysical Research: Atmospheres (1984–2012), 114(D13).

Fu, H., G. Shang, J. Lin, Y. Hu, Q. Hu, L. Guo, Y. Zhang, and J. Chen (2014), Fractional iron solubility of aerosol particles enhanced by biomass burning and ship emission in Shanghai, East China, Science of The Total Environment, 481, 377-391.

Futa, K., and W. Le Masurier (1983), Nd and Sr isotopic studies on Cenozoic mafic lavas from West Antarctica: Another source for continental alkali basalts, Contributions to Mineralogy and Petrology, 83(1-2), 38-44.

Gabric, A. J., R. A. Cropp, G. H. McTainsh, B. M. Johnston, H. Butler, B. Tilbrook, and M. Keywood (2010), Australian dust storms in 2002–2003 and their impact on Southern Ocean biogeochemistry, Global Biogeochemical Cycles, 24(2).

Gabrielli, P., A. Wegner, J. R. Petit, B. Delmonte, P. De Deckker, V. Gaspari, H. Fischer, U. Ruth, M. Kriews, and C. Boutron (2010), A major glacial-interglacial change in aeolian dust composition inferred from Rare Earth Elements in Antarctic ice, Quaternary Science Reviews, 29(1), 265-273.

Gabrielli, P., et al. (2010), A major glacial-interglacial change in aeolian dust composition inferred from Rare Earth Elements in Antarctic ice, Quaternary Science Reviews, 29(1-2), 265-273.

Gaiero, D. M. (2008), Reply to comment by B. Delmonte et al. on “Dust provenance in Antarctic ice during glacial periods: From where in southern South America?”, Geophysical Research Letters, 35(8).

Gaiero, D. M., F. Brunet, J.-L. Probst, and P. J. Depetris (2007), A uniform isotopic and chemical signature of dust exported from Patagonia: Rock sources and occurrence in southern environments, Chemical Geology, 238(1), 107-120.

Gaiero, D. M., J.-L. Probst, P. J. Depetris, S. M. Bidart, and L. Leleyter (2003), Iron and other transition metals in Patagonian riverborne and windborne materials: geochemical control and transport to the southern South Atlantic Ocean, Geochimica et Cosmochimica Acta, 67(19), 3603-3623.

Gao, S., D. A. Hegg, and H. Jonsson (2003), Aerosol chemistry, and light-scattering and hygroscopicity budgets during outflow from East Asia, Journal of Atmospheric Chemistry, 46(1), 55-88.

Gao, Y., Y. J. Kaufman, D. Tanré, D. Kolber, and P. G. Falkowski (2001), Seasonal distributions of aeolian iron fluxes to the global ocean, Geophys. Res. Lett., 28(1), 29-32.

Gao, Y., G. Xu, J. Zhan, J. Zhang, W. Li, Q. Lin, L. Chen, and H. Lin (2013), Spatial and particle size distributions of atmospheric dissolvable iron in aerosols and its input to the

Southern Ocean and coastal East Antarctica, Journal of Geophysical Research: Atmospheres, 118(22), 12,634-612,648.

Gaspari, V., C. Barbante, G. Cozzi, P. Cescon, C. F. Boutron, P. Gabrielli, G. Capodaglio, C. Ferrari, J. R. Petit, and B. Delmonte (2006), Atmospheric iron fluxes over the last deglaciation: Climatic implications, Geophys. Res. Lett., 33(3), L03704.

Gatehouse, R. D., I. Williams, and B. Pillans (2001), Fingerprinting windblown dust in south-eastern Australian soils by uranium-lead dating of detrital zircon, Soil Research, 39(1), 7-12.

Gaudichel, A., M. De Angelis, S. Joussaume, J. Petit, Y. Korotkevitch, and V. Petrov (1992), Comments on the origin of dust in East Antarctica for present and ice age conditions, Journal of atmospheric chemistry, 14(1-4), 129-142.

Gerringa, L. J. A., P. Laan, G. L. van Dijken, H. van Haren, H. J. W. De Baar, K. R. Arrigo, and A. C. Alderkamp (2015), Sources of iron in the Ross Sea Polynya in early summer, Marine Chemistry, 177, Part 3, 447-459.

Gerringa, L. J. A., A.-C. Alderkamp, P. Laan, C.-E. Thuróczy, H. J. W. De Baar, M. M. Mills, G. L. van Dijken, H. v. Haren, and K. R. Arrigo (2012), Iron from melting glaciers fuels the phytoplankton blooms in Amundsen Sea (Southern Ocean): Iron biogeochemistry, Deep Sea Research Part II: Topical Studies in Oceanography, 71–76(0), 16-31.

Gibbs, R., M. Mathews, and D. Unk (1971), The relationship between sphere size and settling velocity, Journal of Sedimentary Petrology, 41(1), 7-18.

Giglio, L., J. T. Randerson, and G. R. Werf (2013), Analysis of daily, monthly, and annual burned area using the fourth-generation global fire emissions database (GFED4), Journal of Geophysical Research: Biogeosciences, 118(1), 317-328.

Gillies, J. A., W. G. Nickling, and M. Tilson (2013), Frequency, magnitude, and characteristics of aeolian sediment transport: McMurdo Dry Valleys, Antarctica, Journal of Geophysical Research: Earth Surface, 118(2), 461-479.

Gingele, F., and P. De Deckker (2005), Clay mineral, geochemical and Sr–Nd isotopic fingerprinting of sediments in the Murray–Darling fluvial system, southeast Australia, Australian Journal of Earth Sciences, 52(6), 965-974.

Glassman, I. (1989), Soot formation in combustion processes, paper presented at Symposium (international) on combustion, Elsevier.

Gore, D., E. Rhodes, P. Augustinus, M. Leishman, E. Colhoun, and J. Rees-Jones (2001), Bunger Hills, East Antarctica: ice free at the last glacial maximum, Geology, 29(12), 1103-1106.

Grand, M., C. I. Measures, M. Hatta, W. T. Hiscock, C. S. Buck, and W. M. Landing (2015), Dust deposition in the eastern Indian Ocean: The ocean perspective from Antarctica to the Bay of Bengal, Global Biogeochemical Cycles.

Grand, M., C. I. Measures, M. Hatta, P. L. Morton, P. Barrett, A. Milne, J. A. Resing, and W. M. Landing (2015), The impact of circulation and dust deposition in controlling the

distributions of dissolved Fe and Al in the south Indian subtropical gyre, Marine Chemistry, 176, 110-125.

Grand, M., C. I. Measures, M. Hatta, W. T. Hiscock, W. M. Landing, P. L. Morton, C. S. Buck, P. M. Barrett, and J. A. Resing (2015), Dissolved Fe and Al in the upper 1000 m of the eastern Indian Ocean: A high-resolution transect along 95°E from the Antarctic margin to the Bay of Bengal, Global Biogeochemical Cycles, 29(3), 375-396.

Greeley, R., and J. Iversen (1985), Wind as a geological process, no. 4 in Cambridge Planetary Science Series, Cambridge Univ. Press, New York, NY, 3(3), 3.2.

Grousset, F., and P. Biscaye (2005), Tracing dust sources and transport patterns using Sr, Nd and Pb isotopes, Chemical Geology, 222(3-4), 149-167.

Grousset, F., P. Rognon, G. Coudé-Gaussen, and P. Pédemay (1992), Origins of peri-Saharan dust deposits traced by their Nd and Sr isotopic composition, Palaeogeography, Palaeoclimatology, Palaeoecology, 93(3), 203-212.

Grousset, F., P. Biscaye, A. Zindler, J. Prospero, and R. Chester (1988), Neodymium isotopes as tracers in marine sediments and aerosols: North Atlantic, Earth and Planetary Science Letters, 87(4), 367-378.

Grousset, F., P. Biscaye, M. Revel, J. Petit, K. Pye, S. Joussaume, and J. Jouzel (1992), Antarctic (Dome C) ice-core dust at 18 ky BP: Isotopic constraints on origins, Earth and Planetary Science Letters, 111(1), 175-182.

Grousset, F., P. Biscaye, M. Revel, J. Petit, K. Pye, S. Joussaume, and J. Jouzel (1992), Antarctic (Dome C) ice-core dust at 18 k.y. B.P.: Isotopic constraints on origins, Earth and Planetary Science Letters, 111(1), 175-182.

Guieu, C., S. Bonnet, T. Wagener, and M. D. Loÿe-Pilot (2005), Biomass burning as a source of dissolved iron to the open ocean?, Geophysical Research Letters, 32(19).

Guieu, C., et al. (2014), The significance of the episodic nature of atmospheric deposition to Low Nutrient Low Chlorophyll regions, Global Biogeochemical Cycles, 2014GB004852.

Gysel, M., M. Laborde, J. Olfert, R. Subramanian, and A. Gröhn (2011), Effective density of Aquadag and fullerene soot black carbon reference materials used for SP2 calibration, Atmospheric Measurement Techniques, 4(12), 2851-2858.

Halstead, M. J., R. G. Cunninghame, and K. A. Hunter (2000), Wet deposition of trace metals to a remote site in Fiordland, New Zealand, Atmospheric Environment, 34(4), 665-676.

Hand, J. L., N. M. Mahowald, Y. Chen, R. L. Siefert, C. Luo, A. Subramaniam, and I. Fung (2004), Estimates of atmospheric-processed soluble iron from observations and a global mineral aerosol model: Biogeochemical implications, J. Geophys. Res., 109(D17), D17205.

Hao, W. M., and M. H. Liu (1994), Spatial and temporal distribution of tropical biomass burning, Global biogeochemical cycles, 8(4), 495-503.

Hasegawa, S., and S. Ohta (2002), Some measurements of the mixing state of soot-containing particles at urban and non-urban sites, Atmospheric Environment, 36(24), 3899-3908.

Hayes, C. T., J. N. Fitzsimmons, E. A. Boyle, D. McGee, R. F. Anderson, R. Weisend, and P. L. Morton (2015), Thorium isotopes tracing the iron cycle at the Hawaii Ocean Time-series Station ALOHA, Geochimica et Cosmochimica Acta, 169, 1-16.

Heimburger, A., R. Losno, and S. Triquet (2013), Solubility of iron and other trace elements in rainwater collected on the Kerguelen Islands (South Indian Ocean), Biogeosciences, 10(10).

Heimburger, A., R. Losno, S. Triquet, and E. Nguyen (2013), Atmospheric deposition fluxes of 26 elements over the Southern Indian Ocean: Time series on Kerguelen and Crozet Islands, Global Biogeochemical Cycles, 27(2), 440-449.

Heimburger, A., R. Losno, S. Triquet, F. Dulac, and N. Mahowald (2012), Direct measurements of atmospheric iron, cobalt, and aluminum-derived dust deposition at Kerguelen Islands, Global Biogeochemical Cycles, 26(4).

Hesse, P. P. (1994), The record of continental dust from Australia in Tasman Sea sediments, Quaternary Science Reviews, 13(3), 257-272.

Hesse, P. P. (1997), Mineral magnetic 'tracing'of aeolian dust in southwest Pacific sediments, Palaeogeography, Palaeoclimatology, Palaeoecology, 131(3), 327-353.

Hesse, P. P., and G. H. McTainsh (2003), Australian dust deposits: modern processes and the Quaternary record, Quaternary Science Reviews, 22(18), 2007-2035.

Hinkley, T. K., and A. Matsumoto (2001), Atmospheric regime of dust and salt through 75,000 years of Taylor Dome ice core: Refinement by measurement of major, minor, and trace metal suites, J. Geophys. Res., 106(D16), 18487-18493.

Hoelzemann, J. J., M. G. Schultz, G. P. Brasseur, C. Granier, and M. Simon (2004), Global Wildland Fire Emission Model (GWEM): Evaluating the use of global area burnt satellite data, Journal of Geophysical Research: Atmospheres (1984–2012), 109(D14).

Hoffer, A., A. Gelencsér, P. Guyon, G. Kiss, O. Schmid, G. Frank, P. Artaxo, and M. Andreae (2005), Optical properties of humiclike substances (HULIS) in biomass-burning aerosols, Atmos. Chem. Phys. Discuss, 5(4), 7341-7360.

Hole, M., and W. LeMasurier (1994), Tectonic controls on the geochemical composition of Cenozoic, mafic alkaline volcanic rocks from West Antarctica, Contributions to Mineralogy and Petrology, 117(2), 187-202.

Hope, B. K. (2008), A dynamic model for the global cycling of anthropogenic vanadium, Global Biogeochemical Cycles, 22(4).

Huang, X., T. Gordon, W. N. Rom, and R. B. Finkelman (2006), Interaction of iron and calcium minerals in coals and their roles in coal dust-induced health and environmental problems, Reviews in mineralogy and geochemistry, 64(1), 153-178.

Huang, X., Y. Song, C. Zhao, M. Li, T. Zhu, Q. Zhang, and X. Zhang (2014), Pathways of sulfate enhancement by natural and anthropogenic mineral aerosols in China, Journal of Geophysical Research: Atmospheres.

Hurst, M. P., and K. W. Bruland (2007), An investigation into the exchange of iron and zinc between soluble, colloidal, and particulate size-fractions in shelf waters using low-abundance isotopes as tracers in shipboard incubation experiments, Marine chemistry, 103(3), 211-226.

Hutchins, D. A., G. R. DiTullio, and K. W. Bruland (1993), Iron and Regenerated Production: Evidence for Biological Iron Recycling in Two Marine Environments, Limnology and Oceanography, 38(6), 1242-1255.

Iinuma, Y., M. Keywood, and H. Herrmann (2015), Characterisation of primary and secondary organic aerosols in Melbourne airshed: the influence of biogenic emissions, wood smoke and bushfires, Atmospheric Environment.

Ito, A. (2011), Mega fire emissions in Siberia: potential supply of bioavailable iron from forests to the ocean, Biogeosciences, 8(6).

Ito, A. (2012), Contrasting the effect of iron mobilization on soluble iron deposition to the ocean in the Northern and Southern Hemispheres, Meteorol. Soc. Japan, 90(0), 167-188.

Ito, A. (2013), Global modeling study of potentially bioavailable iron input from shipboard aerosol sources to the ocean, Global Biogeochemical Cycles, 27(1), 1-10.

Ito, A. (2015), Atmospheric Processing of Combustion Aerosols as a Source of Bioavailable Iron, Environmental Science & Technology Letters, 2(3), 70-75.

Ito, A., and J. E. Penner (2004), Global estimates of biomass burning emissions based on satellite imagery for the year 2000, Journal of Geophysical Research: Atmospheres (1984–2012), 109(D14).

Ito, A., and Z. Shi (2015), Delivery of anthropogenic bioavailable iron from mineral dust and combustion aerosols to the ocean, Atmospheric Chemistry and Physics Discussions, 15(16), 23051-23088.

Jacobs, S. S., A. F. Amos, and P. M. Bruchhausen (1970), Ross sea oceanography and antarctic bottom water formation, Deep Sea Research and Oceanographic Abstracts, 17(6), 935-962.

Jacobsen, S. B., and G. J. Wasserburg (1980), Sm-Nd isotopic evolution of chondrites, Earth and Planetary Science Letters, 50(1), 139-155.

Jacobson, M. Z. (2003), Development of mixed-phase clouds from multiple aerosol size distributions and the effect of the clouds on aerosol removal, Journal of Geophysical Research: Atmospheres (1984–2012), 108(D8).

Jang, H.-N., Y.-C. Seo, J.-H. Lee, K.-W. Hwang, J.-I. Yoo, C.-H. Sok, and S.-H. Kim (2007), Formation of fine particles enriched by V and Ni from heavy oil combustion: Anthropogenic sources and drop-tube furnace experiments, Atmospheric Environment, 41(5), 1053-1063.

Jeong, D., K. Kim, and W. Choi (2012), Accelerated dissolution of iron oxides in ice, Atmospheric Chemistry and Physics, 12(22), 11125-11133.

Jickells, T., et al. (2005), Global iron connections between desert dust, ocean biogeochemistry, and climate, Science, 308, 67 - 73.

Jochum, K. P., U. Nohl, K. Herwig, E. Lammel, B. Stoll, and A. W. Hofmann (2005), GeoReM: A New Geochemical Database for Reference Materials and Isotopic Standards, Geostandards and Geoanalytical Research, 29(3), 333-338.

Johnsen, S. J., W. Dansgaard, H. B. Clausen, and C. C. Langway (1972), Oxygen Isotope Profiles through the Antarctic and Greenland Ice Sheets, Nature, 235(5339), 429-434.

Johnson, K. S., R. M. Gordon, and K. H. Coale (1997), What controls dissolved iron concentrations in the world ocean?, Marine Chemistry, 57(3), 137-161.

Johnson, K., F. Chavez, and G. Friederich (1999), Continental-shelf sediment as a primary source of iron for coastal phytoplankton, Nature, 398, 697 - 700.

Johnson, K., K. Coale, V. Elrod, and W. Tindale (1994), Iron photochemistry in seawater from the equatorial Pacific, Mar Chem, 46, 319 - 334.

Johnson, M. S., N. Meskhidze, V. P. Kiliyanpilakkil, and S. Gassó (2010), Understanding the transport of Patagonian dust and its influence on marine biological activity in the South Atlantic Ocean, Atmos. Chem. Phys. Discuss., 10(11), 27283-27320.

Johnson, B., B. Heese, S. McFarlane, P. Chazette, A. Jones, and N. Bellouin (2008), Vertical distribution and radiative effects of mineral dust and biomass burning aerosol over West Africa during DABEX, Journal of Geophysical Research: Atmospheres (1984–2012), 113(D23).

Johnston, S. W. (2001), The influence of aeolian dust deposits on alpine soils in south-eastern Australia, Soil Research, 39(1), 81-88.

Jong, J., V. Schoemann, D. Lannuzel, P. Croot, H. Baar, and J. L. Tison (2012), Natural iron fertilization of the Atlantic sector of the Southern Ocean by continental shelf sources of the Antarctic Peninsula, Journal of Geophysical Research: Biogeosciences (2005–2012), 117(G1).

Kadko, D., W. M. Landing, and R. U. Shelley (2015), A novel tracer technique to quantify the atmospheric flux of trace elements to remote ocean regions, Journal of Geophysical Research: Oceans.

Kalinske, A. A. (1943), Turbulence and the transport of sand and silt by wind, Annals of the New York Academy of Sciences, 44(1), 41-54.

Kasischke, E. S., and J. E. Penner (2004), Improving global estimates of atmospheric emissions from biomass burning, Journal of Geophysical Research: Atmospheres (1984–2012), 109(D14).

Keeling, R. F., S. C. Piper, and M. Heimann (1996), Global and hemispheric CO2 sinks deduced from changes in atmospheric O2 concentration, Nature, 381(6579), 218-221.

Kellogg, T. B., D. Kellogg, and M. Stuiver (1990), Late Quaternary History of the Southwestern Ross Sea: Evidence from Debris Bands on the McMurdo Ice Shelf, Antarctica, Antarctic Res. Ser. (AGU), 50, 25-56.

Keywood, M. (1999), An evaluation of PM10 and PM2. 5 size selective inlet performance using ambient aerosol, Aerosol Science & Technology, 30(4), 401-407.

Keywood, M. D. (2007), Aerosol composition at Cape Grim : an evaluation of PM10 sampling program and baseline event switches., Baseline Atmospheric Program Australia 2005-2006. 2005-2006 ed. J. M. Cainey, N. Derek, and P. B. Krummel (editors). Melbourne: Australian Bureau of Meteorology and CSIRO Marine and Atmospheric Research, 31-36.

Keywood, M. D., B. Graham, R. W. Gillett, J. G. Gras, and P. W. Selleck (2004), High volume aerosol sampler. Baseline Atmospheric Program (Australia) 2001-200 edited by J. Cainey, N.Derek and P.Krummel. .Bureau of Meteorology CSIRO Atmospheric Research and, Melbourne, Australia: 74-77.

Keywood, M., M. Cope, C. M. Meyer, Y. Iinuma, and K. Emmerson (2015), When smoke comes to town: The impact of biomass burning smoke on air quality, Atmospheric Environment.

Keywood, M., M. Kanakidou, A. Stohl, F. Dentener, G. Grassi, C. Meyer, K. Torseth, D. Edwards, A. M. Thompson, and U. Lohmann (2013), Fire in the air: biomass burning impacts in a changing climate, Critical Reviews in Environmental Science and Technology, 43(1), 40-83.

Khalizov, A. F., H. Xue, L. Wang, J. Zheng, and R. Zhang (2009), Enhanced light absorption and scattering by carbon soot aerosol internally mixed with sulfuric acid, The Journal of Physical Chemistry A, 113(6), 1066-1074.

Kipling, Z., P. Stier, J. Schwarz, A. Perring, J. Spackman, G. Mann, C. Johnson, and P. Telford (2013), Constraints on aerosol processes in climate models from vertically-resolved aircraft observations of black carbon, Atmospheric Chemistry and Physics, 13(12), 5969.

Knight, A. W., G. McTainsh, and R. Simpson (1995), Sediment loads in an Australian dust storm: implications for present and past dust processes, Catena, 24(3), 195-213.

Kobayashi, H., K. Hara, M. Shiobara, T. Yamanouchi, K. Osada, and S. Ohta (2010), Seasonal variation of carbonaceous and metal compositions of atmospheric aerosols at Syowa Station, Antarctica in 2001, Antarctic Record(Tokyo), 54, 554-561.

Koffman, B. G., M. J. Handley, E. C. Osterberg, M. L. Wells, and K. J. Kreutz (2014), Dependence of ice-core relative trace-element concentration on acidification, Journal of Glaciology, 60(219), 103-112.

Koffman, B. G., K. J. Kreutz, D. J. Breton, E. J. Kane, D. A. Winski, S. D. Birkel, A. Kurbatov, and M. J. Handley (2014), Centennial-scale variability of the Southern Hemisphere westerly wind belt in the eastern Pacific over the past two millennia, Climate of the Past, 10(3), 1125-1144.

Kohfeld, K. E., and S. P. Harrison (2001), DIRTMAP: the geological record of dust, Earth-Science Reviews, 54(1-3), 81-114.

Kok, J. F. (2011), A scaling theory for the size distribution of emitted dust aerosols suggests climate models underestimate the size of the global dust cycle, Proceedings of the National Academy of Sciences, 108(3), 1016-1021.

Kok, J. F. (2011), Does the size distribution of mineral dust aerosols depend on the wind speed at emission?, Atmospheric Chemistry and Physics, 11(19), 10149-10156.

Koppmann, R., K. v. Czapiewski, and J. Reid (2005), A review of biomass burning emissions, part I: gaseous emissions of carbon monoxide, methane, volatile organic compounds, and nitrogen containing compounds, Atmospheric Chemistry and Physics Discussions, 5(5), 10455-10516.

Kraemer, S. (2004), Iron oxide dissolution and solubility in the presence of siderophores, Aquatic Sciences - Research Across Boundaries, 66(1), 3-18.

Kraemer, S. M., A. Butler, P. Borer, and J. Cervini-Silva (2005), Siderophores and the Dissolution of Iron-Bearing Minerals in Marine Systems, Reviews in Mineralogy and Geochemistry, 59(1), 53-84.

Krinner, G., and C. Genthon (2003), Tropospheric transport of continental tracers towards Antarctica under varying climatic conditions, Tellus B, 55(1), 54-70.

Krinner, G., J.-R. Petit, and B. Delmonte (2010), Altitude of atmospheric tracer transport towards Antarctica inpresent and glacial climate, Quaternary science reviews, 29(1), 274-284.

Kuma, K., and K. Matsunaga (1995), Availability of colloidal ferric oxides to coastal marine phytoplankton, Marine Biology, 122(1), 1-11.

Kumar, A., M. Sarin, and B. Srinivas (2010), Aerosol iron solubility over Bay of Bengal: Role of anthropogenic sources and chemical processing, Marine Chemistry, 121(1), 167-175.

Kustka, A. B., S. A. Sañudo-Wilhelmy, E. J. Carpenter, D. Capone, J. Burns, and W. G. Sunda (2003), Iron requirements for dinitrogen-and ammonium-supported growth in cultures of Trichodesmium (IMS 101): Comparison with nitrogen fixation rates and iron: Carbon ratios of field populations, Limnology and Oceanography, 48(5), 1869-1884.

Kustka, A. B., et al. (2015), The roles of MCDW and deep water iron supply in sustaining a recurrent phytoplankton bloom on central Pennell Bank (Ross Sea), Deep Sea Research Part I: Oceanographic Research Papers, 105, 171-185.

Laborde, M., P. Mertes, P. Zieger, J. Dommen, U. Baltensperger, and M. Gysel (2012), Sensitivity of the Single Particle Soot Photometer to different black carbon types, Atmospheric Measurement Techniques, 5(5), 1031-1043.

Lamarque, J.-F., T. C. Bond, V. Eyring, C. Granier, A. Heil, Z. Klimont, D. Lee, C. Liousse, A. Mieville, and B. Owen (2010), Historical (1850–2000) gridded anthropogenic and biomass burning emissions of reactive gases and aerosols: methodology and application, Atmospheric Chemistry and Physics, 10(15), 7017-7039.

Lambert, F., A. Tagliabue, G. Shaffer, F. Lamy, G. Winckler, L. Farias, L. Gallardo, and R. De Pol-Holz (2015), Dust fluxes and iron fertilization in Holocene and Last Glacial Maximum climates, Geophysical Research Letters, n/a-n/a.

Lambert, F., B. Delmonte, J. R. Petit, M. Bigler, P. R. Kaufmann, M. A. Hutterli, T. F. Stocker, U. Ruth, J. P. Steffensen, and V. Maggi (2008), Dust-climate couplings over the past 800,000[thinsp]years from the EPICA Dome C ice core, Nature, 452(7187), 616-619.

Lancaster, N., W. G. Nickling, and J. A. Gillies (2010), Sand transport by wind on complex surfaces: Field studies in the McMurdo Dry Valleys, Antarctica, Journal of Geophysical Research: Earth Surface (2003–2012), 115(F3).

Lanci, L., B. Delmonte, V. Maggi, J. R. Petit, and D. V. Kent (2008), Ice magnetization in the EPICA-Dome C ice core: Implication for dust sources during glacial and interglacial periods, J. Geophys. Res., 113(D14), D14207.

Lane, S., B. C. Proemse, A. Tennant, and M. E. Wieser (2013), Concentration measurements and isotopic composition of airborne molybdenum collected in an urban environment, Analytical and bioanalytical chemistry, 405(9), 2957-2963.

Lannuzel, D., M. Grotti, M. L. Abelmoschi, and P. van der Merwe (2015), Organic ligands control the concentrations of dissolved iron in Antarctic sea ice, Marine Chemistry, 174, 120-130.

Lannuzel, D., V. Schoemann, J. de Jong, J. Tison, and L. Chou (2007), Distribution and biogeochemical behaviour of iron in the East Antarctic sea ice, Marine Chemistry, 106(1-2), 18-32.

Lannuzel, D., V. Schoemann, J. de Jong, J. Tison, and L. Chou (2007), Distribution and biogeochemical behaviour of iron in the East Antarctic sea ice, Marine Chemistry, 106(1-2), 18-32.

Lannuzel, D., V. Schoemann, J. de Jong, L. Chou, B. Delille, S. Becquevort, and J. Tison (2008), Iron study during a time series in the western Weddell pack ice, Marine Chemistry, 108(1-2), 85-95.

Lannuzel, D., V. Schoemann, J. de Jong, B. Pasquer, P. van der Merwe, F. Masson, J. Tison, and A. Bowie (2010), Distribution of dissolved iron in Antarctic sea ice: Spatial, seasonal, and inter-annual variability, J. Geophys. Res., 115(G3), G03022.

LaRoche, J., and E. Breitbarth (2005), Importance of the diazotrophs as a source of new nitrogen in the ocean, Journal of Sea Research, 53(1), 67-91.

Latimer, J. C., and G. M. Filippelli (2001), Terrigenous input and paleoproductivity in the Southern Ocean, Paleoceanography, 16(6), 627-643.

Latimer, J. C., G. M. Filippelli, I. L. Hendy, J. D. Gleason, and J. D. Blum (2006), Glacial-interglacial terrigenous provenance in the southeastern Atlantic Ocean: The importance of deep-water sources and surface currents, Geology, 34(7), 545-548.

Law, C., E. Woodward, M. Ellwood, A. Marriner, S. Bury, and K. Safi (2011), Response of surface nutrient inventories and nitrogen fixation to a tropical cyclone in the southwest Pacific, Limnology and Oceanography, 56(4), 1372-1385.

le Roux, J. P. (1994), An alternative approach to the identification of net sediment transport paths based on grain-size trends, Sedimentary Geology, 94(1-2), 97-107.

Legrand, M., and S. Kirchner (1988), Polar atmospheric circulation and chemistry of recent (1957-1983) south polar precipitation, Geophysical research letters, 15(8), 879-882.

Lenes, J., B. Darrow, J. Walsh, J. Prospero, R. He, R. Weisberg, G. Vargo, and C. Heil (2008), Saharan dust and phosphatic fidelity: A three-dimensional biogeochemical model of Trichodesmium as a nutrient source for red tides on the West Florida Shelf, Continental Shelf Research, 28(9), 1091-1115.

Li, F., P. Ginoux, and V. Ramaswamy (2008), Distribution, transport, and deposition of mineral dust in the Southern Ocean and Antarctica: Contribution of major sources, J. Geophys. Res., 113(D10), D10207.

Li-Jones, X., and J. Prospero (1998), Variations in the size distribution of non-sea-salt sulfate aerosol in the marine boundary layer at Barbados: Impact of African dust, Journal of Geophysical Research: Atmospheres (1984–2012), 103(D13), 16073-16084.

Lin, Y. C., J. P. Chen, T. Y. Ho, and I. Tsai (2015), Atmospheric iron deposition in the northwestern Pacific Ocean and its adjacent marginal seas: The importance of coal burning, Global Biogeochemical Cycles, 29(2), 138-159.

Lis, H., Y. Shaked, C. Kranzler, N. Keren, and F. M. M. Morel (2015), Iron bioavailability to phytoplankton: an empirical approach, ISME J, 9(4), 1003-1013.

Liu, J., S. Fan, L. W. Horowitz, and H. Levy (2011), Evaluation of factors controlling long-range transport of black carbon to the Arctic, Journal of Geophysical Research: Atmospheres (1984–2012), 116(D4).

Liu, J., D. L. Mauzerall, L. W. Horowitz, P. Ginoux, and A. M. Fiore (2009), Evaluating inter-continental transport of fine aerosols:(1) Methodology, global aerosol distribution and optical depth, Atmospheric Environment, 43(28), 4327-4338.

Lohmann, U., J. Feichter, J. Penner, and R. Leaitch (2000), Indirect effect of sulfate and carbonaceous aerosols- A mechanistic treatment, Journal of Geophysical Research, 105(D10), 12193-12206.

Lu, H., and Y. Shao (2001), Toward quantitative prediction of dust storms: an integrated wind erosion modelling system and its applications, Environmental Modelling & Software, 16(3), 233-249.

Luo, C., N. M. Mahowald, and J. del Corral (2003), Sensitivity study of meteorological parameters on mineral aerosol mobilization, transport, and distribution, J. Geophys. Res., 108(D15), 4447.

Luo, C., N. M. Mahowald, N. Meskhidze, Y. Chen, R. L. Siefert, A. R. Baker, and A. M. Johansen (2005), Estimation of iron solubility from observations and a global aerosol model, J. Geophys. Res., 110(D23), D23307.

Luo, C., N. Mahowald, T. Bond, P. Y. Chuang, P. Artaxo, R. Siefert, Y. Chen, and J. Schauer (2008), Combustion iron distribution and deposition, Global Biogeochem. Cycles, 22(1), GB1012.

Luo, C., N. Mahowald, T. Bond, P. Y. Chuang, P. Artaxo, R. Siefert, Y. Chen, and J. Schauer (2008), Combustion iron distribution and deposition, Global Biogeochem. Cycles, 22(1), GB1012.

Mackie, D. S., P. W. Boyd, K. A. Hunter, and G. H. McTainsh (2005), Simulating the cloud processing of iron in Australian dust: pH and dust concentration, Geophys. Res. Lett., 32(6), L06809.

Mackie, D., J. Peat, G. H. McTainsh, P. Boyd, and K. Hunter (2006), Soil abrasion and eolian dust production: Implications for iron partitioning and solubility, Geochemistry, Geophysics, Geosystems, 7(12).

Mackie, D. S., P. W. Boyd, G. H. McTainsh, N. W. Tindale, T. K. Westberry, and K. A. Hunter (2008), Biogeochemistry of iron in Australian dust: From eolian uplift to marine uptake, Geochem. Geophys. Geosyst., 9(3), Q03Q08.

Macpherson, A. (1987), The MacKay Glacier/Granite Harbour system (Ross Dependency, Antarctica). A study in nearshore glacial marine sedimentation, 85 pp, Victoria University of Wellington, Wellington.

Maenhaut, W., M.-T. Fernández-Jiménez, I. Rajta, and P. Artaxo (2002), Two-year study of atmospheric aerosols in Alta Floresta, Brazil: Multielemental composition and source apportionment, Nuclear Instruments and Methods in Physics Research Section B: Beam Interactions with Materials and Atoms, 189(1), 243-248.

Maenhaut, W., I. Salma, J. Cafmeyer, H. J. Annegarn, and M. O. Andreae (1996), Regional atmospheric aerosol composition and sources in the eastern Transvaal, South Africa, and impact of biomass burning, JOURNAL OF GEOPHYSICAL RESEARCH-ALL SERIES-, 101, 23,631-623,650.

Magee, J., J. Bowler, G. Miller, and D. Williams (1995), Stratigraphy, sedimentology, chronology and palaeohydrology of Quaternary lacustrine deposits at Madigan Gulf, Lake Eyre, South Australia, Palaeogeography, Palaeoclimatology, Palaeoecology, 113(1), 3-42.

Mahowald, N., K. Kohfeld, M. Hansson, Y. Balkanski, S. P. Harrison, I. C. Prentice, M. Schulz, and H. Rodhe (1999), Dust sources and deposition during the last glacial maximum and current climate: A comparison of model results with paleodata from ice cores and marine sediments, J. Geophys. Res., 104(D13), 15895-15916.

Mahowald, N. M., A. R. Baker, G. Bergametti, N. Brooks, R. A. Duce, T. D. Jickells, N. Kubilay, J. M. Prospero, and I. Tegen (2005), Atmospheric global dust cycle and iron inputs to the ocean, Global Biogeochem. Cycles, 19(4), GB4025.

Mahowald, N. M., S. Engelstaedter, C. Luo, A. Sealy, P. Artaxo, C. Benitez-Nelson, S. Bonnet, Y. Chen, P. Y. Chuang, and D. D. Cohen (2009), Atmospheric iron deposition: Global distribution, variability, and human perturbations*, Marine Science, 1.

Mahowald, N. M., et al. (2010), Observed 20th century desert dust variability: impact on climate and biogeochemistry, Atmos. Chem. Phys., 10(22), 10875-10893.

Marino, F., E. Castellano, D. Ceccato, P. De Deckker, B. Delmonte, G. Ghermandi, V. Maggi, J. R. Petit, M. Revel-Rolland, and R. Udisti (2008), Defining the geochemical composition of the EPICA Dome C ice core dust during the last glacial-interglacial cycle, Geochem. Geophys. Geosyst., 9(10), Q10018.

Marsay, C., P. N. Sedwick, M. Dinniman, P. Barrett, S. Mack, and D. J. McGillicuddy (2014), Estimating the benthic efflux of dissolved iron on the Ross Sea continental shelf, Geophysical Research Letters, 41(21), 7576-7583.

Marticorena, B., and G. Bergametti (1995), Modeling the atmospheric dust cycle: 1. Design of a soil-derived dust emission scheme, J. Geophys. Res., 100(D8), 16415-16430.

Martin, J. H. (1990), Glacial-interglacial CO2 change: the iron hypothesis, Paleoceanography, 5, 1-11.

Martin, C. E., and M. T. McCulloch (1999), Nd-Sr isotopic and trace element geochemistry of river sediments and soils in a fertilized catchment, New South Wales, Australia, Geochimica et cosmochimica acta, 63(2), 287-305.

Martin, J. H., R. M. Gordon, and S. E. Fitzwater (1990), Iron in Antarctic waters, Nature, 345(6271), 156-158.

Martin, J. H., R. M. Gordon, and S. E. Fitzwater (1991), The Case for Iron, Limnology and Oceanography, 36(8), 1793-1802.

Martínez-Garcia, A., A. Rosell-Melé, W. Geibert, R. Gersonde, P. Masqué, V. Gaspari, and C. Barbante (2009), Links between iron supply, marine productivity, sea surface temperature, and CO2 over the last 1.1 Ma, Paleoceanography, 24(1), PA1207.

Martínez-García, A., D. M. Sigman, H. Ren, R. F. Anderson, M. Straub, D. A. Hodell, S. L. Jaccard, T. I. Eglinton, and G. H. Haug (2014), Iron Fertilization of the Subantarctic Ocean During the Last Ice Age, Science, 343(6177), 1347-1350.

Marx, S. K., B. S. Kamber, and H. A. McGowan (2005), Estimates of Australian dust flux into New Zealand: Quantifying the eastern Australian dust plume pathway using trace element calibrated< sup> 210</sup> Pb as a monitor, Earth and Planetary Science Letters, 239(3), 336-351.

McConnell, J. R., G. W. Lamorey, and M. A. Hutterli (2002), A 250-year high-resolution record of Pb flux and crustal enrichment in central Greenland, Geophysical Research Letters, 29(23), 45-41-45-44.

McGillicuddy, D., P. Sedwick, M. Dinniman, K. Arrigo, T. Bibby, B. Greenan, E. Hofmann, J. Klinck, W. Smith, and S. Mack (2015), Iron supply and demand in an Antarctic shelf ecosystem, Geophysical Research Letters.

McGowan, H., and A. Clark (2008), Identification of dust transport pathways from Lake Eyre, Australia using Hysplit, Atmospheric Environment, 42(29), 6915-6925.

McGowan, H. A., B. Kamber, G. H. McTainsh, and S. K. Marx (2005), High resolution provenancing of long travelled dust deposited on the Southern Alps, New Zealand, Geomorphology, 69(1), 208-221.

McLaren, P. (1981), An interpretation of trends in grain size measures, JOURNAL OF SEDIMENTARY RESEARCH, 51(2), 611-624.

McTainsh, G. (1989), Quaternary aeolian dust processes and sediments in the Australian region, Quaternary Science Reviews, 8(3), 235-253.

McTainsh, G., and J. Leys (1993), Soil erosion by wind, Land Degradation Processes in Australia, 188-233.

McTainsh, G., and A. Lynch (1996), Quantitative estimates of the effect of climate change on dust storm activity in Australia during the Last Glacial Maximum, Geomorphology, 17(1), 263-271.

McTainsh, G., J. Leys, and E. Tews (2006), Wind erosion trends for the National State of the Environment Report: Data and Methods, Australia State of the Environment 2006.

McTainsh, G., Y.-c. Chan, H. McGowan, J. Leys, and K. Tews (2005), The 23rd October 2002 dust storm in eastern Australia: characteristics and meteorological conditions, Atmospheric Environment, 39(7), 1227-1236.

Meskhidze, N., and A. Nenes (2006), Phytoplankton and cloudiness in the Southern Ocean, Science, 314(5804), 1419-1423.

Meskhidze, N., W. Chameides, A. Nenes, and G. Chen (2003), Iron mobilization in mineral dust: Can anthropogenic SO2 emissions affect ocean productivity?, Geophysical Research Letters, 30(21).

Meyer, C. P., A. K. Luhar, and R. M. Mitchell (2008), Biomass burning emissions over northern Australia constrained by aerosol measurements: I—Modelling the distribution of hourly emissions, Atmospheric Environment, 42(7), 1629-1646.

Middag, R., H. De Baar, P. Laan, P. Cai, and J. Van Ooijen (2011), Dissolved manganese in the Atlantic sector of the Southern Ocean, Deep Sea Research Part II: Topical Studies in Oceanography, 58(25), 2661-2677.

Mills, M. M., C. Ridame, M. Davey, J. La Roche, and R. J. Geider (2004), Iron and phosphorus co-limit nitrogen fixation in the eastern tropical North Atlantic, Nature, 429(6989), 292-294.

Mitchell, B. G., E. A. Brody, O. Holm-Hansen, C. McClain, and J. Bishop (1991), Light Limitation of Phytoplankton Biomass and Macronutrient Utilization in the Southern Ocean, Limnology and Oceanography, 36(8), 1662-1677.

Moore, J. K., M. R. Abbott, J. G. Richman, and D. M. Nelson (2000), The southern ocean at the Last Glacial Maximum: A strong sink for atmospheric carbon dioxide, Global Biogeochem. Cycles, 14(1), 455-475.

Moore, J. K., K. Lindsay, S. C. Doney, M. C. Long, and K. Misumi (2013), Marine ecosystem dynamics and biogeochemical cycling in the Community Earth System Model [CESM1 (BGC)]: Comparison of the 1990s with the 2090s under the RCP4. 5 and RCP8. 5 scenarios, Journal of Climate, 26(23), 9291-9312.

Morel, F., and N. Price (2003), The biogeochemical cycles of trace metals in the oceans, Science, 300(5621), 944-947.

Morel, F. M., R. J. Hudson, and N. M. Price (1991), Limitation of productivity by trace metals in the sea, Limnology and Oceanography, 36(8), 1742-1755.

Morton, P. L., W. M. Landing, S.-C. Hsu, A. Milne, A. M. Aguilar-Islas, A. R. Baker, A. R. Bowie, C. S. Buck, Y. Gao, and S. Gichuki (2013), Methods for the sampling and analysis of marine aerosols: results from the 2008 GEOTRACES aerosol intercalibration experiment, Limnology and Oceanography: Methods, 11(FEB), 62-78.

Moteki, N., and Y. Kondo (2007), Effects of mixing state on black carbon measurements by laser-induced incandescence, Aerosol Science and Technology, 41(4), 398-417.

Mouillot, F., and C. B. Field (2005), Fire history and the global carbon budget: a 1× 1 fire history reconstruction for the 20th century, Global Change Biology, 11(3), 398-420.

Narcisi, B., J.-R. Petit, B. Delmonte, I. Basile-Doelsch, and V. Maggi (2005), Characteristics and sources of tephra layers in the EPICA-Dome C ice record (East Antarctica): implications for past atmospheric circulation and ice core stratigraphic correlations, Earth and Planetary Science Letters, 239(3), 253-265.

Neff, P. D., and N. A. Bertler (2015), Trajectory modeling of modern dust transport to the Southern Ocean and Antarctica, Journal of Geophysical Research: Atmospheres.

Neff, P. D., and N. A. Bertler (2015), Trajectory modeling of modern dust transport to the Southern Ocean and Antarctica, Journal of Geophysical Research: Atmospheres, 120(18), 9303-9322.

Nicol, S., A. Bowie, S. Jarman, D. Lannuzel, K. M. Meiners, and P. Van Der Merwe (2010), Southern Ocean iron fertilization by baleen whales and Antarctic krill, Fish and Fisheries, 11(2), 203-209.

Nodwell, L. M., and N. M. Price (2001), Direct Use of Inorganic Colloidal Iron by Marine Mixotrophic Phytoplankton, Limnology and Oceanography, 46(4), 765-777.

Novakov, T. (1982), Soot in the atmosphere, in Particulate Carbon, edited, pp. 19-41, Springer.

Oberholzer, P., C. Baroni, M. Salvatore, H. Baur, and R. Wieler (2008), Dating late Cenozoic erosional surfaces in Victoria Land, Antarctica, with cosmogenic neon in pyroxenes, Antarctic Science, 20(01), 89-98.

Oberholzer, P., C. Baroni, J. M. Schaefer, G. Orombelli, S. I. Ochs, P. W. Kubik, H. Baur, and R. Wieler (2003), Limited Pliocene/Pleistocene glaciation in Deep Freeze Range, northern Victoria Land, Antarctica, derived from in situ cosmogenic nuclides, Antarctic science, 15(04), 493-502.

Oshima, N., M. Koike, Y. Zhang, and Y. Kondo (2009), Aging of black carbon in outflow from anthropogenic sources using a mixing state resolved model: 2. Aerosol optical properties and cloud condensation nuclei activities, Journal of Geophysical Research: Atmospheres (1984–2012), 114(D18).

Pacyna, J., and J. Nriagu (1988), Atmospheric emissions of chromium from natural and anthropogenic sources, Chromium in the Natural and Human Environments, 105-123.

Paerl, H. W., K. M. Crocker, and L. E. Prufert (1987), Limitation of N2 fixation in coastal marine waters: Relative importance of molybdenum, iron, phosphorus, and organic matter availability1, Limnology and Oceanography, 32(3), 525-536.

Paerl, H. W., L. E. Prufert-Bebout, and C. Guo (1994), Iron-stimulated N2 fixation and growth in natural and cultured populations of the planktonic marine cyanobacteria Trichodesmium spp, Applied and Environmental Microbiology, 60(3), 1044-1047.

Palmer, T. Y. (1981), Large fire winds, gases and smoke, Atmospheric Environment (1967), 15(10), 2079-2090.

Parekh, P. (1990), A study of manganese from anthropogenic emissions at a rural site in the eastern United States, Atmospheric Environment. Part A. General Topics, 24(2), 415-421.

Paris, R., and K. Desboeufs (2013), Effect of atmospheric organic complexation on iron-bearing dust solubility, Atmospheric Chemistry and Physics, 13(9), 4895-4905.

Paris, R., K. Desboeufs, and E. Journet (2011), Variability of dust iron solubility in atmospheric waters: Investigation of the role of oxalate organic complexation, Atmospheric Environment, 45(36), 6510-6517.

Paris, R., K. Desboeufs, P. Formenti, S. Nava, and C. Chou (2010), Chemical characterisation of iron in dust and biomass burning aerosols during AMMA-SOP0/DABEX: implication for iron solubility, Atmospheric Chemistry and Physics, 10(9), 4273-4282.

Pereira, E., A. Setzer, F. Gerab, P. Artaxo, M. Pereira, and G. Monroe (1996), Airborne measurements of aerosols from burning biomass in Brazil related to the TRACE A experiment, Journal of Geophysical Research: Atmospheres (1984–2012), 101(D19), 23983-23992.

Petit, J. R., and B. Delmonte (2011), Glacial Interglacial Aerosol Input over Antarctica and the Global Hydrological Cycle, Mineralogical Magazine, 75(3), 1.

Petit, J.-R., M. Briat, and A. Royer (1981), Ice age aerosol content from East Antarctic ice core samples and past wind strength, Nature, 293(5831), 391-394.

Petit, J. R., et al. (1999), Climate and atmospheric history of the past 420,000 years from the Vostok ice core, Antarctica, Nature, 399(6735), 429-436.

Petters, M. D., A. J. Prenni, S. M. Kreidenweis, P. J. DeMott, A. Matsunaga, Y. B. Lim, and P. J. Ziemann (2006), Chemical aging and the hydrophobic-to-hydrophilic conversion of carbonaceous aerosol, Geophysical research letters, 33(24).

Pitman, A., G. Narisma, and J. McAneney (2007), The impact of climate change on the risk of forest and grassland fires in Australia, Climatic Change, 84(3-4), 383-401.

Planquette, H., P. J. Statham, G. R. Fones, M. A. Charette, C. M. Moore, I. Salter, F. H. Nedelec, S. L. Taylor, M. French, and A. R. Baker (2007), Dissolved iron in the vicinity of the Crozet Islands, Southern Ocean, Deep Sea Research Part II: Topical Studies in Oceanography, 54(18), 1999-2019.

Porstendorfer, J., G. Butterweck, and A. Reineking (1994), Daily variation of the radon concentration indoors and outdoors and the influence of meteorological parameters, Health physics, 67(3), 283-287.

Pósfai, M., R. Simonics, J. Li, P. V. Hobbs, and P. R. Buseck (2003), Individual aerosol particles from biomass burning in southern Africa: 1. Compositions and size distributions of carbonaceous particles, Journal of Geophysical Research: Atmospheres (1984–2012), 108(D13).

Price, N., and F. Morel (1991), Colimitation of phytoplankton growth by nickel and nitrogen, LIMNOLOGY.

Prospero, J. M. (1996), The atmospheric transport of particles to the ocean, in Particle Flux in the Ocean, John Wiley, Hoboken, N. J.

Prospero, J. M., P. Ginoux, O. Torres, S. E. Nicholson, and T. E. Gill (2002), Environmental characterization of global sources of atmospheric soil dust identified with the Nimbus 7 Total Ozone Mapping Spectrometer (TOMS) absorbing aerosol product, Reviews of geophysics, 40(1), 2-1-2-31.

Pye, K. (1989), Aeolian dust and dust deposits, Academic Press, Harcourt Brace Jovanovich, Publishers.

Radke, L. F., D. A. Hegg, P. V. Hobbs, J. D. Nance, J. H. Lyons, K. K. Laursen, R. E. Weiss, P. J. Riggan, and D. E. Ward (1991), Particulate and trace gas emissions from large biomass fires in North America, Global biomass burning: Atmospheric, climatic, and biospheric implications, 209-224.

Raiswell, R., L. G. Benning, M. Tranter, and S. Tulaczyk (2008), Bioavailable iron in the Southern Ocean: the significance of the iceberg conveyor belt, Geochemical Transactions, 9(1), 7.

Raiswell, R., L. G. Benning, L. Davidson, and M. Tranter (2008), Nanoparticulate bioavailable iron minerals in icebergs and glaciers, Mineral Mag, 72(1), 345-348.

Raiswell, R., L. G. Benning, L. Davidson, and M. Tranter (2008), Nanoparticulate bioavailable iron minerals in icebergs and glaciers, Mineral Mag, 72(1), 345-348.

Ramanathan, V., and G. Carmichael (2008), Global and regional climate changes due to black carbon, Nature geoscience, 1(4), 221-227.

Reid, J. S., and P. V. Hobbs (1998), Physical and optical properties of young smoke from individual biomass fires in Brazil, Journal of Geophysical Research: Atmospheres (1984–2012), 103(D24), 32013-32030.

Reid, J., R. Koppmann, T. Eck, and D. Eleuterio (2005), A review of biomass burning emissions part II: intensive physical properties of biomass burning particles, Atmospheric Chemistry and Physics, 5(3), 799-825.

Reid, J. S., T. F. Eck, S. A. Christopher, P. V. Hobbs, and B. Holben (1999), Use of the Angstrom exponent to estimate the variability of optical and physical properties of aging smoke particles in Brazil, Journal of Geophysical Research, 104(D22), 27,473-427,489.

Resing, J. A., P. N. Sedwick, C. R. German, W. J. Jenkins, J. W. Moffett, B. M. Sohst, and A. Tagliabue (2015), Basin-scale transport of hydrothermal dissolved metals across the South Pacific Ocean, Nature, 523(7559), 200-203.

Revel-Rolland, M., P. De Deckker, B. Delmonte, P. P. Hesse, J. W. Magee, I. Basile-Doelsch, F. Grousset, and D. Bosch (2006), Eastern Australia: A possible source of dust in East Antarctica interglacial ice, Earth and Planetary Science Letters, 249(1-2), 1-13.

Reynolds, R. L., S. R. Cattle, B. M. Moskowitz, H. L. Goldstein, K. Yauk, C. B. Flagg, T. S. Berquó, R. F. Kokaly, S. Morman, and G. N. Breit (2014), Iron oxide minerals in dust of the Red Dawn event in eastern Australia, September 2009, Aeolian Research.

Rhodes, R. H., J. A. Baker, M.-A. Millet, and N. A. N. Bertler (2011), Experimental investigation of the effects of mineral dust on the reproducibility and accuracy of ice core trace element analysis, Chemical Geology, 286(3), 207-221.

Rhodes, R. H., N. A. N. Bertler, J. A. Baker, S. B. Sneed, H. Oerter, and K. R. Arrigo (2009), Sea ice variability and primary productivity in the Ross Sea, Antarctica, from methylsulphonate snow record, Geophys. Res. Lett., 36(10), L10704.

Rich, H. W., and F. M. M. Morel (1990), Availability of Well-Defined Iron Colloids to the Marine Diatom Thalassiosira weissflogii, Limnology and Oceanography, 35(3), 652-662.

Ridgwell, A., and A. J. Watson (2002), Feedback between aeolian dust, climate, and atmospheric CO2 in glacial time, Paleoceanography, 17(4).

Riemer, N., H. Vogel, and B. Vogel (2004), Soot aging time scales in polluted regions during day and night, Atmospheric Chemistry and Physics, 4(7), 1885-1893.

Riemer, N., M. West, R. Zaveri, and R. Easter (2010), Estimating black carbon aging time-scales with a particle-resolved aerosol model, Journal of Aerosol Science, 41(1), 143-158.

Robinson, R. S., M. A. Brzezinski, C. P. Beucher, M. G. Horn, and P. Bedsole (2014), The changing roles of iron and vertical mixing in regulating nitrogen and silicon cycling in the Southern Ocean over the last glacial cycle, Paleoceanography.

Rubin, M., I. Berman-Frank, and Y. Shaked (2011), Dust-and mineral-iron utilization by the marine dinitrogen-fixer Trichodesmium, Nature Geoscience, 4(8), 529-534.

Ruellan, S., H. Cachier, A. Gaudichet, P. Masclet, and J. P. Lacaux (1999), Airborne aerosols over central Africa during the Experiment for Regional Sources and Sinks of Oxidants (EXPRESSO), Journal of Geophysical Research: Atmospheres (1984–2012), 104(D23), 30673-30690.

Rueter, J. G. (1988), IRON STIMULATION OF PHOTOSYNTHESIS AND NITROGEN FIXATION IN ANABAENA 7120 AND TRICHODESMIUM (CYANOPHYCEAE) 1, Journal of Phycology, 24(2), 249-254.

Rueter, J. G., D. A. Hutchins, R. W. Smith, and N. L. Unsworth (1992), Iron nutrition of Trichodesmium, in Marine pelagic cyanobacteria: Trichodesmium and other Diazotrophs, edited, pp. 289-306, Springer.

Running, S. W. (2006), Is global warming causing more, larger wildfires?, SCIENCE-NEW YORK THEN WASHINGTON-, 313(5789), 927.

Ruth, U. (2002), Concentration and size distribution of microparticles in the NGRIP Ice Core during the Last Glacial period, University Bremen.

Saito, M. A., J. Moppett, S. W. Chisholm, and J. B. Waterbury (2002), Cobalt limitation and uptake in Prochlorococcus, Limnology and Oceanography, 47(6), 1629-1636.

Sato, M., S. Takeda, and K. Furuya (2007), Iron regeneration and organic iron(III)-binding ligand production during in situ zooplankton grazing experiment, Marine Chemistry, 106(3-4), 471-488.

Scheiter, S., S. I. Higgins, J. Beringer, and L. B. Hutley (2015), Climate change and long-term fire management impacts on Australian savannas, New Phytologist, 205(3), 1211-1226.

Schroth, A. W., J. Crusius, E. R. Sholkovitz, and B. C. Bostick (2009), Iron solubility driven by speciation in dust sources to the ocean, Nature Geosci, 2(5), 337-340.

Schuck, I. (2009), Mineralogical characterisation and geographic provenance of atmospheric particles in coastal Antarctic ice cores – indicators of past climatic variability, Diploma thesis, Universitat Karlsruhe, Karlsruhe, Germany.

Schulz, M., J. M. Prospero, A. R. Baker, F. Dentener, L. Ickes, P. S. Liss, N. M. Mahowald, S. Nickovic, C. P. r. García-Pando, and S. Rodríguez (2012), Atmospheric transport and deposition of mineral dust to the ocean: implications for research needs, Environmental science & technology, 46(19), 10390-10404.

Schüssler, U., M. Bröcker, F. Henjes-Kunst, and T. Will (1999), P–T–t evolution of the Wilson Terrane metamorphic basement at Oates Coast, Antarctica, Precambrian Research, 93(2–3), 235-258.

Schwertmann, U. (1991), Solubility and dissolution of iron oxides, in Iron nutrition and interactions in plants, edited, pp. 3-27, Springer.

Sedwick, P. N., and G. R. DiTullio (1997), Regulation of algal blooms in Antarctic Shelf Waters by the release of iron from melting sea ice, Geophys. Res. Lett., 24(20), 2515-2518.

Sedwick, P. N., G. R. DiTullio, and D. J. Mackey (2000), Iron and manganese in the Ross Sea, Antarctica: Seasonal iron limitation in Antarctic shelf waters, J. Geophys. Res., 105(C5), 11321-11336.

Sedwick, P. N., E. R. Sholkovitz, and T. M. Church (2007), Impact of anthropogenic combustion emissions on the fractional solubility of aerosol iron: Evidence from the Sargasso Sea, Geochem. Geophys. Geosyst., 8(10), Q10Q06.

Sedwick, P. N., E. R. Sholkovitz, and T. M. Church (2007), Impact of anthropogenic combustion emissions on the fractional solubility of aerosol iron: Evidence from the Sargasso Sea, Geochem. Geophys. Geosyst., 8(10), Q10Q06.

Sedwick, P. N., et al. (2011), Early season depletion of dissolved iron in the Ross Sea polynya: Implications for iron dynamics on the Antarctic continental shelf, J. Geophys. Res., 116(C12), C12019.

Seiler, W., and P. J. Crutzen (1980), Estimates of gross and net fluxes of carbon between the biosphere and the atmosphere from biomass burning, Climatic change, 2(3), 207-247.

Selby, M., J. Rains, and R. Palmer (1974), Eolian deposits of the ice free Victoria Valley, Southern Victoria Land, Antarctica, New Zealand Journal of Geology and Geophysics, 17, 543-562.

Selleck, P. W., M. D. Keywood, J. P. Ward, R. W. Gillett, and K. Boast (2014), Aerosol samplers and chemical composition, 2009-2010 Baseline report, 76-79.

Shao, Y., and L. M. Leslie (1997), Wind erosion prediction over the Australian continent, JOURNAL OF GEOPHYSICAL RESEARCH-ALL SERIES-, 102, 30,091-030,105.

Shaw, E. C., A. J. Gabric, and G. H. McTainsh (2008), Impacts of aeolian dust deposition on phytoplankton dynamics in Queensland coastal waters, Marine and Freshwater Research, 59(11), 951-962.

Shi, Z., M. D. Krom, S. Bonneville, and L. G. Benning (2015), Atmospheric Processing Outside Clouds Increases Soluble Iron in Mineral Dust, Environmental Science & Technology, 49(3), 1472-1477.

Shiraiwa, M., Y. Kondo, N. Moteki, N. Takegawa, Y. Miyazaki, and D. Blake (2007), Evolution of mixing state of black carbon in polluted air from Tokyo, Geophysical Research Letters, 34(16).

Sholkovitz, E. R., P. N. Sedwick, and T. M. Church (2009), Influence of anthropogenic combustion emissions on the deposition of soluble aerosol iron to the ocean: Empirical estimates for island sites in the North Atlantic, Geochimica et Cosmochimica Acta, 73(14), 3981-4003.

Sholkovitz, E. R., P. N. Sedwick, T. M. Church, A. R. Baker, and C. F. Powell (2012), Fractional solubility of aerosol iron: Synthesis of a global-scale data set, Geochimica et cosmochimica acta, 89, 173-189.

Siefert, R. L., A. M. Johansen, and M. R. Hoffmann (1999), Chemical characterization of ambient aerosol collected during the southwest monsoon and intermonsoon seasons over the Arabian Sea: Labile-Fe(II) and other trace metals, J. Geophys. Res., 104(D3), 3511-3526.

Sinclair, K. E., N. A. N. Bertler, and W. J. Trompetter (2010), Synoptic controls on precipitation pathways and snow delivery to high-accumulation ice core sites in the Ross Sea region, Antarctica, J. Geophys. Res., 115(D22), D22112.

Slinn, S., and W. Slinn (1980), Predictions for particle deposition on natural waters, Atmospheric Environment (1967), 14(9), 1013-1016.

Smetacek, V., P. Assmy, and J. Henjes (2004), The role of grazing in structuring Southern Ocean pelagic ecosystems and biogeochemical cycles, Antarctic Science, 16(04), 541-558.

Smetacek, V., et al. (2012), Deep carbon export from a Southern Ocean iron-fertilized diatom bloom, Nature, 487(7407), 313-319.

Smith, W., and D. Nelson (1986), Importance of Ice Edge Phytoplankton Production in the Southern Ocean, BioScience, 36(4), 251-257.

Smith, W. O., and L. I. Gordon (1997), Hyperproductivity of the Ross Sea (Antarctica) polynya during austral spring, Geophys. Res. Lett., 24(3), 233-236.

Sommer, S., D. Wagenbach, R. Mulvaney, and H. Fischer (2000), Glacio-chemical study spanning the past 2 kyr on three ice cores from Dronning Maud Land, Antarctica: 2. Seasonally resolved chemical records, Journal of Geophysical Research: Atmospheres, 105(D24), 29423-29433.

Spokes, L. J., and T. D. Jickells (1995), Factors controlling the solubility of aerosol trace metals in the atmosphere and on mixing into seawater, Aquatic Geochemistry, 1(4), 355-374.

Spokes, L. J., T. D. Jickells, and B. Lim (1994), Solubilisation of aerosol trace metals by cloud processing: A laboratory study, Geochimica et Cosmochimica Acta, 58(15), 3281-3287.

Spokes, L. J., T. D. Jickells, and B. Lim (1994), Solubilisation of aerosol trace metals by cloud processing: A laboratory study, Geochimica et Cosmochimica Acta, 58(15), 3281-3287.

Spolaor, A., P. Vallelonga, J. Gabrieli, G. Cozzi, C. Boutron, and C. Barbante (2012), Determination of Fe2+ and Fe3+ species by FIA-CRC-ICP-MS in Antarctic ice samples, Journal of Analytical Atomic Spectrometry, 27(2), 310-317.

Stafford, R. G., and H. J. Ettinger (1972), Filter efficiency as a function of particle size and velocity, Atmospheric Environment (1967), 6(5), 353-362.

Steffensen, J. P. (1997), The size distribution of microparticles from selected segments of the Greenland Ice Core Project ice core representing different climatic periods, J. Geophys. Res., 102(C12), 26755-26763.

Stephens, M., N. Turner, and J. Sandberg (2003), Particle identification by laser-induced incandescence in a solid-state laser cavity, Applied optics, 42(19), 3726-3736.

Sterle, K. M., J. R. McConnell, J. Dozier, R. Edwards, and M. Flanner (2013), Retention and radiative forcing of black carbon in eastern Sierra Nevada snow, The Cryosphere, 7(1), 365-374.

Tagliabue, A., and K. R. Arrigo (2005), Iron in the Ross Sea: 1. Impact on CO2 fluxes via variation in phytoplankton functional group and non-Redfield stoichiometry, J. Geophys. Res., 110(C3), C03009.

Tagliabue, A., and K. R. Arrigo (2006), Processes governing the supply of iron to phytoplankton in stratified seas, J. Geophys. Res., 111(C6), C06019.

Tagliabue, A., J.-B. Sallee, A. R. Bowie, M. Levy, S. Swart, and P. W. Boyd (2014), Surface-water iron supplies in the Southern Ocean sustained by deep winter mixing, Nature Geosci, 7(4), 314-320.

Tagliabue, A., et al. (2010), Hydrothermal contribution to the oceanic dissolved iron inventory, Nature Geosci, 3(4), 252-256.

Talarico, F., L. Borsi, and B. Lombardo (1995), Relict granulites in the Ross Orogen of northern Victoria Land (Antarctica), II. Geochemistry and palaeo-tectonic implications, Precambrian Research, 75(3), 157-174.

Taylor, S. R., and S. M. McLennan (1985), The continental crust: Its composition and evolution, Pages: 328 pp.

Taylor, S. R., and S. M. McLennan (1995), The geochemical evolution of the continental crust, Rev. Geophys., 33(2), 241-265.

Textor, C., M. Schulz, S. Guibert, S. Kinne, Y. Balkanski, S. Bauer, T. Berntsen, T. Berglen, O. Boucher, and M. Chin (2006), Analysis and quantification of the diversities of aerosol life cycles within AeroCom, Atmospheric Chemistry and Physics, 6(7), 1777-1813.

Trapp, J. M., F. J. Millero, and J. M. Prospero (2010), Trends in the solubility of iron in dust-dominated aerosols in the equatorial Atlantic trade winds: Importance of iron speciation and sources, Geochem. Geophys. Geosyst., 11(3), Q03014.

Tuohy, A., N. Bertler, P. Neff, R. Edwards, D. Emanuelsson, T. Beers, and P. Mayewski (2015), Transport and deposition of heavy metals in the Ross Sea Region, Antarctica, Journal of Geophysical Research: Atmospheres, 120, doi:110.1002/2015JD023293.

Turn, S., B. Jenkins, J. Chow, L. Pritchett, D. Campbell, T. Cahill, and S. Whalen (1997), Elemental characterization of particulate matter emitted from biomass burning: Wind tunnel derived source profiles for herbaceous and wood fuels, Journal of Geophysical Research: Atmospheres (1984–2012), 102(D3), 3683-3699.

Turns, S. R. (1996), An introduction to combustion, McGraw-hill New York.

Uglietti, C., P. Gabrielli, J. W. Olesik, A. Lutton, and L. G. Thompson (2014), Large variability of trace element mass fractions determined by ICP-SFMS in ice core samples from worldwide high altitude glaciers, Applied Geochemistry, 47, 109-121.

Vallelonga, P., P. Gabrielli, K. J. R. Rosman, C. Barbante, and C. F. Boutron (2005), A 220 kyr record of Pb isotopes at Dome C Antarctica from analyses of the EPICA ice core, Geophys. Res. Lett., 32(1), L01706.

Vallelonga, P., C. Barbante, G. Cozzi, J. Gabrieli, S. Schüpbach, A. Spolaor, and C. Turetta (2013), Iron fluxes to Talos Dome, Antarctica, over the past 200 kyr, Climate of the Past, 9(2), 597-604.

Vallelonga, P., et al. (2010), Lead isotopic compositions in the EPICA Dome C ice core and Southern Hemisphere Potential Source Areas, Quaternary Science Reviews, 29(1-2), 247-255.

Van Der Merwe, P., D. Lannuzel, A. Bowie, and K. Meiners (2011a), High temporal resolution observations of spring fast ice melt and seawater iron enrichment in East Antarctica, Journal of Geophysical Research: Biogeosciences (2005–2012), 116(G3).

van der Merwe, P., D. Lannuzel, A. R. Bowie, C. A. Mancuso Nichols, and K. M. Meiners (2011b), Iron fractionation in pack and fast ice in East Antarctica: Temporal decoupling between the release of dissolved and particulate iron during spring melt, Deep Sea Research Part II: Topical Studies in Oceanography, 58(9-10), 1222-1236.

van der Werf, G. R., J. T. Randerson, L. Giglio, G. J. Collatz, P. S. Kasibhatla, and A. F. Arellano Jr (2006), Interannual variability in global biomass burning emissions from 1997 to 2004, Atmospheric Chemistry and Physics, 6(11), 3423-3441.

Wagener, T., C. Guieu, R. Losno, S. Bonnet, and N. Mahowald (2008), Revisiting atmospheric dust export to the Southern Hemisphere ocean: Biogeochemical implications, Global Biogeochem. Cycles, 22(2), GB2006.

Walker, P., and A. Costin (1971), Atmospheric dust accession in South-Eastern Australia, Soil Research, 9(1), 1-5.

Walsh, J. J., and K. A. Steidinger (2001), Saharan dust and Florida red tides: the cyanophyte connection, Journal of Geophysical Research: Oceans (1978–2012), 106(C6), 11597-11612.

Ward, D. (1990), Factors influencing the emissions of gases and particulate matter from biomass burning, in Fire in the Tropical Biota, edited, pp. 418-436, Springer.

Ward, D. E., and C. C. Hardy (1991), Smoke emissions from wildland fires, Environment International, 17(2), 117-134.

Ward, D. E., A. W. Setzer, Y. J. Kaufman, and R. A. Rasmussen (1991), Characteristics of smoke emissions from biomass fires of the Amazon region-BASE-A experiment, Global Biomass Burning: Atmospheric, Climatic, and Biospheric Implications, 394-402.

Ward, D., R. Susott, J. Kauffman, R. Babbitt, D. Cummings, B. Dias, B. Holben, Y. Kaufman, R. Rasmussen, and A. Setzer (1992), Smoke and fire characteristics for cerrado and deforestation burns in Brazil: BASE-B experiment, Journal of Geophysical Research: Atmospheres (1984–2012), 97(D13), 14601-14619.

Warneck, P. (2003), In-cloud chemistry opens pathway to the formation of oxalic acid in the marine atmosphere, Atmospheric Environment, 37(17), 2423-2427.

Wasserburg, G., S. Jacousen, D. DePaolo, M. McCulloch, and T. Wen (1981), Precise determination of SmNd ratios, Sm and Nd isotopic abundances in standard solutions, Geochimica et Cosmochimica Acta, 45(12), 2311-2323.

Wedepohl, K. H. (1995), The composition of the continental crust, Geochimica et Cosmochimica Acta, 59(7), 1217-1232.

Wegner, A., H. Fischer, B. Delmonte, J.-R. Petit, T. Erhardt, U. Ruth, A. Svensson, B. Vinther, and H. Miller (2015), The role of seasonality of mineral dust concentration and size on glacial/interglacial dust changes in the EPICA Dronning Maud Land ice core, Journal of Geophysical Research: Atmospheres, 120(19), 9916-9931.

Weller, R., J. Wöltjen, C. Piel, R. Resenberg, D. Wagenbach, G. KÖNIG-LANGLO, and M. Kriews (2008), Seasonal variability of crustal and marine trace elements in the aerosol at Neumayer station, Antarctica, Tellus B, 60(5), 742-752.

Wells, M., N. Zorkin, and A. Lewis (1983), The role of colloidal chemistry in providing a source of iron to phytoplankton, J Mar Res, 41, 731 - 746.

Whittlestone, S., and W. Zahorowski (1998), Baseline radon detectors for shipboard use: Development and deployment in the First Aerosol Characterization Experiment (ACE 1), Journal of Geophysical Research: Atmospheres (1984–2012), 103(D13), 16743-16751.

Windom, H. L. (1969), Atmospheric Dust Records in Permanent Snowfields: Implications to Marine Sedimentation, Geological Society of America Bulletin, 80(5), 761-782.

Winton, V. H. L., A. R. Bowie, R. Edwards, M. Keywood, A. T. Townsend, P. van der Merwe, and A. Bollhöfer (2015), Fractional iron solubility of atmospheric iron inputs to the Southern Ocean, Marine Chemistry, 177, Part 1, 20-32.

Winton, V. H. L., G. B. Dunbar, N. A. N. Bertler, M. A. Millet, B. Delmonte, C. B. Atkins, J. M. Chewings, and P. Andersson (2014), The contribution of aeolian sand and dust to iron fertilization of phytoplankton blooms in southwestern Ross Sea, Antarctica, Global Biogeochemical Cycles, 28(4), 2013GB004574.

Wolff, E. W., et al. (2006), Southern Ocean sea-ice extent, productivity and iron flux over the past eight glacial cycles, Nature, 440(7083), 491-496.

Wu, J., R. Rember, and C. Cahill (2007), Dissolution of aerosol iron in the surface waters of the North Pacific and North Atlantic oceans as determined by a semicontinuous flow-through reactor method, Global Biogeochem. Cycles, 21(4), GB4010.

Wu, J., E. Boyle, W. Sunda, and L.-S. Wen (2001), Soluble and Colloidal Iron in the Oligotrophic North Atlantic and North Pacific, Science, 293(5531), 847-849.

Wuttig, K., T. Wagener, M. Bressac, A. Dammshäuser, P. Streu, C. Guieu, and P. Croot (2013), Impacts of dust deposition on dissolved trace metal concentrations (Mn, Al and Fe) during a mesocosm experiment, Biogeosciences (BG), 10(4), 2583-2600.

Yamada, Y., H. Fukuda, K. Inoue, K. Kogure, and T. Nagata (2013), Effects of attached bacteria on organic aggregate settling velocity in seawater, Aquatic microbial ecology, 70(3), 261-272.

Yamasoe, M. A., P. Artaxo, A. H. Miguel, and A. G. Allen (2000), Chemical composition of aerosol particles from direct emissions of vegetation fires in the Amazon Basin: water-soluble species and trace elements, Atmospheric Environment, 34(10), 1641-1653.

Zahorowski, W., S. Chambers, and A. Henderson-Sellers (2004), Ground based radon-222 observations and their application to atmospheric studies, Journal of environmental radioactivity, 76(1), 3-33.

Zhang, R., A. F. Khalizov, J. Pagels, D. Zhang, H. Xue, and P. H. McMurry (2008), Variability in morphology, hygroscopicity, and optical properties of soot aerosols during

atmospheric processing, Proceedings of the National Academy of Sciences, 105(30), 10291-10296.

Zhu, X., J. M. Prospero, F. J. Millero, D. L. Savoie, and G. W. Brass (1992), The solubility of ferric ion in marine mineral aerosol solutions at ambient relative humidities, Marine Chemistry, 38(1-2), 91-107.

Zhu, X., J. M. Prospero, D. L. Savoie, F. J. Millero, R. G. Zika, and E. S. Saltzman (1993), Photoreduction of Iron(III) in Marine Mineral Aerosol Solutions, J. Geophys. Res., 98(D5), 9039-9046.

Zhuang, G., R. A. Duce, and D. R. Kester (1990), The Dissolution of Atmospheric Iron in Surface Seawater of the Open Ocean, J. Geophys. Res., 95(C9), 16207-16216.

Zhuang, G., Z. Yi, R. A. Duce, and P. R. Brown (1992), Chemistry of iron in marine aerosols, Global Biogeochem. Cycles, 6(2), 161-173.

Zuberi, B., K. S. Johnson, G. K. Aleks, L. T. Molina, M. J. Molina, and A. Laskin (2005), Hydrophilic properties of aged soot, Geophysical research letters, 32(1).

Zuo, Y., and J. Zhan (2005), Effects of oxalate on Fe-catalyzed photooxidation of dissolved sulfur dioxide in atmospheric water, Atmospheric Environment, 39(1), 27-37.

Appendix A: First author journal publications

Appendix A1: Statement of contribution and publication for paper 1

V.H.L. Winton, A. Bowie, M. Keywood, P. van der Merwe, R. Edwards, 2016. Suitability of high-volume aerosol samplers for ultra-trace aerosol iron measurements in pristine air masses: blanks, recoveries and bugs. *Atmospheric Measurement Techniques Discussions*, doi:10.5194/amt-2016-12, in review.

Statement of co-authorship

I, *Victoria Holly Liberty Winton*, designed and implemented the project, including experimental design, collected, processed and analysed the samples for soluble and total trace element concentrations, and conducted data analysis and manuscript writing of the publication:

V.H.L. Winton, A. Bowie, M. Keywood, P. van der Merwe, R. Edwards. Suitability of high-volume aerosol samplers for ultra-trace aerosol iron measurements: blanks, recoveries and bugs. In prep for *Atmospheric Measurement Techniques.*

Holly Winton

Victoria Holly Liberty Winton

I, as a Co-Author, endorse that this level of contribution by the candidate indicated above is appropriate.

Andrew Bowie

Andrew Bowie (Signature of Co-Author 1)

Melita Keywood

Melita Keywood (Signature of Co-Author 2)

Pier van der Merwe (Signature of Co-Author 3)

R. Edwards

Ross Edwards (Signature of Co-Author 4)

Atmos. Meas. Tech. Discuss., doi:10.5194/amt-2016-12, 2016
Manuscript under review for journal Atmos. Meas. Tech.
Published: 8 April 2016

Atmospheric Measurement Techniques Discussions

Suitability of high-volume aerosol samplers for ultra-trace aerosol iron measurements in pristine air masses: blanks, recoveries and bugs

Holly Winton[1], Andrew Bowie[2,3], Melita Keywood[4], Pier van der Merwe[2], Ross Edwards[1]

[1]Physics and Astronomy, Curtin University, Perth, Western Australia, 6102, Australia
[2]Antarctic Climate and Ecosystems CRC, University of Tasmania, Hobart, Tasmania, 7001, Australia
[3]Institute for Marine and Antarctic Studies, University of Tasmania, Hobart, 7004, Australia
[4]CSIRO Ocean and Atmosphere Flagship, Aspendale, Victoria, 3195, Australia

Correspondence to: V. H. L. Winton (holly.winton@postgrad.curtin.edu.au)

Abstract. Atmospheric inputs of soluble iron (Fe) to the global ocean are an important factor determining marine primary productivity and nitrogen fixation. To investigate soluble aerosol Fe and fractional Fe solubility, marine aerosol sampling has been conducted from a number of platforms including aerosol towers, ship and buoy platforms. A number of these studies have used commercially available high-volume aerosol samplers to collect aerosols from large volumes of air. These samplers are attractive for sampling air from low Fe air masses since they can rapidly concentrate large volumes improving detection limits. Here we investigate the use of a high-volume sampler from the Cape Grim Baseline Air Pollution Station (CGBAPS), Tasmania, Australia to sample aerosol Fe from baseline Southern Ocean air-masses. The study followed the United States Environmental Protection Agency (EPA) standard for the sampling of ambient air using high-volume sampler, and the recommendations and protocols from GEOTRACES community for sampling, sample preparation and digestion of trace element aerosols. Analysis and inspection of exposure blank (one month exposure) filters for Fe, and other metals, revealed significant contamination resulting from passive deposition of local soil, plants and insects. The results of the study suggest that high-volume aerosol samplers may not be suitable for low concentration air masses over the Southern Ocean without some mechanism to hermetically seal the sampler when the baseline sampling criteria are not met.

Atmos. Meas. Tech. Discuss., doi:10.5194/amt-2016-12, 2016
Manuscript under review for journal Atmos. Meas. Tech.
Published: 8 April 2016

Atmospheric Measurement Techniques Discussions

1. Introduction

Aerosols containing iron (Fe) have been investigated over the remote ocean to constrain Fe budgets in surface waters and related biological production. Aerosol sampling for metals such Fe is particularly challenging in these regions where atmospheric concentrations are exceptionally low. Over the Southern Ocean, atmospheric Fe concentrations are extremely low with reported concentrations less than 60 ng m^{-2} of Fe (Bowie et al., 2009; Duce et al., 1991; Gao et al., 2013; Heimburger et al., 2013a; Heimburger et al., 2012; Heimburger et al., 2013b; Prospero, 1996). The low atmospheric concentrations result in low atmospheric fluxes to surface waters. Fertilization experiments in the Southern Ocean have shown that Fe is required for phytoplankton to efficiently undergo photosynthesis and respiration (e.g. Boyd et al., 2007). The Fe-hypothesis (Martin, 1990) has received a lot of interest in the past two decades, whereby the increases in Fe-laden dust, productivity and the degree of nitrate consumption are linked with lowering of atmospheric CO_2 during glacial periods (e.g. Lambert et al., 2015; Martínez-García et al., 2014). Primary production may also be co-limited by other transition metals such as manganese (Mn) (Middag et al., 2011), copper (Cu) (Annett et al., 2008), cobalt (Cu) (Saito et al., 2002), zinc (Zn) (Morel et al., 1991) and nickel (Ni) (Price and Morel, 1991).

From a biogeochemical perspective, it is not the total amount of Fe supplied to the ocean that is important, but the amount that is bio-available, i.e., the amount available for uptake and utilization by living cells. The most common approach to understanding the delivery of Fe-laden aerosols to phytoplankton has been to quantify the solubility of Fe from aerosols, using Fe leaching experiments. Extremely low soluble aerosol Fe concentrations have been observed in the Southern Ocean, for example 0.07-1.3 ng m^{-3} (Gao et al., 2013; Winton et al., 2015). Fractional Fe solubility of mineral dust is typically only 1-2 % of the total Fe content (Baker and Croot, 2010). Ultra-trace metal clean practices and methodologies to limit contamination are required for making reliable measurements of both soluble and total Fe in aerosols from this region. Low blank concentrations from sampling material and during analysis are crucial for reliable measurements (e.g. Bollhöfer et al., 1999; Vallelonga et al., 2002).

Very few estimates exist over the Southern Ocean, partly due to the difficulty of sampling clean baseline air. In remote areas, fixed sampling stations rarely exist due to access difficulties or lack of suitable land masses; this covers the majority of the Southern Ocean. Southern Ocean aerosol Fe solubility estimates have resulted from a combination of ship-based and Subantarctic Island land-based aerosol sampling campaigns (e.g. Bowie et al., 2009; Chance et al., 2015; Gao et al., 2013; Wagener et al., 2008). These studies have used wet and dry aerosol deposition samplers “open collector” (Heimburger et al., 2012) and Volumetric Flow Controlled (VFC) high-volume aerosol samplers (e.g. Falkland Islands, Pers. Comm. Alex Baker). The recent GEOTRACES 2008 intercalibration experiment (Morton et al., 2013) recommends the use of VFC high-volume aerosol samplers for ship-based marine aerosol sampling. In air masses with low particle loading, high volumes of

Atmos. Meas. Tech. Discuss., doi:10.5194/amt-2016-12, 2016
Manuscript under review for journal Atmos. Meas. Tech.
Published: 8 April 2016

Atmospheric Measurement Techniques Discussions

filtered air are required to collect enough material for analysis. To ensure the required mass of sample is collected for analysis, filter substrates are often exposed for long periods of time requiring extra precautions to minimize contamination. Following an international intercalibration experiment between seven laboratories, Morton et al. (2013) recommended Whatman 41 (W41) cellulose fibre filters for low trace element background level applications. This filter substrate can be acid-cleaned to achieve low trace metal blank concentrations (Baker et al., 2006; Morton et al., 2013). Furthermore, W41 filters have a high aerosol particle collection efficiency (e.g. 95 % efficiency for 0.2 µm diameter particles (Stafford and Ettinger, 1972), and 99 % for mineral dust (Li-Jones and Prospero, 1998)). Previous aerosol Fe solubility studies that have adopted these protocols and deployed high-volume aerosol samplers both on ships during marine cruises (e.g. Baker et al., 2006; Chance et al., 2015), and on land either at the top of a tower (for example, the clean air site at the Bermuda atmospheric observatory located 50 m a.s.l. (e.g. Fishwick et al., 2014; Kadko et al., 2015)) or deployed on the rooftop of a building (e.g. Morton et al., 2013).

Most recently, Fe solubility in baseline air over the Southern Ocean has been estimated, using a short time series of archived aerosol filters from Cape Grim Baseline Air Pollution Station (CGBAPS) (Winton et al., 2015). CGBAPS has long been recognized for long-term monitoring of atmospheric species (e.g. Keeling et al., 1996) that are representative of air masses over the remote Southern Ocean. Archived filters from CGBAPS were collected using ultra-trace sampling and methodology previously reported in Bollhöfer et al. (2005). Samplers were deployed at a height of 70 m at the top of a communications tower at CGBAPS, above the turbulent layer. The Bollhöfer et al. (2005) sampler design prevented local soil contamination as filters were mounted inside a weather shelter i.e., cylindrical filter housing that was sealed pneumatically during non-baseline conditions. In order to extend the short aerosol Fe solubility time series of Winton et al. (2015), we have established an Fe aerosol monitoring program at CGBAPS following GEOTRACES sampling and handling protocols for trace metal analysis (Cutter et al., 2010; Morton et al., 2013) and the United States Environmental Protection Agency (EPA) standard, described by (Chow, 1995), for the sampling of ambient air for total suspended particulates (TSP; all particle sizes) and PM10 (particulate matter diameter <10 µm) using high volume sampler for the instrument instalment, calibration and operating procedure. The sampling conditions in Winton et al. (2015) cannot be replicated due to new health and safety requirements at the station that prohibit sampling and personal climbing the tower. Therefore, a new method of sample collection was trialled during this study to assess the suitability of VFC high-volume aerosol samplers within the new framework of health and safety regulations. In the present study, a VFC high-volume aerosol sampler was located on the roof deck (90 m above sea level and 6 m above the ground) at CGBAPS where other VFC high-volume aerosol collectors are located, which collect samples for PM2.5 and PM10 (particulate matter diameter <2.5 µm and <10 µm respectively) aerosol composition using ion chromatography (Selleck et al., 2014), multi-elemental analysis using accelerator based ion beam analysis (e.g. Cohen et al., 2000) and black carbon using light-absorbing techniques (Cohen and Stelcer, 2014).

Atmos. Meas. Tech. Discuss., doi:10.5194/amt-2016-12, 2016
Manuscript under review for journal Atmos. Meas. Tech.
Published: 8 April 2016

As the first step in developing a reliable multi-year Fe time series at the site we investigated a series of filter blanks and baseline aerosol samples. The samples were collected using the EPA standard and GEOTRACES recommended procedures and a VFC high-volume sampler. A combination of Fe leaching experiments, total aerosol digestions, optical light microscopy, scanning electron microscopy (SEM) and enrichment factor analysis were used to assess the reliability of the aerosol samples for Fe solubility studies in baseline Southern Ocean air.

2. Methods

2.1. Study site and aerosol collection

2.1.1 Site details

Cape Grim Baseline Air Pollution Station (40.68 S, 144.69 E) monitors long-term changes in a range of atmospheric species, including greenhouse gases, aerosols, and meteorological parameters. Monitoring occurs during baseline conditions i.e., when the wind direction is between 190º and 280º (Fig. 1a) and the total aerosol particle counts are below a threshold concentration based on the 90th percentile of hourly medians for the previous five years. These conditions occur ~30 % of the time (Keywood, 2007) and are representative of air masses over the remote Southern Ocean.

2.1.2 Aerosol sampler setup

Aerosols were sampled using a VFC high-volume aerosol collector (Lear-Siegler) located on the roof deck at CGBAPS (Fig. 1). We followed the United States EPA standard, described by (Chow, 1995), for the sampling of ambient air for TSP and PM10 using high volume sampler for the instrument instalment, calibration and operating procedure. The sampler was mounted against the northwest side of the roof deck wall. Prevailing winds at the site are from the southwest. Sampling airflow through the collector was automatically triggered during baseline conditions. At the onset of the project the collector was setup to collect TSP. However, optical light microscope inspection of the filters revealed large particles, up to 100 µm in diameter, (see Sect. 3.1.). Microscope images of the particles suggested that they were derived from local soil. Similar soil contamination of CGBAPS filters has been previously reported (Ayers, 2001). To reduce soil contamination a size-selective inlet was installed (PM10) on the sampler partway through the project (Fig. 1).

2.2 Laboratory environment, labware and reagents

2.2.1 Laboratory environment

All cleaning of labware, filters and sample preparation and analysis was conducted in the Curtin University TRACE facility. The TRACE facility is a large multi-stage clean room designed for ultra-trace metal measurements.

Atmos. Meas. Tech. Discuss., doi:10.5194/amt-2016-12, 2016
Manuscript under review for journal Atmos. Meas. Tech.
Published: 8 April 2016

Atmospheric Measurement Techniques Discussions

2.2.2 Reagents

All the apparatus that came in contact with the aerosol filters was acid cleaned following GEOTRACES protocols (Cutter et al., 2010). Nitric acid (HNO_3) and hydrochloric acid (HCl) used throughout the study was high purity (<10 ppt or 0.2 nmol L^{-1} Fe). Both acids were double distilled in-house from Seastar® Instrument Quality (IQ) grade acids (Choice Analytical Pty Ltd, Australia) using an all polytetrafluoroethylene (PFA) acid purification system (DST-1000, Savillex®). Hereafter referred to as ultra-pure acid. This acid was used for both cleaning of labware and filters and for sample and standard preparation. Seastar Baseline® grade hydrofluoric acid (HF) and HNO_3 (Choice Analytical Pty Ltd, Australia) was used in the digestion of aerosol filters. Ultra-pure water (resistivity of 18.2 MΩ-cm, Purelab Classic, ELGA, Germany) was used throughout.

2.2.3 Labware preparation

Low-density polyethylene bottles (LDPE; Nalgene) and polypropylene (PP; Elemental Scientific Inc.) vials were rigorously acid-washed using the following procedure:

1. One week immersion in 3.2 mol L^{-1} IQ grade HNO_3. All labware was rinsed with copious quantities of ultra-pure water between acid baths;
2. One week in 1.2 mol L^{-1} ultra-pure HCl;
3. One week in 0.12 mol L^{-1} ultra-pure HCl;
4. One week in 0.16 mol L^{-1} ultra-pure HNO_3; and
5. One week in ultra-pure water.

Teflon filtration parts used in leaching experiments were cleaned in a series of acid baths on a hotplate at 80 °C for three days. The first bath consisted of 7.9 mol L^{-1} ultra-pure HNO_3, followed by 5.8 mol L^{-1} ultra-pure HCl, then 0.12 mol L^{-1} ultra-pure HCl and 0.16 mol L^{-1} ultra-pure HNO_3, and finally ultra-pure water. Filtration parts were rinsed with copious quantities of ultra-pure water between baths.

2.2.4 Filter preparation

Aerosol collection substrates were all W41 paper sheets (20 x 25 cm; Whatman) acid-washed before use following the method of Baker et al. (2006) and GEOTRACES recommendations (Morton et al., 2013). Briefly, W41 filter sheets were arranged in layers, one at a time, between polypropylene (PP) mesh, in a series of three 0.5 mol L^{-1} ultra-pure HCl baths for 24 hours. Filters were then rinsed three times with ultra-pure water between baths and then placed in a fresh acid bath. Plastic ziplock bags and plastic tweezers were acid-washed using 3 % (0.5 mol L^{-1}) ultra-pure HNO_3 for 2 weeks. Acid-washed filters were stored in individual acid-washed ziplock bags until use.

Atmos. Meas. Tech. Discuss., doi:10.5194/amt-2016-12, 2016
Manuscript under review for journal Atmos. Meas. Tech.
Published: 8 April 2016

Atmospheric Measurement Techniques Discussions

2.3. Sampling procedures and quality control

2.3.1 Filter changing procedure

Loading and changing of aerosol collection substrates was carried out under a laminar flow clean bench at CGBAPS, and aerosol-laden filters were transferred into individual pre-acid-washed ziplock plastic bags immediately after collection and stored frozen until analysis.

2.3.2 Filter blanks and aerosol samples

Four types of filter blanks were analysed during the study: (i) untreated filter laboratory blanks, (ii) acid-washed filter laboratory blank, (iii) procedural filter blanks, and (iv) one-month exposure filter blanks. Procedural blanks consisted of acid-washed filters mounted in the aerosol collector for five minutes, with the air pump off. The one-month exposure blank, was collected by the same method as the procedural blank, but for one month duration. The exposure blank was carried out after the PM10 inlet was installed on the collector. Monthly aerosol sampling (TSP) began in June 2013 and the PM10 size selective inlet was installed in November 2013. Actual samples used for optical and Scanning Electron Microscopy (SEM) observations were CG13TM01 (TSP; sampled between 13 June 2013 and 16 July 2013) and CG13TM08 (PM10; sampled between 28 January 2014 and 25 February 2014). Sampling dates and volumes for blank filters and aerosol samples used in this study are reported in Table 1.

2.3.3 Certified Reference Materials and quality control filters

A certified reference material and a commercial quality control spiked filter were used to validate sample digestion procedures. These included the MESS-3 marine sediment (National Research Council, Canada) and a trace metal spiked quality control nitrocellulose filter (QC-TMFM-A, High Purity Standards).

2.3.4 Sample preparation

Soluble metals were extracted from each type of blank filter. Circular portions (47 mm diameter) were cut out of the blank filter sheets using a punch cutter (designed at Curtin University), which consisted of a sharpened titanium (Ti) circular blade and a PFA backing mount (both acid-washed). Soluble metals including aluminium (Al), Ti, Manganese (Mn), Fe, and lead (Pb) were extracted from the filter using an instantaneous flow-through water leach (e.g. Aguilar-Islas et al., 2010) consisting of three separate passes of 10 mL of ultra-pure water. Three aliquots of each filter blank were leached with three repeated passes of ultra-pure water.

Total trace metal concentrations were determined following recommendations from the 2008 GEOTRACES intercalibration experiment for the analysis of marine aerosols (Morton et al., 2013). All digestions were carried out under high-efficiency particulate arresting (HEPA) filtered air, in a total-exhausting clean-air (ISO Class 5), hot block unit (SCP Science, Canada)

Atmos. Meas. Tech. Discuss., doi:10.5194/amt-2016-12, 2016
Manuscript under review for journal Atmos. Meas. Tech.
Published: 8 April 2016

Atmospheric Measurement Techniques Discussions

fitted with an acid scrubber unit at the University of Tasmania. Circle portions (47 mm) of the filters were digested at 95 ºC for 12 hours with concentrated ultra-pure HNO_3 (1 mL, Seastar Baseline®) and ultra-pure HF (0.25 mL, Seastar Baseline®) in capped PFA vials (15 mL, acid cleaned Savillex®) following Bowie et al. (2010). At the end of the digestion, the samples were evaporated to dryness, reconstituted in 10 % (1.60 mol L^{-1}) ultra-pure HNO_3 (10 mL final volume, Seastar® IQ grade double distilled in-house) and stored at 40 ºC for ~48 hours before analysis. Two certified reference materials (MESS-3 marine sediment, National Research Council, Canada, and QC-TMFM-A spiked trace metals on nitrocellulose filter (TMF), High Purity Standards) were digested alongside the samples to test the digestion recovery procedure. Total digestion recovery for Fe from the MESS-3 CRM was 108 ± 8 % (n=3) and TFM was 99 ± 7 % (n=3). Recovery rates for other trace metals are reported in Supplementary Table 1. Blank concentrations for Savillex® beakers, i.e. the digestion blank, are reported in Table 2.

2.4 High-resolution inductively coupled plasma mass spectrometry analysis

Leachates and resuspended total digests were analysed using high-resolution inductively coupled plasma mass spectrometry (HR-ICP-MS, Element XR ThermoFisher). An auto sampler fitted with an acrylic sample enclosure was used to introduce the sample to the HR-ICP-MS. Measured isotopes and spectral resolutions, along with typical operating conditions, are reported in Supplementary Table 2. The HR-ICP-MS was operated with a jet interface using Ni jet and sample cones and an Apex desolvation unit (Elemental Scientific Inc, ESI) pumped with a Seafast II system syringe pumps (ESI). Samples were analysed in groups of ten bracketed by instrumental blanks (3 % or 0.4 mol L^{-1} ultra-pure HCl (soluble) or HNO_3 (total)), and a quality control standard (QC). The QC standard was prepared from a commercial mixed elemental standard (Cat. #ICP-200.7-6 Solution A, High Purity Standards) by serial dilution. Partial procedural blanks were also determined. These included blanks for the leaching and total digestion procedures. Leaching and total digestion blanks consisted of ultra-pure water processed identically to filter leachates and total digestion samples. All samples and standards were prepared on a similar matrix basis. Leachates were acidified to 1 % (0.12 mol L^{-1}) HCl, and total digests were diluted and presented to the instrument as 3 % (0.5 mol L^{-1}) HNO_3. The sample introduction line was rinsed with 3 % (0.4 mol L^{-1}) ultra-pure HCl (3 % or 0.5 mol L^{-1} ultra-pure HNO_3) between leachate (digest) samples for 1.5 minutes. Standard solutions were prepared by serial dilution from 100 µg mL^{-1} stock solutions using ultra-pure water, with a final HCl (HNO_3) concentration of 1 % or 0.12 mol L^{-1} (3 % or 0.5 mol L^{-1}). Preparation of standards in 1 % or 0.12 mol L^{-1} ultra-pure HCl (3 % or 0.5 mol L^{-1} ultra-pure HNO_3) matrix matched the leachates (digests). Ten-point calibration solutions were measured. Indium (In), at a concentration of 1.5 ppb, was used as an internal standard.

2.5 Optical and Scanning Electron Microscopy

Blank filters (acid-washed laboratory, procedural, and exposure) were examined using optical microscopy to investigate particulate contamination (morphology and particle size). Actual aerosol samples with visible contamination under the optical microscope were further investigated using a SEM (Zeiss Evo 40XVP and Zeiss Neon 40EsB FIBSEM). The SEM

Atmos. Meas. Tech. Discuss., doi:10.5194/amt-2016-12, 2016
Manuscript under review for journal Atmos. Meas. Tech.
Published: 8 April 2016

Atmospheric Measurement Techniques Discussions

was fitted with secondary (SE) and backscatter (BSD) electron detectors and a SiLi energy dispersive X-ray system (EDS) with Oxford Inca software were used to give a qualitative indication of the geochemistry of the particles. The conditions used (kV, spot size, WD and detector) are shown on the SEM images. Filter blanks were carbon-coated prior to SEM examination.

2.6. Air mass back trajectory analysis

Air mass back trajectories were simulated using ANSTO's air mass back trajectory database, based on the NOAA's HYSPLIT v4.0 model (Draxler and Rolph, 2003) for the duration of the one-month exposure blank. Five-day air mass back trajectories were generated for the CGBAPS, based on a starting elevation of 200 m a.g.l., for every hour of every day between 8 November and 10 December 2013. Hindcasts were based on meteorological data of 0.5° x 0.5° resolution generated by the global data assimilation system (GDAS) model downloaded from the NOAA ARL website (ftp://arlftp.arlhq.noaa.gov/archives/gdas0p5).

3. Results

3.1. Optical and Scanning Electron microscopy

Filter blanks and baseline sample filters were inspected by a combination of optical microscopy and SEM. Inspection of acid-washed laboratory and procedural blank filters with an optical microscope showed no obvious sign of particulate contamination. In contrast, the one-month exposure blank and aerosol samples from the aerosol collector (using both the TSP and PM10 inlets) were contaminated with particles up to 100 µm in diameter (Fig. 2-4). Visibly discoloured (orange) patches were also observed on a number of baseline TSP and PM10 filter samples (Fig. 3b). No discoloured patches were found on the blank filters. Baseline sample filters (both TSP and PM10) were inspected using a SEM. Particles were comprised of salt (NaCl, cubical crystals), gypsum, calcium carbonate, mineral dust (identified by the silicon (Si), Fe, Al, Ti EDS signals), and silica was identified on the PM10 filters (Fig. 5). The TSP filters were coated with a broader variety of material compared to the PM10 filters. Particles on the TSP filter were identified as carbonaceous particles, salts, mineral dust, silica sand, spores, and marine aerosol (particles containing magnesium (Mg), strontium (Sr) and barium (Ba); Fig. 6).

3.2. Solubility of contamination-borne particles on blank filters

A typical volume of baseline air collected during a month deployment (ca. 12600 m^3, assuming baseline conditions occur for 30 % of the time (Keywood, 2007)) was used to calculate filter blank concentrations for aerosol samples, and compare them to the aerosol concentrations on a "per cubic meter of air" basis (Morton et al., 2013). Leaching Fe from the blank filters with the use of ultra-pure water gave soluble Fe concentrations for the four types of blank filters, which can be used as a basis for comparison to other studies. The average soluble trace metal concentrations for the three subsamples of each type of filter are reported in Table 3 and Fig. 7. Soluble trace metal concentrations in all blank filters decreased with each

Atmos. Meas. Tech. Discuss., doi:10.5194/amt-2016-12, 2016
Manuscript under review for journal Atmos. Meas. Tech.
Published: 8 April 2016

Atmospheric Measurement Techniques Discussions

additional sequential leach of ultra-pure water (Fig. 7). At least 50 % of soluble trace metals were leached within the first leach i.e., ~65 % of soluble Fe, ~55 % of soluble Al, ~70 % of soluble Ti, ~65 % of soluble V, ~75% of soluble Mn, and ~60% of soluble Pb for the exposure blank filter.

After acid-cleaning the filters, there was a significant decrease in the concentration of soluble Fe, from 200 to 30 pg cm^{-2}. Acid-cleaning the filters also reduced the concentrations of soluble Mn, Pb, and Ti in the leachates, but there was no difference in the soluble V concentrations between acid-washed and untreated filters (Fig. 7). Soluble Al was the only trace metal to increase in concentration (12 to 2600 pg cm^{-2}) after acid-washing the filter; perhaps, due to Al contained within the cellulose filter and further broken down by HCl.

For the procedural blank filters, i.e., those taken to the field and mounted in the VFC high-volume aerosol sampler for five minutes (Table 3), the soluble Fe concentrations (16 pg cm^{-2} of soluble Fe) were similar to the blank acid-washed filters (30 pg cm^{-2} of soluble Fe). This validates the cleanliness of our sample handling procedures. Soluble Ti, V, Mn, and Pb concentrations between acid-washed filter blanks and procedural blanks were also similar. Soluble Al was lower in the procedural blank.

In the month-long exposure blank, a considerable increase in the trace metal concentration was observed; for example, up to 870 pg cm^{-2} of soluble Fe. The concentration of all soluble trace metals was at least an order of magnitude greater in the exposure blank than in the procedural and acid-washed filter blank. Soluble Al displayed the highest concentrations in laboratory, procedure, and exposure blank filters.

3.3. Total trace metal concentrations of contamination-borne particles on blank filters

Similar to the soluble trace metal concentrations, acid-cleaning the filters significantly decreased in the total concentration of all trace metals, except for V where the concentration remained the same (Table 2). Procedural blank concentrations were slightly higher than the acid-washed filters for total Al, total Ti, total V, and total Pb concentrations. The procedural blank total Fe concentration was ~7 pg cm^{-2} lower than the acid-washed filter. Exposure blank total trace metal concentrations were an order of magnitude higher than procedural blank concentrations for all trace metals.

4. Discussion

4.1. Contamination from laboratory procedures, filter handling and site exposure

We used a series of blank filter types to determine the source and quantity of soluble and total Fe contamination. The blank Fe budget consists of Fe introduced to the sample from reagents, ultra-pure water, leaching from plastic bottles and filter substrate, sample collection and handling, and the instrument (Table 4). The instrumental water blank gives an indication of

Atmos. Meas. Tech. Discuss., doi:10.5194/amt-2016-12, 2016
Manuscript under review for journal Atmos. Meas. Tech.
Published: 8 April 2016

Atmospheric Measurement Techniques Discussions

contamination arising from the HR-ICP-MS vial, ultra-pure acids and the instrument. This contribution is ~0.4 pg cm^{-2}. Contamination from the W41 filter substrate is assessed by the difference in Fe between acid-washed and untreated filters. The W41 filters contributes 0.2 ng cm^{-2} (9 pg m^{-3}) of soluble Fe and 7 ng cm^{-2} (0.3 ng m^{-3}) of total Fe to the Fe budget. Thus, acid-washing the filter is crucial for baseline aerosol sampling. Acid-washing of the W41 filters is also necessary when analysing the trace solubility of Mn, Pb, and Ti as acid-washing significantly reduced the contamination arising from the filter substrate alone.

The Fe concentrations of the procedural blanks indicate the contamination acquired throughout the sampling process and handling of filters in the field. The sampling procedure contributes negligible total and soluble Fe to the budget (Table 4). By following ultra-trace protocols (GEOTRACES recommendations), contamination by personal or handling of filters was minimised; blank concentrations in acid-washed laboratory blank filters are similar to or less than procedural blank filters. Furthermore, no evidence of particulate contamination was observed in the acid-washed or procedural blank filters under an optical microscope.

There is considerable contamination derived from filter exposure at the sampling site. The largest source of soluble Fe contamination was evident in the month-long exposure blank. Contamination arising from one-month of site exposure is around 0.03 ng m^{-3} of soluble Fe and 10 ng m^{-3} of total Fe. This is considerable given water soluble Fe concentrations in contamination-free archived filters ranged from 0.01-0.3 ng m^{-3} of soluble Fe and 0.04-5.8 ng m^{-3} of total Fe (Winton et al., 2015). The contamination-free archived filters were sampled using the Bollhöfer et al. (2005) aerosol sampler design (Fig. S1) and a similar Fe water solubility leaching scheme employed here. Thus, in the low concentration aerosol samples, contamination from site exposure (Tables 2 and 3) limits our ability to differentiate between the blank and 'real' signal. We suggest two processes by which contamination occurs during the month-long exposure. Firstly, by a passive deposition on the filters during a month-long sampling period at Cape Grim. Passive deposition contributes the majority (94 %) of Fe to the Fe budget (Table 4). Secondly, as there is no evidence of human-, sampler-, or building-derived (e.g., wood, paint) particles on the filters, the insect, soil, and marine particle contamination is likely a consequence of airborne particles hitting the sampler at high wind speeds. Additionally, insects could fly or crawl into to sampler, as the air inlet is not sealed during non-baseline conditions (Fig. 1). Insect contamination is likely at other sampling sites as indicated by the sampling procedure in the US EPA high-volume sampling standard for the determination of inorganic compounds in ambient air, which recommends that insects be removed with a pair of tweezers.

The total trace metal blank concentrations in acid-washed and untreated W41 filters are similar to those reported by Morton et al. (2013), who use the same acid-washing procedure for cleaning the filters. It is interesting to note that Morton et al. (2013) reports a greater Al concentration on the acid-washed filter than the untreated filter. Our soluble Al blank

Atmos. Meas. Tech. Discuss., doi:10.5194/amt-2016-12, 2016
Manuscript under review for journal Atmos. Meas. Tech.
Published: 8 April 2016

Atmospheric Measurement Techniques Discussions

concentrations were also greater for the acid-washed filter Al suggesting the W41 filters are not suitable for Al studies in Southern Ocean baseline air.

4.2. Passive deposition and back trajectory analysis

The exposure blank, which was left in the aerosol collector with the motor switched off for a one-month collection period, reflects contamination derived from the atmospheric fallout or passive deposition. This type of blank gives an indication of the relative magnitudes of the in-sector active sampling (i.e., pump turned on and controlled by the baseline switch for a month) versus passive deposition. The deposition of particles, is thus, partly dependent on the mixture of in- and out-sector winds during the exposure blank period. The cluster means of five-day air mass back trajectories, for the duration of the month-long exposure blank, show that around half of the trajectories were transported from the non-baseline sector (i.e., over Tasmania) while the other half were baseline marine air (Fig. 7b). The frequency plot in Fig. 7c shows the fetch area of trajectories, which included Tasmania >10 % of the time, and occasionally, the Australian continent (>0.1 %) (Fig. 7b). Furthermore, the high wind speeds at Cape Grim, up 80 km h^{-1} during the exposure blank period (Fig. 7a), potentially transport local dust and vegetation to the sampling site. The wind speed is most important when the sampler is turned off (i.e., non-baseline conditions) as it can transport and deposit local dust and insects through the unsealed air inlet section of the sampler (visible in Fig. 1d). Extreme weather conditions at this site are a concern for aerosol samplers that are not sealed during non-baseline conditions; contamination occurs regardless of whether the sampler is turned on or off. The Bollhöfer et al. (2005) sampler design minimized this source of contamination by pneumatically sealing the sampling when it was turned off.

We use optical microscopy to further assess the impact of passive deposition. Large particles up to 100 µm are observed in the exposure blank (Fig. 2). A mixture of mineral dust, vegetation, and even insects were observed on the exposure blank (Fig. 2). Large particles were still observed on filters after the installation of the PM10 size selective inlet (Fig. 4). An evaluation of PM10 size selective inlet performance in Australia found that PM10 inlets have a d_{50} of 10 µm, i.e., 50 % of particles greater than 10 µm are collected on the inlet (Keywood, 1999). The calibration of the PM10 inlet collection efficiencies is done under certain wind speed conditions and it is likely that the extreme wind speeds at Cape Grim (80 km h^{-1}; Fig 8c) are higher than what the inlet was calibrated in. This may explain why some particles larger than 10 µm are observed on the PM10 sample filter (Fig. 4). These particles could have been deposited on the filter by a combination of high wind speeds when the sampler was running, which lowered the efficiency of PM10 inlet to separate particles <10 µm, and/or passive deposition when the sampler was turned off. Given the large particle size and the wind strength of non-baseline air (Fig. 7), the source of passive deposition is likely local.

Local contamination from the cliff face at Cape Grim has been known to occur for some time (Ayers, 2001), and elemental ratios are used to correct for this local cliff contamination for major ion measurements (Ayers and Ivey, 1988). Due to the

Atmos. Meas. Tech. Discuss., doi:10.5194/amt-2016-12, 2016
Manuscript under review for journal Atmos. Meas. Tech.
Published: 8 April 2016

very weak signal at Cape Grim, fingerprinting (e.g. using elemental ratios or radiogenic isotope ratios) the cliff signal and separating it from the marine particles is challenging. As there is a clear indication of material from the cliff face being blown onto the roof deck during extreme wind events, the soil signal is likely to dominate the marine signal for trace metals. The high concentration of soluble Fe in the exposure blank, sampled at the roof deck height, is as high or higher than soluble Fe in uncontaminated samples collected up the 70 m communications tower (Bollhöfer et al. (2005) sampler design; (Winton et al., 2015). This local contamination will likely mask or dominate the true Fe solubility of baseline aerosols. At Cape Grim, there is no option to install the sampler elsewhere, e.g. higher up on a tower as has been done in the past (Bollhöfer et al., 2005). Using an impactor - for example, with a maximum of six upper stages and a backup filter - may aid in the identification of contamination if the size distribution of the marine aerosol and the cliff debris were known and if those size distributions were significantly different. However, this is likely to result in detection problems of soluble trace metals since the aerosol would be deposited and spread across seven filters instead of one. To overcome this, a PM10 size selective head was installed at Cape Grim to remove the coarse particle size distribution that is not long-range or baseline transport. Cohen and Stelcer (2014) suggested that for non-baseline PM 2.5 samples, windblown soil (estimated from the oxides of Al, Si, Ti, Ca, and Fe) represents about 2 % of the total fine mass at Cape Grim. The remaining fine particle mass comprises sea salt (38 %), black carbon (4 %), and organic matter (5 %). Even if windblown soil only contributes 2 % of the total fine aerosol mass in samples, this could be a large fraction of the trace metal component due to their abundance in the soil particles (Taylor and McLennan, 1985) and significantly affect solubility. The passive deposition of locally-derived particles during out-sector winds will thus have a major influence on the overall aerosol Fe solubility in baseline samples.

The issue of local contamination has also been identified on Kerguelen Island, located in the Indian sector of the Southern Ocean during an aerosol sampling campaign. Using Al/Ti ratios as a tracer of local soil erosion, Heimburger et al. (2013a) found that out of 14 rain samples, only five were free of local contamination and representative of long-range transport particles deposited by rain events. The sampling location has been shown to be a major factor when designing trace metal studies in the Southern Ocean. Other Sub-Antarctic Island sites will likely face similar issues of local contamination such as at Cape Grim and Kerguelen Island. Thus, there is a need for future aerosol campaigns of baseline trace metal solubility to sample aerosols high above the turbulent layer, for example, Cape Verde (30 m) (e.g. Fomba et al., 2012) and Tudor Hill, Bermuda (23 m) (e.g. Fishwick et al., 2014; Kadko et al., 2015).

4.3. Enrichment factor analysis

The Wedepohl (1995) compilation of continental crust composition was used to calculate crustal enrichment factors (EF) to determine the contribution of mineral dust to the observed total elemental concentrations in the blank filters. Total Al was used as a marker for mineral dust. For an element (Z) in a sample, the EF relative to Al is calculated using Eq. (1).

$$EF = \frac{(Z/Al)_{sample}}{(Z/Al)_{crust}} \quad \text{(Eq. 1)}$$

Atmos. Meas. Tech. Discuss., doi:10.5194/amt-2016-12, 2016
Manuscript under review for journal Atmos. Meas. Tech.
Published: 8 April 2016

The enrichment factors of exposure blank filters are used to gauge the level of mineral dust contamination from a month of exposure at the field site. For example, an EF between 0.7 and 2 is considered to be similar to the upper continental crust, implying that these trace metals might have originated from that source. Trace metals had EF between 1.5 – 4.8 (Table 5); this is considered as a similar composition or moderate enrichment, in comparison to the upper continental crust (i.e. EF >0.7). Total Fe does not show Fe enrichment, suggesting that anthropogenic Fe was not a source of contamination to the exposure blank, although it is known to be a source of atmospheric soluble Fe (e.g. Sholkovitz et al., 2012). The low EF values of all trace metals suggest that the trace metals on the exposure blank could have originated from mineral dust sources. The low EFs of all trace metals in the month-long exposure blank that was subject to passive deposition and air masses crossing Tasmania (Fig. 7) are likely to reflect local contamination from crustal sources e.g. mineral dust from the cliff face.

4.4. Recommendations and future work

4.4.1. Importance of microscope observations in trace metal aerosol collection

The main concern when collecting marine-derived trace metal aerosol particles at CGBAPS is that the filters also collect dust from the local cliff-face directly below the sampler at the station, particularly during stormy conditions. The filters are also subject to passive deposition while the wind is out of baseline sector, which is significant because of the already weak signal at CGBAPS. Therefore, microscope observations are a key tool in the identification of local contamination. We recommend that microscope observation becomes a routine practice when measuring the Fe content and solubility in aerosols from the Southern Ocean. For example, insect and vegetation contamination was found in our blank filters only through the use of microscope observations, and this source of contamination would not have been detected by the soluble geochemistry alone.

4.4.2. Bioactivity inside filters

Sporadic discolorations (orange spots) were identified on the PM10, TSP, and month-long exposure blanks. Microscope observations showed that these spots were located inside the ‘depth’ of the filter (Fig. 3b). A possible source for these spots is microbial growth inside the filters. Algae could be living off nutrients e.g. aerosol nitrate in the aerosol-laden filter. Microbes will also accumulate trace metals (Morel and Price, 2003) and affect the solubility. Further work is required to assess these orange spots and determine whether they are an additional source of trace metal contamination.

4.4.3. Aerosol sampler siting and closure requirements for low iron air sampling

Much of the passive deposition contamination found by this study was invisible to the naked eye. However, it was still a significant source of the Fe blank budget compared to the expected Fe aerosol loading. In the case of this study, the sampler was on a platform ~6 m above the ground and exposed to extreme wind conditions. The contamination was primarily due to the lack of an air-tight closure at the sampler intake. As a result, strong winds were able to force particles into the sampler

Atmos. Meas. Tech. Discuss., doi:10.5194/amt-2016-12, 2016
Manuscript under review for journal Atmos. Meas. Tech.
Published: 8 April 2016

and onto the filter. This form of contamination may be decreased by installing the sampler above the surface boundary layer (~50 m); however a hermetic closure is still desirable to keep out air that is out of sector (e.g. Bollhöfer et al., 2005; Winton et al., 2015) (Fig. S1). Due to new work health and safety requirements imposed on the field station, it is not possible to carry out a comparison of sampling on the 70 m tower and roof deck to determine if sampling above the turbulent layer decreases contamination. Ship based high-volume samplers are exposed to particulates from ship exhaust (Edwards, 1999). For similar reasons they should be fitted with a hermetic closure to completely seal off the sampler when the winds are out of sector or the wind speed is too low. For example, Edwards (1999) investigated ship-derived contamination along an upwind/downwind transect of snow on Antarctic sea ice. In contrast to the low upwind iron concentrations, downwind concentrations were up to two orders of magnitude higher than the upwind samples, suggesting that snow is significantly contaminated by material carried in the air from the ship.

5. Conclusion

A VFC high-volume aerosol sampler was installed at CGBAPS under new health and safety regulations, and following ultra-trace protocols and recommendations of the US EAP standard and GEOTRACES community for aerosol sampling. Using a series of blank filter types, we assessed the contribution of Fe contamination during different stages in the sampling, leaching and analysis of baseline Fe solubility at CGBAPS. To do this we used a combination of solubility experiments, microscope observations, and enrichment factor analysis of one-month exposure blank filters. Contamination arising from HR-ICP-MS, lab wear and handling of filters was negligible. Acid-washing the filters substantially reduced Fe leached from the W41 filter substrate. The most significant source of contamination was the passive deposition during aerosol sampling while the wind was out of the baseline sector. This source of contamination cannot be seen with the naked eye, but occurs regardless of whether the sampler is turned on or off. Exposure filters collect insects and dust from the local cliff-face directly below the sampler at the station, particularly during stormy conditions. This is a major concern for collecting marine-derived aerosol Fe particles in baseline air due to the very clean air (weak trace metal signal). As local aerosol debris may be found on filters deployed in high-volume aerosol samplers this type of sampler, in its current configuration, may not be appropriate for sampling marine aerosols representative of a broader region. For Southern Ocean studies, we recommend that (i) the use of microscope observations are a key tool for aiding in the identification of local contamination, (ii) land-based aerosol samplers are sealed during non-collection periods to prevent passive deposition, (iii) ship based aerosol samplers are also sealed when the sector of interest is not being sampled to prevent ship exhaust contamination, and (iv) acid-washed W41 filters are not suitable for studies of Al solubility in very low-level, clean air. Whilst this study shows significant exposure blanks in clean air conditions, this may not be a problem at sites influenced by air-masses containing higher aerosol Fe loadings.

Atmos. Meas. Tech. Discuss., doi:10.5194/amt-2016-12, 2016
Manuscript under review for journal Atmos. Meas. Tech.
Published: 8 April 2016

Atmospheric Measurement Techniques Discussions

Data availability

The dataset for blank filters is available through the Curtin University Research Data repository http://doi.org/10.4225/06/564AB348340D5.

Acknowledgments

This project was funded through Curtin University (Curtin Research Fellowship to R.E.), the University of Tasmania (B0019024 to A.R.B.), the Australian Research Council (FT130100037 to A.R.B.) and the Antarctic Climate and Ecosystems CRC. Access to HR-ICP-MS instrumentation at Curtin University was facilitated through ARC LIEF funding (LE130100029). V.H.L.W. would like to acknowledge the following scholarship support: Australian Postgraduate Award and Curtin Research Scholarship. CSIRO and the Australian Bureau of Meteorology in Australia are also thanked for their continuous support of CGBAPS, and we also thank Sam Clelend, Nigel Somerville and Jeremy Ward who made the collection of aerosol samples possible. Wind speed data for Cape Grim was sourced from the Australian Bureau of Meteorology. The authors acknowledge the use of equipment, scientific and technical assistance of the Curtin University Electron Microscope Facility, which has been partially funded by the University, State and Commonwealth Governments. We thank Phillip Boyd and Edward Butler for use of the high-volume aerosol sampler that was installed at CGBAPS. We appreciate helpful discussion with Alex Baker on contamination issues with high-volume aerosol collection. We thank Alistair Williams, Scott Chambers and Sylvester Werczynski at ANSTO for their contribution to producing air mass back trajectories and plots. We thank and two anonymous reviewers who improved the paper.

Atmos. Meas. Tech. Discuss., doi:10.5194/amt-2016-12, 2016
Manuscript under review for journal Atmos. Meas. Tech.
Published: 8 April 2016

Atmospheric Measurement Techniques Discussions

References

Aguilar-Islas, A. M., Wu, J., Rember, R., Johansen, A. M., and Shank, L. M.: Dissolution of aerosol-derived iron in seawater: Leach solution chemistry, aerosol type, and colloidal iron fraction, Marine Chemistry, 120, 25-33, 2010.

Annett, A. L., Lapi, S., Ruth, T. J., and Maldonado, M. T.: The Effects of Cu and Fe Availability on the Growth and Cu:C Ratios of Marine Diatoms, Limnology and Oceanography, 53, 2451-2461, 2008.

Ayers, G. P.: Influence of local soil dust on composition of aerosol samples at Cape Grim Baseline Atmospheric Program (Australia) 1997-98, 2001. 50-56, 2001.

Ayers, G. P. and Ivey, J. P.: Precipitation composition at Cape Grim, 1977–1985, Tellus B, 40B, 297-307, 1988.

Baker, A. R. and Croot, P. L.: Atmospheric and marine controls on aerosol iron solubility in seawater, Marine Chemistry, 120, 4-13, 2010.

Baker, A. R., Jickells, T. D., Witt, M., and Linge, K. L.: Trends in the solubility of iron, aluminium, manganese and phosphorus in aerosol collected over the Atlantic Ocean, Marine Chemistry, 98, 43-58, 2006.

Baseline: Baseline Atmospheric Program Australia 2009-2010. Edited by Derek. N, Krummel. P. B, Cleland. S. J. Australian Bureau of Meteorology and CSIRO Marine and Atmospheric Research, 2014.

Bollhöfer, A., Chisholm, W., and Rosman, K. J. R.: Sampling aerosols for lead isotopes on a global scale, Analytica Chimica Acta, 390, 227-235, 1999.

Bollhöfer, A., Rosman, K. J. R., Dick, A. L., Chisholm, W., Burton, G. R., Loss, R. D., and Zahorowski, W.: Concentration, isotopic composition, and sources of lead in Southern Ocean air during 1999/2000, measured at the Cape Grim Baseline Air Pollution Station, Tasmania, Geochimica et Cosmochimica Acta, 69, 4747-4757, 2005.

Bowie, A. R., Lannuzel, D., Remenyi, T. A., Wagener, T., Lam, P. J., Boyd, P. W., Guieu, C., Townsend, A. T., and Trull, T. W.: Biogeochemical iron budgets of the Southern Ocean south of Australia: Decoupling of iron and nutrient cycles in the subantarctic zone by the summertime supply, Global Biogeochem. Cycles, 23, GB4034, 2009.

Boyd, P. W., Jickells, T., Law, C. S., Blain, S., Boyle, E. A., Buesseler, K. O., Coale, K. H., Cullen, J. J., de Baar, H. J. W., Follows, M., Harvey, M., Lancelot, C., Levasseur, M., Owens, N. P. J., Pollard, R., Rivkin, R. B., Sarmiento, J., Schoemann, V., Smetacek, V., Takeda, S., Tsuda, A., Turner, S., and Watson, A. J.: Mesoscale Iron Enrichment Experiments 1993-2005: Synthesis and Future Directions, Science, 315, 612-617, 2007.

Chance, R., Jickells, T. D., and Baker, A. R.: Atmospheric trace metal concentrations, solubility and deposition fluxes in remote marine air over the south-east Atlantic, Marine Chemistry, 2015. 2015.

Chow, J. C.: Measurement methods to determine compliance with ambient air quality standards for suspended particles, Journal of the Air & Waste Management Association, 45, 320-382, 1995.

Cohen, D. D., Garton, D., and Stelcer, E.: Multi-elemental methods for fine particle source apportionment at the global baseline station at Cape Grim, Tasmania, Nuclear Instruments and Methods in Physics Research Section B: Beam Interactions with Materials and Atoms, 161, 775-779, 2000.

Cohen, D. D. and Stelcer, E.: Fine particle sampling at Cape Grim, 2009-2010 Baseline report, 2014. 75, 2014.

Cutter, G., Andersson, P., Codispoti, L., Croot, P., Francois, R., Lohan, M., Obata, H., and Rutgers vd Loeff, M.: Sampling and sample-handling protocols for GEOTRACES Cruises, 2010. 2010.

Draxler, R. R. and Rolph, G. D.: Hybrid Single-Particle Lagrangian Integrated Trajectory (HYSPLIT), model, http://www.arl.noaa.gov/ready/hysplit4.html, 2003. 2003.

Duce, R. A., Liss, P. S., Merrill, J. T., Atlas, E. L., Buat-Menard, P., Hicks, B. B., Miller, J. M., Prospero, J. M., Arimoto, R., Church, T. M., Ellis, W., Galloway, J. N., Hansen, L., Jickells, T. D., Knap, A. H., Reinhardt, K. H., Schneider, B., Soudine, A., Tokos, J. J., Tsunogai, S., Wollast, R., and Zhou, M.: The atmospheric input of trace species to the world ocean, Global Biogeochem. Cycles, 5, 193-259, 1991.

Edwards, R.: Iron in modern and ancient East Antarctic snow: implications for phytoplankton production in the Southern Ocean, PhD thesis, University of Tasmania, Hobart, 1999. 1999.

Fishwick, M. P., Sedwick, P. N., Lohan, M. C., Worsfold, P. J., Buck, K. N., Church, T. M., and Ussher, S. J.: The impact of changing surface ocean conditions on the dissolution of aerosol iron, Global Biogeochemical Cycles, doi: 10.1002/2014GB004921, 2014. 2014GB004921, 2014.

Fomba, K., Müller, K., Pinxteren, D. v., and Herrmann, H.: Aerosol size-resolved trace metal composition in remote northern tropical Atlantic marine environment: case study Cape Verde Islands, Atmospheric Chemistry and Physics Discussions, 12, 29535-29569, 2012.

Gao, Y., Xu, G., Zhan, J., Zhang, J., Li, W., Lin, Q., Chen, L., and Lin, H.: Spatial and particle size distributions of atmospheric dissolvable iron in aerosols and its input to the Southern Ocean and coastal East Antarctica, Journal of Geophysical Research: Atmospheres, 118, 12,634-612,648, 2013.

Heimburger, A., Losno, R., and Triquet, S.: Solubility of iron and other trace elements in rainwater collected on the Kerguelen Islands (South Indian Ocean), Biogeosciences, 10, 2013a.

Heimburger, A., Losno, R., Triquet, S., Dulac, F., and Mahowald, N.: Direct measurements of atmospheric iron, cobalt, and aluminum-derived dust deposition at Kerguelen Islands, Global Biogeochemical Cycles, 26, 2012.

Heimburger, A., Losno, R., Triquet, S., and Nguyen, E.: Atmospheric deposition fluxes of 26 elements over the Southern Indian Ocean: Time series on Kerguelen and Crozet Islands, Global Biogeochemical Cycles, 27, 440-449, 2013b.

Kadko, D., Landing, W. M., and Shelley, R. U.: A novel tracer technique to quantify the atmospheric flux of trace elements to remote ocean regions, Journal of Geophysical Research: Oceans, 2015. 2015.

Keeling, R. F., Piper, S. C., and Heimann, M.: Global and hemispheric CO2 sinks deduced from changes in atmospheric O2 concentration, Nature, 381, 218-221, 1996.

Keywood, M.: An evaluation of PM10 and PM2. 5 size selective inlet performance using ambient aerosol, Aerosol Science & Technology, 30, 401-407, 1999.

Keywood, M. D.: Aerosol composition at Cape Grim : an evaluation of PM10 sampling program and baseline event switches., Baseline Atmospheric Program Australia 2005-2006. 2005-2006 ed. J. M. Cainey, N. Derek, and P. B. Krummel (editors). Melbourne: Australian Bureau of Meteorology and CSIRO Marine and Atmospheric Research, 2007. 31-36, 2007.

Lambert, F., Tagliabue, A., Shaffer, G., Lamy, F., Winckler, G., Farias, L., Gallardo, L., and De Pol-Holz, R.: Dust fluxes and iron fertilization in Holocene and Last Glacial Maximum climates, Geophysical Research Letters, doi: 10.1002/2015GL064250, 2015. n/a-n/a, 2015.

Li-Jones, X. and Prospero, J.: Variations in the size distribution of non-sea-salt sulfate aerosol in the marine boundary layer at Barbados: Impact of African dust, Journal of Geophysical Research: Atmospheres (1984–2012), 103, 16073-16084, 1998.

Martin, J. H.: Glacial-interglacial CO2 change: the iron hypothesis, Paleoceanography, 5, 1-11, 1990.

Martínez-García, A., Sigman, D. M., Ren, H., Anderson, R. F., Straub, M., Hodell, D. A., Jaccard, S. L., Eglinton, T. I., and Haug, G. H.: Iron Fertilization of the Subantarctic Ocean During the Last Ice Age, Science, 343, 1347-1350, 2014.

Middag, R., De Baar, H., Laan, P., Cai, P., and Van Ooijen, J.: Dissolved manganese in the Atlantic sector of the Southern Ocean, Deep Sea Research Part II: Topical Studies in Oceanography, 58, 2661-2677, 2011.

Morel, F. and Price, N.: The biogeochemical cycles of trace metals in the oceans, Science, 300, 944-947, 2003.

Morel, F. M., Hudson, R. J., and Price, N. M.: Limitation of productivity by trace metals in the sea, Limnology and Oceanography, 36, 1742-1755, 1991.

Morton, P. L., Landing, W. M., Hsu, S.-C., Milne, A., Aguilar-Islas, A. M., Baker, A. R., Bowie, A. R., Buck, C. S., Gao, Y., and Gichuki, S.: Methods for the sampling and analysis of marine aerosols: results from the 2008 GEOTRACES aerosol intercalibration experiment, Limnology and Oceanography: Methods, 11, 62-78, 2013.

Price, N. and Morel, F.: Colimitation of phytoplankton growth by nickel and nitrogen, LIMNOLOGY, 1991. 1991.

Prospero, J. M.: The atmospheric transport of particles to the ocean, in Particle Flux in the Ocean, John Wiley, Hoboken, N. J, 1996.

Saito, M. A., Moppett, J., Chisholm, S. W., and Waterbury, J. B.: Cobalt limitation and uptake in Prochlorococcus, Limnology and Oceanography, 47, 1629-1636, 2002.

Selleck, P. W., Keywood, M. D., Ward, J. P., Gillett, R. W., and Boast, K.: Aerosol samplers and chemical composition, 2009-2010 Baseline report, 76-79., 2014. 2014.

Sholkovitz, E. R., Sedwick, P. N., Church, T. M., Baker, A. R., and Powell, C. F.: Fractional solubility of aerosol iron: Synthesis of a global-scale data set, Geochimica et cosmochimica acta, 89, 173-189, 2012.

Stafford, R. G. and Ettinger, H. J.: Filter efficiency as a function of particle size and velocity, Atmospheric Environment (1967), 6, 353-362, 1972.

Taylor, S. R. and McLennan, S. M.: The continental crust: Its composition and evolution, 1985.

Vallelonga, P., Van de Velde, K., Candelone, J. P., Ly, C., Rosman, K. J. R., Boutron, C. F., Morgan, V. I., and Mackey, D. J.: Recent advances in measurement of Pb isotopes in polar ice and snow at sub-picogram per gram concentrations using thermal ionisation mass spectrometry, Analytica Chimica Acta, 453, 1-12, 2002.

Wagener, T., Guieu, C., Losno, R., Bonnet, S., and Mahowald, N.: Revisiting atmospheric dust export to the Southern Hemisphere ocean: Biogeochemical implications, Global Biogeochem. Cycles, 22, GB2006, 2008.

Wedepohl, K. H.: The composition of the continental crust, Geochimica et Cosmochimica Acta, 59, 1217-1232, 1995.

Winton, V. H. L., Bowie, A. R., Edwards, R., Keywood, M., Townsend, A. T., van der Merwe, P., and Bollhöfer, A.: Fractional iron solubility of atmospheric iron inputs to the Southern Ocean, Marine Chemistry, 177, Part 1, 20-32, 2015.

Atmos. Meas. Tech. Discuss., doi:10.5194/amt-2016-12, 2016
Manuscript under review for journal Atmos. Meas. Tech.
Published: 8 April 2016

Atmospheric Measurement Techniques Discussions

Table 1: Filter blank and aerosol sampling duration and volume.

	Inlet	Start	Finish	Total sampling time	Total sampling volume (m^3)
Procedural blank	TSP	8/08/2013	8/08/2013	5 minutes	0
Exposure blank	PM10	8/11/2013	10/12/2013	1 month	0
CG13TM01	TSP	12/06/2013	16/07/2013	814.7 hours	59473
CG13TM08	PM10	28/01/2014	25/02/2014	143.3 hours	10461

Atmos. Meas. Tech. Discuss., doi:10.5194/amt-2016-12, 2016
Manuscript under review for journal Atmos. Meas. Tech.
Published: 8 April 2016

Atmospheric Measurement Techniques Discussions

Table 2: Average total trace metal concentration in filtrates. Data for blank filters are corrected for the digestion blank (Savillex® beaker blank). Errors are the standard deviation of the three sub-samples. DL: Detection limit.

Atmos. Meas. Tech. Discuss., doi:10.5194/amt-2016-12, 2016
Manuscript under review for journal Atmos. Meas. Tech.
Published: 8 April 2016

Atmospheric Measurement Techniques Discussions

	Al				Ti				V				Mn				Fe				Pb			
	(ng cm^{-2})	±	(ng m^{-3})	±	(ng cm^{-2})	±	(ng m^{-3})	±	(ng cm^{-2})	±	(pg m^{-3})	±	(ng cm^{-2})	±	(ng m^{-3})	±	(ng cm^{-2})	±	(ng m^{-3})	±	(ng cm^{-2})	±	(pg m^{-3})	±
Instrumental blank (n=10)	0.01	0.004	<0.001	<0.001	<0.001	<0.001	<0.001	<0.001	<0.001	<0.001	0.002	0.002	<0.001	<0.001	<0.001	<0.001	<0.001	<0.001	<0.001	<0.001	<0.001	<0.001	0.005	0.0043
Digestion blank (n=3)	0.67	0.1	0.03	0.01	0.04	0.01	0.002	<0.001	0.01	0.002	0.2	0.1	0.28	0.4	0.01	0.02	0.23	0.2	0.01	0.01	0.02	0.01	1	0.4
Untreated filter (n=3)	5.6	0.3	0.2	0.01	23	10	0.9	0.4	0.01	0.003	0.52	0.1	<DL		<DL		15	2	0.6	0.1	0.08	0.05	3	2
Acid-washed filter (n=6)	4.1	1	0.2	0.05	3.6	1	0.1	0.01	0.01	0.01	0.56	0.3	<DL		<DL		8.0	5	0.3	0.2	0.004	0.01	0.2	0.2
Procedural blank (n=3)	6.3	2	0.3	0.1	7.7	2	0.3	0.1	0.02	0.01	0.76	0.2	<DL		<DL		7.4	2	0.3	0.1	0.01	0.01	0.5	0.3
Exposure blank (n=3)	250	20	9.8	0.9	48	5	1.9	0.2	0.61	0.05	24	2	3.3	0.8	0.1	0.03	260	30	10	1	0.08	0.03	3	1

4 Filter blanks in units of "ng cm^{-2}" were calculated assuming the 47 mm aliquot is representative of the whole filter sheet sample.

5 Filter blanks in units of "ng m^{-3}" were calculated assuming a typical monthly filtered baseline air volume of 12600 m^3 assuming baseline conditions occur 30 % of the time

6 (Keywood, 2007).

Atmos. Meas. Tech. Discuss., doi:10.5194/amt-2016-12, 2016
Manuscript under review for journal Atmos. Meas. Tech.
Published: 8 April 2016

Atmospheric Measurement Techniques Discussions

Table 3: Average trace metal soluble concentration in filtrates. Data for blank filters are corrected for the instrumental blank. Errors are the standard deviation of the three sub-samples.

Atmos. Meas. Tech. Discuss., doi:10.5194/amt-2016-12, 2016
Manuscript under review for journal Atmos. Meas. Tech.
Published: 8 April 2016

Atmospheric Measurement Techniques Discussions

		Al		Ti		V		Mn		Fe		Pb	
		(pg cm^{-2})	±	(pg m^{-3})	±	(pg cm^{-2})	±	(pg m^{-3})	±	(pg cm^{-2})	±	(pg m^{-3})	±	(pg cm^{-2})	±	(pg m^{-3})	±	(pg cm^{-2})	±	(pg m^{-3})	±
Instrumental blank (n=9)		4.9	3	0.2	0.1	1.9	5	0.08	0.2	0.01	0.02	0.0004	0.0008	0.04	0.07	0.002	0.003	0.46	0.3	0.02	0.01	0.14	0.1	0.01	0.01
Untreated filter (n=3)	Leach 1	12	10	0.49	0.4	6.2	8	0.25	0.3	0.97	1	0.04	0.04	60	56	2.4	2	200	180	8.0	7	18	25	0.71	1
	Leach 2	11	7	0.45	0.3	4.7	<DL	0.19	<DL	0.75	1	0.03	0.04	14	7	0.56	0.3	46	24	1.8	0.9	4.3	3	0.17	0.1
	Leach 3	0	0.02	<DL	<DL	1.1	<DL	0.04	<DL	0.14	0.2	0.01	0.01	3.6	2	0.14	0.06	9.4	7	0.37	0.3	0.74	0.6	0.03	0.02
Acid-washed filter (n=3)	Leach 1	2600	180	100	7	1.1	2	0.05	0.07	0.94	0.9	0.04	0.03	7.5	3	0.30	0.1	30	16	1.2	0.6	1.3	1	0.05	0.04
	Leach 2	930	650	37	26	<DL	<DL	<DL	<DL	0.54	0.7	0.02	0.03	4.0	3	0.16	0.1	17	14	0.68	0.6	4.6	7	0.18	0.3
	Leach 3	1700	2800	67	110	<DL	<DL	<DL	<DL	0.12	0.1	<DL	<DL	2.7	1	0.11	0.05	21	29	0.85	1	0.35	0.3	0.01	0.01
Procedural blank (n=3)	Leach 1	620	330	25	13	12	8	0.46	0.3	3.3	2	0.13	0.07	9.7	4	0.38	0.2	16	9	0.63	0.3	2.4	0.4	0.10	0.02
	Leach 2	420	120	17	5	1.9	1	0.07	0.04	0.62	0.2	0.02	0.01	2.0	0.5	0.08	0.02	6.2	3	0.25	0.1	0.92	0.4	0.04	0.02
	Leach 3	540	430	21	17	8.3	<DL	0.33	<DL	0.24	0.1	0.01	<DL	0.82	0.5	0.03	0.02	5.3	2	0.21	0.06	1.1	1	0.05	0.04
Exposure blank (n=3)	Leach 1	54000	21000	2200	850	280	300	11	12	44	10	1.7	0.4	1800	300	70	12	870	490	35	20	26	10	1.0	0.5
	Leach 2	14000	5600	580	220	50	16	2.0	0.6	8.6	4	0.34	0.2	110	100	4.2	4	290	110	12	5	1.6	0.6	0.06	0.03
	Leach 3	8400	3200	330	130	25	10	0.98	0.4	5.9	1	0.23	0.04	22	7	0.88	0.3	170	35	6.7	1	1.1	0.6	0.04	0.03

1 Filter blanks in units of "pg cm^{-2}" were calculated assuming the 47 mm aliquot is representative of the whole filter sheet sample.

2 Filter blanks in units of "pg m^{-3}" were calculated assuming a typical monthly filtered baseline air volume of 12600 m^3 assuming baseline conditions occur 30 % of the time

3 (Keywood, 2007).

Atmos. Meas. Tech. Discuss., doi:10.5194/amt-2016-12, 2016
Manuscript under review for journal Atmos. Meas. Tech.
Published: 8 April 2016

Atmospheric Measurement Techniques Discussions

Table 4: Blank iron contamination budget.

	Total Fe (ng cm^{-2})	Soluble Fe (ng cm^{-2})	Fe blank contribution (ng cm^{-2})	Fe blank contribution (%)
Digestion	[1]0.2		0.2	0.1
Acid	[2]0.0006	[3]0.00004	0.0007	<0.001
Instrument	[4]0.0004	[5]0.0005	0.0009	<0.001
W41 filter	[6]6.6	[7]0.2	6.8	3
Sampling procedure	[8]negligible	[9]negligible	0	<0.001
Month exposure at field site	[10]254	[11]1	255	98
Total	261	1	262	

Method of determination: [1]Digested Savlliex® blank beaker with 0.5 mL of HNO_3 (Baseline Seastar®) and 0.25 mL HF (Baseline Seastar®) (acid and instrument blank subtracted); [2]Assuming certified maximum specification of Seastar Baseline® of HNO_3 and HF is <10 ppt or 0.2 nmol L^{-1} of Fe; [3]Assuming concentration of double distilled in-house HCl from Seastar® IQ grade quality (Choice Analytical Pty Ltd, Australia) is <10 ppt or 0.2 nmol L^{-1} of Fe; [4]Vials filled with ultra-pure water acidified to 3 % or 0.5 mol L^{-1} HNO_3; [5]Vials filled with ultra-pure water acidified to 1 % or 0.12 mol L^{-1} HCl; [6]Total digestion of untreated filter (digestion, instrument and acid-washed filter blank subtracted); [7]Water soluble leach of untreated filter (instrument and acid-washed filter blank subtracted); [8]Total digestion of procedural blank filter (digestion, instrument and acid-washed filter blank subtracted); [9]Water soluble leach of procedural blank filter (instrument and acid-washed filter blank subtracted); [10]Total digestion of exposure blank filter (digestion, instrument and procedural blank filter subtracted); [11]Water soluble leach of exposure blank filter (instrument and procedural blank filter subtracted). Negligible is defined as <0.01 pg cm^3 of Fe.

Atmos. Meas. Tech. Discuss., doi:10.5194/amt-2016-12, 2016
Manuscript under review for journal Atmos. Meas. Tech.
Published: 8 April 2016

Atmospheric Measurement Techniques Discussions

Table 5: Enrichment factors of trace metals relative to Al measured in exposure and procedural blank filters. The composition of the upper continent crust is based from Wedepohl (1995).

	Ti	Fe	Mn	V	Pb
Exposure blank	4.8	2.7	2.0	3.6	1.5

Atmos. Meas. Tech. Discuss., doi:10.5194/amt-2016-12, 2016
Manuscript under review for journal Atmos. Meas. Tech.
Published: 8 April 2016

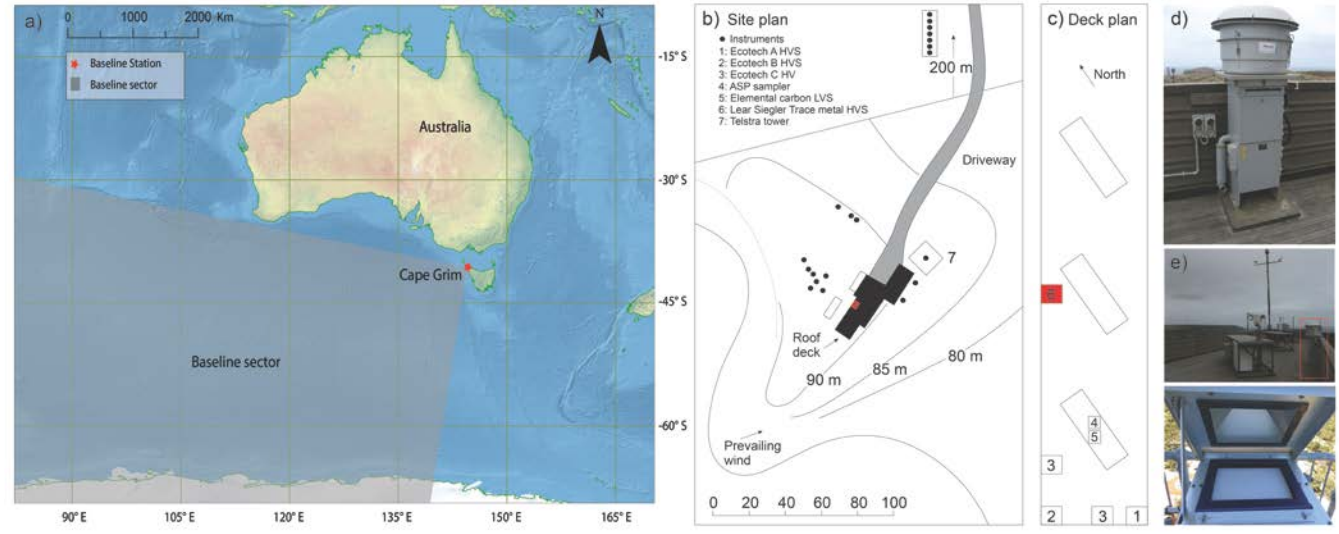

Fig. 1: a) Location of the CGBAPS and the high-volume aerosol sampler installed on the roof deck. Baseline conditions occur when the wind direction is between 190º and 280º and the total aerosol particle counts are below a threshold concentration based on the 90 percentile of hourly medians for the previous five years. b) CGBAPS site plan, b) roof deck plan, d-e) LSA high-volume aerosol sample attached with PM10 size selective inlet (photo credit: Jeremy Ward), f) filter inside the sampler. Panels b) and c) modified from Baseline Report 2009-2010 (Baseline, 2014).

Atmos. Meas. Tech. Discuss., doi:10.5194/amt-2016-12, 2016
Manuscript under review for journal Atmos. Meas. Tech.
Published: 8 April 2016

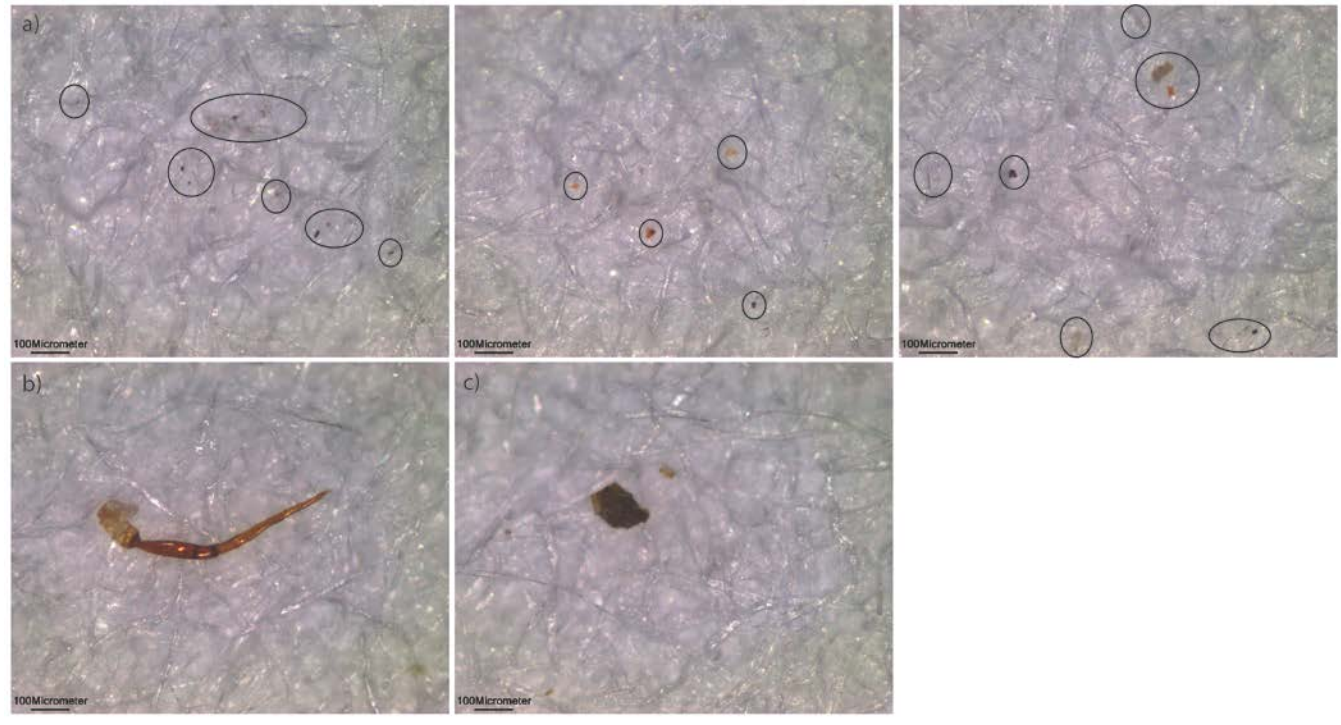

Fig. 2: Optical microscopy images of contaminated exposure blanks showing examples of particles on the filter. a) three examples of windblown particles, b) insect leg, c) large soil particle. Areas of interest are circled.

Atmos. Meas. Tech. Discuss., doi:10.5194/amt-2016-12, 2016
Manuscript under review for journal Atmos. Meas. Tech.
Published: 8 April 2016

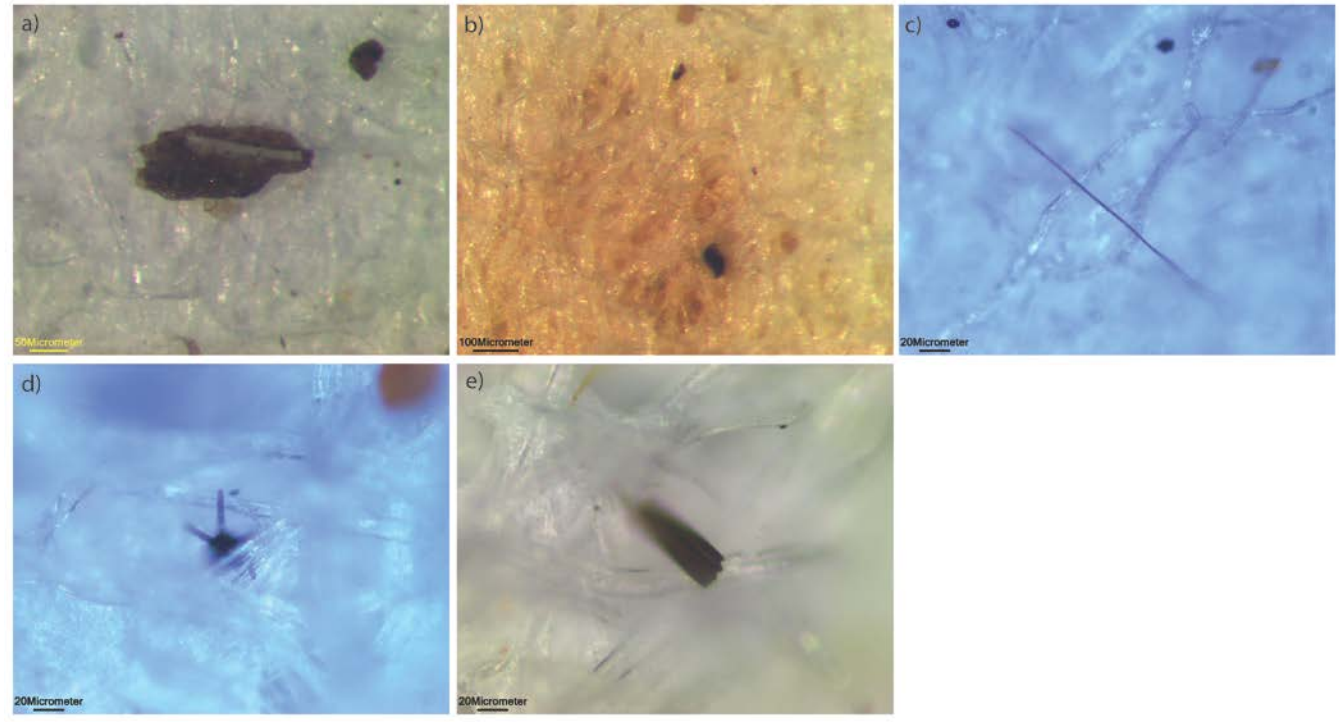

Fig. 3: Optical microscopy images of examples of particles collected on TSP filter (CG13TM01). a) large soil particle, b) orange spot common to many TSP filters, c) hair, d) spore, e) moth spare.

Atmos. Meas. Tech. Discuss., doi:10.5194/amt-2016-12, 2016
Manuscript under review for journal Atmos. Meas. Tech.
Published: 8 April 2016

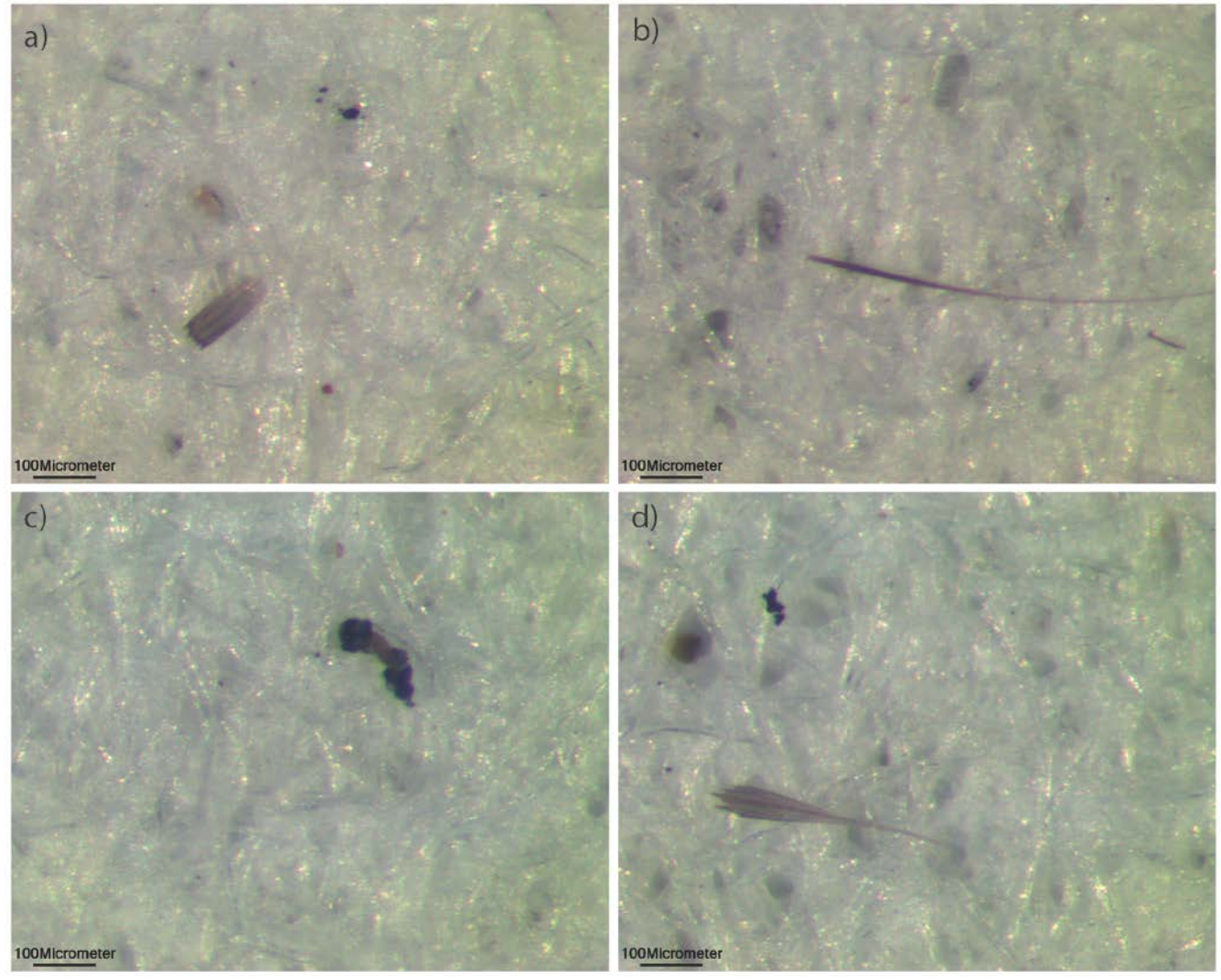

Fig. 4: Optical microscopy images of examples of particles collected on PM10 filter (CG13TM08). a) moth spare, b) grass, c-d) large windblown particles.

Atmos. Meas. Tech. Discuss., doi:10.5194/amt-2016-12, 2016
Manuscript under review for journal Atmos. Meas. Tech.
Published: 8 April 2016

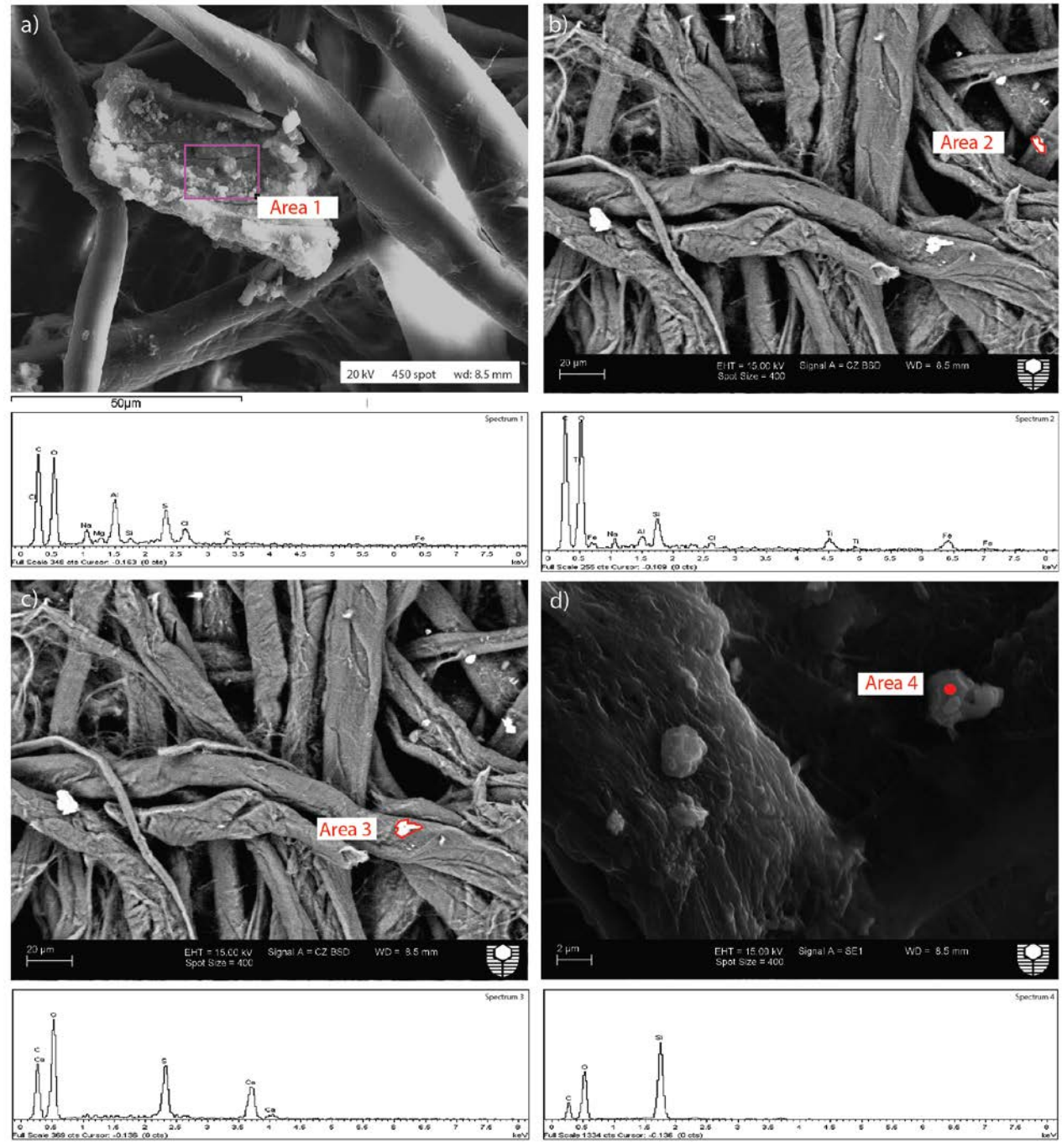

Fig. 5: Scanning Electron Microscope images and spectra of particles on a PM10 filter (CG13TM08). a) salt particle (sodium chloride) (detector: SE, instrument: EVO), b) soil (detector: BSD, instrument: EVO), c) calcium carbonate (detector: BSD, instrument: EVO), d) marine silica (detector: SE, instrument: EVO).

Atmos. Meas. Tech. Discuss., doi:10.5194/amt-2016-12, 2016
Manuscript under review for journal Atmos. Meas. Tech.
Published: 8 April 2016

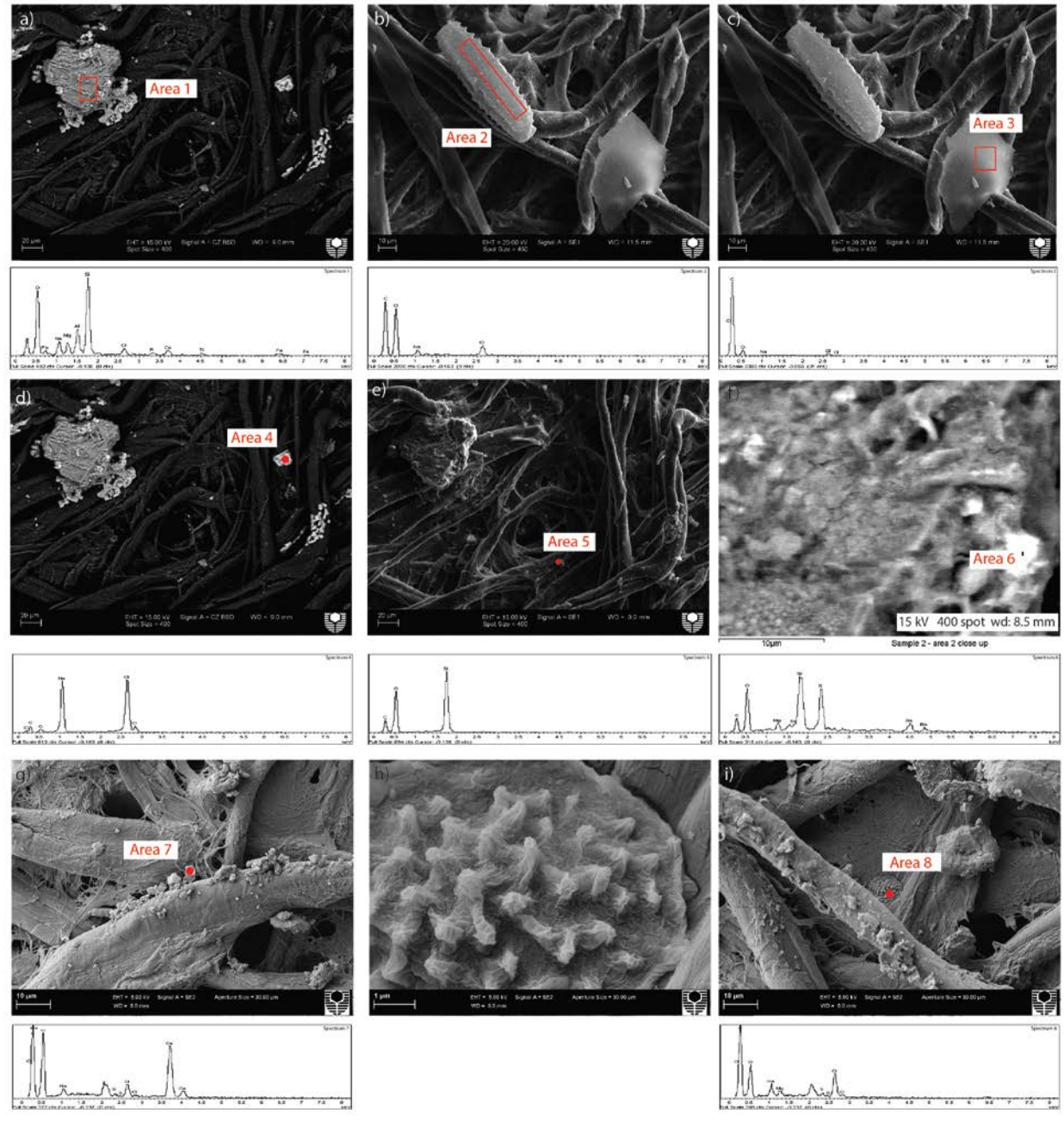

Fig. 6: Scanning Electron Microscope images and spectra of particles on a TSP filter (CG13TM01). a) mineral dust (Fe, Mg, Al, Si, Ti, K) (detector: BSD, instrument: EVO), b) organic material (detector: BC, instrument: NEO), c) organic carbonaceous particle (detector: BC, instrument: NEO), d) cubical salt (sodium chloride) (detector: BSD, instrument: EVO), e) silica sand (detector: BC, instrument: EVO), f) marine aerosol (detector: BSD, instrument: EVO), g) marine aerosol (Mg, Sr, Ba, Cl, Ca, Na) (detector: BC, instrument: EVO), h-i) spore (detector: BC, instrument: EVO).

Atmos. Meas. Tech. Discuss., doi:10.5194/amt-2016-12, 2016
Manuscript under review for journal Atmos. Meas. Tech.
Published: 8 April 2016

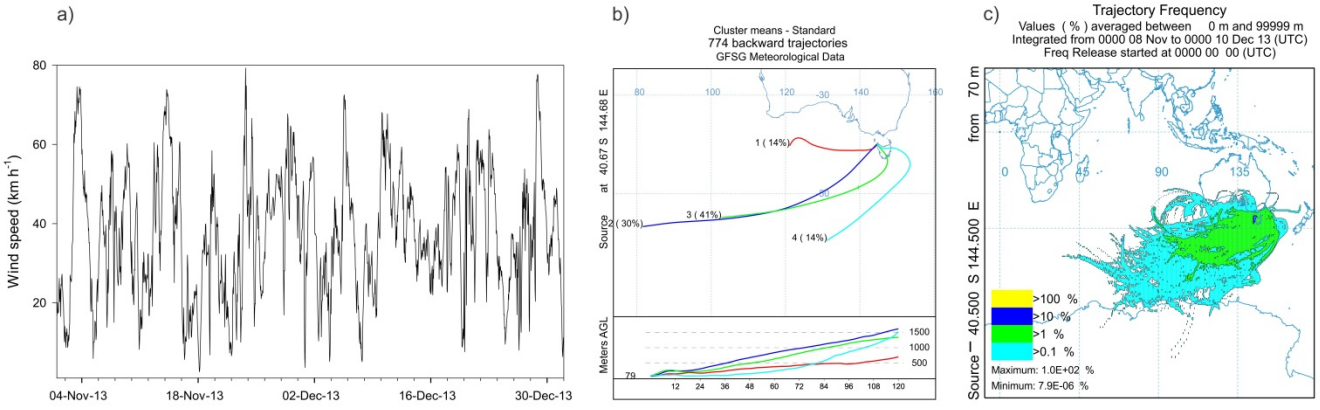

Fig. 7: Wind speed and fetch area of air masses associated with the whole duration of one month long exposure blank from 8 November to 10 December 2013. a) Time series of hourly wind speed (times are in the GMT+10 time zone; data sourced from the Australian Bureau of Meteorology), b) Cluster means of 5 day hourly air mass back trajectories.

Appendix A2: Statement of contribution, copyright license and publication for paper 3

Winton, V.H.L., A.R. Bowie, R. Edwards, M. Keywood, A.T. Townsend, P. van der Merwe, Bollhofer, A., 2015. Fractional iron solubility of atmospheric iron inputs to the Southern Ocean, *Mar. Chem*., 177, Part 1, 20-32, http://dx.doi.org/10.1016/j.marchem.2015.06.006.

Statement of co-authorship

I, *Victoria Holly Liberty Winton*, designed and implemented the project, including experimental design, processed and analysed the samples for water soluble iron, labile iron and total iron, and conducted data analysis and manuscript writing of the publication:

Winton, V.H.L., A.R. Bowie, R. Edwards, M. Keywood, A.T. Townsend, P. van derMerwe, A. Bollhöfer. Fractional iron solubility of atmospheric iron inputs to the Southern Ocean, *Mar. Chem.* (2015), http://dx.doi.org/10.1016/j.marchem.2015.06.006.

Holly Winton

Victoria Holly Liberty Winton

I, as a Co-Author, endorse that this level of contribution by the candidate indicated above is appropriate.

Andrew Bowie

Andrew Bowie (Signature of Co-Author 1)

R. Edwards

Ross Edwards (Signature of Co-Author 2)

M. J. Jarrard

Melita Keywood (Signature of Co-Author 3)

Melita Keywood

Ashley Townsend (Signature of Co-Author 4)

Pier van der Merwe (Signature of Co-Author 5)

Andreas Bollhöfer (Signature of Co-Author 6)

ELSEVIER LICENSE
TERMS AND CONDITIONS

Jun 24, 2015

This is a License Agreement between Holly Winton ("You") and Elsevier ("Elsevier") provided by Copyright Clearance Center ("CCC"). The license consists of your order details, the terms and conditions provided by Elsevier, and the payment terms and conditions.

All payments must be made in full to CCC. For payment instructions, please see information listed at the bottom of this form.

Supplier	Elsevier Limited The Boulevard,Langford Lane Kidlington,Oxford,OX5 1GB,UK
Registered Company Number	1982084
Customer name	Holly Winton
Customer address	Curtin University Bentley, Western Australia 6102
License number	3655641049412
License date	Jun 22, 2015
Licensed content publisher	Elsevier
Licensed content publication	Marine Chemistry
Licensed content title	Fractional iron solubility of atmospheric iron inputs to the Southern Ocean
Licensed content author	V.H.L. Winton,A.R. Bowie,R. Edwards,M. Keywood,A.T. Townsend,P. van der Merwe,A. Bollhöfer
Licensed content date	Available online 12 June 2015
Licensed content volume number	n/a
Licensed content issue number	n/a
Number of pages	1
Start Page	None
End Page	None
Type of Use	reuse in a thesis/dissertation
Portion	full article
Format	both print and electronic
Are you the author of this Elsevier article?	Yes
Will you be translating?	No
Title of your thesis/dissertation	Impact of biomass burning emissions and dust on soluble iron deposition to Australian and Antarctic waters
Expected completion date	Dec 2015
Estimated size (number of pages)	

Elsevier VAT number	GB 494 6272 12
Permissions price	0.00 AUD
VAT/Local Sales Tax	0.00 AUD / 0.00 GBP
Total	0.00 AUD

Terms and Conditions

INTRODUCTION

1. The publisher for this copyrighted material is Elsevier. By clicking "accept" in connection with completing this licensing transaction, you agree that the following terms and conditions apply to this transaction (along with the Billing and Payment terms and conditions established by Copyright Clearance Center, Inc. ("CCC"), at the time that you opened your Rightslink account and that are available at any time at http://myaccount.copyright.com).

GENERAL TERMS

2. Elsevier hereby grants you permission to reproduce the aforementioned material subject to the terms and conditions indicated.

3. Acknowledgement: If any part of the material to be used (for example, figures) has appeared in our publication with credit or acknowledgement to another source, permission must also be sought from that source. If such permission is not obtained then that material may not be included in your publication/copies. Suitable acknowledgement to the source must be made, either as a footnote or in a reference list at the end of your publication, as follows:

"Reprinted from Publication title, Vol /edition number, Author(s), Title of article / title of chapter, Pages No., Copyright (Year), with permission from Elsevier [OR APPLICABLE SOCIETY COPYRIGHT OWNER]." Also Lancet special credit - "Reprinted from The Lancet, Vol. number, Author(s), Title of article, Pages No., Copyright (Year), with permission from Elsevier."

4. Reproduction of this material is confined to the purpose and/or media for which permission is hereby given.

5. Altering/Modifying Material: Not Permitted. However figures and illustrations may be altered/adapted minimally to serve your work. Any other abbreviations, additions, deletions and/or any other alterations shall be made only with prior written authorization of Elsevier Ltd. (Please contact Elsevier at permissions@elsevier.com)

6. If the permission fee for the requested use of our material is waived in this instance, please be advised that your future requests for Elsevier materials may attract a fee.

7. Reservation of Rights: Publisher reserves all rights not specifically granted in the combination of (i) the license details provided by you and accepted in the course of this licensing transaction, (ii) these terms and conditions and (iii) CCC's Billing and Payment terms and conditions.

8. License Contingent Upon Payment: While you may exercise the rights licensed immediately upon issuance of the license at the end of the licensing process for the transaction, provided that you have disclosed complete and accurate details of your proposed use, no license is finally effective unless and until full payment is received from you (either by publisher or by CCC) as provided in CCC's Billing and Payment terms and conditions. If

full payment is not received on a timely basis, then any license preliminarily granted shall be deemed automatically revoked and shall be void as if never granted. Further, in the event that you breach any of these terms and conditions or any of CCC's Billing and Payment terms and conditions, the license is automatically revoked and shall be void as if never granted. Use of materials as described in a revoked license, as well as any use of the materials beyond the scope of an unrevoked license, may constitute copyright infringement and publisher reserves the right to take any and all action to protect its copyright in the materials.

9. Warranties: Publisher makes no representations or warranties with respect to the licensed material.

10. Indemnity: You hereby indemnify and agree to hold harmless publisher and CCC, and their respective officers, directors, employees and agents, from and against any and all claims arising out of your use of the licensed material other than as specifically authorized pursuant to this license.

11. No Transfer of License: This license is personal to you and may not be sublicensed, assigned, or transferred by you to any other person without publisher's written permission.

12. No Amendment Except in Writing: This license may not be amended except in a writing signed by both parties (or, in the case of publisher, by CCC on publisher's behalf).

13. Objection to Contrary Terms: Publisher hereby objects to any terms contained in any purchase order, acknowledgment, check endorsement or other writing prepared by you, which terms are inconsistent with these terms and conditions or CCC's Billing and Payment terms and conditions. These terms and conditions, together with CCC's Billing and Payment terms and conditions (which are incorporated herein), comprise the entire agreement between you and publisher (and CCC) concerning this licensing transaction. In the event of any conflict between your obligations established by these terms and conditions and those established by CCC's Billing and Payment terms and conditions, these terms and conditions shall control.

14. Revocation: Elsevier or Copyright Clearance Center may deny the permissions described in this License at their sole discretion, for any reason or no reason, with a full refund payable to you. Notice of such denial will be made using the contact information provided by you. Failure to receive such notice will not alter or invalidate the denial. In no event will Elsevier or Copyright Clearance Center be responsible or liable for any costs, expenses or damage incurred by you as a result of a denial of your permission request, other than a refund of the amount(s) paid by you to Elsevier and/or Copyright Clearance Center for denied permissions.

LIMITED LICENSE

The following terms and conditions apply only to specific license types:

15. **Translation**: This permission is granted for non-exclusive world **English** rights only unless your license was granted for translation rights. If you licensed translation rights you may only translate this content into the languages you requested. A professional translator must perform all translations and reproduce the content word for word preserving the integrity of the article. If this license is to re-use 1 or 2 figures then permission is granted for non-exclusive world rights in all languages.

16. **Posting licensed content on any Website**: The following terms and conditions apply as follows: Licensing material from an Elsevier journal: All content posted to the web site must

maintain the copyright information line on the bottom of each image; A hyper-text must be included to the Homepage of the journal from which you are licensing at http://www.sciencedirect.com/science/journal/xxxxx or the Elsevier homepage for books at http://www.elsevier.com; Central Storage: This license does not include permission for a scanned version of the material to be stored in a central repository such as that provided by Heron/XanEdu.

Licensing material from an Elsevier book: A hyper-text link must be included to the Elsevier homepage at http://www.elsevier.com . All content posted to the web site must maintain the copyright information line on the bottom of each image.

Posting licensed content on Electronic reserve: In addition to the above the following clauses are applicable: The web site must be password-protected and made available only to bona fide students registered on a relevant course. This permission is granted for 1 year only. You may obtain a new license for future website posting.

17. **For journal authors:** the following clauses are applicable in addition to the above:

Preprints:

A preprint is an author's own write-up of research results and analysis, it has not been peer-reviewed, nor has it had any other value added to it by a publisher (such as formatting, copyright, technical enhancement etc.).

Authors can share their preprints anywhere at any time. Preprints should not be added to or enhanced in any way in order to appear more like, or to substitute for, the final versions of articles however authors can update their preprints on arXiv or RePEc with their Accepted Author Manuscript (see below).

If accepted for publication, we encourage authors to link from the preprint to their formal publication via its DOI. Millions of researchers have access to the formal publications on ScienceDirect, and so links will help users to find, access, cite and use the best available version. Please note that Cell Press, The Lancet and some society-owned have different preprint policies. Information on these policies is available on the journal homepage.

Accepted Author Manuscripts: An accepted author manuscript is the manuscript of an article that has been accepted for publication and which typically includes author-incorporated changes suggested during submission, peer review and editor-author communications.

Authors can share their accepted author manuscript:

- immediately
    - via their non-commercial person homepage or blog
    - by updating a preprint in arXiv or RePEc with the accepted manuscript
    - via their research institute or institutional repository for internal institutional uses or as part of an invitation-only research collaboration work-group
    - directly by providing copies to their students or to research collaborators for their personal use
    - for private scholarly sharing as part of an invitation-only work group on

commercial sites with which Elsevier has an agreement

- after the embargo period
    - via non-commercial hosting platforms such as their institutional repository
    - via commercial sites with which Elsevier has an agreement

In all cases accepted manuscripts should:

- link to the formal publication via its DOI
- bear a CC-BY-NC-ND license - this is easy to do
- if aggregated with other manuscripts, for example in a repository or other site, be shared in alignment with our hosting policy not be added to or enhanced in any way to appear more like, or to substitute for, the published journal article.

Published journal article (JPA): A published journal article (PJA) is the definitive final record of published research that appears or will appear in the journal and embodies all value-adding publishing activities including peer review co-ordination, copy-editing, formatting, (if relevant) pagination and online enrichment.

Policies for sharing publishing journal articles differ for subscription and gold open access articles:

Subscription Articles: If you are an author, please share a link to your article rather than the full-text. Millions of researchers have access to the formal publications on ScienceDirect, and so links will help your users to find, access, cite, and use the best available version.

Theses and dissertations which contain embedded PJAs as part of the formal submission can be posted publicly by the awarding institution with DOI links back to the formal publications on ScienceDirect.

If you are affiliated with a library that subscribes to ScienceDirect you have additional private sharing rights for others' research accessed under that agreement. This includes use for classroom teaching and internal training at the institution (including use in course packs and courseware programs), and inclusion of the article for grant funding purposes.

Gold Open Access Articles: May be shared according to the author-selected end-user license and should contain a CrossMark logo, the end user license, and a DOI link to the formal publication on ScienceDirect.

Please refer to Elsevier's posting policy for further information.

18. **For book authors** the following clauses are applicable in addition to the above: Authors are permitted to place a brief summary of their work online only. You are not allowed to download and post the published electronic version of your chapter, nor may you scan the printed edition to create an electronic version. **Posting to a repository:** Authors are permitted to post a summary of their chapter only in their institution's repository.

19. **Thesis/Dissertation**: If your license is for use in a thesis/dissertation your thesis may be submitted to your institution in either print or electronic form. Should your thesis be published commercially, please reapply for permission. These requirements include permission for the Library and Archives of Canada to supply single copies, on demand, of

the complete thesis and include permission for Proquest/UMI to supply single copies, on demand, of the complete thesis. Should your thesis be published commercially, please reapply for permission. Theses and dissertations which contain embedded PJAs as part of the formal submission can be posted publicly by the awarding institution with DOI links back to the formal publications on ScienceDirect.

Elsevier Open Access Terms and Conditions

You can publish open access with Elsevier in hundreds of open access journals or in nearly 2000 established subscription journals that support open access publishing. Permitted third party re-use of these open access articles is defined by the author's choice of Creative Commons user license. See our open access license policy for more information.

Terms & Conditions applicable to all Open Access articles published with Elsevier:

Any reuse of the article must not represent the author as endorsing the adaptation of the article nor should the article be modified in such a way as to damage the author's honour or reputation. If any changes have been made, such changes must be clearly indicated.

The author(s) must be appropriately credited and we ask that you include the end user license and a DOI link to the formal publication on ScienceDirect.

If any part of the material to be used (for example, figures) has appeared in our publication with credit or acknowledgement to another source it is the responsibility of the user to ensure their reuse complies with the terms and conditions determined by the rights holder.

Additional Terms & Conditions applicable to each Creative Commons user license:

CC BY: The CC-BY license allows users to copy, to create extracts, abstracts and new works from the Article, to alter and revise the Article and to make commercial use of the Article (including reuse and/or resale of the Article by commercial entities), provided the user gives appropriate credit (with a link to the formal publication through the relevant DOI), provides a link to the license, indicates if changes were made and the licensor is not represented as endorsing the use made of the work. The full details of the license are available at http://creativecommons.org/licenses/by/4.0.

CC BY NC SA: The CC BY-NC-SA license allows users to copy, to create extracts, abstracts and new works from the Article, to alter and revise the Article, provided this is not done for commercial purposes, and that the user gives appropriate credit (with a link to the formal publication through the relevant DOI), provides a link to the license, indicates if changes were made and the licensor is not represented as endorsing the use made of the work. Further, any new works must be made available on the same conditions. The full details of the license are available at http://creativecommons.org/licenses/by-nc-sa/4.0.

CC BY NC ND: The CC BY-NC-ND license allows users to copy and distribute the Article, provided this is not done for commercial purposes and further does not permit distribution of the Article if it is changed or edited in any way, and provided the user gives appropriate credit (with a link to the formal publication through the relevant DOI), provides a link to the license, and that the licensor is not represented as endorsing the use made of the work. The full details of the license are available at http://creativecommons.org/licenses/by-nc-nd/4.0. Any commercial reuse of Open Access articles published with a CC BY NC SA or CC BY NC ND license requires permission from Elsevier and will be subject to a fee.

Commercial reuse includes:

- Associating advertising with the full text of the Article
- Charging fees for document delivery or access
- Article aggregation
- Systematic distribution via e-mail lists or share buttons

Posting or linking by commercial companies for use by customers of those companies.

20. **Other Conditions**:

v1.7

Questions? customercare@copyright.com or +1-855-239-3415 (toll free in the US) or +1-978-646-2777.

Marine Chemistry 177 (2015) 20–32

Contents lists available at ScienceDirect

Marine Chemistry

journal homepage: www.elsevier.com/locate/marchem

Fractional iron solubility of atmospheric iron inputs to the Southern Ocean

V.H.L. Winton [a,*], A.R. Bowie [b,c], R. Edwards [a], M. Keywood [d], A.T. Townsend [e], P. van der Merwe [b], A. Bollhöfer [f]

[a] Physics and Astronomy, Curtin University, Perth, Western Australia, Australia
[b] Antarctic Climate and Ecosystems CRC, University of Tasmania, Hobart, Tasmania, Australia
[c] Institute for Marine and Antarctic Studies, University of Tasmania, Hobart, Australia
[d] CSIRO Oceans and Atmosphere Flagship, Aspendale, Victoria, Australia
[e] Central Science Laboratory, University of Tasmania, Hobart, Tasmania, Australia
[f] Environmental Research Institute of the Supervising Scientist, Department of the Environment, Darwin, Northern Territory, Australia

ARTICLE INFO

Article history:
Received 6 November 2014
Received in revised form 2 June 2015
Accepted 5 June 2015
Available online 12 June 2015

Keywords:
Aerosol
Iron
Trace metals
Labile
Bioavailable iron
Cape Grim
Southern Ocean

ABSTRACT

Deposition of iron (Fe) bearing aerosols to Fe deficient waters of the Southern Ocean may drive rapid changes in primary productivity, trophic structure and the biological uptake of carbon dioxide. The fractional solubility (i.e., the ratio of water leachable Fe to total Fe) of aerosol Fe is an important variable determining its availability for biological uptake, and is a function of both particle type and the experimental conditions used to leach the particles. There have been few studies of fractional Fe solubility over the Southern Ocean where the aerosol loading is the lowest in the world. To investigate Southern Ocean aerosol Fe solubility, the fractional solubility of Fe was determined in cryogenically archived Southern Ocean aerosols. Samples were collected at the Cape Grim Baseline Air Pollution Station (CGBAPS), Tasmania, Australia from February 1999 to April 2000. Fractions determined included water soluble Fe (<0.45 μm), labile Fe (>0.45 μm; acetic acid and hydroxylamine hydrochloride leachable Fe) and refractory Fe (>0.45 μm; total digestion using nitric and hydrofluoric acids). Extremely low Fe mass concentrations were observed for baseline Southern Ocean air during the study period. An inverse hyperbolic relationship was observed between fractional Fe solubility (0.5 to 56%) and total Fe mass concentration (0.04 to 5.8 ng m^3; excluding an anomalously high sample). A peak of 4.6 ng m^3 of labile Fe occurred during May/June 1999 and was linked to atmospheric transport from South Western Australia over the Southern Ocean. Bioavailable Fe was estimated by summing the water soluble and labile Fe fractions, and this likely represents the upper bound of long range transport aerosol over the Southern Ocean. The results confirm previous reports of a range of fractional Fe solubility within all atmospheric particles measured and also suggest that a large fraction of the Fe from Australian mineral aerosols is labile and potentially bioavailable.

1. Introduction

Limitation of Southern Ocean primary productivity due to low iron (Fe) availability is well established and has been the focus of a large body of research (e.g. Martin et al., 1990, 1991; Blain et al., 2007). These waters are characteristically replete with nitrate and phosphate and depleted with respect to Fe. In-situ oceanic Fe-fertilisation experiments have demonstrated an almost explosive response of the ecosystem to relatively small additions of dissolved Fe (e.g. Coale et al., 2004; de Baar et al., 2005; Boyd et al., 2007). Inputs of new Fe to pelagic surface waters can occur through upwelling of deep waters (de Baar et al., 1995), deep winter mixing and entrainment (Bowie et al., 2014; Tagliabue et al., 2014), transport from continental margins by ocean currents (Johnson et al., 1999; Elrod et al., 2004), from sea-ice and ice bergs (Sedwick and DiTullio, 1997; Lannuzel et al., 2007, 2008; Raiswell et al., 2008), hydrothermal vents (Tagliabue et al., 2010), deep winter mixing (Tagliabue et al., 2014), and atmospheric aerosol deposition (e.g. Jickells et al., 2005). Aerosol deposition to remote Southern Ocean surface waters is extremely low ranging from 0.3 to 2.5 mg m^{-2} d^{-1}, and has been investigated in relation to the distribution and transport of mineral dust (Duce et al., 1991; Luo et al., 2005; Mahowald et al., 2005; Bowie et al., 2009) and the episodic input of volcanic ash (Narcisi et al., 2005). Episodic changes in mineral dust deposition to the Southern Ocean have been linked to 20th-century climate change and land use modification (Bhattachan and D'Odorico, 2014). Mineral dust proxy records from Antarctic ice cores (Edwards et al., 2006; Gaspari et al., 2006; Spolaor et al., 2012; Vallelonga et al., 2013) and Southern Ocean marine sediments from several regions (e.g. Moore et al., 2000; Martínez-Garcia et al., 2009; Smetacek et al., 2012) display higher deposition rates during glacial stages. Recent Southern Ocean marine sediment studies link enhanced glacial atmospheric Fe

* Corresponding author.
E-mail address: holly.winton@postgrad.curtin.edu.au (V.H.L. Winton).

http://dx.doi.org/10.1016/j.marchem.2015.06.006
0304-4203/

deposition to higher rates of Southern Ocean primary productivity (Martínez-García et al., 2014). While other studies postulate that higher rates of Fe inputs to the Southern Ocean during glacial periods were sourced from the upwelling of water enriched by sediments (Latimer and Filippelli, 2001; Latimer et al., 2006).

Aerosol Fe bioavailability data is required to constrain the biogeochemical impact of present and past atmospheric Fe variability. Aerosol Fe bioavailability will depend on the residence time of the Fe aerosol in the euphotic zone, and thus it is a function of its chemical composition and physical characteristics (e.g. particle size, surface area). Therefore, an upper limit of aerosol Fe bioavailability can be estimated by measuring the instantaneous water solubility (i.e., the concentration of Fe that passes through a 0.2 or 0.45 μm aerosol-laden filter when leached with ultra-pure water) and the labile Fe fraction (i.e., a chemically defined measure using weak acid to estimate the portion of the particulate trace metal pool that is potentially bio-available on the time frame of phytoplankton generation (days) (Berger et al., 2008)) from aerosol particles over longer time scales (Berger et al., 2008; Boyd et al., 2010). Reported values of the Southern Ocean fractional Fe solubility (i.e., the ratio of water leachable Fe to total Fe) range from 0.01 to 90% (Edwards and Sedwick, 2001; Mahowald et al., 2005; Bowie et al., 2009; Baker and Croot, 2010; Heimburger et al., 2013a). This large range may reflect differences in mineral dust concentrations, particle size, atmospheric weathering, cloud chemistry and aerosol leaching methods (Zhuang et al., 1990, 1992; Spokes and Jickells, 1995; Chen and Siefert, 2003; Meskhidze et al., 2003; Bonnet and Guieu, 2004; Mackie et al., 2005; Baker and Jickells, 2006; Buck et al., 2006; Meskhidze and Nenes, 2006; Aguilar-Islas et al., 2010; Trapp et al., 2010). Laboratory studies have indicated that aerosol Fe solubility is enhanced by acid processing (Spokes et al., 1994; Desboeufs et al., 1999), although this relationship was not observed in the remote Atlantic and Pacific ocean (Hand et al., 2004; Baker et al., 2006). An alternative hypothesis for the observed solubility range is that it results from a mixture of aerosol Fe source types with different mineralogy and Fe solubilities (Sholkovitz et al., 2012). Sholkovitz et al. (2012) show that global scale fractional aerosol Fe solubility displays an inverse hyperbolic relationship with the total Fe mass concentration. This relationship is consistent with a low Fe solubility for mineral dust (~1–2%) and the presence of other soluble Fe sources such as those originating from fire and oil combustion with higher Fe solubilities (Chuang et al., 2005; Guieu et al., 2005; Sedwick et al., 2007; Luo et al., 2008; Sholkovitz et al., 2009; Kumar et al., 2010; Paris et al., 2010; Ito, 2011; Gao et al., 2013). Gao et al. (2013) recently measured soluble Fe as Fe(II) in the Southern Ocean southwest of Australia and this species of Fe has been operationally defined as labile (e.g. Chen and Siefert, 2004). Studies of labile Fe species (Fe(II)) over the Atlantic Ocean show that the highest percentage of labile Fe (mean value of 32%) was observed in winter corresponding to low mass concentrations of total Fe and air mass trajectories influenced by anthropogenic activities over North America (Chen and Siefert, 2004). Conversely, the lowest concentrations of labile Fe (mean value 5%) were observed in summer with higher mineral aerosol concentrations associated with African dust.

This study reports fractional Fe solubility and estimates of the upper bound of Fe bioavailability for Southern Ocean aerosols sampled from the Cape Grim Baseline Air Pollution Station (CGBAPS) in Tasmania, Australia. Data from the aerosol samples have previously been reported with respect to lead (Pb) pollution and its source apportionment (Bollhöfer et al., 2005).

2. Methods

2.1. Sampling site

This study used archived aerosol filter samples collected from February 1999 to April 2000 at CGBAPS (40.68° S, 144.69° E), located at the northwest tip of Tasmania, Australia (Fig. 1). Fractions of filters were previously studied for Pb isotopic composition and are described in detail by Bollhöfer et al. (2005). Samples were collected during baseline conditions using a sector-controlled ultra-trace clean aerosol filter system suspended 70 m above the ground (164 m a.s.l.) on a communication tower (~100 m from the ocean, adjacent to 94 m high coastal cliffs). Meteorological baseline air conditions for CGBAPS are described by Ayers et al. (1987) and occur when the winds are from the west to southwest (wind direction from 190 to 280°) (Fig. 1) and total aerosol particle counts are <600 cm^3. These conditions occur ~30% of the time (Keywood, 2007) and are representative of air masses over the remote Southern Ocean.

2.2. Sample collection

Stringent trace-metal clean techniques were used throughout the sampling campaign (Bollhöfer et al., 2005). Briefly, aerosols were collected on 47 mm acid-cleaned polytetrafluoroethylene (PTFE) filters (0.45 μm front, 60 μm back) in single-stage perfluroalkoxy alkane (PFA) filter assemblies (acid-cleaned). The filter assembly housing consisted of trace-metal clean cylindrical inlet units, with a baseline sector controlled pump at the tower base and a pneumatically actuated seal on the top of the inlet unit. The samples were collected over time periods varying from one to seven weeks. Exposure blanks (n = 5), collected with every 3rd to 4th sample, were run as for normal samples but the pump switched off (Bollhöfer et al., 2005). These exposure blanks were used to determine the Fe contribution from sampling, laboratory procedures and analysis. Air volumes were measured using a calibrated gas flow meter. Thirteen cryogenically archived (−18 °C) filter sub-samples (Supplementary Table 1) from the Bollhöfer et al. (2005) study were used in this work to investigate the aerosol Fe mass concentration and fractional Fe solubility.

2.3. Partial filter sizing

During the original study, the filters were cut into halves or quarters with an acid cleaned stainless steel scalpel blade (Bollhöfer et al., 1999, 2005). These filter sub-samples were the focus of this aerosol Fe study. Filter samples were visually inspected in a laminar flow hood under clean-room conditions with minimal handling.

2.4. Aerosol iron leaching experiments

All bottles and filtration parts used in the Fe leaching experiments were acid-cleaned following GEOTRACES protocols (Cutter et al., 2010). Leaching experiments were conducted sequentially using a trace metal clean flow-through reactor (Fig. 2) (e.g. Wu et al., 2007; Aguilar-Islas et al., 2010). This reactor consisted of the sub-sampled filter supported on acid-cleaned 0.45 μm acid cleaned backing filter that was mounted in a single-stage PFA filter assembly with a PFA funnel front face. Leaching solutions were pulled through the reactor under vacuum, into 250 ml low-density polyethylene bottles (LDPE). The PTFE filters were hydrophobic and required exposure to high-purity methanol to initiate water flow. Prior to the leaching experiments, the system was rinsed with several litres of ultra-pure water (>18 MΩ-cm) and ultra-pure 1% HCl (baseline Seastar), followed by another ultra-pure water rinse.

2.4.1. Soluble iron

The instantaneous water soluble Fe fraction (Fig. 2) was investigated using two successive 50 ml aliquots ("a" and "b") of ultra-pure water. The mean procedural blank (n = 10) for this Fe fraction was 0.07 ± 0.005 nmol g^{-1} of soluble Fe. The mean exposure blank (n = 5) was 0.1 ± 0.003 nmol g^{-1} of soluble Fe. The mean ultra-pure water blank (n = 5) was 0.001 ± 0.002 nmol g^{-1}. On average 90% of the water soluble Fe was leached in the first leach. Other ultra-pure water leaching

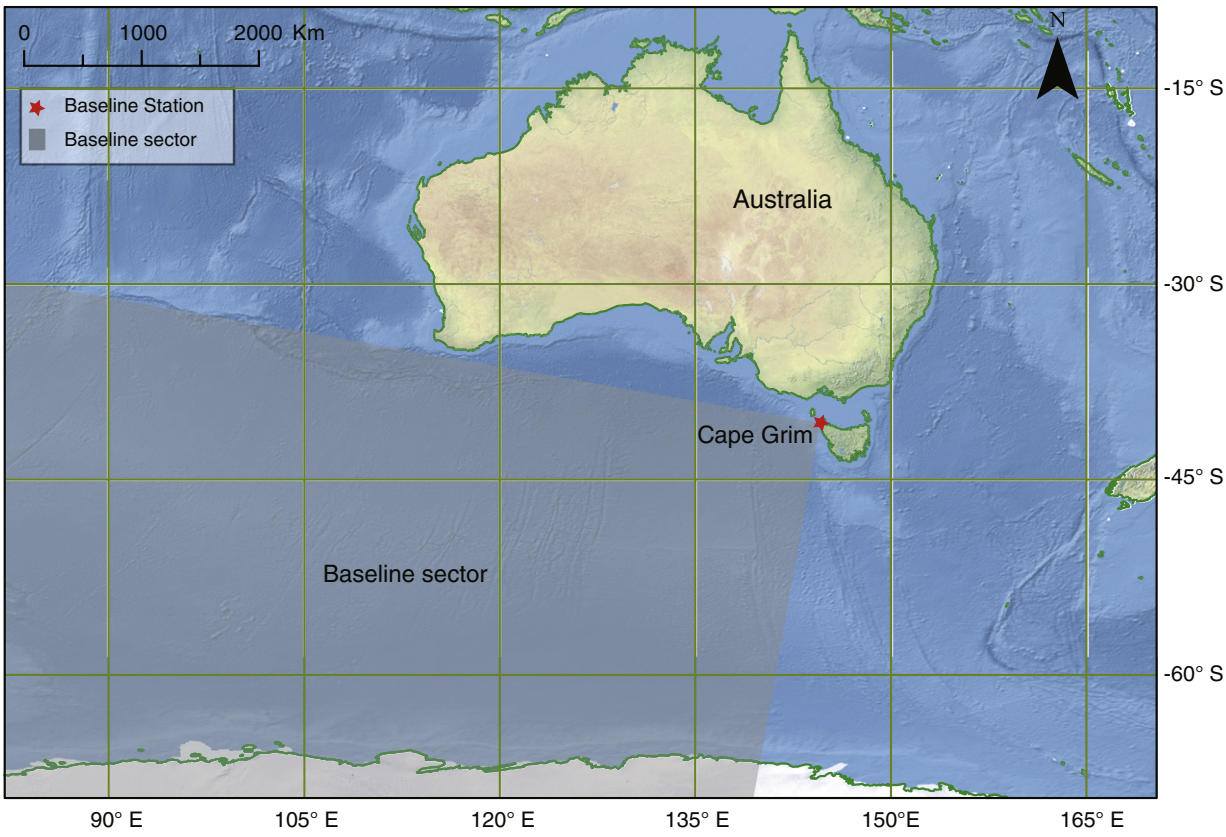

Fig. 1. Map of Australia and the Southern Ocean highlighting the baseline sector associated with CGBAPS.

schemes using multiple leaches have shown that the concentration of soluble Fe exponentially decreases with each successive water leach (e.g. Buck et al., 2006). Thus, even the small volume of leaching solution in the first leach will have captured the majority of instantaneous water soluble Fe.

2.4.2. Labile iron

The method of Berger et al. (2008) was used to determine the labile Fe fraction (Fig. 2) of the aerosol samples. A similar weak acid leaching method to determine labile Fe in aerosols was carried out by Chen and Siefert (2003). The Berger et al. (2008) method uses an acetic acid (HAc) and hydroxylamine hydrochloride ($NH_2OH \cdot HCl$) leach to determine the reactive Fe fraction. A similar method was used in this study with the exception that the filters were water leached prior to exposure to HAc and $NH_2OH \cdot HCl$. In this study, the water leached filters were placed in acid-washed vials, dried under a laminar flow hood and leached with 25% ultra-high purity HAc (Seastar Baseline® 99.9%, <20 ppt Fe) and 0.02 M $NH_2OH \cdot HCl$ (Acros Organics, Belgium, 99%) at 90 °C for 10 min. The short heating step of 90–95 °C is used to access metals found in intracellular proteins that are associated with phytoplankton (Hurst and Bruland, 2007; Berger et al., 2008). This leaching method liberates trace metals associated with biogenic material, Fe

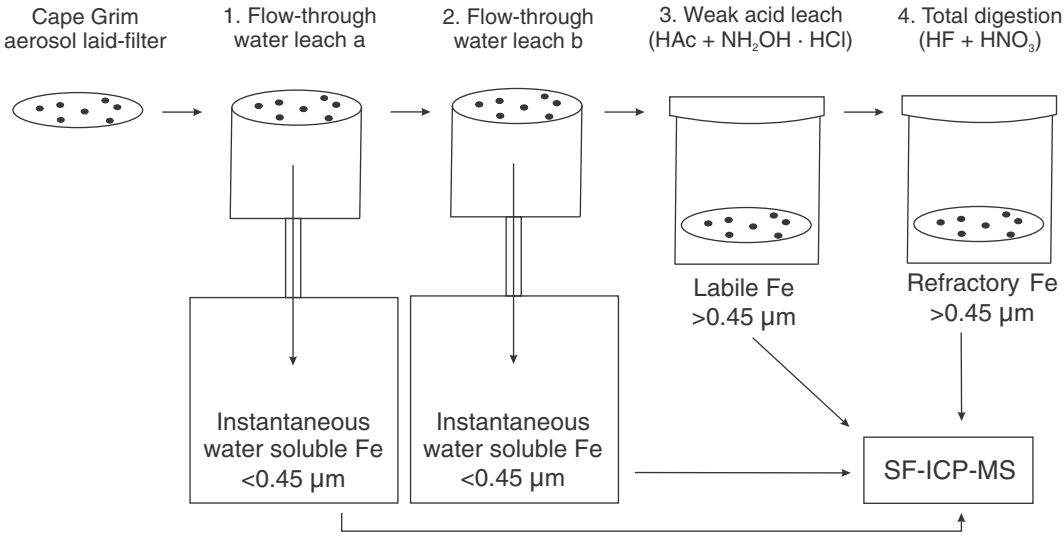

Fig. 2. Schematic showing the different extraction stages to leach soluble, labile and refractory iron from Cape Grim marine aerosols.

and manganese oxyhydroxides and metals that may be adsorbed onto the surface of aluminosilicate clay minerals. Windblown diatoms have been observed in high elevation ice cores significantly inland from the ocean (Burckle et al., 1988). Thus, the possibility that phytoplankton cells are transported in baseline marine air masses cannot be ruled out, although we acknowledge that they most likely constitute a relatively minor mass of the total aerosol loading. The mean labile procedural blank (n = 5) and exposure blank (n = 5) concentrations were 0.03 ± 0.003 and 0.8 ± 0.07 nmol g^{-1} of Fe, respectively. Two exposure blanks were found to have exceptionally high labile Fe concentrations possibly from random contamination (water solubility associated with those exposure blanks did not have high values). Excluding these two high values, exposure blanks averaged 0.2 ± 0.001 nmol g^{-1} of Fe, comparable to the labile procedural blank and water soluble exposure blank concentrations. This blank value was used in labile Fe calculations.

2.4.3. Refractory iron

The refractory Fe fraction (>0.45 μm) was determined following recommendations from the 2008 GEOTRACES intercalibration experiment for the analysis of marine aerosols (Morton et al., 2013). All digestions were carried out under high-efficiency particulate arrestance (HEPA) filtered air, in a total-exhausting clean-air (ISO Class 5), hot block unit (SCP Science, Canada) fitted with an acid scrubber unit. The leached sample filters and filter blanks were digested at 95 °C for 12 h with concentrated ultra-pure nitric acid (HNO_3, 0.5 ml, Seastar Baseline®) and ultra-pure hydrofluoric acid (HF, 0.5 ml, Seastar Baseline®) in capped PFA vials (15 ml, Savillex) following Bowie et al. (2010). At the end of the digestion, the samples were evaporated to dryness, reconstituted in 1% ultra-pure HNO_3 (10 ml final volume, Seastar Baseline®) and stored at 25 °C for ~12 h before analysis. A certified reference material (MESS-3, National Research Council, Canada) of marine sediment was digested alongside the samples to test the digestion recovery procedure. Total digestion recovery for Fe from the CRM was ~90 ± 1.2% (n = 3). Mean refractory procedural blank (n = 3) and exposure blank (n = 5) concentrations were 0.2 ± 0.01 nmol g^{-1} of Fe and 1.0 ± 3.7 nmol g^{-1} of Fe respectively. Two filter blanks were found to have high Fe levels (8.0 nmol g^{-1} and 1.7 nmol g^{-1} of Fe). The digestion of aerosol filters using concentrated HNO_3 and HF at 95 °C could have leached out additional impurities in the PTFE filter than the Bollhöfer et al. (1999) acid cleaning step employed specifically for Pb analysis. Therefore, the high blank levels possibly resulted from a lack of exposure of HF to the PTFE filter substrate prior to sampling (Bollhöfer et al., 1999).

2.4.4. Total iron

The total Fe loading of the filters was estimated as the sum of the individual Fe fractional masses from each step and is given in Eqs. (1) to (3).

$$\text{Water soluble Fe} = \text{water soluble Fe leach “a”} + \text{water soluble Fe leach “b”} \quad (1)$$

$$\text{Bioavailable Fe} = \text{water soluble Fe} + \text{labile Fe} \quad (2)$$

$$\text{Fe total} = \text{bioavailable Fe} + \text{refractory Fe}. \quad (3)$$

2.5. Iron determination by sector-field inductively coupled plasma mass spectrometry

All samples and standards were prepared on a similar matrix basis. Water soluble Fe leachates and total digestion solutions were acidified to 1% (v/v) with ultra-pure HNO_3 (Seastar Baseline®) and spiked with an Indium (In) internal standard. Labile leachates were diluted, and spiked with In and presented to the instrument as a 2.5% (v/v) HAc and 0.02 M $NH_2OH{\cdot}HCl$ solution and 1% (v/v) ultra-pure HNO_3 (Seastar Baseline®). The analysis of the water soluble and labile Fe leachate fractions occurred within 24 h of leaching. All samples were analysed by sector-field inductively coupled plasma mass spectrometry (SF-ICP-MS, Thermo Fisher Scientific ELEMENT 2) at the University of Tasmania. Samples were introduced using an auto-sampler housed in a laminar flow clean-air hood. Typical operating conditions are reported in Supplementary Table 2. Isobaric ^{56}Fe interferences (e.g. $^{40}Ar^{16}O$ and $^{40}Ca^{16}O$) were resolved using a mass resolution of >4000 amu (10% valley definition, medium resolution). Instrumental blanks (1% HNO_3 and 2.5% (v/v) HAc and 0.02 M $NH_2OH{\cdot}HCl$) and a QC standard were measured throughout the analysis sequence at regular intervals. Internal standard normalised ^{56}Fe intensities were quantified using “matrix matched” external standards prepared by serial dilution from traceable commercial primary standards. The results were blank subtracted and corrected for dilution.

2.6. Major cation and anion

Major cation and anion measurements for the period between January 1999 and August 2000 have previously been reported in Keywood et al. (2004), and we use the sodium, sulfate and nitrate data here. Oxalate, not previously reported, was also measured in these samples following the same procedure. The major ion data were obtained using a “Goldtop sampler” installed with a PM10 (particle diameter <10 μm) inlet at CGBAPS (Ayers et al., 1990). Particles were collected on Pallflex filters (EMSB TX 4OH, 120-WW) on a weekly basis. The filter was wetted with methanol before being extracted in 5 ml of ultra-pure water. The sample was then preserved using 1% chloroform. Anion and cation concentrations were determined by suppressed ion chromatography (IC) using a Dionex DX500 gradient ion chromatograph. Anions were determined using an AS11 column and an ASRS ultra-suppressor. Cations were determined using a CS12 column and a CSRS ultra-suppressor.

3. Results

3.1. Aerosol iron mass concentrations

Baseline aerosol concentrations for the different Fe fractions were estimated from the filters by Eq. (4) (assuming a uniform aerosol loading of the filters) and are summarised in Table 1.

$$\text{Aerosol concentration} = \text{Fe fraction mass} * \text{filter sub-sample fraction} / \text{air volume}(m^3; \text{standard temperature and pressure}). \quad (4)$$

With the exception of sample CG5 (4–16 March 1999), extremely low total Fe aerosol mass concentrations, compared to other aerosol Fe studies on a global scale (Sholkovitz et al., 2012), were found and ranged from 0.034 to 5.86 ng m^{-3}. Sample CG5 sampled only 5 m^3 of air but displayed total Fe aerosol concentrations 25 times greater (147.81 ng m^{-3}) than the next largest aerosol sample. This sample was almost entirely comprised of refractory Fe and may have been exposed to local (non-baseline) air. The sample was subsequently excluded from the estimates and further discussion.

Table 1
Fractional aerosol iron concentrations in Southern Ocean baseline air.

Fe fraction	Range (ng m^{-3})	Geometric mean (ng m^{-3})*
Total Fe	0.04 to 5.8	0.8
Refractory Fe	<0.02 to 5.7	0.2
Labile Fe	0.01 to 4.6	0.1
Soluble Fe	0.01 to 0.3	0.07

* n = 13.

3.2. Aerosol iron fractions

The range and geometric mean for the different fractions are shown in Table 1. The total Fe geometric mean mass concentration of 0.77 ng m^{-3} was ~11 times that of soluble Fe (0.07 ng m^{-3}), ~4.8 times the labile Fe (0.16 ng m^{-3}) and ~3.1 times the refractory Fe (0.24 ng m^{-3}) mass concentrations. Fractional estimates relative to total Fe ranged from 0.5% to 56% for soluble Fe, 1.5% to 94.0% for labile Fe, and 4.6% to 97.0% for refractory Fe. The order of the geometric mean fractional estimates was soluble Fe (15%) < labile Fe (32%) < refractory Fe (48%).

3.3. Atmospheric iron dry deposition flux estimates

Estimates of the Fe dry deposition rate (F_{dry}) to adjacent Southern Ocean surface waters were calculated using Eq. (5) from the total and soluble aerosol Fe concentrations ($C_{aerosol}$) using a dry deposition velocity (V_{dry}) of 1.3 cm s^{-1} (Ezat and Dulac, 1995) following Heimburger et al. (2012), and are reported in Table 2. This deposition velocity is based on the dry deposition model of Slinn and Slinn (1980) following the "100-step method" (Dulac et al., 1989) which takes into consideration the size dispersion of particles. We assume a constant deposition velocity is appropriate for the Southern Ocean, as i) the particle size has a narrow size distribution and thus the dry deposition fluxes will exhibit little variability compared to a wide particle size distribution (Arimoto et al., 1985), and ii) the mean wind speeds at Cape Grim have little temporal variability. Furthermore, Duce et al. (1991) report deposition velocities of 0.4 cm s^{-1} for the open ocean and 2 cm s^{-1} for coastal regions and the value of 1.3 cm s^{-1} is within this range.

$$F_{dry} = C_{aerosol} V_{dry\ deposition} \quad (5)$$

4. Discussion

4.1. Baseline iron mass concentrations

Atmospheric Fe mass loadings from 1999 to 2000 are shown in Fig. 3a–d. Total Fe displayed maximum concentrations during May/June 1999 and November 1999 with peak Fe mass concentrations of 5.15 ng m^{-3} and 5.86 ng m^{-3}, respectively. The lowest concentrations occurred from August to November 1999 (austral winter/spring), with a minimum mass concentration of 0.034 ng m^{-3}. The total Fe mass concentrations are amongst the lowest Fe mass concentrations reported in the literature. For example, Bowie et al. (2009) reported total Fe mass concentrations between 5 and 17 ng m^{-3} for marine aerosols collected in a similar region south of Tasmania but sampling all wind sectors. A global compilation of the total aerosol Fe mass data suggests concentrations can reach up to 147 ng m^{-3} for the Southern Hemisphere (Fig. 4) (Sholkovitz et al., 2012). Baseline total aerosol Fe mass loadings are similar to those reported for Syowa Station, coastal East Antarctica (Kobayashi et al., 2010). However, they are lower than estimates over the southwest Australian sector of the Southern Ocean and coastal East Antarctica which average 19 ng m^{-3} and 26 ng m^{-3} respectively (Gao et al., 2013). The authors suggest that the air masses over coastal East Antarctica are influenced by local Antarctic dust, as the total aerosol Fe concentrations were higher than the Southern Ocean, and the aerosols have a coarse particle size distribution.

While the two total Fe peaks were similar with respect to mass concentration, they displayed different characteristics with respect to the leached Fe fractions suggesting different sources and bioavailability. For example, the May/June 1999 Fe peak was primarily composed of labile Fe (~90%) with little refractory Fe (Fig. 3). Conversely, the November 1999 total Fe peak was comprised primarily of refractory Fe, however the contribution of labile Fe to the bioavailable Fe fraction was relatively minor compared to the water soluble contribution. Thus, while the total Fe mass concentrations were similar, the potential bioavailability of the Fe represented by the two peaks was not. The May/June peak was associated with a peak in radon (Fig. 3e) reported by Bollhöfer et al. (2005). Radon is emitted from crustal materials and has a relatively short half-life (3.8 days) making it useful as a tracer of continental air masses (Porstendorfer et al., 1994; Zahorowski et al., 2004). Air mass back trajectories reported by Bollhöfer et al. (2005) combined with the radon data suggest that the labile Fe peak is related to atmospheric transport over South Western Australia.

The highest soluble Fe mass concentrations occurred in February–March 1999 (0.55 ng m^{-3}) and February–March 2000 (0.25 ng m^{-3}; Fig. 3a). However, the soluble Fe concentrations exhibited an extremely low geometric mean soluble Fe concentration of 0.07 ng m^{-3} for the entire data set. These soluble Fe concentrations in baseline air are lower than those reported as Fe(II) for the southwest Australian sector of the Southern Ocean and coastal East Antarctica that range from 0.13–1.3 ng m^{-3} (Gao et al., 2013). Variability in soluble Fe, in this study, essentially tracked the radon concentrations demonstrating a link with continental air masses (Supplementary Fig. 1a). These radon episodes (Fig. 3e) occurred during baseline intervals in May/June 1999, August/October 1999 and January/April 2000 (Bollhöfer et al., 2005). Not surprisingly these time periods encompass the highest Pb concentrations (Fig. 3f) reported by Bollhöfer et al. (2005) which further highlights the link between soluble Fe and continental air masses and potentially anthropogenic emissions.

While, the variability between the labile and soluble Fe with the Bollhöfer et al. (2005) radon and Pb data seemed consistent, the refractory Fe variability bore little resemblance to these time series. The independence of the refractory Fe from the other Fe fractions and radon data was unexpected and difficult to rationalise. For example, the highest refractory Fe concentration occurred during November 1999, coincident with low radon concentrations. A plausible explanation is that this

Table 2
Dry deposition iron fluxes of Southern Ocean baseline air.

Sample	Soluble Fe concentration (ng m^{-3})	Soluble Fe flux (nmol m^{-2} d^{-1})[a]	Total Fe concentration (ng m^{-3})	Total Fe flux (nmol m^{-2} d^{-1})[a]
CG4	0.55 ± 0.04	11 ± 6	1.9 ± 0.1	38 ± 20
CG9	0.17 ± 0.01	3.3 ± 2	0.76 ± 0.02	15 ± 8
CG10	0.34 ± 0.03	6.8 ± 3	5.1 ± 0.2	100 ± 50
CG14	0.01 ± 0.01	0.17 ± 0.1	1.8 ± 0.06	36 ± 20
CG15	0.07 ± 0.01	1.4 ± 0.7	0.26 ± 0.01	5.2 ± 3
CG17	0.04 ± 0.01	0.76 ± 0.4	0.28 ± 0.01	5.7 ± 3
CG18	0.08 ± 0.01	1.7 ± 0.9	0.33 ± 0.01	6.7 ± 3
CG26	0.01 ± 0.01	0.3 ± 0.2	0.68 ± 0.02	14 ± 7
CG28	0.01 ± 0.01	0.14 ± 0.1	0.04 ± 0.00	0.75 ± 0.4
CG23	0.08 ± 0.01	1.7 ± 0.8	5.8 ± 0.2	120 ± 60
CG35	0.25 ± 0.01	5.1 ± 3	0.45 ± 0.01	9.0 ± 5
CG37	0.09 ± 0.01	1.7 ± 0.9	1.4 ± 0.04	27 ± 10
CG40	0.06 ± 0.01	1.3 ± 0.6	1.3 ± 0.04	27 ± 10

[a] The uncertainty in dry deposition fluxes was calculation by propagation of error of the analytical uncertainty and uncertainty in the deposition velocity assumed to be 50%.

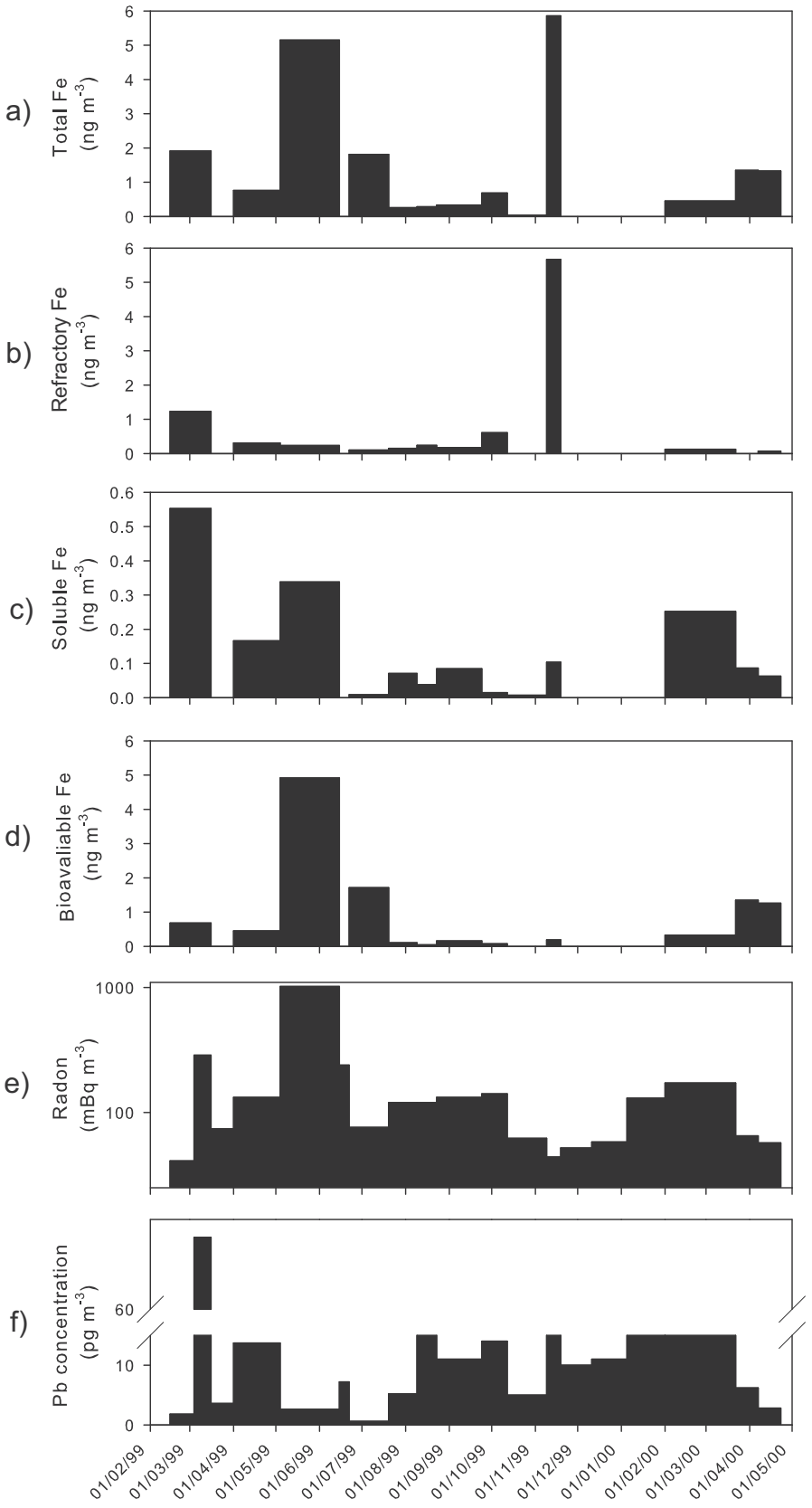

Fig. 3. Time series of aerosol Fe mass concentrations excluding CG5. a) Total Fe concentration, b) refractory Fe concentration, c) soluble Fe concentration, d) bioavailable Fe concentration (i.e., the sum of soluble and labile Fe fractions), e) radon concentration (data source: Bollhöfer et al., 2005), and f) Pb concentration (data source: Bollhöfer et al., 2005).

peak was due to local material blown up to the tower from the cliff face rather than long range transport aerosol. A single mineral grain could contaminate these low concentration samples. However, based on the sample's aerosol Fe mass concentration the data appears uncontaminated by sampling and handling procedures. Bollhöfer et al. (2005) ruled out local soil dust contamination in these aerosol samples by comparing

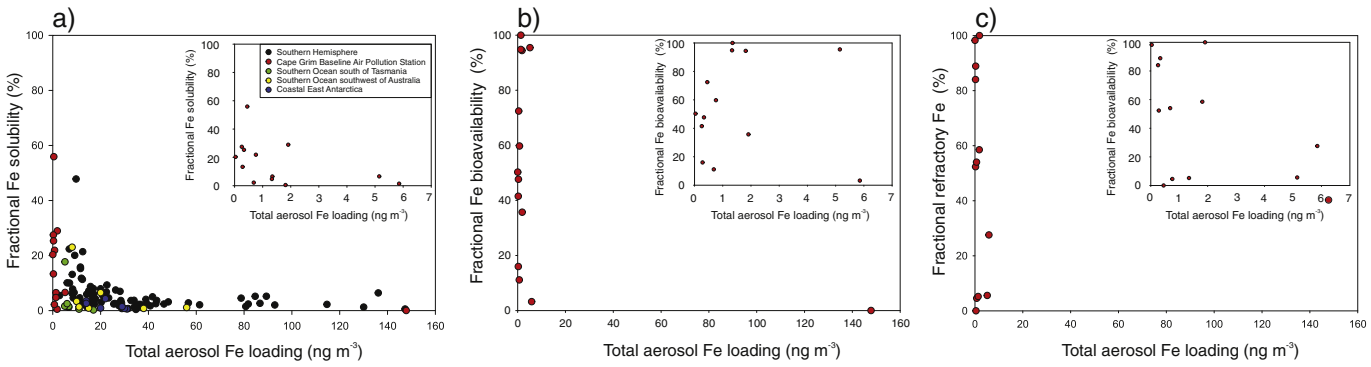

Fig. 4. a) Cape Grim total aerosol Fe mass concentration versus fractional Fe solubility superimposed upon Southern Hemispheric data set (data source: Bowie et al., 2009; Sholkovitz et al., 2012; Gao et al., 2013). Top right inset: Cape Grim data expanded excluding CG5 that sampled a low volume of air. b) Cape Grim total aerosol Fe mass concentration versus fractional Fe bioavailability. c) Cape Grim total aerosol Fe mass concentration versus fractional refractory Fe.

the Pb isotopic composition of the aerosols with that of local soil. Nevertheless, as discussed in the results section, a filter sample from March 1999 was excluded from further assessment due to suspected contamination from local mineral dust sources. If the November 1999 data point is similarly excluded from the interpretation, the refractory Fe variability becomes similar to the soluble Fe and consistent with the radon data (Supplementary Fig. 1b).

4.2. Dry deposition estimates of soluble and total iron

Crude estimates of soluble and total Fe dry deposition fluxes associated with the aerosol samples are reported in Table 2 and range from 0.1 ± 0.07 to 7 ± 3 nmol m^{-2} d^{-1} for soluble Fe and 0.8 ± 0.4 to 116 ± 60 nmol m^{-2} d^{-1} for total Fe over the period April 1999 to March 2000. This period was considered to include samples collected

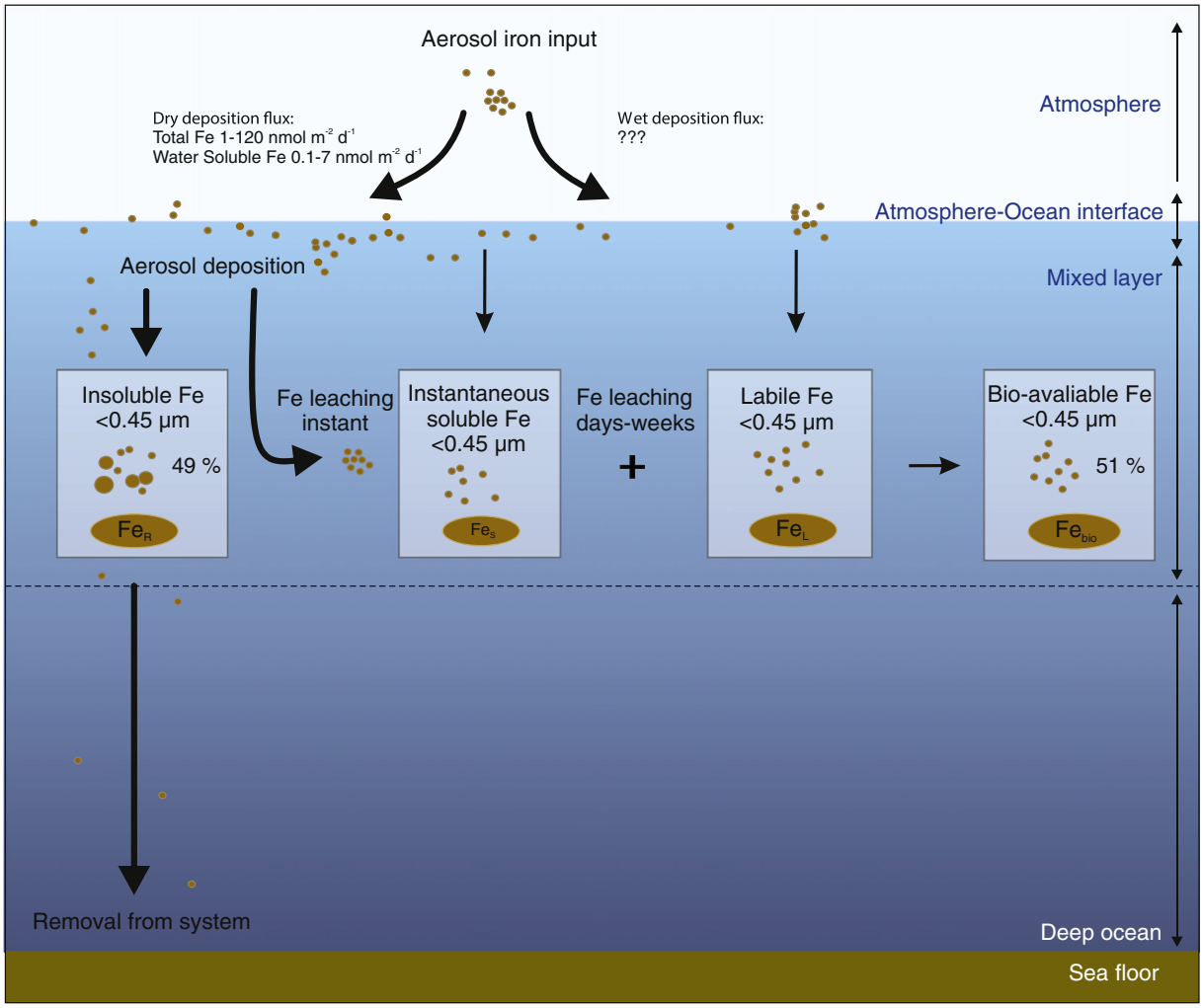

Fig. 5. Schematic of aerosol iron fractions that are potentially bioavailable for uptake by plankton in the Southern Ocean. Fe_R: refractory Fe, Fe_S: soluble Fe, Fe_L: labile Fe, Fe_{BIO}: bioavailable Fe.

with the largest volumes of air over an entire 12 month period, and also closely aligns with the work of Bollhöfer et al. (2005) allowing comparison with their Pb data. The Fe flux estimates for baseline air over Southern Ocean in this study are compared to other aerosol studies from the Southern Ocean. The mean soluble Fe flux (~2 ± 1 nmol m^{-2} d^{-1}) is in good agreement with fluxes of 2.4–7.4 nmol m^{-2} d^{-1} reported by Bowie et al. (2009), 0.04–3.2 nmol m^{-2} d^{-1} reported by Wagener et al. (2008), and 1.8–7.3 nmol m^{-2} d^{-1} reported by Baker et al. (2013) for the South Atlantic. The estimates in this study are lower than those reported at Kerguelen Island, Southern Ocean (400 nmol m^{-2} d^{-1}) where local dust influences the aerosol sample (Heimburger et al., 2013b). Estimates in baseline air may be more representative of the broader Southern Ocean region south of Australia, as the marine air was collected at a higher elevation above the boundary layer and at a site free from local pollution. Estimates of total Fe dry deposition at CGBAPS are significantly lower than those estimated at Kerguelen Island (500–700 nmol m^{-2} d^{-1}) (Heimburger et al., 2013b), at Crozet Island (900 nmol m^{-2} d^{-1}) (Planquette et al., 2007), and in the South Atlantic (100–300 nmol m^{-2} d^{-1}) (Baker et al., 2013). Heimburger et al. (2012) suggest dust fluxes during 2009–2010 were higher during winter and spring, and that the aerosols were crustal in origin. Whereas Heimburger et al. (2013b) showed no seasonal variability in aerosol Fe, they did find an anthropogenic contribution to the Southern Ocean during winter as shown by elevated elemental concentrations of Pb, As, Cr, Cu, and V.

4.3. Fractional iron solubility

The baseline fractional Fe solubility ranged from 0.5% to 56% during the study. Estimates of fractional Fe solubility in the South Atlantic are within this range (2.4% to 20%) (Baker et al., 2013). The lowest values (0.5% to ~3%) at CGBAPS were comparable to the low Fe solubility (1 to 2%) reported for mineral dust (e.g. Baker and Croot, 2010) at relatively high mass concentrations. Furthermore, the low fractional Fe solubility (0.58% to 6.5%) measured as Fe(II) over the southwest Australian sector of the Southern Ocean is thought to be influenced by local Antarctic dust sources (Gao et al., 2013). Mineral dust from Patagonia is also known to be transported into the southern South Atlantic Ocean and on the Antarctic Plateau (Gaiero et al., 2003, 2007; Delmonte et al., 2008). Similar to Sholkovitz et al. (2012), the data in this study displayed an inverse hyperbolic relationship (Fig. 4a) between the total Fe mass concentration and fractional Fe solubility. This relationship has been attributed to the mixing of low Fe solubility mineral dust and other soluble Fe aerosols from sources such as biomass burning and oil combustion (Sedwick et al., 2007). Sholkovitz et al. (2012) reported a synthesis of global aerosol Fe solubility data sets and concluded that the characteristic inverse hyperbolic relationship is common over large regions of the global ocean. Results here are different to other Southern Ocean data, i.e., at the 1–2% fractional Fe solubility limit of mineral dust, the total Fe mass concentrations are very low (<6 ng m^{-3}) compared to the rest of the Southern Ocean where they have been observed up to 140 ng m^{-3}. This aspect of the data may be explained by a lack of both mineral dust and other soluble Fe sources, such as biomass burning, in the exceptionally clean baseline air. Alternatively it is possible that the long cryogenic storage of the aerosol filters resulted in lower concentrations of instantaneously soluble Fe. Jeong et al. (2012) found that the dissolution of iron oxides was enhanced during freezing of aqueous dispersions of Fe oxides. However, the aerosol filters used in this study were stored frozen in a dark and dry environment and are not directly comparable. However, aerosols are archived in ice cores for comparatively longer time periods (e.g. 1 to 1000 years), and Fe solubility studies of ice cores have been used to estimate Fe fluxes and bioavailability. With regards to the instantaneous solubility, Antarctic ice core leaching studies in dilute hydrochloric acid and nitric acid (Edwards and Sedwick, 2001; Edwards et al., 2006; Gaspari et al., 2006; Koffman et al., 2014b) show that a large portion of the Fe bound in frozen mineral particles are not soluble and require up to three months to leach into solution. Furthermore, fractional Fe solubility estimates reported here are within the range of those reported for other studies (e.g. Baker and Croot, 2010) and in particular for aerosols sampled in the Southern Ocean south of Tasmania (Fig. 4a) (Bowie et al., 2009).

4.4. Estimates of iron bioavailability

In order to determine the upper bound of bioavailable trace metals in seawater sourced from atmospheric particles, measurement of both the soluble and labile fractions are necessary (Berger et al., 2008). Commonly used instantaneous water leaching schemes have been suggested to underestimate the fraction of Fe that dissolves in the oceanic mixed layer, as they do not take into account the longer residence time of aerosols in the euphotic zone. Thus, an additional leach is needed to estimate the longer-term release of Fe from atmospheric particles during their residence time in the surface ocean mixed layer (Boyd et al., 2010). This study followed the Berger et al. (2008) rational to estimate the fraction of labile Fe in aerosols. The heating step in this method may overestimate the labile fraction of Fe in aerosols, causing dissolution of Fe that would normally have low bioavailability. Iron solubility increases with temperature (Schwertmann, 1991), and thus the heating step may recover more Fe than the intracellular fraction alone. Despite this, leaching schemes employed to access the labile Fe pool are operationally defined. They are designed to mimic biological processes that take time, but do so in a much shorter and practical timescale in the laboratory. Currently, no leaching scheme takes into account all processes affecting the bioavailability of Fe upon its deposition in the upper water column. For example, grazing is known to impact the bioavailability of Fe contained in particles (Barbeau et al., 1996). Other studies have indicated that the conversion of Fe from particle to dissolved phase in seawater can take place due to photochemistry (Croot et al., 2008; Ellwood et al., 2015). Recently, Lis et al. (2015) observed a relationship between the uptake rate constant of Fe and the surface area of several phytoplankton species. An upper limit to the rate at which Fe-limited phytoplankton can uptake Fe suggests that alternative uptake mechanisms are an advantage in Fe-limited waters, such as a reduction in cell size, or the utilization of Fe from the colloidal or particulate fraction (Nodwell and Price, 2001; Rubin et al., 2011). Colloidal Fe has been found to be an important fraction of the bioavailable Fe pool (Kuma and Matsunaga, 1995; Aguilar-Islas et al., 2010), and further research is required to estimate this fraction over the Southern Ocean.

The leaching scheme used in this study mimics the bi-modal release of Fe, i.e., i) instantaneous soluble Fe and ii) longer term dissolution that is mediated by microbes and/or ligands and photochemistry in the surface mixed layer (Wagener et al., 2008; Wuttig et al., 2013), thereby allowing an estimate of the upper limit of Fe bioavailability over the Southern Ocean. Fractional bioavailable Fe was calculated by summing the fractional Fe solubility and fractional Fe lability (Eq. (3)). Fractional Fe bioavailability ranged from 3 to 100% of the total Fe (Fig. 4b). More bioavailable Fe data is required to investigate the relationship between the total Fe mass concentration and fractional Fe bioavailability and mixing of mineral dust versus combustion aerosol sources (Fig. 4b).

New aerosol Fe supply by dry deposition to the Southern Ocean and the fractions of Fe (soluble, labile, bioavailable and refractory) that are leached from the aerosols upon deposition into surface waters is illustrated in Fig. 5. No wet deposition data is available at the CGBAPS, however estimates of Fe concentrations in rain at Kerguelen Island suggest a concentration of 17 to 32 μg m^{-2} with a fractional Fe solubility of ~70% in rain water (Heimburger et al., 2013a). Wet deposition fluxes of 5.4 to 231 nmol m^{-2} d^{-1} of soluble Fe and 41–-1100 nmol m^{-2} d^{-1} of total Fe for the South Atlantic have been estimated by Baker et al. (2013), and significantly higher wet deposition fluxes of 3700 μmol m^{-2} d^{-1} for the New Zealand region of the South

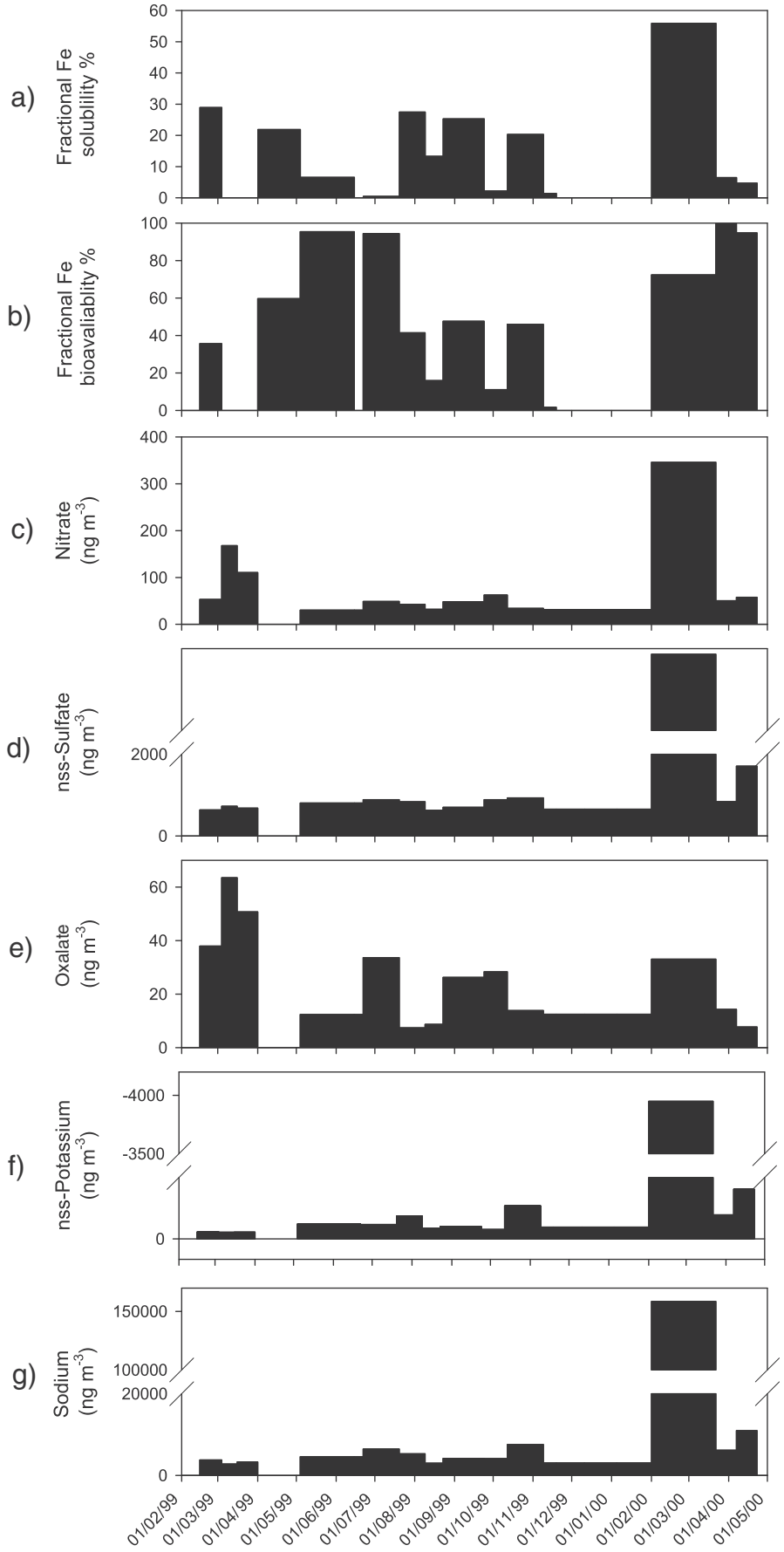
a)
Fractional Fe solubility %
60
50
40
30
20
10
0
b)
Fractional Fe bioavaliablity %
100
80
60
40
20
0
c)
Nitrate (ng m-3)
400
300
200
100
0
d)
nss-Sulfate (ng m-3)
2000
0
e)
Oxalate (ng m-3)
60
40
20
0
f)
nss-Potassium (ng m-3)
-4000
-3500
0
g)
Sodium (ng m-3)
150000
100000
20000
0
01/02/99
01/03/99
01/04/99
01/05/99
01/06/99
01/07/99
01/08/99
01/09/99
01/10/99
01/11/99
01/12/99
01/01/00
01/02/00
01/03/00
01/04/00
01/05/00

Pacific westerlies have been estimated by Halstead et al. (2000). Half of the upper bound of mean fractional Fe bioavailability (50%) from dry deposition at CGBAPS could potentially be bio-available, while the other half is refractory or insoluble and is presumably lost from the surface ocean via settling (Figs. 4c and 5). Aerosol particles associated with instantaneous soluble Fe (i.e., <0.4 μm) will reside in the mixed layer for a time period on the order of years, assuming the mixed layer is between 50 and 200 m (Bowie et al., 2011) and particles with a diameter of 0.4 μm have a settling velocity of 9.5×10^{-6} cm s^{-1} (Gibbs et al., 1971). The residence time of aerosol particles associated with labile Fe is orders of magnitude shorter, and may range between days and weeks (assuming labile Fe over the Southern Ocean range between 0.4 and 5 μm (Delmonte et al., 2002; Delmonte et al., 2013; Koffman et al., 2014a), and this particle size range has a settling velocity between 9.5 x 10^{-6} cm s^{-1} and 1.5 x 10^{-3} cm s^{-1} (Gibbs et al., 1971)). We acknowledge that processes in the ocean can alter sinking rates, such as aggregation of colloids. Moreover, particle dimensions can change, for example with bacterial attachment (Yamada et al., 2013). Labile Fe comprises a large component of total Fe, and this fraction may be slowly released from aerosol particles into the surface mixed layer. Estimates of labile Fe and water soluble Fe, in this study, represent an upper bound of the potential bioavailability of Fe deposited to Southern Ocean. The majority of estimates over the Southern Ocean are based on soluble Fe fractions alone and do not take into consideration labile Fe.

The estimates of bioavailable Fe reported here are relatively high and represent an upper bound of Fe bioavailability over the Southern Ocean. Several factors could account for the high Fe bioavailability found at CGBAPS. Aerosol Fe solubility could be enhanced by cloud chemistry and acid processing (Spokes et al., 1994; Desboeufs et al., 1999; Meskhidze et al., 2003; Kumar et al., 2010), and these processes may play a role in the lability of long range transport aerosol Fe over the Southern Ocean. We compare our fractional Fe bioavailability data to non-sea salt (nss)-sulfate and nitrate aerosol measurements made at CGBAPS (Keywood et al., 2004) (Fig. 6a–d). No significant relationship was found between the acid species and fractional Fe bioavailability during the short time series at CGBAPS. However, in February–March 2000 water soluble Fe made a large contribution to the bioavailable Fe pool (Fig. 6a–b), at a time of high nitrate and nss-sulfate concentrations. During this period, sodium was exceptionally high (Fig. 6g), suggesting the marine aerosol was comprised primarily of sea salt (Mg, K, Cl, and Ca concentrations were also high (Keywood et al., 2004). During this sampling period the average baseline windspeed measured at 10 m of 13.8 m s^{-1} was in the 89th percentile of wind speeds recorded for the period 1998–2005). No relationship between these acid species and fractional Fe solubility was found in other field studies in the remote Atlantic and Pacific Ocean (Hand et al., 2004; Baker et al., 2006). Baker et al. (2013) suggest that the lack of correlation in real samples could be due to a low degree of internal mixing in the aerosol samples rather than due to the lack of acid influence on Fe solubility. Either, the enhancement of Fe bioavailability by acid processing on the surface of the aerosol is not a significant process in the atmosphere over the Southern Ocean, or that it has not occurred in the samples collected in this study because the acidic and Fe-laden aerosol fraction are not in contact with each other, or that our time series is too short to see any relationship, or that the high fractional Fe solubility observed in one sample is related to a large volume of sea salt derived air masses during a particularly strong storm event.

Recently, Fe solubility has been investigated in relation to carboxylic acids, whereby oxalate was most effective at enhancing the fractional Fe solubility in mineral dust (Paris et al., 2011; Paris and Desboeufs, 2013). Paris et al. (2011) show that oxalate complexation increases fractional Fe solubility of hematite, goethite and illite minerals in African dust from 0.0025 to 0.26%. Furthermore, biomass burning is a major source of carboxylic acid and is known to enhance fractional Fe solubility (Fu et al., 2014). A biomass burning source was suggested by Bowie et al. (2009) to account for the high fractional Fe solubility of 17% in an aerosol sample collected over the Southern Ocean south of Tasmania (Fig. 4). We compare the fractional Fe bioavailability data in this study to oxalate measurements made at Cape Grim using methods described in (Keywood et al., 2004) in Fig. 6a–e. The highest concentration of oxalate occurred in March 1999. However, the corresponding sample archive was missing. The May/June peak in fractional Fe bioavailability (where labile Fe contributed a large fraction of the total Fe) corresponds to low oxalate and low nss-potassium (Fig. 6b and e–f). Non sea salt-potassium has been widely used as a biomass burning tracer (e.g. Echalar et al., 1995; Duan et al., 2004; Paris et al., 2010), and the lack of correlation here suggests that biomass burring is not a large contributor to bioavailable Fe at CGBAPS during this study.

The lack of correlation with oxalate at CGBAPS may be related to the type of Fe-bearing minerals in the baseline aerosols. We are unable to determine the atmospheric processes that enhance the fractional Fe bioavailability of marine aerosols during long range transport over the Southern Ocean. This may be related to the extremely clean air masses at CGBAPS. Thus, a longer time series is needed to confirm whether organic complexation or acid processing affects the solubility and bioavailability of aerosol Fe in the Southern Ocean. The temporal variability in aerosol Fe at CGBAPS is most likely related to a mixture of aerosol sources from continental air masses, as discussed above.

5. Conclusions

This paper shows extremely low aerosol Fe concentrations over the Southern Ocean during 1999 to early 2000 and provides estimates for the soluble and total atmospheric Fe flux by dry deposition. The temporal variability of soluble Fe was consistent with the intrusion of continental air masses over the Southern Ocean. The relationship between the fractional Fe solubility and total Fe mass concentration was comparable to other studies that postulated mixed soluble Fe aerosol sources and low mineral dust Fe solubility. Labile Fe comprised a large component of the total Fe and suggested that the soluble Fe may significantly underestimate the potential bioavailability of Fe deposited to Southern Ocean surface waters. However, further studies of labile of Fe are required to understand the significance of labile Fe as determined by the operational here used here. Longer-term studies of Southern Ocean aerosol Fe bioavailability are also required to understand aerosol Fe variability and to characterise sources. Wet deposition Fe estimates remain relatively unknown over the Southern Ocean. Overall the data shows that the Fe bioavailability of present day aerosols is complex and not simply scaled to atmospheric concentrations of mineral dust. It is likely that past variability in the atmospheric deposition of bioavailable Fe to the Southern Ocean is just as complex and that our current understanding of its Quaternary variability may be in need of revision.

Supplementary data to this article can be found online at http://dx.doi.org/10.1016/j.marchem.2015.06.006.

Acknowledgements

This project was funded through Curtin University (Curtin Research Fellowship to R.E.), the University of Tasmania (Rising Stars contract B0019024 to A.R.B.), the Australian Research Council (FT130100037) and the Antarctic Climate and Ecosystems Cooperative Research Centre. Access to SF-ICP-MS instrumentation at UTAS was facilitated through ARC LIEF funding (LE0989539). V.H.L.W. would like to acknowledge the following scholarship support: Australian Postgraduate Award and Curtin University Postgraduate Scholarship. This research would have

Fig. 6. Timeseries of major ions measured at CGBAPS. a) bioavailable Fe concentration (i.e., the sum of soluble and labile Fe fractions), b) nitrate, c) sulfate, d) oxalate, e) sodium (data source for nitrate, sulfate and sodium: Keywood et al. (2004)).

been impossible without the support and dedication of the late Kevin Rosman. Useful discussions with Rachel Shelley over labile iron leaching methods are appreciated. CSIRO and the Australian Bureau of Meteorology in Australia are also thanked for their continuous support of CGBAPS, and we also thank the staff at CGBAPS who made the collection of monthly aerosol samples possible. We thank three anonymous reviewers for their constructive comments which improved this manuscript.

References

Aguilar-Islas, A.M., Wu, J., Rember, R., Johansen, A.M., Shank, L.M., 2010. Dissolution of aerosol-derived iron in seawater: leach solution chemistry, aerosol type, and colloidal iron fraction. Mar. Chem. 120 (1–4), 25–33.

Arimoto, R., Duce, R., Ray, B., Unni, C., 1985. Atmospheric trace elements at Enewetak Atoll: 2. Transport to the ocean by wet and dry deposition. J. Geophys. Res. Atmos. (1984–2012) 90 (D1), 2391–2408.

Ayers, G., Ivey, J., Goodman, H., 1987. Sulfate and methanesulfonate in the maritime aerosol at Cape Grim, Tasmania. Scientific Application of Baseline Observations of Atmospheric Composition (SABOAC). Springer, pp. 371–383.

Ayers, G.P., Ivey, J., Gillett, R., 1990. High Volume Samplers in Baseline Atmospheric Program (Australia) 1988. In: Wilson, S.R., Ayers, G.P. (Eds.), CSIRO Atmospheric Research, Melbourne, Australia, p. 45.

Baker, A.R., Croot, P.L., 2010. Atmospheric and marine controls on aerosol iron solubility in seawater. Mar. Chem. 120 (1–4), 4–13.

Baker, A.R., Jickells, T.D., 2006. Mineral particle size as a control on aerosol iron solubility. Geophys. Res. Lett. 33 (17), L17608.

Baker, A.R., Jickells, T.D., Witt, M., Linge, K.L., 2006. Trends in the solubility of iron, aluminium, manganese and phosphorus in aerosol collected over the Atlantic Ocean. Mar. Chem. 98 (1), 43–58.

Baker, A., Adams, C., Bell, T., Jickells, T., Ganzeveld, L., 2013. Estimation of atmospheric nutrient inputs to the Atlantic Ocean from 50° N to 50° S based on large-scale field sampling: iron and other dust-associated elements. Glob. Biogeochem. Cycles 27 (3), 755–767.

Barbeau, K., Moffett, J.W., Caron, D.A., Croot, P.L., Erdner, D.L., 1996. Role of protozoan grazing in relieving iron limitation of phytoplankton. Nature 380 (6569), 61–64.

Berger, C.J., Lippiatt, S.M., Lawrence, M.G., Bruland, K.W., 2008. Application of a chemical leach technique for estimating labile particulate aluminum, iron, and manganese in the Columbia River plume and coastal waters off Oregon and Washington. J. Geophys. Res. Oceans (1978–2012) 113 (C2).

Bhattachan, A., D'Odorico, P., 2014. Can land use intensification in the Mallee, Australia increase the supply of soluble iron to the Southern Ocean? Sci. Rep. 4.

Blain, S., Queguiner, B., Armand, L., Belviso, S., Bombled, B., Bopp, L., Bowie, A., Brunet, C., Brussaard, C., Carlotti, F., Christaki, U., Corbiere, A., Durand, I., Ebersbach, F., Fuda, J.-L., Garcia, N., Gerringa, L., Griffiths, B., Guigue, C., Guillerm, C., Jacquet, S., Jeandel, C., Laan, P., Lefevre, D., Lo Monaco, C., Malits, A., Mosseri, J., Obernosterer, I., Park, Y.-H., Picheral, M., Pondaven, P., Remenyi, T., Sandroni, V., Sarthou, G., Savoye, N., Scouarnec, L., Souhaut, M., Thuiller, D., Timmermans, K., Trull, T., Uitz, J., van Beek, P., Veldhuis, M., Vincent, D., Viollier, E., Vong, L., Wagener, T., 2007. Effect of natural iron fertilization on carbon sequestration in the Southern Ocean. Nature 446 (7139), 1070–1074.

Bollhöfer, A., Chisholm, W., Rosman, K., 1999. Sampling aerosols for lead isotopes on a global scale. Anal. Chim. Acta 390 (1), 227–235.

Bollhöfer, A.F., Rosman, K.J.R., Dick, A.L., Chisholm, W., Burton, G.R., Loss, R.D., Zahorowski, W., 2005. Concentration, isotopic composition, and sources of lead in Southern Ocean air during 1999/2000, measured at the Cape Grim Baseline Air Pollution Station, Tasmania. Geochim. Cosmochim. Acta 69 (20), 4747–4757.

Bonnet, S., Guieu, C., 2004. Dissolution of atmospheric iron in seawater. Geophys. Res. Lett. 31 (3), L03303.

Bowie, A.R., Lannuzel, D., Remenyi, T.A., Wagener, T., Lam, P.J., Boyd, P.W., Guieu, C., Townsend, A.T., Trull, T.W., 2009. Biogeochemical iron budgets of the Southern Ocean south of Australia: decoupling of iron and nutrient cycles in the subantarctic zone by the summertime supply. Glob. Biogeochem. Cycles 23 (4), GB4034.

Bowie, A.R., Townsend, A.T., Lannuzel, D., Remenyi, T.A., Van der Merwe, P., 2010. Modern sampling and analytical methods for the determination of trace elements in marine particulate material using magnetic sector inductively coupled plasma–mass spectrometry. Anal. Chim. Acta 676 (1), 15–27.

Bowie, A.R., Griffiths, F.B., Dehairs, F., Trull, T.W., 2011. Oceanography of the subantarctic and polar frontal zones south of Australia during summer: setting for the SAZ-Sense study. Deep-Sea Res. II Top. Stud. Oceanogr. 58 (21), 2059–2070.

Bowie, A., van der Merwe, P., Quéroué, F., Trull, T., Fourquez, M., Planchon, F., Sarthou, G., Chever, F., Townsend, A., Obernosterer, I., 2014. Iron budgets for three distinct biogeochemical sites around the Kerguelen archipelago (Southern Ocean) during the natural fertilisation experiment KEOPS-2. Biogeosci. Discuss. 11 (12), 17861–17923.

Boyd, P.W., Jickells, T., Law, C.S., Blain, S., Boyle, E.A., Buesseler, K.O., Coale, K.H., Cullen, J.J., de Baar, H.J.W., Follows, M., Harvey, M., Lancelot, C., Levasseur, M., Owens, N.P.J., Pollard, R., Rivkin, R.B., Sarmiento, J., Schoemann, V., Smetacek, V., Takeda, S., Tsuda, A., Turner, S., Watson, A.J., 2007. Mesoscale iron enrichment experiments 1993–2005: synthesis and future directions. Science 315 (5812), 612–617.

Boyd, P.W., Mackie, D.S., Hunter, K.A., 2010. Aerosol iron deposition to the surface ocean — modes of iron supply and biological responses. Mar. Chem. 120 (1–4), 128–143.

Buck, C.S., Landing, W.M., Resing, J.A., Lebon, G.T., 2006. Aerosol iron and aluminum solubility in the northwest Pacific Ocean: results from the 2002 IOC cruise. Geochem. Geophys. Geosyst. 7 (4), Q04M07.

Burckle, L.H., Gayley, R.I., Ram, M., Petit, J.-R., 1988. Diatoms in Antarctic ice cores: Some implications for the glacial history of Antarctica. Geology 16 (4), 326–329.

Chen, Y., Siefert, R.L., 2003. Determination of various types of labile atmospheric iron over remote oceans. J. Geophys. Res. 108 (D24), 4774.

Chen, Y., Siefert, R.L., 2004. Seasonal and spatial distributions and dry deposition fluxes of atmospheric total and labile iron over the tropical and subtropical North Atlantic Ocean. J. Geophys. Res. 109 (D9), D09305.

Chuang, P.Y., Duvall, R.M., Shafer, M.M., Schauer, J.J., 2005. The origin of water soluble particulate iron in the Asian atmospheric outflow. Geophys. Res. Lett. 32 (7), L07813.

Coale, K.H., Johnson, K.S., Chavez, F.P., Buesseler, K.O., Barber, R.T., Brzezinski, M.A., Cochlan, W.P., Millero, F.J., Falkowski, P.G., Bauer, J.E., Wanninkhof, R.H., Kudela, R.M., Altabet, M.A., Hales, B.E., Takahashi, T., Landry, M.R., Bidigare, R.R., Wang, X., Chase, Z., Strutton, P.G., Friederich, G.E., Gorbunov, M.Y., Lance, V.P., Hilting, A.K., Hiscock, M.R., Demarest, M., Hiscock, W.T., Sullivan, K.F., Tanner, S.J., Gordon, R.M., Hunter, C.N., Elrod, V.A., Fitzwater, S.E., Jones, J.L., Tozzi, S., Koblizek, M., Roberts, A.E., Herndon, J., Brewster, J., Ladizinsky, N., Smith, G., Cooper, D., Timothy, D., Brown, S.L., Selph, K.E., Sheridan, C.C., Twining, B.S., Johnson, Z.I., 2004. Southern ocean iron enrichment experiment: carbon cycling in high- and low-Si waters. Science 304 (5669), 408–414.

Croot, P., Bluhm, K., Schlosser, C., Streu, P., Breitbarth, E., Frew, R., Van Ardelan, M., 2008. Regeneration of Fe (II) during EIFeX and SOFeX. Geophys. Res. Lett. 35 (19).

Cutter, G., Andersson, P., Codispoti, L., Croot, P., Francois, R., Lohan, M., Obata, H., Rutgers vd Loeff, M., 2010. Sampling and Sample-handling Protocols for GEOTRACES Cruises.

de Baar, H.J.W., de Jong, J.T.M., Bakker, D.C.E., Loscher, B.M., Veth, C., Bathmann, U., Smetacek, V., 1995. Importance of iron for plankton blooms and carbon dioxide drawdown in the Southern Ocean. Nature 373 (6513), 412–415.

de Baar, H.J.W., Boyd, P.W., Coale, K.H., Landry, M.R., Tsuda, A., Assmy, P., Bakker, D.C.E., Bozec, Y., Barber, R.T., Brzezinski, M.A., Buesseler, K.O., Boyé, M., Croot, P.L., Gervais, F., Gorbunov, M.Y., Harrison, P.J., Hiscock, W.T., Laan, P., Lancelot, C., Law, C.S., Levasseur, M., Marchetti, A., Millero, F.J., Nishioka, J., Nojiri, Y., van Oijen, T., Riebesell, U., Rijkenberg, M.J.A., Saito, H., Takeda, S., Timmermans, K.R., Veldhuis, M.J.W., Waite, A.M., Wong, C.S., 2005. Synthesis of iron fertilization experiments: from the Iron Age in the Age of Enlightenment. J. Geophys. Res. 110 (C9), C09S16.

Delmonte, B., Petit, J.R., Maggi, V., 2002. Glacial to Holocene implications of the new 27000-year dust record from the EPICA Dome C (East Antarctica) ice core. Clim. Dyn. 18 (8), 647–660.

Delmonte, B., Andersson, P.S., Hansson, M., Schöberg, H., Petit, J.R., Basile-Doelsch, I., Maggi, V., 2008. Aeolian dust in East Antarctica (EPICA-Dome C and Vostok): provenance during glacial ages over the last 800 kyr. Geophys. Res. Lett. 35 (7), L07703.

Delmonte, B., Baroni, C., Andersson, P., Narcisi, B., Salvatore, M., Petit, J., Scarchilli, C., Frezzotti, M., Albani, S., Maggi, V., 2013. Modern and Holocene aeolian dust variability from Talos Dome (Northern Victoria Land) to the interior of the Antarctic ice sheet. Quat. Sci. Rev. 64, 76–89.

Desboeufs, K.V., Losno, R., Vimeux, F., Cholbi, S., 1999. The pH-dependent dissolution of wind-transported Saharan dust. J. Geophys. Res. Atmos. (1984–2012) 104 (D17), 21287–21299.

Duan, F., Liu, X., Yu, T., Cachier, H., 2004. Identification and estimate of biomass burning contribution to the urban aerosol organic carbon concentrations in Beijing. Atmos. Environ. 38 (9), 1275–1282.

Duce, R.A., Liss, P.S., Merrill, J.T., Atlas, E.L., Buat-Menard, P., Hicks, B.B., Miller, J.M., Prospero, J.M., Arimoto, R., Church, T.M., Ellis, W., Galloway, J.N., Hansen, L., Jickells, T.D., Knap, A.H., Reinhardt, K.H., Schneider, B., Soudine, A., Tokos, J.J., Tsunogai, S., Wollast, R., Zhou, M., 1991. The atmospheric input of trace species to the world ocean. Glob. Biogeochem. Cycles 5 (3), 193–259.

Dulac, F., BUAT-MÉNARD, P., Ezat, U., Melki, S., Bergametti, G., 1989. Atmospheric input of trace metals to the western Mediterranean: uncertainties in modelling dry deposition from cascade impactor data. Tellus B 41 (3), 362–378.

Echalar, F., Gaudichet, A., Cachier, H., Artaxo, P., 1995. Aerosol emissions by tropical forest and savanna biomass burning: characteristic trace elements and fluxes. Geophys. Res. Lett. 22 (22), 3039–3042.

Edwards, R., Sedwick, P., 2001. Iron in East Antarctic snow: implications for atmospheric iron deposition and algal production in Antarctic waters. Geophys. Res. Lett. 28 (20), 3907–3910.

Edwards, R., Sedwick, P., Morgan, V., Boutron, C., 2006. Iron in ice cores from Law Dome: a record of atmospheric iron deposition for maritime East Antarctica during the Holocene and Last Glacial Maximum. Geochem. Geophys. Geosyst. 7 (12), Q12Q01.

Ellwood, M.J., Hutchins, D.A., Lohan, M.C., Milne, A., Nasemann, P., Nodder, S.D., Sander, S.G., Strzepek, R., Wilhelm, S.W., Boyd, P.W., 2015. Iron stable isotopes track pelagic iron cycling during a subtropical phytoplankton bloom. Proc. Natl. Acad. Sci. 112 (1), E15–E20.

Elrod, V., Berelson, W., Coale, K., Johnson, K., 2004. The flux of iron from continental shelf sediments: a missing source for global budgets. Geophys. Res. Lett. 31, L12307.

Ezat, U., Dulac, F., 1995. Size distribution of mineral aerosols at Amsterdam-island and dry deposition rates in the Southern Indian Ocean. C. R. Acad. Sci. II 320 (1), 9–14.

Fu, H., Shang, G., Lin, J., Hu, Y., Hu, Q., Guo, L., Zhang, Y., Chen, J., 2014. Fractional iron solubility of aerosol particles enhanced by biomass burning and ship emission in Shanghai, East China. Sci. Total Environ. 481, 377–391.

Gaiero, D.M., Probst, J.-L., Depetris, P.J., Bidart, S.M., Leleyter, L., 2003. Iron and other transition metals in Patagonian riverborne and windborne materials: geochemical control and transport to the southern South Atlantic Ocean. Geochim. Cosmochim. Acta 67 (19), 3603–3623.

Gaiero, D.M., Brunet, F., Probst, J.-L., Depetris, P.J., 2007. A uniform isotopic and chemical signature of dust exported from Patagonia: rock sources and occurrence in southern environments. Chem. Geol. 238 (1), 107–120.

Gao, Y., Xu, G., Zhan, J., Zhang, J., Li, W., Lin, Q., Chen, L., Lin, H., 2013. Spatial and particle size distributions of atmospheric dissolvable iron in aerosols and its input to the Southern Ocean and coastal East Antarctica. J. Geophys. Res. Atmos. 118 (22), 12,634–12,648.

Gaspari, V., Barbante, C., Cozzi, G., Cescon, P., Boutron, C.F., Gabrielli, P., Capodaglio, G., Ferrari, C., Petit, J.R., Delmonte, B., 2006. Atmospheric iron fluxes over the last deglaciation: climatic implications. Geophys. Res. Lett. 33 (3), L03704.

Gibbs, R., Mathews, M., Unk, D., 1971. The relationship between sphere size and settling velocity. J. Sediment. Petrol. 41 (1), 7–18.

Guieu, C., Bonnet, S., Wagener, T., Loÿe-Pilot, M.D., 2005. Biomass burning as a source of dissolved iron to the open ocean? Geophys. Res. Lett. 32 (19).

Halstead, M.J., Cunninghame, R.G., Hunter, K.A., 2000. Wet deposition of trace metals to a remote site in Fiordland, New Zealand. Atmos. Environ. 34 (4), 665–676.

Hand, J.L., Mahowald, N.M., Chen, Y., Siefert, R.L., Luo, C., Subramaniam, A., Fung, I., 2004. Estimates of atmospheric-processed soluble iron from observations and a global mineral aerosol model: biogeochemical implications. J. Geophys. Res. 109 (D17), D17205.

Heimburger, A., Losno, R., Triquet, S., Dulac, F., Mahowald, N., 2012. Direct measurements of atmospheric iron, cobalt, and aluminum-derived dust deposition at Kerguelen Islands. Glob. Biogeochem. Cycles 26 (4).

Heimburger, A., Losno, R., Triquet, S., 2013a. Solubility of iron and other trace elements in rainwater collected on the Kerguelen Islands (South Indian Ocean). Biogeosciences 10 (10).

Heimburger, A., Losno, R., Triquet, S., Nguyen, E.B., 2013b. Atmospheric deposition fluxes of 26 elements over the Southern Indian Ocean: time series on Kerguelen and Crozet Islands. Glob. Biogeochem. Cycles 27 (2), 440–449.

Hurst, M.P., Bruland, K.W., 2007. An investigation into the exchange of iron and zinc between soluble, colloidal, and particulate size-fractions in shelf waters using low-abundance isotopes as tracers in shipboard incubation experiments. Mar. Chem. 103 (3), 211–226.

Ito, A., 2011. Mega fire emissions in Siberia: potential supply of bioavailable iron from forests to the ocean. Biogeosciences 8 (6).

Jeong, D., Kim, K., Choi, W., 2012. Accelerated dissolution of iron oxides in ice. Atmos. Chem. Phys. 12 (22), 11125–11133.

Jickells, T., An, Z., Anderson, K., Baker, A., Bergametti, G., Brooks, N., Cao, J., Boyd, P., Duce, R., Hunter, K., Kawaahata, H., Kubilay, N., LaRoche, J., Liss, P., Mahowald, N., Prospero, J., Ridgewell, A., Tegen, I., Torres, R., 2005. Global iron connections between desert dust, ocean biogeochemistry, and climate. Science 308, 67–73.

Johnson, K., Chavez, F., Friederich, G., 1999. Continental-shelf sediment as a primary source of iron for coastal phytoplankton. Nature 398, 697–700.

Keywood, M.D., 2007. Aerosol Composition at Cape Grim: An Evaluation of PM10 Sampling Program and Baseline Event Switches. Baseline Atmospheric Program Australia 2005–2006. 2005–2006. In: Cainey, J.M., Derek, N., Krummel, P.B. (Eds.), Australian Bureau of Meteorology and CSIRO Marine and Atmospheric Research, Melbourne, pp. 31–36.

Keywood, M.D., Graham, B., Gillett, R.W., Gras, J.G., Selleck, P.W., 2004. High Volume Aerosol Sampler. Baseline Atmospheric Program (Australia) 2001–200 Edited. In: Cainey, J., Derek, N., Krummel, P. (Eds.), Bureau of Meteorology CSIRO Atmospheric Research and, Melbourne, Australia, pp. 74–77.

Kobayashi, H., Hara, K., Shiobara, M., Yamanouchi, T., Osada, K., Ohta, S., 2010. Seasonal variation of carbonaceous and metal compositions of atmospheric aerosols at Syowa Station, Antarctica in 2001. Antarct. Rec. (Tokyo) 54, 554–561.

Koffman, B., Kreutz, K., Breton, D., Kane, E., Winski, D., Birkel, S., Kurbatov, A., Handley, M., 2014a. Centennial-scale variability of the Southern Hemisphere westerly wind belt in the eastern Pacific over the past two millennia. Clim. Past 10 (3), 1125–1144.

Koffman, B.G., Handley, M.J., Osterberg, E.C., Wells, M.L., Kreutz, K.J., 2014b. Dependence of ice-core relative trace-element concentration on acidification. J. Glaciol. 60 (219), 103–112.

Kuma, K., Matsunaga, K., 1995. Availability of colloidal ferric oxides to coastal marine phytoplankton. Mar. Biol. 122 (1), 1–11.

Kumar, A., Sarin, M., Srinivas, B., 2010. Aerosol iron solubility over Bay of Bengal: role of anthropogenic sources and chemical processing. Mar. Chem. 121 (1), 167–175.

Lannuzel, D., Schoemann, V., de Jong, J., Tison, J., Chou, L., 2007. Distribution and biogeochemical behaviour of iron in the East Antarctic sea ice. Mar. Chem. 106 (1–2), 18–32.

Lannuzel, D., Schoemann, V., de Jong, J., Chou, L., Delille, B., Becquevort, S., Tison, J., 2008. Iron study during a time series in the western Weddell pack ice. Mar. Chem. 108 (1–2), 85–95.

Latimer, J.C., Filippelli, G.M., 2001. Terrigenous input and paleoproductivity in the Southern Ocean. Paleoceanography 16 (6), 627–643.

Latimer, J.C., Filippelli, G.M., Hendy, I.L., Gleason, J.D., Blum, J.D., 2006. Glacial–interglacial terrigenous provenance in the southeastern Atlantic Ocean: the importance of deep-water sources and surface currents. Geology 34 (7), 545–548.

Lis, H., Shaked, Y., Kranzler, C., Keren, N., Morel, F.M.M., 2015. Iron bioavailability to phytoplankton: an empirical approach. ISME J. 9 (4), 1003–1013.

Luo, C., Mahowald, N.M., Meskhidze, N., Chen, Y., Siefert, R.L., Baker, A.R., Johansen, A.M., 2005. Estimation of iron solubility from observations and a global aerosol model. J. Geophys. Res. 110 (D23), D23307.

Luo, C., Mahowald, N., Bond, T., Chuang, P.Y., Artaxo, P., Siefert, R., Chen, Y., Schauer, J., 2008. Combustion iron distribution and deposition. Glob. Biogeochem. Cycles 22 (1), GB1012.

Mackie, D.S., Boyd, P.W., Hunter, K.A., McTainsh, G.H., 2005. Simulating the cloud processing of iron in Australian dust: pH and dust concentration. Geophys. Res. Lett. 32 (6), L06809.

Mahowald, N.M., Baker, A.R., Bergametti, G., Brooks, N., Duce, R.A., Jickells, T.D., Kubilay, N., Prospero, J.M., Tegen, I., 2005. Atmospheric global dust cycle and iron inputs to the ocean. Glob. Biogeochem. Cycles 19 (4), GB4025.

Martin, J.H., Gordon, R.M., Fitzwater, S.E., 1990. Iron in Antarctic waters. Nature 345 (6271), 156–158.

Martin, J.H., Gordon, R.M., Fitzwater, S.E., 1991. The case for iron. Limnol. Oceanogr. 36 (8), 1793–1802.

Martínez-Garcia, A., Rosell-Melé, A., Geibert, W., Gersonde, R., Masqué, P., Gaspari, V., Barbante, C., 2009. Links between iron supply, marine productivity, sea surface temperature, and CO_2 over the last 1.1 Ma. Paleoceanography 24 (1), PA1207.

Martínez-García, A., Sigman, D.M., Ren, H., Anderson, R.F., Straub, M., Hodell, D.A., Jaccard, S.L., Eglinton, T.I., Haug, G.H., 2014. Iron fertilization of the subantarctic ocean during the last ice age. Science 343 (6177), 1347–1350.

Meskhidze, N., Nenes, A., 2006. Phytoplankton and cloudiness in the Southern Ocean. Science 314 (5804), 1419–1423.

Meskhidze, N., Chameides, W., Nenes, A., Chen, G., 2003. Iron mobilization in mineral dust: can anthropogenic SO_2 emissions affect ocean productivity? Geophys. Res. Lett. 30 (21).

Moore, J.K., Abbott, M.R., Richman, J.G., Nelson, D.M., 2000. The southern ocean at the last glacial maximum: a strong sink for atmospheric carbon dioxide. Glob. Biogeochem. Cycles 14 (1), 455–475.

Morton, P.L., Landing, W.M., Hsu, S.-C., Milne, A., Aguilar-Islas, A.M., Baker, A.R., Bowie, A.R., Buck, C.S., Gao, Y., Gichuki, S., 2013. Methods for the sampling and analysis of marine aerosols: results from the 2008 GEOTRACES aerosol intercalibration experiment. Limnol. Oceanogr. Methods 11 (FEB), 62–78.

Narcisi, B., Petit, J.-R., Delmonte, B., Basile-Doelsch, I., Maggi, V., 2005. Characteristics and sources of tephra layers in the EPICA-Dome C ice record (East Antarctica): implications for past atmospheric circulation and ice core stratigraphic correlations. Earth Planet. Sci. Lett. 239 (3), 253–265.

Nodwell, L.M., Price, N.M., 2001. Direct use of inorganic colloidal iron by marine mixotrophic phytoplankton. Limnol. Oceanogr. 46 (4), 765–777.

Paris, R., Desboeufs, K., 2013. Effect of atmospheric organic complexation on iron-bearing dust solubility. Atmos. Chem. Phys. 13 (9), 4895–4905.

Paris, R., Desboeufs, K., Formenti, P., Nava, S., Chou, C., 2010. Chemical characterisation of iron in dust and biomass burning aerosols during AMMA-SOP0/DABEX: implication for iron solubility. Atmos. Chem. Phys. 10 (9), 4273–4282.

Paris, R., Desboeufs, K., Journet, E., 2011. Variability of dust iron solubility in atmospheric waters: Investigation of the role of oxalate organic complexation. Atmos. Environ. 45 (36), 6510–6517.

Planquette, H., Statham, P.J., Fones, G.R., Charette, M.A., Moore, C.M., Salter, I., Nedelec, F.H., Taylor, S.L., French, M., Baker, A.R., 2007. Dissolved iron in the vicinity of the Crozet Islands, Southern Ocean. Deep-Sea Res. II Top. Stud. Oceanogr. 54 (18), 1999–2019.

Porstendorfer, J., Butterweck, G., Reineking, A., 1994. Daily variation of the radon concentration indoors and outdoors and the influence of meteorological parameters. Health Phys. 67 (3), 283–287.

Raiswell, R., Benning, L.G., Tranter, M., Tulaczyk, S., 2008. Bioavailable iron in the Southern Ocean: the significance of the iceberg conveyor belt. Geochem. Trans. 9 (1), 7.

Rubin, M., Berman-Frank, I., Shaked, Y., 2011. Dust-and mineral-iron utilization by the marine dinitrogen-fixer Trichodesmium. Nat. Geosci. 4 (8), 529–534.

Schwertmann, U., 1991. Solubility and Dissolution of Iron Oxides, Iron Nutrition and Interactions in Plants. Springer, pp. 3–27.

Sedwick, P.N., DiTullio, G.R., 1997. Regulation of algal blooms in Antarctic Shelf Waters by the release of iron from melting sea ice. Geophys. Res. Lett. 24 (20), 2515–2518.

Sedwick, P.N., Sholkovitz, E.R., Church, T.M., 2007. Impact of anthropogenic combustion emissions on the fractional solubility of aerosol iron: evidence from the Sargasso Sea. Geochem. Geophys. Geosyst. 8 (10), Q10Q06.

Sholkovitz, E.R., Sedwick, P.N., Church, T.M., 2009. Influence of anthropogenic combustion emissions on the deposition of soluble aerosol iron to the ocean: empirical estimates for island sites in the North Atlantic. Geochim. Cosmochim. Acta 73 (14), 3981–4003.

Sholkovitz, E.R., Sedwick, P.N., Church, T.M., Baker, A.R., Powell, C.F., 2012. Fractional solubility of aerosol iron: synthesis of a global-scale data set. Geochim. Cosmochim. Acta 89, 173–189.

Slinn, S., Slinn, W., 1980. Predictions for particle deposition on natural waters. Atmos. Environ. (1967) 14 (9), 1013–1016.

Smetacek, V., Klaas, C., Strass, V.H., Assmy, P., Montresor, M., Cisewski, B., Savoye, N., Webb, A., d'Ovidio, F., Arrieta, J.M., Bathmann, U., Bellerby, R., Berg, G.M., Croot, P., Gonzalez, S., Henjes, J., Herndl, G.J., Hoffmann, L.J., Leach, H., Losch, M., Mills, M.M., Neill, C., Peeken, I., Rottgers, R., Sachs, O., Sauter, E., Schmidt, M.M., Schwarz, J., Terbruggen, A., Wolf-Gladrow, D., 2012. Deep carbon export from a Southern Ocean iron-fertilized diatom bloom. Nature 487 (7407), 313–319.

Spokes, L.J., Jickells, T.D., 1995. Factors controlling the solubility of aerosol trace metals in the atmosphere and on mixing into seawater. Aquat. Geochem. 1 (4), 355–374.

Spokes, L.J., Jickells, T.D., Lim, B., 1994. Solubilisation of aerosol trace metals by cloud processing: a laboratory study. Geochim. Cosmochim. Acta 58 (15), 3281–3287.

Spolaor, A., Vallelonga, P., Gabrieli, J., Cozzi, G., Boutron, C., Barbante, C., 2012. Determination of Fe2+ and Fe3+ species by FIA-CRC-ICP-MS in Antarctic ice samples. J. Anal. At. Spectrom. 27 (2), 310–317.

Tagliabue, A., Bopp, L., Dutay, J.-C., Bowie, A.R., Chever, F., Jean-Baptiste, P., Bucciarelli, E., Lannuzel, D., Remenyi, T., Sarthou, G., Aumont, O., Gehlen, M., Jeandel, C., 2010. Hydrothermal contribution to the oceanic dissolved iron inventory. Nat. Geosci. 3 (4), 252–256.

Tagliabue, A., Sallee, J.-B., Bowie, A.R., Levy, M., Swart, S., Boyd, P.W., 2014. Surface-water iron supplies in the Southern Ocean sustained by deep winter mixing. Nat. Geosci. 7 (4), 314–320.

Trapp, J.M., Millero, F.J., Prospero, J.M., 2010. Trends in the solubility of iron in dust-dominated aerosols in the equatorial Atlantic trade winds: importance of iron speciation and sources. Geochem. Geophys. Geosyst. 11 (3), Q03014.
Vallelonga, P., Barbante, C., Cozzi, G., Gabrieli, J., Schüpbach, S., Spolaor, A., Turetta, C., 2013. Iron fluxes to Talos Dome, Antarctica, over the past 200 kyr. Clim. Past 9 (2), 597–604.
Wagener, T., Guieu, C., Losno, R., Bonnet, S., Mahowald, N., 2008. Revisiting atmospheric dust export to the Southern Hemisphere ocean: biogeochemical implications. Glob. Biogeochem. Cycles 22 (2), GB2006.
Wu, J., Rember, R., Cahill, C., 2007. Dissolution of aerosol iron in the surface waters of the North Pacific and North Atlantic oceans as determined by a semicontinuous flow-through reactor method. Glob. Biogeochem. Cycles 21 (4), GB4010.
Wuttig, K., Wagener, T., Bressac, M., Dammshäuser, A., Streu, P., Guieu, C., Croot, P., 2013. Impacts of dust deposition on dissolved trace metal concentrations (Mn, Al and Fe) during a mesocosm experiment. Biogeosciences 10 (4), 2583–2600.
Yamada, Y., Fukuda, H., Inoue, K., Kogure, K., Nagata, T., 2013. Effects of attached bacteria on organic aggregate settling velocity in seawater. Aquat. Microb. Ecol. 70 (3), 261–272.
Zahorowski, W., Chambers, S., Henderson-Sellers, A., 2004. Ground based radon-222 observations and their application to atmospheric studies. J. Environ. Radioact. 76 (1), 3–33.
Zhuang, G., Duce, R.A., Kester, D.R., 1990. The dissolution of atmospheric iron in surface seawater of the open ocean. J. Geophys. Res. 95 (C9), 16207–16216.
Zhuang, G., Yi, Z., Duce, R.A., Brown, P.R., 1992. Chemistry of iron in marine aerosols. Glob. Biogeochem. Cycles 6 (2), 161–173.

Appendix A3: Statement of contribution, accepted article and copyright license for paper 4

V.H.L. Winton, R. Edwards, B. Delmonte, A. Ellis, P.S. Andersson, A. Bowie, N.A.N. Bertler, P. Neff, A. Tuohy., 2016. Multiple sources of soluble atmospheric iron to Antarctic waters. *Global Biogeochemical Cycles,* 29, doi:10.1002/2015GB005265.

Statement of co-authorship

I, *Victoria Holly Liberty Winton*, designed and implemented the project, including experimental design, processed and analysed the samples for dissolved iron, total dissolvable iron, refractory black carbon, particle size distribution and radiogenic isotopes, and conducted data analysis and manuscript writing of the publication:

V.H.L. Winton, R. Edwards, B. Delmonte, A. Ellis, P.S. Andersson, A. Bowie, N.A.N. Bertler, P. Neff, A. Tuohy. Multiple sources of soluble atmospheric iron to Antarctic waters. In review in *Global Biogeochemical Cycles*.

Holly Winton

Victoria Holly Liberty Winton

I, as a Co-Author, endorse that this level of contribution by the candidate indicated above is appropriate.

R. Edwards

Ross Edwards (Signature of Co-Author 1)

Barbara Delmonte

Barbara Delmonte (Signature of Co-Author 2)

Aja Ellis (Signature of Co-Author 3)

Per Andersson (Signature of Co-Author 4)

Andrew Bowie

Andrew Bowie (Signature of Co-Author 5)

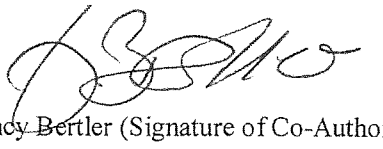

Nancy Bertler (Signature of Co-Author 6)

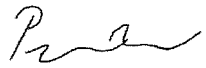

Peter Neff (Signature of Co-Author 7)

Andrea Tuohy (Signature of Co-Author 8)

JOHN WILEY AND SONS LICENSE TERMS AND CONDITIONS

Feb 08, 2016

This Agreement between Holly Winton ("You") and John Wiley and Sons ("John Wiley and Sons") consists of your license details and the terms and conditions provided by John Wiley and Sons and Copyright Clearance Center.

License Number	3804170770531
License date	Feb 08, 2016
Licensed Content Publisher	John Wiley and Sons
Licensed Content Publication	Global Biogeochemical Cycles
Licensed Content Title	Multiple sources of soluble atmospheric iron to Antarctic waters
Licensed Content Author	V.H.L. Winton,R. Edwards,B. Delmonte,A. Ellis,P.S. Andersson,A. Bowie,N.A.N. Bertler,P. Neff,A. Tuohy
Licensed Content Date	Feb 6, 2016
Pages	1
Type of use	Dissertation/Thesis
Requestor type	Author of this Wiley article
Format	Print and electronic
Portion	Full article
Will you be translating?	No
Title of your thesis / dissertation	Impact of biomass burning emissions and dust on soluble iron deposition to Australian and Antarctic waters
Expected completion date	Dec 2015
Expected size (number of pages)	200
Requestor Location	Holly Winton Curtin University DIAP, Building 301 Kent Street Bentley, Australia 6102 Attn: Holly Winton
Billing Type	Invoice
Billing Address	Holly Winton Curtin University DIAP, Building 301 Kent Street Bentley, Australia 6102 Attn: Holly Winton
Total	0.00 AUD
Terms and Conditions	

TERMS AND CONDITIONS

This copyrighted material is owned by or exclusively licensed to John Wiley & Sons, Inc. or one of its group companies (each a"Wiley Company") or handled on behalf of a society with which a Wiley Company has exclusive publishing rights in relation to a particular work (collectively "WILEY"). By clicking "accept" in connection with completing this licensing

transaction, you agree that the following terms and conditions apply to this transaction (along with the billing and payment terms and conditions established by the Copyright Clearance Center Inc., ("CCC's Billing and Payment terms and conditions"), at the time that you opened your RightsLink account (these are available at any time at http://myaccount.copyright.com).

Terms and Conditions

- The materials you have requested permission to reproduce or reuse (the "Wiley Materials") are protected by copyright.

- You are hereby granted a personal, non-exclusive, non-sub licensable (on a stand-alone basis), non-transferable, worldwide, limited license to reproduce the Wiley Materials for the purpose specified in the licensing process. This license, **and any CONTENT (PDF or image file) purchased as part of your order,** is for a one-time use only and limited to any maximum distribution number specified in the license. The first instance of republication or reuse granted by this license must be completed within two years of the date of the grant of this license (although copies prepared before the end date may be distributed thereafter). The Wiley Materials shall not be used in any other manner or for any other purpose, beyond what is granted in the license. Permission is granted subject to an appropriate acknowledgement given to the author, title of the material/book/journal and the publisher. You shall also duplicate the copyright notice that appears in the Wiley publication in your use of the Wiley Material. Permission is also granted on the understanding that nowhere in the text is a previously published source acknowledged for all or part of this Wiley Material. Any third party content is expressly excluded from this permission.

- With respect to the Wiley Materials, all rights are reserved. Except as expressly granted by the terms of the license, no part of the Wiley Materials may be copied, modified, adapted (except for minor reformatting required by the new Publication), translated, reproduced, transferred or distributed, in any form or by any means, and no derivative works may be made based on the Wiley Materials without the prior permission of the respective copyright owner.**For STM Signatory Publishers clearing permission under the terms of the STM Permissions Guidelines only, the terms of the license are extended to include subsequent editions and for editions in other languages, provided such editions are for the work as a whole in situ and does not involve the separate exploitation of the permitted figures or extracts,** You may not alter, remove or suppress in any manner any copyright, trademark or other notices displayed by the Wiley Materials. You may not license, rent, sell, loan, lease, pledge, offer as security, transfer or assign the Wiley Materials on a stand-alone basis, or any of the rights granted to you hereunder to any other person.

- The Wiley Materials and all of the intellectual property rights therein shall at all times remain the exclusive property of John Wiley & Sons Inc, the Wiley Companies, or their respective licensors, and your interest therein is only that of having possession of and the right to reproduce the Wiley Materials pursuant to Section 2 herein during the continuance of this Agreement. You agree that you own no right, title or interest in or to the Wiley Materials or any of the intellectual property rights therein. You shall have no rights hereunder other than the license as provided for above in Section 2. No right, license or interest to any trademark, trade name, service mark or other branding ("Marks") of WILEY or its licensors is granted hereunder, and you agree that you shall not assert any such right, license or interest with respect thereto

- NEITHER WILEY NOR ITS LICENSORS MAKES ANY WARRANTY OR

REPRESENTATION OF ANY KIND TO YOU OR ANY THIRD PARTY, EXPRESS, IMPLIED OR STATUTORY, WITH RESPECT TO THE MATERIALS OR THE ACCURACY OF ANY INFORMATION CONTAINED IN THE MATERIALS, INCLUDING, WITHOUT LIMITATION, ANY IMPLIED WARRANTY OF MERCHANTABILITY, ACCURACY, SATISFACTORY QUALITY, FITNESS FOR A PARTICULAR PURPOSE, USABILITY, INTEGRATION OR NON-INFRINGEMENT AND ALL SUCH WARRANTIES ARE HEREBY EXCLUDED BY WILEY AND ITS LICENSORS AND WAIVED BY YOU.

- WILEY shall have the right to terminate this Agreement immediately upon breach of this Agreement by you.

- You shall indemnify, defend and hold harmless WILEY, its Licensors and their respective directors, officers, agents and employees, from and against any actual or threatened claims, demands, causes of action or proceedings arising from any breach of this Agreement by you.

- IN NO EVENT SHALL WILEY OR ITS LICENSORS BE LIABLE TO YOU OR ANY OTHER PARTY OR ANY OTHER PERSON OR ENTITY FOR ANY SPECIAL, CONSEQUENTIAL, INCIDENTAL, INDIRECT, EXEMPLARY OR PUNITIVE DAMAGES, HOWEVER CAUSED, ARISING OUT OF OR IN CONNECTION WITH THE DOWNLOADING, PROVISIONING, VIEWING OR USE OF THE MATERIALS REGARDLESS OF THE FORM OF ACTION, WHETHER FOR BREACH OF CONTRACT, BREACH OF WARRANTY, TORT, NEGLIGENCE, INFRINGEMENT OR OTHERWISE (INCLUDING, WITHOUT LIMITATION, DAMAGES BASED ON LOSS OF PROFITS, DATA, FILES, USE, BUSINESS OPPORTUNITY OR CLAIMS OF THIRD PARTIES), AND WHETHER OR NOT THE PARTY HAS BEEN ADVISED OF THE POSSIBILITY OF SUCH DAMAGES. THIS LIMITATION SHALL APPLY NOTWITHSTANDING ANY FAILURE OF ESSENTIAL PURPOSE OF ANY LIMITED REMEDY PROVIDED HEREIN.

- Should any provision of this Agreement be held by a court of competent jurisdiction to be illegal, invalid, or unenforceable, that provision shall be deemed amended to achieve as nearly as possible the same economic effect as the original provision, and the legality, validity and enforceability of the remaining provisions of this Agreement shall not be affected or impaired thereby.

- The failure of either party to enforce any term or condition of this Agreement shall not constitute a waiver of either party's right to enforce each and every term and condition of this Agreement. No breach under this agreement shall be deemed waived or excused by either party unless such waiver or consent is in writing signed by the party granting such waiver or consent. The waiver by or consent of a party to a breach of any provision of this Agreement shall not operate or be construed as a waiver of or consent to any other or subsequent breach by such other party.

- This Agreement may not be assigned (including by operation of law or otherwise) by you without WILEY's prior written consent.

- Any fee required for this permission shall be non-refundable after thirty (30) days from receipt by the CCC.

- These terms and conditions together with CCC's Billing and Payment terms and

conditions (which are incorporated herein) form the entire agreement between you and WILEY concerning this licensing transaction and (in the absence of fraud) supersedes all prior agreements and representations of the parties, oral or written. This Agreement may not be amended except in writing signed by both parties. This Agreement shall be binding upon and inure to the benefit of the parties' successors, legal representatives, and authorized assigns.

- In the event of any conflict between your obligations established by these terms and conditions and those established by CCC's Billing and Payment terms and conditions, these terms and conditions shall prevail.

- WILEY expressly reserves all rights not specifically granted in the combination of (i) the license details provided by you and accepted in the course of this licensing transaction, (ii) these terms and conditions and (iii) CCC's Billing and Payment terms and conditions.

- This Agreement will be void if the Type of Use, Format, Circulation, or Requestor Type was misrepresented during the licensing process.

- This Agreement shall be governed by and construed in accordance with the laws of the State of New York, USA, without regards to such state's conflict of law rules. Any legal action, suit or proceeding arising out of or relating to these Terms and Conditions or the breach thereof shall be instituted in a court of competent jurisdiction in New York County in the State of New York in the United States of America and each party hereby consents and submits to the personal jurisdiction of such court, waives any objection to venue in such court and consents to service of process by registered or certified mail, return receipt requested, at the last known address of such party.

WILEY OPEN ACCESS TERMS AND CONDITIONS

Wiley Publishes Open Access Articles in fully Open Access Journals and in Subscription journals offering Online Open. Although most of the fully Open Access journals publish open access articles under the terms of the Creative Commons Attribution (CC BY) License only, the subscription journals and a few of the Open Access Journals offer a choice of Creative Commons Licenses. The license type is clearly identified on the article.

The Creative Commons Attribution License

The Creative Commons Attribution License (CC-BY) allows users to copy, distribute and transmit an article, adapt the article and make commercial use of the article. The CC-BY license permits commercial and non-

Creative Commons Attribution Non-Commercial License

The Creative Commons Attribution Non-Commercial (CC-BY-NC)License permits use, distribution and reproduction in any medium, provided the original work is properly cited and is not used for commercial purposes.(see below)

Creative Commons Attribution-Non-Commercial-NoDerivs License

The Creative Commons Attribution Non-Commercial-NoDerivs License (CC-BY-NC-ND) permits use, distribution and reproduction in any medium, provided the original work is properly cited, is not used for commercial purposes and no modifications or adaptations are made. (see below)

Use by commercial "for-profit" organizations

Use of Wiley Open Access articles for commercial, promotional, or marketing purposes requires further explicit permission from Wiley and will be subject to a fee.

Further details can be found on Wiley Online Library

http://olabout.wiley.com/WileyCDA/Section/id-410895.html

Other Terms and Conditions:

v1.10 Last updated September 2015

Questions? customercare@copyright.com or +1-855-239-3415 (toll free in the US) or +1-978-646-2777.

AGU PUBLICATIONS

Global Biogeochemical Cycles

RESEARCH ARTICLE
10.1002/2015GB005265

Key Points:
- Local and remote sources contribute to Roosevelt Island dust deposition at present
- Dissolved Fe in Antarctic snow appears to be related to both dust and black carbon deposition
- Exceptionally high black carbon, dust, and dissolved Fe concentrations in 2011/2012 austral summer

Supporting Information:
- Text S1, Figures S1–S3, Tables S1 and S2, and captions for Data Sets S1 and S2
- Data Set S1
- Data Set S2

Correspondence to:
V. H. L. Winton,
holly.winton@postgrad.curtin.edu.au

Citation:
Winton, V. H. L., R. Edwards, B. Delmonte, A. Ellis, P. S. Andersson, A. Bowie, N. A. N. Bertler, P. Neff, and A. Tuohy (2016), Multiple sources of soluble atmospheric iron to Antarctic waters, *Global Biogeochem. Cycles*, *30*, doi:10.1002/2015GB005265.

Received 1 SEP 2015
Accepted 3 FEB 2016
Accepted article online 6 FEB 2016

Multiple sources of soluble atmospheric iron to Antarctic waters

V. H. L. Winton[1], R. Edwards[1], B. Delmonte[2], A. Ellis[1], P. S. Andersson[3], A. Bowie[4,5], N. A. N. Bertler[6,7], P. Neff[6,7,8], and A. Tuohy[6,7]

[1]Physics and Astronomy, Curtin University, Perth, Western Australia, Australia, [2]DISAT, Department of Earth and Environmental Sciences, University of Milano-Bicocca, Milan, Italy, [3]Department of Geosciences, Swedish Museum of Natural History, Stockholm, Sweden, [4]Antarctic Climate and Ecosystems CRC, Hobart, Tasmania, Australia, [5]Institute for Antarctic and Southern Ocean Studies, University of Tasmania, Hobart, Tasmania, Australia, [6]Antarctic Research Centre, Victoria University of Wellington, Wellington, New Zealand, [7]National Isotope Centre, GNS Science, Lower Hutt, New Zealand, [8]Now at Department of Earth and Environmental Sciences, University of Rochester, Rochester, New York, USA

Abstract The Ross Sea, Antarctica, is a highly productive region of the Southern Ocean. Significant new sources of iron (Fe) are required to sustain phytoplankton blooms in the austral summer. Atmospheric deposition is one potential source. The fractional solubility of Fe is an important variable determining Fe availability for biological uptake. To constrain aerosol Fe inputs to the Ross Sea region, fractional solubility of Fe was analyzed in a snow pit from Roosevelt Island, eastern Ross Sea. In addition, aluminum, dust, and refractory black carbon (rBC) concentrations were analyzed, to determine the contribution of mineral dust and combustion sources to the supply of aerosol Fe. We estimate exceptionally high dissolved Fe (dFe) flux of 1.2×10^{-6} g m^{-2} y^{-1} and total dissolvable Fe flux of 140×10^{-6} g m^{-2} y^{-1} for 2011/2012. Deposition of dust, Fe, Al, and rBC occurs primarily during spring-summer. The observed background fractional Fe solubility of ~0.7% is consistent with a mineral dust source. Radiogenic isotopic ratios and particle size distribution of dust indicates that the site is influenced by local and remote sources. In 2011/2012 summer, relatively high dFe concentrations paralleled both mineral dust and rBC deposition. Around half of the annual aerosol Fe deposition occurred in the austral summer phytoplankton growth season; however, the fractional Fe solubility was low. Our results suggest that the seasonality of dFe deposition can vary and should be considered on longer glacial-interglacial timescales.

1. Introduction

The Ross Sea is the most biologically productive continental shelf region around Antarctica and an important region for atmospheric CO_2 sequestration [*Arrigo and Van Dijken*, 2007; *Arrigo et al*., 1998, 2008; *Smith and Gordon*, 1997]. Each summer the Ross Sea blooms with phytoplankton [e.g., *Smith and Gordon*, 1997]. Two distinct blooms occur, with each characterized by differences in location, timing, water stratification, and species [*Arrigo and van Dijken*, 2004]. The first bloom occurs in the central Ross Sea polynya north of the Ross Ice Shelf and is dominated by *Phaeocystis Antarctica*. This bloom develops in late October–November when sea ice is still present and terminates as early as mid-December. The second bloom occurs in the southwestern (SW) Ross Sea, is dominated by diatoms, and is much smaller in areal extent. In the Southern Ocean, environmental factors responsible for controlling the rates of phytoplankton production include: grazing [e.g., *Banse*, 1991], temperature [e.g., *Bunt*, 1963], light availability [e.g., *Mitchell et al*., 1991], water stratification [*Tagliabue and Arrigo*, 2006], sea ice extent [*Smith and Nelson*, 1986], trace metal availability [e.g., Fe; *Martin et al*., 1990; *Sedwick and DiTullio*, 1997; *Sedwick et al*., 2011], or a combination of these [e.g., *Arrigo et al*., 2000]. Due to the Ross Sea's capacity to support intense early summer phytoplankton blooms, the seasonally Fe-limited high-nutrient high-chlorophyll (HNHC) regime of the Ross Sea in summer is distinct from the chronically Fe-limited high-nutrient low-chlorophyll (HNLC) offshore waters of the Southern Ocean [*Tagliabue and Arrigo*, 2005].

In situ oceanic iron (Fe)-fertilization experiments have demonstrated a response of the ecosystem to relatively small additions of dissolved Fe (dFe) in the Ross Sea and other sections of the Southern Ocean [*Coale et al*., 2003; *Martin et al*., 1990]. The seasonally Fe-limited HNHC regime in the Ross Sea requires continuous new inputs of dissolved Fe (dFe) to sustain these phytoplankton blooms [e.g., *Fitzwater et al*., 2000; *Sedwick et al*., 2011]. Inputs of new Fe to surface waters in the Ross Sea can occur through upwelling of deep waters, transport from continental margins by ocean currents, melt from sea

ice, icebergs and ice shelves, and atmospheric aerosol deposition [*Atkins and Dunbar*, 2009; *de Jong et al*., 2013; *Gerringa et al*., 2015; *Jacobs et al*., 1970; *Marsay et al*., 2014; *Sedwick and DiTullio*, 1997; *Sedwick et al*., 2011; *Winton et al*., 2014].

In terms of an atmospheric source, the deposition of aerosol Fe to remote Southern Ocean surface waters is extremely low [e.g., *Winton et al*., 2015] and has been investigated in relation to the distribution and transport of mineral dust. Little aerosol Fe data exist for the Ross Sea region. Total dissolvable Fe (TDFe) aerosol fluxes to the Ross Sea from long-range transported dust have been estimated to range between 0.007 and 0.1 mg m^{-2} yr^{-1} [*Edwards and Sedwick*, 2001]. Measurements of local soluble Fe from local dust on sea ice in McMurdo Sound [*Winton et al*., 2014] show that this local Fe source is much larger (2–7 mg m^{-2} yr^{-1}) than that supplied by long-range transport sources [e.g., *Wagener et al*., 2008]. The supplied Fe, however, only contributes to phytoplankton blooms within the localized McMurdo Sound region. On longer timescales, enhanced glacial atmospheric Fe deposition has been linked to higher rates of Southern Ocean primary productivity as observed from recent Southern Ocean marine sediment studies [e.g., *Martínez-García et al*., 2014]. Furthermore, Antarctic ice core records associate higher dust deposition rates with Fe supply during glacial stages [*Conway et al*., 2015; *Edwards et al*., 2006; *Gaspari et al*., 2006; *Vallelonga et al*., 2013]. Dust deposition to Antarctica can be sourced from both remote and local sources [e.g., *Bory et al*., 2010; *Delmonte et al*., 2013]. Dust provenance can be determined from the $^{87}Sr/^{86}Sr$ and $^{143}Nd/^{144}Nd$ radiogenic isotope composition of dust in snow and ice by comparison with potential source areas (PSAs) [*Grousset and Biscaye*, 2005]. This is because the Sr and Nd isotopic composition of dust are primarily related to lithology and the geologic history of parent materials [*Faure*, 1986].

Aerosol Fe bioavailability information is required to constrain the biogeochemical impact of present and past atmospheric Fe variability. Reported values of fractional aerosol Fe solubility range from 0.01 to 90% [*Baker and Croot*, 2010; *Bowie et al*., 2009; *Edwards and Sedwick*, 2001; *Heimburger et al*., 2013; *Mahowald et al*., 2005]. This large range may reflect differences in mineral dust concentrations, particle size, atmospheric weathering, and aerosol leaching methods [*Aguilar-Islas et al*., 2010; *Baker and Jickells*, 2006; *Bonnet and Guieu*, 2004; *Buck et al*., 2006; *Chen and Siefert*, 2003; *Spokes and Jickells*, 1995; *Trapp et al*., 2010; *Zhuang et al*., 1990, 1992]. An alternative hypothesis for the observed solubility range is that it results from a mixture of aerosol Fe sources with different mineralogy and fractional Fe solubility [*Sholkovitz et al*., 2012]. *Sholkovitz et al*. [2012] showed that global scale fractional aerosol Fe solubility displays an inverse hyperbolic relationship with the total Fe concentration. This relationship is consistent with a low fractional Fe solubility for mineral dust (~1–2%) and the presence of other soluble Fe sources, such as those originating from biomass burning and oil combustion with higher fractional Fe solubility [*Chuang et al*., 2005; *Guieu et al*., 2005; *Ito*, 2011; *Kumar et al*., 2010; *Luo et al*., 2008; *Paris et al*., 2010; *Sedwick et al*., 2007; *Sholkovitz et al*., 2009]. Estimates of fractional Fe solubility from fire combustion range from 1 to 60% and may vary in relationship to biomass and fire characteristics as well as that of the underlying terrain [*Guieu et al*., 2005; *Ito*, 2011; *Kumar et al*., 2010; *Luo et al*., 2008; *Paris et al*., 2010]. Over the time period investigated (2010–2012) in this study, Southern Hemisphere biomass burning emissions primarily occurred in the Intertropical Convergence Zone of Africa, Australia, and South America [*Giglio et al*., 2013]. Of these regions, Australia is the closest to the Ross Sea. Biomass burning constitutes a large source of austral dry season aerosol emissions over northern Australia, and episodic austral summer wildfires in southern and eastern Australia [e.g., *Meyer et al*., 2008]. Refractory black carbon aerosols (rBC) are emitted by biomass burning and fossil fuels [*Reid et al*., 2005]. In the Southern Hemisphere, rBC emissions are primarily from biomass burning [*Giglio et al*., 2013] and can be used as a proxy for the long-range transport of biomass burning aerosols to Antarctica. *Bisiaux et al*. [2012] investigated ice core records of rBC deposition to West Antarctica and found annual deposition consistent with austral dry season biomass burning. Thus, Fe associated with rBC may provide information with respect to biomass burning inputs of Fe to the Southern Ocean in this study.

An intermediate depth ice core (764 m) was recently drilled in the framework of the Roosevelt Island Climate Evolution (RICE) project at Roosevelt Island (79.36086°S, 161.64600°W; Figure 1), located on the opposite side of the Ross Sea to McMurdo Sound. Many aspects of atmospheric Fe deposition in marginal areas of Antarctica remain poorly known. In this respect, Roosevelt Island represents an ideal location to investigate the timing and source(s) of soluble Fe deposition to the eastern Ross Sea region. This study investigated the present-day seasonality of fractional Fe solubility and potential sources from mineral dust and rBC at Roosevelt Island.

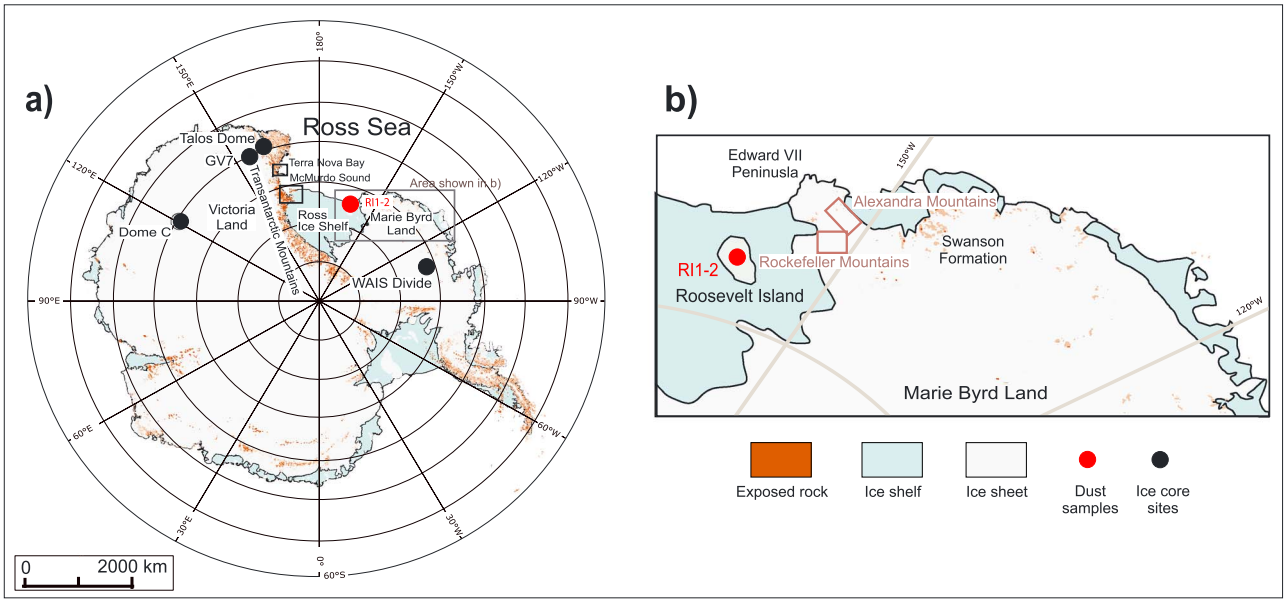

Figure 1. (a) Map of Antarctica showing the location of the Ross Sea. (b) Insert of Marie Byrd Land showing West Antarctic potential source areas and Roosevelt Island dust sample locations (RI1-2). EAIS: East Antarctic Ice Sheet, MDV: McMurdo Dry Valleys, and TAM: Transantarctic Mountains.

2. Methods

A detailed description of the snow sampling procedure, dust, rBC, trace metal solubility, and Sr and Nd isotopic analysis can be found in supporting information Text S1. Briefly, four parallel profiles of ultraclean snow samples were collected at 3 cm resolution from a 1.5 m snow pit. The snow pit was located in a designated clean sector at Roosevelt Island during the 2012/2013 RICE ice core drilling campaign. Parallel profile samples were measured for particle size and concentration (Coulter Counter) [*Delmonte et al.*, 2002], rBC concentration (single particle intracavity laser-induced incandescence photometer (SP2)) [*Sterle et al.*, 2013], $\delta^{18}O$ isotopes (high-resolution laser absorption spectroscopy; Los Gatos Research Liquid-Water Isotope Analyzer), and dissolved and total dissolvable concentrations of sulfur (S), Fe, and aluminum (Al). Dissolved Fe and Al fractions were determined by filtering a 10 mL aliquot of snow melt through a 0.2 μm filter [*Lannuzel et al.*, 2008]. The remaining (unfiltered) sample was leached with 1% HCl (ultrapure) for 3 months to determine the total dissolvable trace metal fraction following *Edwards et al.* [2006] who showed that a 3 month leaching period was required for TDFe concentrations to plateau. Total dissolvable solutions and dissolved leachates were analyzed by high-resolution inductively coupled plasma mass spectrometry (HR-ICP-MS). HR-ICP-MS operating conditions and blank elemental levels are reported in Tables S1 and S2. Stringent trace metal practices were employed at all stages of sample processing and analysis. Sampling vials and filtration gear were rigorously acid cleaned prior to use following GEOTRACES protocols (http://www.geotraces.org/images/stories/documents/intercalibration/Cookbook.pdf). Fractional Fe solubility was calculated using equation (1):

$$\text{Fractional Fe solubility} = \text{dFe} / \text{TDFe} \times 100, \quad (1)$$

where dFe is the soluble or dissolved Fe fraction and TDFe is the total dissolvable fraction.

A reflected light optical microscope (BX51M) was used to confirm the presence of large particles (>10 μm) detected by Coulter Counter (Figure S1). Adjacent to the snow pit, a large volume of surface snow was collected for Sr and Nd isotopic ratios and concentrations of dust for provenance attribution (supporting information Text S1). Dust particles were separated from the snow, and two samples (RI1-2) were spiked, digested, separated from interfering elements and analyzed by TRITON thermal ionization mass following *Delmonte et al.* [2008].

3. Results

3.1. Snow Pit Dating

The dating of the RICE snow pit was based on water stable isotope ratios $\delta^{18}O$ and on concentrations of total dissolved non-sea-salt sulfur (nss-S) (Figure 2) following *Tuohy et al.* [2015]. Non-sea-salt sulfur shows sharp,

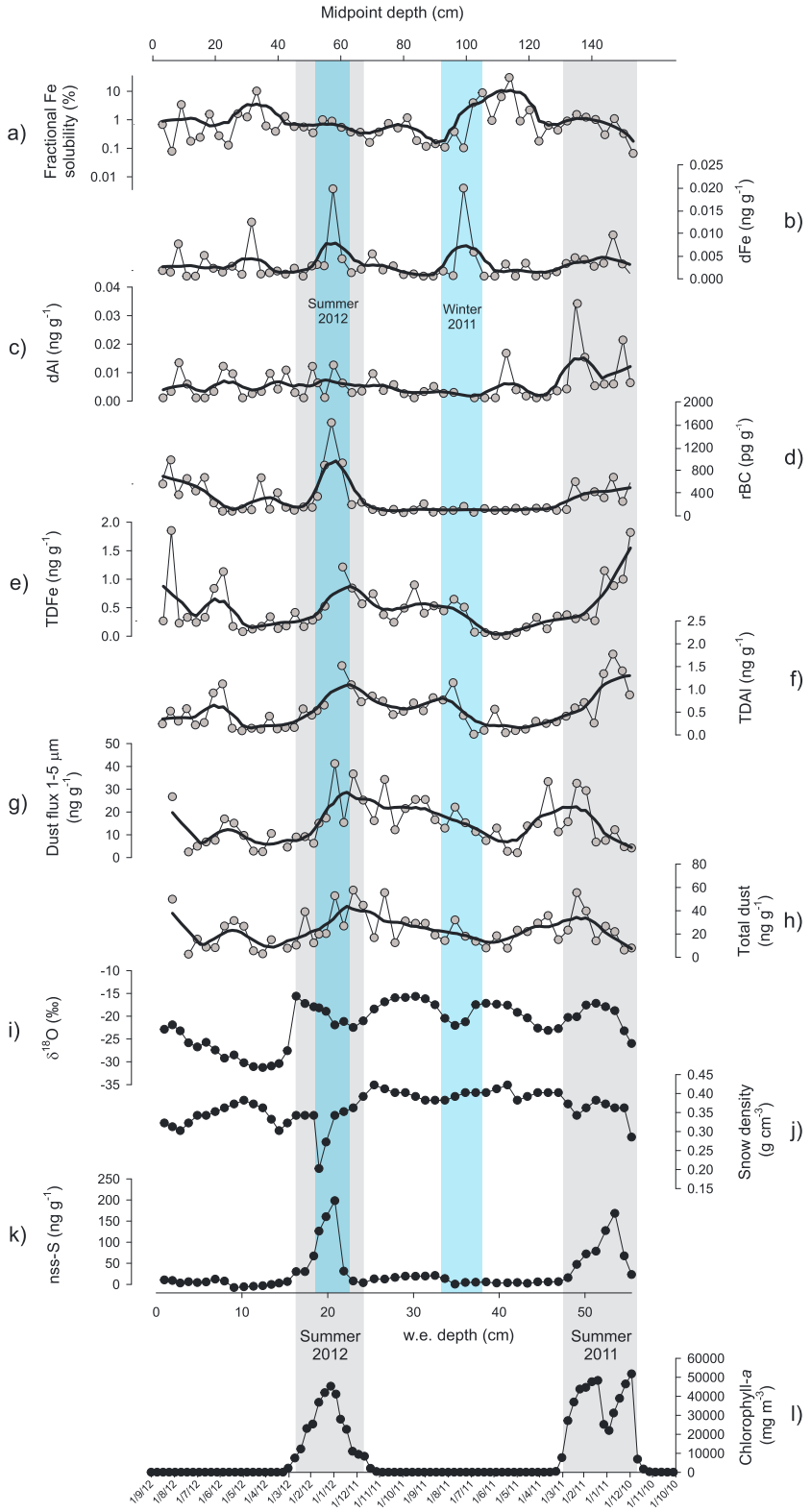

Figure 2. Roosevelt Island snow pit profile showing (a) fractional Fe solubility, (b) dFe concentration, (c) dAl concentration, (d) rBC concentration, (e) TDFe concentration, (f) TDAl concentration, (g) dust concentration for the 1–5 µm fraction, (h) total dust concentration for the 1–30 µm fraction, (i) $\delta^{18}O$, (j) snow density, (k) nss-S concentration, and (l) chlorophyll *a* concentration. Grey bars indicate summer periods. Blue bars highlight the largest periods of dFe deposition. Black lines indicate smoothed data using a 0.15 loess model [*Cleveland and Devlin*, 1988].

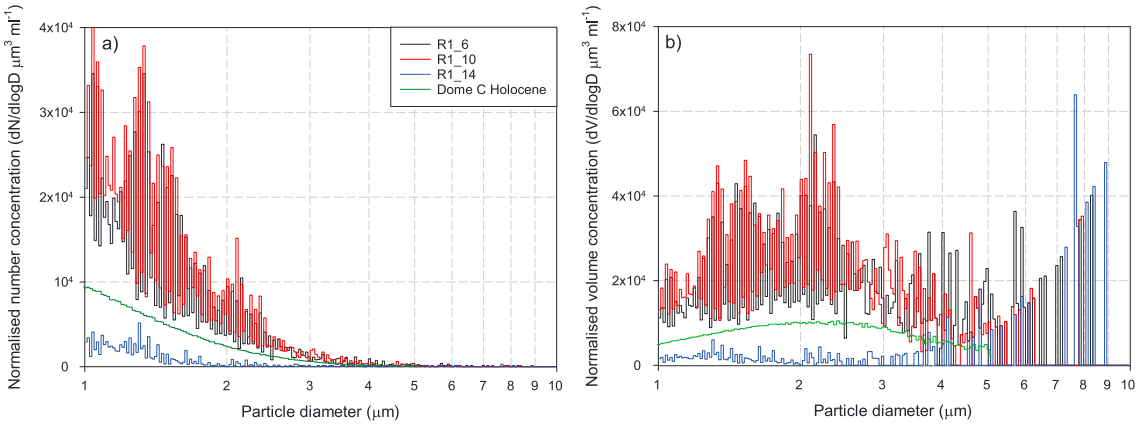

Figure 3. Examples of particle size distributions in the snow pit from Roosevelt Island and comparison to the lognormal particle size distribution of Holocene dust from the Dome C ice core on the East Antarctic Plateau. (a) Normalized size distribution of the number of particles (dN/dlogD) and (b) normalized volume size distribution (dV/dlogD). Samples shown are Blue: RI_14, Black: RI_6, and Red: RI_10. Dome C Holocene particle size distribution from *Delmonte et al.* [2002].

well defined summer peaks. The $\delta^{18}O$ measurements in Antarctic snow and ice often reflect seasonal cycles in temperature [*Dansgaard*, 1954; *Johnsen et al.*, 1972]. However, the upper snow pack at Roosevelt Island contains $\delta^{18}O$ variability within seasons which reflects individual storm events [*Tuohy et al.*, 2015]. Summers were determined as 1 January and were positioned where nss-S peaks aligned with peaks or shoulders of peaks in the $\delta^{18}O$ record. Winters were determined as 1 July where a nss-S trough aligned with a $\delta^{18}O$ trough. Annual cycle counting of nss-S layers shows the snow pit spans a 2 year period from summer 2012/2013 to summer 2010/2011 (Figure 2), with an age uncertainty of ±0.5 year at the base of the snow pit. The snow accumulation rate of the snow pit is estimated to be 0.33 m yr^{-1} water equivalent (w.e.; estimated from nss-S concentration peaks between January 2011 and January 2012), assuming the average annual distribution of snowfall is uniform. These rates are consistent with an accumulation rate of ~0.27 m yr^{-1} ice equivalent from snow stake measurements ~700 m from the snow pit site at Roosevelt Island between 2010 and 2012 (H. Conway, unpublished data, 2015).

To constrain the seasonality of nss-S with known sulfate emissions from phytoplankton [e.g., *Rhodes et al.*, 2009], high-resolution chlorophyll *a* satellite data were downloaded for the Ross Sea region (area defined by 161.175° to −151.125°, −70.078° to −80.0°) (Figures 2k and 2l, SeaWiFS; http://disc.sci.gsfc.nasa.gov/giovanni). The temporal development of Ross Sea polynya phytoplankton bloom ("bloom 2," see section 1.1) was used due to the dominant easterly transport within the Ross Sea [*Sinclair et al.*, 2010]. Comparison of chlorophyll *a* concentration data over the Ross Sea region shows that the bloom develops in November and declines in December in both 2010 and 2011 (Figure 2l). In addition, a hoar layer (with a low snow density of 0.20 g m^{-3}) at ~55 cm depth in the snow pit was compared to nss-S summer maxima (Figures 2i–2l). The age scale independently places this hoar layer in 2011 spring-summer, confirming the validity of the overall age model.

3.2. Seasonal Dust Variability and Particle Size Distribution

The Roosevelt Island snow pit records interannual variability in dust deposition over a 2 year period. The dust concentration in the snow pit ranges from 2 to 41 ng g^{-1} for the 1–5 µm fraction and 2 to 58 ng g^{-1} for the 1–30 µm particle size fraction. We note that two samples have low dust concentrations (<4 ng g^{-1}) close to exposure blank levels (~2 ng g^{-1}). Dust deposition in the snow pit is episodic. The dust record displays two maxima corresponding to summer-spring elevated levels of nss-S in January 2012 and January 2011 (Figures 2g, 2h, and 2k). Lower dust concentrations are observed in winter; however, an episodic dust event is captured during winter 2012. Seasonal dust deposition at Roosevelt Island, primarily during spring-summer, is coherent with an earlier snow pit study from the site that showed higher Al/Na ratios [*Cohen*, 2013] in correspondence with summer peaks of the $\delta^{18}O$ record. At GV7, a peripheral site located on the South Pacific margin of the East Antarctic Ice Sheet (EAIS) in Northern Victoria Land (Figure 1), dust deposition from a snow pit clearly shows spring-summer maxima and winter minima (B. Delmonte, in preparation, 2015). Dust deposition at other locations in Antarctica also exhibits seasonal variability with a maximum in summer (e.g., Berkner Island [*Bory et al.*, 2010], Windless Bight, McMurdo Sound [*Dunbar et al.*, 2009], and South Pole [*Legrand and Kirchner*, 1988]).

Table 1. Nd and Sr Concentrations (in Parentheses) and Isotopic Composition of Roosevelt Island Surface Snow Samples Analyzed in This Study[h]

Sample	Size (μm)	$^{143}Nd/^{144}Nd$	[a] $\pm 2\sigma_{mean}$ *10^6	[b] $\varepsilon_{Nd}(0)$	[c] $\pm 2\sigma$	[Nd] (ppm)	[d] ± (ppm)	$^{87}Sr/^{86}Sr$	[e] $\pm 2\sigma_{mean}$ *10^6	[f] $^{87}Sr/^{86}Sr$ Corrected	[g] $\pm 2\sigma$ *10^6	[Sr] (ppm)	[d] ± (ppm)
RI-1	Bulk	n.d.	n.d.	n.d.	n.d.	3	0.3	0.712173	17	0.712201	17	40	4
RI-2	Bulk	0.512146	50	−9.6	0.3	12	1.2	0.715560	48	0.715588	48	60	6

[a] Internal precision, two standard errors of the mean.
[b] Nd isotopic ratios expressed as epsilon units $\varepsilon_{Nd}(0) = [(^{143}Nd/^{144}Nd)_{sample}/(^{143}Nd/^{144}Nd)_{CHUR}-1] \times 10^4$; CHUR, chondritic uniform reservoir with $^{143}Nd/^{144}Nd = 0.512638$.
[c] Uncertainty estimates based upon external precision for standard runs. Internal precision is used if it exceeds the external.
[d] Error due to difficulty of measuring small sample masses, estimated by repeat measuring of weighting BCR-2 standards (~0.3 mg).
[e] Internal precision, two standard errors of the mean.
[f] Corrected to a National Bureau of Standards 987 $^{87}Sr/^{86}Sr$ ratio of 0.710245.
[g] Uncertainty estimates based upon external precision for standard runs. Internal precision is used if it exceeds the external.
[h] n.d.: no data.

The particle size distribution of dust particles measured from 1 to 30 μm does not approximate a lognormal particle size distribution. Rather, the size distribution of dust particles approaches the theoretical dust emission particle size distribution, parameterized by [*Kok*, 2011a], for particles between 1 and 5 μm in diameter in samples with elevated dust concentrations in both spring-summer periods. The particle size can be seen in some of these highly concentrated spring-summer samples in Figure 3 and compared to the lognormal particle

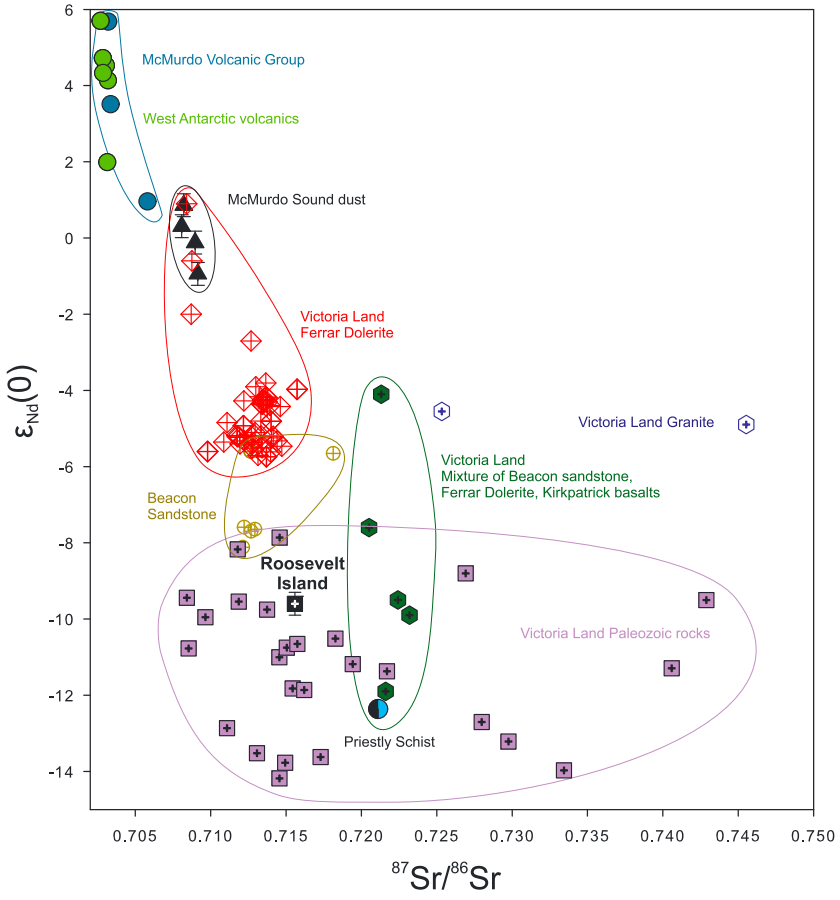

Figure 4. Nd and Sr isotope signature of Roosevelt Island surface snow dust sample. Note only one sample is plotted as there is no Nd data for the second sample. Also plotted are data from Victoria Land sediments from potential dust sources (regolith, glacial deposits, and aeolian sediments) [*Delmonte et al.*, 2004, 2013, 2010] that include different parent lithologies (Victoria Land Ferrar Igneous Provence [*Antonini et al.*, 1999; *Delmonte et al.*, 2004; *Elliot et al.*, 1999; *Fleming et al.*, 1995] and Victoria Land Paleozoic rocks [*Cox et al.*, 2000; *Schüssler et al.*, 1999; *Talarico et al.*, 1995]), volcanic rocks from the McMurdo Volcanic Group and West Antarctica [*Delmonte et al.*, 2004; *Futa and Le Masurier*, 1983; *Hole and LeMasurier*, 1994] and McMurdo Sound dust [*Winton et al.*, 2016].

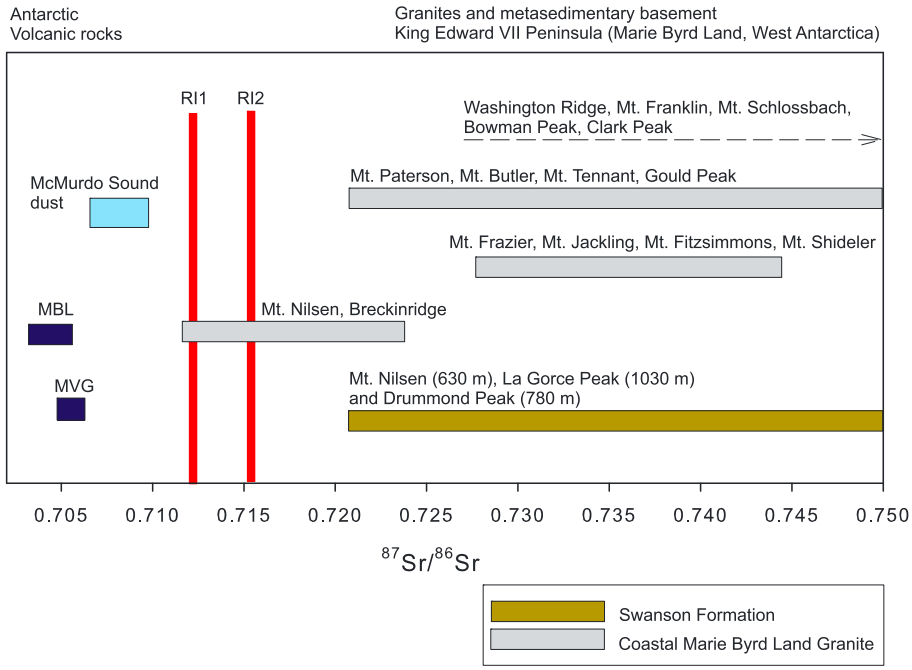

Figure 5. $^{87}Sr/^{86}Sr$ isotopic composition of Roosevelt Island dust compared to McMurdo Sound dust [*Winton et al.*, 2014, 2016], Antarctic volcanic rocks [*Delmonte et al.*, 2004; *Futa and Le Masurier*, 1983; *Hole and LeMasurier*, 1994], and King Edward VII Peninsula, Marie Byrd Land, West Antarctic Granites, and metasedimentary basement rocks [*Adams et al.*, 1995].

size distribution of long-range transported dust to the East Antarctic Plateau. For very low concentration samples, the size distribution of microparticles typically does not show a clear mode. For this reason, other size indicators (fine particle percentage and the coarse particle percentage parameters) were introduced to study long-term dust size variations in central Antarctica [*Delmonte et al.*, 2002]. In this case, longer records of particle size distributions are required to investigate seasonality in particle size distribution at Roosevelt Island. Large particles with an equivalent spherical diameter between 5 and 10 μm were also observed (Figure 3).

3.3. Isotopic Composition of Dust

The Sr and Nd isotopic composition of the two Roosevelt Island dust samples (RI1-2) are $0.7122 < {}^{87}Sr/^{86}Sr < 0.7156$ and $\varepsilon_{Nd}(0) = -9.6$. These data are reported in Table 1 and Figures 4 and 5 with additional isotopic data from Antarctic PSAs. PSAs in Figure 4 are grouped by geographic location.

3.4. Microscope Observations

Mineral dust and volcanic glass (~10 μm in diameter) was present in Roosevelt Island samples, but only a few qualitative optical observations were performed on selected samples from Roosevelt Island (Figure S1). Volcanic glass is a common component of background dust in Antarctica [*Narcisi et al.*, 2005]. These microscopic observations were useful for confirming the presence of particles having a diameter between 5 and 10 μm, thus (a) eliminating the possibility of particulate contamination of sampling equipment and laboratory procedures and (b) validating Coulter Counter observations of relatively coarse particles in the samples.

3.5. Refractory Black Carbon

Deposition of rBC in the Roosevelt Island snow pit is highest during the 2011/2012 summer (Figure 2d). Austral winter background values in 2011 average ~100 pg g^{-1}, and the summer rBC concentrations reached 4 times above background levels in January 2011 and 7 times the background levels in January 2012 (up to ~1.5 ng g^{-1}). The 2011/2012 summer peak in rBC was exceptionally high in comparison to rBC concentrations reported for the West Antarctic Ice Sheet (WAIS) Divide ice core (geometric mean ~80 pg g^{-1}) [*Bisiaux et al.*, 2012]. Additional smaller peaks of rBC concentrations were also found in late winter-spring in 2012 at Roosevelt Island, similar to the timing of rBC deposition at WAIS Divide.

3.6. Dissolved and Total Dissolvable Iron and Aluminum

With the exception of one layer (61.5–64.5 cm depth), TDFe and TDAl concentrations ranged from 0.01 ± 0.001 to 1.9 ± 0.1 ng g^{-1} and 0.01 ± 0.001 to 1.8 ± 0.1 ng g^{-1}, respectively. The higher concentrations from the 61.5–64.5 cm layer were 5.4 ± 0.1 ng g^{-1} of TDFe and 6.7 ± 0.1 ng g^{-1} of TDAl. This depth also displayed high rBC concentrations of 1630 pg g^{-1}. TDFe and TDAl covary in the snow pit (Figures 2e and 2f). A strong relationship was found between the two trace metals ($r^2 = 0.86$; Figure S3a), with maxima occurring in the summer at the same time as rBC and dust in 2011/2012 but not in 2010/2011.

Dissolved Fe concentrations were lower than TDFe and ranged between 0.001 ± 0.0001 and 0.2 ± 0.001 ng g^{-1} (Figure 2b). Although the exposure blank dFe and dAl concentrations are exceptionally low (Table S2), the dFe and dAl blank background is similar to some of the snow pit samples. Due to the extremely low dissolved concentration of the snow pit samples, it is possible that the uncertainty on the blank concentrations could be responsible for some of the temporal variation. Nevertheless, dFe peaked 4 times above the recorded dFe background of 0.02 ng g^{-1}. Two of these maxima occurred in summer 2011/2012 at the same time as peaks in TDFe, TDAl, dust, and rBC concentrations at Roosevelt Island, while the other two peaks occur in the winter when dust rBC, TDFe, and TDAl are low (Figure 2).

4. Discussion

4.1. Atmospheric Dust Deposition and Provenance

Ice cores from the high-elevation East Antarctic Plateau represent a unique archive to investigate long-range dust transport [e.g., *Delmonte et al*., 2004]. In contrast, around the margin of Antarctica, the occurrence of sparse ice-free areas can represent a non-negligible dust source to the local atmosphere [*Bertler et al*., 2005; *Delmonte et al*., 2013]. At these sites, the interpretation of ice core dust records is related to mesoscale dust entrainment, advection, and deposition driven by regional circulation. Roosevelt Island is a low-altitude location (550 meters above sea level), well outside the high-elevation polar plateau. Large expanses of ice-free areas occur around the margins of the Ross Sea (Figure 1), and thus, the dust cycle there is widely different from the East Antarctic Plateau in terms of abundance and origin.

Known dust sources to the western Ross Sea include the Transantarctic Mountains, Terra Nova Bay, and McMurdo Sound [*Atkins and Dunbar*, 2009; *Barrett et al*., 1983; *Dunbar et al*., 2009]. Of these, southern McMurdo Sound is known to be the dustiest location in Antarctica [*Chewings et al*., 2014; *Winton et al*., 2014]. In terms of the western Ross Sea, Sr and Nd isotopic data are only available for McMurdo Sound and some areas in the Transantarctic Mountains [*Cook et al*., 2013, and references therein; *Delmonte et al*., 2004, 2013; *Winton et al*., 2014], although an expansion of the existing isotopic catalog of Antarctic PSAs is in preparation (Blakowski et al., in review) in an effort to deepen the current understanding of Holocene dust input to the periphery of the EAIS. The isotopic signature of these PSAs in the western Ross Sea is plotted in Figure 4 and compared to the signature of Roosevelt Island dust measured in this study. The isotopic composition of one sample representing modern summer snow at Roosevelt Island is markedly different from the fingerprint of McMurdo Sound (Table 1 and Figure 4), i.e., Roosevelt Island dust ($0.7122 < {}^{87}Sr/{}^{86}Sr < 0.7156$ and $\varepsilon_{Nd}(0) = -9.6$) has a more radiogenic $^{87}Sr/^{86}Sr$ signature and less radiogenic $\varepsilon_{Nd}(0)$ signature compared to the volcanic sediments from McMurdo Sound [*Winton et al*., 2014]. Therefore, the isotopic data alone suggest that dust deposited on Roosevelt Island cannot be solely sourced from McMurdo Sound.

In addition, the dust concentrations at Roosevelt Island are lower and the particle size distribution is finer than the dusty McMurdo Sound [e.g., *Chewings et al*., 2014]. An annual dust flux at Roosevelt Island was estimated for the calendar year 2011 (the beginning of the calendar year was taken at each nss-S peak), and the water equivalent depth was calculated from the snow pit density measurements (Figure S2). The estimated dust flux of 6 mg m^{-2} yr^{-1} for the 1–5 μm particle fraction (8 mg m^{-2} yr^{-1} for the bulk 1–30 μm particle fraction) at Roosevelt Island in this study is seven times greater than the equivalent preindustrial East Antarctic dust flux of 0.19–0.75 mg m^{-2} yr^{-1} [*Delmonte et al*., 2013] and also greater than modern modeled and empirical fluxes of dust to the Southern Ocean (0.3 to 2.5 mg m^{-2} d^{-1}) [*Duce et al*., 1991; *Mahowald et al*., 2005; *Wagener et al*., 2008]. The bulk 1–30 μm dust flux at Roosevelt Island is double that found in the WAIS Divide ice core: ~4 mg m^{-2} yr^{-1} over the past two millennia [*Koffman et al*., 2014].

By comparison, the dust fluxes for Roosevelt Island, East Antarctica, and the Southern Ocean are orders of magnitude lower than the dust flux of the McMurdo Sound fine fraction reported by *Winton et al*. [2014], i.e., 460 mg m^{-2} yr^{-1} for the <10 μm fraction.

Larger dust particles (between 5 and 10 μm) represent a non-negligible contribution to the total dust input at Roosevelt Island. The particle size distribution of the dust at Roosevelt Island (Figure 3) is coarser than the distally sourced dust deposited on the East Antarctica Plateau. For example, at Dome C and other sites located in central Antarctica [*Delmonte et al*., 2002], dust particles are mostly within the size interval 1–5 μm in diameter. The only large particles deposited on the central East Antarctic Plateau have been previously associated with tephra layers [*Basile et al*., 2001; *Narcisi et al*., 2005]. Furthermore, the particle size distribution curve can provide additional information about the proximity to the dust source [*Kok*, 2011a, 2011b]. Dust follows a lognormal distribution in ice cores from regions that primarily receive long-range transported dust to the East Antarctic Plateau or central Greenland [*Delmonte et al*., 2002; *Ruth*, 2002; *Steffensen*, 1997], for example, Dome C (Figure 3). However, recent work by *Kok* [2011a, 2011b] has shown that dust near the emission source does not necessarily follow a lognormal distribution. The spring-summer snow pit samples that approach the theoretical dust emission particle size distribution, parameterized by [*Kok*, 2011a], at Roosevelt Island and other sites near the margin of the ice sheet (e.g., WAIS Divide) [*Koffman et al*., 2014], suggest that dust is not traveling as far as long-range transported dust reaching the East Antarctic Plateau which has a lognormal distribution [*Delmonte et al*., 2002] (Figure 3). These spring-summer samples that approach the theoretical dust emission distribution are indicative of local dust sources. Compared to the East Antarctic Plateau, the higher dust flux, particle size distribution approaching the theoretical dust emission distribution and the presence of large particles (>10 μm) observed under the optical microscope and Scanning Electron Microscopy suggests a local Antarctic dust input to Roosevelt Island. This local Antarctic dust input has a distinctly different isotopic fingerprint to modern McMurdo Sound dust emissions (Figure 4).

The Sr and Nd isotopic signature of Roosevelt Island dust in Figures 4 and 5 suggests that dust deposited at Roosevelt Island during summer 2012/2013 could be a mixture of at least two local sources. One end-member is likely volcanic material with relatively high radiogenic Nd and less radiogenic Sr. The other end-member is likely to be much older, with more radiogenic Sr and less radiogenic Nd. Given existing Sr and Nd isotopic data, the sources to Roosevelt Island include eastern Australia, parts of coastal Marie Byrd Land, and most of Victoria Land. Given the relatively high dust flux, the presence of large particles and particle size distribution approaching the theoretical dust emission distribution we first consider local dust sources upwind of Roosevelt Island. The fetch area of 5 day air mass back trajectories for 2011 and 2012 arriving at Roosevelt Island are predominately from West Antarctica, the Pacific Ocean sector of Antarctica, and Victoria Land [*Tuohy et al*., 2015]. Air mass back trajectories and background climatological circulation show prevailing winds cross exposed rock in Marie Byrd Land, West Antarctica before arriving at Roosevelt Island [*Koffman et al*., 2014; *Tuohy et al*., 2015]. Air masses can also arrive at Roosevelt Island via synoptic cyclonic circulation in the Ross Sea [*Koffman et al*., 2014; *Neff and Bertler*, 2015]. Therefore, two potential end-member local dust sources for Roosevelt Island are West Antarctic volcanic material and Victoria Land Paleozoic rocks (i.e., the bedrock that comprises most of northern Victoria Land, effectively upwind of Roosevelt). Figure 4 shows that the isotopic composition of Roosevelt Island dust falls between the isotopic fields of both these end-members. Despite the isotopic similarity of Victoria Land Palaeozoic rocks and Roosevelt Island dust, we believe this West to East dust transport hypothesis is very unlikely, because strong convective uplift would be necessary to uplift dust in the troposphere above the marine boundary layer, where dust is rapidly removed.

In terms of Victoria Land, previous studies have shown that although there is a high dust flux within the McMurdo Dry Valleys [*Ayling and McGowan*, 2006; *Gillies et al*., 2013; *Lancaster et al*., 2010; *Selby et al*., 1974]; little dust exits the valleys [*Winton et al*., 2016]. The long exposure to katabatic winds has winnowed the surface sediment, resulting in a lack of dust and very fine sand-sized material over most of the valley floor [e.g., *Delmonte et al*., 2010; *Selby et al*., 1974]. These air masses do not travel high in the troposphere and when they encounter humidity from the ocean, the dust is scavenged. Although *Bhattachan et al*. [2015] suggest that dust from Taylor Valley in the McMurdo Dry Valleys could supply soluble Fe to the wider Southern Ocean, other studies have discounted the McMurdo Dry Valleys as a major dust (and dFe) source due to the limited transport in this region [*Barrett et al*., 1983; *Bentley*, 1979; *Chewings et al*., 2014; *Winton et al*., 2014, 2016]. Therefore, we suggest that dust sourced from Victoria Land is unlikely to be transported eastward to Roosevelt Island. While Victoria

Land sources should not be completely discarded due to the large expanse of ice-free area and the isotopic signature Victoria Land Paleozoic rocks potentially acting as an end-member dust source, we also consider local sources from Marie Byrd Land that are immediately upwind of Roosevelt Island.

Although Roosevelt Island is completely ice covered, there are patchy ice-free areas (Rockefeller Mountains and Alexandra Mountains and extensive volcanics, e.g., the Executive Committee Range) along the northwesternmost part of Marie Byrd Land, on the King Edward VII Peninsula (Figure 1b), that is adjacent to the eastern Ross Sea. According to *Adams et al*. [1995], the King Edward VII Peninsula is characterized by the presence of three main rock units: (i) a low-grade metasedimentary suite of late Ordovician age, correlated with the Swanson Formation of the Ford Ranges; (ii) a granitoid suite correlated to the Byrd Coast granite and particularly developed in the Rockefeller Mountains, which includes monzogranites and syenogranites; and (iii) the Alexandra Metamorphic Complex formed by migmatitic paragneiss. The Sr isotopic signature of these ice-free areas on the eastern margin of the Ross Sea is compared to Roosevelt Island dust in Figure 5. Whole rock Rb-Sr geochemistry of the Rockefeller and Alexandra Mountains of Edward VII Peninsula show $^{87}Sr/^{86}Sr$ higher than about 0.721 (Swanson Formation) and higher than 0.712 (Byrd Coast Granite) (Figure 5), while Nd isotopic data are not available [*Adams et al*., 1995]. On the contrary, volcanic rocks from Marie Byrd Land and other volcanic provinces show very unradiogenic Sr (McMurdo Sound and Marie Byrd Land volcanic rocks ($0.7026 < {}^{87}Sr/^{86}Sr < 0.7032$ and $2.0 < \varepsilon_{Nd}(0) < 6.9$); Figure 5) [*Futa and Le Masurier*, 1983; *Hole and LeMasurier*, 1994]. On the basis of Sr isotopic data and particle size distribution data indicating that dust at Roosevelt Island may be locally sourced at present-day, we suggest that the summer 2012/2013 Roosevelt Island dust sample represents a mixture of local volcanic dust and crustal material likely deriving from the neighboring granites and metasedimentary rocks of western Marie Byrd Land and possibly Paleozoic rocks from Victoria Land (Figures 4 and 5).

We also consider a remote Southern Hemispheric contribution of long-range transported dust to Roosevelt Island. Distally derived larger particles could reach Roosevelt Island but are not transported further inland to the high-elevation Antarctic interior. The Roosevelt Island isotopic signature is distinctly different to dust deposited on East Antarctica during the preindustrial (1400 A.D. −1800 A.D.; $^{87}Sr/^{86}Sr$ ranging between 0.707468 and 0.708468) and Holocene periods ($^{87}Sr/^{86}Sr$ ranging between 0.707689 and 0.711200) [*Delmonte et al*., 2013], which suggests the eastern Ross Sea has a different dust source to the East Antarctica Plateau. Roosevelt Island falls within the Australian isotopic field, which is characterized by $^{87}Sr/^{86}Sr$ ratios ranging from 0.709 to 0.732 and $\varepsilon_{Nd}(0)$ between −3 and −15 [*Delmonte et al*., 2004; *Revel-Rolland et al*., 2006]. *Revel-Rolland et al*. [2006] and *De Deckker et al*. [2010] suggested that Australia could contribute to the dust input in central East Antarctica. Modeling studies of dust transport to Antarctica from Southern Hemispheric continents [*Krinner et al*., 2010] show that the annual mean concentration of dust in the eastern Ross Sea region of Antarctica is mostly represented by dust derived from Australia, in agreement with former modeling studies [*Albani et al*., 2012; *Li et al*., 2008; *McGowan and Clark*, 2008]. We note, in addition, that the seasonality of Australian dust export to high southern latitudes occurs during spring and summer [*Boyd et al*., 2004; *Mahowald et al*., 2005]; hence, it is synchronous with the dust peaks we observed in the Roosevelt Island snow pit. *Krinner et al*. [2010] clearly showed that the concentration of Australian continental dust tracers is at a maximum at about 150°W, close to Roosevelt Island. Although, dust appears to be mostly concentrated at higher tropospheric levels (about 6000 m) that are well above the altitude of the Roosevelt Island [*Krinner et al*., 2010]. *Neff and Bertler* [2015] and *Tuohy et al*. [2015] highlight the likelihood of air parcels transported to Roosevelt Island: both air mass back trajectories for the 2011/2012 summer season and the average seasonal air mass back forward trajectories from Southern Hemisphere dust sources for the previous 35 years indicate that air can be derived from the South Pacific which includes transport from Australia and New Zealand. Based on the Sr and Nd isotope data of Australian and New Zealand rocks [*Delmonte et al*., 2004; *Revel-Rolland et al*., 2006], an Australian contribution is more likely.

In summary, geochemical evidence excludes McMurdo Sound dust inputs as the dominant dust source to Roosevelt Island at present. The isotopic data and the presence of coarse particles at Roosevelt Island, compared to East Antarctic Plateau dust, suggest a local contribution from coastal regions of Antarctica. Potential dust sources include Marie Byrd Land rock outcrops, West Antarctic outcrops which are currently not well characterized in terms of their Nd and Sr isotopic signature, or other ice-free areas that have an old crust-like signature. These ice-free areas could include Victoria Land, given that the synoptic cyclonic circulation pattern in the Ross Sea region could allow for dust transport from the western Ross Sea to the

Table 2. Summer and Winter Trace Metal Dissolved, Total Dissolvable and Dust Fluxes

	dFe Flux (10^{-6} g m^{-2} y^{-1})	TDFe Flux (10^{-6} g m^{-2} y^{-1})	dAl Flux (10^{-6} g m^{-2} y^{-1})	TDAl Flux (10^{-6} g m^{-2} y^{-1})	Dust Flux1-5 μm (mg m^{-2} y^{-1})	Dust Flux1-30 μm (mg m^{-2} y^{-1})
Summer	0.4	39	0.5	50	2.7	4.1
Winter	0.2	50	0.4	63	2.4	3.2
Annual	1.2	140	2.9	195	5.9	8.8

eastern Ross Sea. We cannot exclude the possibility of an Australian dust contribution, as the isotopic field overlaps with that of Marie Byrd Land and Victoria Land Paleozoic rocks. Both *Bory et al*. [2010] and *Delmonte et al*. [2013] show that local dust sources on the periphery of the ice sheet can significantly influence the dust composition at coastal, low elevation Antarctic ice core sites. Thus, Roosevelt Island could similarly be sourced from a mixture of local and distal dust sources. Further geochemical measurements from the RICE ice core are required to better constrain the dust provenance in the Ross Sea.

4.2. Atmospheric Iron in the Ross Sea Region

4.2.1. Atmospheric Iron Fluxes

Annual dissolved and total dissolvable Fe and Al fluxes for 2011 were calculated using the same method for dust (see section 4.1). Summer and winter dissolved Fe and Al fluxes for the period 2011 to 2012 were also estimated and are reported in Table 2. We estimate an annual dFe flux of 1.2×10^{-6} g m^{-2} y^{-1} and annual TDFe flux of 140×10^{-6} g m^{-2} y^{-1}. The TDFe flux estimate for Roosevelt Island is higher than published Holocene values in Antarctic ice cores, for example, a TDFe flux of 45×10^{-6} g m^{-2} y^{-1} was reported for coastal Law Dome [*Edwards et al*., 2006]. The TDFe flux at Roosevelt Island is also higher than acid leachable fluxes of 7×10^{-6} g m^{-2} y^{-1} at Dome C, East Antarctic Plateau [*Gaspari et al*., 2006], and 90×10^{-6} g m^{-2} y^{-1} at Talos Dome [*Vallelonga et al*., 2013]. Talos Dome is known to be influenced by local dust sources [*Delmonte et al*., 2010], and the higher TDFe flux at Roosevelt Island is likely due to the contribution of local dust sources from Marie Byrd Land and/or Victoria Land. Local dust sources located on the coast of East Antarctica are also known to influence the concentration of aerosol Fe samples collected over marginal waters [*Gao et al*., 2013]. The TDFe flux at Roosevelt Island is orders of magnitude lower than locally derived aeolian Fe from McMurdo Sound (HF and HNO_3 digestible total Fe: 37–121 mg m^{-2} yr^{-1}; water-soluble Fe: 2–7 mg m^{-2} yr^{-1}) [*Winton et al*., 2014]. We acknowledge that these studies are not directly comparable as different methods were employed to determine the total and soluble Fe fractions. It has been demonstrated that both the acid leachable Fe method [*Gaspari et al*., 2006; *Vallelonga et al*., 2013] and the TDFe method [*Edwards et al*., 2006; this study] underestimate the total Fe fraction in snow and ice [*Conway et al*., 2015].

4.2.2. Atmospheric Fractional Iron Solubility

Fractional Fe solubility was calculated using equation (1). Fractional Fe solubility ranged from 0.1 to 30%. Fractional Fe solubility was fairly constant at ~0.7% throughout the record, however dramatically rose above this background to 10 and 30% during winter in 2012 and 2011, respectively. The background fractional Fe solubility (Figure 2a) parallels $\delta^{18}O$ (Figure 2i) suggesting this variability in Fe deposition could be driven by synoptic weather conditions. We note that it is possible that the higher uncertainty associated with extremely low dFe and dAl concentrations in the snow pit could be responsible for some of the variability in the fractional Fe solubility. Additionally, precipitation of Fe(III) during sample melting or removal of oxyhydroxide complexes during filtration through a 0.2 μm filter could lead to underestimation of dFe concentrations and fractional Fe solubility. However, these processes would have had to occur rapidly as snow melting took <2 h and samples were filtered, acidified, and analyzed immediately after melting to minimize such processes.

The data in this study displayed an inverse hyperbolic relationship between the TDFe concentration in snow and fractional Fe solubility (Figure 6). This relationship has been attributed to the mixing of low Fe solubility mineral dust and other soluble Fe aerosols from sources such as biomass burning and oil combustion [e.g., *Sedwick et al*., 2007]. *Sholkovitz et al*. [2012] reported global fractional Fe solubility data sets and concluded that the characteristic inverse hyperbolic relationship is common over large regions of the global ocean. This relationship was also found for baseline air at the Cape Grim Baseline Air Pollution Station (CGBAPS), Tasmania, Australia, representative of the Southern Ocean [*Winton et al*., 2015]. Results here are similar to or greater than CGBAPS with respect to the extremely low TDFe in the exceptionally clean air. The inverse hyperbolic relationship at Roosevelt Island also suggests a mixture of mineral dust and combustion sources of Fe.

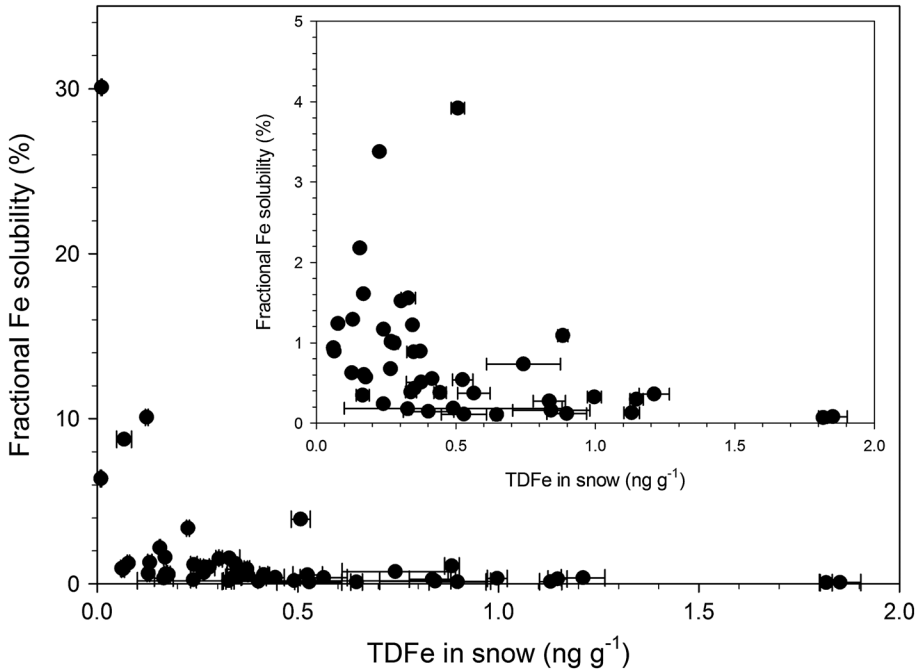

Figure 6. Scatterplot of Roosevelt Island total dissolvable Fe concentration versus fractional Fe solubility. (top right insert) Low concentration data expanded.

Reported values for global fractional Fe solubility of mineral dust are around 1–2% [e.g., *Baker and Croot*, 2010]. Aerosol Fe deposition to remote Southern Ocean surface waters has previously been investigated in relation to the distribution and transport of mineral dust [e.g., *Edwards and Sedwick*, 2001; *Martínez-García et al*., 2014; *Wagener et al*., 2008; *Winton et al*., 2014]. High-elevation East Antarctic ice core records also link higher rates of Fe and dust deposition during glacial periods [*Conway et al*., 2015; *Vallelonga et al*., 2013]. The background fractional Fe solubility of ~0.7% at relatively high TDFe mass concentrations at Roosevelt Island is consistent with a mineral dust source.

Alternatively, the variability in fractional Fe solubility could be driven by changes in dust mineralogy and grain size without necessarily being related to biomass burning sources of soluble Fe. Changes in dust source could supply dust with a higher dFe fraction or where the TDFe dissolves less easily in acid. Furthermore, TDFe can be a highly variable portion of total Fe [e.g., *Conway et al*., 2015; *Tian et al*., 2008]. Seasonal changes in dust provenance at Roosevelt Island are an important topic that deserves further investigation. Some studies have shown that cloud chemistry and atmospheric processing by oxalate and sulfate can enhance the solubility of mineral dust [*Desboeufs et al*., 1999; *Kumar et al*., 2010; *Meskhidze et al*., 2003; *Spokes et al*., 1994]. However, in the remote Atlantic and Pacific Ocean and the Southern Ocean south of Australia, no relationship was observed between acid species and fractional Fe solubility [*Baker et al*., 2006; *Hand et al*., 2004; *Winton et al*., 2015]. Even if the dust source to Roosevelt Island in 2012 was continental Antarctica, e.g., Marie Byrd Land, it is unlikely that atmospheric processing by combustion aerosols (observed in polluted air masses where concentrations of organic acids are high) [*Chuang et al*., 2005; *Ito*, 2015; *Ito and Shi*, 2015; *Kumar et al*., 2010] would enhance the solubility of the Fe contained in the mineral dust. The air masses over Antarctica and the Southern Ocean contain trace concentrations of sulfate and oxalate [*Keywood*, 2007]. However, little is known about the enhancement of fractional Fe solubility in these pristine air masses [*Chance et al*., 2015]. In addition, any enhancement of fractional Fe solubility by oxalate may not be sufficient to account for the high fractional Fe solubility observed in the snow pit. For example, *Paris et al*. [2011] showed that although oxalate complexation increased fractional Fe solubility from 0.0025 to 0.26% in African dust minerals, the fractional Fe solubility remained low. No relationship was found between the samples with a lognormal size distribution and high fractional Fe solubility. Longer records of particle size distribution and fractional Fe solubility at Roosevelt Island are required to investigate whether particle size can explain the variability in fractional Fe solubility.

4.3. Multiple Sources of Atmospheric Dissolved Iron to the Ross Sea

The temporal variability of mineral dust and the biomass burning tracer, rBC, parallels Roosevelt Island atmospheric dFe deposition (Figure 2). Similar to TDFe concentrations, dust and rBC concentrations displayed an inverse hyperbolic relationship with fractional Fe solubility (Figures S3b and S3c). Dissolved Fe deposition to Roosevelt Island is semiannual with elevated deposition in summer and winter during the study period (Figure 2b). The rest of this discussion focuses on the two largest deposition events of dFe highlighted in blue in Figure 2. There were two intervals with high dFe concentrations. There were exceptionally high rBC concentrations in the first interval in summer 2011/2012. While during the second interval in winter 2011, concentrations of rBC were near background levels. In both cases, dust deposition was high indicated by high concentrations of dust, TDFe, and TDAl. During the study period, it appears that dust is the primary source of dFe with additional rBC contributions. In both intervals, the excursion of $\delta^{18}O$ to more negative values suggests that the process by which dFe is deposited at the site is storm related [*Tuohy et al*., 2015]. Multiple sources of dust and rBC may contribute to the atmospheric Fe supply to the Ross Sea, and the absence of an rBC source in winter highlights that the relative importance of the different sources varies seasonally.

4.3.1. Atmospheric Iron Sourced From Mineral Dust

A mineral dust source in summer is evident through (i) covariation of dFe maxima and high dust in 2011/2012 summer-spring (Figures 2e and 2g), (ii) strong correlation between the crustal elements TDFe and TDAl ($r^2 = 0.86$; Figure S3a), (iii) covariation of TDAl and dust in 2011 (Figures S3d and S3e), and (iv) low fractional Fe solubility during summer (~0.7%). For the majority of the record, TDFe and TDAl tracks dust concentration. However, not every dust deposition event leads to higher dFe, for example, in spring 2011. This could be related to differences in the mineralogy of the dust, which varies depending on the dust provenance. Whether the dust provenance switches between seasons is unknown, but it is an important topic that deserves more attention in future. The coarser particle size distribution in summer-spring and Sr and Nd isotopic ratios matching that of nearby Marie Byrd Land, Victoria Land, and Australia suggests that a mixture of different types of local and possibly remote dust sources influences dFe deposition at present.

4.3.2. Atmospheric Iron Sourced From Biomass Burning

Biomass burning may also contribute to the 2011/2012 summer deposition of dFe at Roosevelt Island. Refractory black carbon deposition to Antarctica is linked to Southern Hemispheric long-range transport of biomass burning [*Bisiaux et al*., 2012]. The high fractional Fe solubility during winter in 2011 and 2012 (up to 30%; Figures 2a and 6) indicates that additional atmospheric sources, other than mineral dust or biomass burning, are responsible for high fractional Fe solubility in the winter periods observed in this record. Thus, biomass burning can only account for the high fractional Fe solubility observed in background Southern Hemispheric air during the 2011/2012 summer period covered by the snow pit. Ice core records report rBC as a late winter-spring phenomena in West Antarctica [*Bisiaux et al*., 2012]. Consistent with WAIS Divide, a small late winter-spring time rBC peak is observed in 2012 in this study. However, the exceptionally large 2011/2012 summer rBC peak does not overlap with the time period covered by WAIS Divide rBC record. Longer records of rBC and fractional Fe solubility are needed to test the hypothesis that biomass burning sources of dFe can account for high fractional Fe solubility of aerosols over the Ross Sea.

4.3.3. Timing and Supply of Iron Deposition

Sea ice is a source of dFe to the ocean in the SW Ross Sea, where high dFe concentrations have been observed in the surface waters after considerable sea ice melt [*de Jong et al*., 2013; *McGillicuddy et al*., 2015; *Sedwick and DiTullio*, 1997]. This snow pit record from Roosevelt Island demonstrates that spring-summer dFe deposition occurs during ice-free open water conditions in the Ross Sea, when phytoplankton are blooming (Figure 2l). Around half of the annual TDFe and dFe for 2011 was deposited in the summer, and therefore, the seasonality of dFe deposition needs to be considered on longer glacial-interglacial time scales. Despite high dFe and TDFe deposition in spring-summer, fractional Fe solubility was only ~0.7% at this time. Higher fractional Fe solubility occurs in winter when TDFe is low, and the Ross Sea is seasonally ice covered. Snow on sea ice is a repository for aerosol Fe [*Lannuzel et al*., 2010; *Winton et al*., 2014]. Therefore, deposition of aerosol Fe, with relatively high dFe content, is stored in the surface snow of sea ice during winter. In spring-summer, aerosol Fe with a higher fractional Fe solubility is released and supplied to the ocean as sea ice melts. Regardless of the timing and mechanism in which aerosol dFe is supplied to the Ross Sea, i.e., deposition directly into open water in summer and deposition onto surface snow on sea ice in winter with subsequent release into the ocean during spring-summer sea ice melt, both mechanisms act as a new source of dFe to phytoplankton blooms in spring-summer.

5. Conclusions

A dust flux of 6 mg m^{-2} yr^{-1} for the 1–5 μm fraction and 8 mg m^{-2} yr^{-1} for the bulk 1–30 μm has been estimated for modern dust deposition at Roosevelt Island. Snow pit data from Roosevelt Island reveal dust deposition occurs primarily in the spring-summer season. The higher dust flux at Roosevelt Island compared to the East Antarctic Plateau, the presence of coarse dust particles (>10 μm), the particle size distribution that approaches the theoretical dust emission distribution and the Sr and Nd isotopic ratio of dust deposited on Roosevelt Island suggests a mixture of local and possibly remote dust sources for the present-day. The Sr isotopic composition ($0.7122 < {}^{87}Sr/{}^{86}Sr < 0.7156$) of summer dust in the snow at Roosevelt Island suggests a possible mixing of volcanic and crustal rocks of local origin (i.e., older material, e.g., Paleozoic rock from Victoria Land and parts of Marie Byrd Land and Mesozoic to Cenozoic volcanics). Additional input from remote dust sources cannot be discounted. In this respect, Australia best matches the Roosevelt Island isotopic composition of Sr and Nd. Advection of Australian dust is consistent with modeling studies of modern Australian aeolian transport for the present-day. These dust data from Roosevelt Island provide useful context for the interpretation of the dust record in the 764 m long RICE ice core.

An annual dFe flux of 1.2×10^{-6} g m^{-2} y^{-1} and an annual TDFe flux of 140×10^{-6} g m^{-2} y^{-1} have been estimated for Roosevelt Island for 2011. Deposition of dFe is semiannual occurring in the summer and winter, with half of dFe and TDFe deposition occurring in the summer. The inverse hyperbolic relationship between TDFe concentrations and fractional Fe solubility shows that additional atmospheric sources, other than mineral dust, are responsible for high Fe solubility at different times in the year. There were two intervals with high dFe concentrations in the snow pit: one with exceptionally high rBC concentrations in summer 2011/2012 and the other with rBC concentrations near background levels in winter 2011. In both cases, dust was high. Therefore, mineral dust, from both local and remote sources, is the primary source of dFe to Roosevelt Island with additional input from long-range transport of biomass burning aerosols. Biomass burning may account for the high fractional Fe solubility observed in background Southern Hemispheric air during the summer period. The semiannual nature of Fe deposition to Antarctic waters should be considered when interpreting longer glacial-interglacial time scales of aerosol Fe deposition to the Southern Ocean.

Acknowledgments

This work is a contribution to the Roosevelt Island Climate Evolution (RICE) Programme, funded by national contributions from New Zealand, Australia, Denmark, Germany, Italy, the People's Republic of China, Sweden, UK, and the USA. Logistic support was provided by Antarctica New Zealand (K049) and the US Antarctic Program. We would like to thank Antarctica New Zealand and Scott Base personnel for logistics support. Thank you to the RICE 2012/2013 team for assisting in the collection of samples from Roosevelt Island. V.H.L.W. would like to thank Curtin University for scholarship support (Australian Postgraduate Award and Curtin Research Scholarship). This project was funded by Curtin University, Victoria University of Wellington (RDF-VUW1103), GNS Science (540GCT32), the University of Milano-Bicocca, and the Swedish Museum of Natural History. Access to HR-ICP-MS instrumentation at Curtin University was facilitated through ARC LIEF funding (LE130100029). Thank you to K. Jarrett for technical assistance. Isotopic analyses for dust provenance characterization were carried out at the Swedish Museum of Natural History and were supported by the Department of Geosciences, Swedish Museum of Natural History. The authors acknowledge the use of equipment, scientific, and technical assistance of the Curtin University Electron Microscope Facility, which has been partially funded by the University, State, and Commonwealth Governments. We would like to acknowledge the Norwegian Polar Institute for the use of the Qantarctica package. The data set for the RICE 2012/2013 1.5 m snow pit is available through the Curtin University Research Data repository http://doi.org/10.4225/06/565BCE14467D0 and supporting data are also included as tables in SI files. Additional thanks for the helpful comments and suggestions of Bess Koffman and an anonymous reviewer that aided in revision of this manuscript.

References

Adams, C., D. Seward, and S. Weaver (1995), Geochronology of Cretaceous granites and metasedimentary basement on Edward VII Peninsula, Marie Byrd Land, West Antarctica, *Antarct. Sci.*, *7*(03), 265–276.

Aguilar-Islas, A. M., J. Wu, R. Rember, A. M. Johansen, and L. M. Shank (2010), Dissolution of aerosol-derived iron in seawater: Leach solution chemistry, aerosol type, and colloidal iron fraction, *Mar. Chem.*, *120*(1-4), 25–33.

Albani, S., B. Delmonte, V. Maggi, C. Baroni, J. R. Petit, B. Stenni, C. Mazzola, and M. Frezzotti (2012), Interpreting last glacial to Holocene dust changes at Talos Dome (East Antarctica): Implications for atmospheric variations from regional to hemispheric scales, *Clim. Past Discuss.*, *8*(1), 145–168.

Antonini, P., E. Piccirillo, R. Petrini, L. Civetta, M. D'Antonio, and G. Orsi (1999), Enriched mantle–Dupal signature in the genesis of the Jurassic Ferrar tholeiites from Prince Albert Mountains (Victoria Land, Antarctica), *Contrib. Mineral. Petrol.*, *136*(1-2), 1–19.

Arrigo, K. R., and G. L. van Dijken (2004), Annual changes in sea-ice, chlorophyll *a*, and primary production in the Ross Sea, Antarctica, *Deep Sea Res., Part II*, *51*(1-3), 117–138.

Arrigo, K. R., and G. L. Van Dijken (2007), Interannual variation in air-sea CO_2 flux in the Ross Sea, Antarctica: A model analysis, *J. Geophys. Res.*, *112*, C03020, doi:10.1029/2006JC003492.

Arrigo, K. R., A. M. Weiss, and W. O. Smith Jr. (1998), Physical forcing of phytoplankton dynamics in the southwestern Ross Sea, *J. Geophys. Res.*, *103*(C1), 1007–1021.

Arrigo, K. R., G. R. DiTullio, R. B. Dunbar, D. H. Robinson, M. VanWoert, D. L. Worthen, and M. P. Lizotte (2000), Phytoplankton taxonomic variability in nutrient utilization and primary production in the Ross Sea, *J. Geophys. Res.*, *105*(C4), 8827–8846.

Arrigo, K. R., G. van Dijken, and M. Long (2008), Coastal Southern Ocean: A strong anthropogenic CO2 sink, *Geophys. Res. Lett.*, *35*, L21602, doi:10.1029/2008GL035624.

Atkins, C. B., and G. B. Dunbar (2009), Aeolian sediment flux from sea ice into Southern McMurdo Sound, Antarctica, *Global Planet. Change*, *69*(3), 133–141.

Ayling, B., and H. McGowan (2006), Niveo-eolian sediment deposits in Coastal South Victoria Land, Antarctica: Indicators of regional variability in weather and climate, *Arct. Antarct. Alp. Res.*, *38*(3), 313–324.

Baker, A. R., and P. L. Croot (2010), Atmospheric and marine controls on aerosol iron solubility in seawater, *Mar. Chem.*, *120*(1–4), 4–13.

Baker, A. R., and T. D. Jickells (2006), Mineral particle size as a control on aerosol iron solubility, *Geophys. Res. Lett.*, *33*, L17608, doi:10.1029/2006GL026557.

Baker, A. R., T. D. Jickells, M. Witt, and K. L. Linge (2006), Trends in the solubility of iron, aluminium, manganese and phosphorus in aerosol collected over the Atlantic Ocean, *Mar. Chem.*, *98*(1), 43–58.

Banse, K. (1991), Rates of phytoplankton cell division in the field and in iron enrichment experiments, *Limnol. Oceanogr.*, *36*(8), 1886–1898.

Barrett, P., A. Pyne, and B. Ward (1983), Modern sedimentation in McMurdo Sound, Antarctica, in *Antarctic Earth Science*, edited by R. L. Oliver, P. R. James, and J. B. Jago, pp. 550–554, Antarctic Earth Science Canberra Australian Academy of Sciences.

Basile, I., J. R. Petit, S. Touron, F. E. Grousset, and N. Barkov (2001), Volcanic layers in Antarctic (Vostok) ice cores: Source identification and atmospheric implications, *J. Geophys. Res.*, *106*(D23), 31,915–31,931.
Bentley, P. (1979), *Characteristics and Distribution of Wind Blown Sediments,Western McMurdo Sound, Antarctica*, Victoria Univ. of Wellington, Wellington.
Bertler, N. A. N., P. A. Mayewski, S. B. Sneed, T. R. Naish, U. Morgenstern, and P. J. Barrett (2005), Solar forcing recorded by aerosol concentrations in coastal Antarctic glacier ice, McMurdo Dry Valleys, *Ann. Glaciol.*, *41*(1), 52–56.
Bhattachan, A., L. Wang, M. F. Miller, K. J. Licht, and P. D'Odorico (2015), Antarctica's Dry Valleys: A potential source of soluble iron to the Southern Ocean?, *Geophys. Res. Lett.*, *42*, 1912–1918, doi:10.1002/2015GL063419.
Bisiaux, M., R. Edwards, J. McConnell, M. Curran, T. Van Ommen, A. Smith, T. Neumann, D. Pasteris, J. Penner, and K. Taylor (2012), Changes in black carbon deposition to Antarctica from two high-resolution ice core records, 1850–2000 AD, *Atmos. Chem. Phys.*, *12*(9), 4107–4115.
Bonnet, S., and C. Guieu (2004), Dissolution of atmospheric iron in seawater, *Geophys. Res. Lett.*, *31*, L03303, doi:10.1029/2003GL018423.
Bory, A., E. Wolff, R. Mulvaney, E. Jagoutz, A. Wegner, U. Ruth, and H. Elderfield (2010), Multiple sources supply eolian mineral dust to the Atlantic sector of coastal Antarctica: Evidence from recent snow layers at the top of Berkner Island ice sheet, *Earth Planet. Sci. Lett.*, *291*(1-4), 138–148.
Bowie, A. R., D. Lannuzel, T. A. Remenyi, T. Wagener, P. J. Lam, P. W. Boyd, C. Guieu, A. T. Townsend, and T. W. Trull (2009), Biogeochemical iron budgets of the Southern Ocean south of Australia: Decoupling of iron and nutrient cycles in the subantarctic zone by the summertime supply, *Global Biogeochem. Cycles*, *23*, GB4034, doi:10.1029/2009GB003500.
Boyd, P. W., G. McTainsh, V. Sherlock, K. Richardson, S. Nichol, M. Ellwood, and R. Frew (2004), Episodic enhancement of phytoplankton stocks in New Zealand subantarctic waters: Contribution of atmospheric and oceanic iron supply, *Global Biogeochem. Cycles*, *18*, GB1029, doi:10.1029/2002GB002020.
Buck, C. S., W. M. Landing, J. A. Resing, and G. T. Lebon (2006), Aerosol iron and aluminum solubility in the northwest Pacific Ocean: Results from the 2002 IOC cruise, *Geochem. Geophys. Geosyst.*, *7*, Q04M07, doi:10.1029/2005GC000977.
Bunt, J. S. (1963), Microbiology of Antarctic Sea-ice: Diatoms of Antarctic Sea-ice as agents of primary production, *Nature*, *199*(4900), 1255–1257.
Chance, R., T. D. Jickells, and A. R. Baker (2015), Atmospheric trace metal concentrations, solubility and deposition fluxes in remote marine air over the south-east Atlantic, *Mar. Chem.*, *177*, 45–56.
Chen, Y., and R. L. Siefert (2003), Determination of various types of labile atmospheric iron over remote oceans, *J. Geophys. Res.*, *108*(D24), 4774, doi:10.1029/2003JD003515.
Chewings, J. M., C. B. Atkins, G. B. Dunbar, and N. R. Golledge (2014), Aeolian sediment transport and deposition in a modern high-latitude glacial marine environment, *Sedimentology*, *61*, 1535–1557, doi:10.1111/sed.12108.
Chuang, P. Y., R. M. Duvall, M. M. Shafer, and J. J. Schauer (2005), The origin of water soluble particulate iron in the Asian atmospheric outflow, *Geophys. Res. Lett.*, *32*, L07813, doi:10.1029/2004GL021946.
Cleveland, W. S., and S. J. Devlin (1988), Locally weighted regression: An approach to regression analysis by local fitting, *J. Am. Stat. Assoc.*, *83*(403), 596–610.
Coale, K. H., X. Wang, S. J. Tanner, and K. S. Johnson (2003), Phytoplankton growth and biological response to iron and zinc addition in the Ross Sea and Antarctic Circumpolar Current along 170 W, *Deep Sea Res., Part II*, *50*(3), 635–653.
Cohen, L. (2013), Atmospheric variability and precipitation in the Ross Sea Region, Antarctica, PhD thesis, Victoria Univ. of Wellington, Wellington.
Conway, T., E. Wolff, R. Röthlisberger, R. Mulvaney, and H. Elderfield (2015), Constraints on soluble aerosol iron flux to the Southern Ocean at the Last Glacial Maximum, *Nat. Commun.*, *6*, 7850, doi:10.1038/ncomms8850.
Cook, C. P., et al. (2013), Dynamic behaviour of the East Antarctic ice sheet during Pliocene warmth, *Nat. Geosci.*, *6*(9), 765–769.
Cox, S. C., D. L. Parkinson, A. H. Allibone, and A. F. Cooper (2000), Isotopic character of Cambro-Ordovician plutonism, southern Victoria Land, Antarctica, *N. Z. J. Geol. Geophys.*, *43*(4), 501–520.
Dansgaard, W. (1954), The O18- abundance in fresh water, *Geochim. Cosmochim. Acta*, *6*, 241–260.
De Deckker, P., M. Norman, I. D. Goodwin, A. Wain, and F. X. Gingele (2010), Lead isotopic evidence for an Australian source of aeolian dust to Antarctica at times over the last 170,000 years, *Palaeogeogr. Palaeoclimatol. Palaeoecol.*, *285*(3-4), 205–223.
de Jong, J., V. Schoemann, N. Maricq, N. Mattielli, P. Langhorne, T. Haskell, and J.-L. Tison (2013), Iron in land-fast sea ice of McMurdo Sound derived from sediment resuspension and wind-blown dust attributes to primary productivity in the Ross Sea, Antarctica, *Mar. Chem.*, *157*, 24–40.
Delmonte, B., J. R. Petit, and V. Maggi (2002), Glacial to Holocene implications of the new 27000-year dust record from the EPICA Dome C (East Antarctica) ice core, *Clim. Dyn.*, *18*(8), 647–660.
Delmonte, B., I. Basile-Doelsch, J. R. Petit, V. Maggi, M. Revel-Rolland, A. Michard, E. Jagoutz, and F. Grousset (2004), Comparing the Epica and Vostok dust records during the last 220,000 years: Stratigraphical correlation and provenance in glacial periods, *Earth Sci. Rev.*, *66*(1-2), 63–87.
Delmonte, B., P. S. Andersson, M. Hansson, H. Schöberg, J. R. Petit, I. Basile-Doelsch, and V. Maggi (2008), Aeolian dust in East Antarctica (EPICA-Dome C and Vostok): Provenance during glacial ages over the last 800 kyr, *Geophys. Res. Lett.*, *35*, L07703, doi:10.1029/2008GL033382.
Delmonte, B., et al. (2010), Aeolian dust in the Talos Dome ice core (East Antarctica, Pacific/Ross Sea sector): Victoria Land versus remote sources over the last two climate cycles, *J. Quat. Sci.*, *25*(8), 1327–1337.
Delmonte, B., C. Baroni, P. Andersson, B. Narcisi, M. Salvatore, J. Petit, C. Scarchilli, M. Frezzotti, S. Albani, and V. Maggi (2013), Modern and Holocene aeolian dust variability from Talos Dome (Northern Victoria Land) to the interior of the Antarctic ice sheet, *Quat. Sci. Rev.*, *64*, 76–89.
Desboeufs, K., R. Losno, F. Vimeux, and S. Cholbi (1999), The pH-dependent dissolution of wind-transported Saharan dust, *J. Geophys. Res.*, *104*(D17), 21,287–21,299.
Duce, R. A., et al. (1991), The atmospheric input of trace species to the world ocean, *Global Biogeochem. Cycles*, *5*(3), 193–259.
Dunbar, G. B., N. A. N. Bertler, and R. M. McKay (2009), Sediment flux through the McMurdo Ice Shelf in Windless Bight, Antarctica, *Global Planet. Change*, *69*(3), 87–93.
Edwards, R., and P. Sedwick (2001), Iron in East Antarctic snow: Implications for atmospheric iron deposition and algal production in Antarctic waters, *Geophys. Res. Lett.*, *28*(20), 3907–3910.
Edwards, R., P. Sedwick, V. Morgan, and C. Boutron (2006), Iron in ice cores from Law Dome: A record of atmospheric iron deposition for maritime East Antarctica during the Holocene and Last Glacial Maximum, *Geochem. Geophys. Geosyst.*, *7*, Q12Q01, doi:10.1029/2006GC001307.
Elliot, D. H., T. H. Fleming, P. R. Kyle, and K. A. Foland (1999), Long-distance transport of magmas in the Jurassic Ferrar Large Igneous Province, Antarctica, *Earth Planet. Sci. Lett.*, *167*(1–2), 89–104.
Faure, G. (1986), *Principles of Isotope Geology*, 2nd ed., 589 pp., Wiley, New York.
Fitzwater, S. E., K. S. Johnson, R. M. Gordon, K. H. Coale, and W. O. Smith (2000), Trace metal concentrations in the Ross Sea and their relationship with nutrients and phytoplankton growth, *Deep Sea Res., Part II*, *47*(15-16), 3159–3179.

Fleming, T., K. Foland, and D. Elliot (1995), Isotopic and chemical constraints on the crustal evolution and source signature of Ferrar magmas, north Victoria Land, Antarctica, *Contrib. Mineral. Petrol.*, *121*(3), 217–236.
Futa, K., and W. Le Masurier (1983), Nd and Sr isotopic studies on Cenozoic mafic lavas from West Antarctica: Another source for continental alkali basalts, *Contrib. Mineral. Petrol.*, *83*(1-2), 38–44.
Gao, Y., G. Xu, J. Zhan, J. Zhang, W. Li, Q. Lin, L. Chen, and H. Lin (2013), Spatial and particle size distributions of atmospheric dissolvable iron in aerosols and its input to the Southern Ocean and coastal East Antarctica, *J. Geophys. Res. Atmos.*, *118*, 12,634–12,648, doi:10.1002/2013JD020367.
Gaspari, V., C. Barbante, G. Cozzi, P. Cescon, C. F. Boutron, P. Gabrielli, G. Capodaglio, C. Ferrari, J. R. Petit, and B. Delmonte (2006), Atmospheric iron fluxes over the last deglaciation: Climatic implications, *Geophys. Res. Lett.*, *33*, L03704, doi:10.1029/2005GL024352.
Gerringa, L. J. A., P. Laan, G. L. van Dijken, H. van Haren, H. J. W. De Baar, K. R. Arrigo, and A. C. Alderkamp (2015), Sources of iron in the Ross Sea polynya in early summer, *Mar. Chem.*, doi:10.1016/j.marchem.2015.06.002.
Giglio, L., J. T. Randerson, and G. R. Werf (2013), Analysis of daily, monthly, and annual burned area using the fourth-generation global fire emissions database (GFED4), *J. Geophys. Res. Biogeosci.*, *118*, 317–328, doi:10.1002/jgrg.20042.
Gillies, J. A., W. G. Nickling, and M. Tilson (2013), Frequency, magnitude, and characteristics of aeolian sediment transport: McMurdo Dry Valleys, Antarctica, *J. Geophys. Res. Earth Surf.*, *118*, 461–479, doi:10.1002/jgrf.20007.
Grousset, F., and P. Biscaye (2005), Tracing dust sources and transport patterns using Sr, Nd and Pb isotopes, *Chem. Geol.*, *222*(3-4), 149–167.
Guieu, C., S. Bonnet, T. Wagener, and M. D. Loÿe-Pilot (2005), Biomass burning as a source of dissolved iron to the open ocean?, *Geophys. Res. Lett.*, *32*, L19608, doi:10.1029/2005GL022962.
Hand, J. L., N. M. Mahowald, Y. Chen, R. L. Siefert, C. Luo, A. Subramaniam, and I. Fung (2004), Estimates of atmospheric-processed soluble iron from observations and a global mineral aerosol model: Biogeochemical implications, *J. Geophys. Res.*, *109*, D17205, doi:10.1029/2004JD004574.
Heimburger, A., R. Losno, and S. Triquet (2013), Solubility of iron and other trace elements in rainwater collected on the Kerguelen Islands (South Indian Ocean), *Biogeosciences*, *10*(10), 6617–6628.
Hole, M., and W. LeMasurier (1994), Tectonic controls on the geochemical composition of Cenozoic, mafic alkaline volcanic rocks from West Antarctica, *Contrib. Mineral. Petrol.*, *117*(2), 187–202.
Ito, A. (2011), Mega fire emissions in Siberia: Potential supply of bioavailable iron from forests to the ocean, *Biogeosciences*, *8*(6), doi:10.5194/bg-8-1679-2011.
Ito, A. (2015), Atmospheric processing of combustion aerosols as a source of bioavailable iron, *Environ. Sci. Technol. Lett.*, *2*(3), 70–75.
Ito, A., and Z. Shi (2015), Delivery of anthropogenic bioavailable iron from mineral dust and combustion aerosols to the ocean, *Atmos. Chem. Phys. Discuss.*, *15*(16), 23,051–23,088.
Jacobs, S. S., A. F. Amos, and P. M. Bruchhausen (1970), Ross sea oceanography and Antarctic bottom water formation, *Deep Sea Res. Oceanogr. Abstr.*, *17*(6), 935–962.
Johnsen, S. J., W. Dansgaard, H. B. Clausen, and C. C. Langway (1972), Oxygen isotope profiles through the Antarctic and Greenland ice sheets, *Nature*, *235*(5339), 429–434.
Keywood, M. D. (2007), Aerosol composition at Cape Grim: An evaluation of PM10 sampling program and baseline event switches, in *Baseline Atmospheric Program Australia 2005-2006*, edited by J. M. Cainey, N. Derek, and P. B. Krummel, pp. 31–36, Australian Bur. of Meteorology and CSIRO Marine and Atmospheric Res., Melbourne.
Koffman, B. G., K. J. Kreutz, D. J. Breton, E. J. Kane, D. A. Winski, S. D. Birkel, A. Kurbatov, and M. J. Handley (2014), Centennial-scale variability of the Southern Hemisphere westerly wind belt in the eastern Pacific over the past two millennia, *Clim. Past*, *10*(3), 1125–1144.
Kok, J. F. (2011a), A scaling theory for the size distribution of emitted dust aerosols suggests climate models underestimate the size of the global dust cycle, *Proc. Natl. Acad. Sci. U.S.A.*, *108*(3), 1016–1021.
Kok, J. F. (2011b), Does the size distribution of mineral dust aerosols depend on the wind speed at emission?, *Atmos. Chem. Phys.*, *11*(19), 10,149–10,156.
Krinner, G., J.-R. Petit, and B. Delmonte (2010), Altitude of atmospheric tracer transport towards Antarctica inpresent and glacial climate, *Quat. Sci. Rev.*, *29*(1), 274–284.
Kumar, A., M. Sarin, and B. Srinivas (2010), Aerosol iron solubility over Bay of Bengal: Role of anthropogenic sources and chemical processing, *Mar. Chem.*, *121*(1), 167–175.
Lancaster, N., W. G. Nickling, and J. A. Gillies (2010), Sand transport by wind on complex surfaces: Field studies in the McMurdo Dry Valleys, Antarctica, *J. Geophys. Res.*, *115*, F03027, doi:10.1029/2009JF001408.
Lannuzel, D., V. Schoemann, J. de Jong, L. Chou, B. Delille, S. Becquevort, and J. Tison (2008), Iron study during a time series in the western Weddell pack ice, *Mar. Chem.*, *108*(1-2), 85–95.
Lannuzel, D., V. Schoemann, J. de Jong, B. Pasquer, P. van der Merwe, F. Masson, J. Tison, and A. Bowie (2010), Distribution of dissolved iron in Antarctic sea ice: Spatial, seasonal, and inter-annual variability, *J. Geophys. Res.*, *115*, G03022, doi:10.1029/2009JG001031.
Legrand, M., and S. Kirchner (1988), Polar atmospheric circulation and chemistry of recent (1957-1983) south polar precipitation, *Geophys. Res. Lett.*, *15*(8), 879–882.
Li, F., P. Ginoux, and V. Ramaswamy (2008), Distribution, transport, and deposition of mineral dust in the Southern Ocean and Antarctica: Contribution of major sources, *J. Geophys. Res.*, *113*, D10207, doi:10.1029/2007JD009190.
Luo, C., N. Mahowald, T. Bond, P. Y. Chuang, P. Artaxo, R. Siefert, Y. Chen, and J. Schauer (2008), Combustion iron distribution and deposition, *Global Biogeochem. Cycles*, *22*, GB1012, doi:10.1029/2007GB002964.
Mahowald, N. M., A. R. Baker, G. Bergametti, N. Brooks, R. A. Duce, T. D. Jickells, N. Kubilay, J. M. Prospero, and I. Tegen (2005), Atmospheric global dust cycle and iron inputs to the ocean, *Global Biogeochem. Cycles*, *19*, GB4025, doi:10.1029/2004GB002402.
Marsay, C., P. N. Sedwick, M. Dinniman, P. Barrett, S. Mack, and D. J. McGillicuddy (2014), Estimating the benthic efflux of dissolved iron on the Ross Sea continental shelf, *Geophys. Res. Lett.*, *41*, 7576–7583, doi:10.1002/2014GL061684.
Martin, J. H., R. M. Gordon, and S. E. Fitzwater (1990), Iron in Antarctic waters, *Nature*, *345*(6271), 156–158.
Martínez-García, A., D. M. Sigman, H. Ren, R. F. Anderson, M. Straub, D. A. Hodell, S. L. Jaccard, T. I. Eglinton, and G. H. Haug (2014), Iron fertilization of the Subantarctic Ocean during the last ice age, *Science*, *343*(6177), 1347–1350.
McGillicuddy, D. J., et al. (2015), Iron supply and demand in an Antarctic shelf ecosystem, *Geophys. Res. Lett.*, *42*, 8088–8097, doi:10.1002/2015GL065727.
McGowan, H., and A. Clark (2008), Identification of dust transport pathways from Lake Eyre, Australia using Hysplit, *Atmos. Environ.*, *42*(29), 6915–6925.
Meskhidze, N., W. Chameides, A. Nenes, and G. Chen (2003), Iron mobilization in mineral dust: Can anthropogenic SO_2 emissions affect ocean productivity?, *Geophys. Res. Lett.*, *30*(21), 2085, doi:10.1029/2003GL018035.
Meyer, C. P., A. K. Luhar, and R. M. Mitchell (2008), Biomass burning emissions over northern Australia constrained by aerosol measurements: I—Modelling the distribution of hourly emissions, *Atmos. Environ.*, *42*(7), 1629–1646.

Mitchell, B. G., E. A. Brody, O. Holm-Hansen, C. McClain, and J. Bishop (1991), Light limitation of phytoplankton biomass and macronutrient utilization in the Southern Ocean, *Limnol. Oceanogr.*, *36*(8), 1662–1677.
Narcisi, B., J.-R. Petit, B. Delmonte, I. Basile-Doelsch, and V. Maggi (2005), Characteristics and sources of tephra layers in the EPICA-Dome C ice record (East Antarctica): Implications for past atmospheric circulation and ice core stratigraphic correlations, *Earth Planet. Sci. Lett.*, *239*(3), 253–265.
Neff, P. D., and N. A. Bertler (2015), Trajectory modeling of modern dust transport to the Southern Ocean and Antarctica, *J. Geophys. Res. Atmos.*, *120*, 9303–9322, doi:10.1002/2015JD023304.
Paris, R., K. Desboeufs, P. Formenti, S. Nava, and C. Chou (2010), Chemical characterisation of iron in dust and biomass burning aerosols during AMMA-SOP0/DABEX: Implication for iron solubility, *Atmos. Chem. Phys.*, *10*(9), 4273–4282.
Paris, R., K. Desboeufs, and E. Journet (2011), Variability of dust iron solubility in atmospheric waters: Investigation of the role of oxalate organic complexation, *Atmos. Environ.*, *45*(36), 6510–6517.
Reid, J., R. Koppmann, T. Eck, and D. Eleuterio (2005), A review of biomass burning emissions part II: Intensive physical properties of biomass burning particles, *Atmos. Chem. Phys.*, *5*(3), 799–825.
Revel-Rolland, M., P. De Deckker, B. Delmonte, P. P. Hesse, J. W. Magee, I. Basile-Doelsch, F. Grousset, and D. Bosch (2006), Eastern Australia: A possible source of dust in East Antarctica interglacial ice, *Earth Planet. Sci. Lett.*, *249*(1-2), 1–13.
Rhodes, R. H., N. A. N. Bertler, J. A. Baker, S. B. Sneed, H. Oerter, and K. R. Arrigo (2009), Sea ice variability and primary productivity in the Ross Sea, Antarctica, from methylsulphonate snow record, *Geophys. Res. Lett.*, *36*, L10704, doi:10.1029/2009GL037311.
Ruth, U. (2002), Concentration and size distribution of microparticles in the NGRIP ice core during the last glacial period, Univ. Bremen.
Schüssler, U., M. Bröcker, F. Henjes-Kunst, and T. Will (1999), P–T–t evolution of the Wilson Terrane metamorphic basement at Oates Coast, Antarctica, *Precambrian Res.*, *93*(2–3), 235–258.
Sedwick, P. N., and G. R. DiTullio (1997), Regulation of algal blooms in Antarctic Shelf Waters by the release of iron from melting sea ice, *Geophys. Res. Lett.*, *24*(20), 2515–2518.
Sedwick, P. N., E. R. Sholkovitz, and T. M. Church (2007), Impact of anthropogenic combustion emissions on the fractional solubility of aerosol iron: Evidence from the Sargasso Sea, *Geochem. Geophys. Geosyst.*, *8*, Q10Q06, doi:10.1029/2007GC001586.
Sedwick, P. N., et al. (2011), Early season depletion of dissolved iron in the Ross Sea polynya: Implications for iron dynamics on the Antarctic continental shelf, *J. Geophys. Res.*, *116*, C12019, doi:10.1029/2010JC006553.
Selby, M., J. Rains, and R. Palmer (1974), Eolian deposits of the ice free Victoria Valley, Southern Victoria Land, Antarctica, *N. Z. J. Geol. Geophys.*, *17*, 543–562.
Sholkovitz, E. R., P. N. Sedwick, and T. M. Church (2009), Influence of anthropogenic combustion emissions on the deposition of soluble aerosol iron to the ocean: Empirical estimates for island sites in the North Atlantic, *Geochim. Cosmochim. Acta*, *73*(14), 3981–4003.
Sholkovitz, E. R., P. N. Sedwick, T. M. Church, A. R. Baker, and C. F. Powell (2012), Fractional solubility of aerosol iron: Synthesis of a global-scale data set, *Geochim. Cosmochim. Acta*, *89*, 173–189.
Sinclair, K. E., N. A. N. Bertler, and W. J. Trompetter (2010), Synoptic controls on precipitation pathways and snow delivery to high-accumulation ice core sites in the Ross Sea region, Antarctica, *J. Geophys. Res.*, *115*, D22112, doi:10.1029/2010JD014383.
Smith, W., and D. Nelson (1986), Importance of ice edge phytoplankton production in the Southern Ocean, *BioScience*, *36*(4), 251–257.
Smith, W. O., and L. I. Gordon (1997), Hyperproductivity of the Ross Sea (Antarctica) polynya during austral spring, *Geophys. Res. Lett.*, *24*(3), 233–236.
Spokes, L. J., and T. D. Jickells (1995), Factors controlling the solubility of aerosol trace metals in the atmosphere and on mixing into seawater, *Aquat. Geochem.*, *1*(4), 355–374.
Spokes, L. J., T. D. Jickells, and B. Lim (1994), Solubilisation of aerosol trace metals by cloud processing: A laboratory study, *Geochim. Cosmochim. Acta*, *58*(15), 3281–3287.
Steffensen, J. P. (1997), The size distribution of microparticles from selected segments of the Greenland Ice Core Project ice core representing different climatic periods, *J. Geophys. Res.*, *102*(C12), 26,755–26,763.
Sterle, K. M., J. R. McConnell, J. Dozier, R. Edwards, and M. Flanner (2013), Retention and radiative forcing of black carbon in eastern Sierra Nevada snow, *Cryosphere*, *7*(1), 365–374.
Tagliabue, A., and K. R. Arrigo (2005), Iron in the Ross Sea: 1. Impact on CO2 fluxes via variation in phytoplankton functional group and non-Redfield stoichiometry, *J. Geophys. Res.*, *110*, C03009, doi:10.1029/2004JC002531.
Tagliabue, A., and K. R. Arrigo (2006), Processes governing the supply of iron to phytoplankton in stratified seas, *J. Geophys. Res.*, *111*, C06019, doi:10.1029/2005JC003363.
Talarico, F., L. Borsi, and B. Lombardo (1995), Relict granulites in the Ross Orogen of northern Victoria Land (Antarctica), II. Geochemistry and palaeo-tectonic implications, *Precambrian Res.*, *75*(3), 157–174.
Tian, Z., P. Oliver, A. Veron, and T. M. Church (2008), Atmospheric Fe deposition modes at Bermuda and the adjacent Sargasso Sea, *Geochem. Geophys. Geosyst.*, *9*, Q08007, doi:10.1029/2007GC001868.
Trapp, J. M., F. J. Millero, and J. M. Prospero (2010), Trends in the solubility of iron in dust-dominated aerosols in the equatorial Atlantic trade winds: Importance of iron speciation and sources, *Geochem. Geophys. Geosyst.*, *11*, Q03014, doi:10.1029/2009GC00265.
Tuohy, A., N. Bertler, P. Neff, R. Edwards, D. Emanuelsson, T. Beers, and P. Mayewski (2015), Transport and deposition of heavy metals in the Ross Sea Region, Antarctica, *J. Geophys. Res. Atmos.*, *120*, 10,996–11,011, doi:10.1002/2015JD023293.
Vallelonga, P., C. Barbante, G. Cozzi, J. Gabrieli, S. Schüpbach, A. Spolaor, and C. Turetta (2013), Iron fluxes to Talos Dome, Antarctica, over the past 200 kyr, *Clim. Past*, *9*(2), 597–604.
Wagener, T., C. Guieu, R. Losno, S. Bonnet, and N. Mahowald (2008), Revisiting atmospheric dust export to the Southern Hemisphere ocean: Biogeochemical implications, *Global Biogeochem. Cycles*, *22*, GB2006, doi:10.1029/2007GB002984.
Winton, V. H. L., G. B. Dunbar, N. A. N. Bertler, M. A. Millet, B. Delmonte, C. B. Atkins, J. M. Chewings, and P. Andersson (2014), The contribution of aeolian sand and dust to iron fertilization of phytoplankton blooms in southwestern Ross Sea, Antarctica, *Global Biogeochem. Cycles*, *28*, 423–436, doi:10.1002/2013GB004574.
Winton, V. H. L., A. R. Bowie, R. Edwards, M. Keywood, A. T. Townsend, P. van der Merwe, and A. Bollhöfer (2015), Fractional iron solubility of atmospheric iron inputs to the Southern Ocean, *Mar. Chem.*, *177*(Part 1), 20–32.
Winton, V. H. L., G. B. Dunbar, C. B. Atkins, N. A. N. Bertler, B. Delmonte, P. S. Andersson, A. Bowie, and R. Edwards (2016), The origin of lithogenic sediment in the south-western Ross Sea and implications for iron fertilization, *Antarct. Sci.*, doi:10.1017/S095410201600002X.
Zhuang, G., R. A. Duce, and D. R. Kester (1990), The dissolution of atmospheric iron in surface seawater of the open ocean, *J. Geophys. Res.*, *95*(C9), 16,207–16,216.
Zhuang, G., Z. Yi, R. A. Duce, and P. R. Brown (1992), Chemistry of iron in marine aerosols, *Global Biogeochem. Cycles*, *6*(2), 161–173.

Appendix A4: Statement of contribution and publication for paper 5

V.H.L. Winton, G.B. Dunbar, C.B. Atkins, N.A.N. Bertler, B. Delmonte, P. S. Andersson, A. Bowie, R. Edwards, 2016. The origin of lithogenic sediment in the south western Ross Sea and implications for iron fertilization. *Antarctic Science*, available on CJO2016. doi:10.1017/S095410201600002X.

Statement of co-authorship

I, *Victoria Holly Liberty Winton*, designed and implemented the project, including experimental design, processed and analysed the samples for Sr and Nd isotopic composition, and conducted data analysis and manuscript writing of the publication:

V.H.L. Winton, G.B. Dunbar, C.B. Atkins, N.A.N. Bertler, B. Delmonte, P. S. Andersson, A. Bowie, R. Edwards. The origin of lithogenic sediment in the southwestern Ross Sea and implications for iron-fertilization. In review in *Antarctic Science.*

Holly Winton

Victoria Holly Liberty Winton

I, as a Co-Author, endorse that this level of contribution by the candidate indicated above is appropriate.

17-12-2015

Gavin Dunbar (Signature of Co-Author 1)

Cliff Atkins (Signature of Co-Author 2)

Nancy Bertler (Signature of Co-Author 3)

Barbara Delmonte (Signature of Co-Author 4)

Per Andersson (Signature of Co-Author 5)

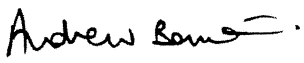

Andrew Bowie (Signature of Co-Author 6)

Ross Edwards (Signature of Co-Author 7)

Antarctic Science page 1 of 11 *(2016)* © Antarctic Science Ltd 2016 doi:10.1017/S095410201600002X

The origin of lithogenic sediment in the south-western Ross Sea and implications for iron fertilization

V.H.L. WINTON[1], G.B. DUNBAR[2], C.B. ATKINS[3], N.A.N. BERTLER[2,4], B. DELMONTE[5], P.S. ANDERSSON[6], A. BOWIE[7,8] and R. EDWARDS[1]

[1]*Physics and Astronomy, Curtin University, Perth, Western Australia, Australia*
[2]*Antarctic Research Centre, Victoria University of Wellington, Wellington, New Zealand*
[3]*School of Geography, Environment and Earth Sciences, Victoria University of Wellington, Wellington, New Zealand*
[4]*GNS Science, National Isotope Centre, Lower Hutt, New Zealand*
[5]*DISAT, Department of Earth and Environmental Sciences, University of Milano-Bicocca, Milano, Italy*
[6]*Department of Geosciences, Swedish Museum of Natural History, Stockholm, Sweden*
[7]*Antarctic Climate and Ecosystems CRC, University of Tasmania, Hobart, Tasmania, Australia*
[8]*Institute for Antarctic and Southern Ocean Studies, University of Tasmania, Hobart, Tasmania, Australia*
holly.winton@postgrad.curtin.edu.au

Abstract: Summer iron (Fe) fertilization in the Ross Sea has previously been observed in association with diatom productivity, lithogenic particles and excess Fe in the water column. This productivity event occurred during an early breakout of sea ice via katabatic winds, suggesting that aeolian dust could be an important source of lithogenic Fe required for diatom growth in the Ross Sea. Here we investigate the provenance of size-selected dust deposited on sea ice in McMurdo Sound, south-western (SW) Ross Sea. The isotopic signature of McMurdo Sound dust ($0.70533 < {}^{87}Sr/{}^{86}Sr < 0.70915$ and $-1.1 < \varepsilon_{Nd}(0) < 3.45$) confirms that dust is locally sourced from the McMurdo Sound debris bands and comprises a two-component mixture of McMurdo Volcanic Group and southern Victoria Land lithologies. In addition, the provenance of lithogenic sediment trapped in the water column was investigated, and the isotopic signature ($\varepsilon_{Nd}(0) = 3.9$, ${}^{87}Sr/{}^{86}Sr = 0.70434$) is differentiated from long-range transported dust originating from South America and Australia. Elevated lithogenic accumulation rates in deeper sediment traps in the Ross Sea suggest that sinking particles in the water column cannot simply result from dust input at the surface. This discrepancy can be best explained by significant upwelling and remobilization of lithogenic Fe from the sea floor.

Received 30 June 2015, accepted 17 January 2016

Key words: Antarctica, dust, dust provenance, iron, McMurdo Sound

Introduction

Atmospheric dust is potentially an important source of dissolved iron (DFe) which is the limiting nutrient required for primary production in vast regions of the remote Southern Ocean, including Antarctica's marginal seas (Sedwick *et al.* 2000, Boyd *et al.* 2010). Despite being seasonally iron (Fe) limited, the high-nutrient, high-chlorophyll regime of the Ross Sea is the most biologically productive continental shelf region in Antarctica, and supports intense phytoplankton blooms in the summer (Arrigo *et al.* 2008). Although the flux of Fe into the Ross Sea plays a critical role in determining its productivity, the origin(s) of this Fe remains poorly constrained (Sedwick *et al.* 2011).

Dust deposition in Antarctica

Global 'background' dust is characterized by fine particles having a mass modal diameter < 5 μm, long atmospheric residence time and modern mass deposition rates in the order of 0.001–0.02 g m^{-2} yr^{-1} in the Southern Ocean (Wagener *et al.* 2008 and references therein). The isolated, snow and ice-covered central East Antarctic Plateau (EAP) has proven to be an excellent location for investigating long-range transport of dust representative of the broader Southern Hemisphere, both at present and in the past (Delmonte *et al.* 2007, 2008). Moreover, the high EAP has much lower accumulation rates of ~ 0.0002–0.0006 g m^{-2} yr^{-1} during the Holocene (Albani *et al.* 2012). Recently, it has become apparent that peripheral areas of the Antarctic ice sheet, close to high elevation ice-free mountain ranges, such as the Transantarctic Mountains (TAM), can receive significant additional dust inputs from exposed Antarctic sources, some of which have been ice-free for millions of years (Delmonte *et al.* 2013 and references therein).

The relative contribution of much smaller, patchy but proximal dust sources to the atmospheric dust load over Antarctica and the Southern Ocean is not well known.

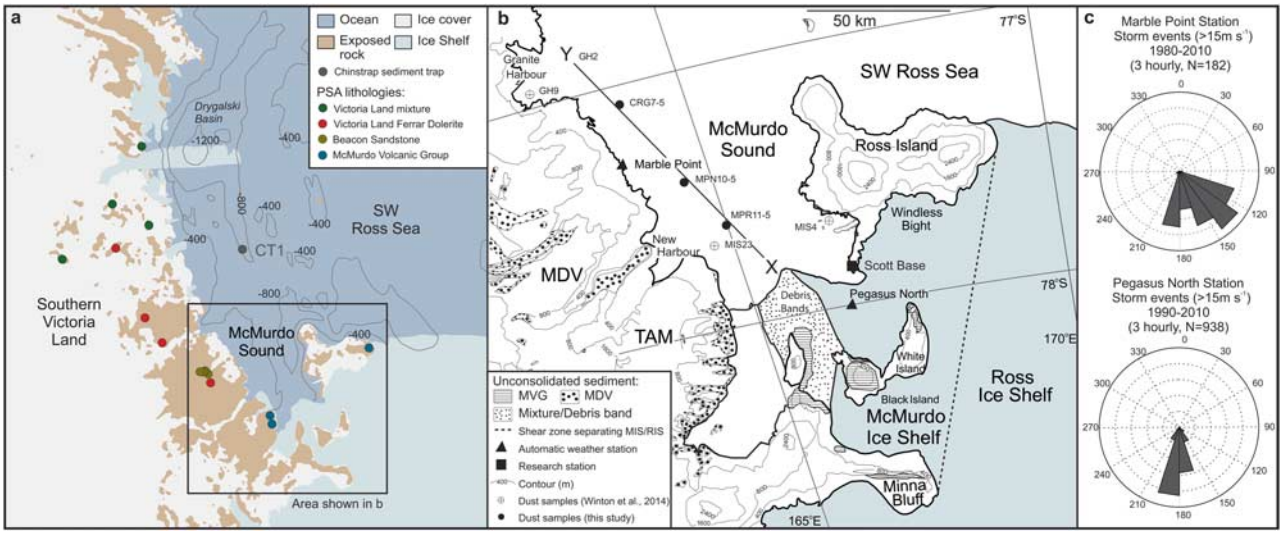

Fig. 1a. Map of the south-western (SW) Ross Sea showing the location of SW Ross Sea Chinstrap sediment trap (CT1). **b.** Insert of McMurdo Sound within the SW Ross Sea showing location of McMurdo Sound snow on sea ice samples (solid: this study, cross: Winton *et al*. (2014), shaded: exposed areas of unconsolidated sediment). Samples are named based on their location: MP = Marble Point, CR = Cape Robert, GH = Granite Harbour, MIS = McMurdo Sea Ice, MDV = McMurdo Dry Valleys, MIS = McMurdo Ice Shelf, MVG = McMurdo Volcanic Group, RIS = Ross Ice Shelf, TAM = Transantarctic Mountains. **c.** Wind roses illustrating the direction of storm events at Pegasus North and Marble Point automatic weather stations (AWS). Locations of AWS shown in Fig. 1b. Modified from Winton *et al*. (2014).

The largest expanse of contiguous ice-free ground in Antarctica is found in the McMurdo Dry Valleys, a series of west-to-east oriented, glacially carved valleys located between the high EAP and the Ross Sea in southern Victoria Land. However, the dustiest known place in Antarctica is located in the south-western (SW) Ross Sea, associated with the so-called 'debris bands' area on the McMurdo Ice Shelf (Kellogg *et al.* 1990) (Fig. 1). In this region, dust deposition flux ($\sim 1\ g\ m^{-2}\ yr^{-1}$) is at least two orders of magnitude greater than fallout of long-range transported dust measured in ice cores from the EAP (Atkins & Dunbar 2009, Delmonte *et al.* 2013, Chewings *et al.* 2014) and is, potentially, an important source of bioavailable Fe to the Ross Sea (Winton *et al.* 2014).

Dust provenance in Antarctica can be determined from the $^{87}Sr/^{86}Sr$ and $^{143}Nd/^{144}Nd$ radiogenic isotope composition of dust in snow and ice by comparison with potential source areas (PSAs) (e.g. Delmonte *et al.* 2010). This geochemical method allows mantle-derived (basaltic rocks, tephra and soils derived from them, weathered and eroded mafic rocks) and crustal-derived sediments and soils to be identified. Both the geochemical fingerprint and particle size of dust deposited on the EAP suggest it originates from arid regions in southern South America during glacial periods (Gaiero *et al.* 2007, Delmonte *et al.* 2008). However, for dust deposition during interglacial periods, that is when dust input to inner Antarctica was extremely low, the source is less certain (Delmonte *et al.* 2007), and an Australian contribution is probable (Revel-Rolland *et al.* 2006, Delmonte *et al.* 2007, 2008). In addition to atmospheric circulation, dust transport efficiency is dependent on particle size; for example, long-range dust deposited on the EAP has a mass modal size of around 2 μm (Delmonte *et al.* 2002). When investigating the provenance of dust, the fractionation of Sr isotopes into different grain size fractions needs to be considered, as there is a correlation between grain size and $^{87}Rb/^{86}Sr$ ratios, and thus $^{87}Sr/^{86}Sr$ ratios. In coarse (fine) grained suspended particulate matter, Sr is enriched (depleted) in less radiogenic Sr isotopic ratios (e.g. Andersson *et al.* 1994). In contrast, Nd isotopic ratios are not influenced to the same extent by particle size (e.g. Andersson *et al.* 1994).

Iron fertilization in the Ross Sea

The Ross Sea is one of the most productive regions in the Southern Ocean and an important oceanic sink for atmospheric carbon dioxide (CO_2) (e.g. Arrigo *et al.* 2008). The environmental factors responsible for controlling the rates of phytoplankton production and incomplete utilization of inorganic macronutrients include: grazing (Banse 1991), temperature (Bunt & Wood 1963), light availability (e.g. Mitchell *et al.* 1991), micro-nutrient availability (e.g. Fe and Mn) (Sedwick & DiTullio 1997, Sedwick *et al.* 2000), or a combination of these (e.g. Arrigo *et al.* 2000). Collier *et al*. (2000) show that a Ross Sea diatom productivity event, captured

during the 1996–97 deployment of moored Antarctic Environment and Southern Ocean Process Study (AESOPS) sediment traps, is correlated with elevated lithogenic particle accumulation rates, excess Fe (determined from high Fe/Al ratios), and with an early breakout of sea ice caused by katabatic winds. They go on to suggest that there may be a causal relationship between the retreat of sea ice, the supply of particulate Fe, and diatom production and export. The source of this lithogenic Fe to the Ross Sea is unknown but could be derived from either dust released into the ocean from melting sea ice from local and/or from distal sources, or new particulate Fe derived from ice shelves, icebergs, upwelling of resuspended continental sediments from the sea floor, Circumpolar Deep Water or some combination thereof.

Multiple sources of new Fe to the Ross Sea region have been identified, which include local dust sourced mainly from the McMurdo Ice Shelf (Atkins & Dunbar 2009, de Jong *et al.* 2013, Chewings *et al.* 2014, Winton *et al.* 2014), sea ice melt (Sedwick & DiTullio 1997, de Jong *et al.* 2013), and lithogenic sediments resuspended from the sea floor (Sedwick *et al.* 2011, de Jong *et al.* 2013, Marsay *et al.* 2014, Gerringa *et al.* 2015). However, the relative importance of these sources for stimulating primary production remains an open question. Winton *et al*. (2014) estimate that the supply of soluble aeolian Fe in dust from the debris bands, southern McMurdo Sound to the adjacent ocean could support up to ~ 15% of primary production in the area. The implication being that Fe supporting the remaining 85% of productivity was derived largely from other sources, such as lithogenic sediment resuspended from the sea floor (Sedwick *et al.* 2011, de Jong *et al.* 2013, Marsay *et al.* 2014, Gerringa *et al.* 2015, Kustka *et al.* 2015, McGillicuddy *et al.* 2015).

As Fe is critical for seasonal phytoplankton growth in the Ross Sea, this study aimed to further investigate the source(s) of lithogenic Fe as a driver of the vast summer phytoplankton blooms in the SW Ross Sea by examining the provenance of lithogenic material sinking in the upper 200 m below sea level (m.b.s.l.) of the water column, and comparing its origin to both known local and global sources. This paper reports the Sr-Nd isotopic composition of i) size-selected dust from snow samples on sea ice from McMurdo Sound, and ii) sediment trap material from the Research on Ocean – Atmosphere Variability and Ecosystem Response in the Ross Sea (ROAVERRS) moorings programme (1996–98) that represents accumulation of sediment settling out of the water column. When investigating PSAs to Antarctica, previous studies have size-selected the PSA samples prior to Sr analysis to be comparable to that of the fine size range of dust deposited in Antarctica (Delmonte *et al.* 2008), and a similar approach is used here.

Methods

Samples used in this study for Nd and Sr isotopic ration and concentration analysis

Previous studies have focused on dust flux and particle size distribution patterns in McMurdo Sound (Atkins & Dunbar 2009, Dunbar *et al.* 2009, Chewings *et al.* 2014). This study is based on the following samples:

- Samples of dust-laden snow collected from sea ice along a south–north X–Y transect in McMurdo Sound, collected in November 2010 and described in Chewings *et al*. (2014) and Winton *et al*. (2014) (Fig. 1b).
- A Ross Sea sediment trap sample from 200 m.b.s.l., collected between 25 December 1997 and 3 January 1998 from the ROAVERRS programme Chinstrap site (76°20.5'S, 165°1.78'E) in the SW Ross Sea. This site was anchored in 830 m water depth in the southern extension of the Drygalski Basin (Fig. 1a).

Sample processing – McMurdo Sound surface snow on sea ice samples

The samples analysed in this work were size-selected in order to be comparable to provenance measurements made of dust from ice core PSAs and with similar studies on dust in Antarctica (e.g. Delmonte *et al.* 2004, 2008, 2010). Both the bulk (all particle sizes) and fine (< 10 μm) fraction of McMurdo Sound dust were analysed to check for particle size induced bias in the isotopic fractionation of samples. The coarse fraction was removed from bulk samples by using a pre-washed 10 μm SEFAR Nitex® open mesh while the fraction 0.4 μm < ∅ < 10 μm was collected on 0.4 μm Isopore™ polycarbonate membranes. After filtration the membranes were put into pre-cleaned Corning® tubes filled with ~ 10 ml of ultra-pure water, and micro-particles were removed from the filter by sonication. Samples were transported to the Department of Geosciences, Swedish Museum of Natural History, Sweden, where the liquid was evaporated in acid-cleaned 15 ml Savillex® beakers. Dry dust samples, ranging between 0.1 and 1.2 mg, were weighed a minimum of five times to obtain a mean weight, which was used for subsequent calculations.

Sample processing – sediment trap samples

Isotopic analysis of bulk sediment revealed that the biogenic fraction of the sediment (up to 70% total mass estimated from AESOPS sediment trap data reported in Collier *et al*. (2000)) incorporated marine Sr, and thus the isotopic signature could not be distinguished from that of

Table I. Nd and Sr concentrations and isotopic composition of McMurdo Sound and Chinstrap sediment trap samples analysed in this study.

Sample	Size (μm)	Location	Date sampled	$^{143}Nd/^{144}Nd$	± 2σmean[a] *10^6	εNd(0)[b]	± 2σ[c]	CNd (ppm)	$^{87}Sr/^{86}Sr$	± 2σmean[d] *10^6	$^{87}Sr/^{86}Sr$ corrected[e]	± 2σ[f] *10^6	CSr (ppm)	Reference
McMurdo Sound														
MPR11-5	Bulk	77°35.44'S 164°31.36'E	Nov 2011	0.512580	12	-1.1	0.2	110	0.708158	6.0	0.708186	8	140	This study
MPR11-5	< 10	77°35.44'S 164°31.36'E	Nov 2011	0.512590	7	-0.94	0.2	220	0.709119	5.3	0.709147	8	320	This study
CRG7-5	Bulk	77°05.44'S 163° 41.86'E	Nov 2011	0.512633	11	-0.10	0.3	38	0.707607	4.2	0.707635	8	510	This study
CRG7-5	< 10	77°05.44'S 163°41.86'E	Nov 2011	0.512632	8	-0.12	0.3	68	0.708943	8.0	0.708971	8	570	This study
MPN10-5	Bulk	77°24.52'S 164°18.60'E	Nov 2011	0.512735	6	1.9	0.4	40	0.706705	13	0.706733	13	6600	This study
MPN10-5	< 10	77°24.52'S 164°18.60'E	Nov 2011	0.512682	8	0.86	0.4	20	0.708188	6.4	0.708216	8	910	This study
GH2	Bulk	76°55.33'S 163°6.17'E	Nov 2009	0.512650	11	0.23	0.3	76	0.707299	12	0.707327	12	890	This study
GH2	< 10	76°55.33'S 163°6.17'E	Nov 2009	0.512654	6	0.31	0.3	72	0.708045	5.8	0.708073	8	620	This study
GH9	Bulk	76°58.36'S 162°52.80'E	Nov 2009	0.512321	5	-6.18	0.3	37	0.712260	5.0	0.712288	8	290	(Winton *et al.* 2014)
MIS4	Bulk	77°40.03'S 166°35.97'E	Nov 2009	0.512815	4	3.45	0.3	56	0.705303	5.0	0.705331	8	800	(Winton *et al.* 2014)
MIS23	Bulk	77°40.03'S 164°35.79'E	Nov 2009	0.51276	6	2.38	0.3	51	0.705608	5.0	0.705636	8	520	(Winton *et al.* 2014)
Ross Sea sediment														
CT1	Bulk	76°20.5'S 165°1.78'E	1997	0.512715	7	1.5	0.3	0.4	0.709008	5.1	0.709036	8	110	This study
CT1-leach	Bulk	76°20.5'S 165°1.78'E	1997	0.512836	8	3.9	0.3	0.5	0.704314	4.4	0.704342	8	20	This study

[a]Internal precision, 2 standard errors of the mean.
[b]Nd isotopic ratios expressed as epsilon units $\varepsilon_{Nd}(0) = [(^{143}Nd/^{144}Nd)_{sample}/(^{143}Nd/^{144}Nd)_{CHUR}-1]x10^4$; CHUR = chondritic uniform reservoir.
[c]Uncertainty estimates based upon external precision for standard runs. Internal precision is used if it exceeds the external.
[d]Internal precision, 2 standard errors of the mean.
[e]Corrected to a NBS987 $^{87}Sr/^{86}Sr$ ratio of 0.710245.
[f]Uncertainty estimates based upon external precision for standard runs. Internal precision is used if it exceeds the external.

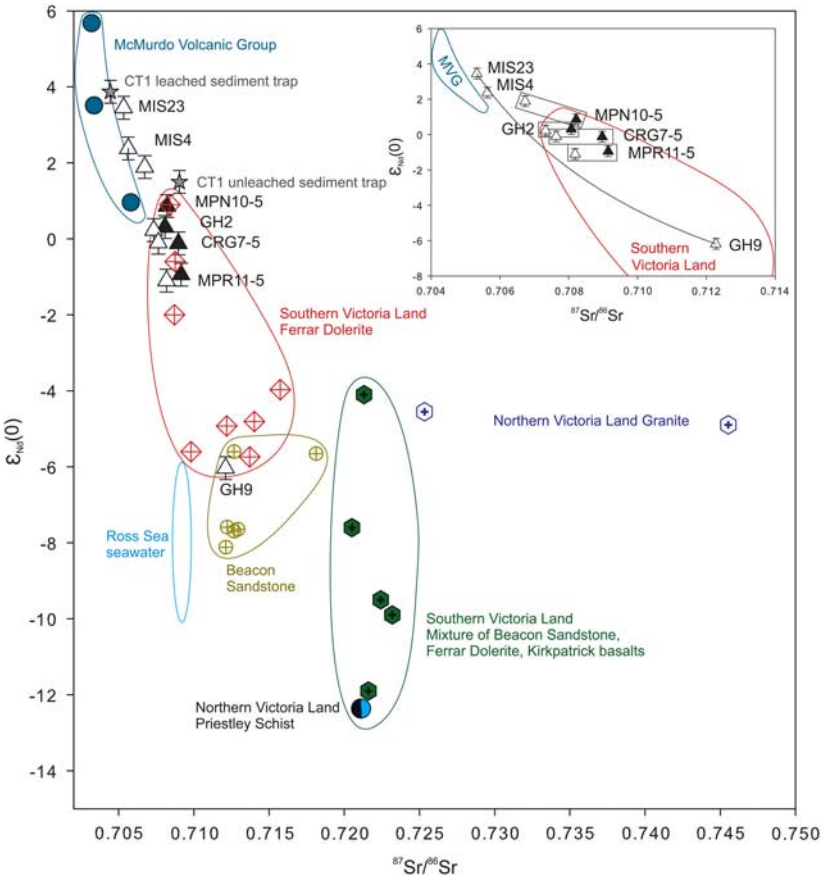

Fig. 2. Nd and Sr isotope signature of fine (black triangles) and bulk (white triangles) McMurdo Sound dust, including bulk McMurdo Sound data (GH9, MIS4 and MIS23; Winton *et al.* 2014), and leached and unleached Chinstrap sediment trap material. Data from southern Victoria Land potential dust sources that include different parent lithologies shown in Fig. 1 (Delmonte *et al.* 2004, 2010, 2013) and the isotopic composition of Ross Sea seawater (Elderfield 1986, Basak *et al.* 2015) are also plotted. Insert top right: McMurdo Sound dust highlighting the fractionation between fine and coarse particle sizes and a hypothetical mixing line between the two end members McMurdo Volcanic Group and southern Victoria Land, Transantarctic Mountains.

seawater (Table I). To remove the biogenic silica and calcium carbonate fraction, the sediment was leached with 6 M HCl in Savillex® beakers and centrifuged following the method of Freydier *et al.* (2001). The lithogenic residue was then rinsed three times with ultra-pure water and dried.

Sample digestion

The chemical treatment of the dust samples and leached sediment, including digestion and elemental separation (Rb-Sr and Sm-Nd) using ion exchange chromatography, was performed at the Swedish Museum of Natural History following the established method of Delmonte *et al.* (2008). The samples were spiked with a mixed $^{147}Sm/^{150}Nd$ spike and ^{84}Sr-enriched spike for the isotope dilution determination of the concentrations. Samples were digested in an acid mixture of 1.5 ml of HNO_3, HF and $HClO_4$ heated to 90°C in closed Savillex® beakers for 24 h. The solution was evaporated to complete dryness on a hot plate and the residue re-dissolved in 4 ml 6 M HCl.

Ion exchange

To achieve separation of potential interfering elements (Fe, Ba, Rb, Sm, Ce and Pr), and obtain high column yield and low blanks, the residue was subjected to chemical procedures described in Delmonte *et al.* (2008). The total blank, including dissolution, chemical separation and mass spectrometry, was frequently monitored in each ion exchange batch and blank concentrations were < 5 pg for Nd and < 130 pg for Sr.

Mass spectrometry

Isotopic analysis of Nd and Sr was performed with a Thermo Scientific TRITON Thermal Ionisation Mass

Spectrometer. Neodymium was loaded mixed with colloidal graphite, Alfa Aesar, on double rhenium filaments and analysed as metal ions in static mode using rotating gain compensation. Concentrations and ratios were calculated assuming exponential fractionation. The calculated ratios were normalized to $^{146}Nd/^{144}Nd = 0.7219$. Epsilon units are calculated as follows:

$$\varepsilon_{Nd}(0) = [(^{143}Nd/^{144}Nd)_{sample}/(^{143}Nd/^{144}Nd)_{CHUR}{}^{-1}] \times 10^4, \quad (1)$$

where CHUR is the chondritic uniform reservoir with $(^{143}Nd/^{144}Nd)_{CHUR} = 0.512638$.

The external precision for $^{143}Nd/^{144}Nd$ is estimated from analysis of the nNdβ standard (Wasserburg *et al.* 1981) by analysing a range, 4–12 ng loads, of nNdβ standard. The external precision becomes larger for smaller loads, with an estimated precision of ~ 40 ppm for small loads, ~ 30 ppm for intermediate loads and ~ 20 ppm for larger loads. These values have been used to estimate the errors for the samples shown in Table I. The mean $^{143}Nd/^{144}Nd$ ratio for the nNdβ was 0.511895 ± 22 ($n = 20$). Literature values for repeated analysis of standard nNdβ (Andreasen & Sharma 2006) yielded $^{143}Nd/^{144}Nd = 0.511892 \pm 3$ (2σ, $n = 23$), and thus no accuracy correction was applied.

Purified Sr samples were mixed with tantalum activator and loaded on a single rhenium filament. Two hundred 8 s integrations were recorded in multi-collector static mode, applying a rotating gain compensation. Measured ^{87}Sr intensities were corrected for Rb interference assuming $^{87}Rb/^{85}Rb = 0.38600$, and ratios were calculated using the exponential fractionation law and $^{88}Sr/^{86}Sr = 8.375209$. External precision for $^{87}Sr/^{86}Sr$, estimated from analysing NBS SRM987 standard, was calculated as ± 0.000016 ($n = 12$), while repeated measurements of prepared CIT #39 seawater gave a reproducibility of ± 0.0000082 or 12 ppm ($n = 21$) which was taken to be the best estimate of the external precision. Accuracy correction was applied to the $^{87}Sr/^{86}Sr$ ratios corresponding to a $^{87}Sr/^{86}Sr$ ratio of 0.710245 for NBS SRM 987 standard (NBS 987: literature value 0.710245, Department of Geosciences value 0.710217 ± 16 ($n = 12$); difference: 0.000028).

The accuracy of the Nd and Sr isotopic composition of small dust samples was determined using the Basalt Columbia River rock standard (BCR-2), a certified reference material. Preparation and analysis of 150–600 µg aliquots of BCR-2 in each batch of ion exchange resulted in a recovery of > 79% ($n = 6$) for concentration and > 99% ($n = 6$) for isotopic composition. Due to the small dust samples and the difficulty of weighing such small masses an Sr and Nd concentration error of ± 10% was estimated by repeated weighing of BCR-2 standards (~ 0.3 mg).

Results

The Sr and Nd isotopic composition of dust are primarily related to lithology and geologic age of parent materials, although the Sr isotopic composition, for particles between 2–50 µm, can also be influenced by size. The Sr and Nd isotopic composition of the fine (< 10 µm) and bulk (all sizes included) dust samples collected in this study are well characterized and reported in Table I and Fig. 2 along with additional isotopic data from McMurdo Sound measured in an earlier study (Winton *et al.* 2014). Samples in Fig. 2 are grouped by geographical location. The samples collected from the snow on sea ice in McMurdo Sound display a narrow isotopic composition ($0.70533 < {}^{87}Sr/^{86}Sr < 0.70915$ and $-1.1 < \varepsilon_{Nd}(0) < 3.45$). Our fine dust (< 10 µm) samples have relatively higher $^{87}Sr/^{86}Sr$ ratios compared to the bulk samples (Fig. 2), consistent with previous studies of size-dependent fractionation (Andersson *et al.* 1994). The Nd isotopes do not fractionate with the particle size (with the exception of MPN10-5 which could be related to the different size fractions originating from different sources; Fig. 2), also consistent with previous studies. The $\Delta^{87}Sr/^{86}Sr$ is ~ 0.00115, that is slightly smaller than the $^{87}Sr/^{86}Sr$ increase of ~ 0.0028 units observed between 63 µm and 2 µm dust particles by Gaiero *et al.* (2007). The isotopic ratios of leached (lithogenic sediment fraction) and unleached (lithogenic and biogenic sediment fraction) Ross Sea sediment obtained from the upper Chinstrap sediment trap (200 m.b.s.l.) are reported in Table I. Leaching had a significant effect on the Sr isotopic ratio of this sample and removed an Sr seawater overprint from the sediment. After leaching, the remaining lithogenic sediment has an isotopic signature between the McMurdo Volcanic Group (MVG) and southern Victoria Land PSAs (Fig. 2).

Discussion

Dust provenance - McMurdo Sound

The overwhelming majority of dust deposited in snow on sea ice in McMurdo Sound is locally sourced. It is not possible to detect any contribution from South American or Australian sources with our approach. Sedimentological, meteorological and geochemical evidence consistently points to the debris bands on the McMurdo Ice Shelf (Kellogg *et al.* 1990) as the dominant local dust source in the McMurdo Sound region (Fig. 1) (Atkins & Dunbar 2009, Chewings *et al.* 2014, Winton *et al.* 2014). Studies of spatial variability of dust and

particle size for the greater McMurdo Sound region show a distinct decrease in particle size and dust flux along transect X–Y (Fig. 1b) as part of a dust plume extending northwards from the debris bands (Atkins & Dunbar 2009, Chewings *et al.* 2014). As the plume extends northwards away from the debris bands the particle size and dust accumulation rate decrease, although secondary elevated patches of both occur near coastal headlands. Overall, dust accumulation declines exponentially from $55\,g\,m^{-2}\,yr^{-1}$ near the debris bands to $\sim 0.2\,g\,m^{-2}\,yr^{-1}$ 120 km north of the debris bands (Atkins & Dunbar 2009, Chewings *et al.* 2014). This northward dust dispersal is consistent with the local meteorology whereby the highest wind speeds, i.e. those most competent with respect to entraining silt and fine sand, are predominately from the south (Fig. 1c), dispersing dust from the debris bands north along the southern Victoria Land coastline.

In addition to sedimentological considerations, geochemical evidence also points to dust being locally sourced. The Sr isotopic composition of modern seawater is homogenous ($^{87}Sr/^{86}Sr = 0.70924$; Elderfield 1986), and has a similar Sr isotopic composition to the geology in McMurdo Sound (Fig. 2). However, the Nd isotopic composition of the local geology and Ross Sea seawater ($-10 < \varepsilon_{Nd}(0) < -6$; Basak *et al.* 2015) is distinguished in Fig. 2, and combined with other provenance indicators (coarse particle size, high dust flux and Fe/Al elemental ratios; Atkins & Dunbar 2009, de Jong *et al.* 2013) allows tracing of dust to local PSAs. Winton *et al.* (2014) report two Sr and Nd isotopic ratios of the bulk sediment from snow on sea ice in southern McMurdo Sound and one from Granite Harbour (Fig. 1). The values are consistent with dust originating from MVG, although within the Granite Harbour embayment there is also evidence for dust derived from TAM lithologies. The possibility that the volcanic signature of McMurdo Sound dust on sea ice is derived from volcanic rocks in Marie Byrd Land can be ruled out ($0.7026 < {}^{87}Sr/^{86}Sr < 0.7032$ and $1.99 < \varepsilon_{Nd}(0) < 6.87$) (Futa & LeMasurier 1983, Hole & LeMasurier 1994) due to the northerly direction of the prevailing winds (Chewings *et al.* 2014).

Consequently, only local PSAs are considered for comparison to the new isotopic dataset. Overall, the Sr isotopic ratios for McMurdo Sound samples analysed in this study, and in Winton *et al.* (2014), are tightly grouped and range between $0.705 < {}^{87}Sr/^{86}Sr < 0.709$ while $\varepsilon_{Nd}(0)$ ranges between $3.45 < \varepsilon_{Nd}(0) < -1.1$. These new isotopic data form a linear array in Fig. 2. McMurdo Sound dust can be considered the result of a two-component mixture derived from isotopically distinct end-members: i) the MVG volcanic rocks and ii) southern Victoria Land lithologies found in the TAM, such as Ferrar Dolerites and sandstones of the Beacon Supergroup (Fig. 2). The narrow range of isotopic ratios of McMurdo Sound dust along the south–north transect X–Y represents northwards dust dispersal downwind from the debris bands, that is a mixture of TAM and MVG sources, with minor localized additions of TAM dust input from coastal outcrops from New Harbour and Marble Point that contribute to the dominant south to north dust plume (Fig. 1). This is consistent with field observations showing sediment on the McMurdo Ice Shelf debris bands is itself a mixture of MVG and TAM lithologies (Kellogg *et al.* 1990).

Previous studies have shown dust deposited within embayments or adjacent to headlands along the south Victoria Land coastline is not widely dispersed (Barrett *et al.* 1983, de Jong *et al.* 2013, Chewings *et al.* 2014). Within the narrow range of isotopic ratios of McMurdo Sound dust, GH9 is isotopically distinct and displays a dominant TAM signature (Fig. 2). This sample is not situated under the main northward-directed dust plume and hence represents localized dust accumulation within the Granite Harbour embayment (Fig. 1). In contrast, the isotopic composition of GH2 lies within the tight cluster of McMurdo Sound dust and thus highlights that the mass of dust on the sea ice immediately seawards of Granite Harbour originates from the south. A single source from the debris bands is also consistent with Fe concentrations within dust samples that were uniform along the transport pathway (Winton *et al.* 2014).

Dust provenance - south-western Ross Sea

The isotopic signature of the lithogenic fraction of sediment from the upper 200 m.b.s.l. Chinstrap sediment trap, located ~170 km north of the debris bands ($^{87}Sr/^{86}Sr = 0.704$, $\varepsilon_{Nd}(0) = 3.9$), falls outside of the isotopic range of dust originating in Australia ($0.709 < {}^{87}Sr/^{86}Sr < 0.763$, $-2.9 < \varepsilon_{Nd}(0) < -15.4$; Delmonte *et al.* 2004, Revel-Rolland *et al.* 2006) and South America ($0.704 < {}^{87}Sr/^{86}Sr < 0.713$, $-8.9 < \varepsilon_{Nd}(0) < -8.3$; Delmonte *et al.* 2004). These two potential Southern Hemisphere sources supply dust to the high elevation EAP at very low deposition rates (e.g. Delmonte *et al.* 2008). The signature of the lithogenic fraction of sediment from SW Ross Sea (Chinstrap) matches that of the local geology and dust on sea ice in McMurdo Sound. Thus, the lithogenic particles, and their associated Fe, collected here are 'locally' sourced from the Ross Sea region (Fig. 2).

Dust transport and deposition - south-western Ross Sea

Deposition of local dust into the SW Ross Sea can occur by direct atmospheric fallout into ice-free surface waters, and release into surface waters by sea ice melt associated with subsequent northwards advection (Atkins & Dunbar 2009, de Jong *et al.* 2013, Chewings *et al.* 2014). The geographical area over which local dust is transported

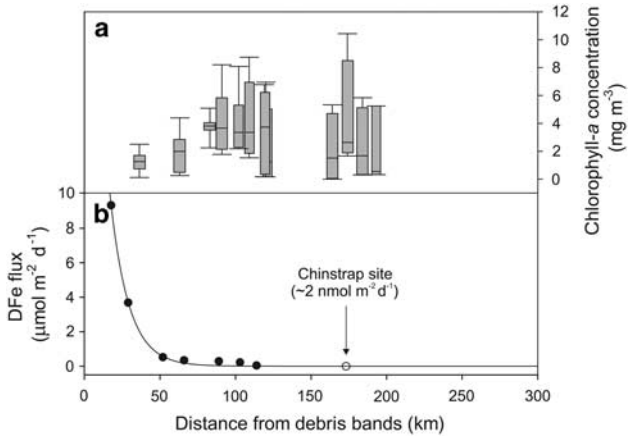

Fig. 3a. Rate of primary production with distance from McMurdo Sound. As the dust flux exponentially decreases, the rate of primary production increases. Primary production inferred from the annual mean chlorophyll *a* concentration (2000–09) in the McMurdo Sound polynya (72.0°S–78.083°S, 160.916°E–179.040°W) from SeaWiFS satellite data (http://giovanni.gsfc.nasa.gov). **b.** Extrapolation of the annual DFe flux from McMurdo Sound into the south-western Ross Sea (DFe data sourced from Winton *et al.* (2014)). The predicted dust flux at the Chinstrap site is estimated at ~ 0.01 g m^{-2} yr^{-1} with a corresponding DFe flux of ~ 2 nmol m^{-2} d^{-1}.

into the Ross Sea, and hence contributes to Fe fertilization, is potentially large. Although dust accumulation measurements only exist up to 120 km from the debris bands and decrease exponentially from the source, local dust deposition probably extends far beyond this point. Extrapolating the dust flux trend observed by Chewings *et al.* (2014) suggests that the Chinstrap site may represent a northern extension of the dust and DFe dispersal pattern reported by Winton *et al.* (2014). The estimated annual accumulation rate from aeolian dust at the Chinstrap site is ~ 0.01 g m^{-2} yr^{-1}, although we do not have accumulation rate data from the Chinstrap sediment trap with which to compare this estimate. Whether or not locally sourced aeolian sediment is the main source of the lithogenic sediment in the Chinstrap site remains somewhat of an open question. However, when the relationship between DFe and phytoplankton productivity in McMurdo Sound is considered we suggest this is unlikely to be the case (Fig. 3).

Implications for iron fertilization

By extrapolating the dust flux trend observed by Chewings *et al.* (2014) and its associated contribution to DFe (Winton *et al.* 2014) into the SW Ross Sea, the upper bound of the DFe at the Chinstrap site from the debris bands can be estimated (Fig. 3). Assuming a lithogenic dust flux of ~ 0.01 g m^{-2} yr^{-1} and an associated total Fe content of 4% and 11% of this Fe is soluble (Winton *et al.* 2014), the maximum DFe flux is estimated to be ~ 2 nmol m^{-2} d^{-1} to the Chinstrap site (Fig. 3). However, when this is considered relative to the spatial distribution of primary production in the SW Ross Sea, using averaged annual Sea-Viewing Wide Field-of-View Sensor (SeaWiFS) satellite chlorophyll *a* data, the gradient in increasing chlorophyll *a* concentration with distance from the debris bands within the McMurdo Sound polynya does not match the pattern of decreasing dust accumulation (Fig. 3). This pattern suggests that DFe from dust does not regulate growth in the SW Ross Sea. A seasonal phytoplankton bloom occurs in the McMurdo Sound polynya SW Ross Sea each summer and is dominated by diatoms. The rate of primary production is greatest in the centre of the McMurdo Sound polynya. As the dust flux decreases and primary production increases with distance from McMurdo Sound, it is difficult to reconcile these patterns at the Chinstrap site assuming only a local dust source (Fig. 3).

Some further insight into the origin of sediment in the water column in the SW Ross Sea may be inferred from the data published by Collier *et al.* (2000). They show a significantly elevated lithogenic accumulation rate in deep AESOPS sediment traps compared to accumulation rates measured in the upper AESOPS sediment traps at other sites in the Ross Sea (e.g. MS-7; 76°30'S, 178°1'W). In addition, lithogenic Fe fluxes between 1–90 µg m^{-2} d^{-1} have been measured for the upper 200 m.b.s.l. AESOPS trap (MIS-7b) and 40–850 µg m^{-2} d^{-1} for the deep trap (MS-7a). The greater mass of sediment and lithogenic Fe flux in the deep traps in the Ross Sea highlight that concentrations of suspended sediment in the water column at these sites cannot simply result from sediment input at the surface (whereby the accumulation in each trap would be the same regardless of depth). Instead, the increase in accumulation with depth probably reflects resuspension and horizontal near-bottom transport processes. While we do not have the data to constrain these processes at Chinstrap we infer, based on the provenance of the lithogenic sediment and distance from known local sources, that the lithogenic sediment accumulating there is most probably dominated by resuspended bottom sediments, potentially from sills either side of the Drygalski Basin but also locally sourced material falling through the water column sourced from atmospheric deposition or ice rafting. Although no Fe flux data for the Chinstrap site are available, future work could examine the relationship between Fe fluxes in the Chinstrap sediment trap and those DFe fluxes reported for locally derived dust at McMurdo Sound.

Despite McMurdo Sound representing the upper bound of locally derived dust and associated DFe to Antarctic waters, previous studies have ruled out local dust as the major source of DFe supply for phytoplankton

blooms in the Ross Sea. Dissolved Fe in McMurdo Sound dust can only support up to 15% of primary production in the region (Winton *et al.* 2014). Furthermore, based on regional scale estimates of dust deposition to the Southern Ocean, primary production triggered by long-range transported dust is likely to be less significant than local dust (e.g. Edwards & Sedwick 2001). Evidence from the extrapolation of the mass accumulation rate to the upper 200 m.b.s.l. Chinstrap trap, the sedimentological study of Chewings *et al.* (2014), sedimentation in the water column, and the low contribution of local aeolian DFe to phytoplankton blooms, suggest that it is unlikely that aeolian dust deposition is the dominant process by which lithogenic Fe is supplied to the water column in the SW Ross Sea. Considered together, these lines of evidence point to a combination of resuspended bottom sediments with smaller additions of local dust sourced from atmospheric deposition or ice rafting as the sources of Fe-bearing sediment to the water column in the SW Ross Sea.

More broadly, Sedwick *et al.* (2011) noted that the phytoplankton-Fe limitation must be overcome by continuous replenishment from new sources to sustain the significant biomass observed over summer. They considered the following as potential sources of new DFe: vertical mixing, lateral advection, aerosol input and dissolution of particulate Fe from any or all of these sources. Consistent with upwelling of DFe as a major source of DFe in the Ross Sea, Marsay *et al.* (2014) reported high DFe concentrations within 50 m of the sea floor in the summer of 2012. Most recently, Gerringa *et al.* (2015) measured seawater DFe concentrations in the 2013–14 summer, and concluded that DFe from the sea floor and land mass sediments are the main sources of DFe which support phytoplankton in the upper mixed layer of the Ross Sea polynya in the early summer. Similarly, phytoplankton blooms in the Pennell Bank region of the Ross Sea are supported by upwelling of DFe (Kustka *et al.* 2015). However, Kustka *et al.* (2015) also highlight the spatial variability of processes supplying DFe in the Ross Sea. For example, circulation patterns around bathymetric features can alter the input of DFe from increased upwelling rates and higher concentrations of DFe. Numerical modelling of DFe supply by McGillicuddy *et al.* (2015) suggests that the largest sources to the euphotic zone are wintertime mixing and melting sea ice (e.g. Sedwick & DiTullio 1997, de Jong *et al.* 2013) with smaller inputs from Circumpolar Deep Water and from melting glacial ice.

Conclusions

Dust extracted from surface snow on McMurdo Sound sea ice enables us to document the present day provenance of dust reaching the SW Ross Sea. Based on our measurements of Sr and Nd isotopic ratios of dust deposited in surface snow on sea ice at McMurdo Sound and in the Chinstrap sediment trap in the SW Ross Sea we conclude the following: i) The Sr and Nd isotopic signature of lithogenic sediment from the upper Chinstrap sediment trap in the SW Ross Sea ($\varepsilon_{Nd}(0) = 3.9$, $^{87}Sr/^{86}Sr = 0.70434$) matches local dust sources. ii) McMurdo Sound has been well characterized in terms of the Sr and Nd isotopic composition of locally derived dust deposited on sea ice. Dust found there displays a narrow isotopic field between $0.70533 < {}^{87}Sr/^{86}Sr < 0.70819$ and $-1.1 < \varepsilon_{Nd}(0) < 3.45$ for the bulk fraction and $0.70807 < {}^{87}Sr/^{86}Sr < 0.70915$ and $-0.94 < \varepsilon_{Nd}(0) < 0.86$ for the fine fraction. Due to Sr isotopic fractionation with particle size, the signature of the fine fraction adds to the PSA database for comparison to Antarctic ice core dust provenance studies. iii) Locally derived dust from McMurdo Sound is unlikely to be the major source of DFe for seasonal phytoplankton blooms in the SW Ross Sea. Although, Sr and Nd isotopic ratios of local dust on sea ice show similarities to lithogenic marine sediment, we acknowledge the limited transport distance of coarse-sized dust in this region. As dust transport varies from year to year, we cannot completely exclude the possibility that local dust can contribute to DFe to the greater Ross Sea region although this is not the dominant source of lithogenic Fe. iv) We surmise that there is significant remobilization and upwelling of Fe from the sea floor that contributes to Fe fertilization of phytoplankton during the summer in the SW Ross Sea. Finally, v) source information of dust inputs to regions, such as the Ross Sea, improves the ability to predict how such supply will change as the climate changes. As local sources are important to the SW Ross Sea, this data could be included in models that predict changes in snow and ice cover in the region.

Acknowledgements

We would like to thank Antarctica New Zealand and Scott Base personnel for logistics support. Thank you to Jane Chewings, Associate Professor Brent Alloway and Assistant Professor Ana Aguilar-Islas for the collection of McMurdo Sound and Granite Harbour dust samples. Additional thanks to Professor Robert Dunbar for Chinstrap sediment trap samples from the ROAVERRS mooring programme. V.H.L.W would like to thank Curtin University (Australian Postgraduate Award and Curtin Research Scholarship) and Antarctic Science (Antarctic Science Bursary) for scholarship and other funding support. This project was funded by Curtin University (Curtin Research Fellowship to R.E.: RES-SE-DAP-AW-47679-1), and New Zealand Ministry of Science and Innovation through contracts to Victoria

University of Wellington (Contracts: VUW0704; RDF-VUW1103) and GNS Science (Contracts: 540GCT32; C05X1001). Isotopic analyses for provenance characterization were carried out at the Swedish Museum of Natural History and were supported by the Department of Geosciences, Swedish Museum of Natural History. Thank you to Karin Wallner and Hans Schöberg for technical support. The isotopic dataset for this paper is freely available from the Curtin University Research Data repository http://doi.org/10.4225/06/5643EBA1C8473. The chlorophyll *a* data was obtained freely from the Sea-Viewing Wide Field-of-View Sensor (http://giovanni.gsfc.nasa.gov/). Additional thanks for the helpful comments and suggestions of Jeroen de Jong and an anonymous reviewer that aided in revision of this manuscript.

Author contributions

V.H.L.W, G.B.D, C.B.A and N.A.N.B designed the research; G.B.D and C.B.A collected the samples; V.H.L.W, B.D and P.S.A prepared the samples and analysed the data; V.H.L.W, G.B.D, C.B.A, B.D and P.S.A evaluated the data; all authors contributed to the interpretation of the data and the writing of the manuscript.

References

Albani, S., Delmonte, B., Maggi, V., Baroni, C., Petit, J.R., Stenni, B., Mazzola, C. & Frezzotti, M. 2012. Interpreting last glacial to Holocene dust changes at Talos Dome (East Antarctica): implications for atmospheric variations from regional to hemispheric scales. *Climate of the Past*, **8**, 741–750.

Andersson, P.S., Wasserburg, G.J., Ingri, J. & Stordal, M.C. 1994. Strontium, dissolved and particulate loads in fresh and brackish waters: the Baltic Sea and Mississippi Delta. *Earth and Planetary Science Letters*, **124**, 195–210.

Andreasen, R. & Sharma, M. 2006. Solar nebula heterogeneity in p-process samarium and neodymium isotopes. *Science*, **314**, 806–809.

Arrigo, K.R., DiTullio, G.R., Dunbar, R.B., Robinson, D.H., VanWoert, M., Worthen, D.L. & Lizotte, M.P. 2000. Phytoplankton taxonomic variability in nutrient utilization and primary production in the Ross Sea. *Journal of Geophysical Research - Oceans*, **105**, 8827–8846.

Arrigo, K.R., van Dijken, G. & Long, M. 2008. Coastal Southern Ocean: a strong anthropogenic CO_2 sink. *Geophysical Research Letters*, **35**, 10.1029/2008GL035624.

Atkins, C.B. & Dunbar, G.B. 2009. Aeolian sediment flux from sea ice into southern McMurdo Sound, Antarctica. *Global and Planetary Change*, **69**, 133–141.

Banse, K. 1991. Rates of phytoplankton cell division in the field and in iron enrichment experiments. *Limnology and Oceanography*, **36**, 1886–1898.

Barrett, P., Pyne, A. & Ward, B. 1983. Modern sedimentation in McMurdo Sound, Antarctica. *In* Oliver, R.L., James, P.R. & Jago, J.B., *eds. Antarctic earth science*. New York, NY: Cambridge University Press, 550–554.

Basak, C., Pahnke, K., Frank, M., Lamy, F. & Gersonde, R. 2015. Neodymium isotopic characterization of Ross Sea Bottom Water and its advection through the southern South Pacific. *Earth and Planetary Science Letters*, **419**, 211–221.

Boyd, P.W., Mackie, D.S. & Hunter, K.A. 2010. Aerosol iron deposition to the surface ocean – modes of iron supply and biological responses. *Marine Chemistry*, **120**, 128–143.

Bunt, J.S. & Wood, E.J.F. 1963. Microbiology of Antarctic sea-ice: microalgae and Antarctic sea-ice. *Nature*, **199**, 1254–1255.

Chewings, J.M., Atkins, C.B., Dunbar, G.B. & Golledge, N.R. 2014. Aeolian sediment transport and deposition in a modern high latitude glacial marine environment. *Sedimentology*, **61**, 1535–1557.

Collier, R., Dymond, J., Honjo, S., Manganini, S., Francois, R. & Dunbar, R. 2000. The vertical flux of biogenic and lithogenic material in the Ross Sea: moored sediment trap observations 1996–1998. *Deep Sea Research II - Topical Studies in Oceanography*, **47**, 3491–3520.

De Jong, J., Schoemann, V., Maricq, N., Mattielli, N., Langhorne, P., Haskell, T. & Tison, J.-L. 2013. Iron in land-fast sea ice of McMurdo Sound derived from sediment resuspension and wind-blown dust attributes to primary productivity in the Ross Sea, Antarctica. *Marine Chemistry*, **157**, 24–40.

Delmonte, B., Petit, J.R. & Maggi, V. 2002. Glacial to Holocene implications of the new 27000-year dust record from the EPICA Dome C (East Antarctica) ice core. *Climate Dynamics*, **18**, 647–660.

Delmonte, B., Robert Petit, J., Basile-Doelsch, I., Jagoutz, E. & Maggi, V. 2007. 6. Late quaternary interglacials in East Antarctica from ice-core dust records. *Developments in Quaternary Sciences*, **7**, 53–73.

Delmonte, B., Andersson, P.S., Hansson, M., Schöberg, H., Petit, J.R., Basile-Doelsch, I. & Maggi, V. 2008. Aeolian dust in East Antarctica (EPICA-Dome C and Vostok): provenance during glacial ages over the last 800 kyr. *Geophysical Research Letters*, **35**, 10.1029/2008GL033382.

Delmonte, B., Basile-Doelsch, I., Petit, J.R., Maggi, V., Revel-Rolland, M., Michard, A., Jagoutz, E. & Grousset, F. 2004. Comparing the Epica and Vostok dust records during the last 220,000 years: stratigraphical correlation and provenance in glacial periods. *Earth-Science Reviews*, **66**, 63–87.

Delmonte, B., Baroni, C., Andersson, P., Narcisi, B., Salvatore, M.C., Petit, J.R., Scarchilli, C., Frezzotti, M., Albani, S. & Maggi, V. 2013. Modern and Holocene aeolian dust variability from Talos Dome (northern Victoria Land) to the interior of the Antarctic ice sheet. *Quaternary Science Reviews*, **64**, 76–89.

Delmonte, B., Baroni, C., Andersson, P.S., Schoberg, H., Hansson, M., Aciego, S., Petit, J.R., Albani, S., Mazzola, C., Maggi, V. & Frezzotti, M. 2010. Aeolian dust in the Talos Dome ice core (East Antarctica, Pacific/Ross Sea sector): Victoria Land versus remote sources over the last two climate cycles. *Journal of Quaternary Science*, 25, 1327–1337.

Dunbar, G.B., Bertler, N.A.N. & McKay, R.M. 2009. Sediment flux through the McMurdo Ice Shelf in Windless Bight, Antarctica. *Global and Planetary Change*, **69**, 87–93.

Edwards, R. & Sedwick, P. 2001. Iron in East Antarctic snow: implications for atmospheric iron deposition and algal production in Antarctic waters. *Geophysical Research Letters*, **28**, 3907–3910.

Elderfield, H. 1986. Strontium isotope stratigraphy. *Palaeogeography, Palaeoclimatology, Palaeoecology*, **57**, 71–90.

Freydier, R., Michard, A., De Lange, G. & Thomson, J. 2001. Nd isotopic compositions of Eastern Mediterranean sediments: tracers of the Nile influence during sapropel S1 formation? *Marine Geology*, **177**, 45–62.

Futa, K. & LeMasurier, W.E. 1983. Nd and Sr isotopic studies on Cenozoic mafic lavas from West Antarctica: another source for continental alkali basalts. *Contributions to Mineralogy and Petrology*, **83**, 38–44.

Gaiero, D.M., Brunet, F., Probst, J.-L. & Depetris, P.J. 2007. A uniform isotopic and chemical signature of dust exported from Patagonia: rock sources and occurrence in southern environments. *Chemical Geology*, **238**, 107–120.

Gerringa, L.J.A., Laan, P., van Dijken, G.L., van Haren, H., De Baar, H.J.W., Arrigo, K.R. & Alderkamp, A.C. 2015. Sources of iron in the Ross Sea polynya in early summer. *Marine Chemistry*, **177**, 447–459.

Hole, M.J. & LeMasurier, W.E. 1994. Tectonic controls on the geochemical composition of Cenozoic, mafic alkaline volcanic rocks from West Antarctica. *Contributions to Mineralogy and Petrology*, **117**, 187–202.

Kellogg, T.B., Kellogg, D. & Stuiver, M. 1990. Late Quaternary history of the southwestern Ross Sea: evidence from debris bands on the McMurdo Ice Shelf, Antarctica. *Antarctic Research Series*, **50**, 25–56.

Kustka, A.B., Kohut, J.T., White, A.E., Lam, P.J., Milligan, A.J., Dinniman, M.S., Mack, S., Hunter, E., Hiscock, M.R., Smith Jr, W.O. & Measures, C.I. 2015. The roles of MCDW and deep water iron supply in sustaining a recurrent phytoplankton bloom on central Pennell Bank (Ross Sea). *Deep-Sea Research I - Oceanographic Research Papers*, **105**, 171–185.

Marsay, C.M., Sedwick, P.N., Dinniman, M.S., Barrett, P.M., Mack, S.L. & McGillicuddy, D.J. 2014. Estimating the benthic efflux of dissolved iron on the Ross Sea continental shelf. *Geophysical Research Letters*, **41**, 7576–7583.

McGillicuddy, D.J., Sedwick, P.N., Dinniman, M.S., Arrigo, K.R., Bibby, T.S., Greenan, B.J.W., Hofmann, E.E., Klinck, J.M., Smith, W.O., Mack, S.L., Marsay, C.M., Sohst, B.M. & van Dijken, G.L. 2015. Iron supply and demand in an Antarctic shelf ecosystem. *Geophysical Research Letters*, **42**, 8088–8097.

Mitchell, B.G., Brody, E.A., HolmHansen, O., McClain, C. & Bishop, J. 1991. Light limitation of phytoplankton biomass and macronutrient utilization in the Southern Ocean. *Limnology and Oceanography*, **36**, 1662–1677.

Revel-Rolland, M., De Deckker, P., Delmonte, B., Hesse, P.P., Magee, J.W., Basile-Doelsch, I., Grousset, F. & Bosch, D. 2006. Eastern Australia: a possible source of dust in East Antarctica interglacial ice. *Earth and Planetary Science Letters*, **249**, 1–13.

Sedwick, P.N. & DiTullio, G.R. 1997. Regulation of algal blooms in Antarctic shelf waters by the release of iron from melting sea ice. *Geophysical Research Letters*, **24**, 2515–2518.

Sedwick, P.N., DiTullio, G.R. & Mackey, D.J. 2000. Iron and manganese in the Ross Sea, Antarctica: seasonal iron limitation in Antarctic shelf waters. *Journal of Geophysical Research - Oceans*, **105**, 11 321–11 336.

Sedwick, P.N., Marsay, C.M., Sohst, B.M., Aguilar-Islas, A.M., Lohan, M.C., Long, M.C., Arrigo, K.R., Dunbar, R.B., Saito, M.A., Smith, W.O. & DiTullio, G.R. 2011. Early season depletion of dissolved iron in the Ross Sea polynya: implications for iron dynamics on the Antarctic continental shelf. *Journal of Geophysical Research - Oceans*, **116**, 10.1029/2010JC006553.

Wagener, T., Guieu, C., Losno, R., Bonnet, S. & Mahowald, N. 2008. Revisiting atmospheric dust export to the Southern Hemisphere ocean: biogeochemical implications. *Global Biogeochemical Cycles*, **22**, 10.1029/2007GB002984.

Wasserburg, G.J., Jacousen, S.B., DePaolo, D.J., McCulloch, M.T. & Wen, T. 1981. Precise determination of Sm/Nd ratios, Sm and Nd isotopic abundances in standard solutions. *Geochimica et Cosmochimica Acta*, **45**, 2311–2323.

Winton, V.H.L., Dunbar, G.B., Bertler, N.A.N., Millet, M.A., Delmonte, B., Atkins, C.B., Chewings, J.M. & Andersson, P. 2014. The contribution of aeolian sand and dust to iron fertilization of phytoplankton blooms in southwestern Ross Sea, Antarctica. *Global Biogeochemical Cycles*, **28**, 10.1002/2013GB004574.